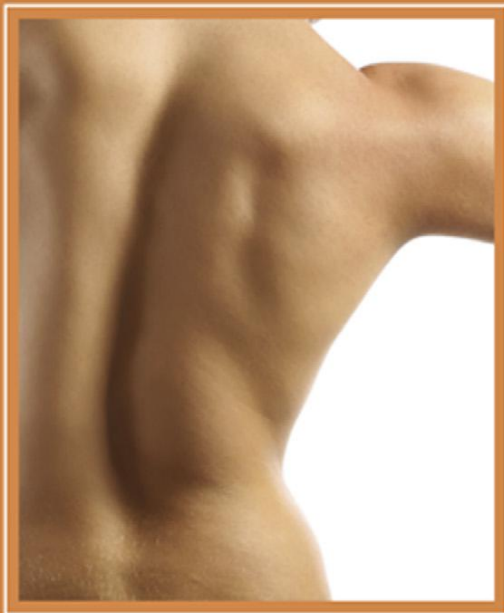


THIRD EDITION

BIOIMPEDANCE & BIOELECTRICITY BASICS



SVERRE GRIMNES
ØRJAN G. MARTINSEN



Bioimpedance and Bioelectricity Basics

This page intentionally left blank

Bioimpedance and Bioelectricity Basics

Third Edition

Sverre Grimnes

Ørjan G Martinsen

*Department of Physics, University of Oslo,
Oslo, Norway and*

*Department of Clinical and Biomedical Engineering,
Oslo University Hospital, Oslo, Norway*



ELSEVIER

AMSTERDAM • BOSTON • HEIDELBERG • LONDON • NEW YORK • OXFORD
PARIS • SAN DIEGO • SAN FRANCISCO • SINGAPORE • SYDNEY • TOKYO

Academic Press is an imprint of Elsevier



Academic Press is an imprint of Elsevier
32 Jamestown Road, London NW1 7BY, UK
525 B Street, Suite 1800, San Diego, CA 92101-4495, USA
225 Wyman Street, Waltham, MA 02451, USA
The Boulevard, Langford Lane, Kidlington, Oxford OX5 1GB, UK

Copyright © 2015, 2008, 2000 Elsevier Ltd. All rights reserved.

No part of this publication may be reproduced or transmitted in any form or by any means, electronic or mechanical, including photocopying, recording, or any information storage and retrieval system, without permission in writing from the publisher. Details on how to seek permission, further information about the Publisher's permissions policies and our arrangements with organizations such as the Copyright Clearance Center and the Copyright Licensing Agency, can be found at our website: www.elsevier.com/permissions.

This book and the individual contributions contained in it are protected under copyright by the Publisher (other than as may be noted herein).

Notices

Knowledge and best practice in this field are constantly changing. As new research and experience broaden our understanding, changes in research methods, professional practices, or medical treatment may become necessary.

Practitioners and researchers must always rely on their own experience and knowledge in evaluating and using any information, methods, compounds, or experiments described herein. In using such information or methods they should be mindful of their own safety and the safety of others, including parties for whom they have a professional responsibility.

To the fullest extent of the law, neither the Publisher nor the authors, contributors, or editors, assume any liability for any injury and/or damage to persons or property as a matter of products liability, negligence or otherwise, or from any use or operation of any methods, products, instructions, or ideas contained in the material herein.

ISBN: 978-0-12-411470-8

British Library Cataloguing in Publication Data

A catalogue record for this book is available from the British Library

Library of Congress Catalog Number

A catalog record for this book is available from the Library of Congress

For information on all Academic Press publications
visit our website at <http://store.elsevier.com/>

Typeset by TNQ Books and Journals
www.tnq.co.in

Printed and bound in the UK



Working together
to grow libraries in
developing countries

www.elsevier.com • www.bookaid.org

Contents

<i>Preface to the Third Edition</i>	xv
<i>Acknowledgments</i>	xvii
<i>Tips to the Reader</i>	xix
Chapter 1: Introduction	1
1.1 What Is Bioimpedance and Biopermittivity?	2
1.1.1 The Difference between AC and DC	3
1.2 What Is Bioelectricity?	3
1.3 How Are the Quantities of Bioimpedance and Bioelectricity Measured and Controlled?	4
1.4 Models	4
1.5 What Are the Applications of Bioimpedance and Bioelectricity?	5
1.5.1 Clinical Applications	5
1.5.2 Laboratory Applications	6
1.5.3 On the Borderline between Medical and Nonmedical Applications	6
1.5.4 Nonmedical Applications	6
1.5.5 Nonbiological Applications Outside the Scope of This Book	6
1.6 Some Unsolved Basic Problems	6
1.7 Who Is Working with Bioimpedance and Bioelectricity?	7
Chapter 2: Electrolytics	9
2.1 Ionic and Electronic DC Conduction	9
2.1.1 Ionization	10
2.1.2 Molecular Bonds	12
2.2 Basic Electrolytic DC Experiment	13
2.2.1 Setup	13
2.2.2 Findings	15
2.2.3 Discussion	15
2.3 Bulk Electrolytic DC Conductance	17
2.3.1 Net Charge of a Particle: The Isoelectric Point	25
2.3.2 Special Electrolytes	26
2.3.3 Conduction and Semiconductor Theory	28
2.3.4 Materials Classified According to Conductivity	29

2.4 Particle Migration and Diffusion	30
2.5 Electrokinetics	33
2.5.1 Flow Caused by Applied Electric Field (Exogen Transport)	34
2.5.2 Flow-Generated Potentials (Endogenic Potentials)	35
2.6 Problems	36
Chapter 3: Dielectrics	37
3.1 Polarization in a Uniform Dielectric	38
3.1.1 Coulomb's Law and Permittivity	39
3.1.2 Three Types of Polarization	41
3.1.3 Induced and Permanent Dipole Moments	42
3.1.4 Clausius–Mosotti and Debye Equations	44
3.1.5 Charge-Dipole and Dipole–Dipole Interactions	44
3.2 Basic Capacitor Experiment	45
3.2.1 Set-up	45
3.3 Complex Variables and Material Constants	47
3.3.1 Immittance and Material Constants: A Survey	49
3.4 AC Polarization and Relaxation in a Uniform Dielectric	51
3.4.1 Relaxation and Dispersion	51
3.4.2 Debye Relaxation (1R-2C) Model	53
3.4.3 Joule Effect and Temperature Rise	60
3.5 Interfacial Polarization	61
3.5.1 Maxwell–Wagner Effects	61
3.5.2 Suspension of Spherical Particles	63
3.5.3 Adsorbed Counterions and Lateral Diffusion (mHz–kHz Range)	65
3.6 Basic Membrane Experiment	67
3.7 Basic Suspension Experiment	70
3.8 Dispersion and Dielectric Spectroscopy	71
3.9 Problems	75
Chapter 4: Passive Tissue Electrical Properties	77
4.1 Basic Biomaterials	77
4.1.1 Water and Body Liquids	77
4.1.2 Proteins	79
4.1.3 Carbohydrates and Saccharides	83
4.1.4 Lipids and the Passive Cell Membrane	83
4.2 Tissue and Organs	85
4.2.1 Tabulated Tissue Conductivity Data	87
4.2.2 Muscle Tissue	89
4.2.3 Nerve Tissue and Impedance	92
4.2.4 Adipose and Bone Tissue	92
4.2.5 Blood	93
4.2.6 Human Skin and Keratinized Tissue	95

4.2.7 Whole Body	105
4.2.8 Postexcision Changes and the Death Process.	106
4.2.9 Plant Tissue.	109
4.3 Special Electrical Properties.	110
4.3.1 Tissue Anisotropy	110
4.3.2 Continuity across Interfaces, Tissue, and Implants	113
4.3.3 Tissue DC Properties	114
4.3.4 Piezo- and Triboelectric Effects	116
4.4 Problems.	117
Chapter 5: Excitable Tissue and Bioelectric Signals	119
5.1 Cell Polarization	120
5.2 Action Potential	122
5.2.1 Ion Channels	123
5.2.2 Channel Gating	123
5.2.3 Cell Potential Model	125
5.2.4 Cell Oscillator	127
5.3 The Neuron.	127
5.3.1 Motor Neuron	128
5.3.2 Brain and Neurons.	129
5.4 Axon Transmission	131
5.4.1 Excitation from the Soma.	131
5.4.2 Exogenous Excitation of the Axon	132
5.4.3 Moving Current Dipole	132
5.4.4 Myelinated Axons	133
5.4.5 The Nerve	134
5.4.6 Synapses	135
5.4.7 Excitation	135
5.4.8 External Electric Excitation	136
5.5 Receptors	138
5.6 Problems.	138
Chapter 6: Geometrical Analysis	141
6.1 Volume Conductors	141
6.1.1 Forward Problem.	142
6.1.2 Inverse Problem.	142
6.1.3 Boundary Value Problem	142
6.2 Sphere Sources, Ideal Three-Dimensional Models.	142
6.2.1 Sphere Monopole Source	143
6.2.2 Constricting/Dispersing Zone	146
6.2.3 CC and PU Dipoles	147
6.2.4 Disk Monopole Source.	150
6.2.5 Ellipsoidal Needle Source	152

6.3 Line Sources, Ideal Two-Dimensional Models	155
6.3.1 Cylinder and Stripe Monopolar Sources	155
6.3.2 Two Parallel Cylinders	157
6.3.3 Ring Monopolar Source	157
6.3.4 Parameter Dependence on Distance from Source	158
6.4 Signal Transfer	158
6.4.1 Fixed Recording Lead, Moving Source	158
6.4.2 Spatial Resolution and Frequency Content, Passage Effect	160
6.4.3 Transfer Lead Vector between Two Dipoles	161
6.4.4 Nonideal Volumes, Reciprocal Lead Field	163
6.4.5 Sensitivity Field	166
6.4.6 Bipolar Measuring Depth	167
6.4.7 Surface Layer	169
6.5 Finite Element Method	169
6.6 Imaging, Electrical Impedance Tomography	171
6.7 Duality of Dielectric and Conductor Theory	176
6.8 Problems	177
Chapter 7: Electrodes	179
7.1 Electrode Pair	179
7.2 Single Electrode	179
7.3 Electrode Metals	180
7.3.1 Test of Polarizability of Electronic Conductors	180
7.3.2 Metal and Electronic Conductor Properties	183
7.4 Contact Electrolytes	184
7.4.1 Contact Media Descriptions	185
7.4.2 “Dry” and Dielectric Contact	188
7.4.3 Skin Preparation	191
7.5 Electrode Double Layer	191
7.5.1 Electric Double Layer, Perpendicular Fields	192
7.5.2 Electric Double Layer, Lateral Fields	196
7.6 DC Potentials, No Current Flow	197
7.6.1 Metal/Ion and Redox Systems	197
7.6.2 The Nernst Equation	199
7.6.3 Electrode Pair DC Voltage	200
7.6.4 Liquid Junction DC Potential, Salt Bridge	201
7.6.5 Membrane Equilibrium (Donnan) Potentials	202
7.6.6 Reference Electrodes	202
7.7 Basic Experiment with DC Current Flow	203
7.8 Faraday’s Law of Electrolysis	208
7.8.1 DC, AC, and Chemical Reaction Reversibility	209

7.9	Electrode Polarization	209
7.9.1	DC Counter Electromotive Voltage	209
7.9.2	Electrode Polarization Impedance in Saline	210
7.9.3	DC/AC Equivalent Circuit for Electrode Processes	214
7.10	Multiple Electrode Systems	219
7.10.1	Half Cells and Electrode Pairs	219
7.10.2	Three-Electrode Systems Monopolar Recording	220
7.10.3	Four-Electrode (Tetrapolar) Systems	223
7.11	Electrode Terminology	226
7.11.1	Probe Concepts, Electric Field Sensor	233
7.12	Electrode Designs	233
7.12.1	Skin Electrodes	233
7.12.2	Skin Electrode Wires	236
7.12.3	Invasive Needle Electrodes	236
7.12.4	Micro- and Nanoelectrodes	239
7.12.5	In vitro Measuring Cells	240
7.12.6	Ponderomotoric Effects and Electrodes	242
7.12.7	Patch Clamp Electrode	244
7.12.8	Nongalvanic Coupling to Tissue	245
7.12.9	Kelvin Probe	251
7.13	Vulnerable Electrode Technology	252
7.14	Problems	253
Chapter 8: Instrumentation and Measurements	255
8.1	General Network Theory, the Black-Box	255
8.1.1	Immittance, Admittance, and Impedance	256
8.1.2	Two-Port Network, Signal Transfer, Conditions	257
8.1.3	Reciprocity	258
8.1.4	Extended Immittance Concepts	259
8.1.5	Step Function Excitation and Time Constant	260
8.1.6	Kramers–Kronig Transforms	260
8.2	Signals and Measurement, Noise	262
8.2.1	DC, Static Values, and AC	262
8.2.2	Periodic Waveforms, Fourier Series	263
8.2.3	Aperiodic Waveforms	271
8.2.4	Spectrum Analysis, Fourier Transforms	273
8.2.5	Time and Frequency Domain	278
8.2.6	General Remarks about Transformation	279
8.2.7	Frequency Filtering	280
8.2.8	Signal Generators	281
8.2.9	Grounded or Not Grounded Patient	282
8.3	Amplifiers, Bridges, Analyzers	283
8.3.1	Black Box Analysis, Amplifiers, Filters	283

8.3.2 Instrumentation Differential Amplifiers	286
8.3.3 Interface Patient and Amplifier, Risk Considerations	288
8.3.4 Power Line Noise Cancellation.	290
8.3.5 Measuring DC Potential and AC Admittance Simultaneously at the Same Skin Site.	293
8.3.6 Bridges, Synchronous Rectifiers, Fast Amplifiers.	294
8.3.7 Lock-in Amplifiers.	295
8.3.8 Microelectronic Lock-in Amplifiers	299
8.3.9 Impedance Analyzers and LCR Meters	302
8.3.10 Time Domain Spectroscopy	309
8.3.11 Time Domain Transmissometry	310
8.3.12 Time Domain Reflectometry.	315
8.4 Nonlinear Phenomena	318
8.4.1 Electrolyte Nonlinearity	318
8.4.2 Electrode Nonlinearity	319
8.4.3 Tissue and Cell Nonlinearity	321
8.4.4 Instrumentation Nonlinearity	327
8.5 Problems.	328
Chapter 9: Data and Models	329
9.1 Models, Descriptive and Explanatory	329
9.1.1 The Model Concept.	330
9.1.2 Description or Explanation?	330
9.1.3 The Best Model.	331
9.2 Equations, Laws, and Equivalent Circuits	332
9.2.1 Coulombs Law	332
9.2.2 Maxwell–Heaviside Equations.	332
9.2.3 Two Ideal Components Equivalent Circuits	335
9.2.4 Debye Models, Three Ideal Components.	342
9.2.5 Constant Phase Element.	344
9.2.6 Cole Equations (1940)	348
9.2.7 Cole–Cole Equations (1941)	357
9.2.8 Symmetrical Distribution of Relaxation Times	358
9.2.9 Nonsymmetrical DRT and Multiple Cole Systems	360
9.2.10 Bidomain Model	367
9.2.11 Memristor Nonlinear Model	367
9.2.12 Universality	369
9.3 Data Calculation and Presentation	370
9.3.1 Measured Data, Model Data.	370
9.3.2 Indexes	371
9.4 Statistical Methods for Bioimpedance Analysis.	371
9.4.1 Hypothesis and Research Design	372
9.4.2 Multiple Variables and Data Reduction (Parameterization)	375

9.4.3 Choice of Statistical Method	376
9.4.4 Validation Methods	386
9.5 More Data Analysis Methods.	394
9.5.1 Multivariate Analysis	394
9.5.2 Clinical Performance	396
9.5.3 Neural Networks	397
9.5.4 Chaos Theory and Fractals	398
9.5.5 Wavelet Analysis	400
9.6 Problems.	403
Chapter 10: Selected Applications	405
10.1 Heart as a Bioelectric Source (ECG)	405
10.1.1 Three Limb Electrodes (Six Limb Leads).	405
10.1.2 Six Chest Electrodes (Six Unipolar Precordial Leads)	411
10.1.3 Cardiac Electrophysiology	412
10.1.4 Vector Cardiography	413
10.1.5 Forward and Inverse Problems.	414
10.1.6 ECG Technology	415
10.1.7 Noise	416
10.2 Other Organs as Bioelectric Sources	416
10.2.1 Brain (EEG, Electroencephalography)	416
10.2.2 Brain (ECOG, Electrocorticography)	417
10.2.3 Eye (EOG, Electrooculography)	417
10.2.4 Eye (Electronystagmography)	417
10.2.5 Eye (ERG, Electroretinography)	418
10.2.6 Stomach (EGG, Electrogastrography).	418
10.2.7 Muscles (EMG, Electromyography)	418
10.2.8 Nerves (Electroneurography)	419
10.2.9 Urology	419
10.3 Electrodermal Activity, Psychophysiology	420
10.3.1 Physiology, Psychophysiology, Stimuli.	420
10.3.2 DC and AC Exogenous Measurements	421
10.3.3 Skin as an Endogenous Bioelectric Source, Skin Potential	422
10.3.4 Potential and Impedance from Same Skin Site	422
10.4 Other Skin Applications	425
10.4.1 Sweat Activity Measurement (Sudologger)	425
10.4.2 Skin Hydration Measurement	425
10.4.3 Skin Diseases	426
10.4.4 Fingerprint Detection	432
10.5 Impedance Plethysmography	433
10.5.1 Ideal Cylinder Models.	433
10.5.2 The Effect of Different Conductivities	435
10.5.3 Models with Any Geometry and Conductivity Distribution	436

10.5.4 Electrical Impedance Myography	437
10.5.5 Rheoencephalography	438
10.6 Impedance Cardiography	440
10.6.1 Stroke Volume Measurements	440
10.6.2 Time Relationships in the Cardiac Cycle	442
10.7 Imaging of Lungs	444
10.8 Body Composition	445
10.9 Defibrillation and Electroshock	450
10.9.1 Defibrillator	450
10.9.2 Electroshock (Brain Electroconvulsion)	452
10.10 Electrosurgery	453
10.10.1 Risk Analysis	455
10.10.2 Embedded Bioimpedance Devices	456
10.11 Cell Suspensions	459
10.11.1 Electroporation and Electrofusion	459
10.11.2 Cell Sorting and Characterization by Electrorotation and Dielectrophoresis	466
10.11.3 Cell-Surface Attachment and Micromotion Detection	467
10.11.4 Coulter Counter	468
10.12 Implanted Active Thoracic Devices	469
10.12.1 Physiologic Impedance Components	470
10.12.2 Fluid Status Monitoring	471
10.12.3 Cardiac Pacemakers	473
10.13 Electrotherapy	474
10.13.1 Electrotherapy with DC	475
10.13.2 Electrotherapy of Muscles	477
10.14 Nonmedical Applications	480
10.15 Discoveries, Innovations	480
10.16 Electrical Safety	482
10.16.1 Threshold of Perception	482
10.16.2 Electrophysiological Hazards	485
10.16.3 Lightning and Electrocution	489
10.16.4 Electric Fence	490
10.16.5 Electroshock Weapon (Taser)	490
10.16.6 Electrical Safety of Electromedical Equipment	491
Chapter 11: History of Bioimpedance and Bioelectricity	495
11.1 Electrocardiogram—Heart Muscle Activity	497
11.2 Electroencephalogram—Brain, Nervous Tissue	498
11.3 Electrodermal Activity—Skin, Sweat Activity	498
11.4 Kenneth S. Cole (1928a,b Papers)	500
11.5 Peter Debye (1929 Book)	501
11.6 Hugo Fricke (1932 Paper)	501

11.7 Kenneth S. Cole (1932 Paper)	502
11.8 Kenneth S. Cole (1940 Paper)	502
11.9 Kenneth S. Cole and Robert H. Cole (1941 Paper)	502
11.10 Herman Paul Schwan (1915–2005)	503
11.11 Surface Potentials Generated by a Bioelectric Source in a Volume Conductor	504
Chapter 12: Appendix	505
12.1 Vectors and Scalars, Complex Numbers	505
12.1.1 Vectors and Scalars.	505
12.1.2 Complex Numbers	506
12.1.3 Sign Conventions	508
12.1.4 Phasor, Sine Wave, and Operator $j\omega t$	509
12.1.5 Some Algebraic Rules for <i>Sine Wave</i> Complex Numbers	509
12.2 Equivalent Circuit Equations	509
12.2.1 Equations for Two Resistor + One Capacitor Circuits	510
12.2.2 Equations for One Resistor + Two Capacitor Circuits	514
12.2.3 Equations for Four-Component <i>Series</i> Circuit (Simple Maxwell–Wagner Model)	517
12.3 Global Symbols	518
12.3.1 Physical Dimensions.	522
References	525
Index	549

This page intentionally left blank

Preface to the Third Edition

Within our field, intriguing new applications have emerged in the period since the second edition of Bioimpedance and Bioelectricity Basics (BBB) appeared six years ago. Medical imaging by bioimpedance has succeeded in going bedside in intensive care units. With new minimally invasive micro-needle electrodes, it is now possible to take rapid electronic biopsies for skin cancer detection. Bioimpedance has made electrosurgery safer by monitoring vessel sealing under coagulation. Such new techniques are described in this edition of the BBB. Also new types of single cell and cell suspension measurements by electrokinetic, ponderomotoric, and micromotion methods are included.

Fourteen years have passed since the first edition of the book appeared. The content of a book like BBB adapts to the continuous progress in basic theory, geometrical analysis, reciprocity, black box modeling, biosignal preamplification, models and laws, statistical methods for bioimpedance analysis, nonlinear phenomena, electrical safety, and many other relevant topics.

Some changes and additions have been made in this edition: An electrode is the most important component of any bioimpedance and bioelectric measuring systems. To make the book easier to read, we have dedicated a specific chapter to electrodes. Furthermore, we have extended the chapter on models with a comprehensive tutorial on statistical analysis of bioimpedance data. We have also included the Kelvin probe, memristor theory, and the concept of universality (scaling properties) and we have expanded the survey on impedance analyzers.

Although this book has been written primarily for graduate and postgraduate students in biomedical engineering and biophysics, we hope it will be useful also for other researchers coming in touch with our area, e.g., from biotechnology in general, electrophysiology, odontology, pharmacy, and plant biology. Some devoted medical doctors in the field of neurology, cardiology, dermatology, clinical chemistry, and microbiology have not been forgotten. We have on certain subjects reverted to an almost “Adam and Eve” approach. In addition, the number of illustrations was high in the first edition, increased in the second edition, and has been increased further in this latest edition. We have not renounced on mathematical equations, but often tried to include an extended discussion on their implications. To keep the book within the “basic” framework, we have imposed certain boundaries: We have excluded magnetism, which is already well covered by Malmuvio and Plonsey (1995). We

have excluded a broader treatment of Electrical Impedance Tomography (EIT), which is now well covered by Holder (2005). We have mainly limited this book to sine wave and step function variables, omitting a more general treatment by the theory of Laplace transforms. And also we have limited the number of application examples.

The first edition of BBB grew out of a certain frustration of having used unnecessarily much time ourselves learning some of the theory and practice of bioimpedance, and out of a certain hope that a new book could pave an easier and more efficient way for people seeking basic knowledge about our discipline. Bioimpedance and bioelectricity must perhaps be considered as rather specialized fields, but obviously based on an extract from scientific basic disciplines. All these disciplines cannot be taught in their full extensions, but with this book it should be possible to gather many of them into *one single subject and one course*. For the newcomer it is also an advantage to be presented a unified set of terminology and symbols, to avoid the start with the silent terminology of the paradigms of each area, bewildering traditions illustrated for instance by the different use of the term “polarization” and such symbols as m and α .

Our background in the fields of biomedical engineering, physics, and instrumentation is of course discernible. All the same we have found it necessary to cover a much broader range of topics. Our emphasis is on systems with galvanic contact with tissue, not so much on the interaction between tissue and airborne electromagnetic fields and waves. A large part has been dedicated to model thinking. The importance of the *geometry* of a measuring system cannot be overemphasized. We hope that the balance between the descriptive and quantitative/theoretical text parts will be appreciated.

Our field offers many challenges. In order to understand the phenomena of interest, a certain basic knowledge of electrochemistry, electronic engineering, physics, physiology, mathematics, and model thinking is needed. And that is exactly what you will find in the chapters of this book.

Acknowledgments

We are greatly indebted to the many colleagues and friends who have contributed to Bioimpedance and Bioelectricity Basics (BBB) by commenting and making suggestions on selected chapters. We are in particular indebted to the late Herman P. Schwan at the University of Pennsylvania for the long discussions that had a significant influence on the first edition. The valuable contributions from Andrew Ahn, Eugen Gheorghiu, David Holder, Javier Rosell, Ramon Bragos, Pere Riu, Leigh Ward, Mart Min, Jan Meijer, Uwe Pliquett, Ronald Pethig, Sebastian Wegner, Stig Ollmar, and many more are highly appreciated. We also thank all our colleagues and friends of the Oslo Bioimpedance Group for the many discussions and invaluable input.

It has been a pleasure to work with Cari Owen and Nicky Carter at Elsevier and we are truly grateful for all their professional help and positive spirit. Last but not least, this book is for the loving memory of Kari and for Kjersti.

Oslo, August 2014
Sverre Grimnes and Ørjan G Martinsen

This page intentionally left blank

Tips to the Reader

A **bold** symbol is either a space vector or a complex number. A nonbold symbol is either a scalar, or a magnitude, or the real part of a vector. In the literature, an intelligent guess often has to be made. A phase angle is denoted by φ , a loss angle by δ . In the literature the loss angle is often called a phase angle, which it of course also is.

Φ is used for a potential difference in space and V for a voltage difference in a circuit. Φ may designate not only the potential at a defined position, but also as a function of position in space, the potential *field* $\Phi(x,y,z)$.

Global symbols used all over the book are tabulated in Table 12.1, and are *not* necessarily explained locally in the text.

Impedance variables such as Z , R , X , ρ , and C_s are preferably used when components are connected in series. *Admittance* variables such as Y , G , B , σ , and C_p are preferably used when components are connected in parallel. *Immittance* is the combined term for both impedance and admittance. It is often used in order to force the reader to be sensitive to the choice: there is no such thing as an immittance equation.

Units are often written in square brackets, e.g., [V] or [volt]

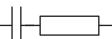
In figures, smooth borderline symbolizes a bounded volume:



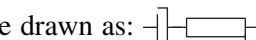
In figures, zigzag borderline symbolizes an infinite volume:



Ideal capacitor and resistor components are drawn as usual:



Electrolytic components with frequency dependent values are drawn as:



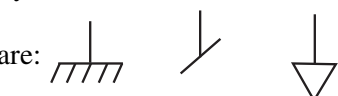
A Wessel diagram is the same as an Argand diagram: a diagram in the complex plane.

Symbol for power line ground (safety and noise) is:



Symbols for a wire from the instrumentation called reference, zero, chassis, shield etc.

are:



The reference wire is to be coupled to an indifferent electrode on the patient. If the wire is grounded in the instrument, the patient will be grounded via the indifferent electrode. A medical instrument will then be of type B. If the wire is not coupled to ground in the instrument, the patient will be floating (F), and the instrument will be of type BF (body floating) or CF (cardiac floating).

The International System of units (SI) is used in Bioimpedance and Bioelectricity Basics (BBB). Notice that the choice of systems also influences the formulas. For instance, Coulomb's law differs by the factor $4\pi\epsilon_0$ between the old centimeter-gram-second (cgs) system ($F = q_1q_2/\epsilon_r r^2$) based on centimeter and not meter, and the SI system ($F = q_1q_2/4\pi\epsilon_r\epsilon_0 r^2$). Or in cgs: $\mathbf{D} = \epsilon_r \mathbf{E}$ and in SI: $\mathbf{D} = \epsilon \mathbf{E}$.

Be aware of the fact that in the literature, $\log x$ may mean the common logarithm $\log_{10} x$ or (in particular in mathematics) the natural logarithm $\ln x$. In BBB $\log x$ means $\log_{10} x$.

Introduction

Bioimpedance, bioelectricity, and the electrical properties of tissue are much about the same things. *Bioimpedance* deals with some passive electrical properties of tissue: the ability to oppose (impede) electric current flow. *Bioelectricity* deals with the ability of tissue to generate electricity, such as done by the heart (electrocardiography). This electricity is endogenic—that is, it is generated by the tissue itself. Bioelectricity is also about how tissue can be controlled by externally applied electricity. Such electricity, together with the electricity used for measuring bioimpedance, is exogenic—that is, it refers to externally applied electricity.

Bioimpedance and bioelectrical methods use electrodes with galvanic coupling to tissue. The instrumentation uses electronic circuitry and wires coupled to the electrodes. The charge carriers flowing in the copper wires are electrons. The charge carriers in living tissue are (with some exceptions) ions. An electrode proper is the site of charge carrier conversion from ions to electrons and vice versa. It is practical to divide problems into circuit problems and field problems. Circuit problems include issues with wires, capacitors, resistors, semiconductors, batteries, and so on. The current flow is confined to the wires; a voltage difference (volt) is measured between two points in the circuitry. Field problems are related to volume conductors and quantities that are a function of position in that volume, such as the potential field $\Phi(xyz)$.

There is a duality in the electrical properties of tissue. Tissue may be regarded as a *conductor* or a *dielectric*. In frequencies of 100 kHz or less, most tissues are predominantly electrolytic conductors. Therefore, we start Chapter 2 with a look at electrolytes. Bulk electrolyte continuity is broken in two important ways: by electrode metal plates and by cell membranes. This break in continuity introduces capacitive current flow segments. At the electrodes, electric double layers are formed in the electrolyte; the cell interiors are guarded by membranes. With high-resolution techniques, it is possible to extract important capacitive (i.e., *dielectric*) properties even at low frequencies, such as 10 Hz. At higher frequencies, such as 50 kHz, the dielectric properties of tissue (discussed in Chapter 3) may dominate. At the highest frequencies, tissue properties become more and more equal to that of water. Pure water has a characteristic relaxation frequency of approximately 18 GHz.

In tissue and the living cell there is an inseparable alliance between electricity and chemistry. Electrolytic theory and electrochemistry therefore form an important basis for

our topics; it is not possible to understand what is going on in tissue during electric current flow without knowing some electrochemistry.

Bioimpedance and bioelectricity is about biomaterials in a broad sense—materials that are living, have lived, or are potential building blocks for living tissue. The tissue of interest may be plant, fruit, egg, fish, animal, or a human body. It may also be dead biological material such as hair or nail, or excised material such as beef or a piece of stratum corneum. The basic building block is the living cell, and a prerequisite for its life is that it is surrounded by an electrolyte solution. Great caution must be imposed on the state of the biomaterial sample. A material may change completely from the living, wetted state with large contributions from interfacial counterion mechanisms, then—via a denaturation or death process—to a more or less dead and dry sample. The extreme end of the spectrums includes a sample that must be measured in a vacuum chamber. It is important to remember this when, for example, ionic versus electronic/semiconductive properties are discussed. Life is so diversified and so complex. For example, bacteria may be in dry surroundings and encapsulated in a sleeping state, and so it is difficult to give them a clear living status.

1.1 What Is Bioimpedance and Biopermittivity?

Impedance is the ratio between voltage and current. It applies to both direct current (DC) and alternating current (AC). *Admittance* is the inverse of impedance—that is, not impede, but admit, current flow. *Immittance* is the combined term for impedance and admittance, so a better and more generic term than bioimpedance is *bioimmittance*.

A dielectric is, traditionally, a dry insulator capable of storing electrical energy. An electrostatic field cannot penetrate a metal but may penetrate through (Greek: dia) the dielectric. The most important dielectric quantity is *permittivity*, or ϵ . Permittivity is the ability to permit storage of electric energy. Under linear conditions and for the same tissue, unity cell admittance (Y), unity cell impedance ($Z = \frac{1}{Y}$), and complex permittivity ϵ all contain the same information, but are presented differently. These quantities are based upon the law of Coulomb (1785) and the equations of Maxwell (1873), discussed in Chapter 9. The Maxwell equations are based on the velocity of light and the fact that light is electromagnetic radiation. There is a direct link between the electrical permittivity of a material and its optical refractive index.

Note the difference between resistance, conductance, impedance, admittance, immittance—and resistivity, conductivity, impedivity, admittivity, immittivity, permittivity. The “-ance” parameters are dependent both on the electrical properties of the sample and the measuring system geometry. The “-ivity” parameters are material constants dependent only on the electrical properties of the sample, not its geometry and dimensions (as discussed in Chapters 3 and 4).

Bioimmittance is frequency dependent. In dielectric or electrolytic models there is a choice between a step (relaxational) and sinusoidal (single-frequency) waveform excitation. As long as the step response waveform is exponential and linear conditions prevail, the information gathered is the same. At high voltage and current levels, the system is nonlinear, and models and parameters must be chosen with care. Results obtained with one variable cannot necessarily be recalculated to other forms. In some cases, one single pulse may be the best waveform because it limits heat and sample destruction.

1.1.1 The Difference between AC and DC

Impedance and admittance are basically AC parameters. It is easy to believe that AC values approach DC values when the AC frequency $\rightarrow 0$ Hz. However, this is not necessarily true because of electrolysis. At sufficiently low frequencies, one polarity lasts long enough to generate irreversible products that change the chemical environment permanently.

1.2 What Is Bioelectricity?

Bioelectricity refers to the electrical phenomena of life processes, and is a parallel to the medical subject electrophysiology. One basic mechanism is the energy-consuming cell membrane ion pumps polarizing a cell, and the action potential generated if the cell is triggered and ion channels opened. The depolarization process generates current flow also in the extracellular volume, which again results in measurable biopotential differences in the tissue. An important part of such activity is intracellular and extracellular single cell measurement results with microelectrodes. Single neuron activity and signal transmission can be studied by recording potentials with multiple microelectrode arrays.

In addition to measure on endogenic sources, bioelectricity also comprises the use of active, stimulating, current-carrying electrodes. Electricity is used clinically for the treatment of patients (electrotherapy), and is discussed in Chapter 10. Low-energy current pulses for nerve excitation are used for pain relief, and also in implanted devices. Organ functions are activated with implanted pacemakers and external muscle stimulators. Small DC currents are used for speeding up the healing of nonunion bone fractures. High-energy methods clearly operate in the nonlinear region. We must be aware that most models treated extensively by textbooks are limited to linear cases. Many applications such as defibrillation or electroporation are performed in the nonlinear range. Defibrillation is a life-saving procedure; electroporation is used for a very short opening of cells. Surgery and ablation are performed using high-frequency currents (electrosurgery).

1.3 How Are the Quantities of Bioimpedance and Bioelectricity Measured and Controlled?

Bioelectricity experiments are performed *in vivo* or *ex vivo* with pickup electrodes and stimulation electrodes. Electrotherapeutic methods use electricity controlled by current or voltage, charge, energy, waveform, and time.

Bioimmittance is measured *in vivo* or *in vitro*. The tissue may be kept alive and perfused under *ex vivo* conditions. Bioimmittance can be measured with two-, three- or four-electrode systems. With four electrodes, one electrode pair is current carrying and the other pair picks up the corresponding potential difference somewhere else in the tissue. If the measured voltage is divided by the applied current, the transfer impedance is calculated. If no voltage is measured, the transfer impedance is zero. This is equivalent to the bioelectricity case in which a signal from the source, such as the heart, is transferred to the skin surface electrodes. Zero transfer impedance does not mean the tissue conducts well, only that no signal transfer occurs. With the bioimpedance two-electrode technique, the transfer factor is eliminated because current application and signal pickup occur at the same site, which means that measured impedance reflects tissue electrical properties more directly.

Single cells are measured with microelectrodes and clamp and patch techniques (see Chapters 7 and 10).

Exogenic current is usually applied with electrodes in galvanic contact with tissue. It is also possible to apply it by a magnetic field without making physical contact with the tissue. Biopotential is difficult but not impossible to measure without galvanic contact.

The technology of the instrumentation is often based on a synchronous rectifier technique because it has superior noise suppression properties, as discussed in Chapter 8. The prerequisite is a reference signal, which is always available in immittance AC measurement systems.

1.4 Models

Science is very much about the use of models, to describe and therefore predict, and to explain and therefore understand. *Bioimpedance and Bioelectricity Basics* emphasizes model thinking, as we see in Chapter 9. The selected model often dictates the measuring method to be used. The interpretation of the results is dependent on the angle of view and the model used. Models, however, have their shortcomings. Important models for bioimmittance are empirical and can, therefore, only describe. Because tissue behaves predominantly electrolytically, a model's treatment of DC conductivity is important. With high-energy pulses or DC, the principle of superposition often is not valid, and different

contributions cannot simply be added. Many high-energy applications such as defibrillation or electroporation are clearly in the nonlinear range; a sine wave excitation does not lead to a sine wave response. Many researchers have been led astray by using an incorrect model, such as using a series model for processes that actually occur physically in parallel. Another example is that a dispersion model presupposes the measured volume is independent of frequency, which is not always the case in a measuring setup. In fact, how to select or limit the measured volume is part of a general problem in bioimpedance.

The classic models for bioimpedance and bioelectricity are mathematical equations and equivalent circuit diagrams with the same electrical behavior as the tissue to be modeled. Others include statistical models, which are used to determine the correspondence between bioelectrical measurements and physiological variables (e.g., tissue characterization).

1.5 What Are the Applications of Bioimpedance and Bioelectricity?

In this book, and in Chapter 10 in particular, we take a look at the many applications of bioimpedance and bioelectricity, including clinical, laboratory, borderline medical and nonmedical, nonmedical, and nonbiological applications.

1.5.1 Clinical Applications

Many clinical applications are well established. Recording bioelectric signals from the heart (electrocardiography) was introduced by Waller in 1887 and brought into clinical use by Einthoven around 1905, and is still an important examination in hospitals worldwide. Electrodermal activity was also started in the 1880s, but it took many decades before the generation mechanism was understood. Electrosurgery was in a similar same position during 1930s. Recording bioelectric signals from the brain (electroencephalography) was introduced during the 1940s, and pacemakers and defibrillators were put into use during the 1960s. Lung plethysmography and respiration rate determination have been used in electrocardiographic monitors for several decades. Split electrodes with bioimpedance monitoring of electrode–tissue contact have been used for many years in critical medical electrode applications.

In the past few years, new applications have emerged. Immittance-based plethysmography is used to measure cardiac output both with transcutaneous electrodes and with pacemaker implants. Electrical impedance tomography is used for lung imaging in intensive care units. Different kinds of skin diagnostic methods are used to treat skin cancer, dermatitis, skin moisture, sweat activity and hyperhidrosis. Pain relief is obtained with transcutaneous electrical nerve stimulators or implanted devices. Organ ischemia and rejection processes can be monitored. Diabetes parameters can be measured. The water balance can be determined together with the monitoring of dialysis treatment. In vivo applications of

electroporation and drug therapy are exploited. Tissue ablation is performed with catheters or endoscopes with radiofrequency current. Tissue characterization is done and needle position can be determined. Joint angles can be determined with skin electrodes. Skin moisture is measured, and sweat activity is logged on several skin sites simultaneously. Skin potential and impedance can be measured simultaneously at the same skin site.

1.5.2 Laboratory Applications

Laboratory-on-a-chip systems use immittance and dielectric variables measured with microelectrodes. In flow sensors, cell properties are measured with microelectrodes, and cell characterization and cell separation are performed. Properties of protein molecules have, for many years, been determined by the established methods of electrophoresis. Electrophoresis is based on the electric charge of cells and proteins, and the driving force exerted by an electric field. All sorts of liquid suspensions with cells or bacteria can be measured with bioimmittance or permittivity. Cell adherence and cell micromotion can be monitored with microelectrodes equipped with a thin surface coating.

1.5.3 On the Borderline between Medical and Nonmedical Applications

Body composition and intra-/extracellular fluid indexes can be determined for monitoring nutrition and physical training. Small portable loggers for heart rate and respiration rate during, for example, bicycling or treadmill exercise have found a large market as a part of the instrumentation for sports medicine.

1.5.4 Nonmedical Applications

Meat quality assessments are made with bioimpedance measurements and multivariate analysis. Fermentation can be monitored in brewery industries. Plant properties can be determined in the living or dead state (wood quality).

1.5.5 Nonbiological Applications Outside the Scope of This Book

Soil quality and humidity can be determined using immittance measurements. Geophysical properties related to oil drilling have been measured with impedance methods since the 1920s (Schlumberger, 1920). Large iron-bar electrodes and current levels of hundreds of ampere are used. Volcanic activity is monitored by impedance on Iceland.

1.6 Some Unsolved Basic Problems

Electromagnetic hazards using bioimpedance and bioelectricity methods must be considered. How is the electric current spread from the electrodes in living tissue? Can we

find the conductivity distribution in living tissue? What is the influence of body macromembranes and anisotropy? To what extent does an externally applied electric current follow blood vessels? Is there really a specific constant-phase mechanism for immittance in biological materials? What are the different mechanisms of the dielectric α -dispersion? What are the mechanisms of counterion relaxation, particularly at the cell membranes? What is the theoretical basis for the nonexponential relaxation so often found? To what extent is it possible to understand tissue properties under nonlinear conditions?

1.7 Who Is Working with Bioimpedance and Bioelectricity?

Industry, research institutes, interventional centers, and universities are all doing basic research within the discipline of bioimpedance and bioelectricity. The goal of the industry is to develop competitive products. The goal of research institutes and universities is to develop new academic knowledge and publish it. Biomedical engineers, biophysicists, mathematicians, electrochemists, and computer scientists are all involved in the development of new methods and new knowledge. On the biological side, physiologists and biologists are important. Medical doctors are often clinically oriented and concerned with applications within their own specialty: anesthesia, cardiology, dermatology, neurology, physical medicine, sports medicine, and surgery.

This page intentionally left blank

Electrolytics

2.1 Ionic and Electronic DC Conduction

An *electrolyte* is a substance with ionic DC conductivity. Intracellular and extracellular liquids contain *ions free to migrate*. In pure electrolytes, the charge carriers are ions, and there is no separate flow of electrons—they are all bound to their respective atoms. Therefore, tissue DC currents are *ionic currents*, in contrast to the *electronic current* in metals. This is not contradictory to a possible local electronic conductance due to free electrons (e.g., in the intracellular DNA molecules). New solid materials such as organic polymers and glasses may contain an appreciable amount of free ions with considerable mobility; therefore, the materials of an electrolytic measuring cell are not limited to liquid media. Some of these solid media show a mixture of ionic and electronic conductivity.

Two *current-carrying electrodes* in an electrolyte are the source and sink of electrons—from electrons of the metal to ions or uncharged species of the electrolyte. *The electrode is the site of a charge carrier shift, or a charge exchange between electrons and ions.*

In a metal, the conductance electrons are free to move; they are similar to an electron gas not linked to particular metal atoms, but with a probability of being at a certain location at a certain time. The metal atoms can be considered bound but ionized; they have lost electrons. Electron transport in a metal involves no transport of metal ions and not even a transport of electrons all of the way. When we supply an electron into a wire end, “another” electron is coming out of the other end. Current flow that seems to be so fast is so only because it is not the same electron entering and leaving. The migration velocity of electrons in a metal is actually very slow—on the order of 0.3 mm/s at rather high current densities. The migration velocity of *ions* in solution is also very slow. As studied by electrophoresis, the ion migration velocity is on the order of 10 mm/s.

At the very low migration velocities, there are no collision phenomena when charge carriers are stopped. The electronic conduction in the vacuum of a cathode ray tube (CRT) is very different. Friction is low and electron velocity is very high—on the order of thousands of meters per second (but with much fewer electrons engaged). When these fast electrons are stopped, there is a collision (e.g., with the phosphor plate that lights up in a CRT or the anode of an X-ray tube, which emits X rays).

Electric current flow in an ionic solution is a more complex event than in a metal. Electron current implies no transport of substance; an externally applied DC current can flow forever without changing the conductor. However, ion current implies a transport of substance. Therefore, an externally applied DC current cannot flow forever without changing the conductor. At first, changes will occur near the electrodes; however, in a closed electrolytic cell with sufficiently long time, the change will spread to the bulk of the electrolyte. Accordingly, *electrolytic long-duration DC conductivity* is a difficult concept in a closed system.

The transfer of electric charge across the solution/electrode interphase is accompanied by an electrochemical reaction at each electrode (electrolysis). *We must keep the phenomenon in the bulk of the solution separate from the phenomenon at the electrodes.*

2.1.1 Ionization

Because the charge carriers of interest are ions, the *ionization* of atoms is of particular interest. The electrons of an atom are arranged in shells. The forces acting between atoms are of electrostatic nature. In electrochemistry, the ionization of an atom is determined by the electron configuration in the *outermost* shell. If this shell is full, then the atom has a noble gas configuration. This is a particularly stable form, implying that a large energy is necessary to remove, or add, an electron and thus ionize such an atom (cf, [Table 2.1](#)).

For hydrogen and helium, the innermost K-shell is also the outermost shell. The K-shell is full with two electrons (the noble gas helium). The next L-shell is full with eight electrons (the noble gas neon). The chemical properties of an atom are determined by the electron

Table 2.1: Electron Shell Configuration for the Lowest Atomic Number Atoms

Protons in Nucleus	Shell			Typical Electro- valency	Ionization Potential, eV	Atom Radius, nm	Positive Ion Radius, nm	Negative Ion Radius, nm
	K	L	M					
H	1	1	0	+1	13.6	0.037	0.00001?	0.154
He	2	2	0	Noble	24.6		N/A	N/A
Li	3	2	1	0	+1	5.4	0.068	N/A
Be	4	2	2	0	+2	9.3	0.044	N/A
B	5	2	3	0	+3	8.3	0.035	N/A
C	6	2	4	0	±4	11.3	0.077	0.016
N	7	2	5	0	-3	14.5	0.070	0.025
O	8	2	6	0	-2	13.6	0.066	0.022
F	9	2	7	0	-1	17.4		N/A
Ne	10	2	8	0	Noble	21.6		N/A
Na	11	2	8	1	+1	5.1	0.097	N/A

Here, ionization potential is the energy necessary to remove the first electron from the valence (outermost) shell. The values for radii depend on how they are measured. N/A, not applicable.

configuration of the outermost shell. These electrons are called *valence* electrons, and their ionization potential (energy necessary to remove an electron) is for most atoms less than 20 eV. Chemical reactions and bonds are related to the valence electrons in the outermost shell; the electrons in the inner shells (affected by X rays) and the nuclei (high-energy nuclear processes) are not affected. Therefore, ordinary chemical methods involve energy levels less than 20 eV. The *electrovalency*, z , of an atom is the number of electrons available for transfer. Thus, the valency for sodium is $z = +1$ and for chlorine is $z = -1$ (cf Table 2.1). A valence electron is a rather broad concept comprising those electrons in the outer shell that may combine with other atoms and form molecules, whether it is by gaining, losing, or *sharing* electrons.

The electrochemical properties are determined by the inclination of an atom to attain noble gas configuration of the outer electron shell. The atoms with few electrons in the outer shell (e.g., H, Li, Na) have a tendency to empty the shell (i.e., lose electrons and form positive ions). The atoms with a nearly filled shell (e.g., O, F) have a tendency to fill up the shell (i.e., gain electrons and form negative ions). “Tendency” here simply means that those configurations are lower energy level forms.

Electronegativity is the relative ability of an atom to gain electrons and become a negative ion. Sodium is clearly not very electronegative, but fluorine is highly electronegative.

Pauling¹ worked out a scale of electronegativity (see Table 2.2).

Table 2.2: Pauling's Scale of Electronegativity for Some Selected Atoms

F	4.0
O	3.5
N	3.0
Cl	3.0
Br	2.8
I	2.5
S	2.5
C	2.5
H	2.1
P	2.1
Fe	1.8
Na	0.9

¹ Linus Pauling (1901–1994), American chemist. Nobel Prize laureate 1954 in chemistry on the structure of proteins (and 1962 in peace). Important work also on chemical bonding and electronegativity and invented the paramagnetic oxygen analyzer.

Electronegativity is not a purely quantitative term, but it is useful in the prediction of the strengths and polarities of ionic bonds between atoms and thus possible electrochemical reactions. In electrochemistry, the use of electrode equilibrium potential tables (Section 7.6) serves the same purpose. The atoms with small electronegativity (e.g., Na) are not inclined to gain an electron at all (it would move the ion away from noble gas configuration), and sodium's natural state is to lose an electron and be a positive ion. Fluorine is very electronegative with a Pauling scale value of 4; its L-shell is filled with just one extra electron. With a value of 2.5, carbon is in a middle position with the ability to lose and gain electrons. *Hydrogen* is in a special position. In principle, hydrogen should be highly electronegative because one extra electron would bring it into a noble gas configuration. However, as we know, hydrogen has a larger tendency to lose an electron and form a proton; therefore, its value is 2.1. Electronegative atoms are on the right-hand side of the periodic system in the three positions preceding a noble gas. A less electronegative atom more easily loses electrons in accordance with small ionization energy (cf, [Table 2.1](#)). The ionization energy does not indicate the energy necessary for an atom to *gain* an electron and thus become a negative ion; this is defined by the *electron affinity*.

2.1.2 Molecular Bonds

Atoms far apart on the Pauling scale tend to form *ionic* molecular bonds, and atoms near each other form *covalent* molecular bonds. The forces acting between atoms in a solid may be grouped in four different types of chemical bonds:

1. Ionic bonding
2. Covalent bonding
3. Metallic bonding
4. Van der Waals bonding

The *ionic* bonds are between unequal atoms. For example, the ionization energy of a sodium atom is small (5.1 eV); therefore, the sodium gives an electron to the highly electronegative chloride. The atoms are ionized, valence electrons are lost or gained, and the coulomb forces are mainly responsible for keeping the ions together in the solid. Because electrons and ions are tightly bound at room temperature, solid ionic crystals generally exhibit no electrical conductivity—neither electronic nor ionic. There are lots of ions, but there is no mobility. In water, the bonds are broken and the ions split (dissociate), causing ionic conductivity.

Covalent bonds are important in molecules formed by atoms of the same atom number (e.g., N₂ in the air or carbon in diamond). The atoms remain neutral, but they share valence electron *pairs*—one from each atom. The sharing of electron pairs always increases the apparent filling of the outermost shell. The number of electrons necessary to obtain a noble gas configuration is the number of *unpaired* electrons. Each shared electron pair is a single *bond*.

Table 2.3: Covalent Bond Lengths

Atom I	Atom II		Bond Length, nm
C	C	Diamond	0.154
C	C	Graphite	0.142
C	H		0.10
C	N		0.147
C	O		0.143
N	N	N ₂	0.11
H	H	H ₂	0.075
O	O	O ₂	0.12
H	O	H ₂ O	0.0965

A carbon atom has four unpaired electrons and can share four electrons with other atoms and form four covalent bonds. Such covalent bonds can be extremely strong (diamond), and the electrons can be locally and strongly bound. Therefore, solid covalent crystals generally exhibit no electrical conductivity—neither electronic nor ionic. In biomaterials, covalent bonds with carbon are very important, and biomaterials usually have no molecular ionic or electronic conductivity. However, the charges in such a molecule may be far apart; thus, very large dipole moments and strong electric polarization may occur (Table 2.3).

The sharing of electron pairs in carbon–carbon covalent bonds may be as a single bond or with double bonds. Single bonds have complete freedom of rotation whereas double bonds are shorter and do not allow free rotation. Therefore, the type of covalent bond is important for such electrical properties as polarization and relaxation time.

In *metals*, the bonds are of the valence type, but the valence electrons are highly mobile and do not belong to particular atoms. This causes the strong electronic conductivity of metals, and the atoms may be regarded as fixed positive ions.

An electron revolving around its nucleus may be considered as a rotating electrical dipole. Such a rotating dipole induces dipoles in neighboring atoms. *Van der Waals* forces are dipole–dipole attractive forces between such atoms. The forces are weak and fall with the sixth power of the interatomic distance. Many organic molecules form aggregates (heterogeneous mass of parts or particles) held together by van der Waals forces.

2.2 Basic Electrolytic DC Experiment

2.2.1 Setup

Now we will give the first and simple illustration of an electrolytic DC current flow system, an *electrolytic cell*.² An electrolytic cell consists of a homogeneous electrolyte

² An *electrolytic* cell is an electrochemical cell used with an externally applied electric current. A *galvanic* cell is an electrochemical cell from which energy is drawn.

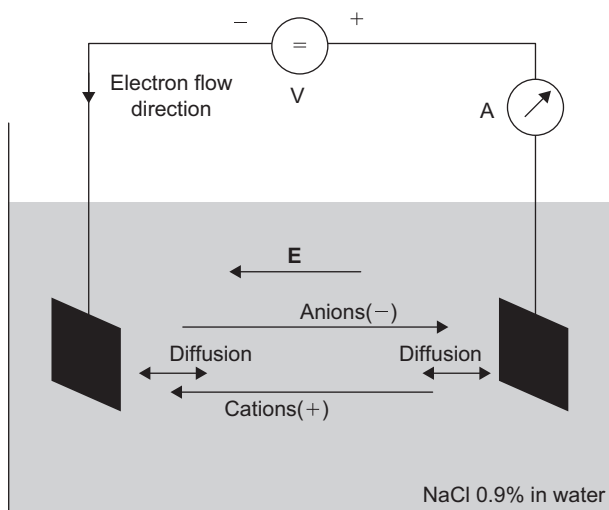


Figure 2.1: The basic bipolar electrolytic experiment, shown with material transport directions.

solution³ with two equal electrodes (Figure 2.1). By homogeneous, we here mean that the solution contains no boundaries or membranes except the two electrodes and the isolating walls of the container. As the electrolyte solution, we chose the most important in the human body—aqueous sodium chloride (NaCl) solution (concentration 0.9% by weight). Dry NaCl is a salt with very low conductivity, but in water the molecule is dissociated by water so that it is split up in two ions: Na^+ and Cl^- . The Na^+ and Cl^- are charge carriers free to migrate in an electric field, thus contributing to DC conductivity.

A DC potential may develop at the electrode metal/solution interphase. The absolute potential of this interphase (half-cell electrode potential) cannot be measured—it must be considered unknown. However, the potential difference between *two* electrodes can be measured with an ordinary voltmeter connected to the two metal wires from the electrodes. If the metals were different, then they could generate a potential difference of 1 V or more. However, here we presume that the *same* electrode material is used and that the measured potential difference is small. We will discuss the case for three different electrode materials important in biological work: *platinum, silver coated with silver chloride (AgCl), and carbon*. To the extent that both electrodes are equal, we have a symmetrical (bipolar) system, and the voltage—current dependence should not be dependent on polarity.

³ If NaCl is dissolved in water, then NaCl is the *solute* (and the electrolyte) and water is the *solvent*; together they are the *solution*.

We connect the DC supply to the electrode metal wires and adjust the voltage so that a suitable DC current flows. An electric field, \mathbf{E} , is accordingly set up in the solution between the electrodes. Positive ions (e.g., Na^+) migrate in the same direction as the E-field all of the way up to the cathode—they are cations. Negative ions (e.g., Cl^-) migrate in the opposite direction in the same directions as the electrons in the wires—they are anions. Anode and cathode are defined from current flow direction and not necessarily from the polarity of the external voltage source. In the bulk of the electrolyte, no change in composition or concentration occurs during the Na^+ and Cl^- migration: The same amount of ions enters and leaves a volume.

We must not forget a second possible transport mechanism different from migration: An ionization of *neutral* species may take place at an electrode. These neutral species cannot be transported to the electrode by migration because they are not charged. The transport caused the diffusion, which is by the concentration gradient near the electrode.

2.2.2 Findings

Platinum Electrodes

We adjust our DC supply to approximately 0.5 V, but no DC current is flowing. We must increase the voltage to approximately 2 V to obtain a DC current, but then the current rapidly increases with voltage. With DC current flowing, gas bubbles are seen on the anode and cathode metal surfaces.

Carbon Electrodes

We must again increase the voltage to approximately 2 V to get a DC current flowing. Gas bubbles are seen on both electrodes, but on the anode an erosion process of the carbon surface seems to take place.

Ag/AgCl Electrodes

Large DC current flows with the voltage supply adjusted to only one-tenth of a volt. No gas bubbles are initially seen on any of the electrodes. At the anode, the color stays the same, but the cathode loses the AgCl layer and a pure silver surface appears after some time.

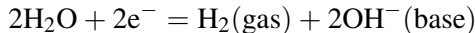
2.2.3 Discussion

With platinum and carbon, an applied DC voltage does not necessarily lead to current flow. There must be energy barriers in the system, and a sufficiently high voltage must be applied to overcome this barrier. It is a nonlinear system that does not obey Ohm's law. It can be shown that the bulk solution obeys Ohm's law; therefore, the energy barrier is not in the bulk but near the electrodes. As we shall see later, the barrier is situated in the double layer formed at the surface of an electrode metal (Section 7.5). When the voltage is

turned on, Na^+ migrates to the cathode and Cl^- migrates to the anode. However, arrival at the electrodes does not lead to an exchange of electrons with the metal; a surface charge is built up opposing the external electric field, and the current stops. An electrode is the interphase at which electronic and ionic conduction meets. Without DC current, there is no electron transfer, no chemical reaction, and no faradaic current.

At the Cathode

With current flowing, anions and cations migrate in opposite directions. The simplest hypothesis dealing with a saline solution would be that Na^+ is discharged at the cathode and Cl^- at the anode. It is not that simple: Na^+ is not discharged at the cathode. Sodium has a very small electronegativity, which means that it takes a large energy and a large negative voltage on the cathode to impose electrons on Na^+ . At much lower voltages, two other processes start: reduction of dissolved neutral oxygen and decomposition of water molecules. Both processes are linked with *noncharged species*, which are transported to the electron transfer sites by diffusion, not by migration. In [Figure 2.1](#), there are two transport mechanisms: migration and diffusion. The reaction of noncharged species at the electrodes must not be overlooked; these species are charged or *ionized* (at least as one step) in the electrode reaction. The concentration of dissolved oxygen is small; therefore, the DC current from the oxygen reduction is not large. As long as our voltage supply is adjusted for a current lower than this current, the oxygen reduction current is sufficient. If a larger current is wanted, then the voltage must be increased so that water is also decomposed. The water reaction at the cathode is



It is actually more complicated—the different versions of the hydrogen ion are active (e.g., the oxonium ion, H_3O^+).

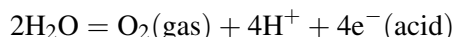
In conclusion, neutral metals and carbon do not have the ability to be reduced; therefore, electrode material cannot be ionized at the cathode and enter the solution. Dissolved oxygen is reduced. At higher currents, free hydrogen gas is also bubbling up, and the solution near the cathode becomes basic. Na^+ need not be considered (but is necessary for the conductivity of the solution so that the voltage drop in the solution is not too high). The positive silver ions of the AgCl are neutralized, and little by little the AgCl layer is decomposed and pure silver appears on the surface. The color changes, but the color of AgCl is not so easy to define. AgCl is photosensitive, and in films exposed to light there are already grains of pure silver, which are gray or black of color.

At the Anode

The electrode reaction at the cathode was not due to the discharge of Na^+ . Is the current at the anode due to the discharge of Cl^- ? Yes. Chloride is highly electronegative, but less

energy is necessary for taking electrons from the chloride ions than from water molecules. Neutral Cl_2 gas is formed at the platinum anode. It does not react with platinum, and it leaves the area as gas bubbles. It *does* react with carbon and destroys the carbon surface. At the AgCl surface, it reacts with silver oxidized by the anode and forms more AgCl . Ag^+ will not enter the solution; if it does, then it will combine with Cl^- and form AgCl . In aqueous solution, the solubility of AgCl is very low; only very small amounts will dissolve in the solvent and it will soon precipitate.

Hydroxide (OH^-) ions may be discharged, but there are few of them and they do not contribute very much to the DC current. With large currents water may be decomposed, and oxygen leaves the area as gas bubbles according to



If oxygen gas is developed, then the solution turns acidic near the anode. The importance of this reaction depends on the current level and what current level the Cl^- concentration will take care of alone.

Therefore, we may conclude that AgCl behaves rather differently from platinum and carbon. Silver undergoes an electrochemical reaction with one of the ions of the electrolyte (Cl^-), and silver may be oxidized or silver ions reduced. The transfer of electrons oxidizing or reducing species at an electrode is called a *redox* process. *The results indicate that if we are to apply large DC currents to tissue, and we are to use noble metals as electrode material directly on the tissue, then the passage of DC current is accompanied by the development of H_2 gas and a basic milieu at the cathode and Cl_2 gas and perhaps oxygen and an acidic milieu at the anode.* However, in real tissue systems (not the model of Figure 2.1), organic molecule redox systems will contribute to additional electrode reactions at low current levels.

What happens if we replace the DC voltage with a sinusoidal AC voltage? If the frequency is sufficiently high (e.g., 1 MHz), then the migration processes in the bulk electrolyte will take place (back and forth), but no accumulation process or reactions will take place at the electrodes. If the frequency is very low (e.g., 0.1 Hz), then the result will depend on the dimensions of the cell and the degree of reversibility of the reactions. If gas has time to bubble away, then the process is certainly irreversible.

2.3 Bulk Electrolytic DC Conductance

According to the Arrhenius⁴ theory of *dissociation*, molecules of acids, bases, and salts react with water molecules to form separate ions. Water *ionizes* the substances, and these

⁴ Svante August Arrhenius (1859–1927), Swedish physicist and chemist. 1903 Nobel Prize laureate in chemistry on electrolytic dissociation theory.

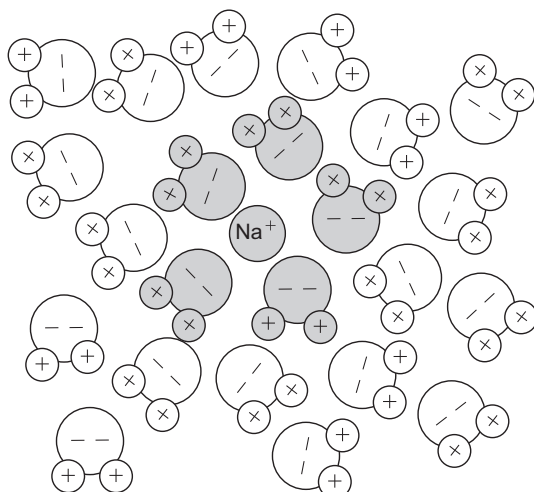


Figure 2.2: Na^+ hydrated by water molecules forming a hydration sheath around it.

ions give their solution the property of conducting electricity. Positive and negative ions free to migrate in the electric field contribute separately to the electric current flow, but because of different mobilities, they do not carry equal portions of the current.

Environment of Ions

In aqueous solutions an ion is not alone. Two zones surround it: the ion attracts ions of opposite sign, and it attracts water molecules. A water molecule has a strong *electric dipole moment*; even if the net charge is zero, water is a polar material. The process of solvent molecules forming a sheath around each electrolyte ion is generally called solvation. When the solvent is water, the process is called *hydration*. Hydration is strong because the water molecules have a large permanent dipole moment. The water molecular sheath stabilizes each ion and hinders ions of the opposite sign to approach so near to each other that they recombine: The substance stays dissociated and ionized. The hydration number is the average number of water molecules forming the sheath. Cations are usually less hydrated, and the hydration sheath less effectively covers large ions. [Figure 2.2](#) shows the hydration process for a sodium ion in water. It is a statistical concept; therefore, *on average*, there are more oriented water molecules (and other ions of opposite sign) near the Na^+ .

Hydration is the buildup of a sheath of *dipoles* around a central ion because of *ion-dipole* forces. According to Debye⁵-Hückel, the central ion is also surrounded by a slight excess

⁵ Peter Joseph Debye (1884–1966), Dutch/American physicist. 1936 Nobel Prize laureate in chemistry on molecular structure and dipole moments.

of *ions* of the opposite charge sign formed by ion–ion forces. They called this an *ionic atmosphere*. The hydration and the ionic atmosphere will increase the effective dimension and reduce the apparent charge of the center ion and thus retard migration.

The ionic atmosphere is a statistical concept. Within the *Debye length* from the central ion, there is an increased probability of finding an ion of opposite charge. A few Debye lengths (on the order of some tenths of nanometers) define a region of space charge where electroneutrality no longer holds. If the charge of an ion suddenly disappeared, then it would take a time on the order of 1 μs for the molecules to rearrange and the ionic atmosphere to disappear. This is an example of a *relaxation time*.

Contributions to Ionic Conductivity

Kohlrausch⁶ showed that conductivity, σ , is composed of separate contributions from anions (−) and cations (+). The current density, \mathbf{J} [A/m^2], of a single anion–cation pair is

$$\mathbf{J} = (nze\mathbf{v})_+ + (nze\mathbf{v})_- = \sigma\mathbf{E} \quad [\text{A}/\text{m}^2] \quad (2.1)$$

$$\sigma = Fc\gamma(\mu_- + \mu_+) \quad [\text{S}/\text{m}] \quad (2.2)$$

Here, n is the number of ions per volume, z is the valency of an atom (number of electrons available for transfer), e is the charge of an electron [C], \mathbf{v} is the velocity of the ion [m/s], F is the Faraday [C/mol], c is the concentration [mol/m^3], γ is the activity coefficient (not all of the electrolyte may be dissociated, and this is taken care of by the activity coefficient γ having a value between 0 and 1.), and μ is the mobility [m^2/Vs]. The current density, \mathbf{J} , of Eq. (2.1) must be summed up with contributions from each negative and positive ion species. Note that it may be difficult to find the activity coefficients of individual ion species because of electroneutrality—an electrolyte cannot consist of only anions or cations.

Equation (2.1) is very important and fundamental; it is the Ohm's law version for volume conductors. It is valid under the assumption of a homogeneous and isotropic medium when the current density and E-field directions are coinciding. Note that current is not the quantity used in this version of Ohm's law but rather current density, \mathbf{J} . Because \mathbf{J} may vary according to the local E-field strength, current must be found by integrating current density over a cross-sectional area. Current [A] is the sum of charges passing a freely chosen cross-section (e.g., of a copper wire) per second (flux) whereas current density [A/m^2] is the sum of charges passing per unit area per second (flux density). Current is a scalar sum of charges per second passing some area not entering the equation (scalar flux); it has no direction in space. Current density is defined by an area oriented in space; therefore, it is itself a vector in space (vector flux density).

⁶ Friedrich Wilhelm Georg Kohlrausch (1840–1910), German physicist. Author of *Lehrbuch der Praktischen Physik*.

The contribution to the total conductivity will come from all free ions according to their concentration, activity, charge, and mobility. The transference number of an ion species is its percentage contribution to the total conductivity.

In the bulk of a solution with free ions, there is *electroneutrality*. In a volume, V [m³], the sum of charges is zero:

$$V \sum (nze)_+ + V \sum (nze)_- = 0 \quad (2.3)$$

If this were not the case, then a space charge would build up, driving excess ions out of the volume. During current flow, equal amounts of charge must enter and leave a solution volume. Electroneutrality is valid for a volume much larger than ionic dimensions.

Electroneutrality does not prevail at boundaries with space charge regions (cf, Section 7.5 on electrical double layers).

The current density according to Eq. (2.1) must be summed for all free ions present; for example, for NaCl Eq. (2.2), current density may be written as

$$\sigma = F(c\gamma)_{\text{NaCl}}(\mu_{\text{Na}} + \mu_{\text{Cl}}) \quad [\text{S/m}] \quad (2.4)$$

The molar conductivity (equivalent conductance), Λ , is conductivity per mole of solute per volume:

$$\Lambda = \frac{\sigma}{c} = \gamma F(\mu_+ + \mu_-) \quad [\text{Sm}^2/\text{mol}] \quad (2.5)$$

Therefore, the molar conductivity is a parameter directly linked with the mobility and not with concentration. The basic unit is [S/m] per [mol/m³], or Sm²/mol. The mobility, μ , is related to the random molecular collisions and corresponding frictional force (viscosity η) experienced by the migrating ion. The frictional force, f , is ideally related to the hydrodynamic radius, a , of the ion according to Stoke's law:

$$f = 6\pi\eta av \quad [\text{newton}] \quad (2.6)$$

The bulk electrolyte solution obeys the linear Ohm's law (Eq. (2.2)). The force on a charge, q , in an E-field is proportional to the electric field strength according to $\mathbf{f} = q\mathbf{E}$. Therefore, the linear Ohm's law shows that ions are not formed by the external field; they are in existence already without a field.

Equation (2.1) is valid also for DC under the condition that electrochemical changes occurring at the electrodes do not spread to the bulk. σ is also considered frequency independent up to at least 10 MHz (Cooper, 1946).

The diameter of many ions has been determined by X-ray diffraction of ionic crystals (dry) (Table 2.1). From Table 2.4, we see that the number of water molecules bound in the sheath around an ion (the *hydration number*) has a certain correlation with the molar

Table 2.4: Molar Conductivity Λ_o [S cm²/mol] in Aqueous Solution at Infinite Dilution and 25 °C

Cation	Λ_o	Hyd	Anion	Λ_o	Hyd
H ⁺ /H ₃ O ⁺	350	-	OH ⁻	198	
Na ⁺	50	5	Cl ⁻	76	0
K ⁺	74	4	HCO ₃ ⁻	45	0
Ca ²⁺	119	10	CO ₃ ²⁻	72	0

Hyd, average number of water molecules in the hydration sheath.

Table 2.5: Relative Atomic Mass = Gram Weight per 1 mol (gram mole)

	Protons	Gram Weight per mol
H	1	1.0
Li	3	6.9
B	5	10.8
C	6	12.0
N	7	14.0
O	8	16.0
F	9	19.0
Na	11	23.0
Cl	17	35.5
K	19	39.1
Ca	20	40.1

conductivity and therefore according to Eq. (2.5) to the mobility (the Ca²⁺ value must be halved for this comparison). This is so because a stronger hydration increases the effective radius of the ion and therefore the friction, and it reduces the effective charge of the ion. Hydration and the ionic atmosphere reduce the molar conductivity.

In practice, *electrolytic concentrations* are often given by weight [g] (e.g., 0.9% NaCl in water meaning 9 g/1000 g = 9 g/L). From the relative atomic mass (Table 2.5), the molar concentration can be found. For example, 23.0 + 35.5 = 58.5 g = 1 mol NaCl; therefore, 0.9% = 9 g/L NaCl = 154 mmol/L.

The conductivity of a given electrolyte solution can be found from the tables of molar conductivity, at least for low concentrations (Table 2.4).

Example

The conductivity of 0.9% NaCl at 25 °C is, according to Eq. (2.5), $\sigma = \Lambda c = (50 + 76) \cdot 0.154 \times 10^{-1} = 1.94$ [S/m].

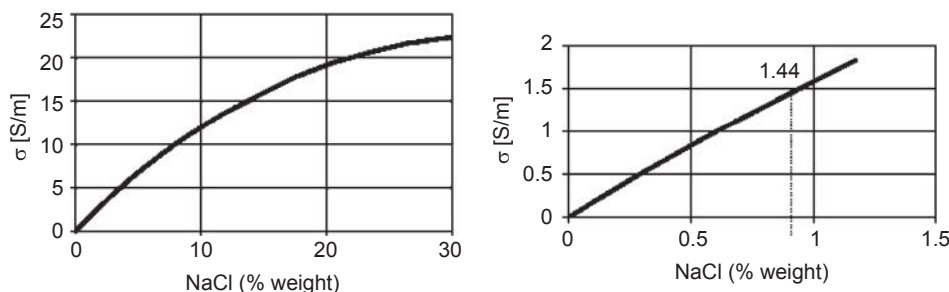


Figure 2.3: Conductivity of NaCl aqueous solution (20 °C).

Figure 2.3 shows how the actual conductivity may be lower because the dependence is not linear. Molar conductivity, Λ_0 , relates to the limiting value at low concentrations. For NaCl, the relationship is quite linear up to the physiological concentration of 0.9% by weight. Sweat concentrations are somewhat lower, urine concentrations vary but may be higher, and seawater concentrations are approximately 3.5%. Much higher concentrations are sometimes used for contact electrolytes (cf, Section 7.4).

At high concentrations, the interaction between ions reduces their mobility. For example, the ions are so tightly packed that their fields interact so that ions of opposite charge form *ionic pairs* (with lower mobility, they become quasi-dipoles). This effect is dependent on solvent permittivity because the electrostatic force between charges and the formation of ionic pairs are stronger the lower the permittivity (Eq. (3.1)). In addition, higher kT gives less coherent ionic atmospheres. Therefore, higher temperature and permittivity give less friction and higher conductivity. According to the *Onsager*⁷ theory, molar conductivity, Λ , is dependent on \sqrt{c} according to $\Lambda = \Lambda_0 - b\sqrt{c}$, where b is dependent on, for example, temperature and viscosity.

Conductivity of Water Itself

Water, hydroxyl, and hydrogen ions have very special electrical properties. Water is strongly polar, but it is also to a small extent an electrolyte in itself. From Table 2.2, we see that the intrinsic conductivity is low, but it is not zero. The small rest conductivity is due to a protonic self-ionizing process. There is a small statistical chance that a water molecule transfers one of its protons to another water molecule in the following way:



⁷ Lars Onsager (1903–1976), Norwegian/American chemist. 1968 Nobel Prize laureate in chemistry for his work on irreversible thermodynamics.

The traditional description of the hydrogen ion, H^+ , alone is not correct. The proton (the hydrogen ion H^+) actually cannot exist as such in water. Without the electron it only consists of the nucleus with a radius of perhaps 10^{-14} m—approximately 4 decades smaller than an ion with electrons in orbit. The electric field near the naked proton is extremely strong, and polar water molecules are immediately attracted; the proton is hydrated and the *oxonium* (*also called hydroxonium or hydronium*) ion, H_3O^+ , is formed. This is also strongly polar and attracts new water molecules, forming H_5O_2^+ and H_9O_4^+ in a dynamic and statistical way. For simplicity, they will all be called a *hydrogen ion* in this book when it is not necessary to differentiate.

A small naked proton has a high mobility and therefore high molar conductivity. The oxonium ion is of more ordinary size; therefore, the molar conductivity actually measured should be in a normal range. However, hydrogen (and OH^-) ions have irregular high molar conductivity (Table 2.4). This is due to the special *proton hopping* mechanism illustrated in Figure 2.4, which is different from ordinary migration. The protons are transferred by hopping directly from water molecule to water molecule by a Grotthuss mechanism instead of being slowed by viscous forces. A part of the mechanism is believed to be a quantum-mechanical tunnel effect, at least at low temperatures. The speed-limiting process is believed to be a necessary rotation of a neighbor water molecule before it can accept a proton—a statistical process. The proton can be considered to hop along a string of water molecules with a statistical net flow in the direction of the E-field. Of course, parallel to the hopping conductance there is the ordinary migration conductance.

Because of their high molar conductivity, the hydrogen ions will often dominate the conductance found. Because of electroneutrality, there are equal numbers H^+ and Cl^- when the strong acid, hydrochloric acid (HCl), dissociates. However, the electrolytic conductivity contribution from the hydrogen ions is approximately 5 times as large as that of Cl^- . From Table 2.4 it is seen that for NaCl the contribution is largest from the Cl^- ions; for potassium chloride the contributions from each ion are approximately equal.

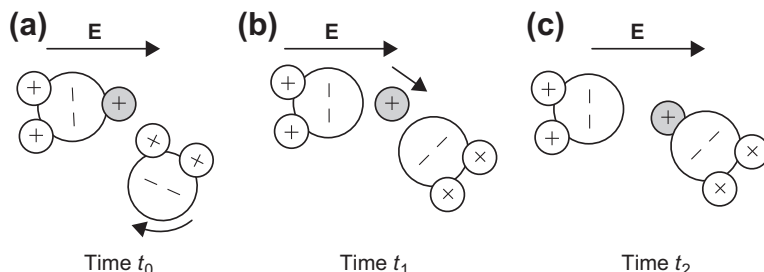


Figure 2.4: Proton Hopping Conductance—Same Molecules at Three Different Moments.
(a) Water molecule rotation, (b) hopping, and (c) new proton position.

Conductivity of Weak Acids

The electrolytes do not only determine conductivity. They are also strongly related to the acid-base balance and the pH ($\text{pH} = -\log [\text{H}_3\text{O}^+]$) of the tissue ($[\text{H}_3\text{O}^+]$ indicates the concentration in moles per liter).

With salts and strong acids, water dissociates all molecules. With weak acids, the situation is different; some of the acid molecules stay undissociated. An example is the conductivity due to dissolved carbon dioxide (CO_2) gas in water. Some of the CO_2 physically dissolved is transformed to carbonic acid (H_2CO_3), which is a weak acid. The Guldberg-Waage^{8,9} law (mass action law) is useful for the calculation of ionic concentrations in such cases. In its original form, the Guldberg-Waage law states that the rate of a chemical reaction is proportional to the *mathematical product* of the mass of the reacting substances and that equilibrium can be expressed by an equilibrium constant characterizing the chemical reaction. In the particular case of a dissociation process, electroneutrality also imposes that the ionic concentrations are equal (for unity valency ions). In the case with dissolved CO_2 , the equilibrium dissociation constant can be set to $K_1 = 10^{-6.3}$. The Guldberg-Waage law then gives

$$\frac{[\text{H}_3\text{O}^+] [\text{HCO}_3^-]}{[\text{H}_2\text{CO}_3]} = K_1 = 10^{-6.3}$$

For such a weak acid, a doubling of the concentration $[\text{H}_2\text{CO}_3]$ leads to a $\sqrt{2}$ increase in $[\text{H}_3\text{O}^+]$ because $[\text{HCO}_3^-]$ must also increase by $\sqrt{2}$ (electroneutrality) so that the product increases by 2. Because of the high molar conductivity of hydrogen ions, the total conductivity of such a solution is dominated by the hydrogen ions; therefore, it is roughly proportional to $\sqrt{[\text{CO}_2]}$, or the square of the partial pressure of the CO_2 gas in equilibrium with the solution.

Accordingly, when water is in equilibrium with air in nature, H_3O^+ and HCO_3^- will contribute to additional DC conductivity and a reduction of pH. The reduction in pH is actually substantial—the pH of pure (nonpolluted) water lowers to 5.7 (acid) when in equilibrium with normal atmospheric CO_2 concentration levels (0.03%).

Water itself is very weakly self-ionized, with a low equilibrium constant, K_w ,

$$[\text{H}_3\text{O}^+] [\text{OH}^-] = K_w = 10^{-14}$$

For electroneutrality $[\text{H}_3\text{O}^+] = [\text{OH}^-]$, which then is equal to 10^{-7} , corresponding to $\text{pH} = 7$. The conductivity according to Eq. (2.5) is

$$\sigma = (\Lambda_+ + \Lambda_-)c = (350 + 198) \times 10^{-7} 10^{-1} = 5.5 \times 10^{-6} \text{ [S/m]}$$

⁸ Cato Maximilian Guldberg (1836–1902), Norwegian mathematician, particularly interested in physical chemistry.

⁹ Peter Waage (1833–1900), Norwegian chemist. Particularly interested in practical applications of chemistry.

Other Factors Influencing Conductivity

The temperature dependence of the conductivity of most ions in aqueous solution is approximately +2.0%/°C. This high temperature dependence results from the decrease in viscosity of water with temperature. The temperature coefficients of H_3O^+ (1.4%/°C) and OH^- (1.6%/°C) are important exceptions and are the result of the different conduction mechanisms of these ions. Viscosity increases with increasing pressure, and the conductivity is reduced.

The conductivity increases at high frequency (>3 to 30 MHz, Debye-Falkenhagen effect). It takes approximately 0.1–1 ns to form an ionic atmosphere, and the time is dependent on the ion concentration. The literature is not clear as to the conductivity frequency dependence of electrolytes such as NaCl, but Cooper (1946) found no variations in the concentration range of 1–4 wt% and frequency range of 1–13 MHz.

As shown, pure deionized water has a low conductivity, but the permittivity is constant up to the lower gigahertz range with a relaxation frequency of approximately 20 GHz (cf, Section 4.1.1).

2.3.1 Net Charge of a Particle: The Isoelectric Point

The charged double layer at the surface of colloidal particles (metallic, semiconductive, nonconductive) and living cells in aqueous solution makes them behave as macro-ions and migrate in an electric field. The net charge of a particle is related to the electrokinetic potential (zeta-potential), which is introduced in Section 2.5.1. This is what occurs by in vitro electrophoresis. In human body liquids, the range of pH is very narrow (7.35–7.45). However, in vitro, it is usually possible to find a pH value at which an amino acid, a protein, or a cell does not migrate. This pH at which no migration occurs is the *isoelectric point*, or sometimes it is a pH *range*. If the particle is conductive, then there is a common charge for the whole particle with a sheath of counter-ions around. When the total charge is zero, no migration occurs. If the particle is not conductive, then we are dealing with local charges and counter-ions, and when the net migrational forces of these are zero, we are at the isoelectric point. The isoelectric point is dependent on the solution used for the examination.

The charge of proteins or cells is the basis for the reciprocal repulsion of particles in a suspension. Loss of charge means losing repulsive forces and implies *clotting* and *precipitation*. Blood coagulation is the result of such a process.

Osmosis is the transport of a solvent through a semipermeable membrane into a more concentrated solution. Reverse osmosis is applying a sufficiently high pressure on the more concentrated side to reverse the transport direction. In medicine, *dialysis* is the separation of suspended colloidal particles from dissolved ions or molecules of small

dimensions by means of their unequal rates of diffusion through the pores of semipermeable membranes. If charged carriers are involved, then applying an electric field can accelerate the process, which is termed *electrodialysis*.

An *ion exchanger* is usually packed into a tube or column through which a solution is made to flow to capture anions or cations. The column arrangement forces the ion–exchange reaction, which is intrinsically reversible, to be completed. The solution flowing down the column continually meets fresh exchanger. When the exchangeable ions do start to emerge from the end of the column, the column has become completely saturated. The column may be regenerated by passing through it a solution of the ions that it originally contained.

2.3.2 Special Electrolytes

Some substances are completely ionized in water (strong acids) whereas others are only partly ionized (e.g., weak acids). Water is often necessary for the ionization or molecule split; for example, pure HCl liquid is an insulator. Many substances dissolved in water are not ionized at all; therefore, they do not contribute to electric conductivity. They are true nonelectrolytes, such as sugar/glucose. The molecules of such substances are not split up (ionized, dissociated) by water. Some may have a symmetrical distribution of charges, with the center of positive and negative charge coinciding. However, many molecules have centers not coinciding, forming permanent dipoles with zero net charge—such substances are called *polar*. Water itself is polar, and a substance must actually be polar to be soluble in water.

NaCl as a dry salt at room temperature is not an electrolyte. The DC conductance is negligible; still, the Na and Cl atoms are ionized, but they are “frozen” so that they cannot migrate.

NaCl dissolved in water is the true electrolyte, and the Na^+ and Cl^- are split and free. Even if NaCl is the true electrolyte, the whole electrolyte solution is often also called just the electrolyte.

Electrolyte Classification

In a solution with colloidal particles, a charged double layer will surround each particle, and the particle may be regarded as a macro-ion. The colloidal particles free to migrate contribute to the solution’s electrical DC conductance, and they may be regarded as a *colloidal electrolyte*. Particles are called colloidal when two of the dimensions are in the range of 1 nm to 1 μm (the third dimension does not have this constraint; e.g., a very thin string).

A *solid electrolyte* is also possible. In liquids, ions generally are more free to move (have a higher mobility) than in solids. Therefore, solid electrolytes at room temperature have a relatively low conductivity.

AgCl is an important molecule for electrode surfaces. The chloride ions (Cl^-) are bound, but the silver metal ions (Ag^+) are genuine charge carriers giving a certain electrolytic ionic conductivity.

The dry glass core in a pH electrode exhibits solid electrolytic conductance, not semiconductive. The electrode is proton sensitive, but the small conductivity in the glass core stems from Li^+ , Na^+ , and K^+ , which have mobilities $10^3\text{--}10^4$ larger than the protons. However, water is absorbed in the leached surface layers of the glass, and there the proton mobility is high and contributes to local DC conductance in an important way.

NaCl as a solid crystal has atoms in ionized form. However, neither the Na^+ nor the Cl^- nor any electrons are free to migrate (at room temperature). There is no DC conductivity: NaCl is an insulator. However, if NaCl is warmed to 800°C , then it melts, the ions are free to migrate with small friction (high mobility), and we have a strong *ionic liquid* or *fused electrolyte*.

There are also *mixed conductors* with ionic and electronic conductance. The sulfides, selenides, and tellurides of silver and lead are examples of this. New plastic materials with ionic conductance have been discovered in polymer chemistry. Nafion is a polymer with ionic conductivity, and it is used in multigas analyzers in anesthesia, where the special high permeability to water is useful.

Some polymers have mixed electronic and ionic conductivity, and some are purely electronic conductors with free electrons similar to a metal or electrons locally linked to centers with electron-donor properties. Carbon as a most basic element for all biochemistry is a very special element that also deserves attention as an electrode material. In the form of graphite, carbon is an electronic conductor, but as diamond it is an almost perfect insulator.

Proteins in the body liquids may be considered as a colloidal electrolyte solute in a water solvent. Contact with water is the natural state of a protein. In more or less dry form, a protein powder loses some of its electrolytic character; it loses the charged double layer on the surface and behaves electrically very differently from protein with water. Such materials may well be mixed conductors—electronic in the dry state and ionic with water content. Keratin is a more or less dry protein found in the natural state of no longer living biological materials such as hair, nails, and the stratum corneum. The water content of such materials is dependent on the relative humidity of the ambient air. The question of ionic or electronic conductivity in proteins is important, and an electronic conduction mechanism must be considered in many cases.

Table 2.6: Concentration of Electrolytes in Body Liquids [meq/L] is Ion Concentration

Cations, meq/L		Anions, meq/L			
	Plasma	Intracellular			
Na ⁺	142	10	Cl ⁻	103	4
K ⁺	4	140	HCO ₃ ⁻	24	10
Ca ²⁺	5	10 ⁻⁴	Protein ⁻	16	36
Mg ²⁺	2	30	HPO ₄ ⁻ + SO ₄ ⁻ + organic acids	10	130
H ⁺ (pH = 7.4)	4 × 10 ⁻⁵	4 × 10 ⁻⁵	Sum	153	180
Sum	153	180			

Milliequivalents [mmol × valency z] per liter, and 0.9% NaCl is 154 mmol.

Body Liquid Electrolytes

The most important ions for extracellular conductance by far are Na⁺ and Cl⁻ (Table 2.6). Note that free protein in plasma are charge carriers with a negative charge (anions) and in this context protein can be regarded as macro-ions and a conductance contributor. This charge is also the basis of DC electrophoresis as an important analytical tool in clinical chemistry (Section 2.5.1). To maintain electroneutrality, an increased protein concentration must increase the concentration of cations or reduce the concentration of other anions. The anion HCO₃⁻ is the bicarbonate related to the transport of CO₂ in the blood; therefore, a change in bicarbonate concentration (anion) will have consequences for the cation concentration.

2.3.3 Conduction and Semiconductor Theory

The charge carriers in metals are electrons that are free to migrate in the energy band called the conduction band (Figure 2.5).

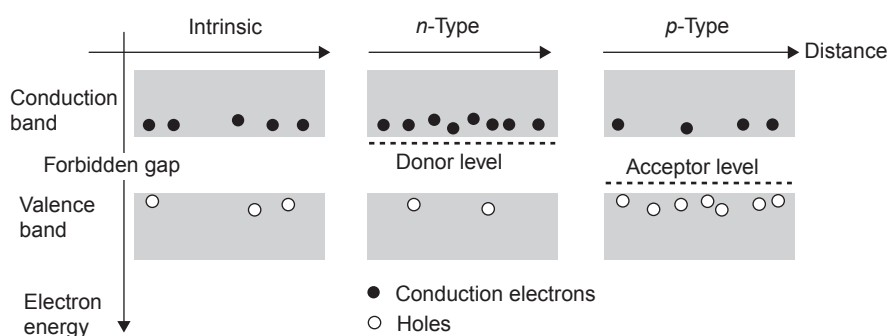


Figure 2.5: Energy levels in a semiconductor without (left) and with impurities. Local impurities create local energy levels (energy wells) as local reservoirs in the forbidden energy gap.

In semiconductors, there is a special valence energy band under the conduction band. With pure (intrinsic) semiconductors, the energy levels in between are forbidden levels, and at room temperature very few electrons statistically have sufficient energy to cross the forbidden band and reach the conduction band; that is, the conductivity is low. For example, the energy gap is 0.7 eV for germanium, 1.1 eV for silicon, and 5.2 eV for diamond (an insulator).

However, with *local impurities* in the material, *local* energy centers may exist in the forbidden gap. Here, electrons reside on energy levels that may be characterized as local energy *wells*. With a certain amount of added energy electrons can come up from the well and reach the conduction band (n-type impurities). This can considerably increase conductivity (extrinsic conduction). According to the nature of the impurities, this added conduction may be by electrons or holes as charge carriers.

The idea of a possible semiconductive mechanism (electrons and holes) in biomaterials is old, as illustrated by the book by Pethig (1979). Later, Takashima (1989) did not mention semiconductivity as a possible mechanism. Indications of an electronic, semiconductive conduction for the DNA molecule have appeared again (Fink and Schönenberger, 1999). Such experiments are performed under nonphysiological conditions in vacuum, which implies that every water molecule free to do so has disappeared.

Ions do not obey these laws of semiconductors. However, the concept of local energy wells can also be adapted to ionic conduction. Debye (1929) proposed a model in which an ion may be translocated between a pair of neighboring energy wells by an applied electric field. With an applied AC field, an ion can be made to hop between these two wells. However, such local hopping does not contribute to DC conduction, only to AC polarization.

2.3.4 Materials Classified According to Conductivity

Materials are often classified according to their DC conductivity as conductors, semiconductors, (electronic), and insulators. For electronic conductors (charge carriers: electrons), this classification is based on energy levels and the Fermi-Dirac statistics of the free electrons. A division between metals and semiconductors is sometimes based on the temperature coefficient of the conductivity, σ : Semiconductors (as for ionic conductors) have a positive $d\sigma/dT$ whereas metals have a negative $d\sigma/dT$.

For ionic conductors, the classification is a little more problematic. They are in the conductivity range of pure semiconductors, but the charge carriers and therefore the conduction mechanism is very different. It is often found with liquid or solid electrolytes that the difference in conductivity is the result of different *mobilities* and not so much a different number of charge carriers ([Table 2.7](#)).

Table 2.7: Electronic or Ionic DC Conductivity, σ , at 20 °C

	e or i	σ [S/m]
Superconductors (low temperature)	e	∞
Silver	e	61×10^6
Copper	e	58×10^6
Aluminum	e	35×10^6
Steel (hard)	e	2×10^6
Mercury	e	1×10^6
Coal	e	17×10^3
Graphite	e	100×10^3
NaCl, fused, 800 °C	i	300
NaCl in water, 25%	i	22
NaCl in water, 5%	i	7
NaCl in water, 0.9% 37 °C	i	2
NaCl in water, 0.9%	i	1.3
Whole blood 37 °C	i	0.7
Muscle 37 °C	i	0.4
Germanium (pure semiconductor)	e	2
Silicon (pure semiconductor)	e	300×10^{-6}
Bone, living	i	10×10^{-3}
Tooth (human enamel)	i?	5×10^{-3}
Ethyl alcohol	i	330×10^{-6}
AgCl	i	100×10^{-6}
Water, deionized	i	4×10^{-6}
Bone, dry	e?	100×10^{-12}
Transformer oil	i?	10×10^{-12}
Mica	e?	10×10^{-15}
PTFE (Teflon)	e	10×10^{-15}
Diamond	e	10×10^{-15}

e, electronic; i, ionic; PTFE, polytetrafluoroethylene.

2.4 Particle Migration and Diffusion

The electrode is the final boundary for ionic migration. Here, some of the ions started, and here they meet a physical hindrance. The metal of an anode may furnish metal ions to the solution, crossing the interphase.¹⁰ Depletion or accumulation of matter and charge may occur at the electrodes, and chemical reactions may also occur. An electrode may also exchange electrons with *neutral species* (e.g., the reduction of dissolved oxygen at a cathode). The transport of neutral species in the bulk of the electrolyte is not by ionic migration but rather a diffusion transport process caused by a

¹⁰ *Interface*: a surface that forms the boundary between two materials (sharp transition). *Interphase*: diffuse transition zone between two phases (e.g., solid/liquid).

concentration gradient. *Diffusion may be as important of a transport mechanism as migration in an electrolytic cell.*

[Equations \(2.1\) and \(2.2\)](#) are to be interpreted according to the kinetic molecular theory of the transport properties of liquids. The charge carriers do not move in an orderly, linear fashion through the liquid. *Diffusion* is the process resulting from random motion of molecules by which there is a net flow of matter from a region of high concentration to a region of low concentration. This process is related to the concepts of Brownian motion, molecular collisions, and the mean free path between collisions. The *migration* of charge carriers in an electric field may be regarded as a special case of diffusion caused by an external influence, not driven by an internal concentration gradient. The transport of charged molecules/ions may be due to concentration gradients and electric fields; *electrodiffusion* is the general term for both of these transport processes. The migrational part is dependent on the electric field. To reduce the migrational effect, an indifferent electrolyte not intervening in the process to be studied may be added to increase conductivity and reduce the electric field. Transport caused by electricity is generally classified as *electrogenic* transport.

Molecular diffusion is described by *Fick's laws*. Consider a simple system in the form of a compartment with unity width and height dimensions and a concentration gradient in the infinite length x direction. Fick's first law is

$$M = -D \frac{\partial c}{\partial x} \quad (2.8)$$

where M is the molar flux density [$\text{mol}/(\text{s} \cdot \text{m}^2)$] and D the diffusion coefficient [m^2/s]. The minus sign indicates that the transport is toward *lower* concentration. During stationary diffusion (e.g., in a tube), [Eq. \(2.9\)](#) shows that a linear concentration will be set up in the diffusion zone out from the electrode surface. Fick's second law is

$$\left(\frac{\partial c}{\partial t} \right)_x = D \frac{\partial^2 c}{\partial x^2} \quad (2.9)$$

Warburg solved this equation already in 1899, finding the concentration waves into the electrolyte at a distance from an AC-polarized electrode surface (cf, Section 7.9.3).

Here is another example. Consider a diffusion process starting in a specified compartment with an infinitely thin (x -direction) band of solute, S [mole per unit width y and depth z], released in the middle of the compartment at $x = 0$ and $t = 0$. By solving Fick's second law under these boundary conditions, the concentration as a function of position x and time t is:

$$c(x, t) = \frac{S}{e^{\frac{x^2}{4Dt}} \sqrt{4\pi Dt}} \quad [\text{mol}/\text{m}^3] \quad (2.10)$$

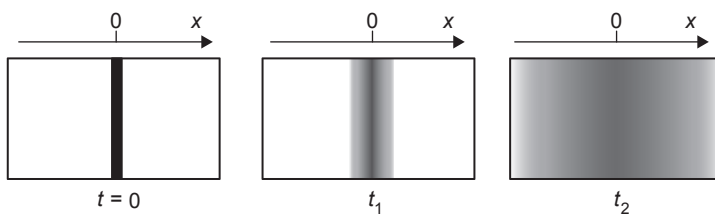


Figure 2.6: Spread of a thin strip of solute by pure diffusion.

The initial conditions correspond to $c(0, 0) = \infty$. \sqrt{Dt} has the dimension of meters and corresponds to the net distance diffused by a molecule in 1 s. Such time dependence is due to the random walk of the molecule. With time, the solute spreads out, and the concentration at the band position ($x = 0$) decreases according to $1/\sqrt{t}$. At a distance x , the concentration at first is very, very small, but then it reaches a maximum and thereafter follows the falling and uniform concentration around the origin (Figure 2.6). With $t \rightarrow \infty$, $c \rightarrow 0$ because the compartment is considered infinite in the x -direction. An electrolytic cell of finite dimensions corresponds to different boundary conditions and a different equation. This is of importance when considering increasing t and the approach toward DC conditions. When the diffusion reaches the boundary of the cell compartment in the x -direction, the process no longer follows Eq. (2.10). With diffusion-controlled processes, new frequency-dependent parameters enter at very low frequencies with a measuring cell of small dimensions (cf, the Warburg impedance, Section 7.9.3).

Equation (2.10) and Figure 2.7 illustrate the diffusion process from an electrode surface positioned at $x = 0$ whether it is the export of reaction products or the import of reactants the other way. Equation (2.10) also illustrates that physical processes in electrochemistry

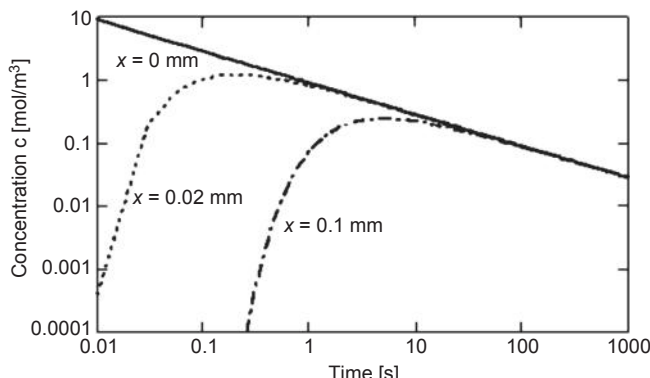


Figure 2.7: Diffusion of a thin strip of solute from position $x = 0$ at $t = 0$ according to Eq. (2.10). Concentration as a function of time with position as parameter. $D = 10^{-9}\text{ m}^2/\text{s}$, $S = 10^{-4}\text{ mol/m}^2$.

do not necessarily follow exponential laws. *This is an important reason why it is often difficult to model electrolytic cells with ideal electronic components.*

The diffusion constant, D , in aqueous solution is on the order of 10^{-11} [m²/s] for large molecules and 10^{-9} for small molecules. This means that the spread of just 1 mm in liquids will take hours for larger molecules whereas small molecules will diffuse approximately 0.1 mm in 1 s. In gases, the values of D are higher. For example, for water molecules in air, $D = 0.24 \times 10^{-4}$ at 1 bar and 20 °C; therefore, without any convection, water molecules will have moved approximately 5 mm in 1 s. Therefore, the spread or mixture of gases in a room across 1 m or more is purely controlled by convection.

2.5 Electrokinetics

There are four electrokinetic effects that are all due to the electric charge of the double layer at the solid/liquid interphase (cf Section 7.5).

In an exogenic E-field:

1. *Electrophoresis* is the migration of charged particles through a liquid.
2. *Electro-osmosis* is a bulk liquid flow through a pore caused by a migrating ionic sheath.

Endogenic E-field generation:

3. *Sedimentation (streaming) potential* is generated because of falling (moving) charged particles.
4. *Sedimentation electric current* is generated when a liquid is pressed through a pore.

The conductivity of the solution involved is of general interest in connection with these effects. High conductivity results in a high current density for a certain E-field strength with a possible temperature increase problem. High conductivity also results in small generated potentials.

However, electrokinetic effects are not restricted to charged particles. Field-induced polarization will make *uncharged* particles move in inhomogeneous or moving electric fields. The resultant forces increase with the volume of the particle and are therefore called body or *ponderomotive* forces. These forces are the basis of phenomena and techniques such as *electrorotation*, *levitation*, *dielectrophoresis (DEP)*, *pearl chain formation*, and *travelling wave DEP* (Fuhr et al., 1996). Electrorotation and traveling wave DEP are techniques in which angular or linear movement of the field relative to the particle produces the desired movement of the particle. On the other hand, inhomogeneous fields can cause levitation, DEP, and pearl chain formation, although pearl chain formation will also occur in homogeneous fields. Ponderomotive effects are obtained with special electrodes generating specialized electric fields; therefore, they are found in Chapter 7, Electrodes (Section 7.12.6).

2.5.1 Flow Caused by Applied Electric Field (Exogen Transport)

Electrophoresis

Free amino acids, proteins, ions, colloidal particles, bacteria, and cells are possible charged particles migrating in an electric field; therefore, they can be studied by electrophoresis. As described in Section 7.5, some molecules of the solvent are attached charges on the particle; hence, some solvent will move together with the particle. This is a part of the electrophoretic effect.

Electrophoretic flux could be calculated from the zeta potential, the permittivity, and the viscosity. Because these quantities are difficult to estimate, electrophoretic mobility is a more practical quantity. Migration velocity is simple to measure, and the different electrophoretic mobility is the basis of a very powerful *in vitro* analytical tool for amino acids and proteins in clinical laboratories (Table 2.8).

Electro-osmosis

Electro-osmosis is the transport of bulk liquid through a pore under the influence of an electric field. The volume of solution transported per unit time, \dot{V} , is

$$\dot{V} = \frac{\zeta \epsilon I \rho}{4\pi \eta} \quad \left[\frac{m^3}{s} \right] \quad (2.11)$$

where ζ is the double-layer zeta potential, ϵ is permittivity, ρ is the resistivity of the liquid, and η is its viscosity. Global symbols are given in Table 12.1.

Electro-osmosis is a kinetic process that is used for the determination of the zeta-potential of a surface/electrolyte solution interphase. It is also a process found in the sweat pores of

Table 2.8: Electrophoretic Mobility
[$10^8 \text{ m}^2/\text{Vs}$] at pH 7.0

Particle	Mobility
Human blood cells	-1
<i>Streptococcus</i>	-1
Methicillin-resistant	
<i>Staphylococcus</i>	-1.5
Proton	+37
Cl^-	-7
Colloidal gold	-3.2
Oil droplets	-3.1

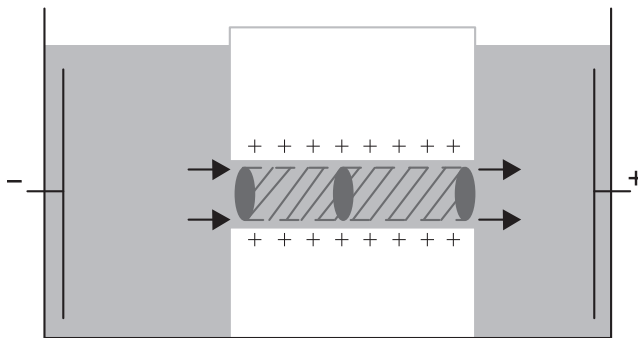


Figure 2.8: Electro-osmosis in a capillary. The double-layer ion sheath migrates, and this brings the inside bulk capillary volume in motion.

human skin. A dry cathode at a skin surface will fill the ducts with liquid/sweat from the deeper skin layers (Figure 2.8).

2.5.2 Flow-Generated Potentials (Endogenic Potentials)

Sedimentation Potential

Charged particles falling through a column filled with an electrolyte solution set up a potential difference between column ends. The falling charge carriers directly represent an electric current flow, which results in a potential difference and hence a flow of charge carriers the opposite direction, opposing the motion of the falling particles. High-conductivity solutions result in small generated potentials.

Streaming Potential

When a liquid is forced through a capillary tube of length L , a potential difference, $\Delta\Phi$, is generated between the ends of the capillary: $\Delta\Phi = \zeta\epsilon\Delta p/4\pi\eta\sigma$. Here, Δp is the pressure difference and ζ is the zeta potential. Using the Poiseuille flow formula, we obtain

$$\Delta\Phi = \frac{2\zeta\epsilon\rho L}{\pi^2 r^4} \dot{V} \quad (2.12)$$

which shows that the potential difference is proportional to the volume flow \dot{V} , the capillary length, and the liquid resistivity. The core electrolyte is neutral, and no electromotive voltage is generated from the bulk flow, only from the ion sheath migration.

2.6 Problems

1. What is the electronegativity of an atom?
2. What is covalent bonding?
3. What is the hydration of an ion?
4. What is the current density at a position in an electrolyte solution where the electric field is 2 V/m and the conductivity is 0.3 S/m?
5. What are the four electrokinetic effects?

Dielectrics

A dielectric may be defined simply as a volume of material placed between the plates of a capacitor for examination by an applied electric field. Traditionally, there is an important difference between dielectric and bioimpedance measurements with respect to the role of water. Etymologically, a *dielectric* is a material that the electric field penetrates (Greek dia meaning through). Conductors do not allow static electric field penetration, and basically a perfect dielectric is a substance without free charges. Synonyms for a perfect dielectric may then be an insulator or a nonconductor; antonyms may be a conductor or an electrolyte.

Living tissues are wet biomaterials and therefore electrolytic *conductors*, with ions free to migrate and therefore with DC conductivity. With living tissue, the situation is therefore complicated, and hydration, double-layer formation, and electrode polarization must be accounted for. A dry dielectric is much easier to handle. There is no galvanic contact with the electrodes and, accordingly, no electrode polarization impedance (see Section 7.9) in series with the dielectric. Complex dielectric theory is well adapted to both wet and dry systems if the necessary precautions because of water are taken.

A more direct definition of a dielectric is a material in which the capacitive (displacement) current is larger than the in-phase current, $\omega C > G$ or $f > \sigma/2\pi\epsilon$. According to this definition, saline ($\sigma = 1 \text{ S/m}$, $\epsilon = 80 \times 8.85 \times 10^{-12} \text{ F/m}$) is a conductor for $f < 250 \text{ MHz}$, and a dielectric for $f > 250 \text{ MHz}$. At sufficiently high frequencies, even a metal becomes a dielectric. The definition is frequency dependent, and this is not very practical for a general grouping of materials. In any case, a material is classified as a dielectric if it has an ability to *store energy* capacitively, not just dissipate it.

Thus tissue may be regarded as a conductor or a dielectric, the choice is ours. An electrolytic conductor is characterized by immittance, a dielectric by permittivity or capacitance. However, as we shall see, the conductivity may be complex and thus take care of a capacitive component as well, and permittivity and capacitance may be complex and also take care of a conductance. Muscle tissue is more a conductor with certain capacitive properties; stratum corneum is more a dielectric with certain conductive properties. We are in a situation that is confusing for users of bioimpedance data (e.g., medical doctors). Some bioimpedance groups characterize tissue by *immittance* terminology, others by *dielectric* terminology. A dermatologist is confronted with skin

characterized by a number of parameters such as capacitance, permittivity, impedivity, impedance, resistivity, resistance, reactance, admittance, admittance, conductivity, conductance, or susceptance. They are different but possibly correct ways of describing a biological material.

There are three mainstream developments of dielectric theories for biomaterials: The eldest, from the time of Coulomb in the eighteenth century, were based upon the relationship between two static electric charges and the mechanical force between them. In the nineteenth century, the Maxwell equations appeared, based upon electromagnetic theory and juxtaposed with light. In the twentieth century came the *Debye* tradition of regarding biomolecules as polar materials with exponential relaxation. However, experimental findings showed that most dielectrics do not show exponential relaxation, but fractional power law relaxation. Fractional power law was the “universal” property. Then came the *Cole* models based upon a new component, the constant phase element (CPE).

Also, a strong confusion has existed ever since electrode polarization was discovered (Fricke, 1932) because tissue polarization and electrode polarization are phenomenologically very equal even if they have different origins.

3.1 Polarization in a Uniform Dielectric

Polarization is a difficult concept, widely but differently used. In Section 7.9, we will focus on the polarization of *electrodes*. In the present section, we will focus on the polarization of *biomaterials*. Basically, we are focusing on static polarization with bound charge carriers. Such polarization is a key concept in understanding the electrical properties of tissue because it covers some very important and characteristic phenomena. We will start with the most general definition of polarization, and then differentiate.

Definition 1

Polarization in a biomaterial volume is the electric field–induced disturbance of the charge distribution in that volume.

The polarization may be *endogenic* (produced by the body itself) or *exogenic* (produced by an externally applied field). Bioimpedance methods are exogenic when *energy is applied* to polarize the system from the outside, for instance by light that is electromagnetic radiation or from an externally applied electric field. The exogenic energy may be stored or dissipated in the dielectric. The membrane of a living cell is polarized because the energy-consuming sodium-potassium pump transfers ions across the membrane so that the cell interior is negatively charged with respect to the extracellular fluid. This is an endogenic polarization mechanism in living tissue.

All materials are polarizable, but vacuum is not (although it can hardly be called a material). With only bound charges, an electric field can only displace charges so that dipoles are formed and the material is polarized. If the biomaterial is dry, double layers (Section 7.5) will not be formed. A dry biomaterial in contact with dry electrode metal forms an interface. With free charges, there are important additional effects from the migration of these in an electric field.

3.1.1 Coulomb's Law and Permittivity

Coulomb's law was published in 1785 and is thus much older than the Maxwell equations. It contained a revolutionary new parameter for an electrical property of a dielectric, the *permittivity* ϵ . Coulomb's law describes the *mechanical force* \mathbf{F} between two *electric* charges q_1 and q_2 at a distance L :

$$F = \frac{q_1 q_2}{L^2 \epsilon_0} \quad \text{In vector form: } \mathbf{F} = \frac{q_1 q_2 \mathbf{L}}{4\pi L^3 \epsilon_0} \quad [N] \quad (3.1)$$

Originally, the law was developed for the permittivity of vacuum ϵ_0 . With vacuum, it was possible to control the accuracy of the equation with very accurate measurements, and it was found that the equation deserved the designation "law" valid for the permittivity of vacuum ϵ_0 . It is an *empirical law*. For a long time, the permittivity was an enigmatic parameter that led, however, to a widespread and fruitful examination of electric properties of materials. It ended up with the permittivity of vacuum having the internationally accepted value of $\epsilon_0 = 8.854\ 187\ 818 \times 10^{-12}$ [F/m], showing that the original idea of the extreme accuracy of Coulomb's law was correct. Also the tight relationship between permittivity, magnetic permeability, and speed of light, all in vacuum, showed that permittivity is a very basic physical constant of vacuum:

$$\epsilon_0 = \frac{1}{\mu_0 c^2} \quad [F/m] \quad (3.2)$$

where c is the velocity of light in vacuum and μ_0 is the magnetic permeability in vacuum.

In our context, it is of course not the properties of vacuum but the permittivity of biological materials that are of interest. It is not always clear whether ϵ is the relative permittivity ϵ_r (dimensionless, often called the *dielectric constant*) or, as in this book, the complete expression $\epsilon_r \epsilon_0$. For vacuum, $\epsilon_r = 1$. There are a lot of subscripts in use for different cases. ϵ_0 does not mean permittivity at zero frequency, but the permittivity of vacuum. ϵ_s means static permittivity. This is not the same as ϵ_{DC} because static is electrostatic with no current flow, whereas DC means current flow but at zero frequency. ϵ_∞ is the permittivity at very high frequencies. And indeed here it may be high frequencies up in the optical range. The relationship between the optical refractive index n and the permittivity is roughly $n = \sqrt{\epsilon_r}$.

The Coulomb force will try to unite charges of opposite sign (even if other forces hinder it at close distance in an atom). Note that *coulomb forces are smaller the larger the permittivity of the medium*. If the medium is water with the large relative permittivity of around 80, the forces are relatively small, and water will tend to break up (dissociate) solute molecules held together by Coulomb forces.

As seen from [Table 3.1](#), the permittivity of water is reduced by the addition of electrolytes. This *dielectric decrement* $\Delta\epsilon_r$ is for 1 mol/L concentration –17 for H^+ , –8 for Na^+ and K^+ , –3 for Cl^- , and –13 for OH^- . It is directly related to the hydration of the ion, because these water molecules are more tightly bound and therefore not so easily polarized as free water molecules. The number of hydrated water molecules around a monovalent ion is of the order of 5 (see Table 2.4).

The concept of *electric field* is derived from Coulomb's law. There is an electric field at a location if a charge there is influenced by a mechanical force \mathbf{f} (space vector) proportional to the charge:

$$\mathbf{E} = \frac{\mathbf{f}}{q} \quad [V/m] \quad (3.3)$$

Table 3.1: Relative Permittivity

	10^2 Hz	10^6 Hz	10^{10} Hz
Gases			
Air (100 kPa)	1.00054		
Liquids			
Carbon tetrachloride	2.2	2.2	2.2
Benzene	2.28	2.28	2.28
Olive oil	3.1		
Chloroform	4.8		
Ethanol	25.7		
Water ($0^\circ C$)	87.7		
Water ($20^\circ C$)	80.1		
Water ($25^\circ C$)	78.5	78.5	65
Water ($25^\circ C$ KCl-0.5 mol/L)	75	75	
Water ($37^\circ C$)	74.3		
Hydrogen cyanide	116		
Solids			
Teflon	2.1	2.1	2.1
Polystyrene	2.6	2.6	2.6
Plexiglas	3.1	2.76	
Ice		4.15	3.2
Glass (pyrex)	5	4.8	4.8
NaCl		5.9	5.9
KCl	5		
AgCl	11		

A free *positive* charge is migrating in the same direction as the \mathbf{E} -field. $\mathbf{E}(x,y,z)$ defines a vector field not linked to a material because it is also defined for vacuum. The work (energy) to bring a charge q from infinity to a location is by convention equal to $q\Phi$ [eV, J]. Φ is the potential at that location, and zero potential is by convention infinitely far away in a space without charges. A *potential difference is work per charge*, $1 \text{ [volt]} = 1 \text{ [joule/coulomb]}$. This is the basis for defining potentials in electrolytic systems and in the electric double layer at electrode or cell membrane surfaces.

The equipotential lines will be perpendicular to the \mathbf{E} and \mathbf{J} vectors, but potential Φ itself is not a vector and has no direction (even if the *change* of Φ has a direction, so Φ has a *gradient* vector, $\mathbf{E} = -\nabla\Phi$). Vector quantities being perpendicular at all points in space are treated with what mathematicians call *conformal mapping*.

3.1.2 Three Types of Polarization

Electronic Polarization

Dipole moment density occurs as a result of very small translational displacements of the electronic cloud with respect to the nucleus, whether in single atoms or in molecules. Displacement of electrons is very fast (picosecond), and the dispersion is in the gigahertz region. Induced dipoles will have the direction of the local E-field and undergo no rotation.

Orientational Polarization

Molecules may form *permanent* dipoles (polar molecules), which of course will also be influenced by an externally applied electric field. A polyatomic molecule is nonpolar if it fulfills certain symmetry criteria. Water molecules are asymmetrical and therefore polar. In polar materials, rotational movements will be caused by the torque experienced by permanent dipoles in electric fields.

Ionic Polarization

This is displacement of positive ions with respect to negative ions. To clarify the division between electronic and ionic polarization: electronic polarization is the displacement of the electron cloud with respect to the nucleus; ionic polarization is the displacement of ions relative to each other. The hydrated sheath around an ion at rest is symmetrical (not really at rest, everything is bumping around at room temperature, we are talking statistically). When current flows, the sheath will lag behind the migrating ion, and the sheath is no longer symmetrical to the ion, cf. the Wien effect (Section 8.4.1). This is local polarization of charges bound to each other.

A molecule with a net charge $\neq 0$ will experience a translational force and therefore try to migrate in a *homogeneous* electric field. A dipole with net charge $= 0$ will *also* experience a translational force, but *only* in an *inhomogeneous* field.

3.1.3 Induced and Permanent Dipole Moments

In dry materials without free charges (e.g., Teflon or dry NaCl), acting as a dielectric between two capacitor plates (Figure 3.1) there is no DC conductance and no local build-up of free charges at dielectric interfaces and no electrolytic polarization, neither in the bulk nor at the electrodes. However, a local disturbance of the distribution of *bound* charges will occur in an imposed E-field. Suppose that two charges are equal but of opposite sign and kept at a small distance and thus hindered to recombine. Such an electric doublet is called a *dipole* (see Figure 6.4). An *atom* with the electrons at a distance from its positive nucleus does not necessarily form a net dipole: the center of the electron cloud may coincide with that of the nucleus. However, every such atom is polarizable because the electrical centers of the charges will be displaced by an *external electric field*. As positive and negative charges move in opposite directions, *dipoles* are formed (*induced*) and the material is *polarized*.

Also, bound ions of the dielectric can move but only locally (translate, rotate) and under strong confinement. *No electric charges are exchanged between the dielectric and the metal electrode plates.*

Electrostatic Dipole Moments

In electrostatic theory, a dipole is characterized by its electrical *dipole moment*, the space vector \mathbf{p} :

$$\mathbf{p} = q\mathbf{L} \quad [\text{Cm}] \quad (3.4)$$

The unit for \mathbf{p} is coulomb meter [Cm], or outside the SI system: the *Debye unit* ($D = 3.34 \times 10^{-30}$ [Cm]). A pair of elementary charges $+e$ and $-e$ held at a distance of 0.1 nm has a dipole moment of 4.8 D, a water molecule has a *permanent* dipole moment of about 1.8 Debye.

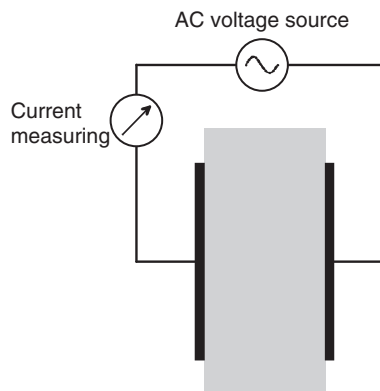


Figure 3.1: The basic capacitor experiment.

The dipole moment \mathbf{p} may be the resultant dipole moment of a molecule, many molecules, or a whole region. Polarization \mathbf{P} [$\text{Cm/m}^3 = \text{C/m}^2$] is the electrical dipole moment *per unit volume* (dipole moment volume density). It is therefore a more macroscopic concept than the dipole moment of molecules or atoms. \mathbf{P} is a space vector having the same direction as the \mathbf{E} -vector in isotropic and linear materials:

$$\begin{aligned}\mathbf{P} &= \mathbf{D} - \epsilon_0 \mathbf{E} = (\epsilon_r - 1) \epsilon_0 \mathbf{E} = \chi \epsilon_0 \mathbf{E} \quad [\text{C/m}^2] \\ \mathbf{D} &= \epsilon \mathbf{E} = \epsilon_0 \mathbf{E} + \mathbf{P} \quad [\text{C/m}^2]\end{aligned}\tag{3.5}$$

\mathbf{D} (either as a surface charge density q_s [C/m^2], or dipole moment volume density [Cm/m^3]) is called the *electric flux density*, or *displacement*. $\chi = \epsilon_r - 1$ is called the *electric susceptibility*¹ of the material. For vacuum, $\epsilon_r = 1$ and $\chi = 0$.

Equation (3.5) shows the relationship between polarization and permittivity. High polarization means high permittivity, $E = 0$ means $P = 0$ and no polarization. *Permittivity is a measure of the amount of dipole moment density created (induced) by an electric field.* Bound charges that can be displaced a long distance L , cause a larger dipole moment, Eq. (3.4), resulting in a higher permittivity. A substance in the liquid state is therefore more strongly polarized than in the solid state; ice has lower permittivity than water. Tissue components such as the proteins are characterized by particularly long distances between charges and can thus have a surprisingly high permittivity. Polarization effects actually are net effects of a constantly changing charge distribution, the degree of disorder increases with temperature according to the Boltzmann factor kT .

Polarization P cannot itself be measured. Dielectric theory is therefore invariably linked with the concept of a capacitor formed by two plates with the dielectric in between (Figure 3.1). The capacitance of this capacitor can be measured and the polarization calculated.

Some molecules are *polar* (e.g., water and many proteins). The *permanent* dipole moments are oriented at random, but with an externally applied electric field they reorient statistically. *Induced* dipoles have the direction of the applied E -field, but if the medium is *polar*, the polarizing E -field also *rotates the permanent dipoles* already in existence (orientational polarization). Polar materials have a large permittivity in addition to the permittivity caused by the induced dipoles of the nonpolar molecules present. The permanent dipoles will experience a rotational force, defined by the *torque* τ :

$$\tau = \mathbf{p} \times \mathbf{E} \quad [\text{Nm}, \text{J}]\tag{3.6}$$

If the charges are bound, the torque will result in a limited rotation. The positions and angles are statistically distributed with less ordering the higher the temperature. As we

¹ Not to be confused with susceptibility in the relation: admittance, conductivity, and susceptibility.

shall see in Section 7.12.6, in a *rotational* \mathbf{E} -field, the *induced* dipoles may lag the external field, and thus also give rise to a torque and continuous rotation.

In some polar media, the dipole moments are “frozen” in positions that statistically result in a net component in a given direction. They are called *electrets*, and they have a net internal \mathbf{P} -field in the absence of an externally applied field. An electret is the electrical equivalent of a permanent magnet. In the form of a thin sheet, the resultant equivalent surface charge density may be of the order of $50 \times 10^{-3} \text{ C/m}^2$. Slowly, the polarization will diminish, but the process may take many years.

The polarization vector \mathbf{P} is composed of all three components:

1. An external field produces new dipoles (induced dipoles)
2. An external field orients the permanent dipoles already there
3. Without an external field, electrets have a permanent net dipole moment

3.1.4 Clausius–Mosotti and Debye Equations

Susceptibility χ is a macroscopic parameter and is correlated with a microscopical factor called the *polarizability* α [Cm^2/V] so that $\mathbf{p} = \alpha \mathbf{E}_L$ where \mathbf{E}_L is the local electric field strength. Then macroscopically $\mathbf{P} = N\alpha \mathbf{E}$, where N is the volume density of atoms or molecules. In nonpolar media there is a simple relationship between the polarization and the molecular structure, the *Clausius–Mosotti* equation:

$$\frac{\epsilon_r - 1}{\epsilon_r + 2} = \frac{N\alpha_e}{3\epsilon_0} \quad (3.7)$$

Equation (3.7) can be extended to also comprise the contribution from polar molecules, demonstrated by one of *Debye*'s equations (c.f. Section 9.2.4):

$$\frac{\epsilon_r - 1}{\epsilon_r + 2} = \frac{4\pi N_A \left(\alpha^2 + \frac{p^2}{3kT} \right)}{v_m} \quad (3.8)$$

where v_m is the molar volume and N_A is Avogadro's constant. The kT -factor is due to the statistical distribution of polar molecules causing the orientational polarization. Eqs (3.7) and (3.8) are in best agreement in gases, in less agreement in liquids, and least in solids. For the last-mentioned cases, Onsager and Kirkwood have extended the theory.

3.1.5 Charge-Dipole and Dipole–Dipole Interactions

Equation (3.4) defines the electrostatic dipole moment $\mathbf{p} = q\mathbf{L}$. The potential field $\Phi(x,y,z)$ from such a dipole is given by:

$$\Phi(x,y,z) = \frac{\mathbf{p} \cdot \hat{\mathbf{r}}}{4\pi\epsilon_0 r^2} \quad (3.9)$$

Table 3.2: Energy Dependence on Distance Between Ions/Dipoles

Interaction	Distance Dependence of \hat{E}
Ion–ion	$1/r$
Ion–dipole	$1/r^2$
Dipole–dipole	$1/r^3$
Dipole–dipole (rotating)	$1/r^6$

where \hat{r} is the unit vector from the dipole to the point (x,y,z) where the potential is to be defined. A prerequisite for this equation is that the dimension of the charges is much smaller than the distance L between them. The potential field is visualized in Figure 6.4. According to Eq. (3.9), the potential falls off as $1/r^2$. Then the energy \hat{E} -field must fall off as $1/r^3$ (see Table 3.2).

In a molecule, there may be local dipoles and single charges in the meaning that the counter charge is far away. Electrostatic forces will occur that basically are of a charge-to-dipole or dipole-to-dipole nature. These forces will be intermolecular and intramolecular and will therefore influence the geometrical form of the molecule.

The static energy \hat{E} related to a point charge q at a distance r from an ideal dipole is:

$$\hat{E} = -\frac{pq}{4\pi\epsilon_0 r^2} \quad (3.10)$$

Table 3.2 shows the static energy dependence on the distance between ions/dipoles. Note that the energy falls off more rapidly when two dipoles rotate at random than under stationary non-thermal conditions (see also Table 6.1).

3.2 Basic Capacitor Experiment

3.2.1 Set-up

In Section 2.2, we treated the electrolytic cell. Now we will introduce a similar cell: the capacitor with two plates (Figure 3.1). The substance we place between the electrode plates is called an electrolyte (in a solution), the substance between the plates of a capacitor is a *dielectric*. In one sense, the difference between Figure 2.1 and Figure 3.1 is not very large. In Figure 2.1, we considered a liquid between metal plates and we studied DC conductance. The material between the plates had a *high* volume density of free charges. In Figure 3.1, we considered a dry solid material such as Teflon with a *low* volume density of free charges, but many bound charges between the metal plates. Both DC and AC current was measured, with a phase sensitive volt/am-meter or displayed on a two-channel oscilloscope.

Findings

Applying a DC voltage of even 10–20 V does not result in a DC current. Applying an AC sinusoidal voltage leads to an AC sinusoidal current, and the current is proportional not

only to voltage amplitude, but also to the signal frequency. The current top comes earlier than the voltage top; the current leads the voltage by almost 90° . As long as this is the case, even large currents do not warm up the dielectric.

Discussion

A capacitive current is an AC current. It is not an electron current of free charges passing between the plates through the dielectric. It is a true current of electrons charging-discharging the capacitor plates, but without electrons leaving or entering the plates. It is a simple relationship between the charge Q [coulomb] on the plates, the voltage [V] between the plates, and the capacitance C [farad] of the capacitor:

$$Q = VC \quad [\text{coulomb}] \quad (3.11)$$

The capacitance C of the capacitor is dependent on the plate area A [m^2], the distance between the plates d [m], and a property of the dielectric between the plates defined already in [Section 3.1.1](#) as *permittivity* ϵ [farad/m]:

$$C = \left(\frac{A}{d}\right)\epsilon \quad [\text{farad}] \quad (3.12)$$

If we apply a sinusoidal AC voltage to the plates as shown in [Figure 3.1](#), the AC current flowing as electrons in the capacitor metal wires will not have its maximum current value at the same time as the voltage maximum occur. The current is *phase shifted* in time. We measure the phase shift in degrees, defining one complete cycle of the AC sinusoidal voltage as 360° or 2π radians. An ideal, steady-state sinusoidal capacitive current is 90° *ahead* of the sinusoidal voltage. It is possible by suitable electronic circuitry to separately measure the *in-phase* (conductive) current (or voltage) component and the 90° out of phase (*quadrature*) (capacitive) current (or voltage) component. It is not sufficient to characterize an AC current only with one number, the amplitude. The current must be characterized with *two* numbers, with the additional number giving information about the phase. The sum of two equal amplitude sine waves is the double amplitude if they are in phase, but constant equal to zero if they are 180° out of phase.

The electric flux density D introduced in [Section 3.1.2](#) represents a displacement of *bound* charges in the bulk of the dielectric. At the capacitor metal plates, D is also the charge per plate area: q/A , but at the plates it is related to the *free* (electron) charge flow corresponding to the measured current in the capacitor wires. The status in the volume of the dielectric is not directly noticeable from the capacitor plates. For the capacitor, the effect of the whole dielectric volume can be reduced to the two layers of bound charges at the surface of the dielectric, each in (almost) contact with the metal plates. These charged layers are “the ends” (this must not be taken too literally; e.g., the charge separation at ordinary field strengths with electronic polarization is very, very small and less than the electron diameter) of the surface dipoles in the dielectric, induced by the external field but bound in the dielectric.

The E-field strength in the dielectric is reduced by the bound charges at the surface of the dielectric. The higher the permittivity, the lower the E-field in the bulk. The E-field is *discontinuous* at the dielectric surface. The electric flux density \mathbf{D} is *continuous* at the dielectric surface as long as there are no free charges there.

3.3 Complex Variables and Material Constants

We revert to the basic capacitor model of [Figure 3.1](#). The *admittance* \mathbf{Y} of the capacitor is (sinusoidal AC voltage u , homogeneous dielectric, and no edge effects):

$$\mathbf{Y} = G + j\omega C = \left(\frac{A}{d}\right)(\sigma' + j\omega\epsilon') \quad (3.13)$$

The current in the capacitor wire $\mathbf{i} = u\mathbf{Y} = uG + ju\omega C$. The conductance G and the current uG comprises all components that are in-phase with u . G is due both to DC conductance and AC *losses* in the dielectric. The j indicates that the $ju\omega C$ current is in quadrature (90° phase shifted) with u , it is a displacement current. AC losses and permittivity ϵ are usually frequency-dependent, but even then \mathbf{Y} is usually equal to $(A/d)\sigma'$ at low frequencies.

Complex Permittivity and Conductivity

It may be useful to treat σ and ϵ as complex quantities in the time domain (e.g., to incorporate dielectric losses and frequency dependence). We then define:

$$\sigma \equiv \sigma' + j\sigma'' \quad [\text{S/m}] \quad (3.14)$$

$$\epsilon \equiv \epsilon' - j\epsilon'' \equiv (\epsilon'_r - j\epsilon''_r)\epsilon_0 \quad [\text{F/m}] \quad (3.15)$$

Note the minus sign in [Eq. \(3.15\)](#) (complex conjugate).

Tissue data are often given with ϵ' and σ' parameters because this is in best agreement with the basic capacitor model ([Figure 3.1](#)) and [Eq. \(3.13\)](#). Of course, tissue data may be given with either *only* complex conductivity or complex permittivity. All three ways are in common use.

Complex Permittivity

Complex permittivity is used when the material is considered as a dielectric (an insulator) with losses. The capacitor is characterized with a complex capacitance or a complex permittivity:

$$\mathbf{Y} = \left(\frac{A}{d}\right)(\sigma' + j\omega\epsilon') = j\omega\mathbf{C} = j\omega\left(\frac{A}{d}\right)(\epsilon' - j\epsilon'') = \left(\frac{A}{d}\right)(\omega\epsilon'' + j\omega\epsilon') \quad [\text{S}] \quad (3.16)$$

Therefore:

$$\epsilon'' = \frac{\sigma'}{\omega} \quad [\text{F/m}] \quad (3.17)$$

σ' is proportional to energy loss per *second* (power loss), ϵ'' to energy loss per *cycle* (*period*). Frequency-independent DC conductivity σ' implies constant energy loss per second and therefore an energy loss per cycle inversely proportional to frequency (Eq. (3.16)). Then ϵ'' diverges when the (angular) frequency approaches zero if σ' is frequency independent. This is why the use of ϵ'' for electrolytic materials may be less attractive.

Complex Conductivity

Complex conductivity σ is used when the material is considered as a conductor with capacitive properties. Complex conductivity is according to the basic capacitor model shown in Figure 3.1, where capacitance and conductance physically are in parallel:

$$\mathbf{Y} = \left(\frac{A}{d}\right)(\sigma' + j\omega\epsilon') = \mathbf{G} = \left(\frac{A}{d}\right)\sigma = \left(\frac{A}{d}\right)(\sigma' + j\sigma'') \quad [S] \quad (3.18)$$

Usually G is a real number in the equation $\mathbf{Y} = G + jB$, but now G is considered complex $= \mathbf{G} = \mathbf{Y}$, thus taking care also of B . Then $\sigma'' = \omega\epsilon' \text{ [S/m]}$, diverging as $f \rightarrow \infty$ (in contrast to ϵ'). This is why σ'' for electrolytic materials may be a less attractive parameter.

Complex Resistivity²

Complex resistivity is not according to the basic parallel model of Figure 3.1; it is linked with impedance and the series equivalent model. Complex resistivity is the inverse of complex conductivity:

$$\text{Equation } \rho = \rho' - j\rho'' = \frac{1}{\sigma} = \frac{(\sigma' + j\sigma'')}{|\sigma|^2} \quad [\Omega m] \quad (3.19)$$

Pay attention³ to the fact that $\rho' \neq 1/\sigma'$, but $\rho = 1/\sigma$ in the meaning $|\rho| = 1/|\sigma|$.

Losses

$\epsilon_r'' = \sigma' / (\epsilon_0 \omega)$ is sometimes called the loss *factor*. The loss *angle* δ of a capacitor is defined so that the ideal capacitor with zero losses also has zero loss angle. This means that $\delta = 90^\circ - \varphi$:

$$\varphi = \arctan \frac{\epsilon'}{\epsilon''} \quad (3.20)$$

$$\delta = \arctan \frac{\epsilon''}{\epsilon'} = \operatorname{arccot} \frac{\epsilon'}{\epsilon''}$$

² Use of “specific resistance” and “specific conductance” for resistivity and conductivity is not recommended. Resistivity has the unit $[\Omega m]$, but “specific” means a quantity per mass, so specific resistance should then have been $[\Omega/kg]$.

³ Historically, there was no problem when only real quantities $\rho = 1/\sigma$ were used. However, with complex quantities, if ρ' is called resistivity, then σ' has no name because $\sigma' = \rho'/|\rho|^2 \neq 1/\rho'$!

$\tan \delta$ is also called the loss *tangent* or *dissipation factor*. $\tan \delta$ is energy lost per cycle divided by energy stored per cycle (rms or peak values).

Care must therefore be taken with regard to the term “phase angle.” In ordinary immittance texts, it is always the tangent of the out-of-phase component divided by the in-phase component. However, in many classical presentations, the loss angle is used instead for characterizing the polarization properties of an electrode: Schwan (1963): symbol δ , Fricke (1932): symbol ψ . Also in the classical Warburg (1899) paper, his angle ψ is the loss angle. Sometimes the loss angle is called the loss angle; sometimes it is called the phase angle.

Modulus Function

It may be useful to have a parameter for the inverse of the permittivity. This is the *modulus function* M :

$$M = \frac{1}{\epsilon} = M' + jM'' \quad [\text{m/F}] \quad (3.21)$$

3.3.1 Immittance and Material Constants: A Survey

Immittance is not a quantity; it is the general term of both impedance and admittance, and in a specific case a quantity must be chosen: either impedance [Ω] or admittance [S]. Such quantities with names ending on –ance are dependent on sample and electrode geometries. Quantities with names ending on –ivity such as impedivity [Ωm], admittivity [S/m], and permittivity [F/m] are *material constants*.

Impedivity and complex resistivity [Ωm] are synonyms. Admittivity and complex conductivity [S/m] are synonyms. With a sample in a measuring in vitro cell like Figure 3.1 or Figure 3.2(a), the material constant complex conductivity can be found from

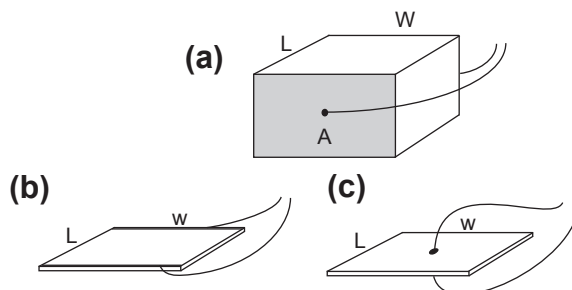


Figure 3.2: Geometrical models. (a) Volume parameters, (b) surface lateral parameters, (c) surface perpendicular parameters.

measured admittance \mathbf{Y} : $\boldsymbol{\sigma} = \mathbf{Y}(d/A)$. The relationship between complex resistivity and measured impedance \mathbf{Z} is: $\rho = \mathbf{Z}(A/d)$. In vivo measurements are difficult to perform in a measuring cell, and it is impossible to go from measured impedance to impedivity with the electric field distribution unknown. Tissue anisotropy and inhomogeneity add to the problems.

In a text, it is often not clear whether ϵ is scalar or complex. If σ or ϵ are complex, they are printed in bold in this book: $\boldsymbol{\epsilon}$ or $\boldsymbol{\sigma}$. If the parameters are not printed in bold, there may be an ambiguity: \mathbf{Y} , \mathbf{Z} , σ and ϵ may mean $|\mathbf{Y}|$, $|\mathbf{Z}|$, $|\boldsymbol{\sigma}|$, $|\boldsymbol{\epsilon}|$, or the real values Y' , Z' , σ' and ϵ' .

σ' , σ'' , ϵ' , and ϵ'' are components of the complex quantities $\boldsymbol{\sigma}$ and $\boldsymbol{\epsilon}$; their somewhat bewildering frequency dependent relationships are:

$$\begin{aligned}\boldsymbol{\sigma} &= j\omega\boldsymbol{\epsilon} & (3.22) \\ \sigma' &= \omega\epsilon'' = G\left(\frac{d}{A}\right) & \sigma'' &= \omega\epsilon' = \omega C\left(\frac{d}{A}\right) = B\left(\frac{d}{A}\right) \\ \epsilon' &= \frac{\sigma''}{\omega} = \frac{Cd}{A} = \left(\frac{B}{\omega}\right)\left(\frac{d}{A}\right) & \epsilon'' &= \frac{\sigma'}{\omega} = \left(\frac{G}{\omega}\right)\left(\frac{d}{A}\right)\end{aligned}$$

If the capacitance of the empty (no dielectric material) cell is C_e (pure capacitance), it is possible to express some interesting relationships:

$$\mathbf{Y} = j\omega C_e \boldsymbol{\epsilon}_r \quad \mathbf{M} = j\omega C_e \mathbf{Z} \quad \mathbf{M} = j\omega C_e / \mathbf{Y} \quad (3.23)$$

Volume Parameters (Figure 3.2(a))

Usually a material is characterized with parameters for volume properties.

$$\begin{aligned}Volume \text{ conductivity } \sigma &= \frac{G \cdot L}{A} \quad [\text{S/m}] \\ Volume \text{ resistivity } \rho &= \frac{R \cdot A}{L} \quad [\Omega \cdot \text{m}] \\ Volume \text{ conductance density } g &= \frac{\sigma}{L^2} \quad [\text{S}/\text{m}^3] \\ Volume \text{ resistance density } r &= \frac{\rho}{A^2} \quad [\Omega/\text{m}^3]\end{aligned} \quad (3.24)$$

Density in physics means the number of items constrained to a defined space (e.g., number of electrons in a volume or on a surface or along a line).

Surface Parameters (Figure 3.2(b) and (c))

Even if a material is often characterized with variables for volume properties, an epithelium or antistatic coating may have a high resistivity with respect to the substrate,

combined with known area but unknown thickness. Then surface parameters may be useful, Eq. (3.25) (w = sample width):

$$\begin{aligned} \text{Surface (lateral) conductivity } \sigma_{\text{sul}} &= \frac{G L}{w} \quad [\text{S}] \\ \text{Surface (lateral) resistivity } \rho_{\text{sul}} &= R \frac{w}{L} \quad [\Omega] \\ \text{Surface (perpendicular) conductivity } \sigma_{\text{sup}} &= \frac{G}{Lw} \quad \left[\text{S/m}^2\right] \\ \text{Surface (perpendicular) resistivity } \rho_{\text{sup}} &= RLw \quad \left[\Omega\text{m}^2\right] \end{aligned} \quad (3.25)$$

Note that the surface lateral parameters are given just in siemens or ohm, as L/w is dimensionless.

The surface parameters are pseudo-material constants because they characterize a given surface or membrane presupposing a given, constant but unknown thickness (e.g., a tissue membrane), and with negligible influence (e.g., from a substrate underneath). If these conditions are not fulfilled, surface parameters are not recommended. Another way is to give values as conductance [S] normalized to e.g., 1 cm^2 , and preferably adding information about the actual surface area used.

As with the volume material constants, the surface pseudo-material constants may be extended to be complex, e.g., surface *lateral* admittance $\sigma_{\text{sul}} = Y L/w$ [S] being composed of surface lateral conductivity $\sigma'_{\text{sul}} = G L/w$ and surface lateral susceptibility $\sigma''_{\text{sul}} = B L/w$. The surface *perpendicular* admittance $\sigma_{\text{sup}} = Y/Lw$ [S/m^2].

3.4 AC Polarization and Relaxation in a Uniform Dielectric

3.4.1 Relaxation and Dispersion

In Section 3.1 about polarization, we considered polarization as a static property of a material, dependent not on time, only on the externally applied field. In an electric field of time varying strength or direction, the charge positions were considered to be synchronous with the instantaneous values of the applied field. However, polarization and the displacement of charges in a material do not occur instantaneously. If the measuring frequency is low enough so that all charges are allowed the necessary time to change their position, polarization is maximal. But with increasing frequency, the polarization and permittivity will decrease.

This time dependence may be characterized by introducing the concept of *relaxation*. It was first used by Maxwell in connection with elastic forces in gases. Later, Debye used it referring to the time required for dipolar molecules to orient themselves. Instead of applying a sinusoidal AC measuring signal and measure (e.g., admittance and phase shift),

the concept of relaxation is linked with a *step function* excitation signal. After a step has disturbed a system under investigation, the system is allowed to *relax* to a new equilibrium; this is the relaxation process. Relaxation occurs in the *time* domain, after a step increase or decrease in the E-field strength. It is described by the parameter *relaxation time*, which is different from the parameter immittance as a function of the frequency of a sine wave excitation.

It is often stated that all electrical properties of biological materials are due to relaxation phenomena. However, the concept of relaxation is not so meaningful with frequency independent DC conductance; the conductance is constant with time and does not relax. When DC voltage is switched on, the current starts immediately.

Impedance theory and relaxation theory often do not include resonance phenomena, as these are usually not found in macro tissue samples in the frequency range from μHz to MHz .

Relaxation time is dependent on the polarization mechanism. Electronic polarization is the fastest mechanism, with relaxation in the higher MHz and GHz regions. Large organic molecules such as proteins may have a particular large permanent dipole moment because of the long distance L between the charges. Because they are so large and have a complex bonding, the rotation and twist can be slow. However, interfacial relaxation may be the most important process and with the longest mean relaxation times of the order of seconds.

Dispersion (frequency dependence according to the laws of relaxation) is the correspondent frequency domain concept of relaxation: permittivity as a function of frequency. Even if the concept of relaxation is linked with step functions, it can of course be studied also with sine waves. An ideal step function contains all frequencies, and dispersion can be analyzed with a step function followed by a frequency (Fourier) analysis of the response signal or with a sinusoidal signal of varying frequency.

As we shall see in the next section, in a simple case of a *single dispersion* with a single relaxation time constant, there will be one permittivity level at low frequencies (time for complete relaxation) and a second *lower* level at higher frequencies (not sufficient time for the relaxation process studied). It will be a transition zone characterized by a frequency window with a characteristic center frequency. Therefore dispersion in relaxation theory often has a somewhat more precise meaning than just frequency dependence. *Simple dispersions are characterized by a permittivity with two different frequency independent levels, and a transition zone around the characteristic relaxation frequency.* In biomaterials, such levels may be found more or less pronounced.

3.4.2 Debye Relaxation (1R-2C) Model

Let us assume only bound charges in a dielectric are placed between two capacitor plates, and that a step increase of DC voltage is applied at $t = 0$. Let us assume that the material has only one relaxation process with a single characteristic time constant, and that the polarization increases according to an exponential curve as a function of time. This is called a *Debye single dispersion*. As a result of the polarization in the dielectric, the surface free charge density $D(t)$ ($=q_s$) at the capacitor plates will increase from one value (D_∞) to another (D_0) as shown in Figure 3.3 and according to the equation:

$$D(t) = D_\infty + (D_0 - D_\infty)(1 - e^{-t/\tau}) \quad (3.26)$$

The subscripts refer to frequency, a sine wave parameter. D_∞ is the surface charge density at $t = 0+$, which is after the step but so early that only apparently instantaneous polarization mechanisms have come to effect (high frequency; e.g., electronic polarization). The capacitor charging current value at $t = 0$ is infinite, so the model has some physical flaws. D_0 is the charge density after so long time that the new equilibrium has been obtained and the charging current has become zero. With a single Debye dispersion, this low-frequency value is called the *static* value (see Section 6.2.1). τ is the exponential *time constant* of the relaxation process.

By Laplace transforming Eq. (3.26), it is possible to find the response in the frequency domain. With $\epsilon' = D/E$, and $C = \epsilon'A/d$, we have:

$$\epsilon(\omega) = \epsilon'_\infty + \frac{\Delta\epsilon'}{(1 + j\omega\tau)} \quad \text{Debye single dispersion equation} \quad (3.27)$$

$$C(\omega) = C_\infty + \frac{\Delta C}{(1 + j\omega\tau)} \quad (3.28)$$

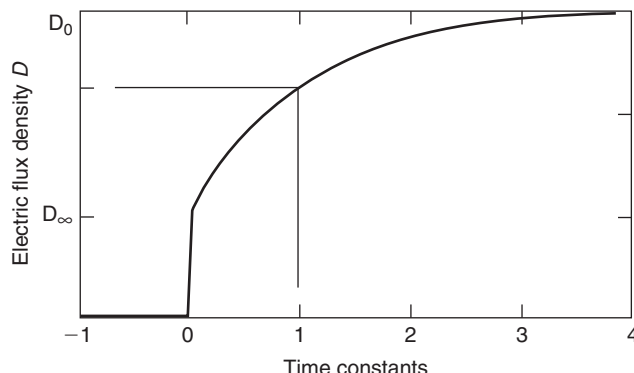


Figure 3.3: Capacitor plate surface free charge q_s (electric flux density D) after an applied voltage step.

Here ϵ and \mathbf{C} are vectors in the time domain. We have already seen the ambiguity that ϵ may mean $|\epsilon|$ or ϵ' . In dispersion theory, this is less a problem, because the parameters used are at frequency extremes, where $\epsilon_s = \epsilon'_s$ and $\epsilon_\infty = \epsilon'_\infty$.

At low frequencies, we measure a frequency-independent capacitance $C_o = C_\infty + \Delta C$. The frequency must be low enough to guarantee that the polarization process can follow. In a sufficiently higher frequency range, we measure another frequency-independent capacitance C_∞ , lower than C_o . The frequency must be sufficiently high so that the polarization process in question cannot follow.

The best equivalent circuit for such behavior is shown in [Figure 3.4](#). [Figure 3.4](#) is the circuit of [Figure 9.12](#) in Section 9.2.4 and [Figure 12.4](#) in Section 12.2.2. With $\tau = R\Delta C$, the complex admittance and capacitance of this equivalent circuit are:

$$\begin{aligned} \mathbf{Y} &= j\omega \mathbf{C} = j\omega C_\infty + \frac{j\omega \Delta C}{(1 + j\omega\tau)} \\ \mathbf{C} &= C_\infty + \frac{\Delta C}{(1 + j\omega\tau)} \end{aligned} \quad (3.29)$$

The in-phase components of [Eq. \(3.29\)](#) are:

$$\begin{aligned} Y' &= \omega \left[C_\infty - \frac{\Delta C \omega \tau}{(1 + \omega^2 \tau^2)} \right] \\ C' &= C_\infty + \frac{\Delta C}{(1 + \omega^2 \tau^2)} \\ \epsilon' &= \epsilon'_\infty + \frac{\Delta \epsilon'}{(1 + \omega^2 \tau^2)} \end{aligned} \quad (3.30)$$

The quadrature loss components are:

$$\begin{aligned} Y'' &= \frac{\Delta C \tau \omega^2}{(1 + \omega^2 \tau^2)} \\ C'' &= \frac{\Delta C \tau \omega}{(1 + \omega^2 \tau^2)} \\ \epsilon'' &= \frac{\Delta \epsilon' \tau \omega}{(1 + \omega^2 \tau^2)} \end{aligned} \quad (3.31)$$

The quadrature component dependence with increasing frequency is from a higher level to a lower, the in-phase component goes through a maximum. C_∞ and ΔC are ideal capacitors. At very high frequencies, C_∞ dominates the total admittance and capacitance. At very low frequencies, R is negligible with respect to the impedance of ΔC , and the two

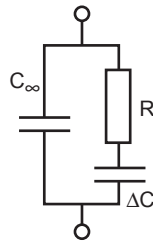


Figure 3.4: Dielectric (1R-2C) model circuit for a debye single dispersion. No DC conductance.

capacitors C_∞ and ΔC are effectively in parallel. So both at high and low frequencies, the circuit is purely capacitive. Correspondingly, ϵ'_∞ and $\Delta\epsilon'$ are real values associated with ideal capacitors. ϵ' is the parameter used, because at very high and very low frequencies $\epsilon'' = 0$ and ϵ is real with values not influenced by R .

The *characteristic relaxation frequency* ω_c is the frequency corresponding to $\omega\tau = 1$ and the maximum ϵ'' . The characteristic relaxation time constant is $\tau = R\Delta C$, and therefore $\omega_c = 2\pi/\tau$. The values of ϵ' and maximum ϵ'' are found from Eqs. (3.30) and (3.31):

$$\begin{aligned}\epsilon'_{\omega\tau=1} &= \frac{\epsilon'_\infty + \Delta\epsilon'}{2} \\ \epsilon''_{\omega\tau=1} &= \frac{\Delta\epsilon'}{2}\end{aligned}\tag{3.32}$$

Maximum value of ϵ'' is therefore not related to the resistor R , but R determines at what characteristic frequency the maximum value will occur.

The power loss W_L in the circuit is (constant amplitude sinusoidal *voltage* = v) (see Section 12.2):

$$W_L = v^2 Y' = \frac{v^2 \Delta C \omega^2 \tau}{(1 + \omega^2 \tau^2)} \text{ [watt]}\tag{3.33}$$

The power loss W_L (constant amplitude sinusoidal *current* = i) is:

$$W_L = i^2 Z' = \frac{i^2 \Delta C \omega \tau}{[(C_\infty + \Delta C)^2 + C_\infty^2 \omega^2 \tau^2]} \text{ [watt]}\tag{3.34}$$

The power loss and heat dissipation do only occur in the resistor, and the two capacitors are ideal components. The frequency dependence of the power loss is dependent on how the circuit is driven. With constant amplitude *voltage*, the power loss goes from zero level at very low frequencies to a defined level v^2/R at high frequencies (as with σ' , see below).

With constant amplitude *current*, the power loss goes from zero level at very low frequencies, through a maximum at the frequency determined by the time constant $\tau = R\Delta C$, and back to zero (like ϵ'' , see below).

Calculating the complex *conductivity* σ , the difference between high- and low-frequency conductance $\Delta\sigma' A/d$ must be $1/R$. $Y = (A/d)(\sigma' + j\sigma'')$, and this must be compared with Y' Eq. (3.30), and Y'' Eq. (3.31):

$$\begin{aligned}\sigma' &= \frac{\Delta\sigma' \omega^2 \tau^2}{(1 + \omega^2 \tau^2)} \quad \text{in-phase (lossy) component} \\ \sigma'' &= \omega C_\infty + \frac{\Delta\sigma' \omega \tau}{(1 + \omega^2 \tau^2)} \quad \text{quadrature (capacitive) component}\end{aligned}\tag{3.35}$$

The in-phase component σ' dependence with increasing frequency is from zero to a finite level, in contrast to ϵ'' , which returned to zero at high frequencies. The last term of the quadrature component equation goes through a maximum, but the first term is proportional to frequency and diverges, just like a capacitive susceptance $B = \omega C$. It is not very logical to characterize a capacitive material with conductivity variables, and some training is necessary for interpreting quadrature conductivity data for dielectrics. $\Delta\sigma'$ is a real number associated with the ideal conductor R . σ' is the parameter used in Eq. (3.35), because at very high and low frequencies σ' and the last part of the equation for σ'' both are real and not influenced by the two capacitors.

A problem with Debye theory and the use of ideal components in the equivalent circuits has been that most dielectrics actually do not follow an exponential discharge curve, but a fractional power discharge curve. This law is called the Curie – von Schweidler's law (Schweidler, 1907). We shall revert to this phenomenon later in Section 9.2.12.

Control Equation

It is an interesting and useful link between three of the variables of Eqs (3.29) and (3.30). If $\tau = R\Delta C = R\Delta\epsilon'/A/d$ and $\Delta\sigma'/A/d = 1/R$, the scalar relationship between $\Delta\epsilon'$, τ and $\Delta\sigma'$ is very simple:

$$\Delta\epsilon' = \tau\Delta\sigma'\tag{3.36}$$

This equation is valid only if there is no DC conductance in parallel with the equivalent circuit and C_∞ . If it is, that part must first be subtracted. σ' is limited to the AC lossy part of the dielectric.

Equation (3.36) represents an efficient tool for a control of measurement results (e.g., of the data presented in Figures 3.5–3.8). It is a special case of the more general

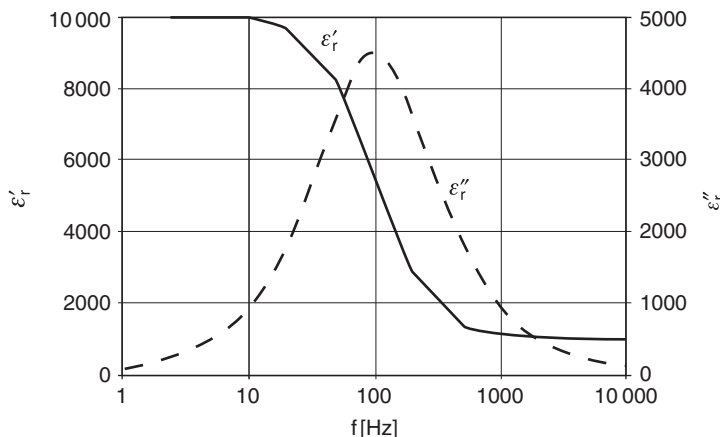


Figure 3.5: Debye single dispersion relaxation, relative permittivity. Values are found in the text.

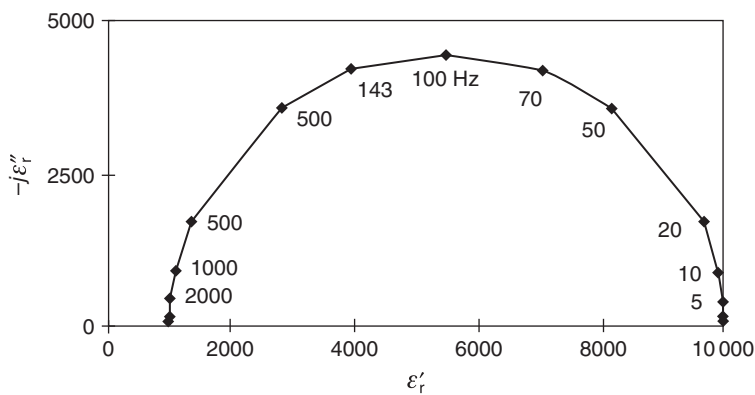


Figure 3.6: Relative permittivity plotted in the wessel diagram, same data as [Figure 3.5](#).

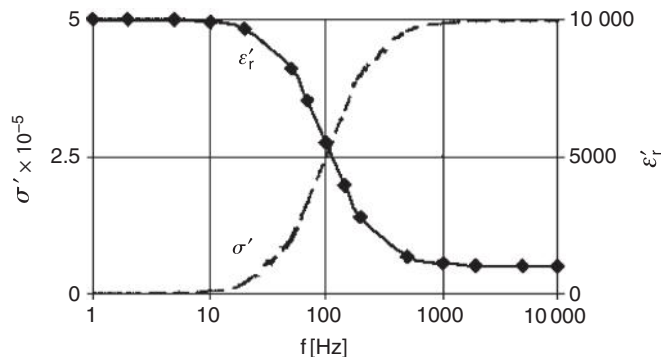


Figure 3.7: Combined permittivity and conductivity plot, same data as for [Figure 3.5](#).

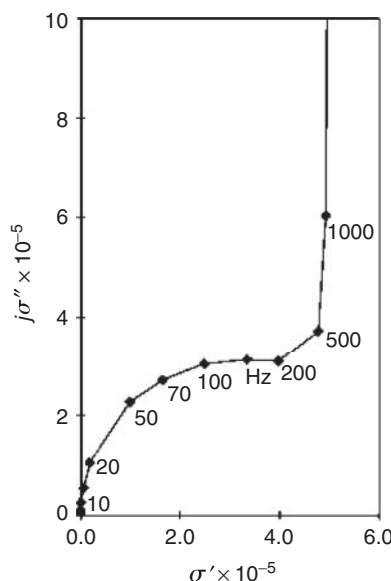


Figure 3.8: Complex conductivity (siemens) in the wessel diagram. A diagram with admittance variables G and B would be similar. Same data as for [Figure 3.5](#).

Kramers-Kronig transform, interconnecting e.g., permittivity and losses as demonstrated in [Figure 3.5](#) and described in Section 8.1.6.

Example, 1R-2C Circuit

[Figure 3.5](#) shows data based on the circuit of [Figure 3.4](#) and [Eqs \(3.30\) and \(3.31\)](#) with chosen values: $\epsilon_{r\infty} = 1000$, $\Delta\epsilon_r = 9000$, $\tau = 1592$ ms. With a ratio $A/d = 20$, this corresponds to $C_\infty = 0.18 \mu\text{F}$, $\Delta C = 1.6 \mu\text{F}$ and $R = 1004 \Omega$.

Almost 80% of the ϵ' -dispersion takes place within one frequency decade, more than 98% in two decades. The ϵ'' -dispersion is broader. It is easy to see that the data are purely capacitive at high and low frequencies.

In the Wessel diagram, the locus of the permittivity is a complete half circle ([Figure 3.6](#)). Also here it is easy to see that the data are purely capacitive at high and low frequencies.

The complex conductivity (same component values) has been plotted as a function of $\log f$ in [Figure 3.7](#). In-phase conductivity σ' increases to the plateau corresponding to $\Delta\sigma = d/RA$.

[Figure 3.8](#) shows the conductivity σ locus in the Wessel diagram. Also here the characteristic frequency is >100 Hz, and in contrast to the permittivity plot with a complete semicircle locus, there is a strong deviation with the σ'' diverging proportional to

frequency. In conclusion, the complex conductivity semicircle is disturbed by the parallel capacitor C_∞ . To obtain a circle, this capacitor must be omitted in the *conductivity* Wessel diagram. Correspondingly, a *permittivity* semicircle would have been disturbed by a parallel conductance G .

The time constant and characteristic relaxation frequency can be defined in more than one way:

- From the transient response ([Eq. \(3.27\)](#))
- From the midpoint of the $\Delta\epsilon$ or $\Delta\sigma$ plotted as a function of $\log f$ ([Figure 3.7](#))
- From the apex of the circular locus of ϵ or σ in the Wessel diagram ([Figure 3.6](#))

Conductance in Parallel, 2R-2C Model

The dielectric Debye equivalent circuit of [Figure 3.4](#) is basically for dry biomaterials without DC conductance. The circuit has no DC conductance; the in-phase component is the lossy part of the relaxation. If it is living tissue it has an ionic DC conductance path in parallel with C_∞ on [Figure 3.4](#). For DC conductance there is no relaxation process, but even so it is not unusual to add this conductance to some of the equations. In the in-phase part of [Eq. \(3.34\)](#), a factor $\sigma_{dc}/\omega\epsilon_0$ (diverging as $f \rightarrow 0!$) is for instance added to ϵ'' . The total in-phase component may then be written on the form:

$$\sigma' = \sigma_{DC} + \frac{\Delta\sigma'\omega^2\tau^2}{(1 + \omega^2\tau^2)} \quad (3.37)$$

Relaxation of Permanent Dipoles (MHz–GHz Region)

The permanent dipoles in a polar dielectric experience a torque by an applied electric field (see [Eq. \(3.6\)](#)). The actual position of each dipole is determined by this externally created torque and the thermal motion of the dipoles. The polarization P is found to be:

$$P = \frac{Np^2F}{3kT} \quad (3.38)$$

Viscosity effects in the dielectric are considered to hinder the rotational movement, and Debye has given the relaxation time τ of this process based on Stoke's law ([Eq. \(2.6\)](#)):

$$\tau = \frac{4\pi\eta a^3}{kT} \quad (3.39)$$

The relaxation time for proteins in water is typically in the micro- to picosecond range (MHz–GHz), and the dielectric decrement of the order of ϵ_0 per gram per liter.

3.4.3 Joule Effect and Temperature Rise

With current flow, an ideal resistor *dissipates* heat energy; the energy is lost as electrical energy. However, an ideal capacitor *stores* electrical energy. In a nonideal capacitor, there are dielectric losses and perhaps losses from a DC current. The stored energy may be partially lost, and completely lost with time (relaxation). As long as a device, a black box or real tissue, has the ability to store electrical energy, it contains some form of capacitors (or inductors).

Energy is the ability for doing work. Potential difference is energy per charge [joule/coulomb]. Energy is measured in *watt seconds* or *joules*, which is the same; or *electron volt* [eV]. Power is the rate of doing work or transferring energy, and is measured in *watt*. Current flow through a copper wire is a flow of electric charge. If the flow occurs with negligible voltage drop, the charge undergoes no energy change. There is no voltage difference, $\Delta V = 0$. A potential difference must be defined in order to delineate the energy of a charge. Power is defined as the product of electric current and voltage difference.

As seen from the outside of the dielectric in the external wires, the instantaneous power W_i delivered from a sinusoidal AC supply to the parallel combination of a capacitor (susceptance B) and a conductor (G), is the instantaneous AC supply voltage multiplied by the instantaneous current in the copper wires:

$$W_i = vi = V_{\text{peak}} \sin\omega t V_{\text{peak}} Y \sin(\omega t + \varphi) \quad (3.40)$$

The instantaneous power W_i is linked with a real electronic current in the copper wires. However, some of this sine wave current is in phase with the applied voltage, and some of it is 90° out of phase. The instantaneous in-phase power W_h is the instantaneous voltage multiplied by the instantaneous in-phase current component. The instantaneous out-of-phase power W_r is the instantaneous voltage multiplied with the instantaneous 90° out-of-phase (*quadrature*) current. To obtain the average power (rate of energy transfer) of the quadrature current ($\varphi = 90^\circ$) (called *reactive power*) over the period T (one cycle), the instantaneous power is integrate over the period (=average energy), and divided by the period (=average power):

$$W_r = \frac{1}{T} \int [V_{\text{peak}} \sin\omega t (V_{\text{peak}} B) \cos\omega t] dt = \frac{1}{T} \left(V_{\text{peak}}^2 \frac{B}{2\omega} \right) [\sin^2\omega t]_0^T = 0 \quad (3.41)$$

The *reactive power* W_r is pumped to and from the capacitor each quarter period, but the net supplied energy is zero. The capacitive, quadrature current just pumps electrons *charging* the plates. The quadrature current causes no heating of the dielectric, but the current in the wires is real and causes heat losses if the *wires* are nonideal.

In the same way the power loss W_L is:

$$\begin{aligned} W_L &= \frac{1}{T} \int \left[V_{\text{peak}} \sin \omega t (V_{\text{peak}} G) \sin \omega t \right] dt \\ &= \frac{1}{T} (V_{\text{peak}}^2 G) \left[\frac{t}{2} - \left(\frac{1}{4\omega} \right) \sin 2\omega t \right]_0^T = \frac{1}{2} V_{\text{peak}}^2 G \end{aligned} \quad (3.42)$$

To find a *root-mean-square (rms)* value of a function of time, the function is first squared, then the mean value is taken, and then the root of the mean. The rms value must be used when power and heat effects are of interest ($W = v_{\text{rms}}^2 / R$). From Eq. (3.42), it is clear that the rms value of a sine wave is $1/\sqrt{2}$ of the peak value. Dealing with other waveforms, the relationships among peak, mean, and rms values will depend on the waveform. Many AC voltmeters *display* rms voltage, but actually *measure* the mean value. Such practice introduces errors for non-sine waveforms.

In the dielectric there is ionic or electronic conduction. In a metallic conductor the free, migrating electrons collide with the lattice of the bound ionized metal atoms, and the electrons transfer their excess energy to the lattice. With electrolytes the charge carriers are ions, and ordinary migration or local displacement is hindered by viscosity-based friction. In both cases the dielectric is heated up and energy dissipated, that is the *Joule* effect.

3.5 Interfacial Polarization

Biomaterials are inhomogeneous dielectrics. In general, the smaller the particles, the larger the surface-to-volume ratio, and the larger the interfacial effects. In contrast to the theories of molecules forming a homogeneous material presented up to now, the relaxation mechanisms to be presented in this chapter are linked to heterogeneity and interfaces: the classical Maxwell–Wagner effects and the counter-ion polarization theories.

3.5.1 Maxwell–Wagner Effects

Maxwell–Wagner effects deal with processes at the interface between different dielectrics. Maxwell–Wagner effects are present also with dry but lossy dielectrics, with wet surfaces additional double layer effects occur. There may be free or bound surface charges at the interface. The potential Φ at the interface must be continuous, or else the E-field strength had to be infinite there. If there is no DC conductance (no free charges) in either of the two dielectrics, the interface cannot be charged by free charges migrating in the applied field. It can be shown that the normal \mathbf{D} -field and the tangential \mathbf{E} -field components are unchanged across such a boundary. If there is a DC conductance in one or both dielectrics, the interface generally will be charged by free charges, and the normal \mathbf{D} -component will not be continuous. Let us analyze Maxwell–Wagner relaxation in a simple model.

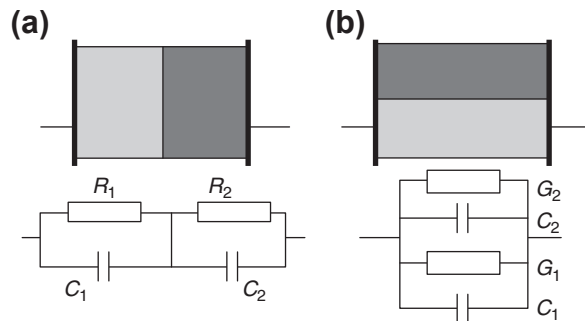


Figure 3.9: Equivalent circuits for the Maxwell–Wagner effect in a simple dielectric model. (a) The slabs in series, and the resistors cause the interface to be charged. (b) The slabs in parallel.

Capacitor with Two Dielectric Layers

Consider two materials, each homogeneous, as two dielectric slabs between the capacitor plates. The models with equivalent circuits are shown in Figure 3.9. Let us consider ideal components and therefore the resistors with frequency-independent values right from DC.

Slabs in Parallel

In Figure 3.9(b), the two slabs are in parallel, and the result becomes very simple as a parallel summation of $G_1 + G_2$ and $C_1 + C_2$.

Slabs in Series

In Figure 3.9(a), the case becomes quite different and much more complicated (see Section 12.2.3). The total immittance, and also the voltage at the interface between the two dielectrics, will be determined by the resistors at low frequencies, but by the capacitors at high frequencies. The analysis of Figure 3.9(a) will be very different dependent on whether a series (impedance) or parallel (admittance) model is used.

If the externally seen *series* capacitance C_{sext} is calculated, it is the series coupling of the two capacitances C_1 and C_2 at high frequencies, but at low frequency, the value of C_{sext} diverges and become infinite.

If the resultant *parallel* capacitance C_{pext} is calculated (Section 12.2.3), we get:

$$\begin{aligned} C_{\text{pext}} &= \frac{(\tau_1 R_1 + \tau_2 R_2)}{(R_1 + R_2)^2} \quad f \rightarrow 0 \\ C_{\text{pext}} &= \frac{C_1 C_2}{(C_1 + C_2)} \quad f \rightarrow \infty \end{aligned} \tag{3.43}$$

Both values converge, at high frequencies with values smaller than at low frequencies. *Thus with the parallel model of the two slabs in series, we have a classical Debye dispersion, with a capacitive decrement ΔC or $\Delta\epsilon'$. This is without postulating anything about dipole relaxation in the dielectric.* Debye dispersion appears and is modeled by two capacitors and two resistors, or even with two capacitors and *one* resistor (one layer without conductivity) as shown in Section 12.2. If the components are ideal (frequency independent), the dispersion will be characterized by one single relaxation time constant.

Maxwell–Wagner dispersion is due to a conductance in parallel with a capacitance for each dielectric, so that the interface can be charged by the conductivity. With zero conductivity in both dielectrics, there is no charging of the interface from free charge carriers. If side one of the dielectric is without conductivity ($\sigma_1 = 0$ and $R_1 = \infty$), then C_{pext} at very low frequencies becomes equal to C_1 . At very high frequencies, the conductivities are without influence.

In an interface without *free* charges, the dielectric displacement \mathbf{D} is continuous across the interface according to Poisson's equation (see Section 4.3.2 on the continuity across interfaces). Because $\mathbf{D} = \epsilon\mathbf{E}$, this indicates that the E-field strength will be smaller on the high-permittivity side. Then the ratio of the current densities on side one and two is:

$$\frac{J_1}{J_2} = \frac{\sigma_1 E_1}{\sigma_2 E_2} = \frac{\sigma_1 \epsilon_2}{\sigma_2 \epsilon_1} \quad (3.44)$$

On the other hand, if $\sigma_1 \epsilon_2 \neq \sigma_2 \epsilon_1$, the difference in current densities indicates that the interface actually is charged. If $\sigma_1 = 0$ and $\sigma_2 > 0$, the interface will be charged.

The conductive path in parallel with the dielectric capacitance causes the Maxwell–Wagner surface charge. *This interface single layer surface charge must not be confused with the double layer charge formed at a wet interphase.* With liquid interphases such as with particles or cells in aqueous media, the double-layer counter-ion effects are additive to the Maxwell–Wagner effects.

3.5.2 Suspension of Spherical Particles

This is a model, for example, for blood or cell suspensions, and the electrolytic solution of interest may then have a considerable ionic conductivity. An analytical solution (Maxwell, 1873) is relatively simple for a *dilute* suspension of spherical particles, and with DC real conductivity as parameters (σ is for the total suspension, σ_a for the external medium, and σ_i for the particles) the relation is (*Maxwell's* spherical particles mixture equation) (Foster and Schwan, 1989):

$$\frac{(\sigma - \sigma_a)}{(\sigma + 2\sigma_a)} = \frac{p(\sigma_i - \sigma_a)}{(\sigma_i + 2\sigma_a)} \quad (3.45)$$

where p is the particle volume fraction. Wagner (1914) extended this to AC cases and the use of complex parameters. Fricke (1924, 1925) extended it for the cases of oblate or prolate spheroids (*Maxwell-Fricke equation*):

$$\frac{(\sigma - \sigma_a)}{(\sigma + \gamma\sigma_a)} = \frac{p(\sigma_i - \sigma_a)}{(\sigma_i + \gamma\sigma_a)} \quad (3.46)$$

where γ is a shape factor and equal to 2 for spheres and 1 for cylinders normal to the field. From such equations, $\Delta\sigma = \sigma_s - \sigma_\infty$ or $\Delta\epsilon = \epsilon_s - \epsilon_\infty$ can be found (subscript s for static values), but the permittivity decrement $\Delta\epsilon$ is often rather small, of the order of a few ϵ_0 . If the particles have a DC conductivity, Maxwell–Wagner effects cause ϵ' as a function of frequency to have an additional slope downwards.

As for the relaxation time, Debye derived a simple expression for a viscosity determined relaxation time of a sphere of radius a in liquid, Eq. (3.39): $\tau = 4\pi a^3 \eta / kT$. The relaxation time is therefore proportional to the volume of the sphere and the viscosity of the liquid.

Maxwell's Eq. (3.45) is rigorous only for dilute concentrations, and Hanai (1960) extended the theory for high-volume fractions:

$$\frac{\epsilon - \epsilon_i}{\epsilon_a - \epsilon_i} \sqrt[3]{\frac{\epsilon_a}{\epsilon}} = 1 - p \quad (3.47)$$

Hanai's equation gives rise to dispersion curves that are broader than the Maxwell-Wagner equation (Takashima, 1989). Similar work had also earlier been done by Bruggeman (1935).

Dilute Suspension of Membrane-Covered Spheres

Equation (3.47) can be extended to comprise spheres in spheres, or sheath-covered spheres. If sheath thickness d is much less than large sphere radius a , the complex conductivity of one sphere inside another sphere is:

$$\sigma = \frac{a \cdot \sigma_{sh} \left(\sigma_i - \left(\frac{2d}{a} \right) (\sigma_i - \sigma_{sh}) \right)}{(1 + d)(\sigma_i - \sigma_{sh})} \quad (3.48)$$

where the subscript i is for sphere material, and sh for the sheath membrane. Equation (3.48) is valid for a sphere without external medium. To have the complete description, the conductivity value from Eq. (3.48) is therefore inserted in Eq. (3.46) for the complex conductivity of the sphere.

For a *cell suspension* with cell membranes dominated by a membrane-capacitance C_m , the equations can be simplified using certain approximations (Schwan, 1957; Foster and Schwan, 1989):

$$\Delta\epsilon = \frac{9paC_m}{4\epsilon_0} \quad (3.49)$$

$$\sigma_s = \sigma_a \left(1 - \frac{3p}{2} \right) \quad (3.50)$$

$$\tau = aC_m \left(\frac{1}{2\sigma_a} + \frac{1}{\sigma_i} \right) \quad (3.51)$$

The full equations (*Pauly-Schwan equations*) are found in Pauly and Schwan (1959). They correspond to a large dispersion resulting from membrane charging effects and a small dispersion at higher frequencies resulting from the different conductivity of the cytoplasm and extracellular liquids. Schwan and Morowitz (1962) extended the theory to small size vesicles of radii 100 nm. With even smaller particles, the two dispersion regions overlap in frequency (Schwan et al., 1970).

The α -dispersion exhibited by cell suspensions could basically be explained by rather complementary mechanisms, formally described by different microscopic models of cell systems, as the ones based either on displacement of counter-ions (Gheorghiu, 1993, 1994) or on shape effects (e.g., exhibited by clusters of interconnected cells as shown by Vrinceanu and Gheorghiu, 1996; Asami et al., 1999; Gheorghiu et al., 2002, 2010). These studies described both α and β dispersions based on unitary microscopic models. The reports emphasizing shape effect on the impedance spectra of (non)spheroidal living cells in suspension have also supported application of time-based impedance spectroscopy assays to noninvasively assess cell dynamics (e.g., cell-cycle progression).

3.5.3 Adsorbed Counterions and Lateral Diffusion (mHz–kHz Range)

In Section 7.5, we analyze the double layer charge in a solution as a function of the perpendicular distance from the solid surface. No double layer formations are considered in the Maxwell–Wagner theory (Section 3.5.1). However, in *wet* systems and in particular with a high volume fraction of very *small* particles, the surface effects from counter-ions and double layers usually dominate. This was shown by Schwan et al. (1962). By dielectric spectroscopy, they determined the dispersion for a suspension of polystyrene particles (Figure 3.10). Classical theories based on polar media and interfacial Maxwell–Wagner theory could not explain such results; the measured permittivity decrement was too large. The authors proposed that the results could be explained in terms of surface (*lateral*) admittance.

Counter Ion Diffusion, Schwartz's Theory

Schwartz (1962) proposed a model with a tightly bound layer of adsorbed counterions on the sphere surface to explain the high permittivity increment found (hundreds of ϵ_0) in a suspension of colloidal particles. Diffusion, and not migration, may govern ionic motion in a double layer. Diffusion processes are not necessarily exponential, but as an

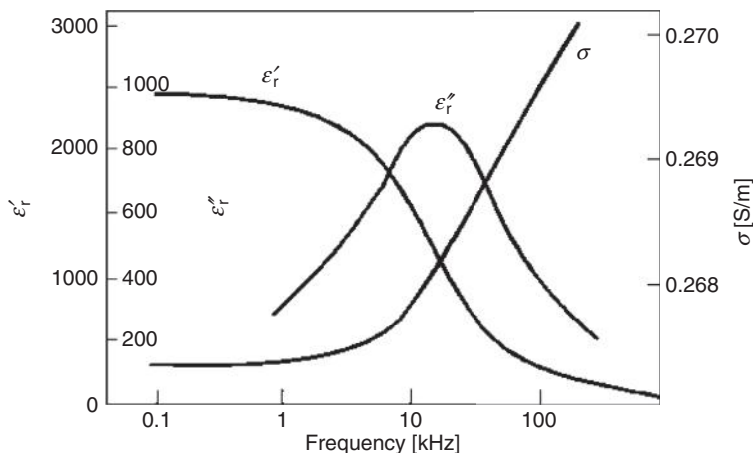


Figure 3.10: Permittivity for a suspension of polystyrene particles. Redrawn from Schwan *et al.* (1962) by permission.

approximation the time constants of such effects are according to the term L^2/D , where L is the diffusion length and D the diffusion coefficient; see Eq. (7.8). This is in contrast to Maxwell–Wagner relaxation, where the RC product, that is resistance and capacitance, determines the time constant. The corresponding relaxation frequencies may be low, in the hertz and kilohertz range. Schwartz developed a theory based upon counter-ion relaxation, where:

$$\tau = \frac{a^2 \epsilon_0}{2\mu kT} \quad (3.52)$$

$$\Delta\epsilon = \frac{9p}{(2+p)^2} \cdot \frac{e^2 a q_s}{\epsilon_0 k T} \quad (3.53)$$

where a = particle radius, μ = counter-ion mobility, and q_s = surface density of charged groups on the particle surface.

In Schwartz's theory, the ions were bound to the double layer and lateral motion within it. A theory is also possible allowing ions to enter or leave the layer from the bulk.

Counterion Diffusion in Pores

Takashima (1989) deduces the expression for the dielectric increment of a suspension of long cylinders by transforming the relations for ellipsoids from rectangular to cylindrical coordinates:

$$\Delta\epsilon = \frac{e^2 \sigma_0 a^2}{bkT} \frac{9\pi p}{2(1+p)^2} \frac{1}{1+j\omega\tau} \quad \text{if } a \gg b \quad (3.54)$$

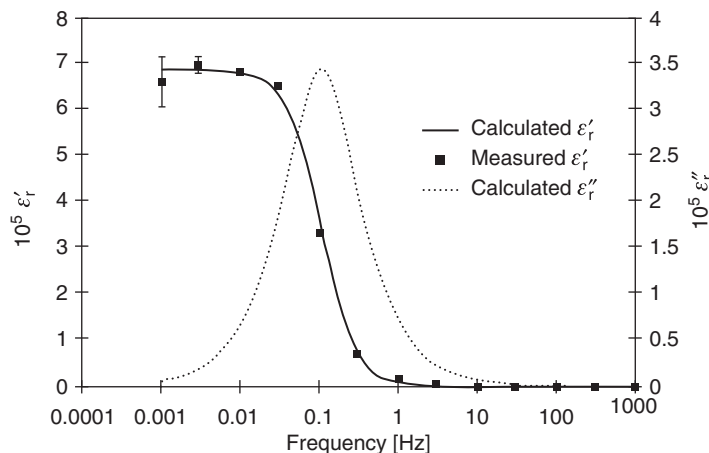


Figure 3.11: Dielectric dispersion of a polycarbonate membrane with pore diameters 100 nm; 1 mm KCl solution; measured and calculated values; DC conductivity omitted. *From Martinsen et al. (1998a), by permission.*

where a is cylinder length and b is cylinder radius. This equation has been found to be applicable also to pores (Martinsen et al., 1998a) and will give a rough estimate of the rate of dielectric dispersion to be expected in sweat ducts and other pore systems.

The electrical properties of microporous membranes in 1 mM KCl solution was investigated in the frequency range 1 mHz to 1 kHz by Martinsen et al. (1998a), using a four-electrode measuring cell (Figure 3.11).

An alpha-dispersion centered around 0.1 Hz was detected and this was assumed to be caused by counter-ion relaxation effects in the pores of the membrane. The membranes used were 6- μm -thick Nuclepore polycarbonate membranes. These membranes have 3×10^8 pores/cm 2 with a pore diameter of 100 nm. The pores are cylindrical with a length equal to the membrane thickness. The surface density of charged groups of the membranes were calculated using streaming potential measurements (see Section 2.5), which enabled the use of Eq. (3.54) for calculation of the dielectric increment. Figure 3.11 shows the measured dispersion together with the calculated real and imaginary part from Eq. (3.54). Other mechanisms that may contribute to the relaxation (e.g., the influence from diffusion of ions in the bulk electrolyte) were not considered in the study.

3.6 Basic Membrane Experiment

Set-up

Let us again consider the electrolyte container with a NaCl 0.9% aqueous solution, but this time divided in two compartments by a membrane (Figure 3.12). A sinusoidal AC current

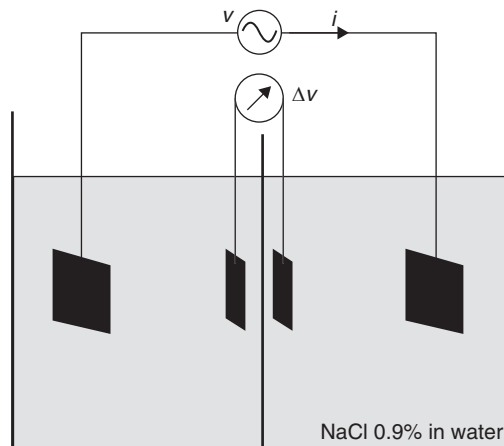


Figure 3.12: The basic membrane experiment.

is applied to the large current carrying electrodes. Two additional voltage pick-up electrodes (no current flow in their wires) are placed on each side of the membrane, and a phase sensitive voltmeter or a two-channel oscilloscope measures the voltage. This four-electrode system eliminates any influence from electrode polarization impedance: The potential drop at the current carrying electrodes does not intervene, and the recording electrodes do not carry any current, so the potential drop in their polarization impedances is zero.

Without Membrane

Without a membrane, an AC voltage Δv is measured. This voltage is proportional to the current through the system, it is in-phase with the current, and the amplitude is independent on frequency. The solution behaves “ohmic”, obeying Ohm’s law (Eq. (2.1)) like a perfect resistor. The voltage is due to the ohmic voltage drop caused by the current density in the bulk volume between the recording electrodes.

Thin Metal Membrane

Then the measured voltage increases, the phase of the recorded voltage lags behind the current, and the amplitude is frequency-dependent.

The conductivity of the metal is more than 1000 times that of the electrolyte, and the metal is thin. The voltage drop in the metal itself must be very small, and the increased measured voltage must be caused by the two double layers formed on each side of the metal plate. These double layers clearly have capacitive properties, and they are in series with the metal.

Let us suppose that there is a thin pore in the membrane. The walls of the pore must also be covered by a double layer. Will counter-ions in that double layer, and ordinary ions in

the pore volume, migrate with the AC E-field? No, because of the high conductivity of the metal the local E-field strength along the axis of the pore will be very small.

Thin Membrane of Insulating Material (No Pores)

The measured voltage difference is very large at low frequencies. At higher frequencies (e.g., >1 kHz), measured voltage is smaller and almost 90° after the applied voltage.

With an insulating material in the membrane, no DC current can flow through the cell. An AC current will flow through the three series coupled capacitors: two double-layer capacitors at each side of the wetted membrane and the capacitor with the membrane itself as dielectric. The measured voltage difference will consist of the voltage drop in the solution between the measuring electrodes, plus the voltage drop across the three capacitors. Most of the reactance will stem from the membrane because its capacitance will be far lower than that of the double layers. At sufficiently high frequencies, the reactance of the membrane capacitors will be so small that the effect of the membrane will disappear, and the phase angle will approach 0°.

Membrane of Insulating Material with Pores

This time the voltage is not so high at low frequencies (e.g., <10 Hz). There is a very small phase shift, less than 5°. At higher frequencies, the voltage difference is falling with frequency and with a 90° phase shift.

The pores form a DC current path. The sum of their conductances is so large that the capacitive effect of the membrane as a dielectric is small at low frequencies. If there are not too many pores, most of the potential difference is over the membrane pores, and the E-field strength in the pores will be high. The counter-ions of the double layer on the pore walls will migrate synchronous with the E-field, and the solution inside the pore will be pumped back and forth by electroosmosis. At higher frequencies, the membrane susceptance will shunt the pores, and voltage across the pore will be reduced. Counterion relaxation will also occur, as shown in [Figure 3.11](#).

Discussion

The most interesting membranes in the field of bioimpedance are of course the membranes in the living body, the cell membranes: the excitable ones in the muscles and the nerve system, and the less excitable ones. In addition, there are membranes both *inside* and *outside* the cells. Inside the cells, there are membranes around some of the organelles. Outside, there are thick, solid macro-membranes around all organs such as the heart, the lungs, the brain, and the intestines (mediastinum).

In tissue, the cell membranes are very small and a part of a living system, quite different from the basic *in vitro* model just shown. However, our simple model is well suited for

artificial membranes. With a special technique it is useful for artificial bilayer lipid membranes very much like the cell membranes. The membrane pore is then closed with a lipid droplet. The droplet gradually becomes thinner until it turns from multimolecular thickness into a single bilayer covering the orifice of the pore. Such a bilayer lipid membrane has important similarities with real cell membranes.

A better model for tissue is the suspension-measuring set-up to be presented in [Section 3.7](#).

3.7 Basic Suspension Experiment

Set-up

Let us consider our electrolyte container again, but let us fill it with a suspension of particles as shown in [Figure 3.13](#), instead of the separating membrane. The electrolyte is still NaCl 0.9% in water. The particles used are small insulating glass or plastic beads. If the particles are sufficiently small ($<0.5\text{ }\mu\text{m}$), the solution is optically clear and the particles will be evenly but randomly distributed in the volume by Brownian movements according to the Boltzmann factor kT . A *suspension* is usually defined as a liquid with *larger* particles. Then, gravitational energy will dominate the kT -factor and a sedimentation process will go on so that the particles will sink to the bottom. The system is unstable, and the concentration in bulk will fall with time. These definitions are rather broad, and several subgroups may be formed. Many molecules are for instance known to *associate* (molecules of *same* kind forming more complex structures, such as water molecules) in solution, and particles may form *aggregates* if their charges are small enough. Macromolecules may form *colloids* with properties dominated by surface properties.

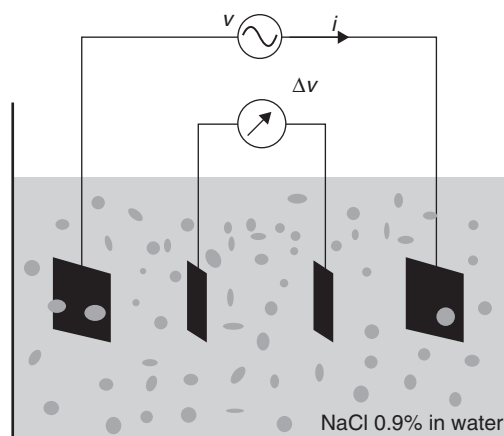


Figure 3.13: The basic suspension experimental model.

Findings

A voltage is measured almost like that found for the basic set-up without a membrane ([Section 3.6](#)). However, a small phase lag is measured, and the voltage decreases somewhat with frequency. The voltage increases with increased particle concentration.

With a high voltage applied, and at a very low frequency <1 Hz, it is possible with a magnifying glass to see the particles moving back and forth synchronously with the AC.

Discussion

In general, the double layer on each particle surface will add capacitance to the system, and therefore the measured voltage will decrease with frequency and lag the current. Note that some of the current passes perpendicular to the double layer of the particles, but some of the current passes parallel to the double layers. Smaller particles have increased surface-to-volume ratios, and therefore result in higher capacitance.

If the particles are *highly conductive* with respect to the solution (metal), this metal is not directly accessible for the current; the double layer must be passed two times. If the concentration of metal particles (fill factor) is increased, the measured voltage will not necessarily decrease; that depends on metal/solution impedance and therefore also the frequency. Above a certain particle concentration, there will be a sharply increased probability of a direct contact *chain* of particles throughout the measured volume segment, the segment will be short-circuited.

If the particles are low conductive (*glass*), the resistance of the suspension at low frequencies will be higher than without particles. Measured voltage is increased, and in addition it will lag the current by a certain phase angle. If the frequency is increased, the susceptance of the sphere volume capacitors will be higher and in the end be determined by the permittivity of the spheres with respect to the solution. With cells the cell membrane surface properties will complicate the case further.

With a sufficiently low frequency, the particles can follow, and we witness how the particles of the suspension are pumped back and forth by *electrophoresis* as a sign of their net electric charge.

3.8 Dispersion and Dielectric Spectroscopy

Schwan emphasized the concept of *dispersion* in the field of dielectric spectroscopic analysis of biomaterials. Dispersion has already been introduced in [Section 3.4.1](#): dispersion means frequency dependence according to relaxation theory. Biological materials rarely show a single time constant Debye response as described in [Section 3.4.2](#). Knowing how complex and heterogeneous living tissue is, the concept of a distribution of

time constants (DRT) should not surprise anyone. Often the distribution also is nonsymmetrical, which cannot come as a big surprise. All such models are covered by the dispersion concept.

Dispersion is therefore a broad concept, and many types of DRTs are possible. The Cole brothers proposed a certain DRT corresponding to the apparently simple Cole–Cole equation (Section 9.2). The Cole–Cole equation presupposes a CPE. However, other distributions than the Cole–Cole type are also found to be in agreement with measured tissue values. The Cole–Cole model is attractive however because the mathematical expressions are so simple. Dispersion models as described below therefore pertain to many types of dispersion mechanisms, among those are also Cole–Cole systems.

Dispersion data are based upon the electrical examination of a biomaterial as a function of frequency, that is, dielectric spectroscopy. Schwan (1957) divided the relaxation mechanisms into three groups, each related to, for example, cell membranes, organelles inside cells, double-layer counter-ion relaxation, and electrokinetic effects. He called them α -, β -, and γ -dispersions (see Figure 3.14). The permittivity of muscle tissue decreases in three major steps corresponding to these dispersions, roughly indicated by Schwan (1957) to correspond to 100 Hz, 1 MHz, and 10 GHz. In the data of Gabriel et al. (1996b), they are situated at lower frequencies: 1 Hz, 1 kHz, and 1 MHz (Figure 4.10). Later, a fourth δ -dispersion has been added in the lower GHz range. There are two possible interpretations of these dispersion groups:

1. The dispersions are linked to defined frequency ranges
2. The dispersions are linked to defined relaxation mechanisms

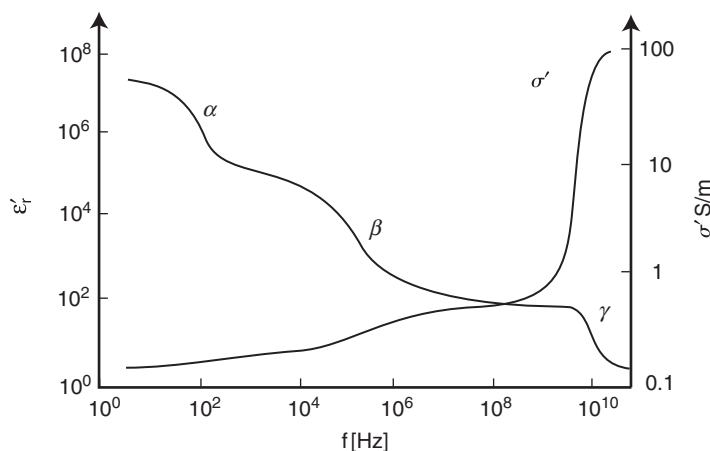


Figure 3.14: Dispersion regions, idealized. Modified from Schwan (1988).

Sometimes dispersions are related to defined frequency ranges, and to a lesser extent to possible relaxation mechanisms.

We do not know so much about the α -dispersion. Newer findings have shown that the α -dispersion must be extended down to the Hz (or mHz) frequency range (Table 3.3). α -dispersion is the first to disappear when tissue dies. Blood has no α -dispersion.

Figure 3.15 shows admittance Wessel plots obtained with four-electrode technique (Grimnes and Martinsen, 2010). The left part of Figure 3.15 is two calf spectra with electrode axis parallel (black) and perpendicular (gray) to the direction of the muscle fibers. Notice how the gray circular arc apparently approaches zero real admittance values at low frequencies.

Dispersions may be described with permittivity or immittivity parameters. Complex permittivity or complex immittivity may be presented in Wessel diagrams as shown in Chapter 9. Wessel diagrams focus data in a narrow frequency range; for broadband spectroscopic data, logarithmic frequency scales are better suited (Figure 3.14).

Table 3.3: Dielectric Dispersions

Type	Characteristic Frequency	Mechanism
α	mHz–kHz	Counter-ion effects (perpendicular or lateral) near the membrane surfaces, active cell membrane effects and gated channels, intracellular structures (e.g., sarcotubular system.), ionic diffusion, dielectric losses (at lower frequencies the lower the conductivity).
β	1 kHz–100 MHz	Maxwell–Wagner effects, passive cell membrane capacitance, intracellular organelle membranes, protein molecule response.
γ	0.1–100 GHz	Dipolar mechanisms in polar media such as water, salts, and proteins.

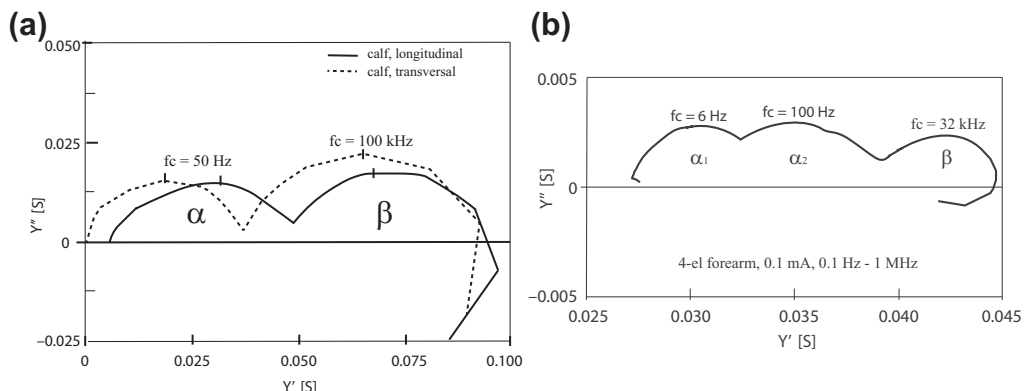


Figure 3.15: Two examples of α -dispersion. (a) Calf, single α -dispersion. (b) Forearm, two α -dispersions.

[Figure 3.14](#) shows that the permittivity in biological materials typically diminishes with increasing frequency, little by little the charges (dipoles) are not quick enough to follow the changes in the E-field. The dispersion regions are here shown as originating from clearly separated Cole–Cole-like systems. Such clearly separated single dispersions can be found with cell suspensions. In tissue, the dispersion regions are much broader and overlap, sometimes as a continuous fall almost without levels and over many decades of increasing frequency (see Section 4.3 on tissue properties and Section 9.2.9 on multiple Cole systems).

A problem with a purely dielectric approach is how to treat the DC conductivity found with living tissue. The conductivity of saline alone is without dispersions below 1 MHz. [Equation \(3.17\)](#) ($\epsilon'' = \sigma'/\omega$) shows that with constant conductivity the quadrature permittivity diverges at lower frequencies. The interpretation for living tissue is therefore easily distorted using the ϵ'' variable. There are two ways out of this: (1) the measured DC conductivity can be subtracted as a nondispersion parameter, or (2) quadrature permittivity is replaced by in-phase conductivity, as shown in [Figure 3.14](#). With subtracted DC conductance, the ϵ'' waveforms would have been peaks (see [Figure 3.5](#)). The conductivity waveform has a continuously increasing level (see [Figure 3.7](#)), and no DC conductance subtraction is necessary when presenting the data. However, the underlying models are different. The electric equivalent circuit for the permittivity parameter is a 1R-2C model, for the conductivity parameter a 2R-1C model (see Section 9.2.7).

The permittivity ϵ'_t for tissue may attain values larger than 10^6 at low frequencies. This does not imply that the capacitive properties of living tissue are dominating at low frequencies (see Table 4.2). The admittance of living tissue is actually dominated by the conductive properties of liquids, and the out-of-phase current is very much smaller than the in-phase current. These effects could not be measured without the introduction of high-resolution measuring bridges, taken into use by Schwan and pioneers before him (see Section 8.3.6). Dispersion is the most common model for explaining the electric behavior of biomaterials, even if electrolytic theory with DC conductivity and electrode phenomena are important factors. The strength of the dispersion concept is that it is very broadly phenomenological, not forcing anybody to consider detailed mechanisms. It is very much Schwan's merit that this field was opened in such a broad way. But the generality is also a problem: dispersion and relaxation concepts can easily be taken as explanations of the machinery behind the phenomena, and they are not. Dispersion relates to the electrical and physical *behavior* of molecules, somewhat opposed to analytical methods such as nuclear magnetic resonance or light spectroscopy examining molecular *structure*. This is partly due to the techniques in analytical chemistry, which are based upon resonance phenomena, whereas dielectric spectroscopy below about 1 GHz is concerned with relaxation, usually presented as a nonresonance phenomenon. However, in the lower GHz region, sharp resonance phenomena are observed for DNA molecules (Takashima, 1989, p. 214).

3.9 Problems

1. Beyond which frequency may copper be considered as a dielectric defined as $B > G$? For copper, use $\epsilon_r = 3$ and $\sigma = 6 \times 10^6$.
2. What is the force in vacuum between two opposite charges of 1 coulomb at distance 1 m?
3. How large is the polarization \mathbf{P} [Cm/m³] in a dielectric with relative permittivity equal to 3?
4. What is the complex admittance \mathbf{Y} of an ideal capacitor with dimensions area 1 cm² and thickness 1 mm, and with a dielectric with $\epsilon_r = 3$ and $\sigma = 2S/m$?
5. What is the complex impedance Z of the same capacitor?
6. An ideal capacitor with dimensions area 1 cm² and thickness 1 mm is measured to have a frequency independent resistance $10^6 \Omega$ and a capacitance of $15 \times 10^{-12} F$. Find the complex permittivity, conductivity, and resistivity of the dielectric.
7. Sketch Figure 3.14 by replacing the σ' parameter with the ϵ''_r parameter.

This page intentionally left blank

Passive Tissue Electrical Properties

4.1 Basic Biomaterials

Hydrogen (63% of the human body's number of atoms), oxygen (25%), carbon (9%), and nitrogen (1.4%) are the four most abundant atoms of the human body. They are all able to form covalent bonds (e.g., water) on the basis of the sharing of electron pairs by two atoms with unpaired electrons in their outer shells (cf, Section 2.1). Most biomolecules are compounds of carbon because of the bonding versatility of this element. Nearly all of the solid matter of cells is in the form of *water, proteins, carbohydrates, and lipids*.

4.1.1 Water and Body Liquids

A short repetition from Chapter 3: Water is a polar liquid with a static relative permittivity of approximately 80 (20°C), falling to 73 at 37°C (Figure 4.1).

The addition of electrolytes such as NaCl or KCl lowers the permittivity proportionally to concentration (e.g., with a dielectric decrement, $\Delta\epsilon_r$, of ~ 4 for a 250 mmol/L concentration of KCl; cf, Section 3.1.1).

The high permittivity is one reason for the dissociative power of water. Ionic bonds are split up so that ions exist in aqueous solutions in a free but hydrated form. Because of the strong dipolar electric field, water molecules are attracted to ions and local charges,

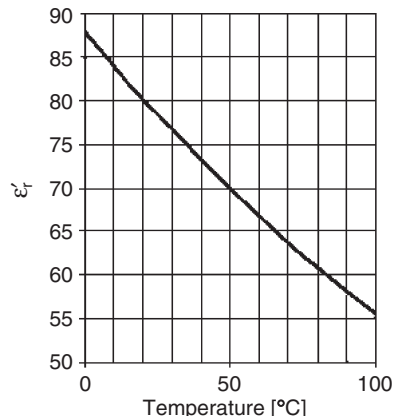


Figure 4.1: Temperature dependence of the relative permittivity of pure water. *Data from CRC (1998).*

forming a hydrated layer (sheet), which tends to neutralize the charge and increase the effective dimensions of the charged particle. The binding of water to protein molecules may be so strong that the water is better characterized as *bound water*. Bound water has different properties than liquid water and must be considered to be a part of the solid and not the liquid phase. A range of bonding energies may be present, corresponding to a scale from free water molecules as liquid via more loosely bound molecules to a very tight bonding when it is very difficult to extract the last water molecules. The similarity of the cytoplasm to a polymer gel rather than an electrolyte liquid, has received increased attention (Pollack, 2001).

Hydrogen ions in the form of protons or oxonium ions contribute to the DC conductivity of aqueous solutions by migration and hopping. Pure water exhibits a single Debye dispersion with a characteristic frequency of approximately 17 GHz (Figure 4.2).

Ice has a static relative permittivity of approximately 92 at 0 °C (at low frequencies, but fallen to <10 already at 20 kHz), slightly anisotropic (~14%), and increasing with lower temperature. The characteristic frequency of the relaxation is much lower than for water, approximately 3 kHz, and with disturbing conductive effects at less than 500 Hz (Hasted, 1973).

The living cell must contain and be surrounded by aqueous electrolytes. In human blood, the most important cations are H^+ , Na^+ , K^+ , Ca^{2+} , and Mg^{2+} , and the most important anions are HCO_3^- , Cl^- , protein⁻, HPO_4^{2-} , and SO_4^{2-} . Note that protein in the blood is considered as a negative (macro)-ion.

The intracellular and extracellular electrolytes are listed in Table 2.6. They cause an electrolytic conductivity on the order of 1 S/m. Up to at least 10 MHz, it is considered to be frequency independent (Cooper, 1946).

Most of the cells of the body only undergo mitosis if they are attached to a surface. Cancer cells are not dependent on such attachment. Blood containing erythrocytes is the best example of a natural cell suspension.

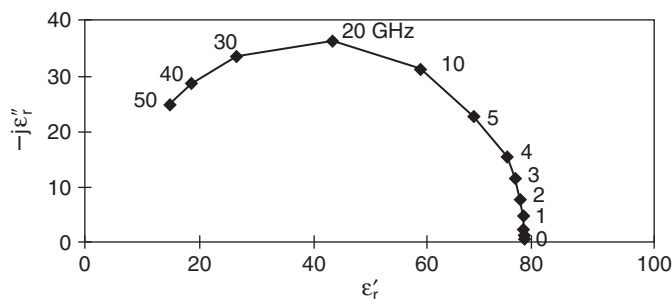
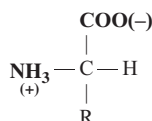


Figure 4.2: Complex relative permittivity of pure water at 25 °C. Data from CRC (1998).

4.1.2 Proteins

Proteins are the most abundant macromolecules in living cells, and 65% of the protein mass of the human body is intracellular. Proteins are the molecular instruments through which genetic information is expressed. All proteins are constructed from 20 amino acids joined by covalent bonds. All 20 amino acids have the following group in common:



This common group is shown in ionized form as would occur at pH 7: The amino group has acquired a proton (NH_3^+), and the carboxyl group has lost one (COO^-). The charges are separated and represent a permanent dipole with zero net charge, and such substances are polar. At pH 7, all amino acids are more or less polar. Even so, the common group is also paradoxically called a “dipolar ion” or a zwitterion because at other pH values it attains a net charge. At low pH values, the NH_3^+ group dominates and the acid is a cation with a net positive charge. At high pH values, the COO^- group dominates and the “acid” is an anion with a net negative charge. The term amino acid may clearly be misleading because in water solution they actually can be an acid (proton donor) or a base (proton acceptor). Even if these conditions mostly are nonphysiological, the acid–base behavior in vitro is valuable for the examination and mapping of amino acids.

The R symbolizes a side chain that determines the properties of each amino acid. The electrical properties of the protein are also strongly dependent on this R-group but only if it is polar or charged. The amino acids are classified according to their R-groups, but the properties of an R-group and therefore the amino acid are very dependent on pH and molecule configuration; therefore, the classification differs in the literature. The following classification for the 20 amino acids may be used at a physiological pH of approximately 7.4:

- Eight of the amino acids are *hydrophobic*; therefore, the R-groups are grouped as nonpolar—they are without net electric charge and have a negligible dipole moment. The net dipole moment of all eight acids is equal to that of the common group.
- Seven are *hydrophilic*; therefore, the R-groups are grouped as *polar*. These polar R-groups have an expected large influence on the dielectric permittivity. Some of them tend to dissociate H^+ so that the amino acid also becomes charged and ionic.
- Two are with negatively charged R-groups; therefore, they have a net negative charge.
- Three are with positively charged R-groups; therefore, they have a net positive charge.

Those amino acids having a net electric charge do migrate in a homogeneous electric field and thus have an electrophoretic mobility. As explained, at a pH value not equal to 7, all

amino acids may be charged. The pH of zero net charge is the *isoelectric point*. For example, glycine has no net charge in the pH range of 4–8; therefore, this is the isoelectric range.

Attempts to interpret the measurements with aqueous solutions of amino acids and peptides with the Clausius–Mossotti equation fail (see Section 3.1.4). Instead, it is a usual practice to characterize the polarizability of biomolecules by a *dielectric increment*, δ . At low concentration, the dielectric increment is the proportionality between the concentration and the permittivity increase for many biomolecules:

$$\epsilon_r = \epsilon_{rps} + \delta c \quad (4.1)$$

where ϵ_{rps} is the relative permittivity of the pure solvent. The unit for the dielectric increment, δ , is per capacitance. The dielectric increment for many amino acids is in the range of 20–200, with dipole moments in the range of 15–50 Debye [D] units (Pethig, 1979).

Electrical Properties of Isolated Amino Acids

In dry form, the polar amino acids may crystallize as a hard material such as NaCl. With nonpolar types, the dry crystal lattice is softer. The electric properties of dry and wetted amino acids are dramatically different. Glycine is the simplest amino acid with only one hydrogen atom as the R side chain. The R-chain is uncharged, but polar, therefore glycine is hydrophilic. In dry form, it forms hard crystals, and Figure 4.3 shows the dielectric dispersion of glycine powder in dry form and with a small (0.67%) water content. The

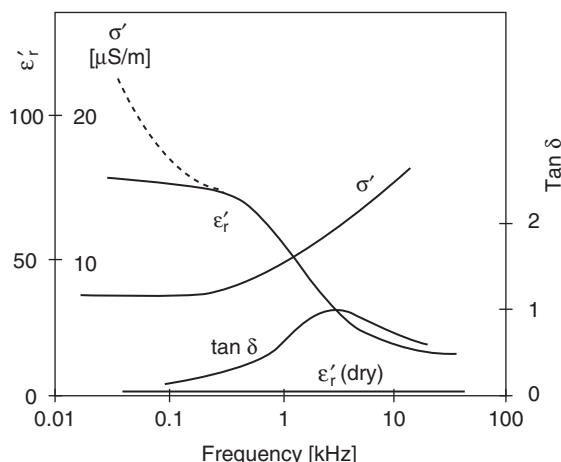


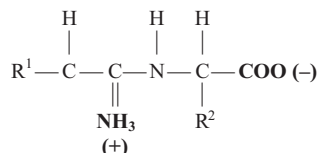
Figure 4.3: Dielectric dispersion for glycine crystals with water content (0.67% and 0%) as a parameter. Two-electrode method, dashed line without correction for electrode polarization.

From Takashima and Schwan (1965), by permission.

permittivity of dry powder is very low and independent of frequency (at least down to 20 Hz). With water, a clear dispersion is apparent with a characteristic frequency of approximately 1 kHz. The size of the crystals has no effect on high- and low-frequency permittivity levels, but the larger the particle size, the lower the characteristic frequency. Protons are believed to play an important role in the water-dependent conductivity of relative dry materials (South and Grant, 1973) because of the hopping conductance mechanism (Figure 2.4).

Peptides are small groups of amino acids, and *polymers* are even more complicated forms of peptides forming *proteins*. A polymer is a general term covering any material built up from a series of smaller units (monomers). Proteins differ from each other because each has its own amino acid *sequence*. Similar to the amino acids, many proteins can be isolated in crystalline and dry forms. A protein may be in the form of a loose strand or a rigid structure. Cross-bindings and foldings are very important for geometrical form, size, and rigidity as well as for function and the electrical properties. Bonds and links are strengthened or weakened according to the charges and distances involved. A change in water solvent concentration may change the electrostatic forces because they are dependent on permittivity (cf, Section 3.3), by which the protein will swell or shrink.

A protein may have a very regular form, such as an α -helix, or a chaotic morphology by *denaturation* at high temperatures or extreme pH values. The denaturation of a protein reduces the solubility in water; therefore, heat coagulation of tissue is accompanied by water liberation. The denatured protein nearly always loses its characteristic biological activities, and the electric properties are often completely changed. This shows the importance of the higher orders of the geometrical (secondary) structure of a protein. For example, a simple peptide may have the form:



As the forms become more complex, very different forms of charge distributions and bonds are possible. The rigidity of the bonds will be important for the electrical relaxation phenomena. In comparison with the displacement of electrons and nuclei during atomic polarization (10^{-15} m), the distance between the charges in a macromolecule can be very large (10^{-8} m). Therefore, the dipole moment of proteins could be very large. However, the symmetry of the electric charges in protein molecules is also surprisingly high. Even with many ionized groups, the dipole moment often corresponds to only a few unit charges multiplied by the length of the molecule. Some proteins actually have a negligible dipole moment and must be regarded as nonpolar.

A protein with many ionized groups is a *polyelectrolyte* if it has a net electric charge. If it is free, then it will migrate in an electric field. Usually it is not free; therefore, it may only undergo local polarization. Because a polyelectrolyte has distributed charges all over the molecule, each charge is sufficiently isolated to attract ions of an opposite charge. A local ionic atmosphere is formed, just like the one formed around ions in strong electrolytes, or even a better analogy is that they are *counterions* just like the counterions forming the electrical double layer. The counterions decrease the DC mobility, and counterion polarization is believed to be very important in many proteins in water solution.

Electrical Properties of Isolated Amino Acids, Peptides, and Proteins

Figure 4.4 shows Cole–Cole plots for glycine (amino acid), glycylglycine (peptide), and albumin (protein). As a biomolecule becomes more and more complicated and large (amino acid–peptide–protein), the frequency exponent $1-\alpha$ of the Cole–Cole equation becomes higher (α lower), indicating a broader distribution of time constants.

A *DNA molecule* consists of two polynucleotide chains (helices). The two chains intertwine with a fixed pitch of 3.4 nm. Two types of base pairs bridge the two helices at a fixed distance of 0.34 nm. The phosphate groups in the nucleotide chains carry negative

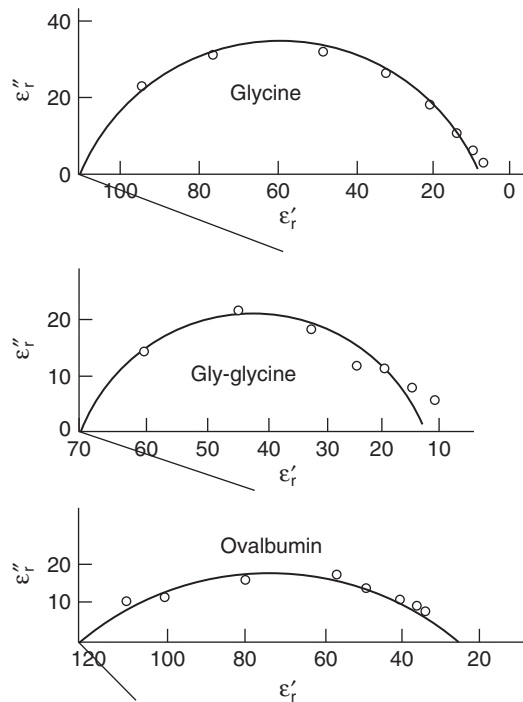


Figure 4.4: Cole–Cole plots for an *amino acid* (glycine with 1.5% water), a *peptide* (glycylglycine with 1% water), and a *protein* (albumin with 11% water). From Takashima and Schwan (1965) by permission.

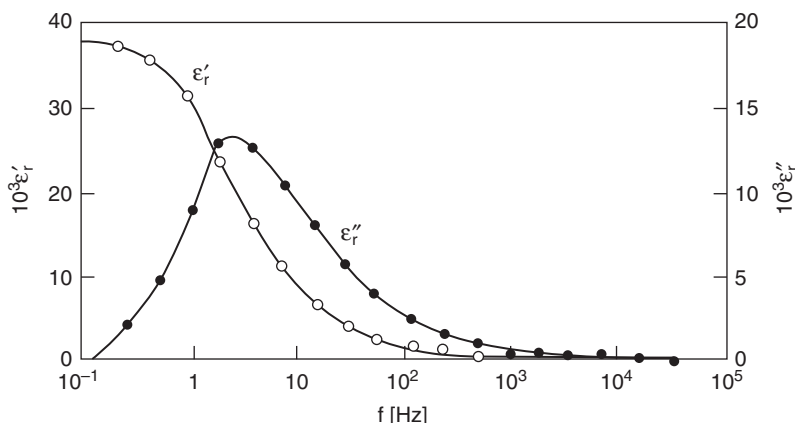


Figure 4.5: Dielectric dispersion of DNA molecules in dilute suspension. *From Takashima (1989), by permission.*

electric charges in water solution. Because of the bridges, the double helix demonstrates considerable rigidity and may be considered as a charged rigid rod. When a DNA solution is heated higher than approximately 80 °C, the two strands unwind and the DNA is changed from a double helix to random coils. The denatured form may in some cases revert to the natural form by a slow cooling process. The dielectric dispersion is shown in Figure 4.5 and is very different in the natural and denatured forms. The polarization found may be due to either the movement of charges along the rod or the turning of the whole molecule. However, the polarization has been shown to be more due to counterion polarization than the orientation process of the permanent dipole. The electrical properties of DNA were also studied by Mandel (1977) and Maleev et al. (1987). A possible resonance phenomenon was discussed by Foster et al. (1987) and Takashima (1989).

4.1.3 Carbohydrates and Saccharides

Carbohydrates and saccharides are the fuels for cell metabolism. They also form important extracellular structural elements, such as cellulose (plant cells), and have other specialized functions. Bacteria cell membranes are protected by cell walls of covalently bonded polysaccharide chains. Human cell membranes are coated with other saccharides. Some saccharides form a jellylike substance filling the space between cells. Some polysaccharides may have a negative charge at a pH of 7, but many carbohydrates are not believed to contribute dominantly to the admittivity of tissue.

4.1.4 Lipids and the Passive Cell Membrane

Lipids are water insoluble, oily, or greasy organic substances. They are the most important storage forms of chemical energy in the body. In our context, one group of lipids is of

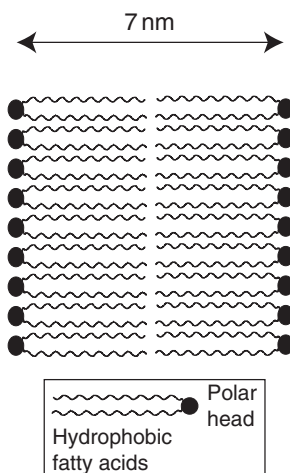


Figure 4.6: Bilayer lipid membrane (BLM), the main component of the cell membrane.

particular importance—the *polar* lipids. They are the major component of the passive cell membranes, and they are an important basis for the capacitive nature of cells and tissue. Polar lipids form micelles (aggregates of molecules, e.g., formed by surface active agents), monolayers, and bilayers. In aqueous systems the polar lipids spontaneously form micelles, by which the hydrophobic hydrocarbon tails are hidden from the water. On the water surface they form monolayers with the hydrophobic tails pointing out toward the air.

The cell membrane is an absolute necessity for life because by it the cell can control its interior by controlling the membrane permeability. If the membrane is destroyed, then the cell dies. The membrane is a layer that separates two solutions and forms two sharp boundaries toward them. The cell membrane consists of *phospholipids* that form a bilayer lipid membrane (BLM) approximately 7 nm thick (Figure 4.6). Each monolayer has its hydrophobic surface oriented inward and its hydrophilic surface outward toward the intracellular or extracellular fluids. The inside of such a bilayer is hydrophobic and lipophilic. A BLM is a very low electric conductivity membrane and is accordingly in itself closed for ions. It lets lipids pass but not water. However, water molecules can pass specialized membrane channels (cf, Chapter 5). The intrinsic conductance is on the order of 10^{-6} S/m, and a possible lipophilic ionic conductivity contribution cannot be excluded.

Even if the conductivity of the BLM itself is very low, the membrane is so thin that the capacitance is very high and the breakdown potential low. The electric field strength with a potential difference of 70 mV and a thickness of 7 nm is 10 kV/mm. This represents a large dielectric strength, but not larger than, for example, Teflon™. In addition, as we shall see, this is not the potential across the bilayer itself but the potential of the bilayer plus the

potential difference of the two electric double layers formed on each surface of the membrane.

A complex coating of special carbohydrates covers the external cell membrane surface, the *glycocalyx*, strongly modifying surface properties. Many of the glycocalyx carbohydrates are normally negatively charged so that living cells repel each other. During fever, the blood sedimentation [mm/h] is increased because the electric charge of the erythrocytes is diminished so that they lump together. According to Stokes law (Eq. 2.6), flow friction is proportional to sphere radius a , whereas the weight is proportional to a^3 : the larger the sphere, the higher the sedimentation velocity (cf, the electrokinetic effects described in Section 2.5).

Some of the carbohydrates are receptor substances binding substances such as hormones, and some are important for the immunological properties of a cell.

An electric double layer covers the wetted outer cell membrane surface. The total cell has a net charge revealed by its electrophoretic mobility. The cell membrane capacitance with the thickness of approximately 7 nm is on the order of $1 \mu\text{F}/\text{cm}^2$. The frequency dependence of the membrane capacitance has been a subject of dispute (Cole, 1972), but the BLM as such is often considered to have a frequency-independent membrane capacitance.

When the potential difference is increased more than 150 mV, the *membrane* breaks down (cf, Section 10.11.1) on electroporation. This must not be confused with the excitation process, in which the ionic *channels* of the membrane suddenly open (cf, Chapter 5).

An artificial BLM may spontaneously take the form of a sphere, enclosing a solution at the inside. Such a sphere is called a *liposome* and has important similarities with a cell. Agitated by ultrasound during formation, they may have a diameter of 10–100 nm; thus, they are smaller than most living cells. Agitated by hand, they may be in the micrometer range.

4.2 Tissue and Organs

Tissue is a very heterogeneous material, and interfacial processes are very important. The cells are of uneven size and have very different functions. There is a large difference between the tissue conductivity—from the liquid tissue flowing through the blood vessels to the myelin sheaths as insulators surrounding the axons of the nerve cells, and to connective tissue specialized to endure mechanical stress to bones and teeth, muscle masses, the dead parts of the skin, gas in lung tissue, and so on. From an electrical point of view, it is *impossible* to regard tissue as a homogenous material.

Let us consider a simple case with a volume of many cells in interstitial fluids (Figure 4.7).

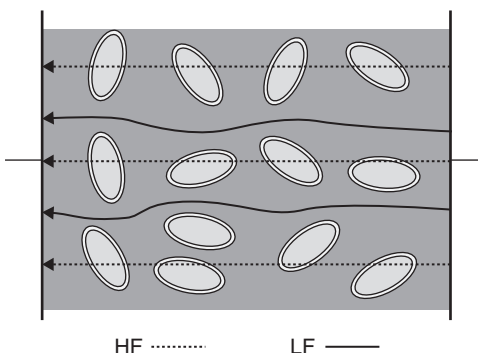


Figure 4.7: Low- and high-frequency current paths in tissue.

The cell membranes are considered to have a high capacitance and a low but complicated pattern of conductivity. At DC and low frequencies, current passes around the cells. Lateral conductance in the double layers is also possible. The cell interior does, to a smaller degree, contribute to current flow. At higher frequencies the membrane capacitance lets AC current pass. The membrane effect disappears, and the current flows everywhere according to local ionic conductivity.

All interfaces give rise to Maxwell–Wagner and counterion polarization effects as described in Section 3.5.

In general, tissue is an anisotropic medium because of the orientation of cells, macromembranes, and organs (Section 4.3.1). Such an anisotropy is a low-frequency phenomenon if it is due to membranes, but not if it is due to, for example, air. Organs are very often compartmentalized, with *macromembranes as compartment walls*. The lung, heart, brain, and stomach all have multilayer membranes, but the largest is the abdominal membrane—the *peritoneum*. These membranes may have a large influence on current flow and endogenic currents between the organs. The gradients of ionic concentration develop electromotive voltages (EMVs) that influence current flow (Nordenstrøm, 1983).

The maximum magnitudes for the different tissue dispersion regions are presented in Table 4.1 (cf., Section 3.8).

Table 4.1: Maximum Dispersion Magnitudes According to Schwan (1963)

	α	β	γ
$\Delta\epsilon_r$	5×10^6	10^5	75
$\Delta\sigma$	10^{-2}	1	80

Extracellular liquids usually dominate the in-phase conductivity. Therefore, the low-frequency *temperature coefficient* is that of electrolytes, approximately $+2\%/^{\circ}\text{C}$. The quadrature ϵ' or Y'' components have a smaller temperature coefficient (e.g., approximately $-0.5\%/^{\circ}\text{C}$) but are dependent on the measuring frequency in relation to the characteristic frequencies of the dispersions. The effect of hyperthermia and freezing on tissue impedance was studied by Yu et al. (2004).

4.2.1 Tabulated Tissue Conductivity Data

It is very difficult to tabulate tissue conductivity, in particular living tissue. Tissue is traditionally classified into four groups in medicine: epithelial, muscle, connective, and nervous tissue. Textbooks in histology may list approximately 35 classifications. Gabriel et al. (1996a) identified over 30 tissue types according to electrical properties. If we leave the macroview and approach cellular levels and the basic tissue building blocks, then the tissue parameter values may change a decade from micrometer to micrometer. This can be illustrated by a thin needle with an insulated shaft and a small exposed tip. **Figure 4.8** shows the measured monopolar impedance as a function of insertion depth in a piece of bacon. There are large differences within apparent similar tissue; therefore, what volume shall a quoted conductivity value be valid for?

Furthermore, the values are dependent on frequency, temperature, water content, blood perfusion, and the status of the body. The electrical properties of tissue will also change under compression (Belmont et al., 2013). The difference between data from human and mammalian animal tissue is usually considered small. The biomaterial may be *in vivo* or *ex vivo* tissue, excised material from freshly killed animals, or human autopsy material obtained a day or two after death.

Electrical tissue data have been tabulated by many authors in many review articles and book chapters: Schwan and Kay (1957), Schwan (1963), Geddes and Baker (1967),



Figure 4.8: Measured modulus of impedance at 10 kHz plotted as a function of insertion depth in a piece of bacon. The mark at $\sim 2 \text{ k}\Omega$ indicates the starting point of the horizontal needle insertion path. Courtesy of Håvard Kalvøy.

Foster and Schwan (1986), Stuchly and Stuchly (1990), Duck (1990), and Holder (2005). Gabriel et al. (1996a) made a literature survey. Their own measurements (Gabriel et al., 1996b) were made with a two-electrode technique and a coaxial probe in the frequency range of 10 Hz to 20 GHz. In that way, the transfer impedance component was eliminated.

Therefore, problems with tabulated values include the following:

- What is the tissue volume the data are averaged over?
- Is the anisotropy given?
- Is it human tissue?
- Are the values valid for living tissue—in vivo, ex vivo, or newly excised—or for dead tissue?
- Is the temperature given?
- Is the frequency dependence given?

In Section 3.8 about dispersions, the use of permittivity or conductivity parameters was discussed. From Section 2.3.4, we know that conductivity is dependent on the density of charge carriers and their mobility. In the frequency range less than 10 MHz, tissue admittance is usually dominated by the conductivity of the body electrolytes, but at higher frequencies it is dominated by the dielectric constant. The electrolytes without cells, in particular urine and cerebrospinal fluid (CSF), have the highest low-frequency conductivity; thus, the higher the cell concentration, the lower the low-frequency conductivity. Tooth, cartilage and bone, lipids, fat, membranes such as the skin stratum corneum (SC), and connective tissue may contain many inorganic materials with low conductivity, but they are very dependent on body liquid perfusion. Tissue conductivity data are tabulated in [Table 4.2](#).

Table 4.2: Tissue Conductivity: Low Frequency and 1 MHz

Tissue	σ [S/m] 1 Hz to 10 kHz	σ [S/m] ~1 MHz	ϕ_{\max} at <10 MHz	Anisotropy
Human skin, dry	10^{-7}	10^{-4}	80°	?
Human skin, wet	10^{-5}	10^{-4}	30°	?
Bone	0.005–0.06		20°	Strong
Fat	0.02–0.05	0.02–0.05	3°	Small
Lung	0.05–0.4	0.1–0.6	15°	Local
Brain (gray matter)	0.03–0.4	0.15	15°	Small
Brain (white matter)	0.03–0.3			Strong
Liver	0.2	0.3	5°	?
Muscle	0.05–0.4	0.6	30°	Strong
Whole blood	0.7	0.7	20°	Flow dependent
Urine	0.5–2.6	0.5–2.6	0°	0
Cerebrospinal fluid (CSF)	1.6	1.6	0°	0
Saline, 0.9%, 20 °C	1.3	1.3	0°	0
Saline, 0.9%, 37 °C	2	2	0°	0
Seawater	5	5	0°	0

In vitro Data

Let us recall that tissue can be characterized by permittivity or admittance. In a unity measuring cell ($A/d = 1$ [m]), the permittivity is: $\epsilon' = C_p$ and $\epsilon'' = G/\omega$. The conductivity is $\sigma' = G$ and $\sigma'' = \omega C_p$.

The poorly conducting membranes of the body and the interfacial polarization thereby cause the permittivity corresponding to α -dispersion in the millihertz to kilohertz range (cf, Section 3.8). At frequencies less than 1 Hz, the capacitive current component vanishes, and the admittance is purely conductive determined by the liquids outside of the outermost membranes. In a frequency range of 0.1–10 MHz, the phase angle is maximal (except for human skin, where it is at much lower frequencies). This is also the Maxwell–Wagner β -dispersion range for the dielectric interfaces, where the susceptance of the cell membranes becomes large and their influence more and more negligible. If there is an anisotropy at lower frequencies, then it has disappeared in this frequency range. The dipolar dispersion of the proteins also appears in this frequency range, and it is still active above 100 MHz. This is the γ -dispersion range, extending all of the way up to the single Debye characteristic frequency of water, centered on 18 GHz. The susceptance is dominating at these high frequencies, and the phase angle may be greater than 80°.

In vivo Data

Magnetic resonance electrical impedance tomography is a new and promising noninvasive method for finding conductivity data in vivo (Oh et al., 2005). Other techniques are invasive, such as by needle or by surgical opening measuring conductivity *in situ* or excised *ex vivo*. The spatial resolution of the measuring electrodes is important with respect to tissue data averaging. In medicine, the *parenchyma* is the typical tissue of the functional element of an organ in contrast to its framework (*stroma*). With a needle electrode with insulated shaft, the size and cutting properties of the tip are important. With a blunt needle, the tissue is pushed during the advancement until the tip suddenly penetrates and the tissue moves back. Thin membranes and tissue interfaces may generate large differences within a fraction of a millimeter ([Figure 4.8](#)).

Tissue immittivity is dependent on body liquid perfusion or tissue ischemia and pathological processes. Local tissue may also be living for a considerable time after the body is dead. Hair and nail is dead tissue, and the SC of the skin is already dead in its natural position.

4.2.2 Muscle Tissue

Muscle tissue exhibits a large α -dispersion and, as shown in [Figure 4.9](#), it may be strongly anisotropic with a low-frequency conductance ratio of approximately 1:8 between transversal and longitudinal directions. In the longitudinal direction, the high conductance

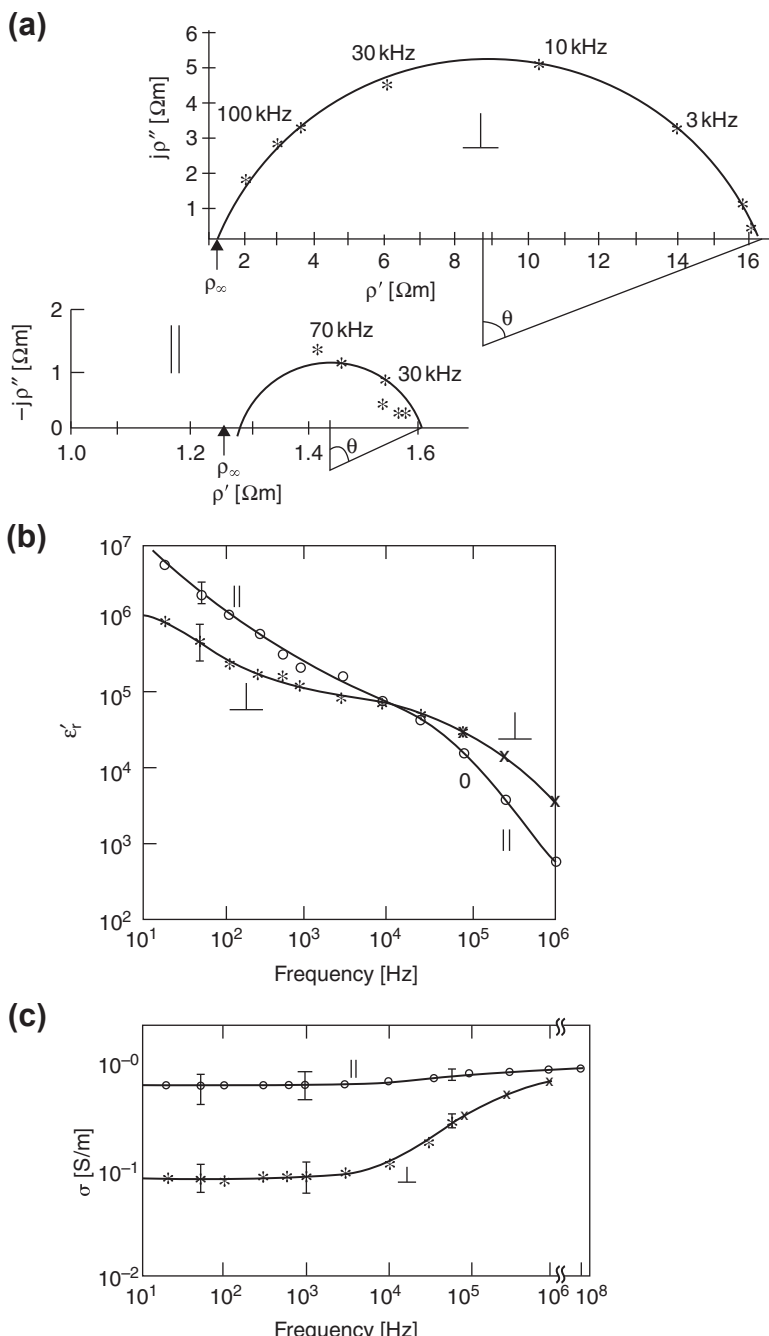


Figure 4.9: Dog excised skeletal muscle (37°C): frequency dependence and anisotropy. Current path: \perp transversal, \parallel longitudinal to muscle fibers. (a) Complex resistivity in the Wessel plane, (b) relative permittivity, and (c) conductivity. Redrawn from Epstein & Foster (1983), by permission.

is not very dependent on frequency, indicating that direct free liquid channels dominate the current path. It has been proposed that the α -dispersion arises from interfacial counterion polarization or from sarcotubular membrane systems in the interior of the muscle fiber. The transversal properties are presumably more dominated by interfacial β -dispersion of the Maxwell–Wagner character.

Figure 4.10 shows another data set presented with permittivity and conductance. In the transversal situation, three to four dispersions are clearly seen. The longitudinal data illustrate how dispersion levels may be almost nonexistent. Dispersion may take the character of one single straight line through many decades of frequency.

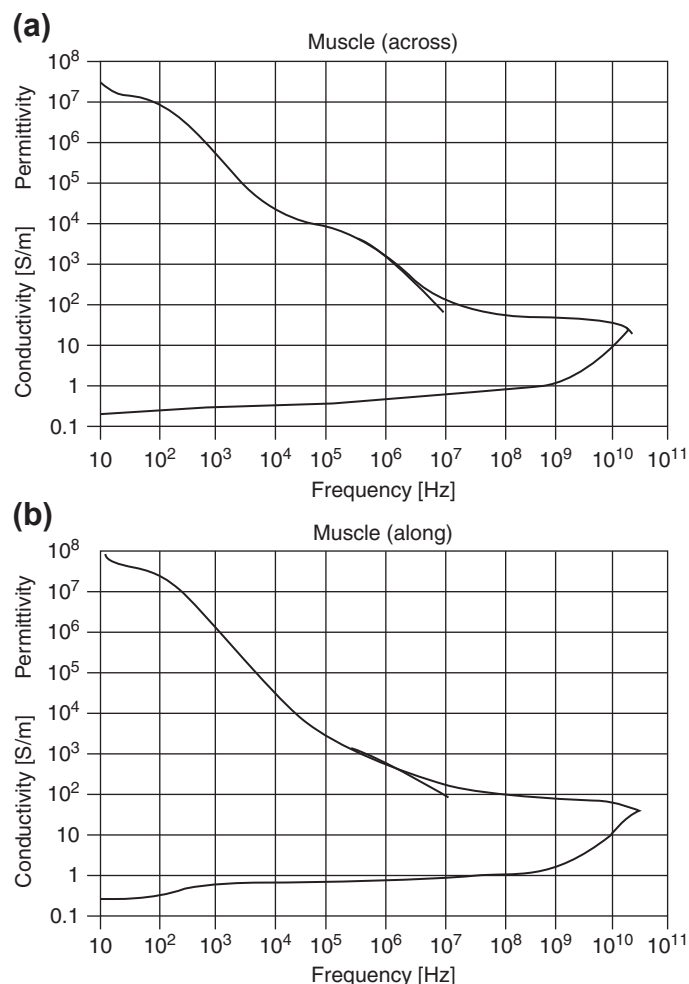


Figure 4.10: Dispersion of muscle tissue: (a) transversal and (b) longitudinal. *From Gabriel et al. (1996b), by permission.*

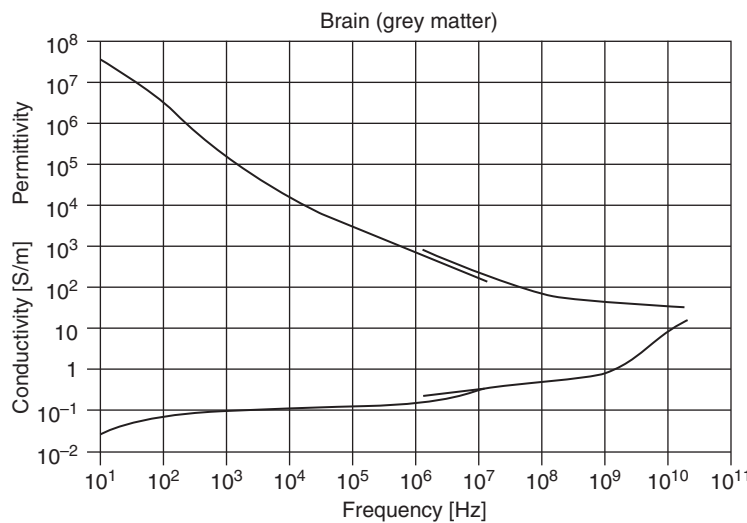


Figure 4.11: Dielectric dispersion of brain tissue. *From Gabriel et al. (1996b), by permission.*

4.2.3 Nerve Tissue and Impedance

The brain is the only tissue with a large volume of nerve tissue. Nerve tissue elsewhere may be regarded as cables, and electrical cable theory is often applied. The insulating properties of the myelin sheath increase the impedance of myelinated nerves.

Oh et al. (2011) and Liston et al. (2012) have modeled and recorded impedance changes in nerves during action potentials. More on action potentials can be found in Section 5.2.

Macroscopical data for brain tissue are shown in Figure 4.11. Note that measurements *in vivo* through the low-conductivity scalp will show quite different data.

There is an ongoing discussion on whether there is a genuine α -dispersion in brain tissue. The work of Gabriel et al. (1996b) and Ranck (1963) indicated β -dispersion at approximately 50 Hz. However, more recent papers (e.g., by Logothetis et al., 2007) show the resistive properties of brain to be flat at these frequencies. Gabriel's recordings have also been criticized by Bedard and Destexhe (2009) because a two-electrode system was used. Wilson et al. (2014) give a good review of relevant literature.

4.2.4 Adipose and Bone Tissue

Figure 4.12 shows the dispersion of adipose tissue. Adipose tissue and in particular bone and bone marrow have a wide spread of permittivity and conductivity that is very dependent on the degree of blood and other liquid perfusion.

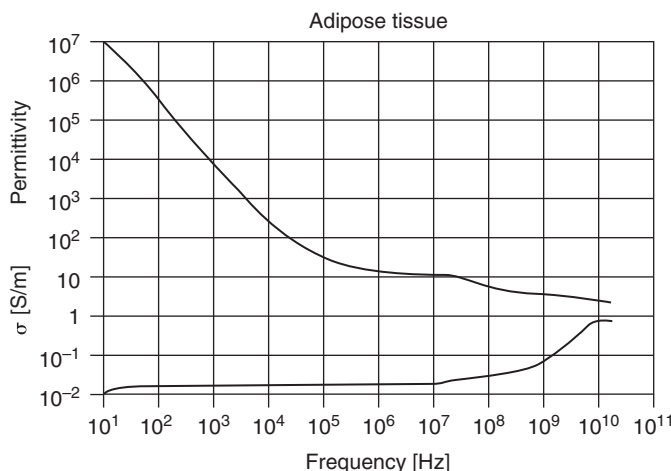


Figure 4.12: Dielectric dispersion of adipose tissue. From Gabriel *et al.* (1996b), by permission.

4.2.5 Blood

Whole blood consists of erythrocytes (containing the hemoglobin) and other cells in plasma. Blood may be studied as whole blood *in vivo*, erythrocytes in suspension, lysed erythrocytes in suspension, as plasma, etc. The erythrocytes are formed as doughnuts with an outer diameter of approximately 10 μm . Plasma is the liquid part with electrolytes and large organic electrically charged molecules. Lysed erythrocytes are destroyed cells with their intracellular material (hemoglobin) emptied into the liquid. The electrical properties of whole blood and lysed blood are of course very different (Figures 4.13 and 4.14). From the Maxwell–Wagner theory, it is possible to find an expression for the conductivity of a suspension of membrane-covered spheres (Section 3.5.1).

The limitation when modeling erythrocytes using spheroids was considered by Gheorghiu (1999). He found that the ellipsoidal model is fairly good when analyzing the impedance spectra of randomly oriented erythrocytes but rather poor whenever oriented erythrocytes are considered. For the latter, microscopic models coping with the actual shape should be considered.

Whole blood exhibits β -, γ -, and δ -dispersion, but curiously enough it exhibits no α -dispersion (Foster and Schwan, 1989). The β -dispersion has a dielectric increment of approximately 2000 centered at approximately 3 MHz (hematocrit 40%). Erythrocytes in suspension have a frequency-independent membrane capacitance with very low losses (Schwan, 1957). The impedance of lysed erythrocytes in suspension shows two clearly separated single relaxation frequencies (Debye dispersions). The α -dispersion is in the lower kilohertz range, and the β -dispersion is in the lower MHz range (Schwan, 1957; Pauly and Schwan, 1966).

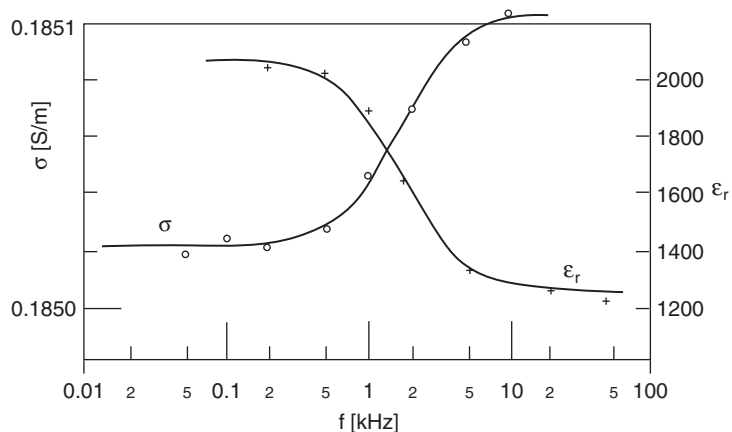


Figure 4.13: Dielectric constant and conductivity of a suspension of lysed erythrocytes. The characteristic frequency is low (~ 1.5 kHz). Note the high-resolution conductivity scale. *From Schwan (1957), by permission.*

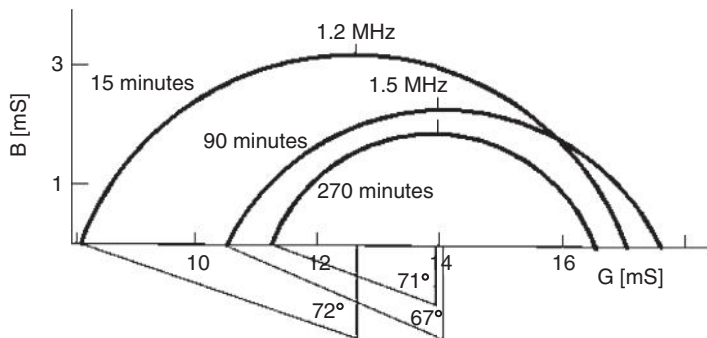


Figure 4.14: Admittance of erythrocytes in natural conditions during sedimentation. *From Gougerot and Fourchet (1972), by permission.*

Figure 4.13 presents an example of the dielectric constant and conductivity of a suspension of lysed erythrocytes, the characteristic frequency of which is low—approximately 1.5 kHz. Figure 4.14 shows the admittance of erythrocytes in natural conditions during sedimentation.

Electrical Properties of Cell Suspensions

Figure 4.13 shows data for a cell suspension. It shows a single dispersion with a characteristic frequency of approximately 1.7 kHz.

The use of dielectric spectroscopy for the characterization of living cells and the possible derivation of cellular parameters such as living cell volume concentration (Figure 4.14), complex permittivity of extracellular and intracellular media, and morphological factors is discussed by Gheorghiu (1996). Another possible application is the electrical measurement of erythrocyte deformability (Amoussou-Guenou et al., 1995).

4.2.6 Human Skin and Keratinized Tissue

Epithelia are cells organized as layers, and skin is an example. Cells in epithelia do form *gap junctions*. In particularly tight membranes, these junctions are special *tight junctions*. The transmembrane admittance is dependent on the type of cell junctions and to what extent the epithelium is shunted by channels or specialized organs (e.g., sweat ducts in the skin).

The impedance of the skin is dominated by the SC at low frequencies. It has generally been stated that skin impedance is determined mainly by the SC at frequencies below 10 kHz and by the viable skin at higher frequencies (Ackmann and Seitz, 1984). This will of course be dependent on factors such as skin hydration, electrode size and geometry etc., but it may nevertheless serve as a rough guideline. A finite element simulation on a concentric two-electrode system used by Yamamoto et al. (1986) showed that the SC accounted for approximately 50% of the measured skin impedance at 10 kHz but only approximately 10% at 100 kHz (Martinsen et al., 1999).

The SC may have a thickness of approximately 10 μm (0.01 mm) to 1 mm or more under the foot. The SC is a solid-state substance, not necessarily containing liquid water, but with a moisture content dependent on the surrounding air humidity. The SC is not water soluble, but it can absorb large amounts of water (e.g., doubling its weight). SC may be considered as a solid-state electrolyte, perhaps with few ions free to move and contribute to DC conductance. The SC contains such organic substances as proteins and lipids, which may be highly charged but bound, and therefore contributing only to AC admittance.

An open question is whether the conductance in SC in addition to the ionic component also has an electronic component (e.g., as a semiconductor).

The SC has been shown to display a very broad α -dispersion (Figure 4.15) that presumably is mainly caused by counterions. Viable skin has electrical properties that resemble that of other living tissue; hence, it displays separate α - and β -dispersions. The interface between the SC and the viable skin will also give rise to a Maxwell–Wagner type of dispersion in the β -range. Although the impedance of the SC is much higher at low frequencies than the impedance of the living skin, the differences in dispersion mechanisms make the electrical properties converge as the frequency is increased. This is the main reason why increased frequency in general leads to measurements at deeper layers in the skin.

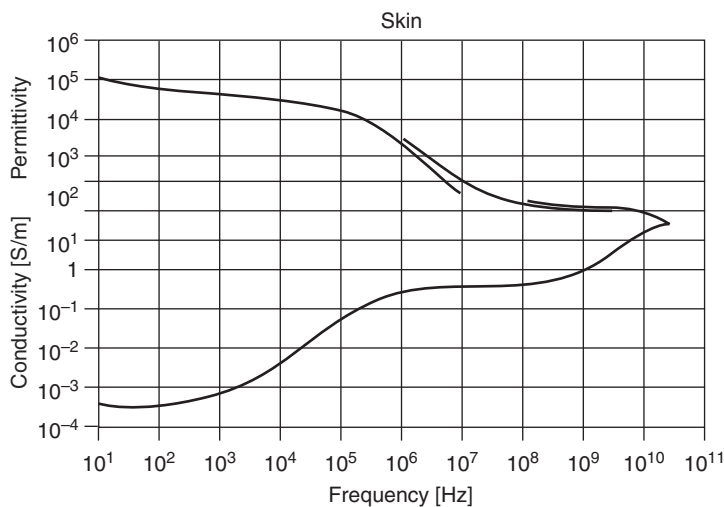


Figure 4.15: Dielectric dispersion of skin tissue. From Gabriel et al. (1996b), by permission.

Yamamoto and Yamamoto (1976) measured skin impedance on the ventral side of the forearm with a two-electrode system and an AC bridge. They used Beckman silver/silver chloride electrodes filled with gel and measured 30 min after the electrodes had been applied. The skin was stripped with cellulose tape 15 times, after which the entire SC was believed to have been removed. Impedance measurements were also performed between each stripping so that the impedance of the removed layers could be calculated. The thickness of the SC was found to be 40 µm, which is more than the common average values found elsewhere in the literature. For example, Therkildsen et al. (1998) found a mean thickness of 13.3 µm (minimum 8 µm/maximum 22 µm) when analyzing 57 samples from nonfriction skin sites on Caucasian volunteers. However, the moisture increase caused by electrode occlusion and electrode gel has most certainly significantly increased the SC thickness.

Knowing the SC thickness enabled the authors to calculate the parallel resistivity and relative permittivity of the removed SC. Furthermore, the resistivity and relative permittivity of the viable skin was calculated by assuming homogenous electrical properties and using the formula for constrictional resistance (cf, Figure 6.3). The resistance of the disk surface electrode is (Eq. 6.17) $R = \rho/4a$. Because $RC = \rho\epsilon_r\epsilon_0$, the relative permittivity of the viable skin can be calculated from the measured capacitance with a similar formula:

$$C = 4a\epsilon_r\epsilon_0 \quad (4.2)$$

The calculated data from Yamamoto and Yamamoto (1976) are presented in Figure 4.16.

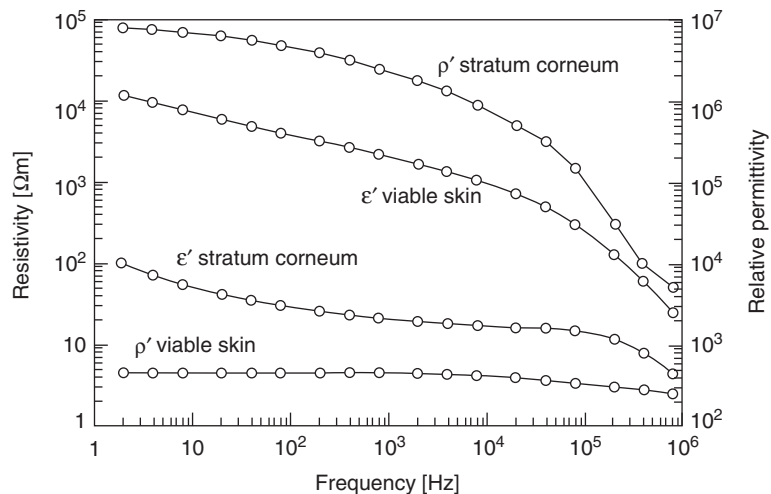


Figure 4.16: Average resistivities and relative permittivities in stratum corneum (SC) and viable skin. Redrawn from Yamamoto and Yamamoto (1976).

These data can also be presented as conductance and susceptance versus frequency, as in [Figure 4.17](#). The very broad nature of the dispersion can easily be seen in this figure. The conductance levels out at low frequencies, indicating the DC conductance level of the skin. The susceptance seems to reach a maximum at approximately 1 MHz, which should then correspond to the characteristic frequency of the dispersion. This frequency response

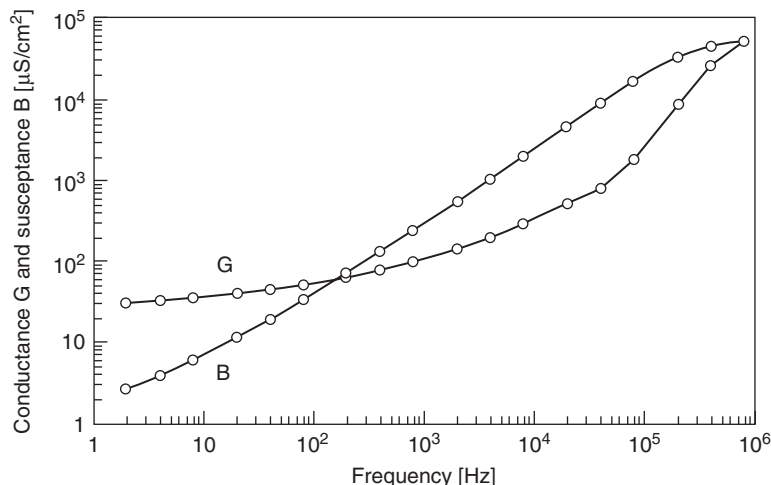


Figure 4.17: Surface admittance density of the stratum corneum as calculated from data presented in [Figure 4.16](#).

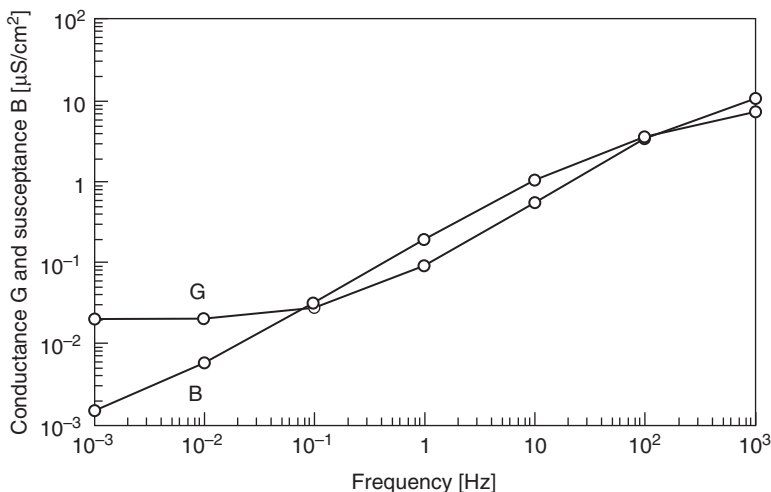


Figure 4.18: Surface admittance density of palmar stratum corneum (SC) in vitro. From Martinsen et al. (1997a), by permission.

is difficult to interpret, and the apparent broad dispersion is most probably a composite of several dispersion mechanisms. The highly inhomogeneous nature of the SC with a significant hydration gradient in brick-like layers of dead, keratinized cells should produce significant dispersion mechanisms in the α and β range.

The frequency response shown in Figure 4.17 can be compared with the admittance data from a 180- μm thick sample of palmar SC in vitro shown in Figure 4.18 (Martinsen et al., 1997a). These measurements were performed with a two-electrode system and hydrogel electrodes at 50% relative humidity (RH). The DC level of this SC sample is much lower than the one shown in Figure 4.17, even after adjusting for the 4.5 times greater thickness of the in vitro sample. This is easily explained from the difference in hydration for the two samples. SC in vivo is hydrated by the underlying viable skin and, in this case, also by the electrode gel. The in vitro skin is in balance with the ambient RH and the hydrogel electrodes do not increase the hydration (Jossinet and McAdams, 1991).

An important finding by Yamamoto and Yamamoto (1976) was that the impedance of the removed SC layers did not produce a circular arc in the complex impedance plane. This is obvious from Figure 4.19, in which the admittance data from Figure 4.17 have been transformed to impedance values and plotted in the complex plane.

Hence, if one plots the data from multifrequency measurements on skin in vivo in the complex plane and uses a circular regression to derive, for example, the Cole parameters, one must be aware of the following: SC alone does not necessarily produce a circular arc, and as described earlier in this chapter, the measured volume or skin layer is highly

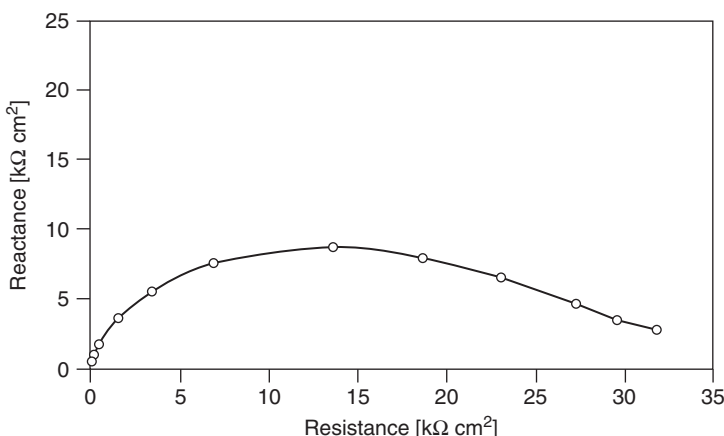


Figure 4.19: The stratum corneum data from Figure 4.17 plotted in the complex impedance plane.

dependent on frequency. Therefore, the derived parameters represent a mixture of different skin layers and different dispersion mechanisms; thus, they are totally ambiguous when used for characterizing conditions of specific skin layers.

Birgersson et al. (2011) showed through mathematical modeling and experiments that the data derived by Yamamoto and Yamamoto (1976) (Figure 4.16) should be adjusted to achieve better agreement between model prediction and experimental findings. Among other things, they pointed out that the cellulose tape stripping procedure used by Yamamoto and Yamamoto is not linear; that is, the amount of SC removed by each tape strip decreases with depth (Lademann et al., 2008). Further progress was made by Birgersson et al. (2013).

Skin admittance varies greatly between persons and between different skin sites on the same person. For example, changes in sweat gland activity and ambient RH during the day or season are also reflected by large variations in skin admittance, mainly because of changes in skin hydration.

Table 4.3 shows the results from impedance measurements at 10 Hz on different skin sites as measured with a 12 cm^2 electrocardiogram (ECG) dry metal plate electrode positioned directly on the skin site after a short breath had been applied to the skin surface (Grimnes, 1983a). The first column presents measurements immediately after the electrode had been applied, and the two subsequent columns give the values after 2 and 4 h, respectively. The first column shows a large variation in the control impedance, which was interpreted as an unstable sweat duct filling during the measurement. The two other columns show stable results at two different levels of control. The values in Table 4.3 clearly demonstrate the large variability in skin impedance on different skin sites and how this changes during a period of skin occlusion.

Table 4.3: Site Dependence of Skin Impedance [$\text{k}\Omega\text{cm}^2$] at 10 Hz

	$\text{k}\Omega\text{cm}^2/\text{k}\Omega$		
	Start	2 h	4 h
Hand: —dorsal side	720/80	210/17	300/33
Forearm: — ventral — distal	250/80	240/17	190/35
Forearm: — ventral — middle	840/80	230/17	360/36
Forearm: — ventral — proximal	560/80	180/17	260/36
Upper arm: — dorsal	840/75	260/16	660/36
Upper arm: — ventral	1000/70	300/16	780/34
Forehead	60/70	36/16	48/35
Calf	325/45	375/17	325/36
Thorax	130/37	110/16	130/35
Palm	200/80	150/17	200/33
Heel	120/60	180/15	120/35

Data represent initial values and values obtained after two intervals of 2 h. Each measurement is compared with the value [$\text{k}\Omega$] obtained from a control pregelled electrocardiogram (ECG) electrode on the ventral forearm.

Reproduced from Grimnes (1983a).

The sweat ducts of the skin introduce electrical shunt paths for DC current. Although lateral counterion relaxation effects have been demonstrated in pores, this effect is presumably negligible in sweat ducts; hence, sweat ducts are predominantly conductive (Martinsen et al., 1998a). However, the DC conductance measured on human skin is not only due to the sweat ducts. Measurements on isolated SC as well as nail and hair reveal conductance values comparable to those found on skin *in vivo* (Martinsen et al., 1997a,b).

Because sweat duct polarization is insignificant, the polarization admittance of the skin is linked to the SC alone. This implies that measurements of capacitance or AC conductance at low frequencies only reflect the properties of the SC.

The series resistance (i.e., the limiting impedance value at very high frequencies) is very small for the SC. In a practical experimental setup, the impedance of the viable skin will in fact overrule this component. The value of this effective series resistance is typically in the range of 100–500 Ω .

Skin Penetrated by External Electrolytes

In low-frequency applications (<100 Hz), the skin impedance is very high compared with the polarization impedance of wet electrodes and deeper tissue impedance. The SC consists of dead and dry tissue, and its admittance is very dependent on the state of the superficial layers and the water content (humidity) of the surrounding air in contact with the skin before electrode onset. In addition, the sweat ducts shunt the SC with a very variable DC conductance. Sweat fills the ducts and moisturizes the surrounding SC. Therefore, the state of the skin and measured skin admittance at the time of electrode

onset is very variable. With low sweat activity and dry surroundings, the skin admittance may easily attain values less than $1 \mu\text{S}/\text{cm}^2$ at 1 Hz.

From the time of onset of a *dry* metal plate, the water from the deeper, living layers of the skin will slowly build up a water contact with the initially dry plate and water content in the SC. A similar process will take place in the skin with hydrogel as contact medium (but here the metal/gel interphase is already established). The processes may take 15 min or more. The water vapor pressure of the hydrogel may be such as to supply or deplete the SC of water dependent on the initial skin conditions.

To avoid the long period of poor contact, a skin drilling technique may remove the SC. Even mild sandpaper rubbing may considerably reduce the initial impedance.

To shorten the long period of poor contact, an electrolytic solution or wet gel is often applied to the skin. The electrolyte concentration of the contact medium is very important. By using high salt concentration, the water *osmotic pressure* in the deeper layers will strongly increase the water transport up through the skin to the high concentration zone. This may be admissible for short-term use (e.g., <0.5 h). For prolonged use, skin irritation may be intolerable. For long-term use, the concentration must be reduced to the range of a physiological saline solution ($\sim 1\%$ of electrolytes by weight).

A surface electrode with the contact electrolyte covering a part of the skin may influence measured skin immittance by four different mechanisms:

1. Changing the water partial pressure gradient in the SC.
2. Osmotic transport of water to or from the contact electrolyte.
3. Penetration of substances from the electrode gel into the SC.
4. Changing the sweat duct filling.

With a dry electrode plate, the moisture buildup and admittance increase in the SC start at the moment of electrode onset. With a hydrogel, admittance may increase or decrease.

With wet gel or a liquid, the initial admittance is high, and with strong contact electrolytes the admittance will further increase for many hours and days (Figure 4.20). Because the outer layers of SC may be wet or dry according to the ambient air, it will not be possible to find a general contact medium that just stabilizes the water content in the state it was before electrode onset; the onset of the electrode will generally influence the parameters measured.

With dry skin, the admittance may be less than $1 \mu\text{S}/\text{cm}^2$ at 1 Hz. A typical admittance of more than $100 \mu\text{S}/\text{cm}^2$ is possible when the SC is saturated by electrolytes and water. The conductivity is very dependent on water content and is believed to be caused, for example, by protons (H^+) and charged, bound proteins that contribute only to AC admittance.

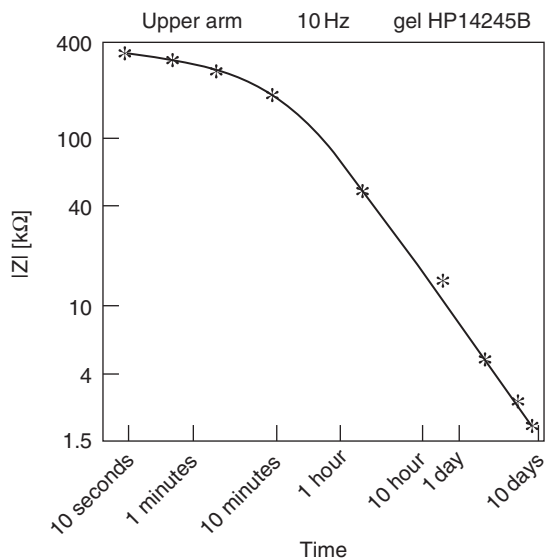


Figure 4.20: Skin impedance as a function of time for an electrocardiogram (ECG) electrode of the commercial, long-term, wet gel, strong electrolyte type. *From Grimnes (1983a), by permission.*

Figure 4.21 shows the dominating effect of sweat duct filling on skin *admittance* and shows clearly how skin capacitance is in parallel and is therefore unaffected by the parallel conductance change.

Hair and Nail

Hair is compactly cemented keratinized cells and grows in *hair follicles* that essentially are invaginations of the epidermis into the dermis. The *sebaceous glands* are located on the sides of the hair follicles. They secrete *sebum* to the skin surface, but the purpose of this secretion is unclear, apart from the fact that it gives a scent that probably is unique to each human being. The problem of acne vulgaris, well known to most young people, is connected to these glands.

The frequency response of hair is not unlike the properties of skin, but typical measured admittance values are, of course, very small, which makes these measurements complicated to perform. Figure 4.22 shows measurements on 100 hair fibers in parallel at different ambient relative humidities (Martinsen et al., 1997b). The hair length was approximately 2 cm.

At 86% RH, the conductance is almost independent of frequency (dominated by DC properties) up to 1 kHz, and at 7% and 62%, only a small increase at the highest frequencies can be detected. The susceptance is increasing linearly at the highest

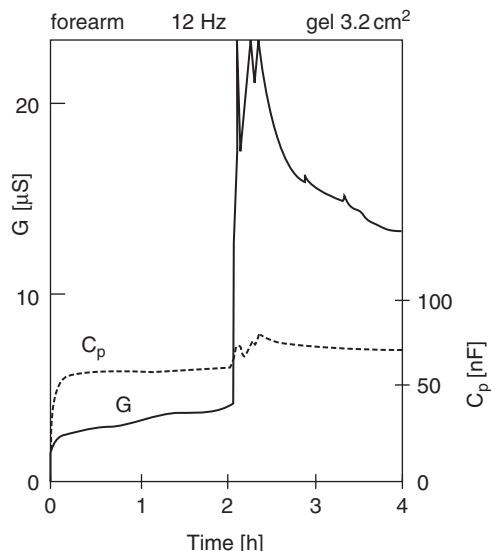


Figure 4.21: In vivo skin conductance and parallel capacitance during abrupt sweat duct filling (sudden physical exercise) and emptying. *From Grimnes (1984), by permission.*

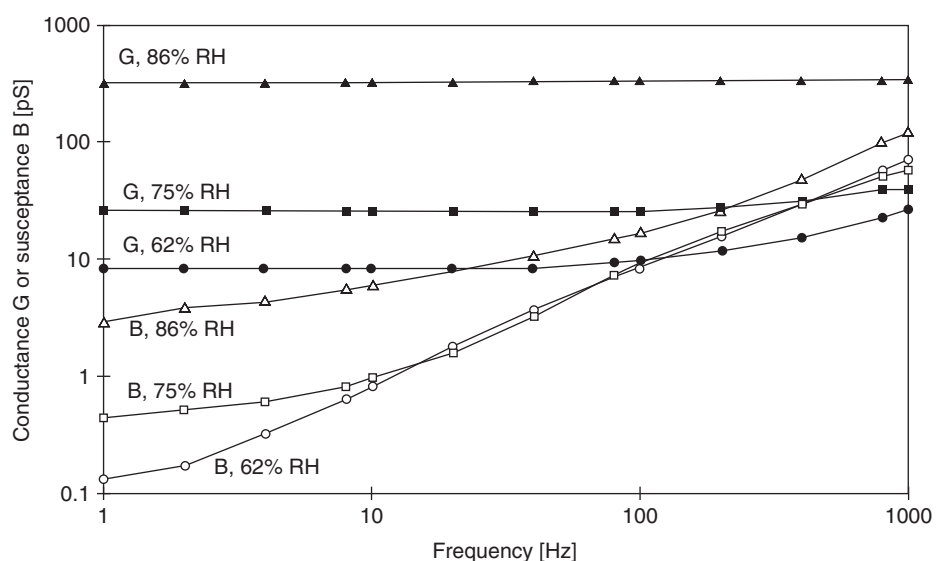


Figure 4.22: Electrical admittance of 100 hair fibers in parallel as function of relative humidity (RH). *Source: Martinsen et al., 1997b.*

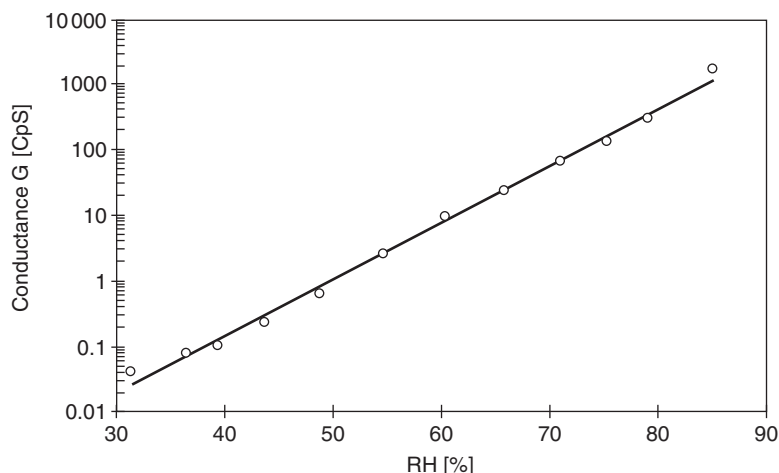


Figure 4.23: Electrical admittance of 50 hair fibers as a function of relative humidity (RH) at 1 Hz. Circles are measured values and the line is logarithmic regression. *Source: Martinsen et al., 1997b.*

frequencies, but it levels off at the lowest frequencies. The frequency at which this flattening starts increases with RH.

Adsorption of water into hair is a very slow process. Robbins (1979) found that the hydration of hair fibers stabilized after a period of 18–24 h after being introduced to an increase in ambient RH. Martinsen et al. (1997b) found that the conductance continued to increase for several days after such a step in RH and concluded that a possible cause of this is that adsorbed water molecules regroup in a way that increases their contribution to the conductivity. They furthermore found desorption to be a very quick process in which the main change in conductance appeared during the first minutes after reducing ambient RH but also with minor changes in conductance for the succeeding few hours.

The electrical admittance of keratinized tissue is typically logarithmically dependent on water content or ambient RH. An example from human hair is shown in Figure 4.23, in which the 1-Hz conductance of 50 fibers in parallel is plotted against ambient RH (Martinsen et al., 1997b).

Nail is also keratinized tissue, but it is harder than SC. This is partly due to the “hard” α -keratin in nail as opposed to the more “soft” β -keratin in SC (Baden, 1970; Forslind, 1970).

Although nail is readily available, and it is easy to perform electrical measurements on the nail, the electrical admittance of human nail has not been extensively investigated.

Figure 4.24 shows the conductance and susceptance of a 450- μm thick nail at 38% RH measured with a two-electrode hydrogel system (Martinsen et al., 1997a).

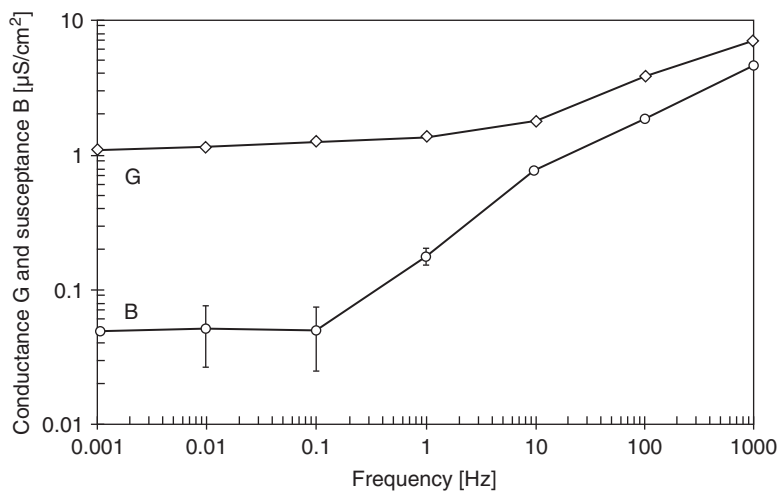


Figure 4.24: Electrical admittance of human nail. Error bars show the uncertainty in low-frequency susceptance data. Nilsen (1997).

The electrical properties of nail resemble those of SC and hair. However, note that the low-frequency susceptance plateau in Figure 4.24 represents a deviation from a simple model with a distribution of relaxation times for a single dispersion mechanism (cf. Section 9.2), and it must be due to another dispersion mechanism such as, for example, electrode polarization, skin layers, etc. The admittance of nail is also logarithmically dependent on water content, as shown in Figure 4.25 (Martinsen et al., 1997c).

4.2.7 Whole Body

Resistance

The value of the impedance between two skin surface electrodes is usually dominated by the contribution of the skin. However, the skin impedance may be negligible if

1. The voltage is high enough for skin electrical breakdown
2. The skin is thoroughly wetted
3. The skin is perforated
4. The effective skin contact area is very large
5. The signal frequency is sufficiently high

Without the skin and with the living body tissue considered purely resistive, the resistance, R , of a body segment is determined by the mean resistivity, ρ ; mean length, L ; and mean cross-sectional area, A , according to $R = \rho L/A$. The resistance can be measured by a four-electrode technique (Freiberger, 1933; Grimnes, 1983a).

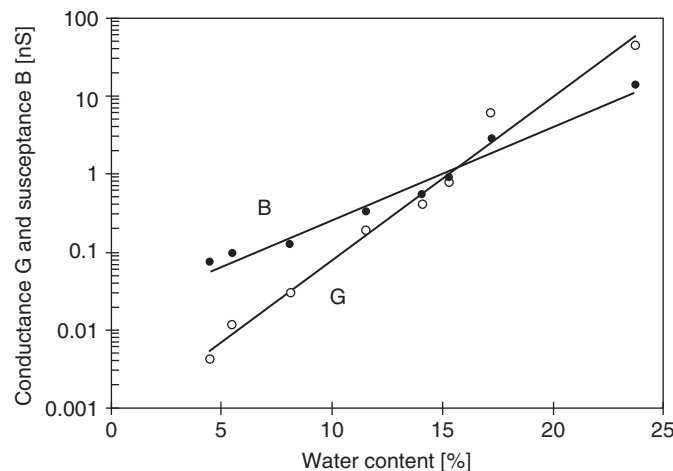


Figure 4.25: Electrical admittance for nail at 80 Hz as function of absolute water content (% weight). The area is 3.14 mm^2 and the thickness is 0.34 mm. Circles represent measured values and the line is the logarithmic regression. Martinsen et al. (1997c).

In Figure 4.26, notice the importance of the cross-sectional area. The resistance is dominated by the contribution from a finger, underarm, and leg, whereas the influence from the chest is negligible. In addition, the current flow may be constricted near the electrodes if the electrodes are small, and an additional *constrictional resistance* must be accounted for (cf., Section 6.2.2). Higher resistance values may also be due to the relatively small well-conducting tissue cross-sectional areas in such joints as the hand/wrist, elbow, and knee.

When skin electrical protection has been broken down during an electrical accident, the volume segment resistance is the current limiting factor (cf., Section 9.14). A description of the body immittance data used for the estimation of body composition is found in Section 10.8.

4.2.8 Postexcision Changes and the Death Process

Tissue metabolism decreases after the tissue has been excised. Often the temperature falls, and measured variations must account for such possible variables. If the tissue is supported by temperature and perfusion systems, then the tissue may be stabilized in a living state *in vitro* (*ex vivo*).

If the tissue is not supported, then irreversible changes will occur, followed by cell and tissue death. If blood flow is interrupted, then the metabolism continues, but in an anaerobic way. Osmosis will cause cell swelling and tissue damage, and a consequence of

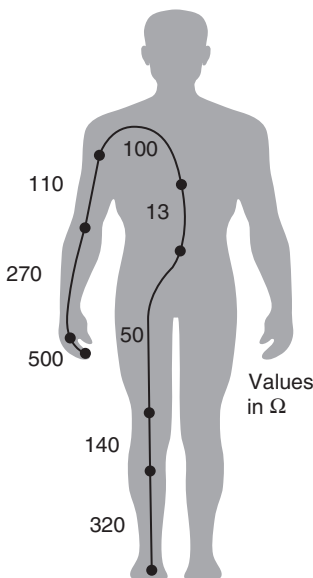


Figure 4.26: Body segment resistance distribution (no skin contribution, no current constriction). Values presented are as found with a four-electrode technique; $500\ \Omega$ is a one-finger contribution. Linear values according to Eq. 2.2 are not very dependent on current density levels.

this is the narrowing of extracellular pathways, which typically gives an increase in the low-frequency ($<10\text{ kHz}$) impedance. A steep increase in low-frequency impedance is also found in tissue with gap junctions when these gap junctions are closed after a certain duration of ischemia. Gap junctions can also produce an additional dispersion at very low frequencies (e.g., in porcine liver at $\sim 7\text{ Hz}$) that vanishes completely when the gap junctions close. Because metabolic products are no longer removed, one will sometimes find a decrease in impedance at high frequencies (e.g., 10 MHz ; Gersing, 1998). In brain tissue, irreversible changes may occur within 5 min at 37°C and in cardiac tissue after 20 min. Impedance spectroscopy has been shown to be of great value for the monitoring of these processes and for the assessment of organ state (Gersing, 1998; Casas et al., 1999).

Figure 4.27 shows the time courses of the electrical resistance at 100 Hz and 10 MHz measured on canine heart muscle treated by perfusion with Custodiol® (Gersing, 1998).

The initial drop in resistance is due to the warming up of the cool tissue sample, and the subsequent drop in 10-MHz resistance is probably caused by accumulation of metabolic products in the tissue (as mentioned previously). The 100-Hz resistance rises steeply after a period of approximately 3 h, indicating the onset of tissue damage. This damage is nonreversible when the upper plateau is reached and the organ cannot be revived. In addition, Salazar (2004) found that bioimpedance measurements enabled differentiation among

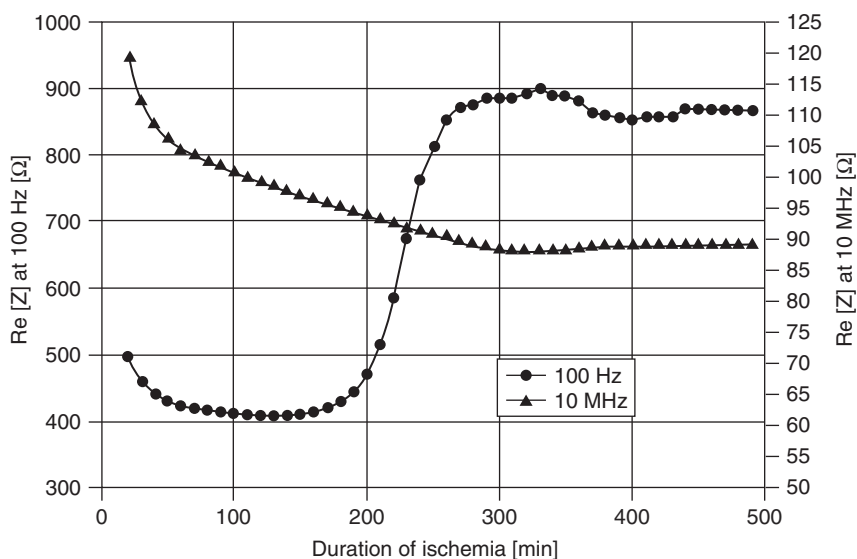


Figure 4.27: Resistances at 100 Hz and 10 MHz of Custodiol® perfused canine heart muscle at 25 °C. From Gersing (1998) with permission.

normal, ischemic, and infarcted myocardium. The general dynamics pattern exhibited by tissue alterations during ischemia was revealed by Gheorghiu and Gersing (1999).

In keratinized tissue such as the outer layers of the human skin and in hair, nail, and horn, the change and ultimate death of the cells are genetically programmed to occur during a period of approximately 30 days. The dead keratinized cells need no intra- or extracellular fluids, and they may be in a dry state with low admittance values.

Bozler and Cole (1935) measured the electrical impedance of frog sartorius muscle from 1.1 kHz to 1.1 MHz. Measurements were first done approximately 2 h after dissection. The tissue was then stimulated to induce contraction, and the tissue was measured again, approximately 3 h after dissection. They found a minor arc of a circle when the data were plotted in the complex impedance plane. Between the relaxed and contracted state, R_0 was found to increase by 75% whereas R_∞ increased only 2%. As usual, R_0 and R_∞ denote the resistances measured at very low and very high frequency, respectively. The significant increase in R_0 was interpreted as a reduced ionic conduction through the cell membranes.

Schäfer et al. (1998) measured the skeletal muscle of rabbits and dogs from 100 Hz to 10 MHz and found a β -dispersion for which the characteristic frequency in the impedance plane typically moved from 20 to 10 kHz and then back to 20 kHz during ischemia. Furthermore, they found the low-frequency resistance to increase during the first 300 min of ischemia, subsequently decreasing up to 850 min and then increasing again. The initial

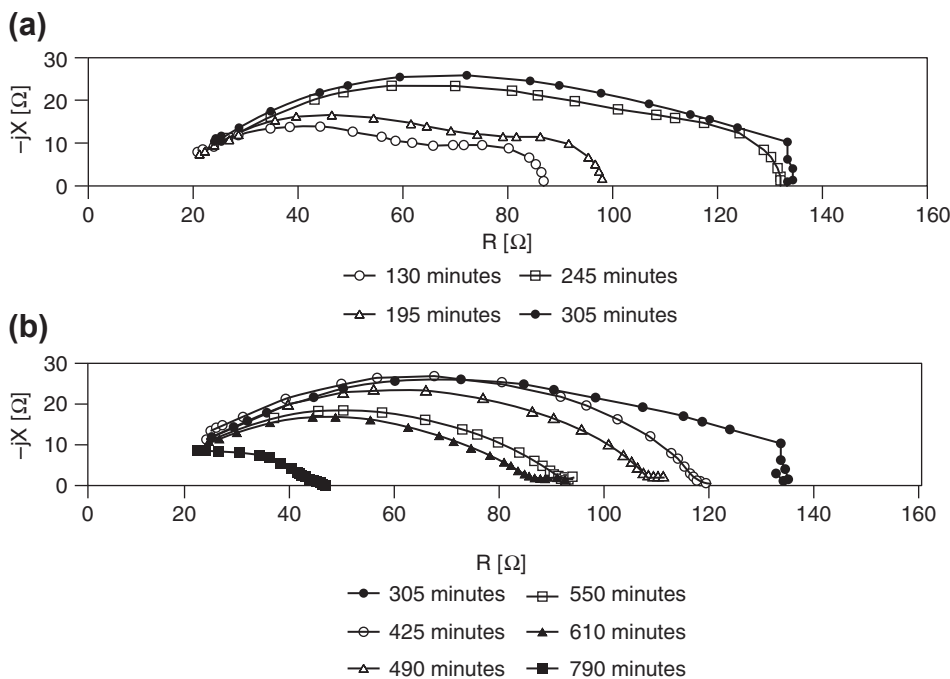


Figure 4.28: Postmortem Wessel plot for fish muscle: (a) first 5 h after death, and (b) next 7 h.

Source: Martinsen et al. (2000), by permission.

increase in resistance is explained as being due to increasing edema because of osmotically induced water shifts, which reduce the extracellular volume. This effect also continues after 300 min, but it is surpassed by a reduced membrane resistance caused by the opening of ion channels leading to a net reduction of the low-frequency resistance. In their model, the membrane resistance reaches a constant level after approximately 850 min whereas the extracellular resistance continues to increase, resulting in a net increase of resistance after 850 min.

Martinsen et al. (2000) presented measurements of the electrical properties of haddock muscle from 1 Hz to 100 kHz as a function of time after the fish was sacrificed (Figure 4.28). Clear α - and β -dispersions were found. Most of the α -dispersion disappeared after a few hours. The low-frequency resistance of the β -dispersion increased during the first 5 h as the fish went into rigor and then decreased as cell destruction developed.

4.2.9 Plant Tissue

In general, plant tissue immittance data are not in accordance with Cole–Cole system models. Nonsymmetrical models of the Davidson Cole and Havriliak–Negami types have

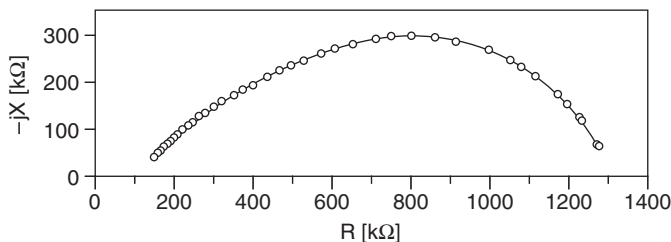


Figure 4.29: Impedance plot for Scots pine needles. From Zhang (1995), by permission.

been used (Zhang et al., 1995). Figure 4.29 shows a Wessel plot with data from Scots pine needles obtained with a two-electrode technique. Air spaces in the needles were believed to have an important influence on the α parameter of the Cole equation and the skewness of the arc. High-temperature dependence has also been reported for plant tissue. Chilcott and Coster (1991) found that a 10 °C increase resulted in more than a doubling of the conductance of *Chara corallina* (an aquatic plant).

4.3 Special Electrical Properties

4.3.1 Tissue Anisotropy

Electrical properties such as permittivity or conductivity are usually dependent on direction in tissue. This is due to morphological patterns in the tissue such as structural lines of muscle fibers, tendons, nerve fibers, and blood vessels. The patterns may be regular or have so small of dimensions that the tissue may be defined as macroscopically homogeneous. The properties of tissue vary strongly according to the dimensional scale; for example, there are heterogeneities at all levels from the muscle as an organ between other organs down to the atomic dimensions of its cell components. All parameter values are actually averaged values of a certain tissue volume.

Dielectric Microscopic Anisotropy

“Microscopic” means that the anisotropy due to nonsymmetrical structures is very small relative to the dimension of the prescribed tissue volume. In the classical electrostatic model there are no free charge carriers; they are all bound to their atoms or molecules. With an applied electric field, the electron cloud is displaced and a dipole moment is generated (cf., electronic polarization, Section 3.1.2). The electric charges are very small (e.g., electrons 10^{-15} m), and their displacement caused by polarization is extremely small ($\approx 10^{-17}$ m). Therefore, in the capacitor model of Figure 3.1, the applied E-field is not disturbed macroscopically by the induced dipoles, only at an atomic scale. However, in a solid dielectric, the charge carriers may be bound differently in different directions

(e.g., crystalline solids), thus resulting in net permittivity anisotropy. In a dielectric with anisotropy, the three vectors of Eq. 3.5, $\mathbf{D} = \epsilon_0\mathbf{E} + \mathbf{P}$, are therefore not necessarily parallel.

Permittivity is usually higher in liquids than in solids (e.g., water/ice) because the charges are more loosely bound in a liquid. A liquid such as water is polar but isotropic when all molecules are free to find their statistical positions.

Bioimpedance Macroscopic Anisotropy

In bioimpedance theory, there are free charge carriers and the current density is $\mathbf{J} = \sigma\mathbf{E}$ (Eq. 2.1). The dimensions of interest are usually much larger than in the dielectric polarization cases, and the applied field is macroscopically disturbed by the anisotropy. For example, take a cubic model of a homogeneous biomaterial as shown in [Figure 4.30](#). In the middle is shown an insulating spheroid implant, which results in a clearly lower net conductivity in the vertical electrode pair (hindering current flow in the constrictional zones of the electrodes, shadowing effect) and a slightly lower net conductivity in the horizontal pair. To the right, a metal implant results in a corresponding anisotropy but with higher net conductivity in the vertical electrode pair. Thus, both implants introduce macroscopical anisotropy.

[Figure 4.31](#) shows how the macroscopical E-field is disturbed and goes parallel to the insulator surface (left) but perpendicular to the metal surface (middle). To the right, a model is shown with small tubes implanted in the biomaterial. If the tubes are of metal, then there is no E-field inside of the tubes and zero current density there. With insulating walls, the E-field direction inside of the tubes is tube axial, and so is the direction of the current density. Outside of the tubes, the local E-field is also parallel with the tube axis. The direction of the local E-field is varying, but Eq. 2.1 is macroscopically correct so that the local current density direction is equal to the local E-field direction. To take care of direction dependence, the conductivity, σ , may be extended to be a tensor. A tensor is a generalization of a vector, and it generally has nine directional components. Only six of

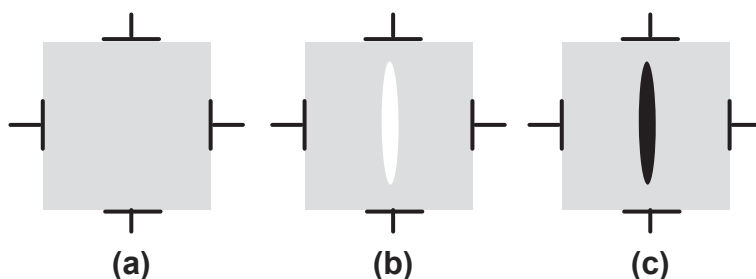


Figure 4.30: Anisotropy Created by Macroscopic Inhomogeneity. (a) Uniform biomaterial, (b) with one spheroid of low conductivity, or (c) with high conductivity.

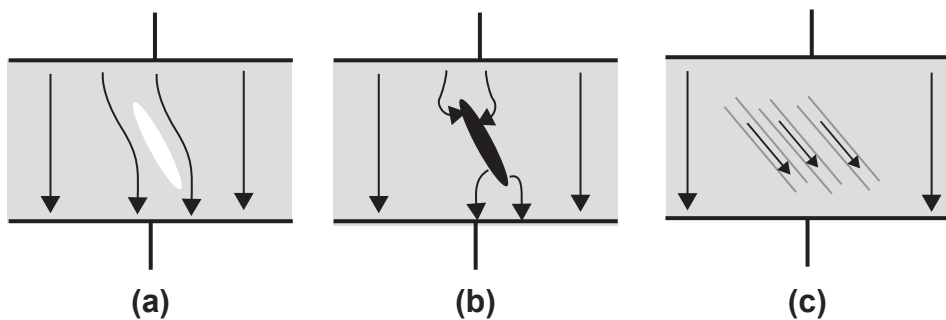


Figure 4.31: Capacitor Model with Homogeneous Conductive Biomaterial. (a) With insulating implant; (b) with metal implant; (c) with inserted well conducting tubes.

them are independent, and by choosing the best coordinate axes with respect to, for example, crystal axes, they reduce to three.

Figure 4.32 illustrates macroscopic anisotropy in a simplified tissue model. In living tissue, conductivity may be 10 times larger in one direction than another. At low amplitude levels the tissue is still linear, and the principle of superposition and the reciprocity theorem are still valid. However, Ohm's law for volume conductors, $\mathbf{J} = \sigma\mathbf{E}$, is not necessarily valid even if it still is linear; the current density direction will not coincide with the E-field direction if the anisotropic structures are sufficiently small.

Frequency Dependence

The models of Figures 4.30–4.32 will exhibit Maxwell–Wagner dispersion. The anisotropy of Figure 4.32 disappears at high frequencies because the capacitive membranes are short-circuited. For example, when anisotropy is caused by air in the lungs, the anisotropy may persist at virtually all frequencies.

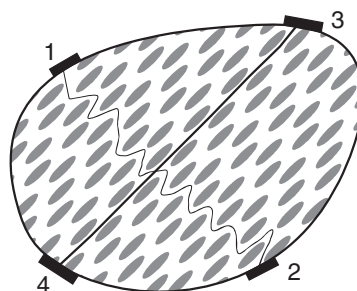


Figure 4.32: Anisotropy in a simplified tissue model. Each ellipse is a cell with cell membranes (cf., Figure 4.7).

Conclusion

Anisotropy implies that the possible selective measurement of defined tissue volumes is disturbed. This leads to serious objections and problems in impedance tomography, numerical modeling such as the finite element method, and immittance plethysmography.

4.3.2 Continuity across Interfaces, Tissue, and Implants

In tissue, an implant may be conductive (metallic) or insulating (Dacron®). Tissues of different electrical properties may result in the bending of current density field lines ([Figure 4.33](#)). At a sharp interface the following rules apply:

1. Potential

The potential is continuous across any interface.

2. Tangential component of \mathbf{E}

The tangential component of \mathbf{E} is continuous across any interface.

3. Normal component of \mathbf{D}

If there are no free charges at the interface, then the normal component of \mathbf{D} is continuous. If there is a surface charge, q_s , then $q_s = \Delta\mathbf{D}$, where $\Delta\mathbf{D}$ is the difference in the normal component of \mathbf{D} across the interface.

Bending of \mathbf{J} in Conductive Materials

A bending of current density field lines occurs at the interface between two homogeneous materials of different conductivity, as shown on [Figure 4.34](#). Let θ be the angle between a

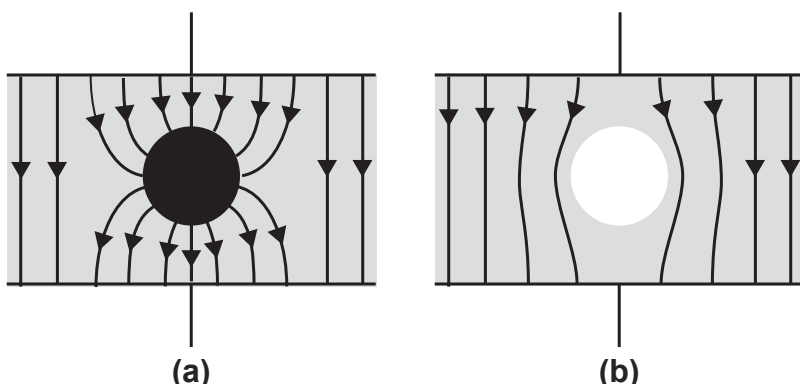


Figure 4.33: (a) Conductive and (b) insulating sphere implanted in a homogeneous material. The current density (electric field) lines are always perpendicular to the metal surface and parallel to the insulator surface.

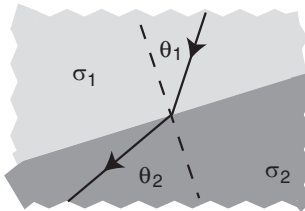


Figure 4.34: Bending of current density field lines.

line of \mathbf{J} and a line perpendicular to the interface. If the volume is large in relation to the interface volume, then

$$\sigma_2 \tan \theta_1 = \sigma_1 \tan \theta_2 \quad (4.3)$$

For example, the field of region one is not an independent variable. Irrespective of how the field was initially the introduction of, for example, a piece of metal in tissue changes the original field so that all field lines become oriented perpendicular to the metal surface. There are some similarities between optical refraction and such line bending; the refraction occurs when light crosses an interface between two optical materials of different refractive index. However, the bending is in some respect quite different: In optics, the introduction of a lens does not change the electromagnetic field in front of the lens.

■ Examples of Eq. 4.3 and Figures 4.33 and 4.34

If region two is a metal so that $\sigma_1 \gg \sigma_2$, then according to Eq. 4.3, $\theta_1 \approx 0^\circ$, showing that the current enters the metal perpendicularly to the surface. Therefore, the tangential E-field strength in the region one side of the interface is small and, according to rule 2, above the tangential E-field strength must be equally small on the region two side. The small E-field strength in region 2 is due to the high conductivity there.

If region two is an insulator so that $\sigma_1 \ll \sigma_2$, then $\theta_1 \approx 90^\circ$, showing that the current avoids the insulator and flows parallel to the insulator surface. Therefore, the tangential E-field strength in the region one side of the interface is high and, according to rule 2, above the tangential E-field strength must be equally high on the region two side. The high E-field strength in region two is due to the low conductivity there.

4.3.3 Tissue DC Properties

Endogenic DC Potentials/Currents

The Nernst equation (Eq. 7.9) defines potential differences as a function of ionic activities, and the Maxwell/Gauss equation defines potential changes as a function of charge densities. We may hypothesize that there are DC potential differences between some of the

organs of the body and that, accordingly, there may be large endogenous electric DC currents flowing between organs. For example, imagine the stomach with its large content of concentrated HCl (Nordenström, 1983).

The most basic DC potential difference is the polarization potential of approximately -70 mV in the cell interior with reference to the extracellular fluids. In addition, the palmar and plantar skin sites are at a negative potential with respect to other skin sites by a magnitude up to -30 to -40 mV DC. This is created by a difference in ionic activities across the skin barrier, with a possible addition of streaming potential waves from sweat propelled up the sweat ducts. The skin potential is shunted by skin sweat duct conductance. Therefore, increased sweat activity, as occurring during a galvanic skin response (GSR), reduces the magnitude of the DC voltage (GSR-DC-wave). GSR is the DC part of the more general concept—electrodermal response (EDR) (cf., Section 10.3).

On the surface of the body, DC recording is moreover used in electro-oculography to determine the position of an eye behind a closed eyelid. Together with GSR, this is one of the few electrophysiological methods making use of DC potentials.

For DC measurement, it is important that the two electrodes are reference electrodes. If the electrodes are made of different metals or surfaces, then a large exogenous DC voltage (possibly >1 V) may be generated. Often the best choice is two silver chloride reference electrodes. They can be coupled to the skin or tissue via electrode gel, as shown in Figure 7.1, or via a salt bridge to reduce the DC offset from liquid junction potentials. An invasive electrode as a neutral electrode is the most stable DC reference with a unipolar skin potential recording system.

Remember that with an exogenous DC source, it is not possible from a pure DC measurement to discern between changes in EMVs and resistance/conductance (cf., Section 7.9.1). Measured DC voltage is not necessarily proportional to the DC resistance of the unknown if a DC constant current is passed through the unknown.

Closed Electric Circuits in the Body

As explained, there are endoelectrogenic sources in the cell membranes. However, it is quite likely that some macroscopic membranes around organs are also the sites of electricity sources. Nordenström (1983) proposed that there are closed DC circuits in the body with the well-conducting blood vessels serving as cables (e.g., a vascular-interstitial closed circuit). These DC currents can cause electro-osmotic transport through capillaries. *Dental galvanism* is the production of electricity by the metals in the teeth.

DC Conductivity

Living tissue is surrounded by extracellular liquids, and these liquids have a DC conductivity of approximately 1 S/m, [Section 4.2.1](#). However, all organs in the body are

surrounded by epithelia, and epithelia with tight junctions between the cells have very low DC conductance. Therefore, measured DC conductivity is very dependent on what sorts of epithelia and lipid bilayers the current has to cross.

Injury Potentials and Bone Fracture Growth

It is well known that the zone of tissue injury is the source of DC potentials. It has often been postulated that bone growth is enhanced if a DC current is supplied to each side of the fracture. Nordenstrøm used DC in an electrochemical treatment of tumors.

4.3.4 Piezo- and Triboelectric Effects

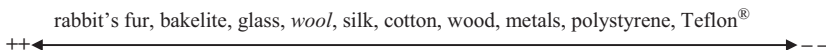
In Chapter 3, we have learnt that an applied electric field induces dipole moments in a dielectric. Such a displacement of charges generally generates a dimensional change in the material. This is called *electrostriction*.

Vice versa, mechanical stress changes the dimensions of the material. This does not usually result in an electrical polarization of the material because most materials have a so-called *center of symmetry* canceling opposite charge displacements. However, crystals lack such a center of symmetry, and they generate an internal polarization, **P**, when mechanically deformed. These materials are called *piezoelectric*, with a direct conversion from mechanical to electrical energy.

Piezoelectric properties have been found in human hair and other keratinized materials. This is also the case for bone and tendon. Bone remodeling has been attributed to piezoelectricity. The theory is that the mechanical stress on a bone generates bioelectricity that in turn influences bone growth. Because most biomaterials exhibit piezoelectric properties, it is not strange that there are many theories postulating piezoelectric effects in tissue; for example, that the transducer mechanism in the inner ear, in the hair follicles, and of touch and vibrational sensitivity is piezoelectric. Results in the literature are often with dry sample, and the question remains as to the importance of piezoelectricity in living, highly conductive tissue.

Triboelectricity (frictional charging) is the generation of charges when two different materials suddenly are separated. All materials, solids and liquids, isolators and metals, display this phenomenon. When two different materials come in mechanical contact, electric charges will be generated at the molecular or atomic level. If the materials are different, then a charge will be generated at the interface between the materials. It is the same mechanism when double layers (Section 7.5) are formed in the liquid having contact with a solid material. This charge will be divided between each surface if they suddenly lose contact. A *triboelectric series* is often set up, but because the position

is very dependent on surface properties, the series often differ. Humidity and cleanliness drastically affect the series. Here is one such series:



Presumably *human hair*, and perhaps dry SC, has a position not too far from wool.

During wintertime, triboelectricity may generate several kilovolts on an insulated person during walking or by blanket movements when the patient's bed is made. If the patient is monitored, then noise will appear on, for example, the ECG recordings (Gordon, 1975). However, the seriousness of the electrostatic problem is linked not only with the generation mechanism but also with the *discharge mechanism*. The volume and surface conductivity of the materials is of the uttermost importance because they determine the discharge time constant. If a person is charged by walking on a floor or taking off some clothing, then the person's capacitance to Earth (e.g., 150 pF) together with the resistance to Earth (e.g., 8 GΩ, $\tau = 1.2$ s), determine the time constant. If the time constant is several seconds, then problems will occur because the charge will stay long enough to cause an electric arc discharge at, for instance, the touch of a metal object. If it is in the millisecond region, then the person is rapidly discharged, and no arc discharge will occur at the touch of a metal object. The conductance of many low-conductivity materials is very dependent on humidity; therefore, the problems are much larger at low ambient RH. This occurs indoors in cold countries during the winter. Under these conditions, cotton is better (have higher conductivity) than most synthetic materials.

Triboelectricity is of great practical interest because it is the basis of all of the problems associated with *electrostatic discharges*. Such discharges represent a risk because they may excite nerves or ignite flammable vapors. The discharge may be perceptible (Section 10.16). Some of the electricity generation is due to the rubbing and separation of skin with textile clothing. Therefore, the triboelectric properties of skin and hair are of interest (combing the hair). When the RH in a room has been 10% for some time, a person can easily be charged to 30 kV with respect to Earth just by walking or rising from a chair. During walking, the electricity generation is determined by the materials of the shoe soles and the floor.

4.4 Problems

1. From data found in Section 4.1, what is the approximate permittivity of water at 37 °C?
2. Are the electrical properties of amino acids dependent on the water content?
3. With a membrane capacitance of $1 \mu\text{F}/\text{cm}^2$ and a membrane thickness of 7 nm, what is the permittivity of the membrane material?

4. How large is the conductivity anisotropy at low frequencies in muscle tissue ([Figure 4.9](#))?
5. Roughly sketch the corresponding ϵ'' curve on [Figure 4.13](#).
6. [Figure 4.26](#) indicates that the resistance of a finger is approximately 500Ω . Calculate the mean resistivity of the finger tissue modeled as a cylinder. Use the dimensions of your own longest finger.

Excitable Tissue and Bioelectric Signals

In living tissue, important communication control is implemented by hormones and nerves. Hormones are slow broadcasting information carriers; nerves are quick prewired point-to-point information carriers. Some cells are not excitable, such as adipose, connective tissue, and blood. They are passive, not under nerve control, and only weakly polarized. However, nerve, muscle, and gland cells are polarized and excitable; within a 1/1000 s, such cells may react on trigger signals. The excitation of a cell is accompanied by an *action potential*. The action potential is the basic bioelectric event and signal source in the body.

In section 4.1.4, the passive cell membrane was described. The membrane is a bilayer lipid membrane (BLM), as shown in Figure 4.6 and Figure 5.1. The membrane of a living

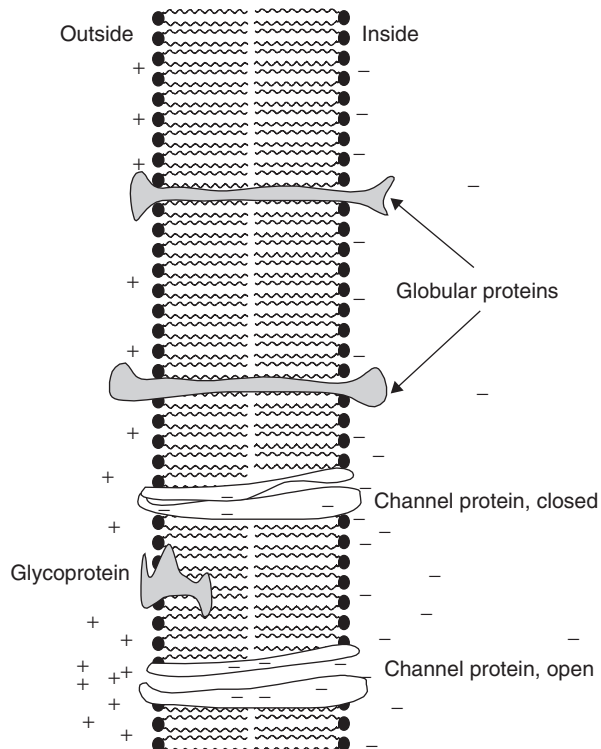


Figure 5.1: Bilayer lipid membrane (BLM) with embedded proteins. A channel macroprotein may form a water channel, an ion channel, or an adenosine triphosphate (ATP)-driven ion pump.

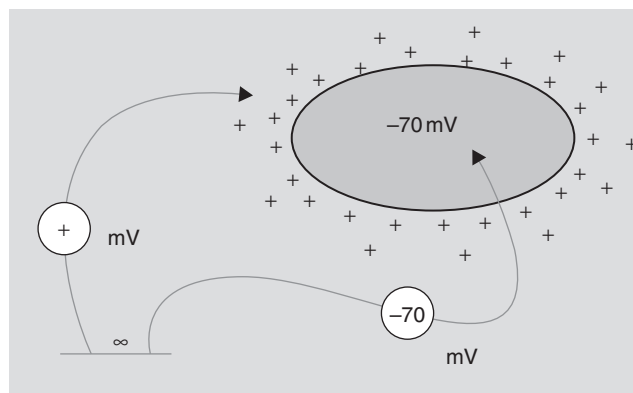


Figure 5.2: The polarized excitable cell.

cell is a most complex and dynamic system. The cell membrane itself is a major barrier to ion flux, but embedded in the membrane there are channels, transporters, and ion pumps. Electrically, they represent shunt pathways in parallel with the BLM, as shown in [Figures 5.1 and 5.3](#). The water channels are a special class of channels, selectively allowing water flux (but without electric charge: no proton or ion flux) in response to osmotic gradients and therefore regulating cell volume swelling or shrinking.

5.1 Cell Polarization

Cell polarization is generated by the ion pumps ([Figure 5.3](#)) using the energy of adenosine triphosphate (ATP) hydrolysis to drive ions against the electrochemical gradient. This energy-consuming mechanism polarizes the cell so that the interior of excitable cells has a potential of about -70 mV with respect to the extracellular electrolytes ([Figure 5.2](#)). Such a pump is a molecular device embedded in the cell membrane, which is capable of generating a net electric current across the membrane and is thus *electrogenic*.

The sodium pump ($\text{Na}^+ - \text{K}^+$ -ATPase) is the most important ion pump. In nerve cells, approximately 70% of its ATP is consumed to fuel sodium pumps. Instead of a direct channel across the membrane, the sodium pump is equipped with a special “box” with a special “door” ([Figure 5.3](#)). Initially, the door is open toward the inside so that three intracellular Na^+ ions with bound ATP enter the box. The door is closed, the box is turned around, and the enclosed ions are released to the outside. There, the pump binds two extracellular K^+ ions with ATP. The pump reorients and releases K^+ into the cell interior. A full cycle has then been completed so that the channel is never open in its total length.

The sodium pump consists of two subunits: The alpha subunit binds ATP and both sodium and potassium ions, whereas the smaller beta subunit determines the position and

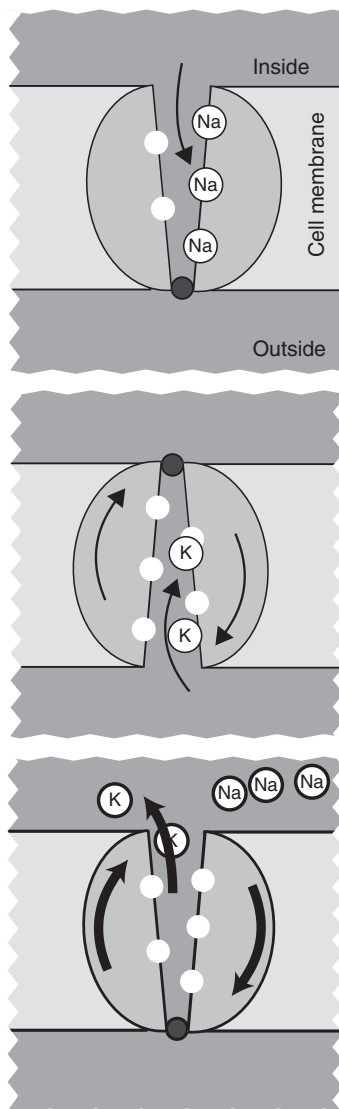


Figure 5.3: $\text{Na}^+–\text{K}^+$ –ATPase pump embedded in a cell membrane.

activation of the alpha unit. The sodium pump translocates a greater electric charge in one direction than the other. Per cycle, it exports three sodium ions Na^+ and imports two potassium ions K^+ , resulting in a net electric current flow out of the cell of one positive ion per cycle. Millions of such pumps in one cell membrane polarize the cell to steady state so that the cell is fully polarized and ready to be triggered. The whole polarization process, such as the number of pumps, their positions, and activity, is under control from aldosterone, catecolamines, insulin, and thyroid hormones, among others.

The Nernst equation (Section 7.6.2) was presented as an equation valid for redox electrode processes in electrochemistry. The Nernst concept is also used for the calculation of the potential difference across a membrane that separates two electrolyte compartments with different ion concentrations. Exchanging the natural logarithm with the common logarithm and putting $n = 1$ and temperature $37\text{ }^\circ\text{C}$, Eq. 7.9 becomes:

$$V = -61 \log\left(\frac{c_e}{c_i}\right) \text{ [mV]} \quad (5.1)$$

where c_i and c_e are the intracellular and extracellular concentrations of one ion species. With external concentration of K^+ , for example, that is 10 times larger than the internal concentration, the intracellular potential is -61 mV .

With more than one ion species present, the extension of Goldman (1943) is used with Na^+ , K^+ and Cl^- ions, for example:

$$V = -61 \log\left(\frac{c_{i\text{Na}^+}P_{\text{Na}^+} + c_{i\text{K}^+}P_{\text{K}^+} + c_{i\text{Cl}^-}P_{\text{Cl}^-}}{c_{e\text{Na}^+}P_{\text{Na}^+} + c_{e\text{K}^+}P_{\text{K}^+} + c_{e\text{Cl}^-}P_{\text{Cl}^-}}\right) \text{ [mV]} \quad (5.2)$$

where P is the permeability [m/s].

The Donnan effect (Section 7.6.5) is a special case for the use of the Nernst concept on membranes. Consider a membrane permeable to all inorganic ions but not to charged macromolecules (proteins) or charged colloidal particles. The presence of such macromolecules on only one side of the membrane will change the distribution of the small ions that are free to cross the membrane.

The polarized potential of excitable human cells is found in the range -40 mV to -90 mV .

Some of the organelles inside the cell, such as mitochondria, have their own membranes, which are presumably built the same way as the cell membrane with BLM and membrane channels.

5.2 Action Potential

A polarized and excitable cell may suddenly be *depolarized*. Gates in ion selective channels suddenly open, and ions flow passively with the electrochemical gradient through the channel until the intracellular charge is more or less neutralized and the gate is again closed. Cole and Curtis studied the nonlinear effects of excitable membranes in the late 1930s. In 1939, Hodgkin and Huxley succeeded in measuring the voltage inside a nerve cell for the first time. They showed that during a nerve impulse the intracellular voltage reversed, such as from -70 mV to $+30\text{ mV}$. Therefore, this could not be due to a simple

short circuiting effect caused by increased membrane conductance; it must be due to an ion flux phenomenon. In a series of five remarkable articles in 1952, they and Bernhard Katz gave the now classical description of the voltage sensitive opening and closing of separate channels for Na^+ and K^+ in the cell membrane. This achievement was awarded with the Nobel Prize in 1963.

5.2.1 Ion Channels

An ion channel is a protein embedded in the cell membrane. The protein consists of an ion filter and a gate. Channels are usually described in terms of their selectivity and gating mechanism. Due to the selective permeability to ions, the cell membrane may be described as an electrochemical membrane. An open channel is highly selective; the permeability for K^+ may, for instance, be 1000–10,000 times higher than for Na^+ . The anion channel macroprotein for Cl^- is very different from the cation channel protein of Na^+ or K^+ , for example (Jentsch, 2002). The selectivity is not due to ion size but to the charge spatial distribution in the filter part of the protein. Channel capacity is high; a K^+ channel can let through 200 million ions per second. If the channel is open only 1 ms, then 0.2 million ions are let through in each trigger event. As a monovalent ion corresponds to an electric charge of 0.16 aC [attocoulomb = 10^{-18} C], this corresponds to a charge of 32 fC. If one cell membrane has 10 million channels, a charge of 0.32 μC flows out of the cell into the extracellular gel.

5.2.2 Channel Gating

Normally, channels have closed gates. A gate can be opened by a voltage change or the arrival of a ligand. If it is voltage-gated, it is the voltage across the cell membrane that determines whether a channel is opened or remains closed. The motor nerve axon has voltage gated sodium and potassium channels.

Figure 5.4 shows the potential and conductance waveforms after stimulus application. There is a delay before the potential starts to increase in the positive direction. Then, the sodium channel gate opens and Na^+ flows into the cell; the cell is depolarized. The potential crosses the zero line and soon reaches its maximum positive potential. The opening of the K^+ gate is slower and the opening time is longer than for Na^+ . After gate closing, the cell repolarizes and the potential goes negative—even more negative than the initial level. During depolarization, the cell can not be retriggered (the *refractory* period) before the cell is repolarized. Figure 5.4 shows the most basic and fastest signal source in the human body, the action potential, and the sudden change in channel conductance. The frequency content of the signal is up to a few kilohertz, but this can only be recorded very near the cell. At a larger distance, the geometry may act as a low-pass filter (Section 6.4.1).

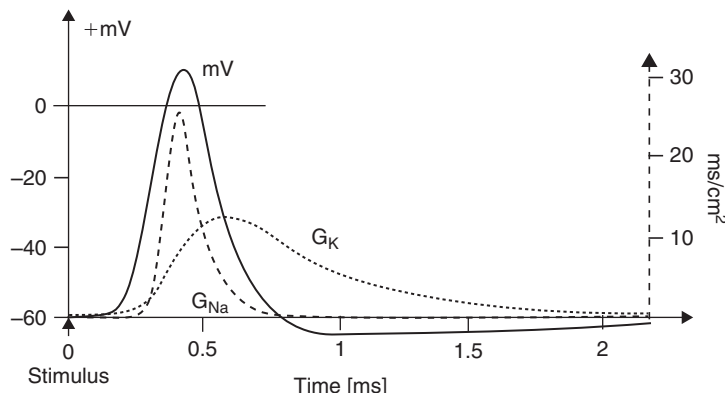


Figure 5.4: Intracellular potential and cell membrane conductance during cell excitation in a mammalian neuron.

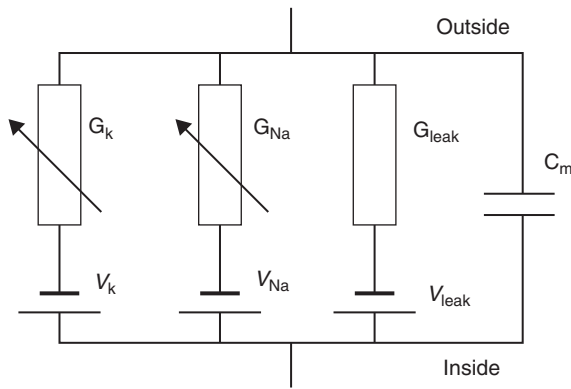


Figure 5.5: A simple electrical model of a cell membrane. *From Hodgkin and Huxley (1952), with permission.*

Each gated channel may be modeled by electromotive voltage (emv) in series with an electrical resistance (Figure 5.5). The BLM membrane capacitance of approximately $1 \mu\text{F}/\text{cm}^2$ is in parallel and is an important time constant parameter of the system. The changes in intracellular potential mean that the membrane capacitance is charged and discharged.

If suddenly the channels (Figure 5.5) open so that the intracellular potential changes abruptly, the ions must also supply a transient discharge current of the membrane capacitance. At the extracellular side, the current is not with respect to a far-away reference electrode, but concentrated to an interstitial fluid zone near the cell. The current flow can be modeled with local current dipoles and is clearly measurable with unipolar or bipolar pickup electrodes in the interstitial liquid. When the cell is depolarizing, cations

and anions flow in all direction through the open channels, but it must be a net flow of anions out of the cell. If the internal mechanical pressure is not to fall or rise, neutral water molecules must also have their gated transport channels.

In the actual situation, there are many channels that may be represented by a surface layer of distributed dipoles. This layer can at a distance be simplified to one net dipole representing one or more cells.

5.2.3 Cell Potential Model

Consider a cell model such as the one in [Figure 5.6](#), with the cell interior completely insulated from the outside by a perfect membrane without channels. The intracellular and extracellular electrolytes are very conductive. The interior has been polarized by an initial transport of some cations out from the interior and into the extracellular volume.

The interior has a well-defined electrical capacitance with respect to the outside. Double layers are formed in the electrolyte/membrane interphase both internally and externally. The measured intracellular potential includes the potential of these charged double layers ([Section 7.5](#)). A double layer has a thickness on the order of 0.1–10 nm, and the cell membrane is approximately 7 nm. The total measured BLM capacitance, double layers included, is about $1 \mu\text{F}/\text{cm}^2$. The charge q necessary to obtain a voltage U across a capacitor is $q = CU$ [coulomb]. With a cell radius of $2 \mu\text{m}$, the membrane area is $A = 4\pi r^2 = 50 \times 10^{-12} [\text{m}^2]$. With $V = 60 \text{ mV}$, the charge is $q = 0.5 \text{ pC}$. Because a

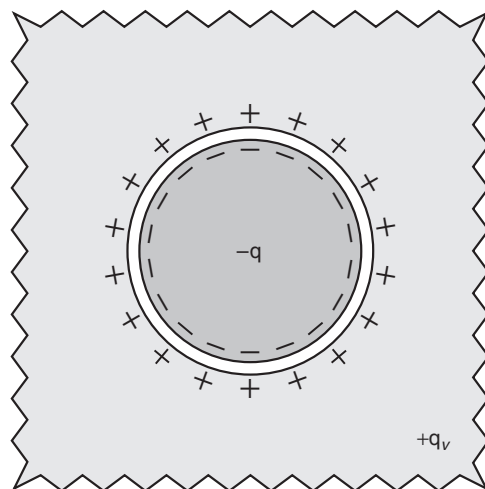


Figure 5.6: Static cell model with perfect insulating tight membrane and conductive electrolytes. Initially, some intracellular cations have been transported out of the cell into the extracellular infinite volume.

monovalent ion has a charge of 0.16 aC, approximately 3 million monovalent ions must have been removed from the cell interior to obtain 60 mV. This calculation is not based upon the Nernst concept because the permeability of the membrane is zero. The calculation is based upon the charge of the membrane capacitance.

The basic capacitor model (Chapter 3) is a dielectric between two metal plates with free electrons. In the cell model, the metal plates are replaced by electrolytes with free ions. In the static case with no leakage across the membrane, there is no current flow inside or outside the cell. At the inside membrane, a *surface charge density* q_{sf} of free ions neutralizes the electric field in the membrane plus the double layer charges, so that the cell interior has $E = 0$ and no current flow. There is electroneutrality in the bulk, but surface charges at the interphase. The intracellular bulk volume has a potential, but zero electric field strength. The membrane has a bound surface charge density q_{sb} , which will reduce the membrane E-field to $(q_{sf} - q_{sb})/\epsilon_0$. Thus, the E-field in the membrane is *less* than the potential difference divided by the membrane thickness.

Can the intracellular static voltage be measured from the outside without a unipolar electrode penetrating the membrane? The intracellular net charge creates a charged layer at the outside surface of the cell. In this way, the cell will migrate in an applied extracellular electric field, and this migration can be measured (electrophoresis). The charges are very near the cell membrane surface, and in the extracellular bulk electrolyte no potential related to the intracellular charge can be measured.

Now let us introduce passive ion channels in the membrane of a polarized cell ([Figure 5.7](#)). The channels are normally closed, but now suddenly opened. Due to the potential difference, cations will immediately start to migrate into the negative cell interior. A current density field is suddenly created both intra- and extracellularly. The extracellular current density vector field \mathbf{J} and the potential field Φ are related by Eq. 2.1: $\nabla \Phi = -\mathbf{J}/\sigma$. The current is generated by the ionic flow, and it terminates on the membrane capacitor in a discharge/charge process.

An *action potential* can accordingly be measured by nearby electrodes with a unipolar or bipolar technique.

The cell potential models of [Figures 5.6 and 5.7](#) are very simplified in order to obtain a basic understanding of the current density and potential fields. They represent a macro view of a system with very small dimensions; in particular, the thickness of a human cell membrane is only approximately 7 nm and the channel protein charge positions are accurate to within an ångstrom (0.1 nm). In addition, the real cell membrane is covered by a very dynamic system of receptor molecules and other components. Also, electrolytes in contact with proteins have thin charged double layers formed at the interphase.

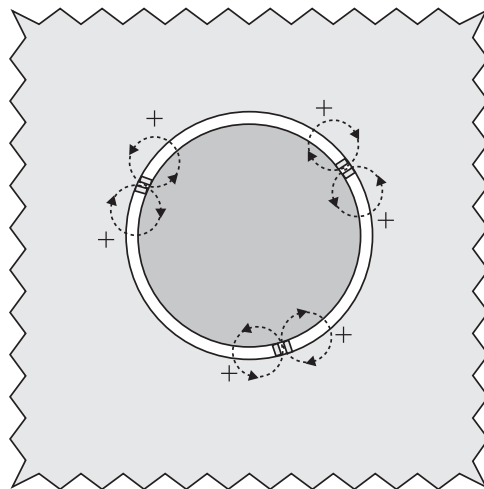


Figure 5.7: Polarized cell just after the opening of three ionic channels resulting in a sudden inflow of cations.

5.2.4 Cell Oscillator

Figure 5.5 shows a leakage conductance in parallel with the other ion channels. If the leakage current is larger than the net pumping current, the cell is slowly depolarized; if it is voltage gated, it may reach the trigger level. The cell has become a free-running oscillator with a frequency determined by the trigger level, the membrane capacitance, and the balance between the polarizing and leakage currents.

5.3 The Neuron

A neuron (nerve cell) consists of: (1) soma (cell body), (2) dendrites, (3) transmission part (fiber), and (4) output terminals (synapses). The cell nucleus and organelles are in the soma; organelles are also spread out along the axon. Dendrites represent the neuron input and a single long axon the output. Neurons have very different forms and sizes with respect to axon length (up to 1 m), number of dendrites, size and position of the soma, and number of presynaptic terminals (up to 100,000).

Figure 5.8 shows some typical neuron morphologies. The motor neuron is found in the spinal cord. It is an efferent type bringing information from the central nervous system (CNS) to a muscle or gland, for example. The receptor type is an afferent neuron with a special direct axon coupling between the receptor and the CNS. The pyramid morphology is found in the cortex of the brain.

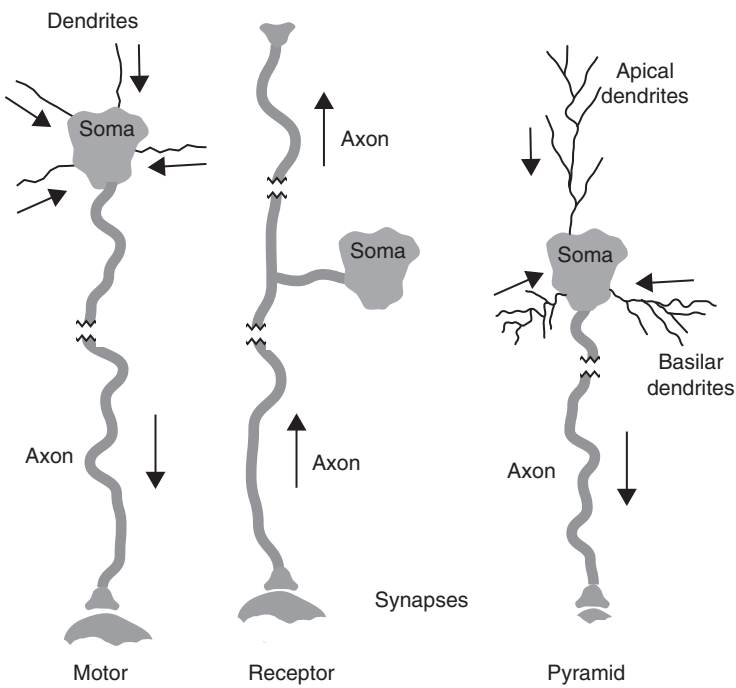


Figure 5.8: Typical neuron morphologies.

5.3.1 Motor Neuron

Figure 5.9 shows an example of a motor neuron (neuron with an axon leaving the CNS). Presynaptic terminals from other neurons are connected to the dendrites and also directly to the soma. Presynaptic terminals on the dendrites are excitatory; approximately 5% of all dendrites are directly on the soma and most of them are inhibitory. One neuron has one

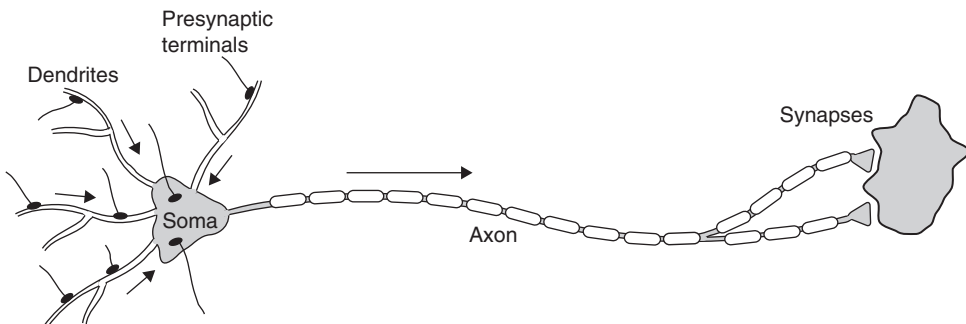


Figure 5.9: Motor neuron with myelinated axon.

soma and one axon. The changeover zone between the axon and the soma is the hillock. The inhibitory presynaptic terminals on the soma are almost a gate for the excitatory signals from the dendrites on their way to the hillock. The soma integrates all inputs, and the response is all or nothing. If the neuron is triggered, the action potential starts in the hillock. The excitation then spreads down the axon to the end where the axon terminates in one or more synapses, coupled, for instance to a muscle, gland, or another neuron.

The neuron may respond not only to electrical input; mechanical pressure and chemical substances may also act as input signals. The difference between a neuron and a receptor may thus be small ([Section 5.5](#)).

5.3.2 Brain and Neurons

The three most important parts of the brain are the cerebrum, brainstem, and cerebellum. They are covered by several membranes. Between the skull and the brain, there are three membranes (meninges): dura mater (two layers), arachnoid (resembling a spider's web), and pia mater. The pia mater is in direct contact with the cortex, and between the pia mater and the arachnoid there is space for the highly conductive cerebrospinal fluid (CSF).

The cortex is the outer part of the cerebrum. The phylogenetic newest part is the human cortex, the neocortex. It is 2–5 mm thick, covers all convolutions of the cerebrum, and probably comprises about 10 billion neurons with about 1000 billion connections. The cells of the cortex are of three types: granular, fusiform, and pyramidal. Cortical neurons are strongly interconnected and are the principle source for the electroencephalogram signals registered on the head. The superficial layer is often referred to as *gray matter*. The cells there are of two types: pyramidal and nonpyramidal. The next layer is white matter, consisting of axons and connective tissue. The cortex is organized vertically (z-direction) in six layers (lateral x–y direction) and in the sensory cortex also in vertical columns. A neocortical column may have a diameter of about 0.5 mm. The neurons in a column communicate in short range x–y directions and longer range z-directions. Axons may be oriented vertically through some of these layers, or laterally to neighboring areas. Some cortical areas have primary somatic sensory functions (e.g., vision or hearing) and other primary motor functions (e.g., hand skills). Large areas cannot be assigned to any specific function.

The brainstem is a prolongation of the spinal cord and is the eldest part of the brain, taking care of basic functions necessary in all vertebrates.

The cerebellum is a motion computer optimized for rapid movement control in animals and humans.

Electrical Properties

Section 4.2 and Table 4.1 give some basic electrical properties of tissue relevant for the brain. [Figure 5.10](#) shows a simple electrical model of the brain with the layers to be passed by an electrical current. The cortical brain with its neurons is the main endogenous signal source. The pia mater and the scull have low conductivities, the brain and scalp have medium conductivity, and the blood and CSF have high conductivities. The skull is a mechanically strong bone structure with relatively low electrical conductance estimated as being about 20 times lower than that of the scalp or the brain (Oostendorp et al., 2000). This ratio is important because it determines, for instance, the current path between current carrying scalp electrodes. If the current-carrying electrodes are near to each other, a large part of the current may flow in the scalp with a small penetration into the brain. These two layers result in substantial signal attenuation from the endogenous sources to the surface pickup electrodes.

[Figure 5.11](#) illustrates the signal attenuation effect of layers between the pickup electrodes and a current dipole volume. Let the dipole be supplied by a constant current. The arrows symbolize the magnitude and direction of the current density generating potential differences at the electrodes. [Figure 5.11\(a\)](#) illustrates the direct contact with the cortex, resulting in a rather high pickup voltage u_1 . [Figure 5.11\(b\)](#) shows that with a poorly conducting layer (e.g., skull), the current density in the skull will be small; however, the resistivity is high so that $u_2 \approx u_1$ as long as the layer is thin with respect to dipole length. [Figure 5.11\(c\)](#) shows that a second well-conducting layer (e.g., scalp) has been added. Current will pass perpendicularly through the skull into the scalp, easily pass the scalp, and then return through the skull to reach the minus pole. However, the current density in the top layer will be small and, as the resistivity also is low, u_3 will be smaller than u_1 . The skull/scalp combination has a signal attenuation effect dependent on the conductivity ratio between the layers and the thickness of the layers.

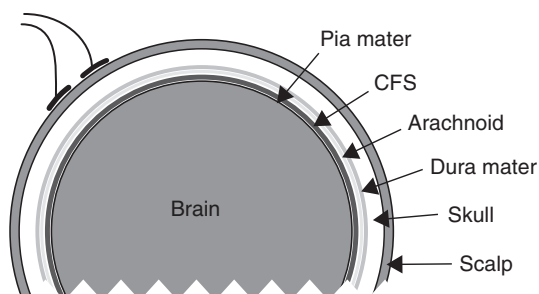


Figure 5.10: Model of the brain with membranes, skull, and scalp.

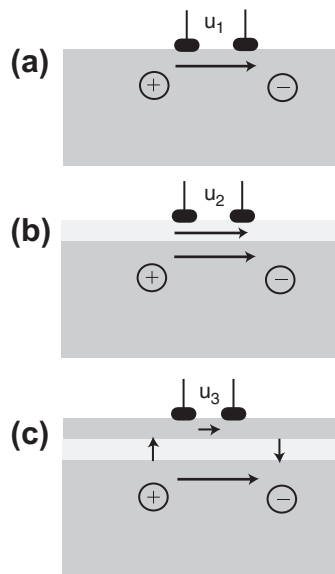


Figure 5.11: Signal transfer from deep current dipole to surface pickup electrodes and the effect of layers. (a) Without layer. (b) With poorly conducting layer. (c) With well-conducting layer on top of the poorly conducting layer. Arrows represent direction and magnitude of E-field.

5.4 Axon Transmission

The brain is the only organ with a large volume of nerve tissue. Nerve tissue elsewhere may be regarded as cables with coupling nodes (plexus), and electrical cable theory is often applied. The naked axon diameter is of the order of $20 \mu\text{m}$, and the length can be 1 m.

5.4.1 Excitation from the Soma

The excitation front shown in [Figure 5.12](#) is initiated by the soma, enters the axon, and propagates to the right. The velocity in a naked, nonmyelinated axon is low (C-fiber) and of the order of 1 m/s. If the sum of the depolarization and repolarization time is 1 ms, the length of the depolarized part is thus 1 mm (outside the drawing in [Figure 5.12](#), bottom). It is clear from [Figure 5.12](#) that the border line between polarized and nonpolarized part of the axon can be treated as the orientation of a dipole field generated by the membrane current. In the extracellular electrolyte, current flows from the positive (polarized) part to the negative (depolarized) part as shown on [Figure 5.12](#) and according the usual convention in the literature. The current is accompanied by a

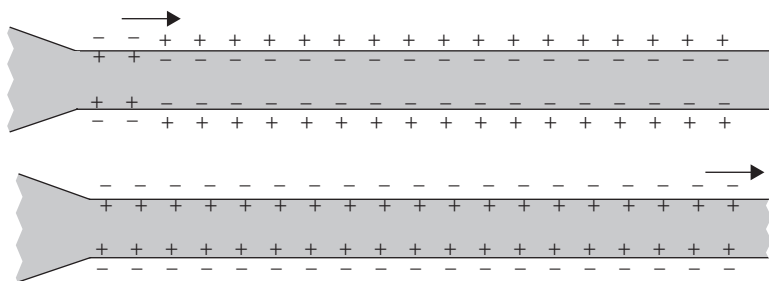


Figure 5.12: Upper: The soma on the left initiates an action potential transmission along the axon. Lower: A later snap-shot.

potential field, and therefore the action potential can then be measured by extracellular electrodes.

5.4.2 Exogenic Excitation of the Axon

The axon has no unidirectional mechanism. If triggered by an external current anywhere between its ends, the impulse propagation will go in both directions, as shown on [Figure 5.13](#). How will the soma react?

5.4.3 Moving Current Dipole

The propagation of the action potential signal through tissue is occurring with an accompanying low-pass filtering effect (Section 6.4.1).

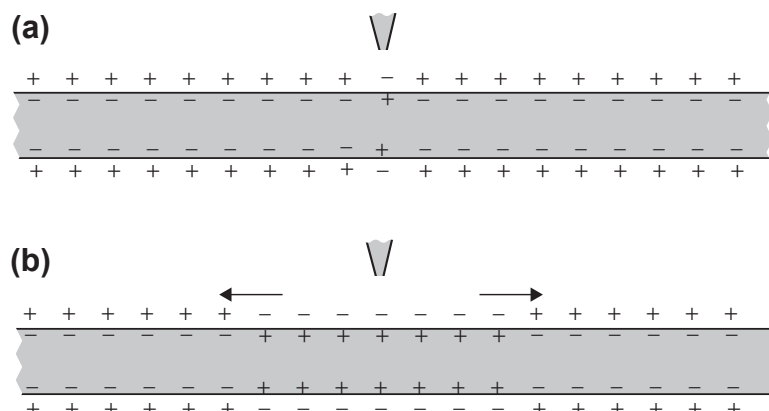


Figure 5.13: (a) Initial external excitation by a unipolar electrode and (b) propagation in both directions.

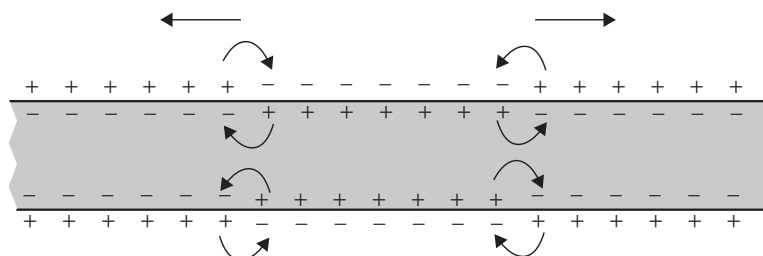


Figure 5.14: Moving dipoles in both directions as a result of an exogenous excitation. Arrows symbolize conventional current direction from plus to minus (direction of cation flow).

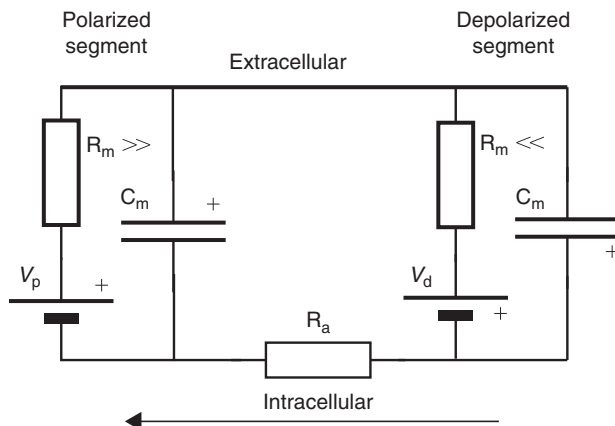


Figure 5.15: Equivalent circuit of fig. 5.14 for the axon action potential propagation process in the direction of the arrow. Per axon length, R_a is the intracellular resistance, R_m is the membrane resistance, and C_m is the membrane capacitance. V is the Goldman-related emv (Eq 5.2).

The current flow directions indicated in Figure 5.14 are so that the intracellular flow is in the direction of the impulse propagation. When making an equivalent electric circuit for the process (Figure 5.15), the thin axon interior has a much larger resistance R_a than the large volume extracellular resistance, which therefore is omitted. The current is the charging/discharging current of the membrane capacitance. The propagation velocity is to a large extent determined by the time constant of the axon resistance and the membrane capacitance: $\tau = R_a C_m$.

5.4.4 Myelinated Axons

The propagation velocity in a nerve fiber can be increased by myelination of the axon. For unmyelinated fibers, the propagation velocity increases with the square root of the fiber diameter; in thin fibers, it can be as low as 0.5 m/s (Table 5.1). The myelin sheath

Table 5.1: Nerve Diameter and Propagation Velocity.

		Diameter [μm]	Velocity [m/s]	Example of Function
α	Myelinated	15–20	60–100	Skeletal muscle
β	Myelinated	5–15	30–90	Vibration, high precision touch
γ	Myelinated	1–10	6–60	Muscle spindle
δ	Myelinated	1–5	6–30	Deep pressure
C	Unmyelinated	0.5–2	0.5–2	Sympathetic, pain, tickle, crude touch and pressure

surrounds the axon like the insulation of an electric cable. The myelin may be thicker than the axon itself (about 20 μm) and is made of a lipid with very low conductivity. The axon membrane thickness is effectively increased, and the effective capacitance decreased. The myelin sheath is interrupted about every millimeter by a node of Ranvier. The result is a higher velocity, up to 100 m/s. A Ranvier node is a few microns of naked cell membrane. The result is propagation in a saltatory way from node to node (Figure 5.16).

5.4.5 The Nerve

A nerve is a collection of nerve fibers (fascicles). Axons must be electrically isolated from each other to maintain channel separation. Each axon, naked or with myelin, is therefore spirally enwrapped by a thin sheath or membrane (neurilemma). Axons are grouped in a bundle (funiculus) surrounded by its own sheath of connective tissue (perineurium). Within a bundle, the fibers are packed with interstitial connective tissue (endoneurium). Many bundles constitute a nerve. The outermost part of a nerve is a sheet of connective tissue (epineurium). A nerve bundle usually contains both efferent fibers (motor fibers, signal direction toward periphery) and afferent fibers (receptor signals toward CNS).

As each of these sheets and membranes have different thicknesses and conductivities, they play an important role in determining current density fields and the exogenic excitation threshold.

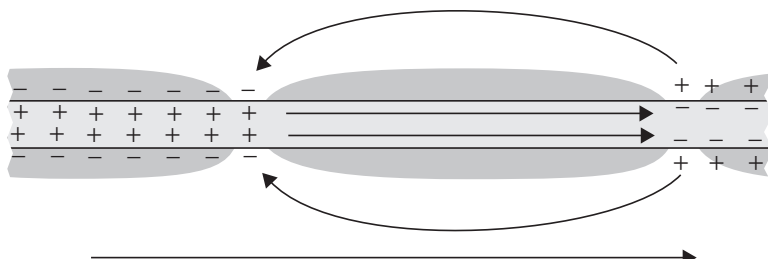


Figure 5.16: Myelinated axon, with saltatory propagation from node to node.

5.4.6 Synapses

The synapse is the region where signal coupling between, for example, two neurons takes place. In the synapse, the signal may pass, may be blocked, or may be modified. In the animal world, there are two types: the chemical and the electrical synapse.

Chemical Synapses

Most of the synapses in the CNS are chemical. A ligand gated membrane channel may be directly activated by neurotransmitters secreted at the synapse by the transmitting neuron. The neurotransmitter acts on receptor proteins called ligands on the surface of the receiving neuron. The chemical synapse allows only unidirectional traffic. The neuron that secretes the neurotransmitter is presynaptic; the signal receiving neuron is postsynaptic. The chemically activated ion channels in the postsynaptic neuron are called ligand activated channels. Over 30 different neurotransmitters are known, and they have excitatory or inhibitory effects depending on the receptor properties. Neurotransmitters are substances such as adrenaline, acetylcholine, or dopamine conveying signal transmission across the synapses.

Electrical Synapses

In the electrical synapse, the distance between the cell membranes are just a few nanometers and much shorter than in the chemical synapse. The joining membranes open a direct channel between the intracellular compartments in the form of small tubules (*gap junctions*), allowing direct ionic flow. Gap junctions are found in the visceral smooth muscles and in the cardiac muscle. Gap junctions allow direct signal transmission in both directions between neighboring muscle cells so that each cell does not need a direct innervation.

Target Tissue

Target tissues are often the other neurons. The action potential arrives along an axon, which splits up in several synapses. These act as presynaptic terminals on other neurons. Other target tissue types are muscles, where a part of the muscle called a muscle group is innervated. Other targets are internal organs, blood vessels, intestines, and glands (eyes, sweat, saliva, tears, endocrine).

5.4.7 Excitation

Neuron excitation is dependent on the total information entering from all presynaptic terminals. Because there are thousands of inputs, no single input has any decisive influence. The inhibitory inputs have largest influence because there are much fewer inhibitory than excitatory presynaptic terminals.

In the nerve system, there is summation—both spatial and temporal. This is easily illustrated with skin receptors. If a variable skin contact area electrode is used for the examination of electric current perception, it is found that the current density threshold is dependent on the contact area. As the area is increased, the current density threshold is lower because of the summation effect of the receptor responses in the skin (Martinsen et al., 2004). Because of the temporal summation, the excitatory signals must be synchronized in order to trigger the neuron. However, slow changes of the presynaptic DC levels may also make a cell more or less excitable. Such level shifts are according to the Nernst concept and are also under hormonal control.

5.4.8 External Electric Excitation

A current carrying electrode is used to trigger (excite, pace) a nerve. The electrode may be on the skin (transcutaneous excitation), as a needle inserted through the skin, as a catheter electrode, as a part of an active implant, or as a microelectrode into an exposed nerve or axon.

Trigger Parameters

The choice of the best parameter for defining a trigger level is difficult. The level may be expressed as current [mA], current density [mA/mm^2], voltage [V], electric field [V/m], charge [C], energy [J or Ws], or power [W].

We have seen that a cell basically must move a net number of ions in order to approach the trigger level ([Figure 5.7](#)). For a single cell, the charge was calculated to be of the order of 0.5 pC. The polarized cell is positively charged at the external cell surface. Therefore, there is reason to believe that a short negative polarity pulse from an external electrode would decrease the membrane potential and thus be excitatory. This is according to experimental evidence: the trigger level is lower with negative pulses.

Basically, we may guess that the preferred parameter is electric charge [coulomb], being the membrane capacitance charge. However, with extracellular electrodes, we do not have direct access to the cell interior, and most of the charge supplied by the electrodes is lost in the tissue volume far from the cell. The current density near the cell surface therefore is the basic parameter, or alternatively the electric field.¹ As the current density or electric field usually are unknown, it is common practice to use accessible parameters—that is, those which can be measured in the electrode lead wires: current, charge, energy, or power. Usually, a current controlled rectangular pulse generator is used. The pulse duration

¹ Actually, the two major organizations that set up guidelines for exposition to low-frequency electromagnetic fields now identify the electric field inside the body (outside the cell) as the relevant quantity, and have abandoned the current density for that purpose. ANSI/IEEE C95.6:2002, ICNIRP 2010.

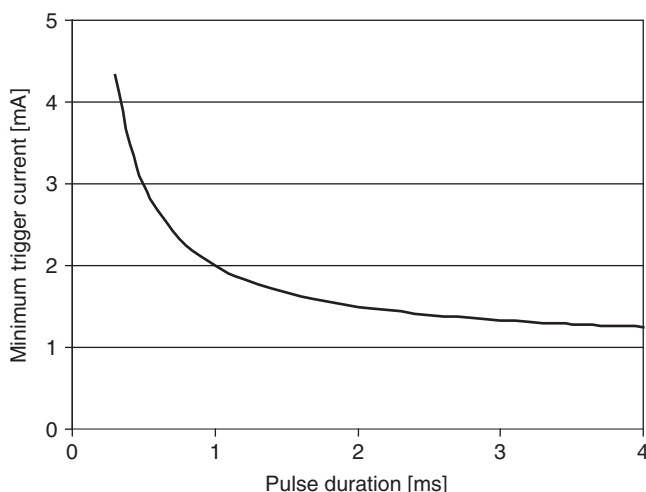


Figure 5.17: Current level versus pulse duration, according to the hyperbolic rheobase model.

and current level are selected, which then actually is the charge $q = It$. If the generator voltage waveform also is measured, the power or energy can be determined. A defibrillator pulse is defined with the energy parameter [Ws or joule]. This is from practical reasons because the pulse is delivered by a large charged capacitor. A pacemaker pulse is also given as current and pulse duration, which is in reality electric charge.

Waveforms

The most used current waveform is rectangular monophasic or biphasic. With defined electrode/tissue geometry, there is a relationship between the pulse duration and the current level necessary for nerve excitation. [Figure 5.17](#) shows an example; as the pulse duration increases, the necessary current approaches asymptotically a baseline current called the rheobase. The chronaxie is the pulse duration with the double rheobase current.

Weiss (1901) and the Lapicque (1907) presented slightly different models of current-duration relationships for rectangular pulses (Reilly, 1998). Weiss used the equation

$$I = I_0 \left(1 + \frac{\tau}{t} \right) \text{ (hyperbolic)} \quad (5.3)$$

and Lapicque used:

$$I = I_0 \left(1 - e^{-\tau/t} \right)^{-1} \text{ (exponential)} \quad (5.4)$$

where I is the minimum current for excitation with a pulse width t , τ is a time constant characteristic for the nerve tissue and electrode geometry, and I_0 is the

rheobase current. τ for motor nerves may be approximately 0.3 ms and for myocard 3 ms.

[Figure 5.17](#) shows a calculated current-duration graph with linear scales based on the hyperbolic model with normalized values: rheobase current 1 mA and chronaxie 1 ms. In the hyperbolic model, the chronaxie is equal to the time constant. The charge necessary for triggering is constant at short pulse durations and increasing with longer pulses. The energy necessary for triggering goes through a minimum near the chronaxie.

The empirical current-duration relationship is in somewhat better accordance with the hyperbolic model than the exponential, but the exponential model is directly derived from the electric circuit model with a current source supplying an ideal resistor and capacitor in parallel. The empirical current-duration relationship is different for myelinated and naked axons. Also, it must be remembered that the excitation process is nonlinear and not easily modeled with ideal electronic components.

Electrotonus and rheobase are further discussed in Section 10.13.

5.5 Receptors

Receptors transduce specific types of energy into a nerve signal. The nerve signal being electrical actually means that receptors qualify as purely biological biosensors. They are selective and have a narrow range of stimulus energy levels. There are five types of receptors:

1. Mechanoreceptors (skin, joint, ear, vessel, muscle)
2. Thermal receptors (warm and cold)
3. Chemical (itch, taste, smell, carbon dioxide, oxygen)
4. Pain (nociceptors)
5. Electromagnetic (eye)

A receptor may consist of free nerve endings or specialized organelles. Some of them couple to axons, not dendrites. Nociceptors are coupled to slow, thin, nonmyelinated axons (C-fibers). Muscle spindle receptors monitor the muscle tension and the electrotonus. Some receptors are sensitive to static energy levels; other monitors the rate of change of stimulus energy, such as the Pacinian corpuscles, which are sensitive to vibration.

5.6 Problems

1. Use the Nernst equation to find the potential difference across a cell membrane where the concentration of potassium on the outside is 5 times higher than on the inside. Should the calculation have been done with the Goldman equation?

2. Calculate the change in intracellular potential if 2 million Na^+ ions are transported out of the cell. The cell diameter is $10 \mu\text{m}$, membrane capacitance is $1 \mu\text{F}/\text{cm}^2$, ion charge is 1.6×10^{-19} [coulomb], and $q = \text{UC}$.
3. Find the difference between the Weiss and Lapique equations if $t/\tau = 10$.
4. Define an action potential. Must it be measured with an intracellular microelectrode?

This page intentionally left blank

Geometrical Analysis

Important electrical characteristics of an electrode/tissue system are determined solely by the geometrical configuration. To clarify this important function, the systems to be treated in Chapter 6 are simple models suited for basic analysis and mathematical treatment as well as computational approaches such as finite element analysis (Section 6.5). In bioimpedance systems, the biomaterial is usually an ionic wet conductor, and the current carrying electrodes are polarized. However, in this chapter, the models are idealized in several ways. Biomaterial is considered homogeneous and isotropic. An electrode is considered isoelectric (superconducting metal). Only DC systems without polarization phenomena and frequency dependence are considered. Then a *potential* difference between two points in tissue space is equal to the *voltage* difference found between two circuit wires connected to the same two points, $\Phi_{12} = V_{12}$. If the value of the potential is known everywhere in space Φ can be interpreted as a potential *field* $\Phi(x,y,z)$, V is simply the voltage difference between two defined points in a wired electric circuit. Φ is a scalar quantity [energy per charge = volt], the current density \mathbf{J} is a space vector and has a current density vector field $\mathbf{J}(x,y,z)$.

All models are volume models, but the field from a long straight cylinder has no changes in the direction of the cylinder axes. For this reason or because of symmetry (e.g., spheres), simplified calculations and two-dimensional presentations give all necessary information for many basic geometry models. This is true when the imaging plane cuts through, for example, the sphere center or cylinder axis.

6.1 Volume Conductors

Figure 6.1 shows two current-carrying (CC) electrodes connected to a tissue volume. In the electrode wires, the flow of electrons is confined to the wires. When the electrode dimensions are smaller than the tissue volume dimension, the ionic current spreads out from a source electrode so that the current density falls with distance from the electrode. Voltage and current in the electrode wires are measured and define the immittance. However, in the tissue volume, the current flow must be defined with both magnitude and direction, and the parameter is current density \mathbf{J} [A/m^2], a spatial vector. The current density field $\mathbf{J}(x,y,z)$ cannot easily be measured and the current density field is often unknown.

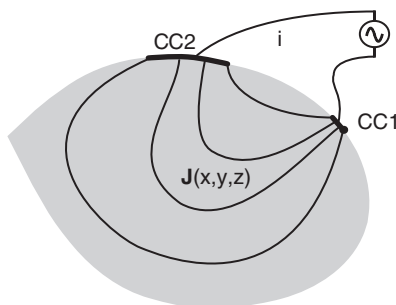


Figure 6.1: Current i [A] in the electrode wires and current density J [A/m^2] in the tissue volume.

The lines drawn in the tissue show current flow direction, the proximity of two lines is the current density magnitude. i is easily measured and known; the $J(x,y,z)$ field is difficult to map and often unknown.

6.1.1 Forward Problem

To find the potential field in tissue caused by a known signal current source is a *forward* problem. The tissue may be inhomogeneous, anisotropic, and of finite dimensions.

Examples are given in [Section 6.2](#). Usually there is one unique solution to a posed problem.

6.1.2 Inverse Problem

In electrophysiology, a body surface potential is often recorded, with the purpose of characterizing the unknown bioelectric source in position, size, and direction. To go from measured potentials in a known conductive medium and calculate back to the source properties is called an *inverse* problem. Usually there are *infinitely* many possible solutions to a posed problem (see Figure 8.11(c)). Important classical patient examination methods such as electrocardiogram and electroencephalogram are aimed at characterizing properties of the source organ, and are thus based upon more or less empirical solutions to the inverse problem.

6.1.3 Boundary Value Problem

In impedance tomography, the problem is a *boundary value* problem. From recorded potentials caused by exogenic current injection, the distribution of conductivity is to be found.

6.2 Sphere Sources, Ideal Three-Dimensional Models

The monopolar sphere is the most basic geometry in the sense that *any* electrode in an infinite homogeneous medium reverts to a symmetrical spherical geometry at

Table 6.1: Parameter Dependence on Distance r from Different Sources in a Homogeneous Medium

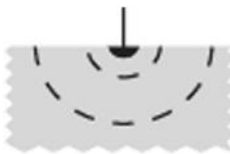
Source	Unipolar PU Φ , [V]	Dipolar PU $\Delta\Phi$ [V], E [V/m], J [A/m ²]	W_v [W/m ³]
Long rod	$\sim \ln(r^{-1})$	$\sim r^{-1}$	$\sim r^{-2}$
Sphere	$\sim r^{-1}$	$\sim r^{-2}$	$\sim r^{-4}$
Dipole	$\sim r^{-2}$	$\sim r^{-3}$	$\sim r^{-6}$

sufficiently large distance. At distance, any electrode geometry corresponds to an equivalent sphere radius.

The spherical coordinate system with the coordinates r , θ , and ϕ is of course well suited for spherical sources. A sphere in a homogeneous medium *disperses* the current radially out in all directions. Because the surface area of a sphere is $4\pi r^2$, the current density falls proportional to r^{-2} . As we shall see, this is in contrast to a line source where the current density falls proportional to r^{-1} (Table 6.1). Because the current spreads out in all directions, a three-dimensional (3D) analysis is necessary, but in a homogeneous medium any plane through the sphere center will show the same two-dimensional (2D) plot.

6.2.1 Sphere Monopole Source

The conductance G of a superconducting hemisphere of radius a , half submerged in a half-infinite homogeneous biomaterial and with a concentric half-spherical reference electrode infinitely far away, is:

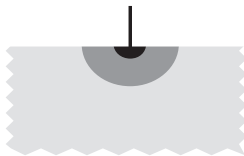


$$G = \sigma 2\pi a \quad [\text{S}] \quad R = \frac{\rho}{2\pi a} \quad [\Omega] \quad (\text{hemisphere}) \quad (6.1)$$

In a real case with a metal electrode in an electrolyte solution, the electrode polarization impedance resulting from the surface layer is physically in series with the electrolytic resistance given by Eq. (6.1). Equation (6.1) shows that the electrolytic resistance is inversely proportional to *radius a* (or circumference $2\pi a$) of the electrode. However, the electrode *polarization impedance* is inversely proportional to a^2 (surface area $2\pi a^2$). Therefore, the influence of the electrode polarization can be made as small as wanted by increasing the sphere radius. Alternatively, by reducing the electrode radius sufficiently, it

will be possible to measure polarization or electrode surface properties selectively, without influence from the electrolytic series resistance.

The resistance contribution of a finite hemispheric *shell* of radius r on the metal sphere of radius a is:



$$R = \frac{\rho}{2\pi} \left(\frac{1}{a} - \frac{1}{r} \right) \quad [\Omega] \quad (\text{hemispheric shell, } r \geq a) \quad (6.2)$$

Accordingly, 99% of the total resistance is within a sphere of radius $100a$, and 90% within a sphere of radius $10a$. The resistance value measured with a small spherical monopolar electrode may therefore show good spatial selectivity. A concentric hemisphere is an equipotential surface, and the surface can therefore be covered by a thin metal sheet acting as one electrode. It is not a neutral electrode until r is large. As a neutral electrode, a hemispherical electrode with $r \rightarrow \infty$ is equal to an infinite area bottom plate at infinite distance (Figure 6.2).

Injecting a current I into a hemisphere, the current density \mathbf{J} in the tissue volume in radial direction is:

$$J = \frac{I}{2\pi r^2} \quad [\text{A/m}^2] \quad (\text{hemisphere, } r \geq a) \quad (6.3)$$

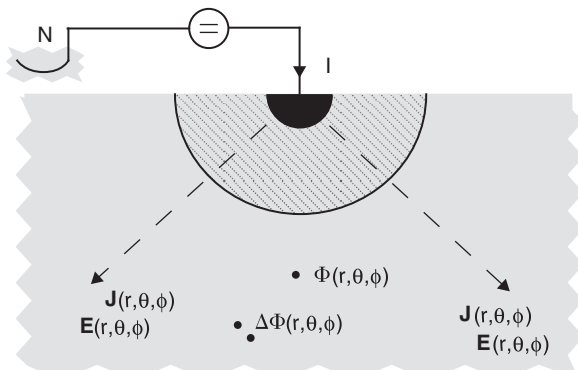


Figure 6.2: Vector fields caused by a monopolar, hemispherical surface source shown with a corresponding arbitrary equipotential hemisphere. N is an ideal neutral electrode infinitely large at infinite distance.

The voltage V is applied relative to the infinitely remote reference electrode with $V = 0$ (Figure 6.2). The current I to the hemisphere electrode is $I = V\sigma 2\pi a$. The scalar potential field Φ in the medium (forward problem) is:

$$\Phi = \frac{Va}{r} = \frac{\rho I}{2\pi r} \quad [\text{V}] \quad (\text{hemisphere}, r \geq a) \quad (6.4)$$

Notice that V is a voltage supplied by an external wire circuit, Φ is a potential in space.

From Eq. (2.2), $\mathbf{E} = \mathbf{J}/\sigma$ where \mathbf{E} is the *electric field strength* [V/m]. Because $I = V\sigma 2\pi a$, the electric field \mathbf{E} is from Eq. (6.3):

$$\mathbf{E} = \frac{Va \hat{\mathbf{r}}}{r^2} \quad [\text{V/m}] \quad (\text{space vector}, r \geq a) \quad (6.5)$$

where $\hat{\mathbf{r}}$ is the unity radius vector, dimension [1]. The potential difference in a pick-up dipole of length \mathbf{L}_{pu} is:

$$\Delta\Phi = \frac{Va \mathbf{L}_{pu} \cdot \hat{\mathbf{r}}}{r^2} \quad [\text{V}] \quad (r \geq a) \quad (6.6)$$

Note that as sphere radius, $a \rightarrow 0$, then $G \rightarrow 0$ (Eq. (6.1)). With applied voltage V , the potential at the electrode surface $\Phi_a = V$ ($r = a$, Eq. (6.4)). The whole potential drop Φ occurs at the electrode if $a \rightarrow 0$, and no current flows. This is not the result of a polarization; it is a pure function of geometry. However, with applied current I and $a \rightarrow 0$, then at the electrode surface $\Phi_a \rightarrow \infty$, $E_a \rightarrow \infty$ and $J_a \rightarrow \infty$.

Power density $W_v = EJ$ is:

$$W_v = \frac{\sigma(Va)^2}{r^4} = \frac{\rho(\frac{1}{2}\pi)^2}{r^4} \quad [\text{watt}/\text{m}^3] \quad (\text{hemisphere}, r \geq a) \quad (6.7)$$

Power density falls off extremely rapid with distance from the electrode, and the equation formulates the basis of unipolar electrosurgery (Section 10.10). It shows that the diathermy effect is concentrated to a very narrow sheath around the electrode, and with little tissue damage elsewhere in the tissue. The temperature rise ΔT in a tissue volume is:

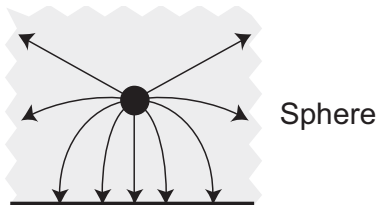
$$\Delta T = \frac{J^2}{\sigma} \frac{t}{cd} \quad [^\circ\text{C}] \quad (6.8)$$

where c is specific heat capacity (e.g., for water 4.2 kJ per kg and $^\circ\text{C}$) and d is the density. With a current density of $J = 200 \text{ mA/cm}^2$, $\sigma = 1 \text{ S/m}$ and $d = 1000 \text{ kg/m}^3$, the temperature rise in the tissue per second is $1 \text{ }^\circ\text{C}$. This is under adiabatic conditions, for example, with no cooling effects from the surroundings (e.g., no blood flow).

Sphere and Conductive Plate

Previously we have analyzed the hemisphere in a half-infinite homogenous medium. The model is changed if the sphere is in a medium of limited dimensions or if

homogeneity is disturbed by, for example, a conductive plate. Let us take the case of an infinite medium but a conductive plate at a finite distance from the sphere. The resistance and conductance can be found from the nonideal current carrying dipole solution ([Eq. \(6.16\)](#)) because the current density field is unchanged if the plane isoelectric area is replaced by a thin metal plate. With respect to the dipole solution, the resistance is halved and the conductance doubled (whole sphere and plate immersed in an infinite medium):



$$G = \sigma 4\pi a \left(1 + \frac{a}{L} + \left(\frac{a}{L}\right)^2 + \left(\frac{a}{L}\right)^3 + 2\left(\frac{a}{L}\right)^4 + 3\left(\frac{a}{L}\right)^5 + \dots \right) \quad (L > 2a) \quad (6.9)$$

where L is two times the distance between the sphere center and the plate, and short circuit between sphere and plate occurs at $L = 2a$.

6.2.2 Constricting/Dispersing Zone

The zone near a small source or sink electrode is the *spreading, dispersing, or constricting zone* of the current path, [Figure 6.3](#). In the spreading zone of a half-sphere, the resistance R is $\frac{\rho}{2\pi} \left(\frac{1}{a} - \frac{1}{r}\right)$ according to [Eq. \(6.2\)](#). However, $R = \rho L/A$ is in the segmental zone in [Figure 6.3](#). With a small sphere, the total resistance will be dominated by the constricting resistance, and then is a monopolar system.

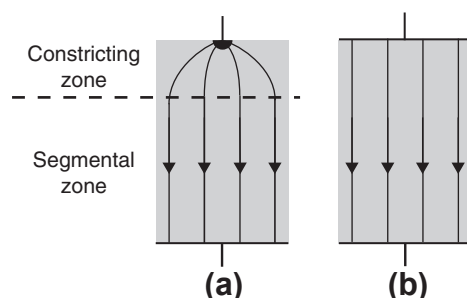
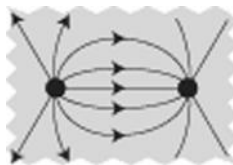


Figure 6.3: Current constriction. (a) Monopolar system where the resistance is increased by the smaller electrode and current constricting geometry; (b) bipolar system.

6.2.3 CC and PU Dipoles

The current carrying (CC) dipole is the most fundamental bioelectric model of endogenic signal sources in biology; the current from the dipole spreads out in the body and must eventually return to the dipole to close the electric circuit. The living cell may be regarded as dipoles spread out on the cell surface area, for example, the cell membrane (Section 5.1). The action potential of a nerve cell may be regarded as being generated by dipoles under motion (see [Section 6.4.1](#)). The sum of millions of muscle cells may be considered equivalent to one single dipole (the heart vector).



The dipole is well known from *electrostatic theory*: by *duality* the electrostatic dipole equations can be used for CC dipoles. Such duality has a limited validity range; this is further discussed in [Section 6.7](#). The CC dipole is defined with two CC spheres of radius a and center-to-center distance \mathbf{L}_{cc} resulting in a dipole moment \mathbf{m} :

$$\mathbf{m} = \mathbf{IL}_{cc} \quad [\text{Am}] \quad (6.10)$$

The direction of \mathbf{L}_{cc} is the dipole axis.

Technically Ideal CC Dipole

An *ideal* CC dipole mathematically defined is a dipole in an *infinite homogeneous* medium where $I \rightarrow \infty$, $a \rightarrow 0$ and $\mathbf{L}_{cc} \rightarrow 0$, keeping \mathbf{m} constant. However, in physics and engineering, the concept of infinitely small CC *points* with infinite current density is not ideal. *We will therefore define the current dipole as technically ideal also with $a > 0$ if $\mathbf{L}_{cc} \gg a$ and the dimensions of the homogeneous volume are much larger than \mathbf{L}_{cc} . The technically ideal current carrying dipole uses the same equations as the mathematically ideal dipoles.*

If the superposition theorem is valid, the scalar potential field can be found by simply adding the potential contribution from each sphere (a forward problem):

$$\Phi = \frac{Ip}{4\pi} \left(\frac{1}{r_1} - \frac{1}{r_2} \right) \quad [\text{V}] \quad (\text{mathematically ideal CC dipole}) \quad (6.11)$$

where r_1 and r_2 are the distances from each sphere to the pick-up (PU) position of Φ .



Equation (6.11) may be expressed with the dipole moment $\mathbf{m} = \mathbf{IL}_{cc}$ and as a vector dot product valid if $r \gg \mathbf{L}_{cc} \gg a$:

$$\Phi = \frac{\rho(\mathbf{m} \cdot \hat{\mathbf{r}})}{4\pi r^2} \quad [\text{V}] \quad (\text{technically ideal CC dipole far away}) \quad (6.12)$$

The vector dot product indicates the directional sensitivity shown in **Figure 6.4**. The potential falls as r^{-2} (**Table 6.1**) in all radial directions except for the special case of \mathbf{r} being perpendicular to \mathbf{m} , then $\Phi = 0$ for any distance.

Equation (6.13) shows the PU potential pick-up from the CC dipole. \mathbf{r}_1 and \mathbf{r}_2 are the distance from the CC dipole to each of the PU dipole poles. In this way, the local electric field strength \mathbf{E} [V/m] in the $\mathbf{r}_1 - \mathbf{r}_2$ direction is measured. $\mathbf{r}_1 - \mathbf{r}_2$ is actually the length of the PU dipole: \mathbf{L}_{pu} .

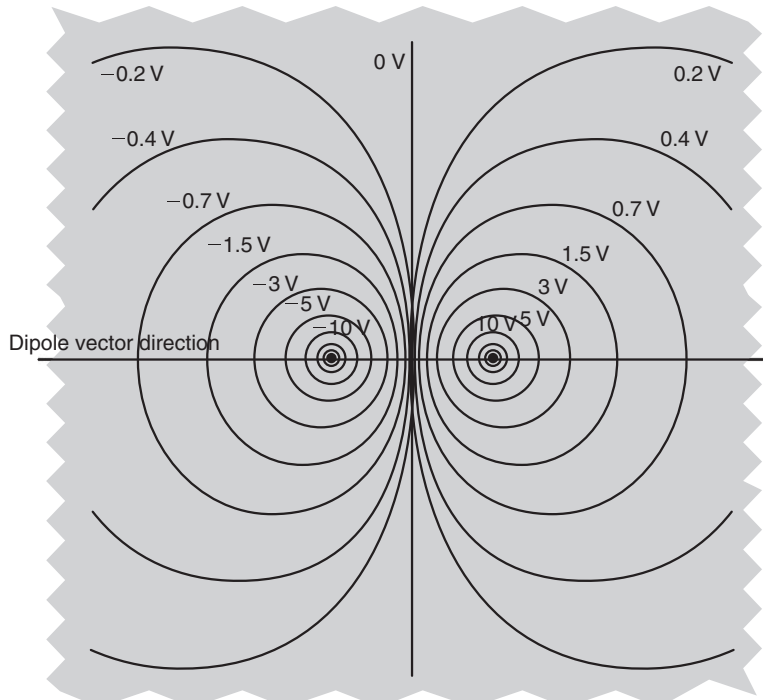


Figure 6.4: Equipotential lines in any plane through a current dipole axis, not referred to as a Cartesian coordinate system. High density of equipotential lines in the center is only due to the arbitrarily chosen voltage range.



$$\Delta\Phi = \left(\frac{\rho}{4\pi r^3} \right) \mathbf{m} \cdot (\mathbf{r}_1 - \mathbf{r}_2) \quad [\text{V}] \quad (\text{technically ideal CC dipole far away}) \quad (6.13)$$

Notice that the Eqs (6.11)–(6.13) do not refer to a coordinate system. Notice also that the dot product is defined with the vectors mathematically moved to obtain a common starting point; physically they are separated by the distance r .

The resistance of the ideal dipole is simply the resistance of one whole sphere multiplied by two:

$$R = \frac{\rho}{2\pi a} \quad G = \sigma 2\pi a \quad (\text{technically ideal CC dipole}) \quad (6.14)$$

Then a large part of the medium between the spheres does not contribute to the resistance.

Figure 6.4 illustrates the potential distribution in a plane through a dipole axis (homogeneous infinite conductive medium). Such equipotential lines are of course the same for any such plane (cylinder coordinates). The model is based upon two CC spheres at a distance L_{cc} apart. Each electrode may be regarded as a unipolar electrode in their proximity zone of the current path, with equipotential lines as concentric circles. Further away, the equipotential lines are not circular. However, in cable theory (Section 6.3), with the poles of **Figure 6.4** being considered as long wires, these equipotential lines are circular but eccentric.

Ideal Pick-up Dipole

Equation (6.13) gave the potential difference $\Delta\Phi$ between two points in the field of a technically ideal current dipole. This potential difference can be picked up by an ideal recording dipole. Such an ideal dipole is not CC and the dipole spheres may therefore approach points. Let the distance r between the two dipoles be large and the PU dipole length L_{pu} be small so that $r_1 \approx r_2 = r$, $\mathbf{r}_1 - \mathbf{r}_2 = \mathbf{L}_{pu}$ and therefore:



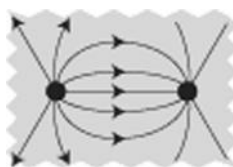
$$\Delta\Phi = \left(\frac{\rho}{4\pi r^3} \right) \mathbf{m} \cdot \mathbf{L}_{pu} \quad [\text{V}] \quad (\text{technically ideal CC dipole and ideal PU dipole at long distance}) \quad (6.15)$$

$\mathbf{m} = IL_{cc}$ is the source, and the mathematically defined ideal current dipole is with $L_{cc} \rightarrow 0$ and $I \rightarrow \infty$, whereas \mathbf{m} is constant. [Equation \(6.15\)](#) shows that the ideal PU dipole is not like this: the potential difference is proportional to L_{pu} , so that sensitivity is lost if $L_{pu} \rightarrow 0$. *The ideal PU dipole is with point spheres but finite dipole length.*

The double dipole model with one current carrying and one PU dipole far away from each other is an important analytical model for studying transfer functions in media (see [Section 6.4.3](#) on the lead field).

Non-Ideal Current Dipole

If the condition $L_{cc} \gg a$ is not met, the superposition theorem is not valid because the introduction of a second superconducting sphere disturbs the current density lines from the first sphere. The conductance of two spheres immersed in an infinite homogeneous medium is:



$$G = \sigma 2\pi a \left(1 + \frac{a}{L} + \left(\frac{a}{L}\right)^2 + \left(\frac{a}{L}\right)^3 + 2\left(\frac{a}{L}\right)^4 + 3\left(\frac{a}{L}\right)^5 + \dots \right) \quad (6.16)$$

(two whole spheres, $L > 2a$)

This equation takes care of the effect that each sphere has on the other. Half-immersed in the surface of a semi-infinite medium the conductance according to [Eq. \(6.16\)](#) is halved. If $L \gg a$, [Eq. \(6.16\)](#) simplifies to [Eq. \(6.1\)](#). Using the factors written out in [Eq. \(6.16\)](#), the error of [Eq. \(6.16\)](#) is $<1\%$ down to the length $L = 3a$ ($L = 2a$ represents short circuit). At $L = 4a$, the ideal dipole solution ([Eq. \(6.1\)](#)) gives only 75% of the true value obtained with [Eq. \(6.16\)](#).

If the conductivity of the spheres is equal to the conductivity of the medium, the current density is not disturbed, but we still have the problem of how to connect the end of the wire to the sphere.

6.2.4 Disk Monopole Source

The disk can be regarded as a flattened sphere (*oblate ellipsoid of revolution*) and the needle as a stretched sphere (*prolate ellipsoid of revolution*). A spheroid is the same as an ellipsoid of revolution.

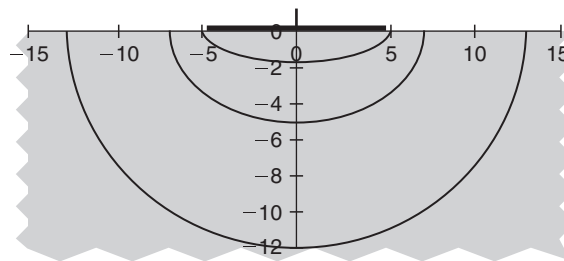
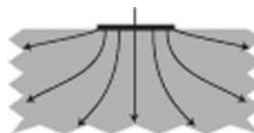


Figure 6.5: Equipotential lines caused by a current-carrying disk electrode at the tissue surface.



Analytical solutions are possible because by letting the length of the axis of revolution tend to 0, we end up with a disk. If positioned on the surface, it is the most common of all electrode geometries. We then discover the often overlooked fact that current is not injected evenly under the surface of such a plate electrode.

Figure 6.5 shows a 2D cut through the center of a surface disk electrode on a conducting homogenous medium. It shows the potential field with a current-injecting electrode plate of radius $a = 5$ units. The equipotential lines are themselves spheroids; at a distance $>2a$, they rapidly approach a spherical shape. But near the electrode edge, the distance to an equipotential spheroid is much smaller than at the center, indicating a higher current density at the edge.

Each confocal spheroid in Figure 6.5 is an equipotential surface and may be regarded as a possible electrode, with unchanged equipotential lines outside the electrode. The only difference is that the conductance G of such a spheroid will increase with size. The conductance of the surface disk with radius a is found to be:

$$G = \sigma 4a \quad R = \frac{\rho}{4a} \quad (\text{one side}) \quad (6.17)$$

Compared with Eq. (6.1), a disk has therefore only $2/\pi$ times less conductance than a sphere of the same radius, independently of a . As for the sphere, the conductance is proportional to the electrode circumference, not the area (Figure 6.6).

At the surface of a disk electrode (Figure 6.6), the current density \mathbf{J} as a function of the radius r is:

$$\mathbf{J} = \frac{I}{2\pi a \sqrt{a^2 - r^2}} \quad (r < a, \text{ one side}) \quad (6.18)$$

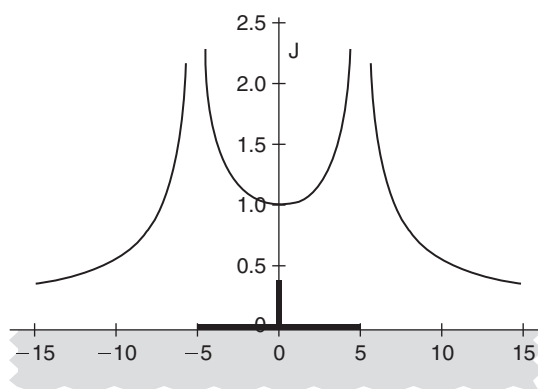


Figure 6.6: Current density in the tissue surface layer caused by a disk electrode.
 $J = 1$ corresponds to the current density of a spherical electrode with the same radius, half immersed in the tissue.

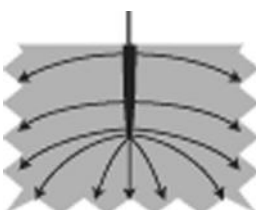
The direction of \mathbf{J} is perpendicular to the metal surface except at the edge, which is a singular curve where the current also leaves the edge in directions of the tissue surface. Current density therefore diverges at the edge. The edge is therefore outside the zone of linearity. There are many misconceptions in the literature, with current density under a surface electrode considered uniform. The current density in the disk center is the same as on the surface of a sphere of the same radius a . The potential field in the tissue is:

$$\Phi = \frac{2V}{\pi} \arctan \frac{\sqrt{2a}}{\sqrt{(r^2 - a^2) + \sqrt{(r^2 - a^2)^2 + 4a^2z^2}}} \quad (6.19)$$

when the disk is lying in the xy -plane symmetrical to the origin. The tissue surface potential ($z = 0$) is then $(2V/\pi) \arctan ((r/a)^2 - 1)^{-0.5}$.

6.2.5 Ellipsoidal Needle Source

This geometry is important as a model for invasive electrodes, often used in neurophysiology with insulated shaft and an open half-ellipsoid-like end as the active electrode. The conductance of a half-ellipsoid of revolution in a half-infinite homogeneous medium is:



$$G = \sigma \frac{2\pi\sqrt{L^2 - a^2}}{\ln \frac{L + \sqrt{L^2 - a^2}}{a}} \quad (\text{half ellipsoid of revolution}) \quad (6.20)$$

where a = rotational radius and L = half long axis.

Equation (6.20) is for a noninsulated half-ellipsoid inserted from the surface. When the needle shaft is insulated so that when the needle is inserted from the surface and penetrates deeper into the tissue, the model may be regarded as a gradual change towards a full-length ellipsoid in an *infinite* medium. The conductance given by Eq. (6.20) would then be doubled. A slightly different model is to consider the half-ellipsoid positioned at the end of an insulating rod.

For needles, the diameter d is a more practical dimension than radius a , so if $d = 2a$ is inserted in Eq. (6.20) and if $L \gg d$, the equation simplifies to:

$$G = \sigma \frac{\pi 2L}{\ln \frac{4L}{d}} \quad R = \rho \frac{\ln \frac{4L}{d}}{\pi 2L} \quad (L \gg d) \quad (6.21)$$

Figure 6.7 shows how small influence the needle diameter has on the needle conductance (resulting from the logarithmic factor in Eq. (6.20)). An equivalent sphere is a sphere with the same conductance as a given needle. The equivalent sphere to a noninsulated needle of diameter $0.1 L$ and needle length $L = 0.5$ has a diameter of about $0.3 L$. Reducing the

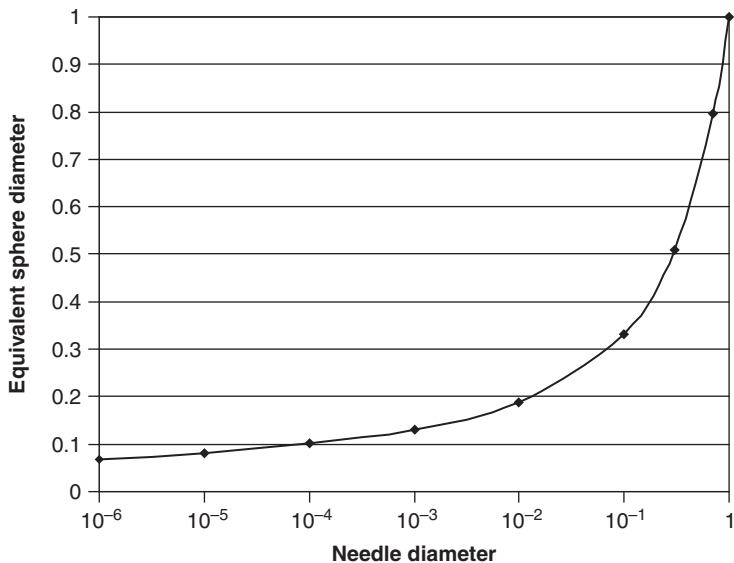


Figure 6.7: Equivalent sphere diameter as a function of needle diameter, equivalent sphere, and needle having equal conductance. Needle half axis length $L = 0.5$.

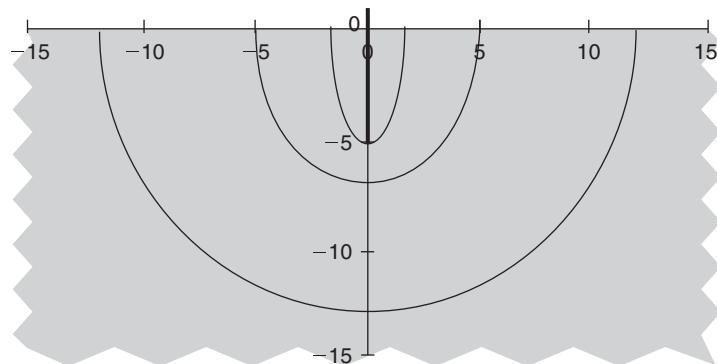


Figure 6.8: Equipotential lines of a noninsulated current injecting needle (prolonged spheroid of maximum diameter 0.4 units and length 5 units).

needle diameter further down three decades ($0.0001 L$) only reduces the equivalent sphere diameter to $0.1 L$. Needle length is the dominant factor. This is a general rule for the electrical properties of electrodes: it is the largest dimension that is the determining factor.

Figure 6.8 shows the equipotential field lines caused by a CC needle electrode having the form of a long, thin ellipsoid. The potential drop is very significant near the needle tip.

Figure 6.9 shows the needle surface current density as a function of depth, normalized with $J = 1$ at the electrode tip. If such a noninsulated needle is used for nerve excitation, most of the current will be injected from the shaft, but at threshold the excitation occurs only at the tip.

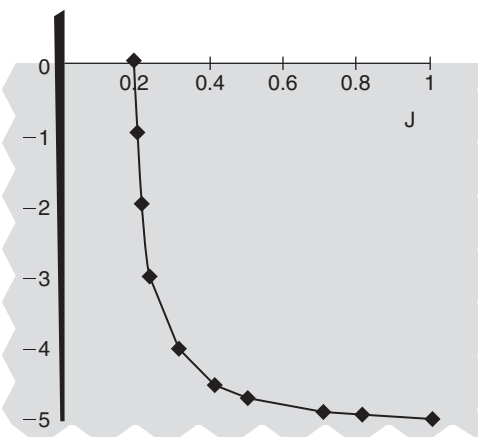
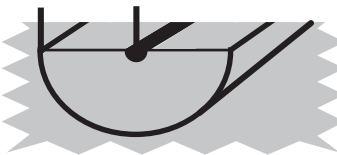


Figure 6.9: Needle surface current density as a function of depth. Needle dimensions: maximum diameter 0.4 units, length 5 units.

6.3 Line Sources, Ideal Two-Dimensional Models

Like the sphere, a cylinder of infinite length also spreads the current radially, but not in the length direction. The cylindrical coordinate system with the coordinates z , r , and ϕ is of course well-suited for line sources. The sphere has double curvature, the cylinder single-curvature geometry. The surface area of a cylinder segment of length L is $2\pi rL$ and the current density accordingly falls proportional to r^{-1} (sphere: r^{-2} , Table 6.1). The line source spreads the current deeper than a sphere of the same radius.



A cylinder of length L and limited by two insulating plates perpendicular to the cylinder axis has the same electrical properties as the infinitely long cylinder per length L .



6.3.1 Cylinder and Stripe Monopolar Sources

Figure 6.2 is relevant, but this time the black electrode must be interpreted not as a sphere but a cut through an infinitely long half-immersed cylinder. The resistance and conductance of a half-immersed cylinder is:

$$R = \frac{\rho}{\pi L} \ln \frac{r}{a} \quad \frac{G}{L} = \frac{\sigma \pi}{\ln \frac{r}{a}} \quad (r \geq a, \text{ hemicylinder, infinitely long}) \quad (6.22)$$

Here L is not the cylinder length because that is infinite: L is the length of a cylinder segment. The radius of the half-immersed cylinder is a , and r is the radius of a chosen outside concentric hemicylinder in the tissue volume. R is the resistance between two cylinders and in contrast to the sphere, R diverges if $r \rightarrow \infty$.

The surface of a cylinder segment is $2\pi rL$, and if I is the current fed into that cylinder segment the current density in tissue is:

$$J = \frac{I}{L} \frac{1}{\pi r} \quad [\text{A/m}^2] \quad (r \geq a, \text{ hemicylinder}) \quad (6.23)$$

It is not possible to define a finite potential at $r = \infty$ because a certain current I then results in an infinite potential because R diverges. With an infinitely long cylinder, only potential *differences* can be defined and Eq. (6.24) describes a quantity often called the “logarithmic potential” for this difference between two points at distance r_1 and r_2 :

$$\Delta\Phi = \frac{I\rho L}{\pi} \ln \frac{r_1}{r_2} \quad [\text{V}] \quad (r \geq a, \text{ hemicylinder}) \quad (6.24)$$

If the surface of the cylinder is defined as $r_1 = a$, the potential at distance r in the tissue is:

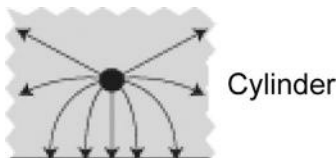
$$\Phi = \frac{I\rho L}{\pi} \ln \frac{a}{r} \quad [\text{V}] \quad (r \geq a, \text{ hemicylinder}) \quad (6.25)$$

According to Eq. (6.25), the potential at $r = \infty$ is $-\infty$ V and at the cylinder surface 0 V. In comparison the potential of a sphere is zero at infinite distance.

Because the current density field has no changes in the axial direction, the calculations are simplified to 2D problems. Around the ends of a *finite* length rod in an infinite conductive medium, the problem is no longer 2D, and the best analytical approach is to turn to an ellipsoid geometry (see following section on finite length rod).

Infinite Cylinder and Conducting Plate

The two parallel-cylinder solution (section 6.3.2) is directly applicable to a complete cylinder discussed previously (e.g., with an infinite metal plate), because the current density field is unchanged if the isoelectric plane surface is covered by a thin metal sheet. The resistance is halved and the conductance doubled (see Eq. (6.26)):



$$R = \frac{\rho}{2\pi L} \ln \left\{ \frac{D}{2a} + \sqrt{\left(\frac{D}{2a} \right)^2 - 1} \right\} \quad \frac{G}{L} = \frac{2\sigma\pi}{\ln \left\{ \frac{D}{2a} + \sqrt{\left(\frac{D}{2a} \right)^2 - 1} \right\}} \quad (6.26)$$

where D is two times the sphere center to plane distance. If $D \gg a$, this simplifies to

$$\frac{G}{L} = \frac{2\sigma\pi}{\ln \frac{D}{a}} \quad (6.26a)$$

Finite Length Rod

The needle equations Eqs (6.20) and (6.21) are also valid if a needle ellipsoid with full-length $2L$ is turned 90° so that its long axis is parallel to the surface, and with the ellipsoid half immersed. This is perhaps the best analytical model for a finite length rod.



6.3.2 Two Parallel Cylinders

The resistance and conductance of two half-immersed cylinders are:



$$R = \frac{2\rho}{\pi L} \ln \left\{ \frac{D}{2a} + \sqrt{\left(\frac{D}{2a} \right)^2 - 1} \right\} \quad \frac{G}{L} = \frac{\sigma\pi}{2 \ln \left\{ \frac{D}{2a} + \sqrt{\left(\frac{D}{2a} \right)^2 - 1} \right\}} \quad (6.27)$$

where D is the distance between the cylinder centers. If $D > 20a$, this is equal to the double resistance of the single cylinder (Eq. (6.22)) to an accuracy better than 0.1%.

6.3.3 Ring Monopolar Source

The conductance of a ring-formed cylinder of ring radius R and cylinder radius a in a half-infinite volume is:



$$G = \sigma \frac{2\pi^2 R}{\ln \frac{8R}{a}} \quad (\text{half immersed}) \quad (6.28)$$

Just as for the ellipsoid needle, we see that the conductance is not very dependent on cylinder radius a , it is the length $2\pi R$ that is important.

6.3.4 Parameter Dependence on Distance from Source

Table 6.1 showed distance from source dependences. Important consequences of the values are: The current density falls less rapid from a cylinder than a sphere source. Power density and therefore temperature rise falls extremely rapid with distance from a CC sphere (see electrosurgery in Section 10.10).

6.4 Signal Transfer

A basic bioelectric model is the dipole, both as a signal source and signal receiver. In *ideal volumes* (homogenous infinite size, tissue with linear isotropic electrical properties), analytical solution can be found as already shown. Even if analytical solutions cannot be found with finite volumes and heterogeneous tissue, transfer functions may be determined from measurements or calculations. The dipole is well-suited for analytical models.

6.4.1 Fixed Recording Lead, Moving Source

The basic model for signals derived from the action potential of a nerve cell axon is a *free* current carrying dipole vector with fixed moment $\mathbf{m} = IL_{cc}$, Eq. (6.10). We will now go into a more detailed description of the axon model because it so clearly demonstrates how the registered waveforms are so dependent on the PU electrode lead, and how the tissue geometry, the axon included, acts as a low-pass filter.

A technically ideal (Section 6.2.3) current dipole with constant moment moves with constant velocity along the x -axis in an ideal volume, Figure 6.10. The monopolar and bipolar potentials are calculated at a fixed point on the y -axis at distance $5L_{cc}$ and $10L_{cc}$. The monopolar and bipolar potentials are calculated using Eq. (6.11) with $I_p = 2000\pi$. The potential values in Figures 6.11 and 6.12 can therefore be compared.

Unipolar Recording

The potential contribution from each dipole sphere is added according to Eq. (6.11). Equation (6.12) shows that with the dipole moment \mathbf{m} and the distance \mathbf{r} in the same direction the potential falls off as r^{-2} . This is in accordance with the maximum amplitudes at Figure 6.11(b) for the recording electrode distances $5L_{cc}$ and $10L_{cc}$. In Figure 6.11(a),

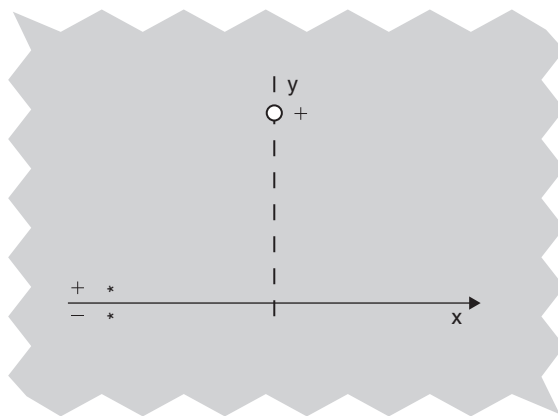


Figure 6.10: Moving current dipole (*) with fixed position unipolar recording electrode.

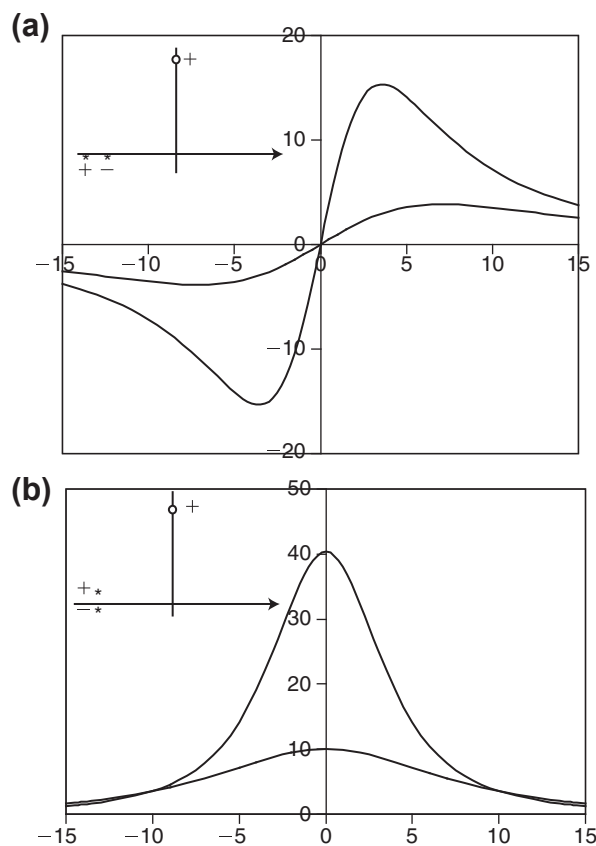


Figure 6.11: Unipolar potentials from a current dipole moving along the horizontal x -axis. Dipole length is L_{cc} ; the unit of the x -axis is L_{cc} . The recording electrode is at distance $5L_{cc}$ and $10L_{cc}$: (a) horizontal dipole orientation, biphasic waveforms, and high spatial resolution; (b) vertical dipole orientation, monophasic waveforms, and largest signal amplitude of all geometries.

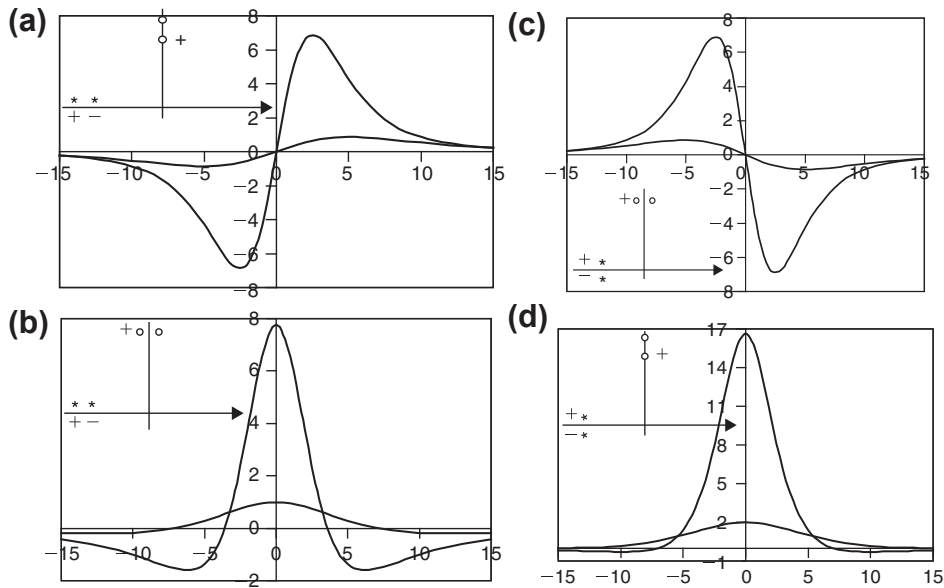


Figure 6.12: Bipolar potentials from a current dipole source. Conditions as for [Figure 6.11](#) with the recording dipole length $L_{pu} = L_{cc}$.

however, the r^{-2} agreement is not so precise because the maxima do not occur at the same x value for the two distances.

Bipolar Recording

Bipolar PU electrodes actually measure the electric field strength. The potentials are calculated at each PU electrode and subtracted. [Equation \(6.13\)](#) indicates that the potential difference $\Delta\Phi$ falls off more rapidly with distance than the unipolar case. In [Figure 6.12](#), the $\Delta\Phi$ fall is between r^{-2} and r^{-3} .

This is confirmed by [Figure 6.12](#), which shows a large positional discriminative property. The waveform in [Figure 6.12\(b\)](#) is even triphasic. [Figure 6.12\(a\) and \(c\)](#) show biphasic waveforms with a large high-frequency content, but the recorded voltage difference is small.

6.4.2 Spatial Resolution and Frequency Content, Passage Effect

All the bipolar recordings show higher discriminative power than the unipolar recordings. The bipolar waveforms therefore have higher frequency components.

The curves at distance $10d$ are less steep and with less high-frequency components. *The distance to the signal source act as a low-pass filter.* This is not due to tissue

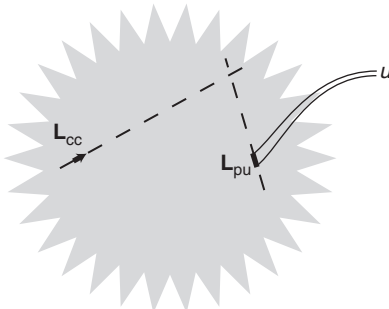


Figure 6.13: Two ideal dipoles far away from each other in an infinite, homogeneous conductor volume. Their axes need not cross each other. The left dipole is current carrying (\mathbf{L}_{cc}); the right dipole (\mathbf{L}_{pu}) picks up signals transferred from \mathbf{L}_{cc} .

electrical properties, only to different geometrical angles of view. It is in accordance with, for example, the high content of high-frequency signals found in electromyelogram signals obtained with recording electrodes near to a large muscle mass. It is like standing at a distance from a road where cars pass. The nearer you are to the road, the more intense is the noise at car passage, but the shorter the noise duration. At a long distance from the road, a low noise starts early, but does not reach a high noise maximum at passage.

6.4.3 Transfer Lead Vector between Two Dipoles

We have just calculated the recorded potential from a moving dipole source in an ideal infinite volume. The potential recorded from an endogenic electrical source is as we have seen very dependent on the position of the PU electrodes with respect to the source (Figures 6.10 and 6.11). We will now analyze signal transfer between *two* ideal dipoles in more detail.

Figure 6.13 shows a general model with two ideal dipoles in an infinite, homogeneous medium. One technically ideal dipole is CC (dipole length \mathbf{L}_{cc}); the other ideal dipole is for signal PU (dipole length \mathbf{L}_{pu}). Their axes need not cross each other.

Equation (6.15) gave the potential difference from a current carrying technically ideal dipole. Technically ideal CC dipole is explained in Section 6.2.3. Putting $\mathbf{m} = \mathbf{IL}_{cc}$ we have:

$$\Delta\Phi = u = \left(\frac{l\rho}{4\pi r^3} \right) \mathbf{L}_{pu} \cdot \mathbf{L}_{cc} \quad [\text{V}] \quad (6.29)$$

(technically ideal CC dipole far away from the PU dipole)

It is clear from this equation that it does not matter which dipole is CC and which is PU, in accordance with the principle of reciprocity. We separate the part of Eq. (6.29) associated with the PU dipole and call it the *lead vector* \mathbf{H} :

$$\mathbf{H} = \left(\frac{\rho}{4\pi r^3} \right) \mathbf{L}_{pu} \quad [\Omega/m] \quad (\text{Lead vector of ideal pick-up dipole}) \quad (6.30)$$

The lead vector¹ defines a transfer factor between the CC and PU dipoles. It depends on the resistivity ρ of the medium, the distance r between the dipoles, and the PU dipole length vector \mathbf{L}_{pu} . The scalar signal u created by a current dipole $\mathbf{m} = I\mathbf{L}_{cc}$ is:

$$u = \mathbf{H} \cdot \mathbf{m} \quad [V] \quad (\text{technically ideal dipoles}) \quad (6.31)$$

Vector \mathbf{H} has a free starting point but fixed magnitude and direction according to Eq. (6.30). The current dipole \mathbf{m} is bound, but may vary in current I and length \mathbf{L}_{cc} .

The transfer impedance Z_t is defined as u/i in the external wires, so from Eq. (6.29):

$$Z_t = \left(\frac{\rho}{4\pi r^3} \right) \mathbf{L}_{pu} \cdot \mathbf{L}_{cc} \quad [\Omega] \quad (\text{technically ideal CC dipole far away from the PU dipole}) \quad (6.32)$$

Z_t is a scalar in space, but may be a time vector \mathbf{Z}_t related to a frequency dependence of ρ . Both the lead vector \mathbf{H} and the scalar transfer impedance Z_t are transfer factors between the CC and PU dipoles. The relationship between them is: $Z_t = \mathbf{H} \cdot \mathbf{L}_{cc} \quad [\Omega]$.

The Einthoven triangle is an example of a recorded voltage u (the electrocardiogram signal) modeled as the dot product of the *lead vector* of a bipolar PU electrode pair and the bound *heart dipole vector* \mathbf{m} (see Section 10.1).

In-Line Surface Dipoles

For surface electrodes, simple analytical solutions can be found if we return to Eq. (6.11). Equation (6.11) is valid for all technically ideal CC dipoles without any restrictions on the distance to the potential PU positions. Let us call the two CC electrodes CC1 and CC2 with dipole length \mathbf{L}_{cc} , and the two PU electrodes PU1 and PU2 with dipole length \mathbf{L}_{pu} . If the two dipoles are on the same plane surface, the geometry is completely determined by three vectors: the two dipole vectors and one vector giving the distance between them. If they are in-line, three scalars must be known, Figure 6.14.

¹ Schmitt (1957) called the lead vector \mathbf{H} transfer impedance. This may be misleading both because impedance is a spatial scalar, whereas \mathbf{H} is a spatial vector and with dimension $[\Omega/\text{meter}]$.

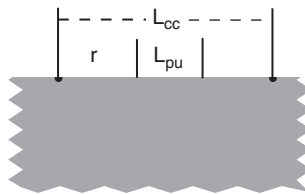


Figure 6.14: Two dipoles oriented in-line on a plane, infinite tissue surface.

Because the upper half-infinite volume is taken away, the potential of Eq. (6.11) for a given current is doubled. For the in-line geometry of Figure 6.14, the voltage difference is:

$$\Delta\Phi = \frac{I\rho}{2\pi} \left(\frac{1}{r} - \frac{1}{L_{pu} + r} - \frac{1}{L_{cc} - r} + \frac{1}{L_{cc} - L_{pu} - r} \right) \quad (6.33)$$

(technically ideal surface dipoles in line)

If the electrodes are equally spaced with distances d , the voltage difference is:

$$\Delta\Phi = \frac{I\rho}{2\pi d} \quad (\text{technically ideal surface dipoles in line}) \quad (6.34)$$

and the transfer impedance Z_t

$$Z_t = \frac{\rho}{2\pi d} \quad (\text{technically ideal surface dipoles in line}) \quad (6.35)$$

The model of Figure 6.14 is based upon contact hemispheres for the PU electrodes with radius $a \rightarrow 0$, but for the CC electrode $a > 0$ according to our definition of a technically ideal CC dipole. The system is therefore not necessarily reciprocal if the two dipoles are swapped. In Figure 6.14 therefore $r \geq a$.

Equations (6.29–6.35) are the basic equations for three- and four-electrode systems according to the model of two ideal dipoles. Notice that all these analytical models presuppose ideal dipoles; that is, electrode sphere radii are much smaller than dipole length, distance between dipoles is much larger than dipole lengths, and infinite homogeneous isotropic medium.

6.4.4 Nonideal Volumes, Reciprocal Lead Field

Figure 6.15 illustrates a situation with a finite and inhomogeneous volume where \mathbf{m} is the dipole source, symbolizing for instance the heart vector. Under such conditions, the dipole equations are not exact solutions, and a more realistic approach according to limited conductor volumes and inhomogeneous tissue must be found. To find the lead vector \mathbf{H} under more realistic conditions, the concept of *reciprocal excitation* was introduced (McFee and Johnston, 1953). *Reciprocal excitation is to let the PU electrodes be CC with*

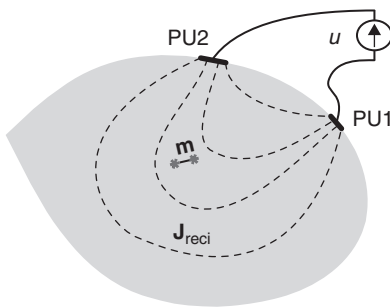


Figure 6.15: Sensitivity of a PU electrode pair to a dipole source \mathbf{m} is directly related to the reciprocal current density generated by the PU electrodes at the source position.

a unity current of 1 A (in contrast to their intended use as zero current PU electrodes). The current density vector field $\mathbf{J}'_{reci}(x,y,z)$ generated by a unit current excitation is called the reciprocal *lead field*, dimension [1/m²].

Initially, the lead field is often unknown, but may be found by finite element method (FEM) modeling (Section 6.5) to the extent that the volume dimensions and resistivity distribution are known. The lead *field* illustrates the sensitivity distribution of the PU electrodes for CC electrodes or biological processes somewhere in the finite volume. The measured signal u is:

$$u = \iiint \rho \mathbf{J}_{cc} \cdot \mathbf{J}'_{reci} dv \quad [\text{V}] \quad \text{The general transfer signal equation} \quad (6.36)$$

u is of course proportional to the excitation current density J_{cc} , so J_{cc} has the dimension [A/m²]. To get rid of the unit current concept, we may equally well use $\mathbf{J}' = \mathbf{J}/I_{reci}$ [1/m²] where I_{reci} is any current level supplied in the PU electrode wires. The equation is then:

$$u = I_{reci}^{-1} \iiint \rho \mathbf{J}_{CC} \cdot \mathbf{J}_{reci} dv \quad [\text{V}] \quad (6.37)$$

Because $\mathbf{J} = \sigma \mathbf{E}$ (isotropic case), we may equally well express u as a function of the two electrical fields:

$$u = I_{reci}^{-1} \iiint \sigma \mathbf{E}_{CC} \cdot \mathbf{E}_{reci} dv \quad [\text{V}] \quad (6.38)$$

The transfer impedance Z_t between the CC and PU electrodes is:

$$Z_t = \iiint \rho \mathbf{J}'_{CC} \cdot \mathbf{J}'_{reci} dv \quad [\Omega] \quad \text{The general transfer impedance equation} \quad (6.39)$$

It is still possible to use the lead vector concept (e.g., from the example shown in Figure 6.14). The lead vector of the PU dipole is not a vector field; it is the total

sensitivity of a lead under ideal (homogeneous, infinite, isotropic) conditions. However, in real cases, the PU electrodes may be at a large distance from each other on the body surface, and it is less evident that they shall be considered as a dipole. But even with the highest geometrical and tissue complexities, the tissue can always be considered linear with the current and voltage levels generated by life processes. Therefore the principle of superposition is valid, and any space vector can be decomposed to its Cartesian x-y-z components. Each direction can be treated separately and later added to form one resultant vector. For instance, the relation $u = \mathbf{H} \cdot \mathbf{m}$ may still be useful if two sets of PU electrodes are used with individual lead vectors and simultaneous measurement of the two lead voltages from the same source. The individual vectors are added so that the direction of the source dipole vector \mathbf{m} can be determined. This is used for the determination of the electrical axes of the heart (Section 10.1).

A lead vector \mathbf{H} is determined by the geometry and conductivity distribution of the signal PU system, and is valid for one tissue volume and one set-up with all electrode and source positions and distributions defined and constant. Changing one PU electrode or source position, leaving all other factors constant, results in another lead vector \mathbf{H} .

Optimum electrode configuration is crucial to focus the measurements on the desired tissue volume (see e.g., Song et al., 2005). The sensitivity of a transfer impedance measurement in a limited volume with four surface electrodes can be determined by studying the dot product according to Eq. (6.39) (see Figure 6.16). In some volume positions where the vectors are perpendicular to each other, the measured impedance is insensitive to local resistivity changes. In other positions, the angle is $>90^\circ$; in those positions, the sensitivity is reversed. Again we must point out that *the transfer impedance is not an ordinary impedance, it is a transfer factor between an input and output port. If, for example, $Z_t = 0$ this is not because the tissue is so well conducting, it is because there is no signal transmittance from the source dipole to the PU dipole. It is only with the one port two-electrode technique that tissue immittance is measured without influence from transmission properties.*

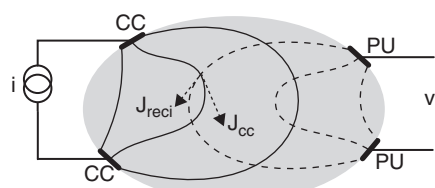


Figure 6.16: Four-electrode system with current density and reciprocal current density lines. Sensitivity is illustrated at one point, the dot product; therefore, the sensitivity there is small because the two current density vectors are almost perpendicular to each other.

Swapping the PU and CC pairs does not change the transfer impedance as long as the system is electrically linear (reciprocity). This is valid for both tripolar and tetrapolar electrode systems.

6.4.5 Sensitivity Field

The lead vector \mathbf{H} is a transfer factor determining signal amplitudes in a PU electrode pair from, for example, a certain biological source activity in a fixed position. So \mathbf{H} is a *sensitivity parameter* of the whole lead system, a large lead vector means large signal transfer. From Figure 6.14, it is clear that higher signal amplitudes are recorded from a dipole source near the electrodes and their constricted current zones of high current density. If the reciprocal current density is negligible in a volume, dipole sources in that volume do not contribute to the recorded signal.

The transfer impedance Z_t between the CC electrode pair and the PU electrode pair is given by Eq. (6.39). The contribution of each voxel is $\rho \mathbf{J}'_{\text{reci}} \cdot \mathbf{J}'_{\text{cc}}$, and we define the sensitivity S of a tissue voxel as:

$$S = \mathbf{J}'_{\text{reci}} \cdot \mathbf{J}'_{\text{CC}} \quad [1/\text{m}^4] \quad (6.40)$$

The sensitivity S is a factor determining the influence of the local resistivity on the total result, the impedance contribution of a voxel is $\rho S dv$. If an interesting physiological process is going on somewhere in the tissue, the PU electrode pair should be situated so that the volume is in a high sensitivity zone of the PU electrodes. In Section 10.5 on plethysmography, for instance, the sensitivity for detecting small local changes in tissue conductivity is discussed.

In a two-electrode system (bipolar or monopolar), the forward and reciprocal current densities are identical, so therefore:

$$Z = \iiint \rho |\mathbf{J}'|^2 dv \quad S = |\mathbf{J}'|^2 \quad (6.41)$$

where \mathbf{J}' is the unity current density [$1/\text{m}^2$]. If the medium is homogeneous the resistivity ρ is constant and can be placed outside the integration sign, then the contribution of a voxel is simply a function of $|\mathbf{J}'|^2$.

Sensitivity may be defined according to any transfer function; our interest is on impedance sensitivity. The spatial variation of S is the *sensitivity field*. At the neutral electrode in a unipolar system, \mathbf{J} is low, so the contribution of the tissue there will be negligible. In a tube with cross-sectional area A and $\mathbf{J} = I/A$ constant, Eq. (6.41) reverts to the well-known $R = \rho L/A$. For the unipolar hemisphere on the tissue surface, Eq. (6.3) shows that \mathbf{J} is proportional to r^{-2} . From Eq. (6.41), Z is proportional to $|\mathbf{J}'|^2$, and the contribution of a

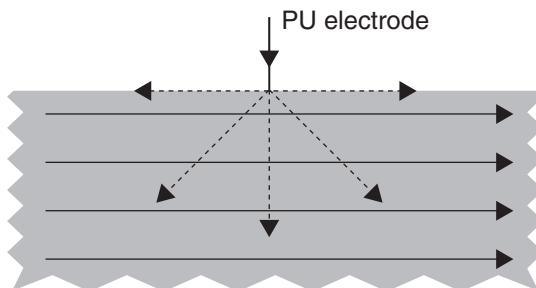


Figure 6.17: Sensitivity of a PU electrode in a uniform current density field.

voxel falls very rapidly as r^{-4} . However, at the same time, the *number* of voxels in a spherical shell increases as r^2 , so the contribution of a shell falls as r^{-2} . It is of course a general phenomenon that the number of voxels increases in a current spreading geometry with falling \mathbf{J} and falling contribution of each voxel.

Zero Sensitivity, the Symmetry Paradox

Figure 6.17 illustrates reciprocal current injection by a small contact area PU electrode into an infinite volume of homogeneous and isotropic material with uniform current density \mathbf{J}'_{cc} . From the reciprocally excited PU electrode, the current spreads out in a hemispheric symmetrical geometry in accordance with Figure 6.1. The reciprocal current density \mathbf{J}'_{reci} near the electrode is very high, and one may be led to believe that the sensitivity is high in this zone. The voxels lying in the vertical line from the PU electrode have zero sensitivity because the reciprocal current line is perpendicular to the horizontal current lines. Near the surface, the dot product $\mathbf{J}'_{reci} \cdot \mathbf{J}'_{cc}$ is very high near the PU electrode. However, as long as we are inside the symmetrical zone of reciprocal current density, the contribution from the left and right side volumes with respect to the PU electrode position are equal but with opposite signs. The volume of the symmetrical zone is dependent on the reciprocal current path (e.g., whether it is a bipolar or unipolar PU electrode system). The paradox is that the symmetrical very high sensitivity region has zero net sensitivity; all contributions cancel. In conclusion, such an electrode configuration will be very sensitive to asymmetry in the tissue near the PU electrode, and the recording may easily be unstable and noisy. Increased PU electrode contact area will reduce the problem, but this implies current disturbance of the \mathbf{J}'_{cc} field.

6.4.6 Bipolar Measuring Depth

Constant Area Disks, Varying Distance

The distance between two surface electrodes will influence measuring depth, Figure 6.18. If the bipolar electrodes are driven from a constant amplitude voltage source, the total current and in particular the current density will decrease with increasing distance.

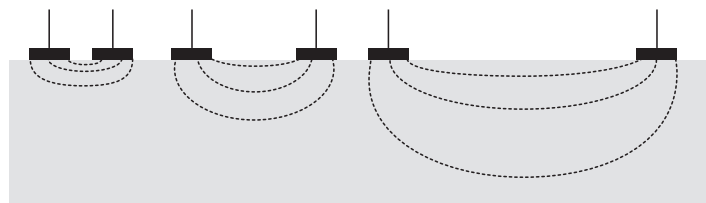


Figure 6.18: Measuring depth as a function of spacing distance between equal electrodes.

In addition, the relative contribution of the deeper layers will increase. Even so, the sensitivity is proportional to the current density squared, so a given volume of tissue proximal to the electrodes is more important for the result than the *same volume* in the deeper layers. By varying the distance between the electrodes, it is therefore possible to control the measuring depth. Ollmar and Nicander (1995) varied the measurement depth by inserting a third active current carrying electrode between the two measuring electrodes.

Constant Distance, Varying Disk Area

Measuring depth is not so dependent on electrode dimensions. This is illustrated in [Figure 6.19](#) with equal electrode center distances. With the narrow gap on the right figure, the sensitivity in the gap will be high. On the other hand, the number of voxels there is small and the number of low sensitive voxels is very high. The local gap sensitivity can be increased much more by keeping the narrow gap, but reducing the electrode areas.

By using multiple surface electrodes, it is possible to reduce the measuring depth somewhat ([Figure 6.20](#)). Such electrodes are often made in the form of metal strips, not disks. Measuring depth is determined *both* by the strip width and the distance between the strips.

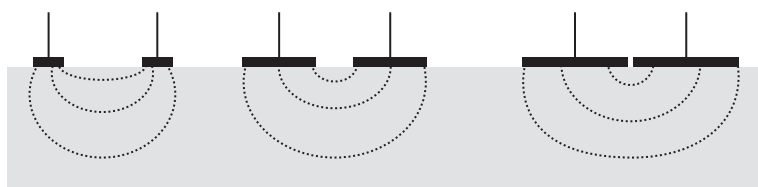


Figure 6.19: Measuring depth as a function of electrode dimensions, constant distance between electrode centers.

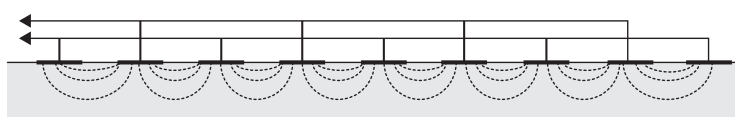


Figure 6.20: Multiple surface electrodes.

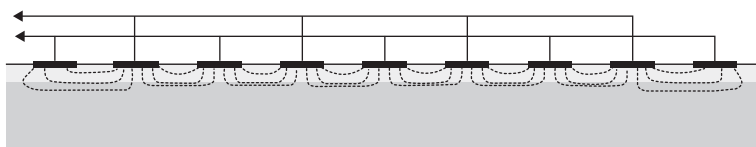


Figure 6.21: Surface electrodes on poorly conducting surface layer.

6.4.7 Surface Layer

If a homogenous volume is covered by a poorly conducting homogenous layer, the current will go more or less perpendicular right down to the well-conducting layer (Figure 6.21). The whole volume of the poorly conducting layer will dominate measuring results. Dependent on the conductivity ratio and upper layer thickness/edge to edge distance, a certain part of the current will still go the shortest way through the poorly conducting layer.

6.5 Finite Element Method

Maxwell's equations are discussed in Section 9.2.2. Any problem in regard to the distribution of current or electric field in a homogeneous or composite material can be solved with these equations if the excitation and electrical properties of the materials are known. There are in general two different types of problems to be solved in differential equations: *initial value* problems and *boundary value* problems. Initial value problems arises when the values of the unknowns are given at a particular point (e.g., at a given time), and the values at future times are to be computed. Boundary value problems arise when the values on the boundary of a material are known, and the values of the interior are to be computed. The latter is a common situation in bioimpedance research where, for example, the current distribution in tissue is to be computed from a given excitation from surface electrodes.

Because the differential equations that describe the behavior of our system, in this case the Maxwell equations, basically describe an infinite-dimensional object, we must use a finite-dimensional approximation to represent the solution. There are two main forms of such approximation, *finite differences* and *finite elements*. In the finite difference method, the differential equation describing the continuous change of the values can, for example, be replaced with an approximation describing the slope of change between a finite number of discrete points, called mesh points. Danilov et al. (2013) showed that the use of adaptive tetrahedral meshes significantly reduces the number of mesh elements and hence the associated computational cost, compared with rectangular meshes, without sacrificing model accuracy.

The FEM involves dividing the modeled geometry into small subregions called elements. The unknown solution is then expressed as the weighted sum of basis functions, which are polynomials in each element. The differential equation is then used in each element to compute the weight used for the basis function of that particular element in the total sum. Each calculation introduces a small error but the errors will in the ideal case diminish as the number of points or elements is increased. There is no guarantee however for some ill-posed problems that the sum of an increasing number of diminishing errors will not have a large effect. It is therefore highly recommended to verify any algorithms or computer software of the sort before use by first solving similar problems that have an analytical solution.

Earlier in Chapter 6, we treated some simple electrode/tissue geometries with mathematical analytical solutions. Of course, tissue morphology and composition is so that analytical solutions most often cannot be found. It is therefore necessary to take a more engineering approach: to make a realistic geometrical model of the tissue and electrode system, immittance distribution included. Then let a computer calculate current density vectors and equipotential lines on the basis of a chosen mesh.

In principle, the computer programs may calculate complex 3D models with frequency dependent tissue parameters. However, the computing time may be long, and accordingly time-consuming to experiment with the model. It is important to define the problem in the simplest possible way, and in a way adapted to the software used. If the 3D problem can be reduced by symmetry to two dimensions, and if a DC/purely resistive problem definition can be used, results are more easily obtained.

Finite element models can be used to analyze both simple measurement systems such as the one in [Figure 6.22](#), and more complex systems based on 3D data such as magnetic resonance imaging scans (Pettersen and Høgetveit, 2011). The minimum input data are electrode stimuli currents and conductivity for all materials for a stationary simulation. It is possible to expand the model by adding relative permittivity for all materials to enable time or frequency-domain simulations. Frequency-dependent input parameters, such as those from Gabriel et al. (1996b), can be added to the model to further enhance the simulation. After simulations are done, we have access to all output data for virtually all spatial points in the model, such as current density and potential and derived values such as sensitivity and volume impedance density (z) may be calculated. A variety of graphics output is possible, such as current path lines as shown in [Figure 6.22\(a\)](#) or sensitivity for a plane beneath the electrode surface as shown in [Figure 6.22\(b\)](#). Pure numerical results such as the expected transfer impedance can be found by integrating z over the entire volume. If we instead integrate z over a smaller volume, such as the sphere in [Figure 6.22](#), we can find how much that particular volume contributes to the final transfer impedance. A model of our measurement

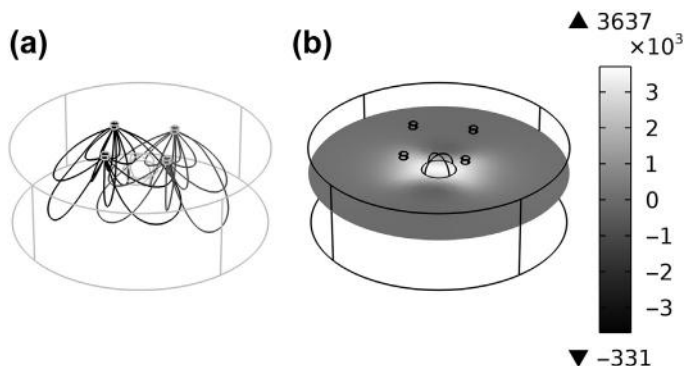


Figure 6.22: Illustration showing current paths and sensitivity in a simulation of a tetrapolar impedance measurement system. Four electrodes on top of the model and a spherical object in the center of the model below the electrodes: (a) Current paths for the two current-carrying electrodes are the dark lines to the left, and the current paths for the reciprocal currents are the gray to the right. (b) Sensitivity distribution in a slice through the model in the same level as a spherical object inside the model. The darkest regions indicate negative sensitivity. Courtesy of Fred Johan Pettersen.

problem may provide insight in what we really measure and what changes in the results may be caused by. This may again aid us to find an optimum measurement configuration for a given problem.

6.6 Imaging, Electrical Impedance Tomography

See also an application of electrical impedance tomography (EIT) in Section 10.7.

A mapping of the immittance distribution in a tissue layer (tomography) is possible with an electrode system of multiple skin surface electrodes. In EIT, a current (about 1 mA) is typically injected in one electrode pair and the voltages between other electrodes are recorded (Rosell et al., 1988b; Bayford and Tizzard, 2012). Current injection is then successively shifted so that all electrode pairs are used. The reciprocal theorem can serve as a control of system linearity. A frequency on the order of 50 kHz is commonly used, so a complete set of measurements with, for example, around 50 electrodes can be performed in less than 0.1 s. The images obtained have a resolution of about 1 cm at 10 cm tissue depth.

One of the fundamental problems of anatomical imaging based on single-frequency impedance measurements is that the absolute impedance is difficult to determine accurately because of the uncertainty in the position of the electrodes. Impedance imaging has hence until recently mainly been concerned with impedance changes resulting from physiological or pathological processes. With the introduction of multifrequency EIT, the possibility of tissue characterization based on impedance spectroscopy has been realized (Riu et al., 1992, 1995). If the frequency response varies significantly between different

organs and tissues, it will be easier to achieve anatomical images because the images will be based on characteristic changes of impedance with frequency rather than the absolute value of the impedance. Indexes such as the relation between measured data at two frequencies may be used, but, because of the differences in characteristic frequencies for the dispersions of different tissues, it has been proved difficult to choose two frequencies to match all types of tissue. Hence, typically 8–16 frequencies are used. Brown et al. (1994a) used seven frequencies from 9.6 to 614 kHz in a 16-electrode thorax measurement and computed from the measured data several parameters from a three-component electrical model. They also adapted the measured data to the Cole impedance equation (see Section 9.2). Indexes were furthermore made by using the 9.6 kHz data as a reference and they concluded that it may be possible to identify tissues on the basis of their impedance spectrum and the spectrum of the changes in impedance. Blad (1996) proposed another approach in a preliminary study on imaging based on the measurement of characteristic frequency.

In principle, the method of mapping tissue immittance distribution is not limited to a slice. By increasing the number of electrodes, volume acquisition is equally possible. One of the potential benefits from 3D EIT is that it could take into account that the current spreads out of the imaging plane of 2D EIT. However, the complexity of both the EIT hardware and software will increase considerably by introducing this third dimension. Some important achievements in the pursuit of 3D EIT were, for example, presented in *Nature* in 1996 (Metherall et al., 1996).

Typical, EIT systems involve 16–32 electrodes in any one plane and operate at frequencies between 10 kHz and 1 MHz. The Sheffield Mark III system (Brown et al, 1994a,b) uses 16 electrodes and injects current and measures potential drop between interleaved neighboring electrodes to reduce cross-talk ([Figure 6.23](#)). They measured on frequencies between 9.6 kHz and 1.2 MHz and used a current of 1 mA p–p. A total of 64 measurements are made at each frequency when driving odd numbered electrodes and measuring at even numbered electrodes.

As explained in [Section 6.4.5](#), the sensitivity of the measurement to a given local change in admittivity is given by the dot product of the current density vectors resulting from injecting current through the two pairs of current and potential electrodes, respectively. The sensitivity may be highest close to the current injecting or potential PU electrodes and lowest toward the center of the medium, depending on the size of the electrodes and the distance between them.

Some of these problems have also been addressed by the Adaptive Current Tomographs systems of the group at Rensselaer Polytechnic Institute (Gisser et al., 1987). They have built 32 and 72 electrode systems with as many independently controllable sources as electrodes. This allows all electrodes to excite the unknown region. Measurements are also

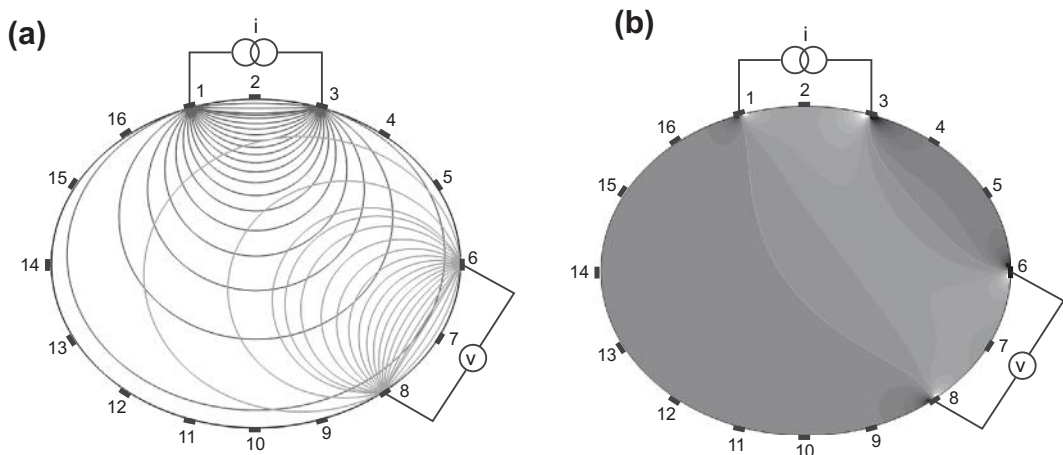


Figure 6.23: Applying current and measuring potential difference between interleaved electrodes in a homogenous medium: (a) Current density lines between electrodes 1 and 3 and reciprocal current lines between electrodes 6 and 8; (b) corresponding sensitivity field distribution — white lines showing zero sensitivity (where the current density lines are orthogonal) — positive sensitivity (light grays) between these lines and negative sensitivity (dark grays) outside the lines.

obtained from all electrodes simultaneously. This scheme allows many different patterns of current to be applied, some of which have low spatial frequencies, which are relatively insensitive to small errors in electrode placement. It also permits higher current densities in the body interior without excessive currents at any skin site, increasing the distinguishability of small inhomogeneities at greater depth from the electrodes. Isaacson has shown how to generate the best sets of current patterns to apply to the unknown region.

Recent work of this group has focused on imaging breasts using radiolucent electrodes attached to a mammography machine (Kao et al., 2007; Saulnier et al., 2007). This allows accurate control of electrode placement, which is important for making static images. The reconstruction algorithms designed by Isaacson permit static image reconstruction with good fidelity. The algorithms also reconstruct a full 3D volume in a few slices of tissue between the electrode planes. The system now used is a 72-electrode system capable of imaging at seven frequencies in the band from 3.3 kHz to 1 MHz, acquiring and displaying all seven images in 6 s. Off-line analysis of these spectra has developed a scheme that can distinguish malignant tissue from normal and benign abnormalities with promising sensitivity and specificity.

Contactless data acquisition techniques are also used in EIT. Such systems may involve coils for inducing currents and electrodes for measuring voltage or they may be totally

contactless when magnetic coils or capacitive coupling are used both for the current excitation and for measuring the voltage response (Scaife et al., 1994; Gencer and Ider 1994). Tozer et al. (1998) describe a system in which currents at 10 kHz, 100 kHz, and 1 MHz are passed axially in the body (between head and feet) and the resulting magnetic field in the body is measured by means of small search coils. The measured magnetic fields are related to current distribution by the Biot-Savart² law that, among other things, states that the intensity of the magnetic field set up by a current flowing through a wire is inversely proportional to the distance from the wire. Korjenevsky and Cherepenin (1998) present an all-magnetic system that comprises coils both for inducing current and for measuring voltage. Their system works in the frequency range 10–20 MHz and measures phase shifts between excitation and response, which is found to be proportional to the integral of the conductivity of the medium. The high frequency typically used for such all-magnetic systems has, however, so far reduced their clinical utility.

This has been challenged by the Graz group, which is developing both hardware and image reconstruction algorithms for simultaneous multifrequency magnetic induction tomography at a low frequency band (50 kHz–1 MHz) (Scharfetter et al., 2003; Hollaus et al., 2004). The latest system consists of 16 transmitter coils and 16 planar gradiometers as receiver coils with an analog bandwidth of 50 kHz–1.5 MHz, which covers a good part of the β -dispersion of many tissues (Rosell et al., 2001). At each acquisition time, eight of the 16 excitation coils are simultaneously driven by individual power amplifiers with up to 3 A_{pp} at multiple frequencies. These amplifiers are ampere-configured as current sources so that every coil termination is high enough so as not to perturb the field of all other coils. For encoding the excitation coils, their individual carrier frequencies differ by 200–500 Hz. In this way, every excitation frequency is split into eight subcarriers within a bandwidth of 1.6–4 kHz so that they can be approximately considered as a single peak in the comparatively flat tissue spectrum. The theoretical acquisition speed is up to 10 frames/s. Image reconstruction is carried out either from state differential or from frequency differential datasets with a regularized one-step Gauss-Newton-approach (Merwa et al., 2003; Scharfetter et al., 2006a,b; Brunner et al., 2006). Iterative solutions have been tested but not yet evaluated with real data. Gursoy et al. (2011) combined EIT, magnetic induction tomography, and induced-current EIT in multimodal tomography and achieved an improvement of about 20% in image resolution by combining the techniques.

Cross-talk is by no means the only instrumentation problem experienced in EIT. Rosell and Riu (1992) discussed the significant common-mode voltage sensed by the potential

² Jean-Baptiste Biot (1774–1862) and Félix Savart (1791–1841). French scientists. Biot was author of “Traité élémentaire d’astronomie physique” (1805) and accompanied J.-L. Gay-Lussac in 1804 on the first balloon flight undertaken for scientific purposes.

measuring electrodes. They proposed a method called common-mode feedback and obtained an improvement of 40 dB in the measurements at frequencies up to 10 kHz. Bragos et al. (1994) designed wideband single and floating current sources for EIT based on current-mode components and with DC feedback, and the effect of electrode size on images of different objects in saline tanks was described by Newell et al. (1998).

The methods for constructing images from immittance measurements may be divided into *single-pass* and *iterative* processes. In single-pass methods, a single mathematical operation is performed on the measured data. Although the conceptual simplicity of the method makes it unsuitable for static imaging where the images are based on the absolute immittance values measured, it works well for dynamic imaging where the images are based on changes in the time or frequency domain. Single-pass methods can be further divided into backprojection and sensitivity matrix methods. Backprojection is a commonly used technique in X-ray computed tomography imaging where the values of a measured profile are distributed in pixels through the thickness of the object and the accumulated value in each pixel after profiles have been measured in different angles, are used for imaging. A high-pass filtering technique is also normally used on the image to reduce artificial blurring of the contour of the organ produced by the backprojection. The sensitivity matrix is the matrix of values by which the conductivity values can be multiplied to give the electrode voltages. The matrix describes how different parts of the measured object influence on the recorded voltages because of the geometrical shape of the object. The sensitivity matrix has to be inverted to enable image reconstruction. This operation is not uncomplicated and many techniques have been suggested (see Morucci et al., 1994).

Iterative methods are mostly used for static imaging. An intelligent guess of the distribution of, for example, conductivities in the tissue is made initially in the iterative algorithm. The forward problem (see [Section 6.1.1](#)) is then solved to calculate the theoretical boundary potentials that are compared with the actual measured potentials. The initial guess is then modified to reduce the difference between calculated and measured potentials and this process is repeated until this difference is acceptably small. The calculation for the boundary potentials may, for example, be performed by means of the FEM (see [Section 6.5](#)).

Because of poor resolution, the range of clinical applications has so far been limited. Examples are imaging of gastric function (Mangnall et al., 1987; Smallwood et al., 1994), pulmonary ventilation (Harris et al., 1987), perfusion, brain hemorrhage (Murphy et al., 1987), hyperthermia (Griffiths and Ahmed, 1987; Gersing et al., 1995), epilepsy and cortical spreading depression (Holder, 1992), and swallowing disorders and breast cancer (Jossinet, 1996). EIT has also been applied to assess the unilateral pulmonary function

with a standard 16 electrode system (Serrano et al., 2002) and also using reduced electrode sets (Serrano et al., 2004). Also, tidal volume monitoring seems feasible, at least in healthy volunteers, with better results in men than in women (de Lema et al., 2006; Balleza et al., 2007).

A fundamental difficulty is also the considerable anisotropy found in the electrical properties of, for example, muscle tissue. No satisfactory solution of how to deal with anisotropy in EIT has yet been proposed. For anisotropic electrical impedance imaging, see, for example, Lionheart (1997). The obvious advantages of the method are speed of acquisition and relatively low-priced equipment. Two European concerted action programs on EIT (originally called applied potential tomography) resulted in a high-activity research period. This was described in a comprehensive review article by Boone et al. (1997), following the completion of the last program.

A first major commercial breakthrough occurred with the introduction of the PulmoVista 500 (see Chapter 10.7). It is interesting to note that the success was not due to a pursuit in the complex technological direction: not a large number of electrodes, not multifrequency measurements, not large instrumentation, no 3D solution, and no special adaption toward a well-defined clinical goal. Instead a large effort was made toward simple and small technology and the evaluations in steps: stationary equipment for laboratory, smaller equipment for evaluation with animals and healthy test persons, then building a model specially adapted for clinical use, and after five years of evaluation by multiple intensive care clinics, then at last entering the commercial market. See Chapter 10.7 and also Chapter 10.15 on innovation.

Impedance plethysmography is closely related to tomography because both are concerned with the recording of local tissue immittivity variations or distributions. Impedance plethysmography is the measurement of immittance changes due to respiration or perfusion and is described in more detail in Section 10.5.

6.7 Duality of Dielectric and Conductor Theory

A biomaterial can be characterized as a conductor or a dielectric. If the system is linear, the complex conductivity and the complex permittivity contain the same information. It is therefore natural that many of the formulas of dielectrics have their corresponding conductor versions and vice versa. Dual parameters are for instance:

$$\begin{aligned}\epsilon &\Leftrightarrow \sigma \\ \mathbf{D} &\Leftrightarrow \mathbf{J} \\ q_v &\Leftrightarrow I_v\end{aligned}$$

where I_v is the current source density.

In physics and engineering, the duality has its limitations not present in the pure mathematical equations:

It is the problem of *range*: $|\sigma|$ may approach zero (vacuum) and infinite (superconductors), whereas the lowest value of $|\epsilon|$ is ϵ_0 (vacuum) and the highest value at least in living tissue does not approach infinity.

It is a problem with the principle of *superposition*: In electrostatic theory, the charge carrier, for example, an electron or ion, is considered vanishing small (point charge) so that the field from a single charge is not disturbed by the introduction of a second charge: the fields of several charges can simply be added. To measure exogenic immittivity, a current flow is injected into the conductor. The CC electrodes cannot be points; they must have a certain size to limit the current density and the local heat dissipation. Then the introduction of a second electrode may disturb the field from the first electrode, with the consequence that the principle of superposition is no longer valid.

Electrostatic theory deals with the field of one point charge. The other charge of opposite polarity is infinitely far away. This is a parallel to the situation with a monopolar CC electrode, [Figure 6.1](#). With the *electrostatic dipole*, we have two charges of opposite polarities separated by a length L and without DC current flow. The current dipole is used in materials with DC conductivity so that DC current will flow. The dipole moment of an *electrostatic* dipole is $\mathbf{p} = q\mathbf{d}$ [Cm]. An *ideal* electrostatic dipole is a dipole where $q \rightarrow \infty$ and $d \rightarrow 0$, keeping the dipole moment constant. Many potential equations are based on the model of point charges and the principle of superposition. The *CC* dipole model is defined with two CC spheres of radius a separated by a distance \mathbf{d} resulting in a dipole moment $\mathbf{m} = I\mathbf{d}$ [Am]. An *ideal* current dipole would then be a dipole where $I \rightarrow \infty$, $a \rightarrow 0$ and $\mathbf{d} \rightarrow 0$, keeping \mathbf{m} constant. The ideal dipole as a *mathematical* model is not necessarily problematic but in physics and engineering it is not “ideal.” The concept of CC *points* is unacceptable. The driving potential and the dissipated power density would diverge in the constricting zone.

6.8 Problems

1. A sphere of radius 1 cm is positioned in an infinite medium of resistivity $1 \Omega\text{m}$.
 - a. Calculate the resistance between the sphere and an infinite large and distant counter electrode.
 - b. Calculate the resistance with a spherical counter electrode at distance 10 cm.
 - c. Calculate the resistance with an infinite area plate counter electrode at distance 10 cm.
2. Consider a large plastic cylinder of diameter 80 cm filled with saline of $\rho = 2 \Omega\text{m}$. In the center is placed an electrical equivalent heart dipole of moment 10 mAcm.

- Calculate the measured voltage in two PU electrodes 10 cm apart, parallel to the heart dipole and at distance 10 cm. Consider the case to be ideal according to [Section 6.2.3](#).
3. Make a comparison between the two-electrode system (resistance of two hemispheres far away from each other according to [Eq. \(6.1\)](#) is $R = \rho/\pi a$) and the four-electrode system of [Eq. \(6.35\)](#).
 4. Find the dipole current of a heart vector with the following parameters given: $u = 1 \text{ mV}$, $L_{pu} = 0.3 \text{ m}$, $L_{cc} = 1 \text{ cm}$, $r = 5 \text{ cm}$, $\rho = 2 \Omega\text{m}$. Consider [Eq. \(6.29\)](#) is valid.

Electrodes

7.1 Electrode Pair

An electrode is a unique device, it cannot function alone. It takes two current-carrying (CC) electrodes to send an electric current through the body: a source and a sink. At a certain DC voltage, no current flows, and the electrode pair is in *equilibrium*. The applied voltage can be changed so that a current flows. This change is called an *overvoltage*. The current then flows through the CC electrodes, and they are therefore polarized.

Also, it takes two pick-up (PU) electrodes to record the biopotential difference between two body contact sites. Negligible current flows through the two PU electrodes. The biopotential signal is generated by electrical activity in a body organ; the source is endogenic. Bioimpedance can be measured with four electrodes: two CC electrodes and two PU electrodes. This implies a signal transmission from the CC pair to the PU pair. The signal source is exogenic. Bioimpedance can also be measured with only two electrodes. Each electrode then functions both as a PU and a CC electrode.

7.2 Single Electrode

In the electrode copper wire, the charge carriers are free electrons. In tissue, the charge carriers are free ions, positive or negative. The electrode is where the change of charge carriers takes place.

[Figure 7.1](#) shows an example of a generic skin electrode. The copper wire from the instrumentation connects to a silver foil at the top of a sandwich structure. The underside

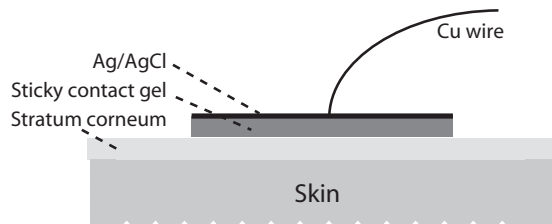


Figure 7.1: Generic skin surface electrode with sticky contact gel in contact with the skin beneath and a silver chloride (AgCl) layer on top, covering a thin silver foil in contact with a copper wire to be connected to the instrumentation.

of the foil is covered by a thin layer of silver chloride (AgCl). The AgCl layer is in contact with a layer of contact electrolyte gel. When a metal with electrons as charge carriers comes in contact with an electrolyte with ions as charge carriers, an electric double layer is formed at the surface of the metal plate in the electrolyte. The double layer is very thin and more or less depleted of charge carriers. This is where the conversion from electron to ion (or vice versa) charge carriers takes place.

7.3 Electrode Metals

By metal, we mean a conductor with electrons as the dominant charge carrier. In this context, *carbon* is within the definition of a metal.

The electric double layer is the most central part of an electrode. It is a very thin layer formed at the sharp boundary (interphase) between an electronic conductor and an ionic conductor (e.g., between a metal plate and an electrolyte). The double layer is described in [Section 7.5](#). The electronic conductors are described now and the ionic conductor (contact electrolyte) will be described in the next [Section 7.4](#) ([Table 7.1](#)).

Often the mechanical strength of the metal is an important property (e.g., in the shaft of a needle electrode). Biocompatibility may be critical if a metal comes in contact with living tissue (e.g., with metals used in sterile invasive electrodes). Flexible large electrodes of nickel may generate allergy in human skin. This can be prevented by using an electrolytic salt bridge between the electrode metal and the tissue.

7.3.1 Test of Polarizability of Electronic Conductors

[Figure 7.2](#) shows a test set-up by which it is possible to check the polarizability of metals (Cooper, 1946).

In [Figure 7.2\(a\)](#), DC current pulses of 10 uA and 1-s duration are applied to a CC electrode pair in a saline solution. The polarization properties of these CC electrodes do not matter as long as the generator is of a controlled current type. Two other equal metal electrodes are used as PU electrodes, and it is this electrode pair that is under study. They are loaded with a resistor of 750 k Ω , so they are slightly CC and therefore polarized. The equivalent electric circuit ([Figure 7.2\(b\)](#)) comprises the parallel coupling of a resistor R_{pol} and a capacitor C_{pol} characterizing the polarizability of a measured pair. A nonpolarizable electrode has a small R_{pol} , a polarizable electrode has an R_{pol} much larger than the load 750 k Ω . C_{pol} together with R_{pol} determine the time constant.

[Figure 7.3](#) shows pick-up voltages obtained with six different electrode metals. The silver chloride electrode pair is the best one ($R_{\text{pol}} \approx 75 \text{ k}\Omega$); pure silver is much worse ($R_{\text{pol}} > 10 \text{ M}\Omega$) because the square waveform is totally distorted. The transfer resistance

Table 7.1: Electronic Conductor Materials

Metal	Properties	Use
Ag/AgCl	Stable DC reference, low DC polarization, not biocompatible	Skin surface electrocardiogram, electromyogram
Platinum metals	Noncorrosive, biocompatible, polarizable	Needles, implants
Gold	Noncorrosive, less biocompatible than platinum	Needles
Titanium	Highly biocompatible	Implants
Stainless steel	Mechanically strong, noncorrosive, highly DC polarizable and noisy, very alloy-dependent	Needles
Tin, lead	Low noise, soft and moldable	Electroencephalogram
Nickel	Thin flexible plates, skin allergic reactions	Skin surface
Silver, zinc, iron, aluminum	Pharmaceutical or bactericidal properties	DC therapy and skin iontophoresis
Carbon	X-ray translucent, soft and flexible multiuse rubber plates and wires	Skin surface electrocardiogram, electromyogram
Polymers	Also found as ionic or mixed versions, special consideration must be taken for the ionic contact medium. May be a part of the contact electrolyte	Skin surface
Mercury	In research laboratories. Unique as a mercury dripping electrode with the metal surface continuously renewed	

Metals listed are usually alloys. In practice, oxides are formed covering the surface (except for dripping mercury), and also on the noble metals and their alloys. Use of different metals in an electrode pair may generate large DC voltages that may saturate the input stage of biopotential amplifiers.

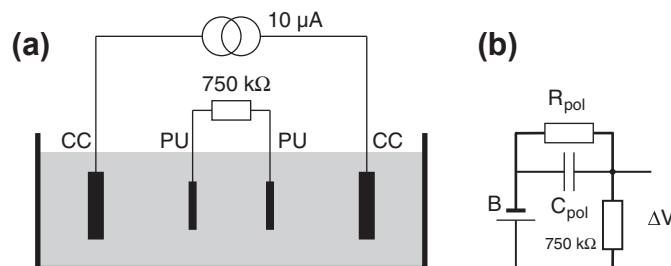


Figure 7.2: Metal dependence of polarizability. (a) Four-electrode system in 0.9% saline. (b) Equivalent electric circuit for the loaded PU electrode pair. B is the unloaded PU signal; output from six different metals as shown in [Figure 7.3](#) as registered with 750 k ohm load resistance. See text.

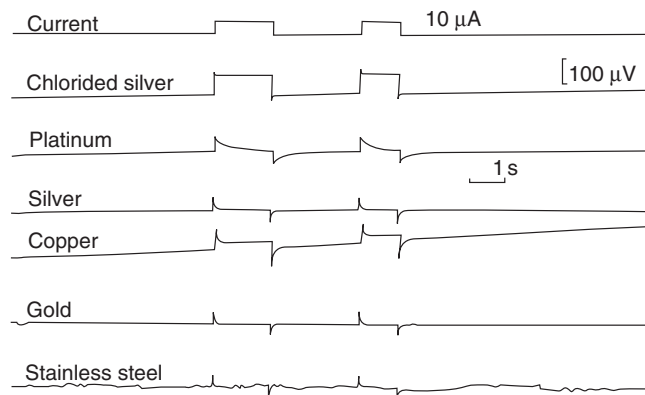


Figure 7.3: Measured voltage ΔV with six different pick-up electrode metals (see [Figure 7.2](#)).

between the CC and PU electrodes is $R = V/I = 100 \mu\text{V}/10 \mu\text{A} = 10 \Omega$. For platinum, the time constant is roughly 0.5 s , so that $C_{\text{pol}} = 0.5 \text{ s}/0.75 \text{ M}\Omega = 0.7 \text{ fF}$. Highly polarizable electrodes are dominated by a large C_{pol} with little influence from a large R_{pol} . As soon as the capacitor is charged, no more current flows and the output voltage is zero. According to [Figure 7.3](#), silver, gold, and stainless steel are all highly polarizable. But notice that replacing the load resistance of $750 \text{ k}\Omega$ with a much higher resistance will reduce the polarizing current through the PU electrodes, reduce the polarization, and reduce the waveform distortion.

[Figure 7.4](#) shows the result of a clinical measurement of biopotentials with three different metals in the PU electrodes. The signal source is endogenic: electro-oculography registrations are related to eye position and are measured with DC response biopotential amplifiers. It is clear that AgCl is the only material making the electrodes sufficiently nonpolarizable.

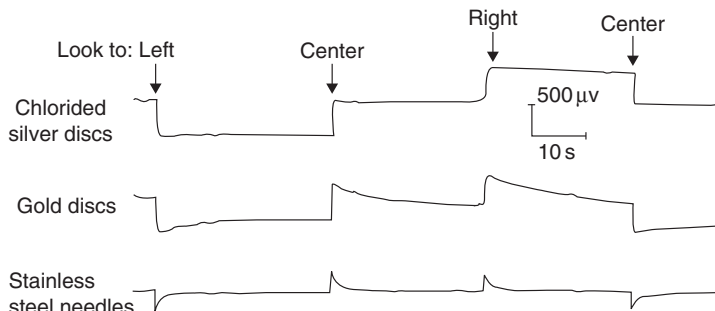


Figure 7.4: Recording of eye movements with different electrode metals. Electrode positions: 1 cm from the outer canthus of each eye. *Source:* Cooper et al. (1980).

7.3.2 Metal and Electronic Conductor Properties

Ag/AgCl

This is a much used electrode metal (*silver covered by silver chloride*) in biology and medicine for DC applications both because it is simple and because it has a well-defined DC potential not very dependent on DC current flow. It is therefore a nonpolarizable DC reference electrode. It usually consists of silver metal covered by an AgCl layer, often electrolytically deposited. Ag and AgCl are toxic and cannot be used in long-term living tissue contact. A salt bridge is often used to remove the electrode metal from direct tissue contact.

Wet AgCl is a solid ionic conductor. With DC current flow, the AgCl layer will increase in thickness if it is deposited on silver metal anode. The polarization impedance will go through a minimum and thereafter increase as a function of AgCl-layer thickness (see the following section). As a cathode with DC current flow, the layer will diminish and eventually be stripped of. We are left with a pure silver surface with quite different properties (e.g., with much higher polarization impedance and a different equilibrium potential) (Figure 7.3).

To produce an AgCl electrode, the silver is placed as the anode in a solution of, for example, 0.9% sodium chloride (NaCl). The optimum result is dependent on both the current density and quantity of electricity used; often the current density is of the order of 1 mA/cm^2 , and the quantity of electricity 1000 mA s/cm^2 (Geddes, 1972). Optimum values are not necessarily the same for minimum impedance and maximum DC voltage stability, and they are dependent on actual electrode surface area. The best AgCl-layer thickness also depends on the desired mechanical durability and the possible quantity of electricity that may be passed the opposite direction without stripping off the AgCl layer during use. A monopolar nerve stimulating electrode is nearly always used as cathode, and will therefore gradually strip of an AgCl layer. AgCl may also be *sintered* to form bulk AgCl; the surface can then be rubbed and thus be used many times.

Platinum Metals

Platinum electrodes are in certain ways the opposite of AgCl electrodes. Platinum is biocompatible and therefore highly suitable for invasive electrodes and implants. Even if it is highly DC-polarizable, it is still suitable for DC potential measuring applications under strict zero DC current conditions. Together with other noble metals and their alloys, they are also preferred as CC electrodes in contact with living tissue, in particular for pacemaker-implanted catheter electrodes. For pacing electrodes, Greatbatch (1967) found large differences between the pure noble metals and their alloys, except for Pt and Pt 90%, Ir 10%.

The platinum electrode can be improved by an active electrolytic process forming a platinum black surface. The reduced polarization impedance is due to an increased effective metal surface area (fractal surface). The electrode is prepared in an electrolyte containing (e.g., 3% platinum chloride), with the platinum as the cathode. Platinum black is deposited on the surface, and also here there are optimum values for current density and quantity of electricity: a current density of about 10 mA/cm^2 and a quantity of electricity (charge) of about $30,000 \text{ mA s/cm}^2$ is recommended (Schwan, 1963). Best results are obtained if the platinum surface is sandblasted before platinum black deposit. However, the surface may be fragile, and a protein layer formed with tissue contact may easily smooth the micro-rough surface and increase polarization impedance. Platinum black electrodes are best stored in distilled water and short-circuited (Schwan, 1963).

Titanium Alloys

Typically, titanium alloys have been the materials of choice for medical implants. The Ti-6Al-4V alloy is generally considered chemically inert, compatible with human tissue, and resistant to corrosion by human body fluids. However, the small percentages of vanadium and aluminum contained in the alloy are potentially toxic. Pure titanium is chemically and biologically more compatible with human fluids and tissue, but it is too weak for prostheses that must bear heavy loads, such as leg or hipbone implants.

7.4 Contact Electrolytes

The contact medium is an ionic conductor positioned between the electronic conductor and the tissue. Insulating materials such as glass that depend purely on displacement currents are a special group. The purpose of the contact electrolyte is to:

- control the metal-electrolyte interface
- form a high-conductance salt bridge from the metal to the skin or tissue
- ensure small junction potentials
- enable the metal–electrolyte interphase to be kept at a distance from the tissue
- fill out spaces between an electrode plate and tissue
- moisten a poorly conducting skin with electrolytes

The contact medium represents an electrolytic volume DC resistance in series with the polarization and tissue impedances.

The metal/electrolyte interface area is called the *electrode area* (EA). EA may be the plane area or include a surface roughness or fractal factor. The interface area of the contact medium and the tissue is called the *effective electrode area* (EEA). Skin surface electrodes are often EEA > EA ([Figure 7.30](#)). Electrolyte-filled glass micro-electrodes are often EEA < EA.

On tissue, the contact area is very important:

- large EA implies low electrode polarization impedance
- small EEA may imply geometrically dependent on current constriction effect (see Figure 6.3) and a larger influence from the tissue or electrolyte volume near the electrode.
- large EEA for *recording* electrodes implies low noise, an averaging effect, and loss of spatial resolution.
- large EEA for *stimulating* electrodes implies higher excitable tissue volume and a summation effect in the nerve/muscle system.

The stratum corneum layer of nonwetted human skin is strongly variable and may be very poorly conductive. As we shall see, the skin is often dominating the electrical properties of an electrode used for recording endogenic signal sources such as the ECG. This skin influence is therefore treated here. For additional information on skin electrical properties, see Chapter 4.

7.4.1 Contact Media Descriptions

Wet Gel or Paste with Electrolytes

The mechanical or viscous properties of the contact medium are important, and often the electrolyte is thickened by a gel substance or contained in a sponge or soft clothing. Commercial electrocardiogram (ECG) electrodes are often delivered as pregelled devices for single use, and the medium may contain preservatives to increase storage life, or quartz particles for abrading purposes on the skin.

Generally, the ionic mobility and therefore the conductivity in a high viscosity paste are lower than in a liquid. Wet electrolytes of high concentration ($>1\%$) penetrate the skin actively, with a time constant often quoted to be of the order of 10 min (Tregear, 1966; Almasi et al., 1970; McAdams et al., 1991b). However, actually the process is not exponential (as diffusion processes are not), and may go on for hours and days (Grimnes, 1983a) (see Figure 4.20). The penetration is stronger the higher the electrolyte concentration, but also more skin irritating. NaCl is better tolerated by human skin at high concentration than most other electrolytes. [Figure 7.5](#) shows the electrolyte penetration into the skin the first 4 h after electrode onset to the skin. Impedance at 1 Hz is dominated by stratum corneum electrolyte content, with less than 1% contribution from the electrode's own small-signal polarizing impedance. If sweat ducts are filled or have recently been filled, the conductance of the ducts shunts the high impedance of the dry stratum corneum.

The conductivity σ of some often used contact creams/pastas are: Redux creme (Hewlett Packard) 10.6 S/m, Electrode creme (Grass) 3.3 S/m, Beckman-Offner paste 17 S/m,

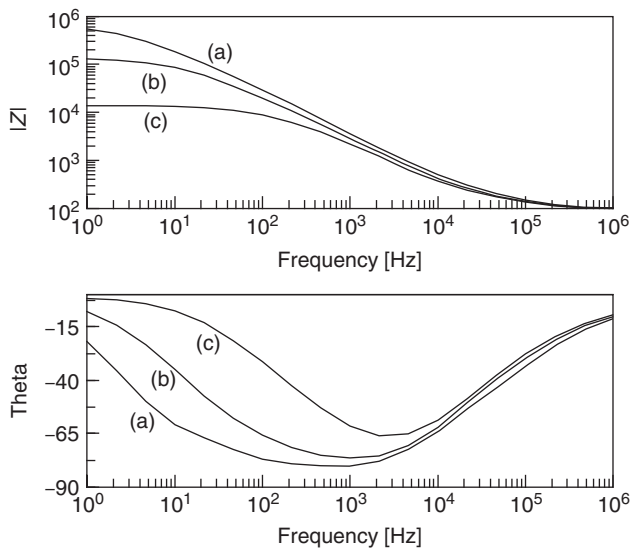


Figure 7.5: Spectra of skin impedance plus electrode polarization and the effect of wet contact electrolyte-skin penetration. Values just after electrode onset (a) and after 1 (b) and (c) 4 h. One commercial pregelled ECG electrode on forearm, skin wetted area 3 cm^2 .

NASA Flight paste 7.7 S/m, and NASA electrode cream 1.2 S/m. NASA Flight paste contains 9% NaCl, 3% potassium chloride (KCl), and 3% calcium chloride (CaCl), in total 15% (by weight) of electrolytes. Thick electroencephalogram (EEG) paste may contain as much as 45% KCl.

In comparison, 0.9% NaCl (by weight) physiological saline solution has a conductivity of 1.4 S/m; most gels are therefore strong electrolytes. Seawater contains about 3.5% salts, and the Dead Sea contains $>25\%$ salts with a composition of 50% MgCl₂, 30% NaCl, 14% CaCl₂, and 6% KCl. That is quite different from seawater salt (NaCl 97% of total salt content). The Dead Sea is called “dead” because its high salinity prevents plants and fish from living there.

Experience has shown that the stronger the gel, the quicker the penetration into the skin and sweat ducts. However, skin reactions such as skin irritation and reddening are also faster. For a quick ECG examination, stronger gels can be used; for monitoring during days, the contact gel must be weak. Most people appreciate hours of bathing in seawater, so a salt content of 3.5% should in many cases be acceptable.

For electrodermal activity (Chapter 10.3), a contact wet gel must have a low salt content to assure rapid emptying of the ducts.

Salt Bridges

Usually it is an advantage to have the electrode metal at a distance from the tissue. An example is shown in Figure 7.6. Movement in the junction's tissue, gel, or metal generates noise. The metal may be less biocompatible and may irritate the living tissue.

Human skin impedance is usually much higher than electrode polarization impedance (Grimnes, 1983a). As they are physically in series, Figure 7.6, electrode polarization impedance can often be neglected in skin applications. In Figure 7.6, R_{cnstri} is related to the current constricting zone of the electrode (see Figure 6.3).

In some skin applications, the electrode polarization impedance may still be a source of error. With solid gel contact electrolytes, the series resistance of the contact medium may be disturbing at higher frequencies. When the stratum corneum is highly penetrated by electrolytes (Figure 7.5), the skin impedance is so low ($50\text{ k}\Omega$) that the electrode polarization impedance becomes important.

Skin impedance is of great concern both for recording and current carrying applications. High electrode impedance and relatively low amplifier input impedance has been a problem in ECG right from the time of Einthoven, who used large electrolyte containers with the limbs deeply immersed. A classical study for ECG applications is by Geddes and Baker (1966). Rosell et al. (1988a) measured the impedance of skin coated with gel, but otherwise unprepared, and found that for 1 cm^2 , the impedance at 1 Hz varied from $10\text{ k}\Omega$

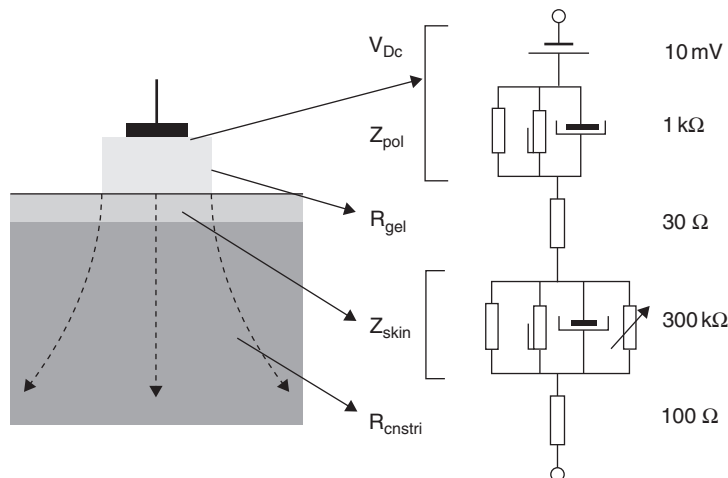


Figure 7.6: Skin surface electrode geometry and its equivalent electric model. Right: Typical values at 10 Hz for a commercial wet gel ECG electrode. Note that Z_{skin} before contact electrolyte penetration is >99% of the total impedance.

to $1 \text{ M}\Omega$ and at 1 MHz was always close to 120Ω . They measured at sites typically used for ECG, impedance plethysmography, impedance cardiography, and electrical impedance tomography and stressed the importance of considering these values for designers of biopotential amplifiers. Also McAdams and Jossinet (1991b) reexamined the problem with respect to the increased demands posed by the renewed interest in high-resolution ECG recording. See Chapter 4 for more information on skin electrical properties.

Solid Gel (Hydrogel), with or without Adhesive Properties

Hydrogels are crosslinked polymers. They can contain more than 99% water by absorption. The process is accompanied by strong swelling, but polymers are not dissolved. Gelatin is a natural substance and an example of a hydrogel. A solid gel may constitute both the contact electrolyte and the adhesive surface. Solid gels have natural or synthetic hydrocolloids (McAdams et al., 1991b). They do not wet the skin, and when applied to the skin the gel may moisten the skin or the skin may moisten the gel. Water transport is diffusion controlled to the material with the lowest partial pressure of water. In contrast to wet gels, the effective electrode area, when applied to the skin, is rather constant and well-defined. Hydrogels as skin contact medium have been found to give smaller parallel DC conductance and higher capacitance coupling than wet contact media (McAdams et al., 1991b). This implies less wanted properties the lower the frequency, but desired properties in high-frequency applications such as for electrosurgery plate electrodes.

The importance of choosing the correct type of electrode gel is obvious from [Figure 7.7](#). Tronstad et al. (2010) measured low-frequency conductance with a solid gel electrode (a) and a wet gel electrode (b) on the abdomen of a test subject. The two time-courses are markedly different. The conductance measured with the solid gel decreases in the first minutes. This is probably because of decreased sweat activity from the passive person. After some seconds of physical exercise, the conductance increases, however, indicating increased sweating. The wet gel of electrode (b), however, penetrates the stratum corneum, giving a steady increase in conductance even if the person is passive. The gel will also penetrate into the sweat ducts and because it is better conducting than the sweat, the measured conductance will actually decrease when the gel is replaced by sweat during increased sweating. Hence, this negative conductance wave is a pure artifact produced by the electrode gel.

7.4.2 “Dry” and Dielectric Contact

“Dry” Plate Contact

Putting a dry metal disk on dry human skin results initially in a quick step admittance increase. It corresponds to the stratum corneum as a dielectric between the two plates

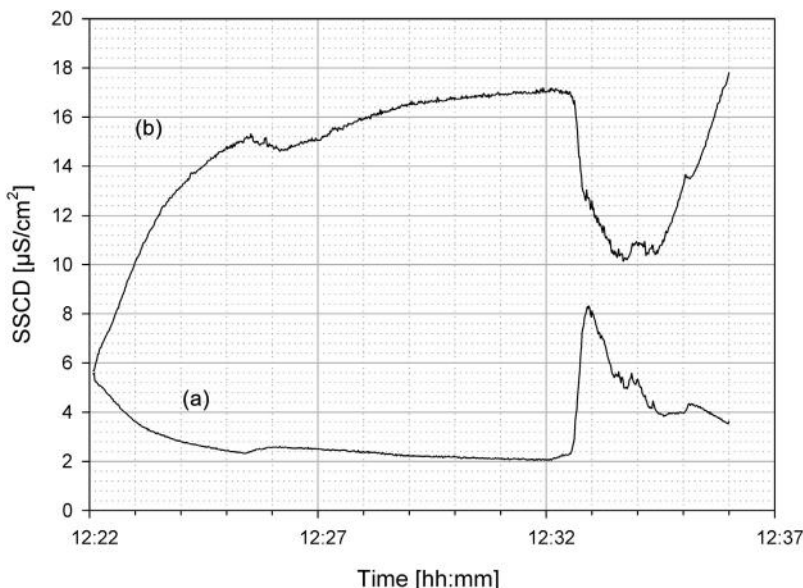


Figure 7.7: Measurements on the abdomen with solid gel (a) and wet gel (b) electrode. A 2-min exercise period was performed between 12:32 and 12:34. *From Tronstad et al. (2010) with permission.*

(Figure 3.1) formed by the electrode metal plate and the electrolytic ionic conductive layer in the living part under the dead stratum corneum layer. Water molecules from the imperceptible perspiration immediately start to cover the metal plate, making ionic contact between the metal plate and the skin surface. After the initial step, there is a rapid admittance rise as the natural water of the skin gradually wets the dry metal surface. It is possible to stabilize the first minute or so by applying a short breath toward the dry plate or the skin (see Grimnes, 1982). Before disk onset the water content of the superficial layers of the stratum corneum is determined by the partial pressure of water vapor in the surrounding air, and on the recent sweat activity. After some hours, the conditions may become more like the applied wet gel case.

Dielectric Dry Contact Plate

Figure 7.8 shows a capacitive electrode system. One half-cell is an ordinary indifferent electrolyte-skin electrode. In the other half-cell, the electrolyte has been replaced by a dielectric so that there is no galvanic coupling between the electrode metal plate and the skin. The dielectric is usually a thin layer of a chloride or oxide of the metal in the electrode plate. The metal plate functions as a substrate for the thin dielectric that can be made from anodizing or oxidizing silver, aluminum, silicon, or titan. The dielectric must be robust and endure humidity and sweat arriving from the skin. The capacitance between the metal plate and the skin is dependent on contact area, dielectric thickness, and

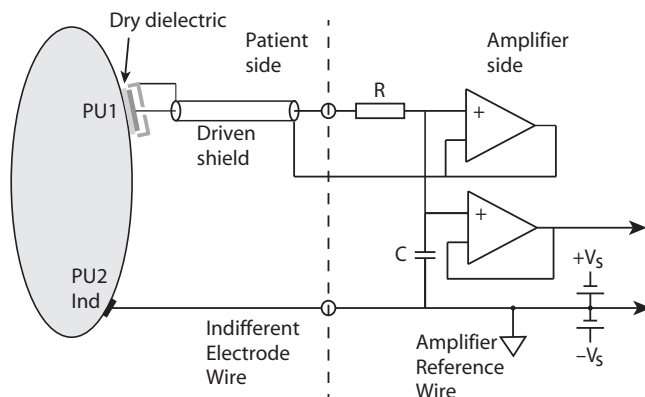


Figure 7.8: Capacitive monopolar PU electrode with skin-to-dielectric contact. Indifferent electrode can serve many capacitive electrodes.

permittivity. Capacitance values can be found in the range 0.1–10 nF. Resistance ought to be of the order of $1\text{ G}\Omega$, but if the dielectric is brittle and sweat can penetrate the dielectric, then slowly the electrode will be more galvanic. There is no well-defined supply of bias current for the two noninverting inputs of the operational amplifiers (opamps).

Noise is a problem with capacitive electrodes. In Figure 7.8, active shielding is used around the electrode and the electrode cable. The low-pass filter RC protects the two opamps against electrostatic discharges. Figure 10.33 shows that an electrostatic discharge lasts just a few microseconds.

Tissue Liquid Electrolytes

Invasive electrodes usually have metal in direct contact with the tissue. The metal must then be biocompatible for the duration of tissue contact. The electrical properties will be dependent on the metal and the tissue.

Electric Arc

A special ionic contact medium, to skin or any tissue surface, is a gas *plasma*. Plasma is an ionized, and therefore conductive, gas. The ionization process is high electric field-induced, and the process is enhanced in inert gas atmospheres such as argon.

In its simplest form, an arc may be drawn from a needle electrode to the skin surface. The arc will seek high conductive spots like the sweat duct orifices. The arc may be DC or AC driven, and in air about 2000 V/mm distance is necessary for ignition with a steady state current in the microampere range.

A single spark is the usual contact medium with electrostatic discharges in daily life situations (Section 10.16).

In electrosurgery, argon is used as a gas medium for radiofrequency (RF) coagulation of tissue surfaces. The argon gas flow guides the arc and facilitates the spread coagulation over a larger area. At the same time, oxygen reactions are impeded, and thus carbonization of tissue occurs.

7.4.3 Skin Preparation

Even a light abrasion of the skin surface is a surprisingly effective way of lowering the skin impedance the first half-hour or so. This is because dry stratum corneum contributes more than 99% of the total electrode impedance (10 Hz, see [Figure 7.6](#)). Because the stratum corneum is very thin, about 10–15 µm except on palmar and plantar sites, removing just 5 µm of surface layers can be quite effective.

Washing the skin with tap water will lower the impedance. Washing with alcohol may remove ions of saline, and the impedance may initially increase.

Other methods have also been tried in order to avoid the high impedance of the skin. Vitreous carbon buttons have been implanted in the skin, and tattooing techniques have been used for depositing colloidal carbon in the skin (Hoenig et al., 1978). Black dot areas of about 8 mm in diameter showed reduced impedance at 1 Hz. The effect was reported to be equally active after more than 2 years.

Collodion

Collodion is a syrupy compound of pyroxylin (nitrocellulose), ether, and alcohol. It dries up to a transparent, tenacious film used as a typical protectant. Collodion is widely used to glue electrodes to the head for EEG.

7.5 Electrode Double Layer

Double layer is a much broader concept than just what we meet in an electrode at the interface between the metal and the electrolyte. It is a contact phenomenon because two different molecular structures meet and a rearrangement must take place in the transition zone. It is generated at the contact boundary between two phases, either or both of which may be solid, liquid, or gas. It is a molecular phenomenon generated by the abrupt meeting of two different molecular structures, and the two materials may be of different or same phases. For instance, when two dry solid state plane blocks are in sliding contact, the double layer is the place of friction. Static electricity is generated when two such blocs are suddenly separated (see [Section 4.3.4](#)). When two different liquids are in contact, a double layer is formed in the interphase. Ions in the bulk electrolyte are free to move, but approaching the double layer they are gradually bound by the charge distribution in the double layer. At the metal side the atoms or molecules are strictly bound and hence only

the surface contributes to the double layer. The double layer therefore only extends into the electrolyte side and not the metal side.

We must not be deceived by the seemingly simple construction of an electrode: a metal plate in contact with an electrolyte. Many critical processes are hidden in the nanometer thin double layer:

1. The energy barrier in a double layer depleted of charges.
2. The exchange of electrons from the metal plate with the ions of the contact electrolyte.
3. The site of chemical redox reactions when an externally electric current is applied.
4. The nonlinear properties of the double layer.
5. The DC potential generated in the double layer.
6. The special RF properties of the double layer.
7. The ability to adsorb or desorb substances at the double layer.
8. Electrode polarization impedance or counter emf.

7.5.1 Electric Double Layer, Perpendicular Fields

At the metal/liquid interphase, the conversion from *electronic* to *ionic* conduction occurs. The electrode metal is the source or sink of electrons, and *electron transfer* is the key process whereby the electrode exchanges charges with the arriving ions, or ionizes neutral substances (a second mechanism of charge transfer is by oxidation of the electrode metal: the metal leaves the surface as charged cations and enters the solution). Without electron transfer, there is no chemical electrode reaction, no DC electrode current, and no faradaic current. In the solution at the electrode surface, the electric *double layer* is formed as soon as the metal is wetted. Electron transfer takes place somewhere in the double layer.

An electrical potential will be generated across the interphase according to the Poisson Eq. (7.1). This effect is particularly pronounced at the interphase between a solid and a polar medium, as with water, where the surface charges of the solid will attract counterions from the polar medium. When the polar medium is a liquid where the ion mobility is high, the formation of an electric double layer will therefore take place in the liquid phase.

In this chapter, the double layer charge will be treated as a function of the distance *perpendicular* to the surface. In the next section, we will treat counterion movements *lateral* along the surface.

Simple Helmholtz Layer

The double layer can be thought of as a molecular capacitor, where one *plate* is represented by the charges in the metal and the other *plate* by the ions at a minimum distance in the solution. The distance between the “plates” is of molecular dimensions

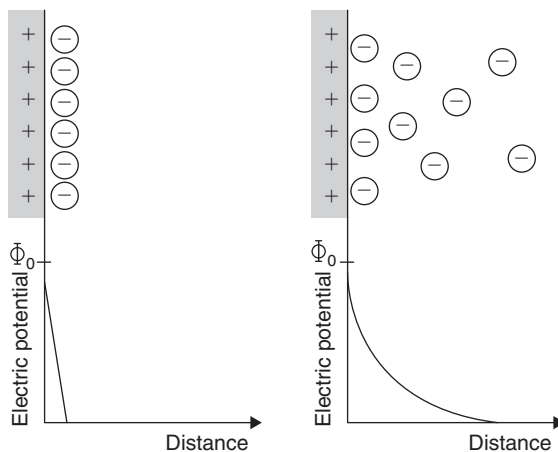


Figure 7.9: Helmholtz' (left) and Gouy-Chapman's (right) model of the electric double layer and electric potential as a function of distance from the electrode surface.

(e.g., in the order of 0.5 nm), so the capacitance values are enormous. This simple model of the electric double layer was introduced by Helmholtz in 1879, and is *valid only for rather high-concentration electrolyte solutions* (Figure 7.9 left). In this simplest model, the double layer is depleted from charges. In more dilute solutions, the transition will not be so abrupt and the thickness of the double layer will *increase*. The thickness is related to the distance from the metal surface at which the ions can escape to the bulk by thermal motion. In that case, the counterion atmosphere will be more like the ionic atmosphere around an individual ion; this is commonly referred to as the *diffuse electric layer*.

General Theory of Gouy-Chapman

In the combined theory of Gouy and Chapman, the exchange of counterions between the double layer and the bulk solution due to thermal motion is taken into account. Both coulomb forces and thermal motion hence influence the equilibrium distribution of counterions in their model for the diffuse double layer (Figure 7.9, right).

The assumptions for their theory are, among others:

1. The surface charge is continuous and uniform.
2. The ions in the solution are point charges.

The electric potential in the double layer is given by the Poisson equation:

$$\nabla^2 \Phi = -\frac{q_{vf}}{\epsilon_0} \quad (7.1)$$

where Φ is the electric potential, q_{vf} is the volume density of free charges, and ϵ is the permittivity of the medium, and furthermore by the Boltzmann equation:

$$n_i = n_0 \exp\left(\frac{-W_{\text{el.}}}{kT}\right) \quad (7.2)$$

where n_i is the concentration of an ion “i” at a given point, determined by coulombic forces and thermal motion, n_0 , is the concentration in the bulk solution and the electric work $W_{\text{el.}} = z_i e \Phi$, where z_i is the charge per ion. The Poisson equation for the diffuse double layer will then be:

$$\nabla^2 \Phi = \frac{2z_e n_0}{\epsilon} \sinh\left(\frac{ze\Phi}{kT}\right) \quad (7.3)$$

We then introduce:

$$\kappa = \sqrt{\frac{2z^2 e^2 n_0}{\epsilon k T}} \quad [1/\text{m}] \quad (7.4)$$

where $1/\kappa$ is referred to as the thickness of the double layer (also called the Debye length), and is used in the simplifications of Eq. (7.3). In physiological electrolyte solutions it is about 10 nm, smaller the higher the electrolyte concentration.

Debye-Hückel Approximation

The Debye-Hückel approximation may be used if the surface potential is small:

$$\Phi_0 \ll \frac{kT}{ze} \quad (7.5)$$

(approximately 25 mV for a monovalent electrolyte at 25°C). The simplification will then be made by replacing $\sinh(x)$ with x .

For a spherical double layer, the solution using the Debye-Hückel approximation, will be:

$$\Phi = \Phi_0 \frac{a}{r} \exp[-\kappa(r - a)] \quad (7.6)$$

For a flat double layer (i.e., when $a \gg 1/\kappa$), the solution will be

$$\Phi = \Phi_0 \exp(-\kappa x) \quad (7.7)$$

General Theory of Stern

The theory of Gouy-Chapman becomes inadequate when κ and/or Φ_0 are large. The theory of Stern takes the finite size of the counter-ions and their binding properties at the surface, into account. The diffuse layer is divided into an inner layer (the Stern layer) and an outer

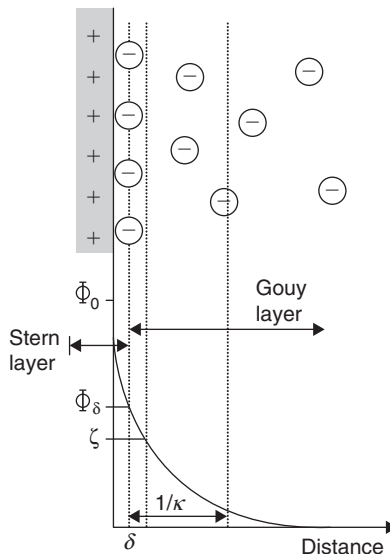


Figure 7.10: Stern's model of the diffuse electric double layer.

layer (the Gouy layer), as shown in Figure 7.10. The Stern layer includes any adsorbed layer of ions. It is separated from the Gouy layer at the Stern plane at a distance δ from the surface. This distance corresponds roughly to the radius of a hydrated ion. The ions are adsorbed in the Stern layer according to the Langmuir adsorption isotherm. The theory of Gouy-Chapman is still applicable in the Gouy layer, but Φ_0 is replaced by Φ_δ , which is the potential at the Stern plane. In case of strong specific adsorption in the Stern layer, Φ_0 may be smaller than Φ_δ , or they may have opposite polarity. The potential at the Stern plane, Φ_δ , may in most cases be assumed to be equal to the so-called zeta (ζ)-potential, which is the electrokinetic potential which can be determined experimentally by means of, for example, electrophoresis or streaming potential measurements. The zeta-potential is the potential at the shear plane between the charged surface and the liquid (i.e., the potential at the boundary of, for example, a moving particle with its adsorbed ions). The Stern theory is complicated, and will not be treated in any detail in this book. Stern theory should be used when the surface potential is high, or when the solution is concentrated so that a significant part of the potential drop occurs in the Stern layer. Gouy-Chapman theory may be adequate also at higher concentrations if the surface potential is small.

Grahame made a further division of the Stern layer into the inner Helmholtz layer and outer Helmholtz layer. These layers are separated by the inner Helmholtz plane at a distance from the surface corresponding to the radius of nonhydrated specifically adsorbed ions. These ions are smaller than the counterions, and the inner Helmholtz plane is hence located between the Stern plane and the surface. The outer Helmholtz layer is limited by the outer Helmholtz plane, which is identical to the Stern plane.

7.5.2 Electric Double Layer, Lateral Fields

Schwarz Theory for a Suspension of Spheres

Schwarz wanted to use the theories of electric double layers to describe the measured α -dispersion of particle suspensions. He considered the case of an electric double layer at the surface of a spherical particle, as shown in [Figure 7.11](#).

The counterions will be electrostatically bound to the surface charges of the sphere, but will be *free* to move laterally along the surface. When an external field is applied, the positive counter ions in [Figure 7.11](#) will move toward the cathode, but without leaving the surface of the sphere (this polarization effect is largely exaggerated in [Figure 7.11](#)). The reestablishment of the original counter-ion atmosphere after the external field is switched off, will be diffusion-controlled, and the corresponding time constant according to Schwarz theory is

$$\tau = \frac{a^2}{2D} \quad (7.8)$$

where $D = \frac{\mu kT}{e}$ and a is the particle radius.

Later Improvements of Schwarz Theory

Schwarz theory provides a practical tool for analyzing measured data, but the theory has been criticized for neglecting the diffusion of ions in the bulk solution near the surface. Efforts have been made by, among others, Dukhin, Fixman and Chew, and Sen to employ Gouy-Chapman theory on particle suspensions, but the resulting theories are very complex and difficult to use on biological materials. Mandel and Odijk (1984) have given a review of this work.

Simplified models that use the Gouy-Chapman theory have been presented by, for example, Grosse and Foster (1987), but the assumptions made in their theory limits the utility of the model.

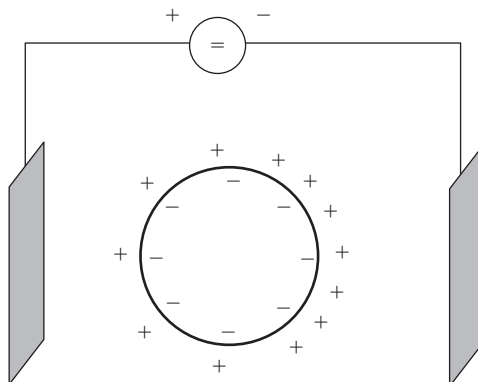


Figure 7.11: Counter-ion polarization near the surface of a spherical particle.

Effect of Hydration

Hydration of ions is due to the dipole nature of water. In the case of a cation in water, the negative (oxygen) end of the neighboring water molecules will be oriented toward the ion, and a sheet of oriented water molecules will be formed around the cation. This sheet is called the primary hydration sphere. The water molecules in the primary hydration sphere will furthermore attract other water molecules in a secondary hydration sphere, which will not be as rigorous as the primary sphere. Several sheets may likewise be involved until at a certain distance the behavior of the water molecules will not be influenced by the ion.

7.6 DC Potentials, No Current Flow

With zero DC current in the electrode wire, the electrode is at equilibrium. A polarization still existing must therefore be endogenic. Even with zero current flow in the electrode, wire local currents may flow caused by inhomogeneities of the metal surface or contact with a nonisoelectric tissue area. Endogenic polarization is important and manifests itself by a polarization immittance measured with low AC currents so that the system is linear (see Section 8.4).

7.6.1 Metal/Ion and Redox Systems

Metal/Ion Systems

According to Nernst, metals have a tendency to send their ions into a solution as solvated particles. The potential difference arises from this transfer of positive metal ions across the double layer, with a resulting negative potential on the metal surface. The standard potential of such a metal/ion half-cell are shown in [Table 7.2](#), the reference electrode is the *hydrogen electrode*. Volta's original findings were in rough accordance with this table. The least noble metals have the largest tendency to send their ions out into the solution generating the most negative electrode potentials. For noble metals, the number of metal ions sent out in the solution may be small, and the potential must then be measured under the most strict zero current conditions.

Redox Systems

With an external DC power supply connected to the electrolytic cell, the applied voltage that gives *no DC current flow* in the external circuit corresponds to the *equilibrium potential* of the half-cell (or actually the cell). It is the same voltage as read by a voltmeter with very high input resistance and virtually no current flow (pH meter). In electrochemistry, *potentiometry* is to measure the potential of an electrode at zero current flow, which is when the cell is not externally polarized. To understand the equilibrium potential with zero external current, we must introduce the concept of *electrode reaction*.

Table 7.2: Metal/Ion Equilibrium Potentials

Metal/Metal Ion	V_o [volt]
Li/Li ⁺	-3.05
K/K ⁺	-2.93
Na/Na ⁺	-2.71
Al/Al ³⁺	-1.66
Zn/Zn ²⁺	-0.76
Fe/Fe ²⁺	-0.44
Ni/Ni ²⁺	-0.25
Sn/Sn ²⁺	-0.14
Pb/Pb ²⁺	-0.13
H₂/H⁺	0
Carbon	Dependent on structure
Cu/Cu ²⁺	+0.34
Ag/Ag ⁺	+0.80
Pt/Pt ²⁺	+ ~1.2
Au/Au ³⁺	+1.50

and link it with an electric current in the external circuit. An electrode reaction going rapidly both ways (ionization/de-ionization, reduction-oxidation) is called *reversible*. A pure redox system presupposes an inert electrode metal with no metal ion transfer to the solution. At the electrode the redox system is:

anode is the *electron sink*, where ions or neutral substances lose electrons and are oxidized: $\text{red} \rightarrow \text{ox} + \text{ne}$.

cathode is the *electron source* where ions or neutral substances gain electrons and are reduced: $\text{ox} + \text{ne} \rightarrow \text{red}$.

However, an element that is *oxidized* loses electrons but the element is referred to as the reducing agent. Memory rule: OIL—Oxidation Is Loss (of electrons).

Likewise, an element that is *reduced* gains electrons and is referred to as the oxidizing agent.

The metal/ion half-cell generates a potential by the exchange of *metal ions* between the metal and the electrolyte solution. In contrast, a *redox* half-cell is based upon an exchange of *electrons* between the metal and the electrolyte solution. So actually there are two sets of standard potential tables, one for metal/ion half-cells ([Table 7.2](#)) and one for redox half-cells ([Table 7.3](#)). The half-cell potential is of course *independent* of the interphase area,

Table 7.3: Standard Equilibrium Electrode Potentials for Some Redox Systems

Electrode	Electrode Reaction	V_o [volt]
Pt	$2H_2O + 2e^- \leftrightarrow H_2 + 2OH^-$	-0.83
Pt	$O_2 + 2H_2O + 2e^- \leftrightarrow H_2O_2 + 2OH^-$	-0.15
Pt	$2H^+ + 2e^- \leftrightarrow H_2$	0
Carbon	$\rightarrow ?$?
AgCl	$AgCl + e^- \leftrightarrow Ag + Cl^-$	+0.22
Calomel		+0.28

because equilibrium potential is without current flow. As soon as the cell is externally polarized and a current is flowing, electrode area is of interest (current density).

7.6.2 The Nernst Equation

The Nernst equation relates the redox process and the potential giving zero current flow. In the solution of an electrolytic cell, it indicates the *redox equilibrium potential V with zero DC current flow*:

$$V = V_o + \left(\frac{RT}{nF} \right) \ln \left(\frac{a_{ox}}{a_{red}} \right) \quad \text{The Nernst equation} \quad (7.9)$$

Here V_o is the standard electrode potential of the redox system (with respect to the hydrogen reference electrode at 1 mol concentration), n is the number of electrons in the unit reaction, R is not resistance but the universal gas constant, and F is the Faraday constant (see [Section 7.8](#)). a_{ox} and a_{red} are *activities*, $a = \gamma c$, where c is the concentration and γ is the activity *coefficient*. $\gamma = 1$ for low concentrations (no ion interactions), but < 1 at higher concentrations. The half-cell potentials are referred to standardized conditions, meaning that the other electrode is considered to be the standard hydrogen electrode (implying the condition: pH = 0, hydrogen ion activity 1 mol/L). The Nernst concept is also used for semipermeable membranes with different concentration on each side of the membrane (see [Section 7.6.4](#)).

In [Eq. \(7.9\)](#), the RT/nF factor can be substituted with -61 mV for room temperature and using the common instead of the natural logarithm. Then the Nernst equation becomes:

$$V = V_o - 0.061 \log \left(\frac{a_{ox}}{a_{red}} \right)$$

The Nernst equation presupposes a *reversible* reaction: that the reaction is reasonably fast in both directions. This implies that the surface concentration of reactants and products are maintained close to their equilibrium values. If the electrode reaction rate is slow in any direction, the concentration at the electrode surface will not be equilibrium values, and the Nernst equation is not valid, the reactions are *irreversible*.

For metal cathodes, the activity of the reduced forms a_{red} is 1, and the equation, for example, for an AgCl electrode is:

$$V = V_{\text{AgCl}/\text{Ag}} - \left(\frac{RT}{F} \right) \ln a_{\text{cl}^-} \quad (7.10)$$

where R is the universal gas constant.

According to Eq. (7.10), the DC potential is only dependent on the activity of the Cl^- anion in aqueous solution (and temperature). The silver–silver chloride electrode is an example of an “electrode of the second kind:” the electrode metal (AgCl) is in equilibrium with a low solubility salt of its ions (Ag^+).

7.6.3 Electrode Pair DC Voltage

If different metals are used in a PU electrode pair, the different half-cell potentials may easily create a DC voltage output of 1 V or more. This may represent a source of noise and may saturate the input stage of the biopotential amplifier used. Inhomogeneous surfaces may create local potential differences, local DC current flow, and local corrosion, even with zero current flow in the electrode wires. If an AgCl surface is partly stripped its coating so that some pure silver surface appears, the DC voltage will change and the noise level will increase (see Table 7.2 for half-cell potentials).

Two *equal* AgCl plates immersed in a homogeneous chloride electrolyte, will in practice generate <1 mV DC, under well-controlled conditions just a few microvolts.

The *noble metals* in saline solution are highly polarizable, and the DC voltage will be unstable and poorly defined unless under strict zero current conditions. Metal alloy inhomogeneity will create noise as a function of local current flow between different parts of the metal surface. The noise generation of stainless steel electrodes is very dependent on the alloy composition (see Section 7.3).

According to Tables 7.2 and 7.3, two different electrode materials in the same electrolyte solution may generate 1 V or more. Superimposed on signals in the microvolt range, this may create noise and be a problem for the input amplifiers. If both electrode surfaces are of, for example, stainless steel in saline, there are not necessarily any redox reactions at the surface at all. The voltage is not well defined and may easily attain 100 mV or more, the system is highly polarizable and the output voltage noisy. But even strongly polarizable electrode metals such as stainless steel, platinum, or mercury have an electrode reaction if the applied DC voltage is high enough. This is both on the anodic and cathodic side, but the reactions are irreversible and therefore not redox reactions.

Under zero current condition, many metal electrodes are of interest in biological work. The platinum electrode for instance becomes an interesting redox potential recording

electrode. An inert platinum electrode may actually be used in potentiometry in the bulk of a redox system, during titration or in, for example, seawater analysis. With zero current, the inert platinum will pick up the redox equilibrium potential of the process.

7.6.4 Liquid Junction DC Potential, Salt Bridge

Between two dissimilar electrolyte solutions a potential difference is created, just like between a metal and an electrolytic solution. By Brownian motion, the ions randomly walk with a velocity proportional to the Boltzmann factor kT . The corresponding E-field will have a direction to slow down the rapid ions and accelerate the slow ones in the interface zone. The resulting potential difference is called the *liquid junction potential* (Φ_{lj}) and follows a variant of the Nernst equation called the *Henderson* equation:

$$\Phi_{lj} = \frac{\mu^+ - \mu^-}{\mu^+ + \mu^-} \frac{RT}{nF} \ln \frac{c_1}{c_2} \quad [\text{volt}] \quad (7.11)$$

where R is the universal gas constant and μ^+ and μ^- are the mobilities of cations and anions, respectively. In biological application, it must be remembered that adsorbed species at the electrode surface may change the half-cell potentials.

The liquid junction potential is usually less than 100 mV. For instance, for a junction of different concentrations of NaCl and with $c_1 = 10c_2$, the dilute side is 12.2 mV negative with respect to the other side.

Salt Bridge

The salt bridge usually represents a low resistance bridge to the tissue and makes an effective contact with only a small liquid junction potential. The solution may be in the form of a liquid, a paste, a gel, or a hydrogel. The ionic mobilities are less the higher the viscosity of the medium, and the liquid junction potential thus changes according to Eq. (7.11).

The liquid junction DC potential generated by a salt bridge is minimized if the mobilities of the ions used are as equal as possible, see Eq. (7.11). This is, for instance, the case for K^+ and Cl^- , and a salt bridge therefore often contains a strong KCl electrolyte. Then it may be necessary to impede the strong electrolyte from reaching the tissue or measuring cell, by introducing a rather tight plug or filter. The influence of the cations Na^+ , K^+ , and Ca^+ is different on living cells and tissue, so the choice between NaCl, KCl, or CaCl may be very important.

The K^+ Cl^- ions have about the same mobilities, and therefore KCl creates a lower liquid junction potential than, for example, NaCl. The liquid junction DC potential can be kept small by inserting a salt bridge between the solutions, so that there will be two junctions

instead of one. By using a concentrated solution of KCl in the bridge, it can be shown that the two junction potentials will tend to be equal and be dominated by the concentrated salt solution, but with opposite sign so that they more or less cancel.

In electrophysiology requiring DC stability, AgCl electrodes are widely used. They may be used with a salt bridge filled with saturated KCl. Even if the salt solution is immobilized with agar gel at the tissue side, potassium is known to influence excitable cells, and it may be preferable to use NaCl 0.9% instead. A liquid junction DC potential must then be accounted for.

DC measurements of skin potentials are of particular interest. Often palmar skin is at about -20 mV with respect to an invasive electrode or a nonpalmar skin surface electrode. Such a voltage is very dependent on the contact electrolyte used, dependent on the liquid junction potential between the salt bridge and the natural electrolytes (sweat) of the skin. It is found that the measured DC voltage is very dependent not only on the concentration of the salt, but also on the cations (e.g., Na^+ , K^+ , Ca^+) used.

7.6.5 Membrane Equilibrium (Donnan) Potentials

The liquid junction potential was defined with no membrane separating the two media. A membrane separating an electrolyte in two compartments is often selectively permeable (e.g., rather open to water), but less permeable to certain ions or larger charge carriers. The selectivity may be due to the mechanical dimensions of pores, or charge dependent forces.

With different concentrations on each side, such membranes generate an osmotic pressure difference. With different ionic concentration also an electrical potential difference is generated. This is called the *Donnan potential difference*, Φ_d :

$$\Phi_d = \left(\frac{RT}{F} \right) \ln \frac{a_1}{a_2} \quad [\text{volt}] \quad 7.12$$

where a_1 is the activity of a specified ion on compartment side one and R is the universal gas constant.

7.6.6 Reference Electrodes

In the field of bioimpedance, by far the most important nonpolarizable electrode for stable DC potential measurement is the *AgCl electrode*. This is because all tissue liquids contain some Cl^- ions, and because the electrode can be made very small (e.g., with just a small chlorided silver wire). The half-cell potential relative to a standard hydrogen electrode at 25°C in an aqueous solution is $+0.222\text{ V}$. Under ideal conditions such an electrode can be reproducible to $\pm 20\text{ }\mu\text{V}$. Thus two equal electrodes in the same solution should have zero

potential difference to within $\pm 40 \mu\text{V}$. This precision is quoted under the assumption of virtually no DC current flow.

The most cited reference electrode is the *platinum-hydrogen* electrode, and electrode DC potentials are often given relative to such an electrode. It is an important electrode for absolute calibration, even if it is impractical in many applications. The platinum electrode metal is submerged in a protonic electrolyte solution, and the surface is saturated with continuously supplied hydrogen gas. The reaction at the platinum surface is a hydrogen redox reaction: $\text{H}_2 \leftrightarrow 2\text{H}^+(\text{aq}) + 2e$, of course with no direct chemical participation of the noble metal. Remember that the standard electrode potential is under the condition: $\text{pH} = 0$ and hydrogen ion activity 1 mol/L at the reference electrode. Thus the values found in tables must be recalculated for other concentrations. Because of the reaction it is a hydrogen electrode, but it is also a platinum electrode because platinum is the electron source or sink, and perhaps a catalyst for the reaction.

7.7 Basic Experiment with DC Current Flow

In Figure 2.1, a basic experiment with two equal electrodes was described. To study electrode reactions a little further, we must be able to differentiate between cathodic and anodic processes. We therefore change the set-up shown in Figure 2.1. Instead of two equal electrodes, we reduce the area of one of them to be, for example, $<1/100$ of the other ([Figure 7.12](#)).

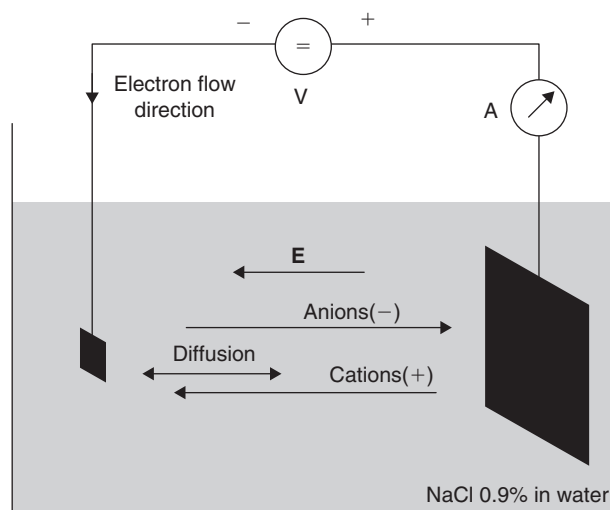


Figure 7.12: Monopolar electrode system, cf. Figure 2.1.

With no current through the electrolytic cell, it does not matter whether the electrodes are large or small; the equilibrium potentials are the same. But with current flow, the current density and therefore the voltage drop and the polarization, will be much higher at the small electrode. An increased potential drop will occur in the constrictional current path near the small electrode, and in general the properties of the small electrode will dominate the results. The small electrode will be the electrode studied, often called the *working electrode*. It is a *monopolar* system, meaning that the effect is determined by *one* electrode. The other electrode becomes the *indifferent* or *neutral* electrode. Note that this division is not true in potentiometry, electrode area is unimportant under no-current conditions.

We let the external DC voltage change slowly (e.g., ramp voltage from a polarograph), and we record the DC current (Figure 7.13). In electrochemistry, this is called *voltammetry* (volt-am-metry), the application of a varying voltage with the measurement of current. *Ampereometry* is more generally the measurement of current with a constant amplitude voltage.

Polarography is voltammetry, preferably with the dripping mercury electrode and with a diffusion-controlled current in a monopolar system.

The electrolyte (Figure 7.12) is as usual NaCl 0.9% in water. With a *platinum* working electrode, there will be no DC current over a rather wide voltage range (Figure 7.13(a)). The *incremental* DC resistance $R = \Delta V / \Delta I$ is large in this range ($\Delta I \approx 0$). With beginning oxygen reduction, R is small, but at the current plateau (diffusion controlled oxygen transport to the cathode) R is again large. With silver–silver chloride (Figure 7.13(b)) R is small, even at zero DC current. The system is nonlinear, and care must be taken with regard to the use of linear models.

With a sufficiently large voltage of any polarity, DC faradaic current flows and we have an *electrode reaction* at the platinum surface. R falls to smaller values. Evidently large *activation energy* is necessary to obtain electron transfer and an electrode reaction.

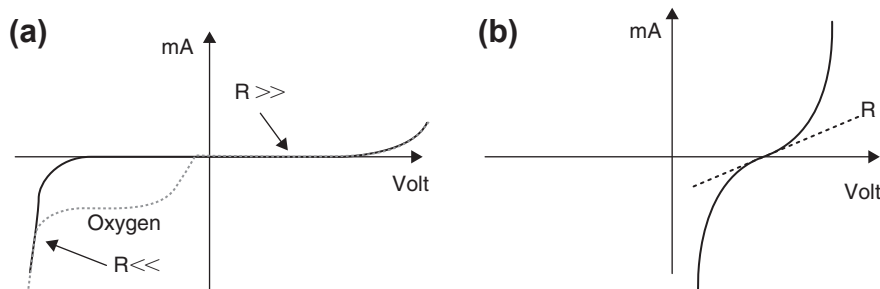


Figure 7.13: DC monopolar electrode current. Working electrode: (a) platinum, (b) silver–silver chloride.

It is not likely that this reaction involved chemical reaction with platinum, or that platinum metal entered the solution as ions. However, in our basic experiment of Figure 2.1, we did consider the effect of dissolved oxygen. With a suitable negative voltage, the neutral oxygen is reduced at the cathode, left curve stippled. This reaction causes a faradaic current. However, when the negative voltage is large enough, we reach a *current plateau*, again with a large incremental R. Then the electron transfer is no longer the rate limiting factor, but the diffusion of oxygen to the cathode. At the cathode surface the concentration of oxygen is approximately zero, all available oxygen is reduced immediately. *The current is diffusion controlled.* The oxygen molecules are neutral in the solution and are not migrating in the electric field, they move because of the concentration gradient. At the platinum surface they are ionized (reduced), accepting electrons. This is the principle of the polarographic oxygen electrode. If we increase the voltage to about -1.4 V, a much larger DC current flows, and the decomposition of water with bubbles of H_2 appears.

Now let us change to a small silver/silver chloride working electrode (Figure 7.13(b)). Even with a small deviation ΔV from the equilibrium voltage with zero current, the ΔI will be large, and in either direction. Even at the equilibrium voltage, R is rather small. We have an immediate, large electrode reaction. This is the nonpolarizable electrode, even with relatively large DC currents the charge distribution does not change very much, neither do the DC potentials. With a positive overvoltage on the electrode, the $AgCl$ layer thickens, with a negative overvoltage it becomes thinner and is at last stripped off. Then we have changed the electrode surface to a pure silver electrode, and with a different equilibrium potential.

Suppose a small AC signal is superimposed on the DC voltage. At equilibrium, DC voltage with no DC current, the AC current will flow in both directions because it is a reversible redox electrode process at the $AgCl$ surface. With a DC current, the small AC current will be superimposed on the larger DC current, and thus just change the reaction rate a small amount.

As seen in Figure 7.14, the resultant AC current will depend on the local slope of the DC current curve. The slope defines the *incremental resistance*:

$$R = \frac{\Delta V}{\Delta I} \quad [\Omega] \quad (7.13)$$

The incremental resistance varies according to the DC (*bias*) level. Because the DC current curve is not linear, it is clear that with large amplitudes the current response will not be a sine wave even if the superimposed AC voltage is a pure sine wave. Because of the capacitive properties of the cell, the current will not be in phase with the applied sine voltage.

From the curves on Figure 7.14, it is clear that by changing the frequency and record the AC current it is possible to examine electrode processes and find out how quick they are.

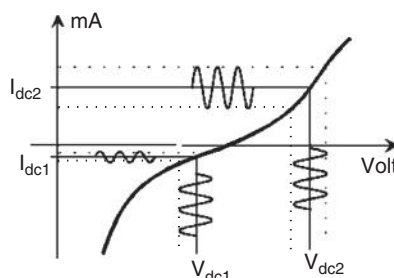


Figure 7.14: DC (bias) voltage with superimposed AC. The resulting AC current is dependent on the slope of the DC current curve.

By studying the harmonic content of the current waveform as a function of DC voltage and AC amplitude/frequency, nonlinearity phenomena can also be studied.

With no redox reactions (e.g., by using a platinum electrode in saline), the small AC voltage will result in an AC current dependent on double-layer capacitance and other components.

The voltage deviation ΔV from equilibrium necessary for a certain DC current flow is called the *overvoltage*. With small deviations, there is a linear relationship between ΔV and electrode current I , but with larger ΔV it is strongly nonlinear. An overvoltage is linked with an external current and therefore the electrode is externally *polarized*.

In *cyclic voltammetry*, the voltage is swept like in polarography, but at a predetermined voltage level the sweep is reversed and the cycle ends at the starting voltage. More than one cycle may be used, but usually the recorded current curve changes for each cycle. The single-cycle experiment must therefore not be confused with a steady state AC condition. Two examples are shown in [Figure 7.15](#).

As the sweep is linear, the x -axis is both a voltage and time axis. The charge transferred from the sweep generator to the cell is therefore proportional to the area between the curve and the x -axis ($=0$ mA). If the enclosed areas over and under the x -axis are equal, no net charge is supplied to the system. The currents may be due either to double-layer charging, sorption at the metal surface, or electrode reactions.

The electrolytic cell voltammograms in [Figure 7.15](#) are with irreversible (a) and reversible (b) processes. The irreversible process represents a net charge transfer to the cell, because very little reverse current is present. During voltage sweep a non-faradaic charge current will also flow to or from the double layer capacitance. The current steps at the sweep ends represent the reversal of such a capacitive charging current. In the reversible process, most of the charge is returned, the redox reaction is reversed.

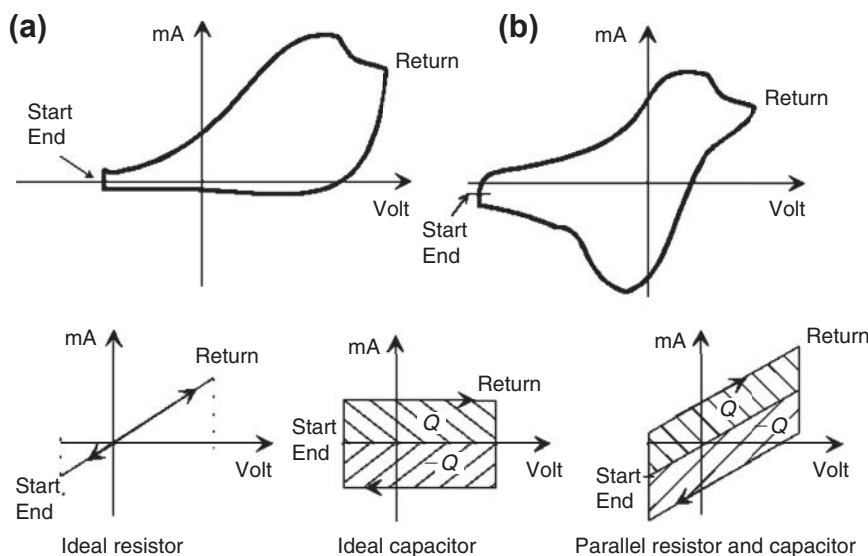


Figure 7.15: Cyclic voltammograms. Top: Electrolytic cell (a) irreversible reaction, (b) reversible. Bottom: with ideal components.

With an ideal resistor instead of the electrolytic cell, the current curve is the same straight line, and a charge transfer equal to the double of the area under the line is transferred.

With an ideal capacitor the charging current I is $I = CdV/dt$. When dV/dt is constant, I is constant; when dV/dt changes sign, I changes sign. The area under the current curve is Q , and the same charge $-Q$ is returned at the return sweep. No net charge is transferred to the capacitor. The current to the parallel RC components is then the sum of electrolyte, and the platinum electrode is the worst possible choice. Another example is the dropping mercury electrode in an indifferent electrolyte, with a perfectly smooth surface continually renewed. No reversible charge transfer occurs within a rather broad range of DC voltage (oxygen-free solution).

To obtain a well-defined potential *also with a variable DC current flowing*, a reversible electrochemical reaction is necessary at the electrode. Usually this implies that there must be redox reactions, with easy both way electron transfers. Such an electrode with easy electron transfer is called a *nonpolarizable electrode*.

A redox reaction is not only dependent on the electrode material, but also on the electrolyte solution. As we have seen, platinum was highly polarizable in the NaCl solution. However, if the surface is saturated with dissolved hydrogen gas, a redox system is created (H/H^+), and then the platinum electrode becomes a *nonpolarizable reference electrode*. Surface oxidation, adsorption processes, and organic redox processes may reduce the polarizability and increase the applicability of a platinum electrode in tissue media.

One type of electrode has no defined DC voltage at all, the ideally *polarizable electrode*. It can attain any potential; it is just a double-layer capacitor that can be charged to any voltage if the necessary charging current is supplied. No electron transfer occurs; there is no free charge carriers cross the double layer or flow in the solution. With a real electrode, this implies virtually zero DC current within a certain range of applied voltage. A platinum electrode in NaCl aqueous solution is a practical example. As a current-carrying DC reference electrode in NaCl, it is useless.

7.8 Faraday's Law of Electrolysis

With current flow in the electrode wire the electrode is polarized by the current, this is an exogenic polarization. The current flow may generate a chemical reaction at the electrode surface. In the solution, there is a two-way flow of ions and there are charge carriers of both signs. In the metal wires of the electrodes, there is only one type of charge carriers of one sign, the electrons. The charge of one electron is exactly equal to that of one proton (with opposite sign): $1.6 \cdot 10^{-19}$ [C], the smallest known charge called the *elementary charge*.

In the solution, the current spreads out from the current carrying electrodes, and we must use *current density* [A/m^2] as quantity instead of current (see Eq. (2.3)). A *flux* is the flow rate through a cross-sectional area, so current density is a flux density. But the total sum of ionic charges passing through the solution is the current density integrated over the whole cross-sectional area, and per second this must equal the electronic current I in the external electrode wire.

A sum of electric charges q is also a *charge* and is also called a *quantity of electricity* Q , with the unit (coulomb). If 1 A flows through a cross-sectional area in 1 s, 1 C has passed. Faraday¹ found that the reaction products are proportional to the quantity of electricity passed. The Faraday constant F is the charge of 1 mol of electrons; 1 mol is the number 6×10^{23} , and as the elementary charge is 1.6×10^{-19} [C], the Faraday constant $F = 96\,472$ [C/mol]. *Faraday's law of electrolysis* links the amount of reaction products at the electrode to a quantity of electricity Q :

$$M = \frac{Q}{Fz} \quad [\text{mol}] \quad \text{Faraday's law of electrolysis} \quad (7.14)$$

where M is the substance produced and z is the valency of the element produced.

Faraday's law of electrolysis defines the term *electrolytic* as follows: an electrolytic system is a system that basically is characterized by Faraday's law. A current creating a reaction

¹ Michael Faraday (1791–1867), English physicist and chemist (natural philosopher), found the laws of electromagnetic induction and of electrolysis. A self-educated man who knew very little mathematics.

at an electrode according to Faraday's law is called a *faradaic current*². Nonlinearity in electrode electrodes is treated in Section 8.4.2.

7.8.1 DC, AC, and Chemical Reaction Reversibility

Faraday's law is basically a DC equation. The quantity of electricity may be obtained with a DC current, a current pulse or an AC current. A DC current implies faradaic current only. A pulse current has an additional capacitive, non-faradaic current component. Using a sufficiently high AC frequency, each polarity period is very short and if the reaction has a high degree of reversibility the actual net electrolysis product may be very small. But if the frequency is sufficiently low, each polarity lasts so long that reaction products in the form of a surface layer or gas production makes the process both nonlinear and irreversible.

7.9 Electrode Polarization

Polarization was defined in Chapter 3. Polarization in *tissue* was treated in Section 3.1; here Section 7.9 is about *electrode* polarization.

In most cases, electrode polarization is a nuisance because it is only the tissue impedance that is of interest. Electrode polarization impedance introduces errors in tissue impedance measurements.

In electrochemistry, an electrolytic cell is said to be polarized if a current flows through the cell. A CC electrode is therefore a polarized electrode. Recording electrodes (PU electrodes) are in general not considered to be polarized. However, a metal electrode may be positioned in a region that is not isoelectric, or the metal surface properties may vary. The result is local current flow and endogenous polarization *without any current in the external electrode wire*.

Polarization comprises both dynamic and static properties. An AC voltage u connected to a skin electrode pair generates an AC current in the electrode wires. The impedance is $Z = u/i$ and it comprises both the tissue impedance and the double electrode polarization impedances. They are physically coupled in series. Can we avoid the electrode contribution?

7.9.1 DC Counter Electromotive Voltage

A DC voltage connected to a skin electrode pair generates a DC current in the electrode wires. The resistance $R = V/I$, but V comprises both the tissue voltage drop and the

² Faradic current is the pulse current from an induction coil used for muscle stimulation.

electrode voltage drop. The electrode voltage drop may be dependent on charging or discharging batteries or capacitors and so may vary with time. The electrode voltage must be subtracted from the external applied DC voltage; it represents a varying counter electromotive voltage (emv) generated by the electrode. How can we avoid the counter emv contribution?

Fundamentally impedance is an AC concept. When DC special parameters are used, two examples are the Faraday law of electrolysis and the concept of counter emv. If the electrode circuit model comprises a chargeable battery or a capacitor, the DC current will charge such components, and little by little the current will decrease. This corresponds to a counter emv. It is a polarization voltage, not a polarization resistance.

7.9.2 Electrode Polarization Impedance in Saline

Platinum Black Electrode

The impedance is shown in Figure 7.16 for black platinum in a physiological saline solution, one of the lowest polarization impedance systems known. Schwan's data are for a 1.4 mm^2 platinum disk, but here recalculated for 1 mm^2 and given as impedance series values. If

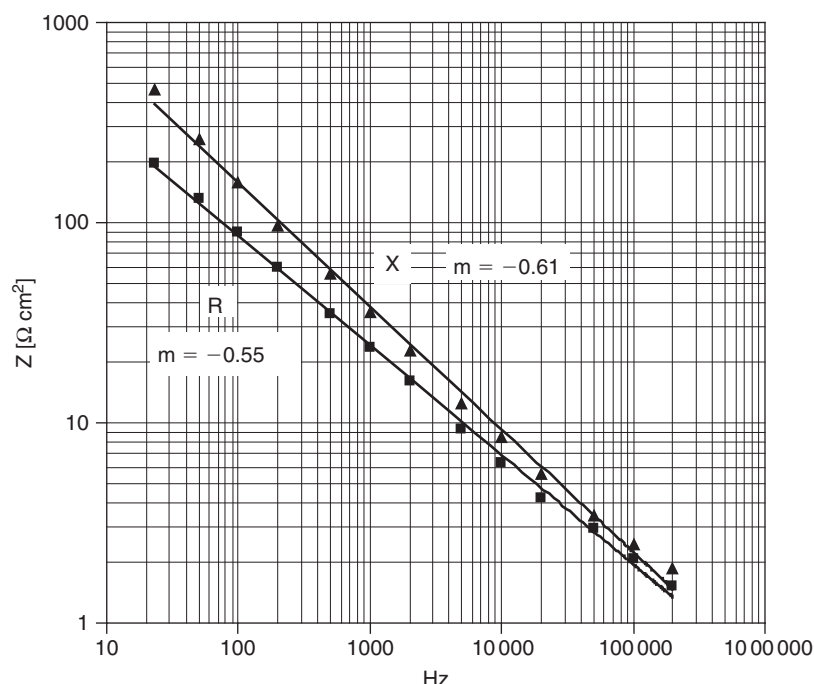


Figure 7.16: Polarization impedance for monopolar platinum black electrode in physiological saline solution. Constrictional series resistance subtracted. *Data from Schwan (1963), by permission.*

inversely proportional to EA, the values correspond to an impedance $|Z|$ less than 1Ω for 1 cm^2 at 1000 Hz. The exponential factor for the reactance X is $m = -0.61$ ($R^2 = 0.996$). If Fricke's law is valid, this corresponds to a phase angle $\varphi = m \times 90^\circ = -54.9^\circ$ and a loss tangent $\tan\delta = 0.39$. The resistance R exponent factor for the whole frequency range is $m = -0.55$ ($R^2 = 0.998$), corresponding to a phase angle $\varphi = -49.5^\circ$. As is easily seen on [Figure 7.16](#), the ratio X/R and therefore also $|\varphi|$, diminish with increasing frequency. Instead of whole range exponents, local exponents for a limited frequency range may be examined, and a useful accordance with Fricke's law is found even if φ is a function of frequency (Schwan, 1963).

The parallel capacitance calculated from the data of [Figure 7.16](#) is not a pure double-layer capacitance, it is too frequency-dependent. It must be due to redox or sorption processes at the platinum surface, or the fractal surface of black platinum. Under optimum conditions, it is possible to obtain capacitance values of the order of $50 \mu\text{F/mm}^2$ at 20 Hz (Schwan, 1963). A polished and etched platinum surface has a capacitance on the order of $0.5 \mu\text{F/mm}^2$ at 20 Hz, 1/30 of the value for the platinum black surface shown in [Figure 7.16](#).

Silver Chloride Wet Gel Electrode

[Figure 7.17](#) showed that platinum black is a preferred electrode metal element with respect to low polarization impedance. However, it may easily be polarized by a DC current, and for such cases an Ag/AgCl electrode is usually preferred. Typical immittance plots for one pregelled Ag/AgCl ECG electrode obtained from two electrodes in front to front contact (no tissue in between) is shown in [Figure 7.17](#). The data were obtained with a constant amplitude current of $1 \mu\text{A/cm}^2$ rms, corresponding to a single electrode maximum (1 mHz) voltage of 2.5 mV rms.

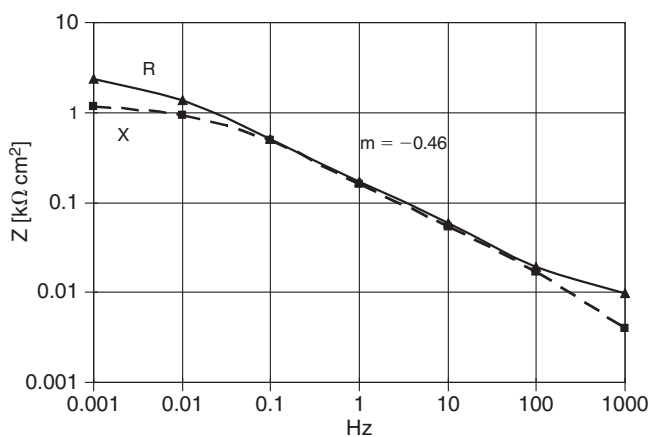


Figure 7.17: AgCl electrode polarization impedance with pregelled wet electrolyte. Two ECG commercial electrodes measured front to front, contribution of one electrode.
Gel area 3 cm^2 .

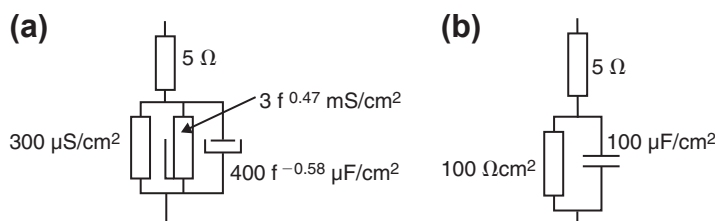


Figure 7.18: Equivalent circuits for the electrode polarization impedance found with one AgCl/wet-gel electrode. (a) with frequency-dependent CPE components ($m = 0.47$); (b) more simplified version with ideal components, valid around 10 Hz (ECG).

A possible interpretation of these data is: At high frequencies, the series resistance of the electrolyte dominates (frequency independent value of about 5Ω , Figure 7.18(a)), the low value indicates a strong, highly conductive electrolyte. At low frequencies, the parallel admittance of the polarization process at the AgCl surface dominates. Accordingly the *high-frequency* results must be analyzed from the *impedance* plot. The low-frequency admittance plot is not shown here but indicates a DC leakage parallel to the polarization process of approximately 0.3 mS . In the medium frequency range from about $0.1\text{--}100 \text{ Hz}$ (3 decades), the phase angle is constant equal to about 43° , so the polarization immittance is dominated by a constant phase element (CPE). The frequency exponent m of the admittance in the same range is found to be 0.47 , which multiplied by 90° is also about 43° . The CPE is therefore of a Fricke type.

Two possible electrical equivalent circuits are shown in Figure 7.18. Such equivalent circuits are often given in the literature in the most simplified way with ideal components as shown for 10 Hz in Figure 7.18(b). Important characteristics of an electrode are lost by such a simplification. For two-electrode tissue measurements, the immittance of the equivalent circuit of Figure 7.18 is a source of error physically in series with the tissue, and must either be negligible, or be subtracted as impedance from the measured impedance.

Hydrogel/Aluminum Electrode

Figure 7.19 shows the same data for hydrogel and aluminum electrode metal. Series resistance flattens out at about 1500Ω at higher frequencies; left part of the diagram of Figure 7.19. This corresponds to a conductivity of the hydrogel equal to $\sigma = 6 \text{ mS/m}$ (gel thickness 1 mm). Accordingly, the polarization impedance down to about 0.1 Hz of this hydrogel electrode is purely resistive and dominated by the frequency independent resistance of the gel.

The conductivity of the hydrogel contact medium is much smaller than for the wet gel (Figure 7.18 showing a series resistance of only about 5Ω). With such a high series resistance, the visible constant phase frequency range of the CPE is reduced to a small

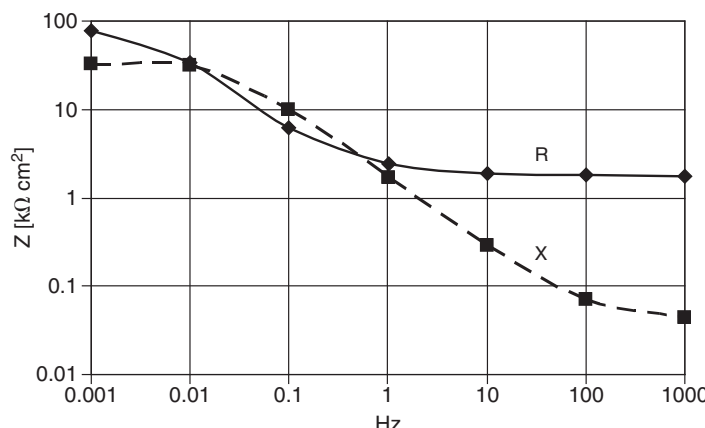


Figure 7.19: Electrode polarization impedance for 5 cm² skin contact area hydrogel/aluminum electrode. Two ECG commercial electrodes front to front; contribution of one electrode.

zone around 0.1 Hz. The polarization admittance $|Y|$ of the metal-electrolyte interphase is about 20 $\mu\text{S}/\text{cm}^2$ at 0.01 Hz, and consequently is much lower than for the AgCl/wet-electrolyte case with about 600 $\mu\text{S}/\text{cm}^2$ at 0.01 Hz. At the lowest frequencies, B is almost proportional to frequency, indicating a relative static capacitance ($B = \omega C$). Because of the large series resistance, it is difficult to assess in accordance with Fricke's law directly. However, it is possible to subtract the presumed static series resistance from measured R , and then proceed the analysis from there.

The series capacitances of some other metal/electrolyte interfaces are given by Geddes (1972). They are always lower than the AgCl or platinum black electrodes in 0.9% NaCl. For stainless steel, it was given as 40 $\mu\text{F}/\text{cm}^2$ at 20 Hz ($\approx 500 \mu\text{S}/\text{cm}^2$).

The series resistance in these models may be regarded as an access resistance to the electrode interface, dependent on electrolyte conductivity and geometry, but not linked to the polarization processes. As such it belongs to the chapter on contact media, and should be subtracted from measured electrode impedance when analyzing polarization immittance.

The series resistance may often be regarded as a short salt bridge with a high-conductivity electrolyte solution. The salt bridge resistance may be a problem at high frequencies. Electrodes for plethysmography for instance are used around 50 kHz, and the polarization impedance is then so low that the series resistance may be the dominant factor. This is particularly true with hydrogel contact media as shown in [Figure 7.19](#).

Difference between Electrolyte and Tissue as Contact Media

A contact electrolyte is a homogeneous material. The current distribution may be uniform with the metal closing the cross-sectional area of a measuring cell tube. Otherwise, it will

be a current spread from the electrode with a constrictional effect near the electrode, perhaps with an edge effect if it is a surface plate electrode. Even if the current density always may be unevenly distributed, there is one fundamental difference if the metal is in direct contact with tissue. At low frequencies, the cells will have a shadow effect because the poorly conducting cell membranes force the current to go around the cells in the interstitial liquid. The current density may vary locally and have much higher values than the average. The effective polarization impedance may be higher than the values found with a homogeneous electrolyte. Schwan (1992a) found that electrode polarization impedance increased with higher concentration of cells in suspension.

Electrolyte Concentration

A polarization ratio can be defined as the ratio of polarization impedance to the bulk resistance of the electrolyte. Mirtaheri et al. (2005) measured the ratio as a function of frequency (10^{-2} – 10^3 Hz) and NaCl concentration (2.4–77.0 mmol/L) and found that the polarization ratio diminished as a function of concentration regardless of electrode material. Medical stainless steel ratio was concentration independent but had high electrode polarization impedance values compared with the other metals studied. Aluminum showed small ratio changes at low concentrations. However, the changes were more pronounced at higher concentrations. Gold, platinum, and silver showed a moderate concentration dependency at low concentrations.

7.9.3 DC/AC Equivalent Circuit for Electrode Processes

The faradaic polarity-dependent DC currents are not only dependent on the applied DC voltage, but also on elapsed time. With a small change in excitation voltage, it takes a certain time to reach a new current level. The four processes to be considered are:

1. A faradaic component: the rate of *electron transfer* to the electroactive species of the solution (occurring near/at the electrode surface in the double layer)
2. A faradaic component: the amount of species that can be *transported to* the reaction site from the bulk of the electrolyte, and the amount of reaction products that can be transported away *from* the reaction site
3. Electric *charging* of the double layer
4. *Sorption* of species at the electrode surface.

The mechanisms and speed of the *electron transfer process* have long been discussed. Does it take the electron a long time to meet the particle ion, or is the ion immediately ready to donate or accept an electron? When a chemical reaction is to occur, the species approach one another to a necessary close distance. In an electrode reaction, the ions enter the outer part of the double layer, and the chance increases of gaining or losing electrons. If the electroactive species are ions, what is the effect of the hydration sheath and ionic

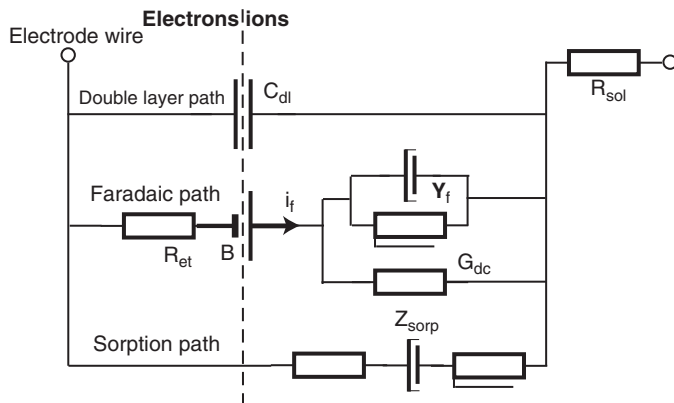


Figure 7.20: Electric equivalent circuit for the three-electrode processes.

atmosphere surrounding them? Must a part of it be stripped off? The reacting partners must possess sufficient energy (translational, vibrational, rotational) to obtain reaction. The concept of necessary *activation* energy is therefore important. Sodium is very electropositive, thus wanting to get rid of electrons. From these scales the most probable electrode reactions can be predicted.

A possible but rough electrical DC/AC equivalent circuit for the electrode processes is shown in Figure 7.20. The electrodic part consists of three principal current paths in parallel. The elements are Cole-like as discussed in Section 9.2, and some of the used component symbols indicate that their values are nonideal, frequency-dependent.

As for the electrode processes, DC parameters are actually contraindicated, because a DC study should be performed with virtually zero applied overvoltage to be in the linear region. By using a superimposed AC signal of sufficiently small amplitude at $f > 0$, the model may be a linear model, and the values of the components of the equivalent circuit may vary according to the applied DC voltage or current.

The Series Resistance

The bulk of the electrolyte obeys Ohm's law, Eq. (2.2). Accordingly, the bulk electrolyte is modeled as an ideal resistor R_{solu} in series with the electrode components. This is to indicate that bulk electrolytic conductance is considered frequency independent, but dependent on the geometry and possible current constrictional effects. If the bulk electrolyte is replaced by tissue, a more complicated equivalent circuit must replace R_{sol} , and we are confronted with the basic problem of division between tissue and electrode contributions.

The series resistance causes an overvoltage due to a simple IR-drop ($\Delta V = IR_{sol}$) in the solution. Actually this is not due to a polarization process. However, it is often practical to

include it in the total overvoltage and the electrode polarization concept. The IR drop is proportional to current, and can be reduced by the addition of a suitable strong electrolyte not intervening with the processes of interest (*indifferent* electrolyte). It can also be reduced by introducing a reference electrode reading the potential very near to the working electrode, and connect all three electrodes to a potentiostat.

Double Layer Path with Leakage

With a dripping mercury electrode the surface is ideal and the double layer is modeled as a pure, frequency independent capacitor, somewhat voltage-dependent. The capacitance values are very high because of the small double-layer thickness, C_{dl} is about $20 \mu\text{F}/\text{cm}^2$. With solid electrode materials, the surface is of a more fractal nature, with a distribution of capacitive and resistive properties. The actual values are dependent on the type of metal, the surface conditions, the type of electrolyte, and the applied voltage. The capacitance increases with higher electrolyte concentration. The double-layer capacitor is inevitable; it is there as long as the metal is wetted. C_{dl} may dominate the circuit if there are no sorption or electrode reaction processes, or if the frequency is high.

Surface Sorption AC Path

The additional capacitive impedance Z_{sorb} is due to the adsorption and desorption of species at the electrode surface. These species do not exchange electrons with the electrode surface, but change the surface charge density and therefore cause a pure AC current path. A current-limiting resistor in series may model the processes with a Cole-like element without DC conductance (drawn as a series constant phase element because it is in series with a resistor, see Section 9.2). Z_{sorb} may dominate the circuit in the middle and higher Hz and lower kHz frequency range. Sorption currents are AC currents, and as the adsorption/desorption may occur rather abruptly at a certain DC voltage, these currents may be very dependent on the applied DC voltage. Sorption currents may dominate noble metal electrodes, so the measurement of their polarisation impedance must be performed under controlled DC voltage.

Electrode Reaction DC/AC Path (Faradaic)

The metal and the electrolyte also determine the DC half-cell potential, modeled by the battery B. If there is no electron transfer, R_{et} is very large and the battery B is decoupled, the electrode is then polarizable with a poorly defined DC potential. But if there is an electrode reaction, R_{et} has a lower value and connects an additional admittance in parallel with the double layer admittance. This current path is through the *faradaic impedance* Z_f , and the current is the faradaic current i_f . Faradaic current is related to electrode reactions according to Faraday's law (Section 7.8). The faradaic impedance may dominate the equivalent circuit in the lower Hz and sub-Hz frequency range and at DC. The faradaic impedance is modeled by a complete Cole-like series system. It consists of the resistor R_{et}

modeling the electron transfer, in series with a Cole-like parallel element of *admittance* Y_f related to slow processes (mass transport and slow electrode reactions) and therefore introducing time delays necessitating an equivalent admittance and not just a conductance.

The electron transfer resistance R_{et} is related to the *activation energy* and to the extent electroactive species have reached sufficiently near the electrode surface so that acceptance or give off of electrons can occur. If the electrode voltage is not sufficient to create electron transfer and an electrode reaction, R_{et} will be very large. R_{et} is purely resistive, which means that there is little transfer time delay. The process is almost immediate, but energy and therefore probability dependent. R_{et} is clearly current dependent, and for nonpolarizable electrodes it is small for all DC current values. For polarizable electrodes, it is very large at zero DC current. R_{et} is clearly a nonlinear element. It only dominates to the extent that electron transfer is the current-limiting process. Under that condition, the concentration of active species at the electrode is independent of current flow. Then the relationship between the *overvoltage* ΔV and the electrode current I is given by the *Butler-Volmer* equation:

$$I = I_o[\exp(\psi k \Delta V) - \exp(-(1 - \psi)k \Delta V)] \quad (7.15)$$

where I_o is the exchange current present when the external current is zero, the exponent ψ is called the *transfer coefficient*, and $k = zF/RT$. At equilibrium voltage with no external current, there may actually still be large reducing and oxidizing local currents that externally cancel, this is I_o .

The slow process *admittance* Y_f is related to reactions that are rate limited by the necessary time of transport to or from the electrode active sites, and the time of accompanying chemical reactions. If the faradaic current is limited by *diffusion alone*, the immittance is called *Warburg* immittance. R_{et} is then negligible, and the current is determined by Y_f . The electron transfer flux and the chemical reaction rate are so high that the process is controlled by diffusion alone. Diffusion is a transport process only dependent on concentration gradients (see Section 2.4). The diffusion may be of reactants to the electrode, or reaction products *away* from the electrode, both influencing Y_f . Warburg (1899) was the first to solve Fick's second law (Eq. (2.9)) for an electrolytic cell under AC conditions. He presumed a diffusion-controlled process with negligible migrational effects. He found that under ideal conditions, the concentration at the electrode surface is $+45^\circ$ and the voltage -45° out of phase with the applied current, independently of the applied frequency. Such an ideal and purely diffusion controlled electrolytic cell is therefore a perfect model for a CPE. He found that the concentration wave spreads out longer in the electrolyte the lower the applied frequency, [Figure 7.21](#).

The penetration will be delayed and can be described by a damped sine wave, so that both lower and higher than the bulk concentration may exist. It is like the slow penetration of

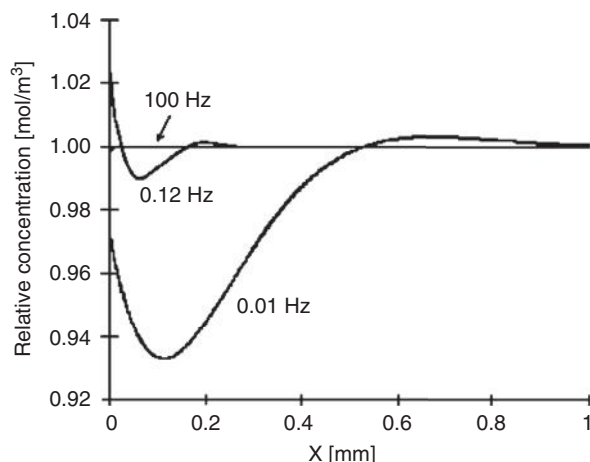


Figure 7.21: Concentration wave into the electrolyte as a function of distance from the electrode surface, with the frequency of the applied current as parameter. $D = 10^{-9} \text{ m}^2/\text{s}$, arbitrary current and zero current concentration.

changing cold and warm weather into a housing wall or the ground. He found the diffusion zone defined as the distance δ from the electrode at which the concentration wave is reduced to $1/e$ of its value at the electrode to be:

$$\delta = \sqrt{\frac{2D}{\omega}} \quad [\text{m}] \quad (7.16)$$

where D is the diffusion constant. The diffusion zone length δ may therefore extend all the way to the counter current carrying electrode at low frequencies. With $D = 10^{-9} \text{ m}^2/\text{s}$ and at $10 \mu\text{Hz}$, δ is 14 mm. To introduce negligible phase distortion, the cell length should then be several centimeters long. Pure 45° properties will only be found if convection effects are negligible during the period. A purely diffusion controlled electrode reaction has an *infinite length Warburg admittance* with a constant (frequency independent) phase angle $\varphi = 45^\circ$. A more general *finite-length Warburg admittance* does not have the same constant phase character (MacDonald, 1987).

The thickness of an electric double layer is about 0.5 nm with strong electrolytes, about the same size as the ions, and perhaps 10 nm in dilute solutions (diffuse double layer). The thickness of a diffusion zone in unstirred solutions is enormously much larger. The diffusion zone length is not dependent on concentration (as long as D is constant).

The influence of the electron transfer resistor R_{et} and the slow process admittance Y_{sp} on the total faradaic impedance is determined by which factor is reaction rate-limiting. It is possible to study this by plotting the faradaic impedance as a function of frequency in a log–log plot, or in the Wessel diagram and look for circular arcs (see Section 9.2).

The term *electrode polarization immittance* is sometimes related to the total immittance of the equivalent circuit of [Figure 7.20](#), but it is sometimes useful to exclude the series resistance R_{sol} if it has the character of being an access resistance to the electrode processes. Without electrochemical reaction, measured currents are due to double layer components and sorption. The term electrode polarization immittance should more often either be avoided or defined. The processes involved are of a very different nature, and in a measuring set-up different variables must be controlled dependent on what effects are to be studied. The electrode immittance of an electronic conductor in contact with 0.9% NaCl is of special interest to us. Data for such interfaces are found in [Section 7.4](#).

7.10 Multiple Electrode Systems

7.10.1 Half Cells and Electrode Pairs

From electrochemistry, our discipline has borrowed important terminology. One electrode with electrolyte is called a *half-cell* to underline that one electrode is not enough. Two electrodes, an electrode *pair*, are needed to close the electric circuit so that electric *current* can flow (CC electrodes). A whole cell is two electrodes both submerged in the same electrolyte (e.g., in a glass dish).

Also when a *potential* is to be measured, two PU electrodes must be used. The potential of each electrode is either measured individually with respect to a third electrode and then subtracted or the *potential difference* between the two PU electrodes are measured directly without the use of a third electrode. DC voltage measured is the sum of the equilibrium potentials of the two electrodes, plus the potential difference in the tissue between them. The tissue potential may be membrane potentials, for instance the skin DC potential. If the two electrodes are made of different metals (e.g., steel and platinum), a DC voltage of hundreds of millivolt may be generated by the electrode pair (battery effect).

If *impedance* is to be measured the electrodes must be connected to an AC current source. The two CC electrodes, the membrane, and the electrolytes all contribute. As they are physically in series the contributions must be added.

The behavior of an electrode pair depends on the application, is it to be CC or is it to be potential reading (PU) with negligible current flow? If it is a PU pair the skin contact *area* is less important, but the skin *site* may be very important. If both electrodes are on skin sites that are under the same nervous control (same dermatome), the potential difference will be small or negligible and with no signal the bipolar lead is useless. But if one of the electrodes are on an indifferent (passive) skin site the signal may be large, the lead is monopolar and useful.

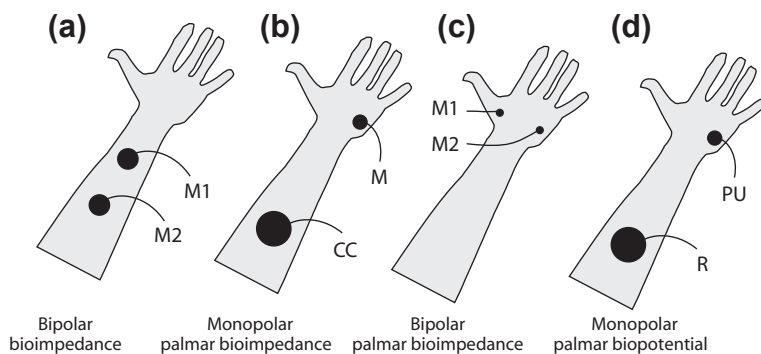


Figure 7.22: Four examples of electrode pairs.

Figure 7.22(a) is with two equal contact area electrodes on the forearm. With equal neuroactivity in the skin, the two electrode potentials change with the same amount and no signal is recorded, the lead is useless for measuring biopotential difference. But as a bioimpedance lead, it will be sensitive for neuroactivity under both electrodes, and an impedance signal will be recorded. This is an important conclusion: *an electrode pair can behave very differently dependent on whether potential difference or impedance is to be measured.*

Figure 7.22(a and b) show one large area electrode on the forearm and a small electrode at the neuroactive palmar site. In example (b), the lead is monopolar for bioimpedance. If the large electrode is on an indifferent skin site, it could also measure monopolar palmar potential, example (d).

Figure 7.22(c) with both contact areas on palmar sites, the lead is useful for bioimpedance but useless for biopotentials.

7.10.2 Three-Electrode Systems Monopolar Recording

Three-electrode systems correspond to a *two port, three-terminal network* equivalent (see Section 7.1). Because there are two ports, it is the *transfer parameters* that are measured even if one CC and one PU electrode are common. Figure 7.23 shows the principle (Grimnes, 1983a). The current flows between the M and C electrodes and the R electrode is a PU electrode without current flow.

In a two-electrode unipolar impedance system, it may be difficult to estimate a possible contribution from the neutral electrode. Often only a zone of the current path proximal to the measuring electrode is of interest (e.g., when measuring skin admittance). In such cases, the distal volume segment of the current path is a disturbing part. It may also be difficult to work with a sufficiently large neutral electrode in some situations. By adding a third electrode, Figure 7.24, it becomes easier to control the measured tissue zone. The

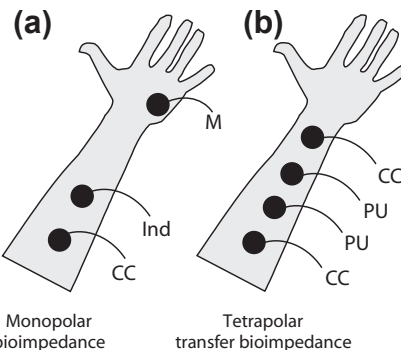


Figure 7.23: Three- and four-electrode systems.

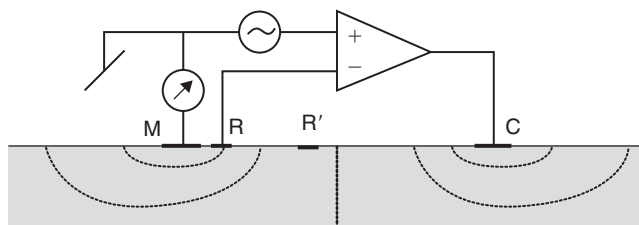


Figure 7.24: Three-electrode geometry and circuit, equipotential lines shown in tissue presuppose homogeneous biomaterial. The position of electrode R determines the sensitivity field of the electrode system.

set-up has the measuring electrode M common both for current injecting and voltage recording.

With just the measuring electrode M and the electrode C, the resultant current is dependent on the impedance of both electrodes plus the tissue in between. By measuring the voltage u on a potential recording electrode R (no current flow and no polarisation) with respect to M, the admittance Y of M is: $\mathbf{Y} = \mathbf{i}/\mathbf{u}$. In a practical set-up this is effectively done with an opamp as shown. The circuit guarantees that the potential on R is equal to the excitation voltage, so it is a constant voltage, admittance reading circuit. What is then included in measured \mathbf{Y} ?

1. The polarization impedance of electrode M
2. A tissue volume zone proximal to M, with gradually reduced contribution (sensitivity) at increasing distance from M.
3. Negative sensitivity in parts of the volume between the R and C electrodes.

One interesting feature with this circuit is that if there is a capacitively coupling of 50/60 Hz mains leakage current to the patient, the necessary AC current is supplied by the current-carrying counter electrode. This current is supplied by the opamp,

does not pass the measuring electrode, and is therefore not recorded by the transresistance amplifier (Section 8.3.1).

The circuit of Figure 7.24 is also the principle of a *potentiostat*, with the reference electrode controlling the voltage of the electrode M.

From Figure 6.3, we know that a spherical electrode alone has a larger sensitivity in the constricted zone of the electrode for purely geometrical reasons. Using a surface disk M electrode, tissue near the electrode edge also influences the result to a larger extent than tissue elsewhere (Section 6.2.2).

If the geometry is fixed, the electrodes included, the R and the C wires may be swapped with no change in measured admittance (reciprocity). This is an important circuit quality test. The polarization impedance of C and the impedance of R should not influence the results, but if any of the electrodes are too small that electrode may be in the nonlinear region so that the reciprocity test fails.

The metal of the R electrode should be recessed (Figure 7.24), or the metal should be narrowed in the current flow direction, to impede current flow from being attracted away from the lower admittivity tissue surface layers.

The three-electrode opamp circuit of Figure 7.24 has a problem if the M and R electrodes are of different metals and so generate a DC voltage difference (Section 7.6.3). The same problem occurs if the tissue generates an endogenic DC voltage. The palmar sites may for instance generate up to -50 mV with respect to the underarm. The opamp will generate a DC current to drive the opamp inputs to zero volt difference, and the whole system may inadvertently be under steady polarization.

Example: Intracellular Voltage Clamp, Three-Electrode

Figure 7.25 shows a similar three-electrode voltage intracellular clamp circuit. A problem with the circuits is that two micro-electrodes must be introduced through the cell membrane.

A single invasive electrode may be used, with constant current injection simultaneously with the voltage recording by the same electrode. Electrode polarization will be included in

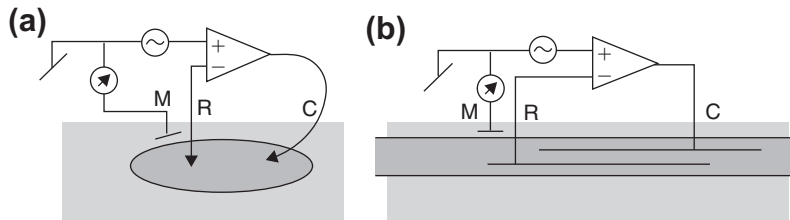


Figure 7.25: Intracellular three-electrode voltage clamp circuits. (a) ellipsoid cell form, (b) nerve cell axon.

the voltage reading. Here it is also likely that the M and R electrodes are dissimilar and may generate a DC voltage. To diminish this problem, a sample-and-hold circuit can be used, so that that a reference voltage is read before current is switched on. In current flow mode, the sampled reference voltage is subtracted from the instantaneously recorded voltage and the voltage clamp circuit drives a current necessary to obtain a clamp to the voltage difference.

7.10.3 Four-Electrode (Tetrapolar) Systems

If the effect of the zones proximal to the current carrying electrodes and the polarization impedance of the electrodes themselves are to be reduced, the four-electrode system is preferred. Such four-electrode systems correspond to a *two-port, four-terminal network* equivalent (see Section 8.1). Because there are two ports, these systems actually measure *transfer parameters* between the ports. This means that if for instance impedance is measured to $0\ \Omega$, this does not necessarily imply high-conductivity tissue, but rather no signal transfer from CC to PU electrodes.

In vitro Example: Tube

An in vitro example with a liquid filled tube is shown (Figure 7.26). Let us first analyze the tube as a two-electrode system with the two-tube endplates as PU electrodes and a dipole moment \mathbf{m} positioned somewhere in the volume. The PU voltage can be found with Eq. (6.31): $u = \mathbf{H} \cdot \mathbf{m}$. The lead vector \mathbf{H} can be found from Eq. (6.30), \mathbf{J}_{reci} is uniform all over the tube and equal to $1/A$, where A is the cross-sectional area of the tube. Integrating Eq. (6.30) $\mathbf{H} = z\rho/A$, where \mathbf{z} is the unity vector in direction of the tube axis. From Eq. (6.30), the recorded voltage from the current dipole \mathbf{m} is: $u = \rho/Az \cdot \mathbf{m}$.

As a four-electrode system, the measured segment is determined by the position of the two PU electrodes R and R', or more exact: by the position of their electrolyte/salt bridge

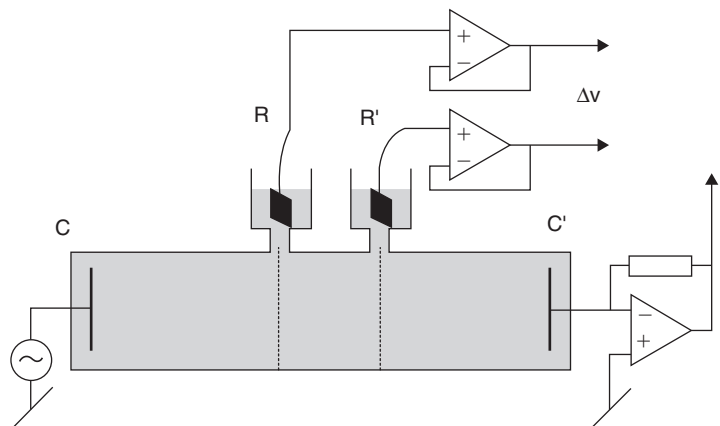


Figure 7.26: Four-electrode system, tubular in vitro version.

connections to the measuring cell. The two dashed equipotential lines indicate this. The transfer resistance can be calculated from Eq. (6.39), but the reciprocal current density field is not easily found. As we know the answer to be $R = \rho L/A$ where L is the distance between the PU electrodes, we can calculate back and find that the dot product $\mathbf{J} \cdot \mathbf{J}_{\text{reci}}$ integrated over the whole volume is equal to $1/A^2$ irrespective of the PU pair position as long as they are oriented in the axial direction. With inhomogeneity, there will be zones of negative sensitivity at the salt bridge orifices on the sides toward the C and C' electrodes. According to the reciprocity theorem, [Section 7.1](#), the transfer impedance is unchanged if the CC and PU pairs are swapped, if the system is electrically linear.

Current is recorded with a current-reading opamp. The PU electrodes are connected to one buffer amplifier each. No current is flowing in the electrode leads, and the electrodes can therefore not be externally polarized (but internal currents may polarize them, see the following section). Electrolyte/salt bridge connections are used to be able to increase the electrode metal area to increase electrode admittance and reduce noise ([Figure 7.26](#)).

Large electrodes directly into the measuring cell will disturb ionic current flow pattern, and polarization will occur on the metal surface. The electrode metal should not be in direct contact with the electrolyte, but should be recessed ([Figure 7.27](#)). The electrolyte is contained in a tube with isolating walls, and if a part of this wall is substituted by electrode metal, the current will prefer the high-conductivity path of the metal. The current lines will deviate from the path parallel to the tube walls, and in one part of the area the current will enter, in the other part it will leave. Thus the electrodes are polarized, but not by a current in the external leads. The polarization may not be uniform over the electrode surface area, and the polarization will occur according to local current direction and polarization admittance. When the metal is recessed, the current will also deviate into the electrolyte of the bridge path, but the current will not pass any metal surface, and no polarization will occur.

In vivo Example 1

[Figure 7.28](#) shows a four-electrode in vivo skin surface version. The two recording electrodes define to a certain extent the measured segment. When the geometry is

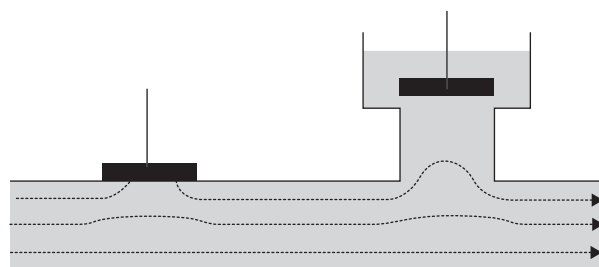


Figure 7.27: The nonrecessed electrode to the left implies polarization from the current entering and leaving the metal.

analyzed with Eq. (6.39), it will be seen that the sensitivity is negative in parts of the zone between the CC and PU electrodes and positive between the PU electrodes. The zones are not sharply delimited, and it is only the sensitivity field together with the resistivity distribution which gives all necessary information about the contribution of each voxel. There is, for example, no contribution from voxels where \mathbf{J}_{rec} and \mathbf{J} are perpendicular to each other.

To reduce the proximal zone contribution, and sometimes for anatomical reasons, it may be advantageous to place the PU electrodes *outside* the CC electrodes, instead of inside as shown in [Figure 7.28](#). If the system is linear, transfer immittance should be the same if the CC and PU electrodes are swapped; compare the reciprocity theorem.

In vivo Example 2

[Figure 7.29](#) shows an in vivo transfer impedance spectrum obtained with four electrodes positioned on the forearm.

The spectrum shows two dispersions plus an inductive dispersion, which drives the phase positive at 1 MHz. Both the current density field \mathbf{J}_{CC} and the reciprocal current density field \mathbf{J}'_{CC} of the PU electrodes, are unknown.

Aliau-Bonet and Pallas-Areny (2012, 2013) have studied the effect of body capacitance to ground in four-electrode bioimpedance measurements and found that stray capacitance between the measured body and ground could lead to inductive artifacts and resonance behavior.

Four-electrode systems are commonly used on humans both with skin surface electrodes or on probes meant for different body cavities. It could also be used by implantable devices

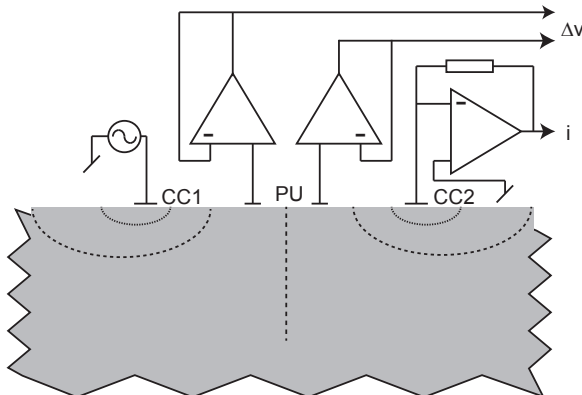


Figure 7.28: Four-electrode system, in vivo version. Equipotential lines are dashed. The position of the PU electrodes determines the tissue segment measured and the size of the proximal zones measured by CC1 and CC2.

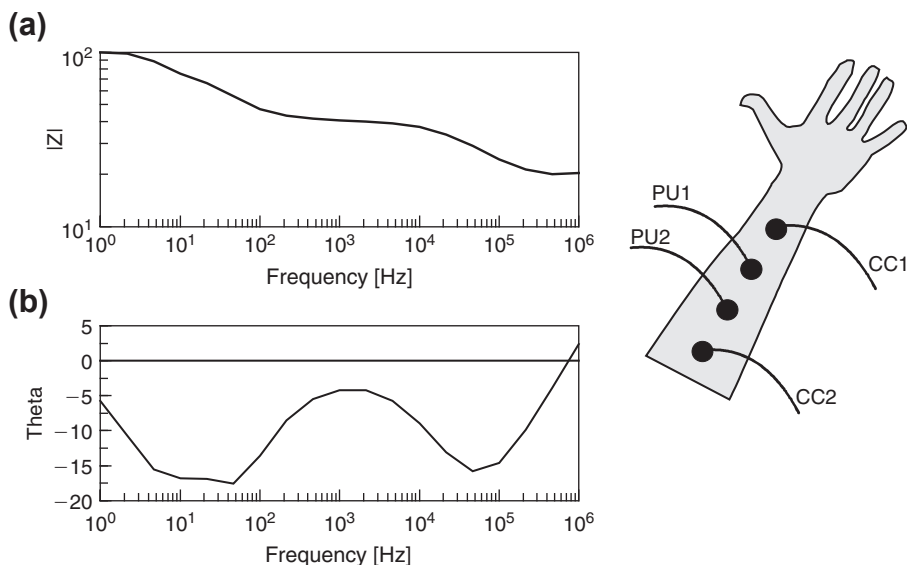


Figure 7.29: Transfer impedance frequency spectrum from forearm; impedance modulus (a) and phase angle (b).

where an example is Bogonez-Franco et al. (2013), who developed an implantable miniature bioimpedance monitor with a four-electrode system and a ZigBee transceiver for telemetry.

Sometimes more specialized results can be achieved by using more than four electrodes: Rabbani et al. (1999) combined two orthogonal four-electrode systems to achieve a more localized zone of measurement sensitivity in what he called focused impedance measurements. Kwon et al. (2012) showed that a system using 16 miniature electrodes was able to outperform the four-electrode system in sensitivity and impedance estimation. With this method, they were also able to recover anisotropic properties from the measured object.

7.11 Electrode Terminology

In this book there are about 40 different terms covering different types of electrodes and electrode system. They come from many fields: electrochemistry, physics, medicine, electrophysiology, cardiology, and neurology. Some have Latin, some have Greek origins. Some of them have rather vague meanings, examples are ground, amplifier common reference, neutral, indifferent, monopolar. Some are synonyms, such as PU electrode = recording electrode. We have tried to put together a list to give you a chance of surveying this slightly chaotic topic.

Electrode

Device from which the shift from electronic to ionic conduction (or vice versa) occurs.

CC electrode

Current-carrying electrode. CC electrodes are polarized because they are current carrying. A *dipolar* current injecting electrode pair uses two equal electrodes, each electrode contributing in the same way (current dipole). The dipole is the *most fundamental model* of a bioelectric endogenous signal source.

PU electrode

A pick-up electrode record tissue potential under zero current condition and are therefore not polarized. PU electrodes measure electric potential difference.

A bipolar PU electrode pair lead measures the local potential difference and is therefore actually also an electric field strength [V/m] probe. If the conductivity is known, it is also a current density probe since $J = \sigma E$. Because the electric field is a vector field and the bipolar lead has an orientation being the length L_{pu} between the PU electrodes, the measured voltage is the dot product: $v = E \cdot L_{pu} = J \cdot L_{pu}/\sigma$. The larger the electrode area, (1) the larger the averaging effect, (2) the lower the spatial resolution, (3) the lower the signal source impedance (less noise, better high-frequency response).

Recording electrode = PU electrode

Indifferent electrode

1. PU electrode situated on an inactive skin site. The other electrode is then situated on an active skin site. This constitutes a monopolar system. If both electrodes are situated on an active skin site, no signal (potential difference) is measured. Function is independent of surface area (as are all PU electrodes), but small electrodes pick up more noise. Not CC, current density $J = 0$. Indifferent electrode shall be situated far from bioelectric sources. Examples: ECG: right leg, other extremities, Wilson terminal. EEG: ear flip, nose. Electrodermal activity: elbow.
2. The indifferent electrode wire can be coupled to the reference wire of the preamplifier to minimize the common mode voltage and noise.

The indifferent electrode is in many ways problematic. Bipolar potential measurement with both PU electrodes on active skin sites may be useless, so a monopolar lead must be chosen: one active PU electrode and one indifferent PU electrode. The ideal indifferent electrode shall have zero potential, which can only be achieved in an infinite electrolyte volume with the electrode at infinite distance from signal sources.

Wilson's (central) terminal

Supposed to represent an indifferent electrode. Summing (averaging) the potentials of more than one PU electrode (e.g., the right arm, left arm, and left leg electrodes

in ECG). Can be used together with one or more monopolar electrodes forming monopolar leads.

Unpolarized electrode

In equilibrium with no current flow in the electrode wire.

Polarized electrode

Polarized by a current flow in the electrode wire.

Polarizable electrode

With considerable change in the half-cell potential as a function of current flow.

Nonpolarizable electrode

Only small changes in the half-cell potential as a function of current flow.

Invasive electrode

Positioned in living tissue. In most cases, it is sterile.

Noninvasive electrode

Does not penetrate protective barriers of tissue (e.g., skin surface electrode).

Sterile electrode

Constructed so that it can be sterilized by temperature, chemicals, or radiation.

Nonsterile electrode

To be used on healthy skin or as an electrode more remote from living tissue.

Biopotential

It is not so easy to describe a monopolar *potential* reading electrode. Such a PU electrode is functioning under zero current conditions. The measured potential is then independent of the skin contact area. It is monopolar in the meaning that only one of the electrodes is in contact with an active tissue area. The other electrode must either be at a passive skin area so that it is *indifferent*, or the potential can come from the average potential of two or more electrodes like the Wilson terminal.

With many electrodes in a one- or two dimensional-array, it is possible to either measure two and two electrodes as bipolar, or/and measure each electrode with respect to an indifferent site or Wilson terminal. Such techniques are used in ECG, EEG, and electrical impedance tomography.

Table 7.4: The Number of Electrodes and Confusion from Words with Latin and Greek Origins

Latin	Greek	Meaning in Potential Measurements
Unipolar	Monopolar	One electrode dominant in a nonsymmetrical system of two or more electrodes
Bipolar	Dipolar	Two equal electrodes in a symmetrical system
Tripolar	Tripolar	Three-electrode system
Quadro-polar	Tetrapolar	Four-electrode system

Monopolar-bipolar electrode systems

The terms monopolar-dipolar are of Greek origin and are preferably used for current carrying systems in this book. The terms unipolar and bipolar are of Latin origin and are often used for signal PU electrode systems. The terminology in the literature is confusing (see [Table 7.4](#)), and it is practically impossible to be consistent.

Monopolar means that the result in some respects depends only on one of the electrodes. The other electrodes being neutral or indifferent; for example, a system of three electrodes: monopolar measuring (M), reference (R), and CC.

A *monopolar* current carrying electrode system has one small electrode as the *active (working, source)* electrode, and the other one as a large area *neutral (sink)* electrode.

A *monopolar* signal PU electrode system has one electrode in contact with active tissue and the other one as a (large) indifferent electrode.

Bipole or dipole without current flow

Signal obtained from two electrodes, one in contact with active tissue and the other in contact with passive tissue.

Bipole or dipole without current flow plus a third indifferent electrode

Each potential from the dipole electrodes is measured relative to the indifferent electrode and the results are subtracted to obtain the dipolar voltage difference. An advantage is that each electrode can be checked whether it is in contact with active tissue.

Bipole or dipole with current flow

In living tissue, there are no monopolar endogenous sources; all sources are dipoles.

Three-electrode monopolar system

Two bipolar CC electrodes plus PU reference electrode (see Section 8.3).

Tetrapolar system

System with two ports and four electrodes: one port with two PU electrodes and one with two CC electrodes. Measures *transfer impedance* from CC port to PU port (see [Section 7.10.3](#)).

Active electrode

1. CC electrode with high current density; for example, for electrosurgery or nerve stimulation, synonym with working electrode.
2. PU electrode situated on a site of neurogenic activity.

Working electrode

CC monopolar electrode with high current density (e.g., for electrosurgery or nerve stimulation).

Passive electrode

PU electrode in contact with tissue without neurogenic activity.

Source – sink electrodes

DC applications follow the old definition that current direction is from plus pole (source) to minus pole (sink): source electrode has positive polarity, sink electrode has negative polarity. In AC applications: arbitrarily defined to understand better the function of an electrode system.

Lead

An electrode pair and their two wires are called a *bipolar* lead. A *unipolar/monopolar* lead is with one PU and an indifferent electrode or a wire from Wilson's terminal. A lead may be defined physically as two signal wires with an associated recording electrode system. It may also be defined conceptually as an information channel receiving information from a signal recording electrode system.

Electrode array

Arrangement of many electrodes in a one-dimensional (e.g., equally spaced along a needle shaft) or two-dimensional pattern.

Floating system (general term)

Electrode system with no coupling to ground.

Ground electrode (general term)

A large noninsulated rod or wire buried into the ground under the building. The dimensions and materials of the walls, ceiling and floor usually have sufficient electric

conductance to make a Faraday cage (shield) for each room. If the house is made of poorly conductive materials (e.g., dry wood) only small Faraday shielding effect will be obtained.

Ground wire (general term)

Yellow/green wire in an electrical power cable connected to the ground (earth) of the building where electromedical equipment is used. It serves two purposes: one increases electrical safety and the other reduces noise. It is not supposed to be current-carrying in a fault-free system. Often (wrongly) used synonymous with the reference wire of the preamplifier. Antonym: not grounded = floating.

Ground, reference, and indifferent electrodes

In Einthoven's early time without ECG amplifiers, there was no need for a "ground" electrode, the galvanometer was a floating input device. But mains supplied amplifiers needed a "ground" electrode to reduce noise, and it was the right leg that was chosen for that purpose. Later safety philosophy advocated that the patient should be electrically floating with respect to ground (see Section 10.16.2). This implied that "ground" was not ground in the meaning the ground wire of the mains. Instead "ground" is the indifferent electrode, meaning that the amplifier and the patient are connected together so that they roughly are at the same potential. But then we also had the ECG tradition that in unipolar leads the reference may be not only one electrode, but, for example, a Wilson terminal, used as "zero" or indifferent reference. In our book, ground means the protective ground electrically connected to the building and the room, supplied by the mains. The purpose of a reference wire is to obtain potential equalization between the patient's indifferent electrode and the electronic circuitry, the reference wire. The indifferent electrode is usually an electrode on the right leg. A neutral or indifferent electrode may also be a part of a unipolar electrode system, and is usually obtained by summing the potentials from more than one electrode; see the Wilson terminal and [Section 7.10.4](#).

With an ideal current dipole in an infinite volume, zero potential will exist in all directions if the distance to the dipole is large enough. Unfortunately, an indifferent (neutral) ECG electrode does not exist because the human body is not large enough. If we go out in one direction along a limb, the limb proper is isoelectric with respect to the heart activity, but not with respect to other sources (e.g., respiration). If we go out along a second limb that too will be isoelectric; however, the potential will not be equal to that of the first limb. Therefore none of them represents a true indifferent electrode.

Because this is an unsolvable problem, the ideal unipolar lead does not exist. Nonideal solutions are to use one electrode at some remote point (e.g., at a limb or an earlobe). Another solution is to add the voltages picked up by more than one electrode, such as two limb electrodes (augmented leads) or three limb electrodes (Wilson central terminal).

Reference electrode

1. With three-electrode monopolar amplifier (see [Figure 7.24](#)).
2. Electrode being a part of a calibration system (see [Section 7.6.6](#)).

Reference wire of the preamplifier

The amplifier's reference wire is the electronic zero of the electronic circuitry. The reference wire of the amplifier may be floating or referred to ground. The wire is connected to the indifferent electrode wire of the person to be measured; it is the system for potential equalization between the measured person and the instrumentation.

Neutral electrode

As a part of a monopolar electrode system: electrode without influence on the measurement results or on power delivery (electrosurgery). Neutral means that the current density at the electrode surface is so low that the effect of current flow is negligible. In particular used for a monopolar impedance recording CC electrode with a surface area much larger than the monopolar electrode. May also refer to an electrode situated at an inactive skin site.

The neutral CC electrodes are also called indifferent, silent, passive, or dispersive electrodes. The ideal CC neutral electrode is an enormous spherical electrode infinitely far away and at zero potential. In real situations, it may be difficult to obtain large enough electrode areas with low enough current density, and the neutral electrode has a disturbing effect. This implies that there may by all sort of intermediate versions between true monopolar and dipolar systems. A special way of creating a more ideal neutral system with a small electrode is to use two of them in an active opamp circuit ([Section 7.2.7](#)).

Neutral PU electrodes are also called indifferent or reference electrodes. A PU electrode may be more or less indifferent depending on its area and position with respect to signal sources. The ideal unipolar models presuppose an enormous spherical neutral electrode, infinitely far away and at zero potential. In a limited tissue volume such as the human body, the ideal indifferent electrode is not feasible, and we use the concept of *quality* of an indifferent electrode. A practical approach is to take the average potential of several electrodes (e.g., Wilson's central terminal in ECG). It is not ideal to connect electrodes of different potentials resulting in exchange current flow between them, but each electrode may first be connected to a buffer amplifier.

Plate electrode

Synonym with neutral electrode in electrosurgery.

Isoelectric, equipotential cable

If zero potential difference is measured in a region, the region is *isoelectric*. A line designating tissue at the same potential is an equipotential *line*, a cable connecting

two electrodes in separate regions so that the regions have the same potential is called an *equipotential cable*.

Immittance and transmittance

A one-port (dipolar) electrode system measures *immittance*. The two electrodes function both as CC and PU electrodes. A two-port four-electrode system measures *transmittance* (transfer immittance): for example, with current injected in one port and voltage recorded at the other port (the black box, [Section 7.1](#)). The electrode pairs of current injection and voltage recording may be interchanged: if the reciprocity theorem is valid, the transmittance is the same. For the reciprocity theorem to be valid, there are no constraints on geometry, only on, for example, system linearity as outlined in [Section 8.1.3](#). The reciprocity theorem is not based on geometry but on network theory, and is therefore treated in [Section 8.1](#).

7.11.1 Probe Concepts, Electric Field Sensor

An *electrode pair* is a *sensor* measuring the potential difference between two electrodes. Knowing the distance between them the sensor is also an *electric field sensor*:

$$\mathbf{E} = \frac{\Delta u}{\mathbf{L}} \quad [\text{volt/m}] \quad (7.17)$$

where Δu is the potential difference between the electrodes, \mathbf{E} is the electric vector field strength, and \mathbf{L} is the vector length between the electrodes.

A *probe* is perhaps the most general term comprising sensing components, housing and cable (e.g., ultrasound probe). A probe can have one or several electrode pairs mounted. *Sensor* may be the same as a probe, or only the sensing components (e.g., temperature sensor). *Biosensor* is a sensor using biomaterials as one of the sensing components. A hair hygrometer is a biosensor because the length of a biomaterial depends on the relative humidity of the air. *Medical sensor* is a sensor made for use in medicine. A *transducer* is the part converting a physical quantity into an electric signal (e.g., a pressure transducer).

A wet electrode is a *galvanic electrode*, meaning that it can accept DC current flow. However, bioimpedance electrodes need not have galvanic contact with tissue, the contact may be by displacement (capacitive) currents via a thin Teflon or glass membrane; or air coupled. An electrode functions by *electric* fields. Time-varying *magnetic* fields may also produce electric currents in tissue, stimulating nerves or producing potential differences that can be picked up by electrodes.

7.12 Electrode Designs

7.12.1 Skin Electrodes

The most used skin surface electrode is the recessed type, [Figure 7.30\(a\)](#). The metal plate is at a certain distance from the tissue surface. The electrolyte is guarded in a rigid

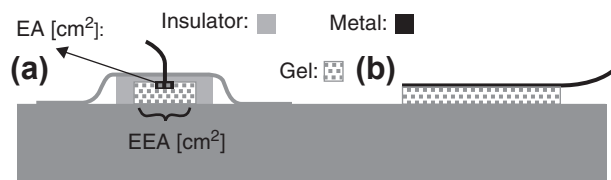


Figure 7.30: Skin surface electrode designs. (a) Recessed metal with gel in stiff cup; (b) electrode with hydrogel contact electrolyte.

container for mechanical support and to minimize evaporation. The electrolyte solution is often supported or contained in a sponge. In this way, the metal/solution interphase is clearly defined, and the total electrode impedance can easily be measured by connecting two electrodes face to face. Streaming potentials (electrokinesis) can be annoying if the solution is moved with respect to the metal during patient movements, but with the recessed electrode the interphase is stabilized and motion artifacts minimized.

The area of the skin wetted or in contact with the electrolyte solution is called the *effective electrode area* of the electrode. EEA is a dominating factor determining electrode/skin impedance. EEA may be much larger than the metal area in contact with the solution (EA), which determines the polarization impedance. The electrode is fixed with a tape ring outside the EEA. Electrolyte penetrating the tape area increases EEA, but reduces the tape sticking area. Pressure on the electrode does not squeeze electrolyte out on the skin surface because of the rigid container construction.

Figure 7.30(b) shows an electrode with solid contact gel. The gel is sticky and serves both as contact electrolyte and for electrode fixation. For this electrode, $\text{EEA} = \text{EA}$. The electrolyte conductivity is rather low because the solution is a gel with low ionic mobility. Electrolyte series resistance may be the dominating factor of electrode/skin impedance at high frequencies. This may introduce problems for use (e.g., for impedance plethysmography around 50 kHz). With this electrode type the skin is not wetted. With such constructions it is possible to make an electrode with a very large $\text{EEA} > 100 \text{ cm}^2$, and obtain efficient skin contact over the whole contact area by using a rather thick gel. For neutral electrode plates in high-frequency electrosurgery, the conductivity of the gel may deliberately be chosen low, so that the electrode functions mostly by capacitive coupling.

Band electrodes are used as large-surface, low-impedance electrodes with the additional attractive feature of *reducing the current constrictional effect* found with smaller disk electrodes. This is important in two electrode applications such as impedance.

Plethysmography and body composition estimation. In Figure 7.31, the usual configuration is shown with the current carrying electrodes CC and CC' as the outer electrodes. Consider the consequence of swapping the current carrying and recording electrodes.

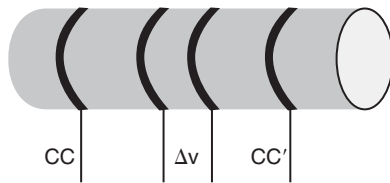


Figure 7.31: Band electrodes.

Multiple-Point Electrodes

The problem with a plate electrode in some applications is the covering effect on the tissue. With a multiple-point electrode, humidity for instance can escape from the surface. Dependent on tip sharpness and electrode pressure the points may penetrate the superficial layers.

Concentric Ring Electrodes

Barnett (1937) used a three-electrode system with a 6 cm^2 ring electrode as measuring electrode on the upper arm (Figure 7.32). He used Monel metal covered by flannel soaked in normal saline. The current carrying counter electrode was positioned symmetrical on the other side of the arm. The reference electrode was concentric to the measuring ring electrode. This is an efficient geometry for eliminating much of the deep tissue series impedance. He measured in the frequency range 2–42 kHz. With a four-electrode technique, he also measured deep tissue contribution.

Yamamoto et al. (1986) used a two-electrode quasibipolar system, with the large electrode having about 10 times the area of the small one. The concentric electrodes were positioned spring mounted in a tube to secure a constant electrode mechanical pressure on the tissue

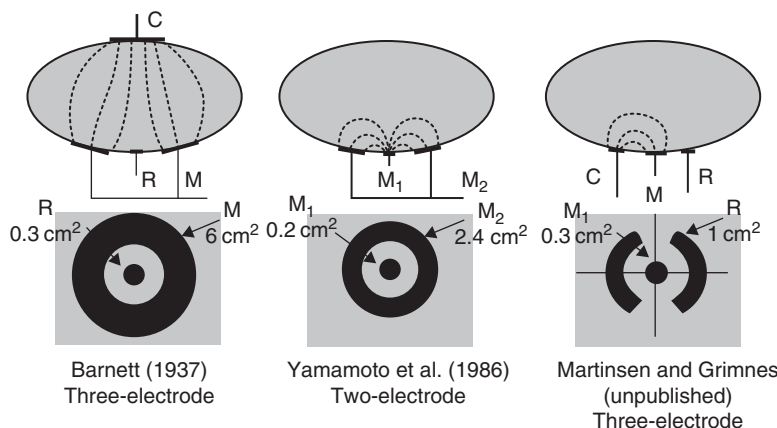


Figure 7.32: Concentric ring electrodes.

surface. With a third CC electrode, it has also been used as a part of a three-electrode system (Martinsen et al., 1996).

Martinsen and Grimnes used a three-electrode concentric ring system with the outer ring split in two parts, one used as reference electrode (R) and the other as current carrying (C) electrode. In this way, the reference electrode picks up a potential closer to that of the measuring electrode, so that deeper tissue series impedance contribution is reduced.

7.12.2 Skin Electrode Wires

See [Figure 7.33](#) and [Section 7.13](#). The electrode wire is a trivial but very important part of the electrode. There are many things to consider: the best cable track, no wire drag on the electrode, and minimal weight of the electrode connector. Very flexible wire, perhaps shielded? The best is to have no connector at the electrode side, a wire with prefabricated direct entry into the electrode.

With an electrode connector, the left version in [Figure 7.33](#) has the problem that to connect, pressure must be applied that can squeeze contact electrolyte out and make the skin contact area unstable. The connector in the middle can be fixed without any vertical pressure and squeeze effect.

On the left side of [Figure 7.33](#), the wire connectors on the equipment side are shown. These are insulated to prevent accidental contact to current carrying conductors after the electrode has been fixed to the patient but not yet connected.

7.12.3 Invasive Needle Electrodes

Electrodes as shown in [Figure 7.34](#) are used in anesthesia, EMG, and neurology. For mechanical strength, they can be made of stainless steel, with outer diameter around 1 mm or less. As seen, a metal shaft may be used also as reference electrode. Because of small



Figure 7.33: Skin electrode wires. Courtesy Tormod Martinsen.

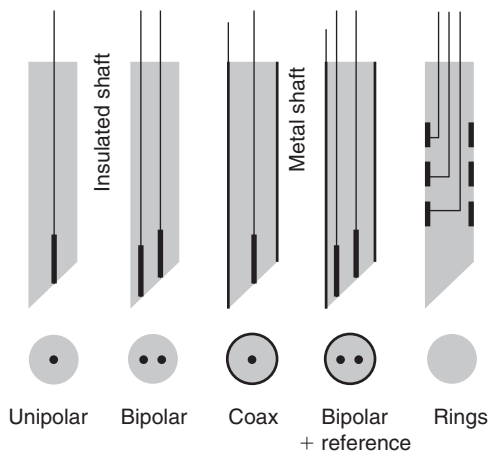


Figure 7.34: Needle electrode cross-sections.

EA and according to Section 6.1, the total electrode impedance may be high and dominated by electrode polarization impedance. A needle tip may look bright and shining, but the magnified surfaces shown in [Figure 7.35](#) shows “fractal” surface increase and debris from the manufacture. This may lead to unstable polarization impedance on the tip.

Hollow needles are used for injection or aspiration of liquid samples. The external shaft may be insulated by, for example, lacquer layer insulation; the internal tube is usually

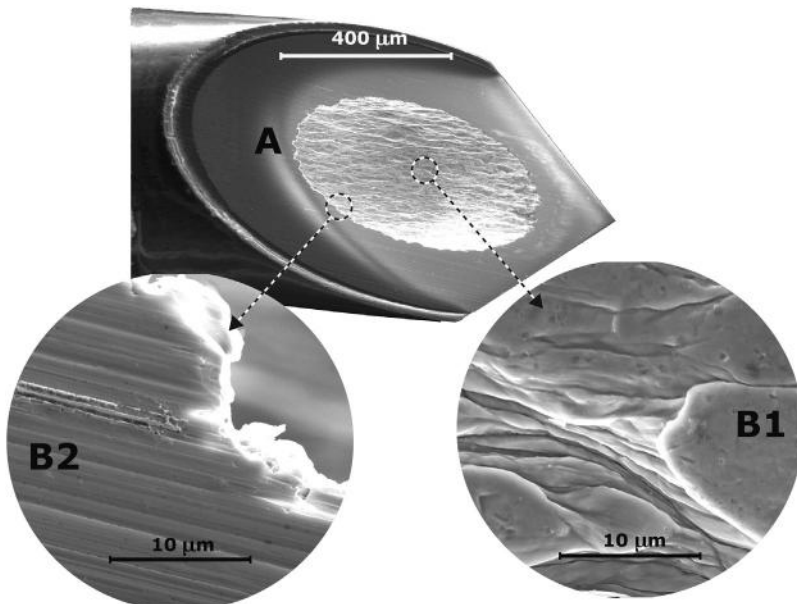


Figure 7.35: Hollow needle electrode magnified. Courtesy Håvard Kalvøy.

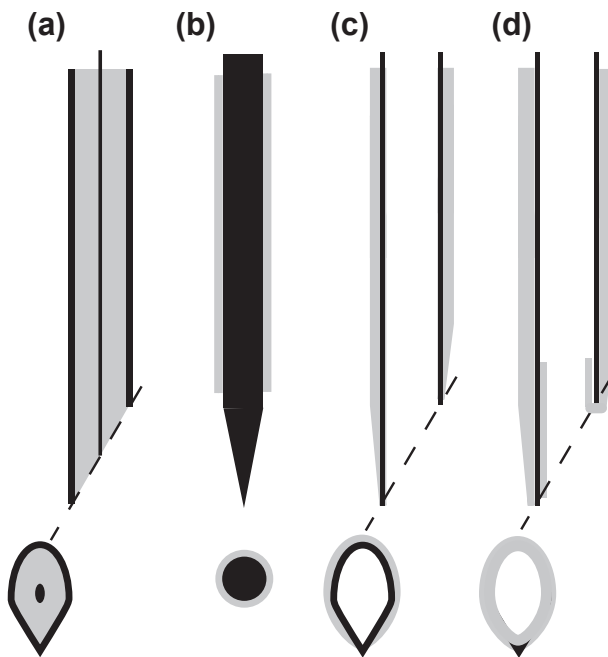


Figure 7.36: Needle models with insulation. (a) Coaxial small EA with exposed metal shaft; (b) massive needle with insulated shaft; (c) hollow injection needle with internal metal contact; (d) hollow injection needle with internal end insulation. (a), (c), and (d) with bevel end cut.

not insulated. The tip of the needle is exposed as an oval ring or a small tip area ([Figures 7.36 and 7.37](#)).

Impedance of Needle Electrode in Living Tissue

[Figure 7.37](#) shows the monopolar impedance spectrum measured with a thin insulated needle inserted in porcine living tissue. The 90% sensitivity zone is roughly a sphere of about 3 mm centered at the exposed needle tip. Above ≈ 10 kHz the data are dominated by tissue properties, below ≈ 1 kHz by electrode polarization impedance.

Tissue Dependence of Polarization Immittance

An important finding from [Figure 7.37](#) was that the polarization impedance was tissue dependent, in accordance with the findings of Schwan (1992a).

With such data combined with multivariate analysis, it is possible to determine the type of tissue that surrounds a needle tip and also the position of the needle tip.

Another example of the use of needle electrodes for tissue characterization is Mishra et al. (2012), who used an impedance-sensing biopsy needle to separate between malignant and benign prostate tissue in a clinical setting.

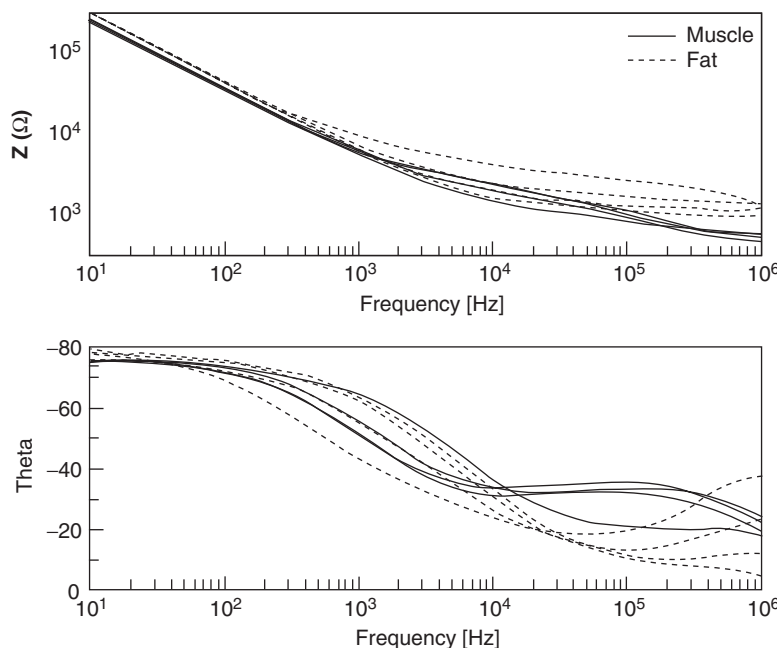


Figure 7.37: Monopolar impedance of insulated needle with exposed tip *in situ* in living porcine tissue. Impedance data dominated by electrode polarization below ≈ 1 kHz. Notice, however, polarization impedance dependence on tissue type. Courtesy of Håvard Kalvøy.

7.12.4 Micro- and Nanoelectrodes

Monopolar recordings in the intracellular space are made with a small transmembrane electrode in contact with the cytoplasm, and a larger extracellular electrode in the interstitial liquid. The tip of the electrode must be small enough to penetrate the membrane without too much damage and not too much plasma/electrolyte leakage. Squid giant axons have diameters up to $1000\text{ }\mu\text{m}$, and in such studies the diameter of the penetrating part may be of the order of $50\text{ }\mu\text{m}$. For ordinary cell sizes, tips down to $1\text{ }\mu\text{m}$ diameter are used.

The electrode itself may be the end of a *metal needle* or the end of a fluid-filled *glass capillary (micropipet)*. The electrical characteristics of these two types are very different, and they have their characteristic application areas. The metal electrode has poor DC properties, and is best for recording fast action potentials. The micropipet electrode is better suited for recording DC or slowly varying DC potentials (Figure 7.38).

The *metal needle* can be made of tungsten, stainless steel, platinum alloys, etc., and it is possible to fabricate tip diameters down to $1\text{ }\mu\text{m}$. It is necessary to isolate the shaft except the tip. A lacquer or glass coating can do this. A description of how to make them can be

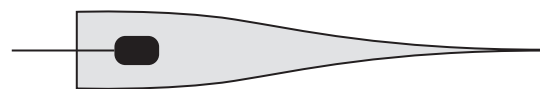


Figure 7.38: Glass micropipette electrode.

found in Geddes (1972). The metal surface exposed to the electrolyte is very small (on the order of $10 \mu\text{m}^2$), and accordingly the polarization impedance may be several megaohm, increasing at lower frequencies and making the electrodes less suited for DC measurements. The frequency response is dependent on the polarization impedance and the distributed stray capacitance. The stray capacitance depends on the length of the needle shaft in contact with fluids and the thickness of the isolating layer.

The glass *micropipette* electrode is filled with an electrolyte, usually 3 M KCl. Such a high concentration is used to lower the electrode resistance, but the infusion of this electrolyte into the cell must be minimized. A liquid junction potential of some megavoltage will be generated by the concentration gradient at the tip. The electrode is fragile. During muscle studies the glass capillary end may easily break when the cells are excited. The micropipette electrodes are made with orifice diameters down to $1 \mu\text{m}$. The small tip and its length and diameter determine to a large extent the electrical properties of the electrode, and its resistance may easily attain $100 \text{ M}\Omega$. The electrode surface is often AgCl, and the EA can easily be made so large that electrode polarization impedance error is negligible. It is a purely resistive electrode; however, with a distributed stray capacitance because of the glass dielectric in contact with the inner electrolyte and external tissue liquids.

The ordinary use of a micropipette electrode is monopolar. Double pipette electrodes are sometimes used with only one penetration of the cell membrane. One pipette is current carrying and the other is recording in a three-electrode set-up.

Another example of the use of small electrodes is Jahnke et al. (2013), who used a flexible microelectrode array to separate between brain and tumor tissue *in vivo*.

For *cellular patch clamp electrode*, see [Section 7.12.7](#).

7.12.5 In vitro Measuring Cells

Some material constants with a homogeneous cylinder of biomaterial is: $\sigma = GL/A$, $\epsilon = CL/A$, and the resistivity $\rho = RA/L$. The ratio A/L [m], or L/A [1/m] is the *cell constant* of a measuring cell. In general, the cell constant can be determined for other geometries than the cylinder, so that it is easy to derive the unknown conductivity, permittivity, or resistivity from measured results. In the latter case, it is of course important that the measuring cell is completely filled with the sample biomaterial.

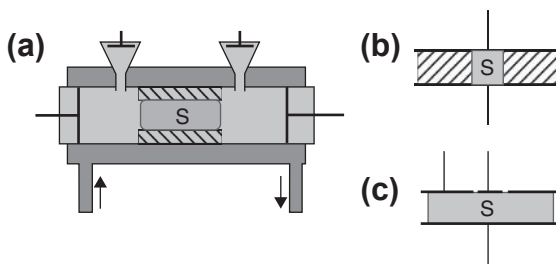


Figure 7.39: Measuring cells for tissue samples (S). (a) Four-electrode liquid filled system, temperature-controlled; (b) sample confined by isolating material; (c) guard ring (kept equipotential with center electrode).

If sample size varies, it is easier to use a *guard ring* (Figure 7.39(c)) around the measuring electrode and kept at the same voltage. The effect of stray fields or current constriction is then reduced.

If the measurement is to be performed under ex vivo conditions, the tissue is to be kept alive by controlling the temperature and the extracellular fluids. Also with dead samples, temperature and extracellular liquid control may be necessary. For “dry” dead samples, control of the *ambient air humidity* may also be necessary.

One way of reducing the effect of electrode polarization is to increase the impedance of the sample by increasing its length. To compensate for the polarization impedance further, several methods are possible:

1. Four-electrode system (tetrapolar) (see Section 7.1.3)
2. Measure electrode polarization impedance separately and subtract
3. Substitute the unknown with a known sample for calibration
4. Vary the measured sample length (e.g., in suspensions)

Method numbers 2 and 3 are based on the assumption that the metal/liquid interphase and thus the polarization impedance is invariable. This is not always the case. Measuring on “dry” samples for instance implies poor control of the contact electrolyte. Also a sample may contain local regions of reduced conductivity near the electrode surface. The currents are then canalized with uneven current density at the metal surface (shielding effect).

Electrode polarization impedance, in particular at low frequencies, is then dependent on the degree of shielding. An example of method 4 is Krizaj and Pecar (2012), who described such a method for removing the contribution from electrode polarization impedance on measured impedance data of a suspension of microcapsules.

There is also an increasing interest for developing practical electrode systems for impedance-based monitoring of cell growth and other cellular processes in chambers or scaffolds. Examples are Lu et al. (2013), who used a multielectrode bioimpedance system

to monitor cell growth, and Sarro et al. (2012), who developed a four-electrode system with interdigitated micro-electrodes to monitor cell adhesion.

7.12.6 Ponderomotoric Effects and Electrodes

Dielectrophoresis

Dielectrophoresis (DEP) is the movement of dielectric particles in an inhomogeneous electric field. The force \mathbf{f} on a charge is $\mathbf{f} = q\mathbf{E}$, so if the net charge is zero, there is no force. A dipole has net charge = 0 and will experience a torque in an electric field, but no translational force. However, in an inhomogeneous field, there is also a translational force on a dipole. Consider a spherical noncharged particle in a medium. It is polarized in an electric field and if there is a field gradient $\nabla\mathbf{E}$, there is a force \mathbf{f} on the particle (Pethig, 1979) given by:

$$\mathbf{f} = (\mathbf{p} \cdot \nabla)\mathbf{E} = 2\pi a^3 \Re \left[\frac{\epsilon_2(\epsilon_1 - \epsilon_2)}{(\epsilon_1 + 2\epsilon_2)} \right] \nabla\mathbf{E}^2 \text{ [N]} \quad (7.18)$$

where \mathbf{p} is the induced dipole moment, subscript 1 is for the particle, and 2 for the medium. [Equation \(7.17\)](#) is the basic equation for DEP and shows that, depending on the relative polarizability of the particle with respect to the medium, the particle will move either in the direction of the field gradient (positive DEP) or in the opposite direction (negative DEP). The electrophoretic and dielectrophoretic mechanisms can be completely separated, and Pohl (1958) adopted the term dielectrophoresis to identify this distinction. Only DEP gives a net force in an AC electric field, the \mathbf{E}^2 term has no polarity dependence. One problem with [Eq. \(7.17\)](#) is that it does not account for surface and double layers on wet surfaces. Two useful review articles on DEP are Pethig (2010, 2013). See Section 10.11.2 for applications of DEP.

Electrorotation

Particles suspended in a liquid will experience a torque in a rotating \mathbf{E} -field (Arnold and Zimmerman, 1982). A dipole is induced in the particle. Because the polarization process (redistribution of charges) is not immediate, the induced dipole will lag the external field and a frequency dependent torque will exist. It can be shown that the torque is dependent on a relaxation time constant identical to the time constant in the theory of β -dispersion (Schwan, 1985). Cell rotation is therefore a direct physical manifestation of dispersion. Theory predicts that the torque may have two maxima, usually of opposite sign (corotation and antirotation) and is given by (Zhou et al., 1995):

$$\Gamma = -4\pi a^3 \Im \left[\frac{\epsilon_2(\epsilon_1 - \epsilon_2)}{(\epsilon_1 + 2\epsilon_2)} \right] \nabla\mathbf{E}^2 \quad (7.19)$$

Rotation also occurs in nonrotating external fields, and onset is often at a sharply well-defined frequency. The rotation is therefore also called *cellular spin resonance*. One

possible mechanism is the dipole–dipole interaction between neighbor cells. The peak rotation frequency is many decades lower than the excitation frequency, the latter being in the β -dispersion range (MHz).

Cellular spin resonance indicates various physiological states of living or dead cells, and also represents a method for cellular manipulations. It should, for example, be possible to rotate intracellular organelles with respect to the whole cell.

Levitation

Negative dielectrophoresis causes particles and cells to be repelled from regions of high electric field strength. This effect can be used to levitate particles over, for example, a planar array of electrodes. A common geometry is a four-electrode field trap with electrodes forming the sides or corners of a square and with the particle levitated over the center of the square. The viscous forces from the medium will damp the motion of the particle.

Traveling Wave Dielectrophoresis

If the E-field in an electrorotation chamber was made to move in a linear rather than an angular manner, an interesting combination of dielectrophoretic and electrorotation effects will occur. The principles are shown in Figure 7.40, where phase-shifted cosine voltages are applied to facing electrodes along an array of such electrodes. Only particles experiencing negative dielectrophoresis will move along the interelectrode channel. They will otherwise be trapped at the electrodes by positive DEP.

As shown previously, the dielectrophoretic effect depends on the real part of the induced dipole moment and the electrorotation effect on the imaginary part of the induced dipole moment. Both these effects contribute to the motion of the particle in the traveling wave chamber. Viable cells will typically exhibit negative

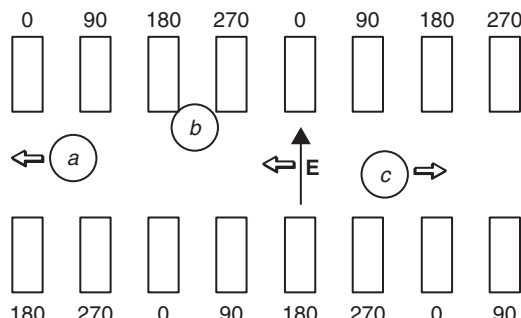


Figure 7.40: Traveling wave DEP achieved by using cosine voltages with the indicated phase relationships as excitation on each pair of facing electrodes. The electric field will travel from right to left in this example. Particle a could be a nonviable cell, b a cell trapped by positive dielectrophoresis, and c a viable cell.

dielectrophoresis at low frequencies (typically <10 kHz) and in a frequency window below this frequency, where the imaginary part of the induced dipole moment is positive, the cell will move in the opposite direction of the traveling electric field. Below this frequency window, the cell will be levitated over the electrode array. For nonviable cells, the negative dielectrophoretic effect will typically occur at high frequencies over 1 MHz. The corresponding imaginary part of the dipole moment will be negative and the cell will hence travel in the direction of the moving field (Wang et al., 1993).

Pearl Chain Formation

A dielectric particle disturbs the local **E**-field, so even in a homogeneous external field there is a local gradient. Two neighboring dielectric particles will therefore be attracted to each other. They form a dipole and will be oriented in the direction of the **E**-field. In a homogeneous field, cells will therefore tend to form pearl chains in the direction of the **E**-field. In a gradient field the pearl chains will protrude from the electrode surface (Schwan and Sher, 1969).

7.12.7 Patch Clamp Electrode

The patch clamp technique with its great versatility has been a most important tool in the study of excitable cells. Figure 7.41 illustrates the main components of the technique. A glass pipette with a very small opening (diameter $\approx 1\ \mu\text{m}$) is filled with an electrolyte in contact with a metal electrode for current and potential recording. The pipette is brought in contact with a cell membrane and suction applied to make a tight seal around a tiny area (patch) comprising (e.g., one membrane channel). The suction brings the pipette-extracellular liquid resistance up, for example, from $50\ \text{M}\Omega$ to $50\ \text{G}\Omega$; the suction creates a *gigaseal*. When a channel opens, all ions therefore flow through the pipette and is measured as electrons in the electrode wire. The arrangement shown in Figure 7.41 is called the *cell-attached patch clamp technique*.

Local membrane destruction can be made by suddenly applying a short strong burst of suction. A hole is created in the cell membrane so that the pipette is in direct electrolytic contact with the cell interior. Electrical potentials and currents from the entire cell are measured and are therefore called the *whole-cell recording technique*. The hole may also be used to inject substances into the interior of the cell.

The *inside-out patch technique* is to retract the pipette that is in the cell-attached configuration so that a small vesicle of membrane remains attached. By exposing the tip of the pipette to an external electrolyte, it is possible to control the medium to which the intracellular surface of the membrane is exposed. Alternatively, if the pipette is retracted while it is in the whole-cell configuration, the membrane ruptured ends at the tip of the

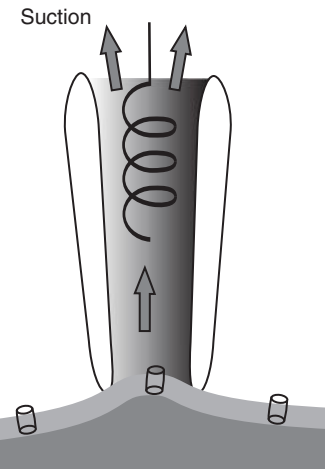


Figure 7.41: Patch clamp electrode.

pipette can anneal so that a membrane patch is produced that has its extracellular surface exposed. This arrangement, called the *outside-out patch technique*, is optimal for studying how channel activity is influenced by extracellular chemical signals, such as neurotransmitters.

7.12.8 Nongalvanic Coupling to Tissue

Magnetic Coupling to Tissue

A time-varying magnetic field causes an induced emv in a conducting medium according to *Faraday's law of induction* (more generally formulated in Maxwell's Eq. (7.12)):

$$v = \frac{-\partial\phi}{\partial t} \quad (7.20)$$

where ϕ is the magnetic flux (in weber or volt-seconds) through a closed loop, and v is the voltage between the loop ends if the loop is open. In volume conductors, the loops are effectively closed and the induced potential causes a flow of electric current. Such currents induced by time-varying magnetic fields are called *eddy currents*. The induced eddy current density will be higher the higher the medium conductivity. Induced low-frequency currents will therefore follow high conductive paths (blood vessels), and avoid low-conductivity areas (lung and bone tissue, myelin). With the fast switching ($100 \mu\text{s}$) of the high gradient magnetic fields (25 mT/m) used in magnetic resonance imaging (MRI), the current density in the body is approaching the threshold of perception. This is analogous to the use of skin surface coils for the stimulation of superficial nerves. Bickford and Fremming (1965) demonstrated the feasibility of magnetic nerve stimulation. Barker et al. (1982) found that it is possible to stimulate the human motor cortex. With a suitable skin surface coil of a diameter of about 10 cm, a short millisecond pulse with a peak current of the order of 5000 A creates a local

maximum field of a few tesla. Even if the magnetic field strength falls off with distance, the induced current in a nerve just under the coil is sufficient for excitation. The excitation threshold is dependent on the magnetic field direction. The ordinary single-coil construction gives maximum field strength distributed over the whole circle corresponding to the coil windings, with only a small contribution in the coil center. Double coils are used to focus the field strength. The inductance of the coil and the high current level and short pulse time correspond to a high voltage across the coil ends and thus a high local electric field in addition to the magnetic field. The mechanical forces acting on the coil windings are considerable, and with repeated pulses heat development must also be considered.

Eddy currents will set up their own magnetic fields, *opposing the external field*. The magnetic field will therefore be attenuated as function of depth (*skin effect*). The *skin depth* (depth of penetration) δ in the case of a uniform, plane electromagnetic wave propagating in a volume conductor with a magnetic permeability μ is:

$$\delta = \frac{1}{\sqrt{\pi f \sigma \mu}} \quad (7.21)$$

Because the wave may be reflected at the surface, the initial value corresponds to the value just inside the medium. [Equation \(7.20\)](#) must be used with care, because the far-field conditions of a *wave* are not fulfilled at lower frequencies.

The skin depth will be deep if the conductivity is low and the frequency low. According to [Table 7.5](#), magnetic alternating fields are not very much attenuated by the presence of a human body at frequencies below 1 MHz. Casañas et al. (2004) used a frequency of 28 kHz to measure iron overload in the human liver. At frequencies used in MRI (e.g., 60 MHz for 1.5 T systems), the attenuation and phase shift are considerable.

Magnetic Resonance Imaging

In MRI, the field coupling to the body is as purely magnetic as possible. It is obtained by three sets of coils: the static main field coils (e.g., 1 T), the gradient coils (e.g., 30 mT/m with rise and fall times in the microsecond range), and the RF coils (e.g., with separate transmitting such as peak power of 10 kW at 60 MHz and receiving coils).

Table 7.5: Skin Depth δ as a Function of Frequency and Material

σ (S/m)		δ @ 60 Hz	δ @ 1 kHz	δ @ 1 MHz	δ @ 3 GHz
$5.8 \cdot 10^7$	Copper	8.5 mm	2 mm	66 μ m	1.2 μ m
$1 \cdot 10^5$	Graphite	210 mm	50 mm	1.6 mm	29 μ m
5	Sea water	30 m	7 m	2 m	4 mm
1	Physiological saline	67 m	16 m	4.5 m	8.9 mm

In a superconducting coil, the voltage across the coil ends is zero, and so there is no additional E-field applied to the patient. Gradient coils and RF coils however have a considerable voltage difference between the coil ends to drive the necessary current. If not shielded, such coils therefore produce an electric field in addition to the magnetic field.

Magnetic Fields from Endogenic Current Sources

All electric currents are accompanied by magnetic fields. With the invention of the Superconducting Quantum Interference Device as an extremely low magnetic field (10^{-9} T) detector, it has become possible to measure the magnetic fields from the small endogenic currents of the body, even from the small sources in the heart and the central nervous system. This has opened up a whole new field of measurements analogous to their electric counterparts: MKG (EKG), MEG (EEG), and so on. However, these interesting subjects are outside the scope of this book, and the reader is referred to the book by Malmivuo and Plonsey (1995).

Capacitive Coupling to Tissue

A nongalvanic electric field coupling to tissue is a capacitive coupling. Accordingly, it is more efficient the higher the signal frequency used, according to $B = \omega C$. For low frequencies (e.g., <1 Hz) and at DC, nongalvanic coupling cannot be used. However, for example, the coupling from the power lines is of interest in hazard analysis, even when the coupling is at several meter distances and the frequency is only 50/60 Hz.

Static Electric Field Coupling to Tissue

An ideal dielectric is a material that allows internal E-fields because the material has no free charge carriers and therefore no DC conductivity. With a conductor like the human body, being exposed to an external static field, does not allow internal static E-fields, the charges on the surface are rearranged so that the internal E-field strength is zero. *An externally applied static E-field to the human body therefore has no effect on internal organs, only on the skin.* However, applied alternating E-fields result in tissue currents and internal E-fields. At high electric fields, corona discharge will occur.

Low-Frequency Electric Field Coupling to Tissue

Humans are exposed to electric fields from power lines in their daily life. The power lines inside buildings expose us to 50/60 Hz E-fields, and in usual situations some tenths of a microampere is measured if a well-insulated person is grounded via an ammeter. Such small currents are perceptible for humans under certain conditions (*electrovibration*, Section 10.16.1). Outdoors, a much higher current can be measured if the person is under a high-voltage power line. Calculations show that at low frequencies (e.g., power line frequencies 50/60 Hz), the field strength in a human's interior is far smaller than the external field strength (Foster and Schwan, 1989). Except for the skin, the tissues of the body to the first

approximation may be considered to be equipotential. However, this is not true for small-signal measurements: 1 μA 50/60 Hz through, for example, an arm with a total resistance of about 500 Ω (Section 4.3) results in a voltage difference of 0.5 mV. This is certainly not a negligible signal when ECG signals of the same magnitude are to be measured (see Section 6.2). The current density distribution in such cases was studied by Guy et al. (1982).

The effect of an applied alternating E-field may be analyzed as an ordinary capacitor coupled system (Chapter 3). The tissue of interest may be modeled as a part of the dielectric, perhaps with air and other conductors or insulators. The analysis of simple geometries can be done according to analytical solutions of ordinary electrostatic equations as given in Chapter 6. Real systems are often so complicated that analysis preferably is done with the Finite Element Method (FEM) (Chapter 9).

A simple first approximation calculation can be done, for example, with a model consisting of a conductor cylinder of radius a at distance $D/2$ from an infinite plane conductor. The capacitance per meter conductor is:

$$C = \frac{2\pi\epsilon}{\ln \frac{D}{a}} \quad (7.22)$$

With $D = 2$ m and $a = 1$ mm, C is of the order of 7.6 pF/m (and not very dependent either on a or on D !). The current is $i = u\omega C$ per meter, and with 60 Hz and 130 V this gives 0.35 μA per meter wire. Such a simplified model with a person as the plane conductor is therefore in rough agreement with measured currents from power cord couplings found in actual situations. With a completely insulated person, the AC voltage of the person is the mains voltage with respect to ground reduced by the voltage division caused by the power cord/person and person/ground capacitances. If the person is grounded, the system can be regarded as a monopolar system. The grounding point is the point of high current density (active electrode). The whole body skin surface area is the low current density capacitively coupled neutral plate. Possible effects are to be found at the active electrode site.

For bioimpedance measurements a bipolar electrode may be used covered by an insulating layer of Teflon or glass. This is further analyzed by FEM (see Section 5.5). Another example of capacitive electrode coupling is diathermy, see the following section.

High-Frequency Electric Field Coupling to Tissue

Short wave diathermy uses a frequency around 27 MHz, corresponding to a wavelength of about 12 m. The tissue is placed in the near-field of an applicator capacitor (or coil), and the local power density W_v (watt/m³) is everywhere given by the equations $W_v = \sigma E^2 = J^2/\sigma$. The corresponding adiabatic temperature rise per second $\Delta T/t$ as a function of current density (or E-field strength) under adiabatic conditions is given by

$\Delta T/t = J^2/(\sigma' c \cdot d)$, where d is mass density (for water: 1000 kg/m^3) and c the heat capacity (for water: 4.2 kJ/kg and $^\circ\text{K}$).

A certain selectivity between tissue doses is of interest, and from these equations it may be deduced that with constant amplitude voltage (E-field strength), the tissue of highest conductivity has the largest power dissipation and temperature rise. This is true in a homogeneous medium, but in the inhomogeneity of real tissues the opposite may also be true. Consider a capacitor with two equal slabs of materials with unequal conductivities *in series*. With DC parameters, it is easy to show that the ratio between the power densities in slabs 1 and 2 when $\sigma_1 \ll \sigma_2$, is:

$$\frac{W'_1}{W'_2} = \frac{\sigma_2}{\sigma_1} \gg 1 \quad (7.23)$$

The current density is the same in the two slabs, and it is determined by the slab with lowest conductivity, σ_1 . Slab 1 with the *lowest* conductivity also has the highest E-field strength, and will therefore have the highest power density.

If the two slabs are side by side *in parallel*, the situation will be opposite. The E-field strength is the same in both slabs, but the current densities are not. The material with *highest* conductivity will have the highest current density and the highest power density.

With an *inductive* coil coupling, the circulating currents in the tissue are eddy currents, which are proportional to tissue conductivity (see Section 8.1). The corresponding rules for inhomogeneous materials can easily be worked out.

2000 MHz = 2 GHz corresponds to a wavelength of about 15 cm, and the tissue is partly in the near-field and partly in the far-field. At higher microwave frequencies the conditions are more and more of a far-field type, so we are dealing with electromagnetic *radiation* properly speaking (see Section 8.1.1.2). The electromagnetic fields of microwave diathermy are determined not only by incident radiation, but also on reflected energy from interface zones of changing impedance (e.g., at skin, fat, bone surfaces).

Nongalvanic Coupling by Electromagnetic Waves (Far-field Radiation)

The electromagnetic fields at a distance from the source larger than about 10 times the wavelength propagate as a far-field electromagnetic *wave*. Near-field components have vanished. More than 3 m away from a 1 GHz antenna, the fields thus are dominated by the electromagnetic wave. Examples of electromagnetic wave coupling to tissue are, for example, microwave heating, or a person in front of a radar antenna.

Even higher frequencies correspond to IR, visible, and ultraviolet light. In this range, electromagnetic waves more and more behave like a stream of photons, particles without charge, and rest mass. Planck's law $\Delta E = \hbar\nu$ defines the correspondence between photon

Table 7.6: Depth of Penetration of an Electromagnetic Wave into Tissue

	Saline	Muscle	Fat
433 MHz	2.8 cm	3 cm	16 cm
2.5 GHz	1.3 cm	1.7 cm	8 cm
10 GHz	0.2 cm	0.3 cm	2.5 cm

energy ΔE and frequency v . The higher the frequency, the higher the photon energy. In the ultraviolet spectrum, the photon energy has increased to about 5 eV, enough to excite the outer electrons of an atom. The radiation is then *ionizing*, representing a rather well defined hazard to living tissue. Even higher energy photons, partly absorbed by tissue, are used in diagnostic X-ray, but these subjects are outside the scope of this book.

Passing through homogenous tissue attenuates an electromagnetic wave, **Table 7.6**. Fat with low conductivity has least attenuation.

In addition, reflection and scattering occurs in tissue. For frequencies < 100 GHz and wavelengths > 3 mm, the wave obeys the laws of reflection and not scattering. *Rayleigh* scattering is the dispersion of electromagnetic radiation by *small* particles having a radius less than approximately 1/10 the wavelength of the radiation. Rayleigh scattering is strongly frequency dependent: the higher the frequency, the more powerful the scattering. When the radius of curvature of tissue is *larger* than the wavelength, geometrical scattering (planar reflection) occurs. This effect is frequency independent, and the basis of lenses and the laws of reflection.

The reflection and transmission of a plane wave at a planar tissue interface depend on the frequency, the polarization, and angle of incidence of the wave as well as the complex dielectric constant of the tissue. The reflection coefficient R from (and the transmission T through) an interface of two media with intrinsic impedance Z_1 and Z_2 are:

$$R = \frac{Z_2 - Z_1}{Z_2 + Z_1} \quad (7.24)$$

$$T = \frac{2Z_2}{Z_2 + Z_1}$$

Here, T and R are field coefficients, as opposed to power transmission/reflection coefficients.

The specific absorption rate (SAR) of non-ionizing electromagnetic radiation with frequencies < 100 GHz is defined (sine waves, W/kg) as:

$$\text{SAR} = \frac{\omega \epsilon_0 \epsilon''}{2\rho} |E_i|^2 [\text{W/kg}] \quad (7.25)$$

where ρ is mass density (kg/m^3). This equation does not take into account possible absorption of magnetic energy related to the magnetic permeability of tissue. It also does not necessarily relate ϵ'' and all the absorbed power to heat and temperature rise.

7.12.9 Kelvin Probe

The Scanning Kelvin Probe is a state-of-the-art device that measures surface electrical potential without actually contacting the sample. Its operation can be grossly summarized as follows (Figure 7.42): A probe tip is positioned close to the skin, creating a type of capacitor; the probe tip acts as a plate, whereas the skin acts as the contralateral plate and the potential difference between the two (V_s) generates a charge on the probe tip; the probe tip oscillates to vary the distance from the skin (d_0 = tip-to-sample distance, $2d_1$ = probe oscillation amplitude); because capacitance is inversely related to distance, the oscillation changes the capacitance and alters the charge on the probe tip; this generates a measurable current which is used to calculate the potential difference between the tip and sample; with a constant work potential seen with the metallic tip, the skin surface potential can be determined.

Older versions of the Kelvin Probe derived the specimen surface potential by applying a constant potential to the vibrating tip and adjusting the amplitude until the tip-to-specimen potential difference effectively reached zero (thus no detectable electrical current in the circuit). This approach, however, was prone to imprecisions as any ambient electrical fields would contribute to some detectable current. More recent versions of the Scanning Kelvin Probe uses an “off null” detection method where a constant potential of sufficient amplitude is both added and subtracted (not simultaneously) to the vibrating tip to create two data points “off null”; for example, sufficiently disparate from the “null” condition where tip and specimen electrical potentials are equal (Baikie et al., 1999). Using a clever linear interpolation method, both the tip-to-sample potential difference and a surrogate distance measure can be calculated. This approach reportedly confers the device with two features: (1) high signal levels, 1000 times larger than the conventional approach and (2) independent reporting of the tip to sample spacing to within 1 micron

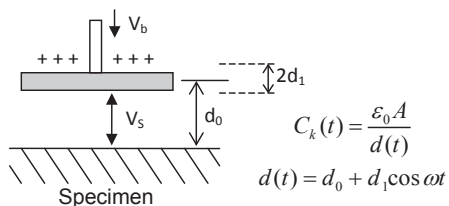


Figure 7.42: Kelvin probe principles. Tip and specimen are capacitively coupled. Charges on the tip change with probe oscillation. V_s = voltage difference between tip and sample.

(Baikie et al., 1991a,b; Baikie and Estrup, 1998). This latter condition importantly guarantees that initial surface potential settings are identical each time the measurement is performed and avoids changes in spacing during a surface potential topography scanning.

Traditionally, the Kelvin Probe has been used to study the surface properties of metals and semiconductors. In these cases, the charge carrier is well defined (i.e., electron) and the surface potential measurements clearly impart information about the materials work function. In biological tissue, however, the charge carriers are typically ionic, and fixed molecular constituents have insulating and polar properties that may modify the surface volume electrical fields and thus alter the derived surface potential measurements in ambiguous ways. It may be for this reason that the Kelvin Probes has not been commonly applied to biological specimens, much less to *in vivo* tissues. Earliest applications of a Kelvin Probe to measure macroscopic electrical biopotentials occurred in the 1990s when the stalk of the corn shoot was measured during steady growth and exposure to light (Baikie et al., 1999). Subsequently, it has been applied to the study of human skin wound (Nuccitelli et al., 2008) and acupuncture points (Gow et al., 2012), but Kelvin Probe studies involving biological samples have otherwise been infrequent. The appeal for the application of Kelvin Probe to biological studies arises from its noncontact approach and its capacity to bypass the electrode-tissue confounders that commonly plague many conventional bioelectrical measurement devices. Moreover, the Kelvin Probe does not utilize intercalating dyes, strong electrical currents, or ionizing beams that may interfere or harm active physiological processes.

Based on recent theoretical and computational analyses, the Kelvin Probe performs in two distinct ways when applied to biological tissue: the specimen can be treated either as a perfect dielectric when the charge relaxation rate is slow or as a highly conductive material (much like metal) when the charge relaxation rate is rapid (Ahn et al., 2012). Because of their rapid relaxation rate and increased permittivity, biomaterials tend to fall into the latter category, and in samples that range from wet/dry skin to cerebral spinal fluid or tendons, the Kelvin Probe can readily obtain surface potentials as if it were a highly conductive metal. This does not, however, preclude the many potential challenges that frequently accompany the study of biological (particularly, *in vivo*) samples: irregular surfaces, presence of interfering hair or microorganisms, dynamic physiological processes, physical movement, local temperature and humidity changes (which can alter the vibrating tip work function), and ambient electrical fields.

7.13 Vulnerable Electrode Technology

An electrode pair is a sensor. Experience shows that in many cases the electrodes are the most vulnerable part of bioimpedance/electricity equipment. Perhaps 85% of problems are due to electrodes and their wires/cables. The demands on electrodes may be special and

hard: They are the only part of equipment that sometimes has to be sterile or biocompatible. It must perhaps endure use in water, rain, bath, or shower. Electrodes may be low cost and well adapted to single use with no spread of contamination between users. Even low cost and seemingly simple, here are some reasons to consider:

1. Electrodes are to be in stable contact with the patient and cannot be so well protected as a more remote electronic instrumentation box.
2. Electrode fixation to the patient deteriorates with use. Sticky contact gel may dry out and gradually loose contact or have unstable contact generating noise in the measurement. Useful remedies are silicon belts, plasters also on each electrode, rubber bands, and rings.
3. Insensitive to outside pressure to the electrode? Electrolyte squeezed out on the skin increasing the EEA.
4. If electrode connections to the instrument are by wires, these wires are very exposed. Also such wires may send out or receive disturbing signals (antenna effect).
5. Cables, wires, and connectors. Remedies: light and flexible wires, carefully prepared wire tracks, and wire fixation with small wire loops allowing patient to move without wire pulling the electrode. Each electrode wire before leaving the body could be terminated in a small box, with common cable further from the body up to the electronic instrument. Tiny box with preamplifiers near the patient. Prewired electrodes are without the weight of local connector and plug.
6. Wireless connection between electrodes and instrument has many advantages. A consequence is that sensors must be mounted inside a thin local box with batteries and wireless local communication. Best-quality connectors and plugs, perhaps watertight construction. All connectors situated remote from the patient, as lightweight as possible, and without boxes that may increase the weight.
7. Wet gel or other gels/liquids/electrolyte seepage reaching the electrode metal and the copper wire can generate unstable electrode performance and noise. Wet gel squeezed out on the skin short-circuiting neighbor electrodes. Electrode handling in general well planned, for example, will electrode endure patient heavy sweating or taking a shower?
8. Pregelled electrolyte drying out. Use solid gel contact electrolyte when possible. “Best before” marking of pregelled types.

Intended use may be very different. To be used during sleep, indoor, outdoor, or in a boat fresh or salt water. Is the patient lying unconscious in a car/ambulance bed? Is the purpose long-time monitoring or a short examination?

7.14 Problems

1. Which electrodes have six different metals in [Figure 7.2\(a\)](#)?
2. What requirements must the plate electrode fulfill?

3. What is faradaic current?
4. What is a double layer? Does it have capacitive properties?
5. With a Pt wire and an AgCl covered silver wire as electrodes in the same solution, what is the voltage generated by the electrode pair?
6. What is incremental resistance?

Instrumentation and Measurements

8.1 General Network Theory, the Black-Box

In many cases, we will regard our biological material, together with the necessary electrode arrangements, as an unknown “black box.” By electrical measurement, we want to characterize the content of the box (we do not have direct access to the key to open the lid!). We want to use the data to *describe* the electrical behavior, and perhaps even *explain* some of the physical or chemical processes going on in the box, and perhaps discern between electrode and tissue contributions. The description must necessarily be based upon some form of *model* (e.g., in the form of an *equivalent* electric circuit), mimicking measured electric behavior. We may also want to link properties to distinct tissue parts or organ parenchyma behavior. A basic problem is that always more than one model fits reasonably the measured electric behavior. The equivalent circuit is the tool of the electronic engineers and facilitates their interpretation of the results, simply because they are trained and used to interpret such diagrams. As discussed in Section 9.1, the equivalent model may also go further and be of a more explanatory nature.

The black box may be assumed to “contain” the whole body, a part of the body, just an organ, or just a cell, together with the electrodes. It may also be assumed to contain not the real things, just the *equivalent model circuit* of the tissue of interest.

We will now give a very general description of the black box and how to characterize it electrically, irrespective of the box content. The black box may be considered to contain the real tissue with electrodes for excitation and response measurement, or our model in the form of an electric *network* as a combination of *lumped* (discrete) electrical components. The network may be with two, three, or four external *terminals* (compare the number of electrodes used). A pair of terminals for excitation or recording is called a *port*. The treatment is so general that the content can be characterized with global variables not particularly linked with electrophysiology.

A very general box is the four-terminal type with two ports, [Figure 8.1\(a\)](#). This is the box corresponding to the four-electrode systems described in Section 7.10.3: two pick-up (PU) electrodes in the electrical field generated by two current-carrying (CC) electrodes.

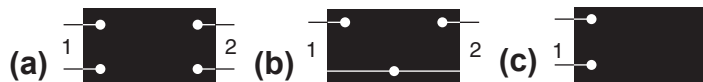


Figure 8.1: Black boxes. The two boxes (a) and (b) allow for *transfer* parameters from one port to the other. Box (c) is a one-port, two-terminal box with only *driving point* parameters possible.

8.1.1 *Immittance, Admittance, and Impedance*

Immittance is the general term covering the duality of admittance and impedance.

Driving point immittance is defined with excitation and response at the same port, the result is not influenced by any contribution from transmittance components. There are two possible ratios: v_1/i_1 (impedance) and i_1/v_1 (admittance).

Transmittance is defined with excitation and response at different ports. The *transfer function* $\mathbf{H}(\omega)$ of voltages at two different ports is:

$$\mathbf{H}(\omega) = \frac{v_2}{v_1} \quad [\text{dimensionless}] \quad (8.1)$$

Such a dimensionless function is used to emphasize signal transmission and not tissue characteristics.

Transmittance may be *transfer admittance* or *transfer impedance*. The four external variables of a two-port black box (Figure 8.1(a)) are v_1 and i_1 (first port), v_2 and i_2 (second port). There are four possible ratios: v_1/i_1 , v_2/i_2 , v_1/i_2 and v_2/i_1 . These ratios may be inverted so actually there are eight possible ratios. If the signals are sine waves, most of the ratios have their special names:

Transfer Admittance

A two-port four-electrode black box may use port 1 for controlled current excitation and port 2 for zero current potential measurement. The ratio excitation current to measured potential is called admittance [siemens]. However, it is *transfer admittance*, implying that the transfer admittance is a transmission parameter and therefore strongly dependent on the distance between port 1 and 2. Therefore transfer admittance is not directly characterizing the tissue.

Transfer Impedance

If port 1 is used for controlled voltage excitation and port 2 for (zero voltage) current measurement, the ratio voltage to current is impedance [ohm]. However, it is *transfer impedance* implying that the impedance is a transmission parameter and therefore strongly dependent on the distance between port 1 and 2. Therefore transfer impedance is not directly characterizing the tissue.

We have seen that many types of ratios can be formed between the different variables of a two-port black box. It may be confusing that the term impedance alone is used for any ratio between voltage and current when the “transfer” designation is not used. There are examples from other professions to make one-word designations: If in electronic circuit design a circuit is a current-to-voltage amplifier, the ratio of interest is v_o/i_i , which is a resistance. Such an amplifier has therefore been given the one-word designation *transresistance* amplifier. In a field effect transistor, the input voltage controls the output current and the ratio i_o/v_i is called *transconductance*.

8.1.2 Two-Port Network, Signal Transfer, Conditions

Each port has two terminals: one port is for excitation (input) and the other for output. Because linearity is a prerequisite (Section 8.4), all signals are sinusoidal if the excitation is so. Each signal is voltage or current. The four external variables of a two-port black box (Figure 8.1(a)) are v_1 and i_1 (first port), v_2 and i_2 (second port). One class of variables is with both ports CC, another with one CC and the other zero current-voltage reading. The last version is preferable because then two of the electrodes are not polarized.

The one-port two-electrode network measures the driving point admittance of the tissue without any transmission component. The two-port, four-electrode network measures the transfer admittance from one port to another. It can be completely defined with four ratios (constants) characterizing the network, and four variables. Here we will introduce two equation sets:

The *admittance* equation set for a two-port network:

$$i_1 = Y_{11}v_1 + Y_{12}v_2 \quad (8.2)$$

$$i_2 = Y_{21}v_1 + Y_{22}v_2 \quad (8.3)$$

Y_{11} or Y_{22} is the driving point admittance and measured with excitation and response at the same port. The *transfer admittances* Y_{12} and Y_{21} are defined as:

$$Y_{12} = \frac{i_1}{v_2} \quad (v_1 = 0, \text{ port 1 short-circuited}) \quad (8.4)$$

$$Y_{21} = \frac{i_2}{v_1} \quad (v_2 = 0, \text{ port 2 short-circuited}) \quad (8.5)$$

The variable v is independent, i is dependent, and both transfer admittances are specified with one of the ports *short-circuited*.

The *impedance* equation set for a two-port network is:

$$v_1 = Z_{11}i_1 + Z_{12}i_2 \quad (8.6)$$

$$v_2 = Z_{21}i_1 + Z_{22}i_2 \quad (8.7)$$

Driving point impedance Z_{11} or Z_{22} is measured with excitation and response at the same port. The *transfer impedances* are defined as:

$$Z_{12} = \frac{v_1}{i_2} \quad (i_1 = 0, \text{ port 1 open}) \quad (8.8)$$

$$Z_{21} = \frac{v_2}{i_1} \quad (i_2 = 0, \text{ port 2 open}) \quad (8.9)$$

The variables i are independent, v are dependent, and both transfer impedances are specified with one of the ports *open*.

Conditions

For the network theory presented, there are certain conditions to be met if the theory is to be valid; namely that the network is:

1. *Linear*. Impedance values must be independent of v or i , both the principle of *superposition* and *proportionality* must hold. Most of the systems of our interest are not linear at DC, but may have a linear amplitude range at AC: sometimes a broader range, the higher the frequency.
2. *Passive*. The energy delivered to the network must be positive for any excitation waveform, and all currents or voltages must be zero without excitation. As we know, tissue with electrodes does not fulfill this last requirement; we know, for instance, that it contains cells with endogenous ionic pumps.
3. *Causal*. The network response must be nonanticipatory (e.g., there must be no response before an excitation has been applied). Important in Fourier analysis, for instance the phase response of a capacitive network at the onset of a sine wave excitation. Often, phase analysis actually presupposes that the sine wave has been there long before the time of analysis.

A somewhat different measuring principle is to record the voltage at a port and record the reduced signal as a function of shunting the recording port with different load impedances (Mørkrid et al., 1980).

8.1.3 Reciprocity

In black box theory the excitation (input) and output ports must be defined, the transmission direction must be defined. A network is *reciprocal*¹ if the ratio between excitation and response remains unaltered when the ports of excitation and response are interchanged. Then the transfer immittances are equal, $Y_{12} = Y_{21}$ and $Z_{12} = Z_{21}$. Tissue is reciprocal only if it is

¹ This is the *reciprocity theorem* and originates from Helmholtz. In mechanical engineering, a similar type is known as the *reciprocal theorem* and originates from Maxwell.

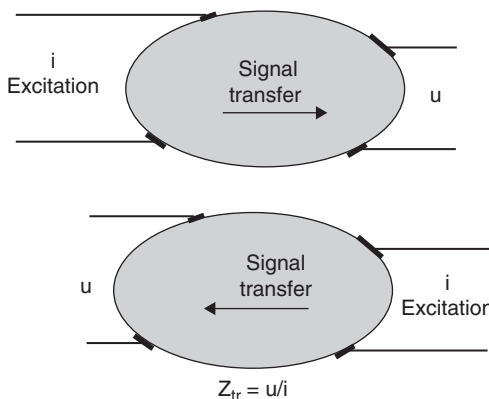


Figure 8.2: Reciprocity.

linear and passive. A network of passive components may be reciprocal, but the insertion of a transistor makes it nonreciprocal. The transistor is a one-direction signal device.

The reciprocity theorem is illustrated in [Figure 8.2](#). At the top the configuration is with excitation input current from the left and signal output voltage to the right. At the bottom, the reciprocal wire connection is shown; electrodes remain fixed. It is with excitation current CC on the right side and output voltage PU on the left side. The transfer impedance Z_{transfer} is unaltered. In both cases, only the CC electrodes carry current, whereas the PU electrodes are with zero current so they are not polarized. If the CC electrodes are driven with controlled current, the influence of their polarizing impedance also has been removed. In the case of [Figure 8.2](#), the reciprocal configuration is in general the best because the upper left electrode has the smallest contact area. It is therefore best to have no current flow in its wire. The risk is that CC electrodes may be polarized to the extent that they are outside their linear range. If so, the reciprocity property is lost. From [Figure 8.2](#), it is quite clear that there can be no rectifying properties in the measured volume. Signal transfer cannot be hampered by any one-way action. At first the reciprocity may be counterintuitive; the current paths are not the same, so the initial reaction is usually that the theorem cannot be true!

8.1.4 Extended Immittance Concepts

The classical immittance concept is linked to sine waves. The driving point admittance of a black box port is for instance defined as the ratio $\mathbf{Y} = \mathbf{i}/\mathbf{v}$, where \mathbf{v} is a sine wave as the independent variable. However, such ratios may be defined also for other waveforms than DC or sine waves. The immittance concept may be extended by the *Laplace² transform*.

² Pierre Simon de Laplace (1749–1827), French mathematician. Famous for his work on differential equations and on probability, even so an extreme determinist.

By replacing the imaginary frequency variable $j\omega$ by an extended complex frequency variable $s = \sigma + j\omega$ (here σ is not conductivity), it is possible to define, for example, impedance not only in the angular frequency ω -domain, but also in the s -domain. The impedance of a capacitor of capacitance C is, for example, in the frequency domain: $Z(\omega) = 1/\omega C$, and in the s -domain: $Z(s) = 1/sC$. The Laplace transforms of some very important excitation waveforms are very simple: for example, for a unit impulse it is 1, a unit step function $1/s$, a ramp $1/s^2$, etc. That is why the excitation with, for example, a unit impulse is of special interest examining the response of a system. In the extended immittance definition, calculations with some nonsinusoidal waveforms become very simple. Even so, Laplace transforms are beyond the scope of this book.

8.1.5 Step Function Excitation and Time Constant

Immittance theory is based upon *sinusoidal* excitation and sinusoidal response. In relaxation theory (and cell excitation studies), a *step* waveform excitation is used, and the time constant is then an important concept. If the response of a step excitation is an exponential curve, the time constant is the time to reach 63% of the final, total response. Let us for instance consider a series resistor-capacitor (RC)-connection, excited with a controlled *voltage* step, and record the current response. The current as a function of time $I(t)$ after the step is: $I(t) = (V/R)e^{-t/RC}$, the time constant $\tau = RC$, and $I(\infty) = 0$.

However, if we excite the same series RC-circuit with a controlled *current* step and record the voltage across the RC circuit, the voltage will increase linearly with time ad infinitum. The time constant is infinite. Clearly, the time constant is dependent not only on the network itself, but on how it is excited. *The time constant of a network is not a parameter uniquely defined by the network itself.* Just as immittance must be divided between impedance and admittance dependent on voltage or current driven excitation, there are two time constants dependent on how the circuit is driven. The network may also be a three- or four-terminal network. The time constant is then defined with a step excitation signal at the first port, and the possibly exponential response is recorded at the second port.

Many dielectrics do not show exponential discharge curves, but fractional power curves. This has led to new models of “Universality” (see Section 9.2.12).

The step waveform contains an infinite number of frequencies, and the analysis with such nonsinusoids is done with Laplace transforms.

8.1.6 Kramers–Kronig Transforms

If the real part of a linear network function of frequency is known over the complete frequency spectrum, it is possible to calculate the imaginary part (and vice versa). There is a relationship between the real and imaginary part of an immittance (or ϵ' and ϵ''), given

by the Kramers–Kronig transforms (KKTs). In theory there is no additional information in, for example, the real data when the imaginary data are known. Of course, a double data set increases accuracy and makes a control of data quality possible.

KKTs are tools brought to network theory by the work of Kramers (1926) and Kronig (1929) on X-ray optics. Just as the reciprocity theorem, they are purely mathematical rules of general validity in any passive, linear, reciprocal network of a *minimum phase shift* type. By minimum-phase networks, we mean ladder networks that do not have poles in the right half plane of the Wessel diagram. A ladder network is of minimum phase type; a bridge where signal can come from more than one ladder is not necessarily of the minimum-phase type. The transforms are only possible when the functions are finite-valued at all frequencies. With impedance $\mathbf{Z} = R + jX$ the transforms are:

$$R(\omega) - R(\infty) = \frac{2}{\pi} \int_0^{\infty} \frac{fX(f) - \omega X(\omega)}{f^2 - \omega^2} df \quad (8.10)$$

If we seek DC values, ω is set to zero and we get:

$$R(0) - R(\infty) = \frac{2}{\pi} \int_0^{\infty} \frac{X(f)}{f} df = \frac{2}{\pi} \int_{-\infty}^{+\infty} X(\ln f) d(\ln f) \quad (8.11)$$

$$X(\omega) = -\frac{2\omega}{\pi} \int_0^{\infty} \frac{R(f) - R(\omega)}{f^2 - \omega^2} df \quad (8.12)$$

$$\varphi(\omega) = \frac{2\omega}{\pi} \int_0^{\infty} \frac{\ln|Z(f)|}{f^2 - \omega^2} d\ln f \quad (8.13)$$

The frequency of integration f is from zero to infinite. The resistance or reactance or modulus of impedance $|Z|$ must therefore be known for the complete frequency spectrum. Dealing with one dispersion only, the spectrum of interest is limited to that of the dispersion. When the frequency range is limited and the number of measurement points is reduced, some error is committed when obtaining one impedance component out of the other (Riu and Lapaz, 1999).

With *admittance* $\mathbf{Y} = G + jB$, the transforms are:

$$G(\omega) - G(\infty) = \frac{2}{\pi} \int_0^{\infty} \frac{fB(f) - \omega B(\omega)}{f^2 - \omega^2} df \quad (8.14)$$

If we seek DC values, ω is set to zero and we get:

$$G(0) - G(\infty) = \frac{2}{\pi} \int_0^{\infty} \frac{B(f)}{f} df = \frac{2}{\pi} \int_{-\infty}^{+\infty} B(\ln f) d(\ln f) \quad (8.15)$$

The corresponding *permittivity* KKTs are:

$$\epsilon'(\omega) - \epsilon'(\infty) = \frac{2}{\pi} \int_0^{\infty} \frac{f\epsilon''(f)}{f^2 - \omega^2} df \quad (8.16)$$

$$\epsilon''(\omega) = \frac{2\omega}{\pi} \int_0^{\infty} \frac{\epsilon'(f) - \epsilon'(\infty)}{f^2 - \omega^2} df \quad (8.17)$$

If we seek static (DC) values, ω is set to zero and we get:

$$\epsilon'(0) - \epsilon'(\infty) = \frac{2}{\pi} \int_0^{\infty} \frac{\epsilon''(f)}{f} df = \frac{2}{\pi} \int_{-\infty}^{+\infty} \epsilon''(\ln f) d(\ln f) \quad (8.18)$$

Consequently, the area under one dispersion loss peak is independent on the distribution of relaxation times. These equations also represent a useful check for experimental data consistency.

8.2 Signals and Measurement, Noise

8.2.1 DC, Static Values, and AC

DC (direct current) is a current flowing in the same direction all the time (*unidirectional* current). The abbreviation “DC” is so much used that it is common language to say DC current (tautology) and DC voltage (contradictory). A DC may be constant, but may also fluctuate or an AC may be superimposed, as long as the sum never changes direction. Any DC and AC signal may be added, but if the system is *nonlinear*, the response will not be equal to the sum of the individual signal responses. The DC current may be pulsed, but if the current changes direction in the cycle, it is an AC.

A *galvanic* current is the same as a DC current, and the term is used in particular for therapeutic applications and in electrochemistry. Anode and cathode are not defined from voltage polarity, but current direction. A galvanic (electrolytic) cell produces (passes) DC. If it does not, it is a dielectric cell and only displacement AC passes. Even so, an in-phase current may pass the cell, but it is due to dielectric losses and not DC conductance. Thus in-phase components are not the same as DC components.

Stable values are constant values, the term *static* values corresponds to steady-state conditions and can be used for a DC potential or voltage, but not so well for a DC current that is in disagreement with *electrostatic* conditions. In dielectric relaxation theory, the subscripts often refer to frequency (e.g., D_0) (Section 3.4.2); the charge density at $f = 0$, that is such a long time after the excitation step that the new equilibrium has been obtained and the charging current has become zero. With a single Debye dispersion, this low-frequency value is called the *static* value (see Section 3.4.2). Static also means without current flow, without magnetic field generation. D_0 could therefore equally well have been called D_s , with s for “static.” This is the case for the symbol of permittivity, where low frequency permittivity is ϵ_s , whereas ϵ_0 is the vacuum permittivity.

AC (alternating current) is a current steadily changing direction. The abbreviation is so much used that it is common language to say AC current (tautology) and AC voltage (contradictory). We also say constant AC voltage (contradictory), but we mean constant amplitude AC voltage.

DC compared with a sine wave AC when $f \rightarrow 0$

When a sine wave frequency approaches 0 Hz, corresponding to a period of, for example, an hour or more, the signal may for a long time be regarded as a slowly varying DC. Strong DC polarization effects may have time to develop at the electrodes, and capacitive susceptance is very small according to $B = \omega C$.

To maintain linear conditions in electrolytic systems, the signal amplitude must be reduced $\rightarrow 0$ as $f \rightarrow 0$ (see Section 8.4.1). Except in the bulk of an electrolyte (see Eq. 2.2), *DC conditions are therefore virtual unobtainable in electrolytic systems* (see also the Warburg impedance concept described in Section 7.9.3). This is well illustrated with the logarithmic frequency scale, where both infinitely high and infinitely low frequencies are equally off-scale and unattainable. With electronic (not ionic) conduction and ordinary resistors, perfect DC conditions represent no difficulty, and these can therefore only be idealized *models* of electrolytic systems.

8.2.2 Periodic Waveforms, Fourier Series

A *periodic* waveform repeats itself exactly at regular time intervals (the period T). It is predictive: at any moment in the future we can foresee the exact value. According to Fourier, any periodic waveform can be considered to be the sum of a *fundamental* sine wave of frequency $f_1 = 1/T$, and sine waves at certain discrete frequencies, the *harmonics* ($2f_1$, $3f_1$, $4f_1$, and so on). A periodic waveform is an idealized concept; the waveform is to have lasted and to last forever. At the time we start and stop it, other frequency components than the harmonics appear as transients.

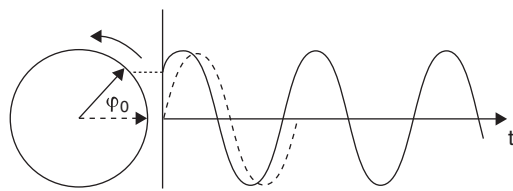


Figure 8.3: The sine wave, with a dashed reference sine wave.

The sine wave is a very special periodic waveform in the sense that it is the only waveform containing just one frequency: the fundamental frequency. Why does just the *sine wave* have such special qualities?

It is derived from the circle, [Figure 8.3](#), it is the projection of a rotating radius (see the phasor, Section 12.1.4). If the rotation is steady, the waveform is sinusoidal. A sinusoidal is characterized by its *frequency* f (Hz, periods per second) or the *period* $T = 1/f$ (second). *Angular frequency* ω must be used for trigonometric functions and to emphasize the relationship with the angle of the rotating radius. $\omega = 2\pi f = 2\pi/T$ is the number of rotations (in radians or degrees) per second. T is the time of one complete rotation. $\varphi = \omega t$ is the angle of rotation during the time t . A frequency independent phase shift or a reference value φ_0 may be added: $\varphi = \omega t + \varphi_0$.

If the sine wave is symmetrical around 0, it has no DC component and is described by the equation:

$$v(t) = V_o \sin(\omega t + \varphi_0) \quad (8.19)$$

$$\int v dt = -V_o \cos(\omega t + \varphi_0) = -V_o \sin(90^\circ - \omega t - \varphi_0) \quad (8.20)$$

$$\frac{dv}{dt} = V_o \cos(\omega t + \varphi_0) = V_o \sin(90^\circ - \omega t - \varphi_0)$$

The time derivative as well as the time integral of a sine wave is also a sine wave of the same frequency, but phase-shifted 90° . The relationship between a sine wave and the circle is seen more directly in the complex notation of a radius \mathbf{r} rotating around the origin in the Wessel diagram:

$$\mathbf{r}(t) = r_o e^{j\omega t + \varphi_0} = r_o [\cos(\omega t + \varphi_0) + j \sin(\omega t + \varphi_0)]$$

Because the time derivative of an exponential is the same exponential, then $\partial(e^{j\omega t})/\partial t = j\omega e^{j\omega t}$. That is why integration and derivation in the equations describing the behavior of electrical circuits can be replaced by algebraic operations with the $j\omega$ instead of the $\partial/\partial t$. *This is under the assumption that all signals are sine waves of the same frequency.*

A phasor and a sine wave are given with respect to some reference sine wave. In [Figure 8.3](#), the reference is dashed, and the waveform of interest *leads* the reference by about 45° .

The peak value is called the *amplitude* V_p , φ is the *phase angle*. To define φ , we must define a reference sine wave; for instance, the known excitation signal. Although the mean value of a full period is 0, it is usual to quote the mean of half a period: $2V_p/\pi$. The *rms* (root mean square) value is $V_p/\sqrt{2}$.

The Sum and Product of Two Sine Waves

To simplify the equations and the discussions, we presuppose two sine waves of *equal amplitude*, symmetrical around zero.

The *sum* of two such sine waves of different frequencies is:

$$f(t) = \sin \omega_1 t + \sin \omega_2 t = 2 \sin\left(\frac{\omega_1 + \omega_2}{2}t\right) \cdot \cos\left(\frac{\omega_1 - \omega_2}{2}t\right) \quad (8.21)$$

The *product* of two sine waves of different frequencies is:

$$f(t) = \sin \omega_1 t \cdot \sin \omega_2 t = \frac{1}{2} \{ \cos [(\omega_1 - \omega_2)t] - \cos [(\omega_1 + \omega_2)t] \} \quad (8.22)$$

Case 1: $\omega_1 = \omega_2 = \omega$

With a constant phase difference φ between the sine waves, $\omega_1 t = \omega t$ and $\omega_2 t = \omega t - \varphi$:

$$\text{Sum: } f(t) = \sin \omega t + \sin(\omega t - \varphi) = 2 \cos \frac{\varphi}{2} \sin\left(\omega t - \frac{\varphi}{2}\right) \quad (8.23)$$

The *sum* is as a *pure sine wave* at the fundamental frequency, phase-shifted, with double amplitude when $\varphi = 0^\circ$ and zero amplitude with $\varphi = 180^\circ$. No new frequencies appear, in accordance with the law of superposition valid for a linear system.

$$\text{Product: } f(t) = \sin \omega t \cdot \sin(\omega t - \varphi) = \frac{1}{2} [\cos \varphi - \cos(2\omega t - \varphi)] \quad (8.24)$$

This is an important equation, proving the creation of a new frequency in a nonlinear system where the laws of superposition no longer are valid. A *DC component and a pure sine wave of double the frequency (2. harmonic component) have appeared; the fundamental frequency has disappeared*. The equations are illustrated in [Figure 8.4](#).

Frequency Spectrum Analysis Fundamentals (see [Eq. 8.24](#) and [Figure 8.4](#))

- The product of two sine waves of equal frequency and phase difference not 90° contains a DC component.
- The product of a sine and cosine wave of equal frequency contains no DC component.
- Thus by multiplying a given signal function with a reference sine wave, the DC component of the product is proportional to the in-phase signal component at the reference frequency.

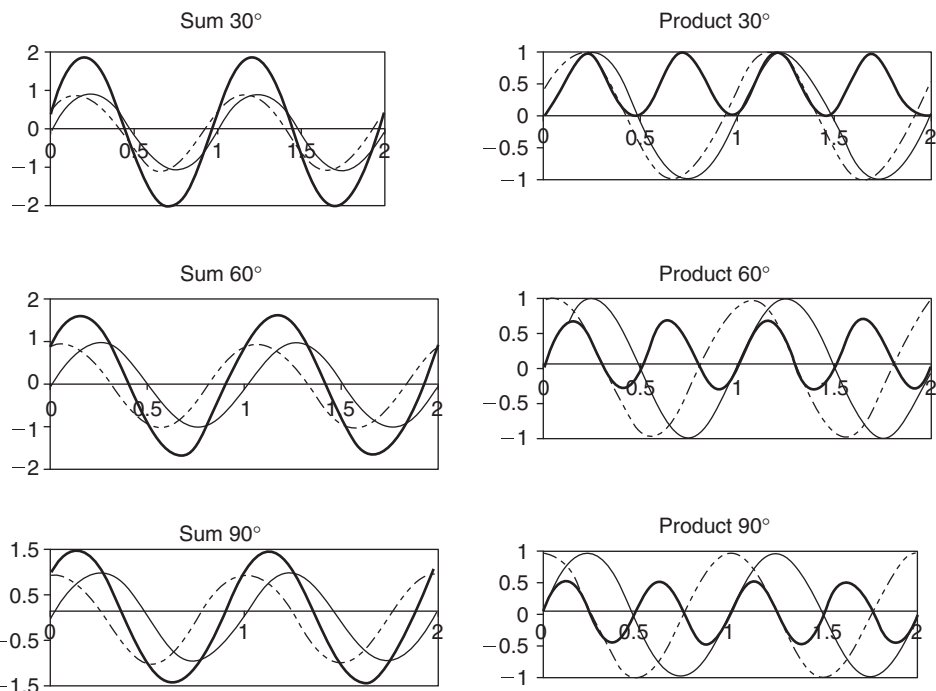


Figure 8.4: Sum and product of two equal amplitudes (=1) equal frequency sine waves, phase shifted by various amounts: 30° (top), 60° (middle), and 90° (bottom). Notice the DC component of the product (right hand side). Example is with amplitude = 1 (e.g., volt), $f = 1$ Hz so that the time scale is in seconds.

The low-pass filtered result is a DC voltage proportional to the cosine of the phase difference between the signals; quadrature signals ($\varphi = 90^\circ$) are thus canceled. The peak-to-peak amplitude of the 2. harmonic component is half the fundamental and independent of the phase.

[Equation 8.24](#) formulates the basis for the lock-in amplifier and frequency spectrum analysis (Fourier analysis). In the lock-in amplifier, one sine wave is the stable reference signal supplied by the experimental setup. The other sine wave is the measured response variable, usually containing also other nonsynchronized signals and noise.

In tissue and at electrodes, the linear case corresponds to low-level excitation. The nonlinear case and the creation of new frequencies correspond to high-level excitation (the nonlinearity in the form of multiplication is of course only one possible form).

Input signal with DC component:

$$f(t) = (V + \sin \omega t) \cdot \sin(\omega t - \varphi) = \frac{1}{2} [\cos \varphi - \cos(2\omega t - \varphi)] + V \sin(\omega t - \varphi) \quad (8.24a)$$

This is a realistic situation because electrodes often generate a DC offset voltage V . Equation 8.24a shows that the fundamental frequency reappears, but does not contribute to a low-pass-filtered output signal. This is because we have a true sinus multiplication. If the reference signal is a square wave as it often is in simpler chopped phase sensitive rectifiers, the input DC appears also in the output as an error signal.

Case 2: $\omega_1 \neq \omega_2$

$\omega_1 \approx \omega_2$

If $\omega_1 \approx \omega_2 \approx \omega$, Eqs 8.23 and 8.24 can be used by introducing a slowly varying phase shift φ .

The most important effect for the *sum* (Eq. 8.23) is the corresponding varying amplitude according to the $\cos(\varphi/2)$ factor. The sum is a sine wave of frequency ω with amplitude changing at the low beat frequency $\omega_1 - \omega_2$ from the double value to zero. The new waveform does not contain any new frequencies, and there is no DC component. This is illustrated in Figure 8.5(a) and (b). The curve is contraintuitive because it may easily be taken as a waveform containing the sum and beat frequencies, which it does not. It is the fundamental sine wave with slowly varying amplitude at the beat frequency 0.125 Hz. The picture is different when the frequency difference is larger, Figure 8.5(c) and (d). Now it is clearly seen that high-frequency sine wave is simply superimposed on the slow sine wave.

In the *product* (Eq. 8.24) waveform, the DC level changes at the low beat frequency $\omega_1 - \omega_2$ according to the factor $\cos \varphi$. This is a true DC component created by the nonlinear effect. However, it has zero mean value over a beat frequency period, and thus does not contribute to a DC component after low-pass filtration. The second harmonic component has constant peak-to-peak amplitude but a phase varying at the beat frequency.

Large difference between ω_1 and ω_2

Now the discussion is based on Eqs 8.21 and 8.22. It is clear from Figure 8.5(c) and (d), that the *sum* waveform is just the 1 and 8 Hz signals with no phase shifts. However, the *product* waveform has a new higher frequency (the sum $8 + 1 = 9$ Hz). When studying Figure 8.5(c) and (d), the waveform is amplitude modulated with an envelope frequency of 1 Hz. The frequency difference component of 7 Hz ($8 - 1 = 7$ Hz) is difficult to see.

In radio communication systems, the signal with frequency ω_1 is called the carrier and ω_2 the modulation, and $\omega_1 \gg \omega_2$. The amplitude modulated signal from a perfect multiplier under these conditions does not contain the low-frequency signal ω_2 , just the upper and lower sideband frequencies $\omega_1 + \omega_2$ and $\omega_1 - \omega_2$. They are very near to the carrier frequency and can therefore be transmitted through the ether.

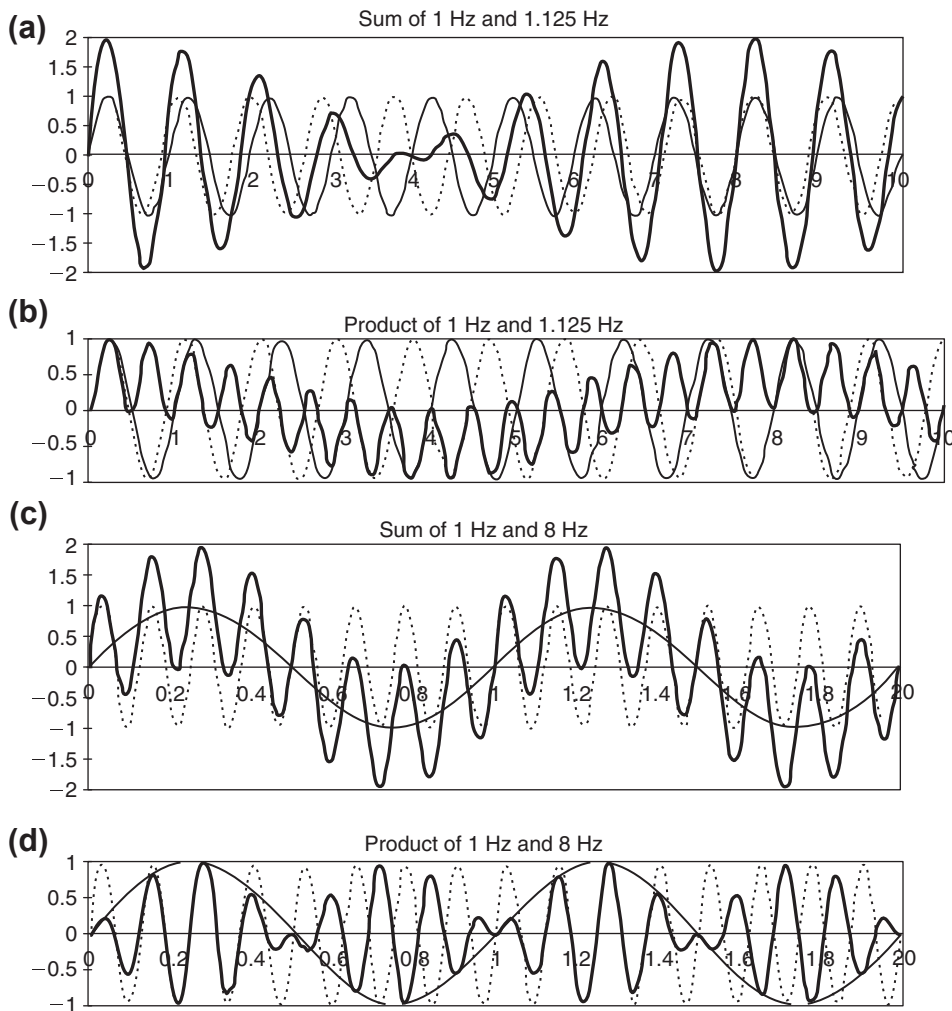


Figure 8.5: Different frequencies. Sum and product of two equal amplitude ($=1$) sine waves: (a), (b) 1 Hz & 1125 Hz sine waves ($\omega_1 \approx \omega_2$); (c), (d) 1 and 8 Hz sine waves.

It is clear from these discussions that the waveforms in the time domain may be difficult to interpret correctly, and it is the mathematical treatment that gives the correct answers.

The Sum of a Fundamental Sine Wave and Its Harmonic Components: Fourier Series

The only waveform containing just one frequency is the sine wave. A periodic waveform can be created by a sum of sine waves, each being a harmonic component of the sine wave at the fundamental frequency determined by the period. This is illustrated in Figure 8.6(a), showing the sum of a fundamental and its third and fifth harmonic

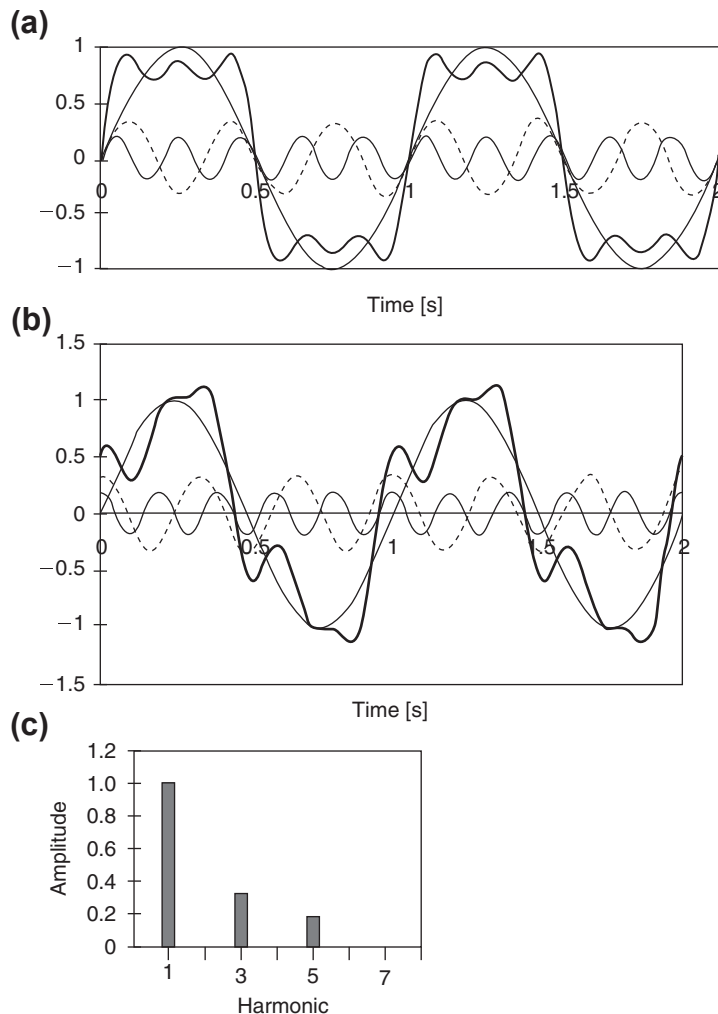


Figure 8.6: Summation of harmonic sine waves, waveform dependence of phase relationships.
Amplitude of fundamental sine wave = 1. Time domain; (a) in-phase harmonics,
(b) phase-shifted harmonics. (c) Amplitude magnitude line frequency spectrum, equal for
both cases.

components. It indicates that uneven harmonic components may lead to a square wave, with a precision determined by the number of harmonic components included.

Figure 8.6(c) shows the frequency spectrum of the waveform. It is a *line* or *discrete* spectrum, because it contains only the three discrete frequencies. Continuously repetitive waveforms have line spectra, and their periodicity is composed only of the fundamental and its harmonic components.

Fourier formulated the mathematical expression for the sum of the fundamental and its harmonics. The condition is that a fundamental period of a waveform $f(t)$ can be determined, and that the waveform $f(t)$ is extended outside its defined interval so that it is *periodic* with period 2π .

$$f(t) = \frac{a_0}{2} + \sum_{n=1}^{\infty} (a_n \cos n\omega_1 t + b_n \sin n\omega_1 t) \quad (8.25)$$

where a_n and b_n are the amplitudes of each harmonic component n , a_0 is the DC component, and ω_1 the angular fundamental frequency defining the period 2π .

According to the Fourier series Eq. 8.25, any periodic waveform is the sum of a fundamental sinusoid and a series of its harmonics. Notice that, in general, each harmonic component consists of a sine and cosine component. Of course, either of them may be zero for a given waveform in the time domain. Such a *waveform synthesis* (summation) is done in the time domain, but each wave is a component in the frequency domain. The *frequency spectrum* of a periodic function of time $f(t)$ is therefore a *line spectrum*. The amplitudes of each discrete harmonic frequency component is:

$$a_n = \frac{1}{\pi} \int_{-\pi}^{\pi} f(t) \cos(n\omega_1 t) dt \quad (8.26)$$

$$b_n = \frac{1}{\pi} \int_{-\pi}^{\pi} f(t) \sin(n\omega_1 t) dt \quad (8.27)$$

$$\mathbf{A}_n = a_n + jb_n \quad (8.28)$$

$$A_n = \sqrt{a_n^2 + b_n^2} \quad (8.29)$$

$$\varphi = \arctan\left(\frac{b_n}{a_n}\right) \quad (8.30)$$

Because the waveform is periodic, the integration can be limited to the period interval 2π as defined by ω_1 . However, the number n of harmonic components may be infinite. The presentation of a signal in the time or frequency domain contains the same information; it is a choice of how data are to be presented and analyzed.

Figure 8.6 illustrates how two rather different waveforms in the time domain may have the same amplitude magnitude A_n frequency spectrum. The amplitude magnitude frequency spectrum does not contain all necessary information; the phase information is lacking. For each harmonic component, both the sine and cosine (Eqs 8.26 and 8.27) or the magnitude and phase (Eqs 8.29 and 8.30), must be given, a magnitude and a *phase spectrum*. The amplitude \mathbf{A}_n is a vector; therefore, amplitude magnitudes A_n cannot just

be added as scalars. A given waveform is the sum of only one unique set of sine and cosine harmonics.

An infinite number of harmonics must be added to obtain, for instance, a true square wave. The Fourier series for a periodic square wave of unit amplitude is (see [Figure 8.6\(a\)](#)):

$$f(t) = \frac{4}{\pi} \sum_{n=1,3,5,\dots} \frac{1}{n} \sin n\omega_1 t \quad (8.31)$$

This square wave can therefore be realized as the sum of only sine components.

Any waveform with sharp ascending or descending parts, like the square wave or sawtooth, contains large amplitudes of higher harmonic components. The triangular pulses contain more of the lower harmonics. No frequencies lower than the fundamental, corresponding to the repetition rate, exist. The waveform may contain a DC component; if it is symmetrical around zero, the DC component is zero. However, if the waveform is started or stopped nonsynchronized with the period, it is no longer periodic. During those nonperiodic intervals, the Fourier series approach is no more valid.

By using nonsinusoids as excitation waveforms, a system is excited at several frequencies simultaneously. If the system is linear, the response of each sine wave can be added. If the system is nonlinear, new frequencies are created influencing the frequency spectrum. The square wave to the left of [Figure 8.7](#) has no DC component. One of the ramps in the middle is used in scanning devices such as polarographs. As drawn, the waveform has a DC component. The pulse to the right has a DC component dependent on the repetition frequency.

8.2.3 Aperiodic Waveforms

These are the waveforms of bioelectricity, because the repetition rate of, for example, the respiration or the heart is not perfectly periodic.

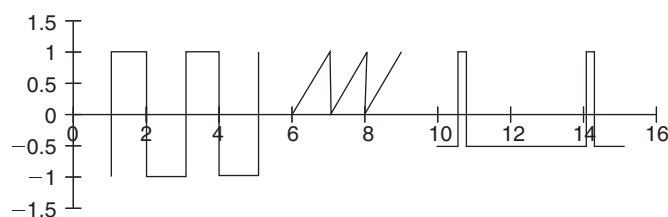


Figure 8.7: Square, ramp, and pulse periodic waveforms.

Single Pulse or Step

A single pulse or a step function excitation is the basis of relaxation theory. Power dissipation and temperature rise may for instance impede the use of repeated waveforms, and single pulse excitation is necessary. A single pulse is a pulse waveform with repetition interval $\rightarrow \infty$, it has a *continuous* frequency spectrum as opposed to a line spectrum. The *unit impulse* (delta function) waveform is often used as excitation waveform. It is obtained with the pulse width $\rightarrow 0$ and the pulse amplitude $\rightarrow \infty$, keeping the product = 1. The frequency spectrum consists of equal contributions of all frequencies. In that respect, it is equal to white noise (see the following section). Also, the infinite amplitude of the unit pulse automatically brings the system into the nonlinear region. The unit impulse is a mathematical concept; a practical pulse applied for the examination of a system response must have limited amplitude and a certain pulse width.

What then is the frequency content, for example, of a single rectangular pulse? It can be found from the periodic waveform by letting the period $\rightarrow \infty$. The frequency spectrum $F(\omega)$ of a positive pulse of amplitude A and duration T is:

$$F(\omega) = \frac{2A}{\omega} \sin \omega \frac{T}{2} \quad (8.32)$$

Note that the frequency spectrum as defined by $F(\omega)$ in Eq. 8.32 is *amplitude per angular frequency*. Equation 8.32 defines a continuous frequency spectrum; *all frequencies* are present except the discrete frequencies $1/T$. This may be regarded as another way of saying that the periodicity of a single pulse does not exist, it has no characteristic harmonics. All these frequency components must also be a function of time: all components must be zero before the single pulse has arrived (see the causality criterion, Section 8.1.2). During and after the pulse, the frequency spectrum components build up and decay, with time constants depending on the filters used to record them. Another illustration of a *frequency spectrum as a function of time* is the frequency analysis of speech or music. Biological events do not occur strictly periodically, and it is therefore a general need for doing a frequency analysis as a function of time. To have good resolution in the time domain, the time interval used should be short. But a short time interval makes it impossible to analyze low frequencies. This is the basis for the special Short Time Fourier Transform presented by Gabor (1946).

White Noise Waveform

Like the sine wave containing only one frequency, white noise signal is the other extreme containing all frequencies of equal amplitudes. As with the sine wave or unit impulse, white noise is an ideal concept. It is a fractal curve; any enlargement will just bring up similar curves. It is an interesting excitation waveform, because the system is examined at all

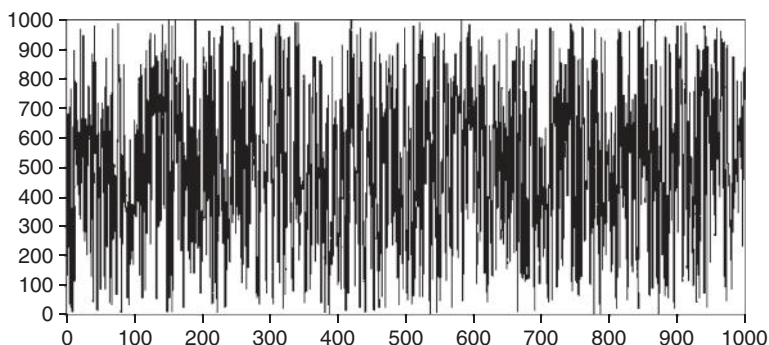


Figure 8.8: White noise in the time domain. One thousand samples of arbitrary numbers between one and 1000. Mean (DC) value = 500.

frequencies simultaneously. White noise is a curve where the value in the future cannot be predicted; there is an equal probability of any amplitude at any moment. Both the unit pulse and white noise is represented by a flat frequency spectrum. However, the ideal unit pulse is of infinite short time duration, whereas the ideal white noise is of infinite long time duration.

However, because amplitude in any system is limited, we do not have absolute white color of the noise found in a system. Also our total sampling time is limited. The curve in [Figure 8.8](#) is calculated for a certain time interval Δt . Based on [Figure 8.8](#), we evidently can say nothing about a possible periodicity for times $>\Delta t$ (frequencies below $1/\Delta t$). In general, any amplitude is possible; noise must therefore be described by a value averaged over a defined time interval. Usually the rms value is used. This is practical because noise is related to energy according to Boltzmann, Einstein, and the interpretation of Brownian motions (random walks).

[Figure 8.8](#) shows a computer-generated curve in which the computer was asked to generate 512 random numbers (periodic samples at the x -axis) of values between one and 1000 (amplitude at the y -axis). These choices are related to the graphical limitations of the illustration. [Figure 8.8](#) therefore does not illustrate ideal white noise because both the number of samples and the amplitudes are limited. The waveform is somewhat counterintuitive, because visual inspection may easily give the impression of periodicities.

8.2.4 Spectrum Analysis, Fourier Transforms

Frequency Spectrum (Fourier) Analysis

The *time domain* is well known from daily life experience, it is, for example, the way a signal is recorded as a function of time as an electrocardiogram (ECG) waveform.

From the waveform in the time domain, the components can be found in the *frequency*

domain: a search for periodicity. In the frequency domain, we have seen the line spectra of *periodic* signals. But the heart does not beat regularly. The heart rate varies both in a noisy way and by the way it is controlled by nervous and biochemical systems. Making a frequency analysis of an ECG waveform will therefore not give a *line* spectrum; the spectrum will have a more *continuous* character. Regular heart beats at sleep correspond to more pronounced line spectra than those obtained during variable physical activity. The frequency spectrum of an electronic driven pacemaker, however, is a line spectrum. A periodic waveform occupies a line spectrum; an aperiodic waveform occupies a continuous frequency spectrum.

There are several ways of finding the frequency spectrum of a time domain waveform, periodic or aperiodic. By sending the signal into a filter bank, the output of each filter represents the signal content as a function of time (both frequency and time domain!) within the frequency passband of the filter. The result is not optimal because the output of each filter is an amplitude magnitude, the phase information is lost. In [Section 8.2.2](#), we have just shown that by multiplying the waveform to be analyzed by a sine wave, the DC value of the result indicates the amplitude content at that frequency. By multiplying also by a 90° phase-shifted signal, information about the phase relationships in the waveform may also be obtained. This must be repeated at each frequency of interest, and therefore is a slow procedure. Instead of these analog methods, the signal can be digitized and treated by a mathematical algorithm called a fast Fourier transform. In such ways, the frequency content can be extracted; this is the Fourier³ or spectrum analysis. Such an analysis is a search for periodicities in a waveform.

The Fourier *series* with discrete harmonics was introduced in [Section 8.2.2](#).

Mathematically, the Fourier *transform* of a function (periodic or nonperiodic) in the time domain $f(t)$, to the corresponding function in the frequency domain $F(\omega)$, is described by:

$$F(\omega) = \int_{-\infty}^{\infty} f(t) e^{-j\omega t} dt \quad (\text{to frequency spectrum from time domain}) \quad (8.33)$$

The inverse Fourier transform is then:

$$f(t) = \int_{-\infty}^{\infty} F(\omega) e^{j\omega t} d\omega \quad (\text{to time domain from frequency spectrum}) \quad (8.34)$$

Note that by multiplying by the complex expression $e^{j\omega t} = \cos \omega t + j \sin \omega t$, both the in-phase and quadrature components, and thus the phase information, is taken care of. When dealing with signals defined, for example, as volt, $F(\omega)$ represents the signal distributed in

³ Joseph Fourier (1768–1830), French mathematician. Participated as scientist in the Napoleon military expedition in Egypt 1798–1801.

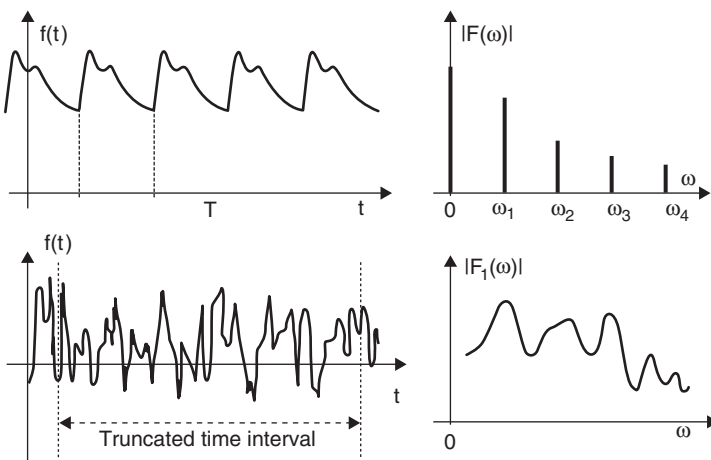


Figure 8.9: Top: Periodic waveform with a line harmonic frequency spectrum. Bottom: Nonperiodic waveform has a continuous frequency spectrum. Line spectrum amplitude [volt]. Continuous spectrum amplitude [volt $\sqrt{\text{sec}}$].

the frequency spectrum: the *density of signal amplitude per frequency bandwidth*. The unit may be, for example, $\mu\text{V}/\text{Hz}$. In general, there will be two spectra: one in-phase spectrum and one quadrature spectrum, or one amplitude spectrum and one phase spectrum. Thus $F(\omega) = F'(\omega) + jF''(\omega)$, or $F(\omega) = |F(\omega)|e^{j\phi(\omega)}$, and $|F| = (F'^2 + F''^2)^{1/2}$. Because of the phase dependence, the amplitudes at each frequency are not simply additive.

Equation 8.33 is the integral, and thus a more general form of Eq. 8.25. The integral form can, for example, be used for periodic signals when the pulse interval $\rightarrow \infty$, that is for a single pulse (Eq. 8.32). Note also the nonrealistic integration over the complete frequency spectrum from $-\infty$ to $+\infty$, and that the frequencies are not limited to the harmonics. As we have seen, the integration interval is not a problem with periodic waveforms; the waveform can easily be extended without limitation. With aperiodic waveforms, approximations introducing errors must be made (see the following section).

According to Eq. 8.33, there may be a non-zero signal density at any frequency, thus a *continuous spectrum* is possible. With periodic waveforms, only *line* spectra were possible; this is illustrated in Figure 8.9.

The *energy* of a waveform pulse is proportional to the square of voltage or current in a time interval. According to Plancheral's theorem (a special case of the more general Parseval's theorem⁴), the *energy* corresponding to an ideal resistor and a voltage or current

⁴ Parseval des Chênes (1755–1836), French mathematician. Forced to flee France after writing poems critical to the Napoleonic government.

waveform $f(t)$ computed in the time domain, is equal to the energy computed in the frequency domain:

$$\int_{-\infty}^{\infty} f^2(t)dt = \int_{-\infty}^{\infty} |F(\omega)|^2 d\omega \quad (8.35)$$

For steady-state conditions, the integral diverges and *power* (energy per time interval) spectra is used. Note that the magnitude $|F(\omega)|$ used in Eq. 8.35 implies that the information contained in the phase relationships is lost in the power spectrum. Or stated more positively: power spectra are not sensitive to phase relationships and values may just be added.

When dealing with power spectra related to, for example, rms voltage v_{rms}^2 according to $W = v_{rms}^2/R$, $|F(\omega)|^2$ represents the distributed power spectrum: the *density of signal power per frequency bandwidth*. The unit for $F(\omega)$ (e.g., when dealing with noise spectra) may be $\mu V_{rms}/\sqrt{Hz}$. When the spectrum is plotted with amplitude per \sqrt{Hz} on the y -axis and frequency on the x -axis and scaled so that the area under the $F(\omega)$ curve is equal to the total rms value in the time domain (Plancheral's theorem), the spectrum is called a *power density spectrum*. A less stringent definition is simply that a spectrum is called a *power spectrum* when the function is squared before analysis.

Aperiodic Signal in a Limited Time Interval

With a recorded waveform, we generally must assume that it represents the sum of nonsynchronized aperiodic signals, for example, from exogenous sources and endogenous activities such as respiration, peristaltic movements, heart beats, and nerve activities. In addition, there may be wideband noise and noise at discrete frequencies, for example, from the power line 50- or 60-Hz fundamentals.

In a practical case, the waveform to be analyzed must be of limited time duration. This is particularly clear when the analog signal has been digitized for computer analysis. Thus a long-lasting waveform must be *truncated* with a finite sampling time. Errors are introduced when such a waveform is analyzed, because the Fourier transform (Eq. 8.33) presupposes that the integration interval is infinite. When the end value (trailing edge) is not equal to the start (leading) value, the abrupt change of level corresponds to high-frequency components introduced by the truncation. Generally, truncation results in sharp discontinuities in the time domain and the additional frequency components in the frequency spectrum are called *leakage*.

To reduce the leakage effect, the signal can be amplitude weighted around the leading and trailing edges, so that the signal starts and ends near zero value. A Hanning or Blackman truncation function is often used for this purpose.

The truncated time interval also defines the lowest frequency that can be analyzed; nothing can be said about sine wave components with half-periods longer than the time analyzed.

In conclusion, the truncation introduces errors resulting from leakage, and the (totally sampled) interval limits the lowest frequency analyzed. In addition, the limited sampling frequency may also introduce errors when an analog waveform is to be digitized. The sampling frequency must be higher than twice the highest frequency to be analyzed (*Nyquist criterion*). If this is not the case, *aliasing* errors (frequency folding) are introduced. If the sampling frequency cannot be increased, the signal must be low-pass filtered before analysis, so that the Nyquist criterion is met for all signal components reaching the analyzer.

Correlation and Convolution

In electroencephalogram (EEG) waveforms, it may not be easy to visually estimate whether there is interdependence between the waveforms from two different leads.

Correlation analysis is used to find common periodicities of two functions (waveforms): $f_1(t)$ and $f_2(t)$. We have seen that if we multiply two sine waves of the same frequency, the DC value of the product is proportional to the cosine of the phase difference φ between them (Eq. 8.24). We can therefore calculate the product as a function of delaying one of the waveforms with respect to the other, and look for maxima corresponding to $\varphi = 0$.

Mathematically, for each time t , the correlation value $c(t)$ can be found by summing up the products of one of the waveforms and a time displaced version of the other:

$$c_{\text{cor}}(t) = \int_{-\infty}^{\infty} f_1(\tau)f_2(t + \tau)d\tau \quad (8.36)$$

The correlation will be maximal if one signal can be displaced with respect to the other until they fluctuate together. The correlation function $c(t)$ will be a more or less noisy sine wave symmetrical around $t = 0$. The decay of the amplitude envelope from $t = 0$ indicates the degree of correlation: the slower the decay, the higher the correlation. If $f_1(t) = f_2(t)$, *autocorrelation* is done by delaying a copy of the function itself and perform the integration of Eq. 8.34. The process will be much the same as a Fourier analysis, a search for periodicity.

For the sake of completeness, the *convolution* transform shall also be mentioned because it is so closely related to cross-correlation:

$$c_{\text{con}}(t) = \int_{-\infty}^{\infty} f_1(\tau)f_2(t - \tau)d\tau \quad (8.37)$$

The plus/minus sign in the integrand is the only difference between the integrals of cross-correlation and convolution. Convolution is a powerful mathematical tool strongly related also to the Fourier transform. By performing a usual logarithmic transform, a

multiplication is simplified to a summation, and then the antilogarithmic transform brings up the result. In a similar way, *convolving* two functions in the time domain corresponds to a *multiplication* of the same functions in the frequency domain. The convolving action implies a folding in the frequency domain, represented by the term $(t - \tau)$. In the integrand of the correlation transform there is no folding process in the term $(t + \tau)$.

Signal Averaging

If a synchronization signal is available from the stimulus source, special noise-reducing techniques are available. The response of an organism to a stimulus is called an *evoked potential* or *event-related* signal. The technique is somewhat similar to the principle of a lock-in amplifier (Section 8.3.7). By recording the response as a function of time after a stimulus, store it, repeat the stimulus many times, each time sum the response with the last sum, and we gradually increase the signal to noise ratio. Nonsynchronized waveforms will cancel out in the long run. It can be shown that the signal-to-noise ratio increases with \sqrt{N} , where N is the number of stimuli (see Eq. 8.45 in Section 8.3.7). The signal-to-noise ratio limits are related to the variability of the responses, both with respect to amplitude and time. Applications are, for example, within hearing, brain stem evoked potentials, EEG with visual stimuli, electrodermal response.

Other Forms of Signal Processing

- An important *time domain* analysis method is the *probability density function* of finding a certain signal amplitude value. This is simply histograms of the amplitude window values versus the number of counts in each amplitude window.
- Recording the number of *zero crossings* per time interval.
- *Bispectral* analysis. Instead of phase spectra obtained in Fourier analysis where the phase relates to the start of the epoch, the bispectrum correlates the phase between different frequency components. Used in EEG.
- *Wavelet analysis*. This is treated in Section 9.5.5.

8.2.5 Time and Frequency Domain

With increasing interest in time-resolved impedance measurements but also with the demand of parallel measurements, fast methods based on time domain approach move more and more into the focus. Although time and frequency domain are well defined, they are often not clearly presented. Especially, when the impedance spectrum changes with time, a joint analysis in terms of time and frequency dependence is often accompanied by uncertainties in wording.

The transformation between time and frequency domain requires linear and time invariant systems. Practically, linear refers to the relation between current and voltage within the

observed range, whereas time invariant denotes negligible changes of the transfer function within the measurement time.

Frequency domain in general means the description of any physical quantity, X, as a function of frequency, $\omega = 2\pi f$, as independent variable: $X = f(\omega)$.

Having time, t, as independent variable, yields time domain: $X = f(t)$.

The physical quantities describing passive electrical behavior of material in time and frequency domain are clearly distinguished. The complex, frequency-dependent impedance (impedance spectrum) exists only in the frequency domain, whereas the impulse answer is the respective property in the time domain. A single relaxation process yields a dispersion region (e.g., β -dispersion) with a characteristic frequency (e.g., ω_B) in the frequency domain that corresponds to a relaxation strength and relaxation time (time constant) in the time domain.

In joint time-frequency analysis, impedance is presented as function of time. This however, does not mean that time and frequency domains are mixed together. Any impedance at a given time should be considered as time invariant that is true for any time interval approaching zero. The consequence is that the impedance should change negligibly within the smallest given time interval. Sophisticated, nonlinear models for time variant impedances are not considered here.

A popular way to monitor a spectrum with respect to the time (e.g., voltage or acoustic signals) is windowed transformation. A window propagates through the signal and a transformation (preferentially Fourier transform) is applied within this window only. The window function approaches zero toward plus and minus infinite. Popular windows are rectangular window or Gaussian window (Garbor transformation). The width of the window limits the spectrum toward low frequency. It should be noted that by using periodic excitation signals, which are common in bioimpedance measurements, rectangular windowing with the window size matching the period of the stimulus is always preferred, whereas for active signals (such as electromyographical signals) Gaussian windowing is the better choice.

A typical way to show the result is the two-dimensional diagram of spectrum versus time where each point in time contains a complete spectrum along the y-axis.

8.2.6 General Remarks about Transformation

The common tool for obtaining the spectrum in the frequency domain from a time function is the Fourier transformation. This exhibits some limitation like a frequency vector, which is multiple integers of the fundamental frequency. Moreover, it requires periodic signals. Practically, periodic signals should be used in their entire length;

otherwise, a leakage effect with partial corruption of the spectrum occurs. The fast Fourier transformation algorithm is most popular, but exhibits some shortcomings. It requires the length of the equally spaced sample vector as a power of two. If this is not given, algorithms usually add zeros (zero padding, e.g., FFT—function in Matlab).

It is often worth tuning the transformation algorithm to get what is wanted. For calculation of random lines within the Fourier spectrum (equidistant frequencies), discrete Fourier transformation or sparse Fourier transformation is a good choice (Görtzel algorithm). For assessing a small window within the spectrum but with high-frequency resolution, z-transformation (Chirp-z-transformation) can be used. A popular algorithm is the Bluestein algorithm. The latter solutions are especially helpful for single shot signals. The continuous analogy is the Laplace transformation.

8.2.7 Frequency Filtering

High-Pass Filter

To eliminate DC from an AC signal, a blocking capacitor is inserted. Together with a resistor they form a high-pass filter, Figure 8.10(a). The time constant is RC , and the so called 3 dB corner frequency f_o is $1/2\pi RC$. At that frequency, the phase shift is 45° , and the amplitude has dropped to 63%. This is clear from the transfer function:

$$H(\omega) = \frac{v_o}{v_i} = \frac{(\omega^2 R^2 C^2 + j\omega RC)}{(1 + \omega^2 R^2 C^2)} \quad \varphi = \arctan\left(\frac{1}{\omega RC}\right) \quad (8.38)$$

The phase shift is: At f_o : $\varphi = 45^\circ$, at $10f_o$: $\varphi = 5.7^\circ$, and at $100f_o$: $\varphi = 0.57^\circ$. The phase shift in a filter is thus substantial even far away from the corner frequency in the passband, and the frequency must be much higher than the corner frequency to ensure negligible phase shift.

If a repetitive signal is applied to the tissue electrodes via a high-pass filter, no DC polarization is possible.

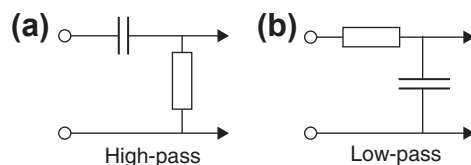


Figure 8.10: (a) High- and (b) low-pass filters.

Low-Pass Filter

The low-pass filter (LPF) (Figure 8.10(b)) is passing low frequencies and DC. The transfer function is:

$$H(\omega) = \frac{v_o}{v_i} = \frac{(1 - j\omega RC)}{(1 + \omega^2 R^2 C^2)} \quad \varphi = \arctan(-\omega RC) \quad (8.39)$$

The same precaution holds for the phase shift: to ensure low phase shift, the frequency must be much lower than the corner frequency. These low-pass filtering effects are an important source of error when reading signals through such high-impedance systems as microelectrodes because of inevitable stray capacitance between the inner conductor and the surrounding tissue.

The LPF is also easily realized with a capacitor in parallel with the feedback resistor of the operational amplifier (opamp) circuits of Figure 8.12(b) and (d).

Measurement of Immittance with an Endogenic Signal Source

It is possible to determine the immittance of an electrode system without the use of exogenic signal sources. An endogenic signal is recorded, and the electrode system is loaded with a known admittance in parallel. The *reduction* in signal amplitude is measured as a function of the admittance load. The source immittance can be then be calculated. The method has been used for checking the influence of a limited input impedance of ECG amplifiers (Geddes and Valentinuzzi, 1973), and the estimation of signal source impedance of implanted pacemaker electrodes (Mørkrid et al., 1980).

8.2.8 Signal Generators

The Constant Amplitude Voltage Output (Voltage Clamp)

From the mains and our use of batteries, we are well acquainted with the constant amplitude voltage supply. The ideal voltage supply has zero internal resistance. It supplies the set voltage from no load (load resistance ∞ , open circuit) to full load (minimum load resistance and maximum current). Two ideal voltage sources cannot be coupled in parallel. In series, the voltages are added.

With $V = \text{constant}$, Ohm's law $I = V/R = VG$ shows that the current is proportional to G , not to R .

The Constant Amplitude Current Output (Current Clamp)

There are no constant amplitude current supplies in our daily life surroundings, so we are not so well acquainted with this sort of supply. It may be constructed in two ways: either by electronic circuitry or by a voltage supply with a large series resistance.

The ideal current supply has infinite internal resistance. It supplies the set current from no load (load resistance 0Ω , short circuit) to full load (maximum load resistance and maximum voltage). To leave a current supply open-circuited is the same as leaving a voltage supply short-circuited. Two ideal current sources cannot be coupled in series. In parallel, the currents are added.

With $I = \text{constant}$, Ohm's law $V = RI = I/G$ shows that the voltage is proportional to R , not to G .

Choice of Supplies

The power dissipated as a function of load resistance R is:

$$W(R) = RI^2 = \frac{V^2}{R} \quad (8.40)$$

We realize from these equations the important difference between using a constant amplitude current or a constant amplitude voltage supplying a variable load resistance. The current—voltage characteristic of the black box may decide the choice of constant amplitude voltage or current.

8.2.9 Grounded or Not Grounded Patient

In a building, there are construction materials forming the ceiling, floor, and walls of a room. The materials used may have a certain electrical conductivity. We must remember that the dimensions are very large, so that even a small conductivity may result in appreciable conductance according to $G = \sigma A/L$. These materials form a Faraday cage around a room, and it is of interest to have electrical access to this cage. That is one of the functions of the household *ground wire*. The ground wire follows as an integrated part of the power cables supplying every room with electricity. In our context, the importance of the ground wire is not that it is connected to the Earth, but to the building and the room we are in. The ground wire is of interest with respect to noise (*functional grounding*) and safety (*safety grounding*). Therefore, the net plug of electromedical class I equipment contains three wires: the two power line wires and the ground wire with the color yellow/green according to the international standard IEC-60601. In every medically used room, the power outlets shall be equipped with the yellow/green ground wire. Electromedical equipment may also be of class II with *double insulation*, then there is no safety ground wire in the flexible power cord of the equipment.

For safety reasons, we ideally wish to have a floating (not grounded) patient (person), because if the patient by accident touches a CC noninsulated metal part, no current will flow through the patient. Therefore, modern electromedical equipment is usually designed with a *floating applied part* of type body floating (BF) or cardiac floating

(CF) (see Section 10.16.6). The *applied part* is the part of the equipment that by intention is in physical contact with the patient. B means body, C cardiac, and F floating. F-type equipment is designed with a *galvanic separation* between the applied part and the rest of the equipment. Some equipment still grounds the patient; that is, type B.

Electronic circuitry with operational amplifiers is usually supplied from a symmetrical power supply, for example, ± 12 V. This implies three power wires to the amplifier: +12, 0, and -12 V. The 0 V wire is called the amplifier's *reference wire* (or chassis wire). The reference wire is used for connecting local shields of, for example, cables or chassis. It is often floating; that is, not connected to ground. The symbols for reference and ground are shown in Figure 8.13, lower right. The reference wire may also be grounded to reduce noise (functional grounding) or to increase safety (protective grounding).

8.3 Amplifiers, Bridges, Analyzers

Circuitry for impedance measurements has changed dramatically since the first measurements were performed on biological tissue. The development of digital electronics and the incorporation of computer power in almost all instruments have had an important impact on the possibilities of studying the passive electrical behavior of biomaterials over a wide frequency range, and with a speed that was not feasible only a few years ago. Only a brief summary of some of the techniques will be given in this section.

8.3.1 Black Box Analysis, Amplifiers, Filters

Let us consider a black box containing some series combination of ideal components: one resistor, one or no battery, and one or no capacitor. By external measurements, we shall find the component values in three different cases.

First, DC method. We are told that there is only one resistor in the black box. To find the resistance value R, we apply a known DC voltage V (Figure 8.11(a)). From measured current I, the resistance is calculated: $R = V/I$. Now let somebody go into the black box and add the ideal battery B in series with the resistor (Figure 8.11(c)). The DC current will of course change. How can we know from the outside whether the DC current change was

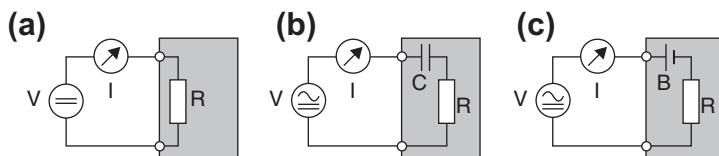


Figure 8.11: Basic black box—measuring problems.

due to a change in resistance, or an additional electromotive voltage (emv) in the black box? We cannot.

Second, DC method. To find out, we must add something to the measurement. For instance, by varying V, the current I also varies. By applying $V = 0$, we still have a current flowing, which must be $I = V_B/R$. We can then assume that there must be a battery in the circuit.

Third, DC/AC method. To obtain this information, we actually have to superimpose a varying signal, an AC voltage, on the DC voltage. In addition, this manual method cannot be used if we want to continuously monitor changing values of V_B and R .

If R and B are nonideal with current depending values, as in an electrolytic electrode system, the DC approach cannot be used. A better approach is to superimpose a *small, continuous* sine wave voltage on the applied DC voltage. Our current measuring device must then be able to measure both AC current with phase and DC. The battery (being ideal with zero internal resistance) will not influence the AC current, and we consequently measure the resistance of R at AC, but a different “R” at DC. Because there is no phase shift, we then know that the battery is in the circuit. If we repeat the measurement on many frequencies and the results are identical, we know that there is no capacitor inside the black box.

What if the battery B is replaced by a capacitor C ([Figure 8.11\(b\)](#))? With the sine wave superimposed, the current will be phase-shifted. From a single frequency measurement, we can find the RC values by the impedance formula $Z = R + 1/j\omega C$.

The DC current will decay from the value found when the applied voltage was switched on. The voltage V_c on the capacitor depends on the charge and the capacitance according to $V_c = Q/C$. Just like the battery, it stores energy and it can give this energy back. The capacitor voltage represents a voltage that changes the current I in the same way as a battery. The AC current will not change during the charging of the capacitor, so constant impedance reveals that the DC current decay must be caused by a gradually increased capacitor charge.

If the battery is also inserted, it cannot necessarily be detected from the outside because it is blocked by the capacitor. A battery *may be* regarded as a very large capacitor with a nearly constant charge and voltage, so large a capacitance that its reactance ($1/\omega C$) may be negligible. Also an ideal battery has zero internal resistance (reactance). However, the battery generates an emv from a chemical reaction. The capacitor is a dry system with energy stored in the dielectric, and a voltage according to $V = Q/C$. It is a matter of definition whether the capacitor voltage shall be called a counter-emv; in this book, only emv from electrolytic net charge distributions will be regarded as such.

Operational Amplifiers

The opamp is an amplifier with two inputs (inverting and noninverting). They are always used with negative feedback, and have so large amplification that the voltage difference between the inputs is negligible (Figure 8.12(c)). It may be used as single-ended voltage amplifier (negligible input current) as in Figure 8.12(d), or as a current amplifier (negligible voltage drop at the input), called a *transresistance* or *transimpedance* amplifiers (Figure 8.12(b)) for making a voltage output. It is not suited to measure a differential voltage without loading the measured circuit; this is done by a special circuit (often composed of three operational amplifiers) called an *instrumentational amplifier*, treated in Section 8.3.2.

These amplifiers are active devices in which the inputs need a certain bias current and must operate within the limits of the power supply voltage. The power supply wires and the reference wire (0 V), as illustrated in Figure 8.12(a), are frequently omitted on most circuit diagrams. Notice that the inputs are galvanically separated neither from the output, nor from the power supply. Transcouplers or optocouplers are needed if galvanic separation is necessary (Min et al., 2006).

Figure 8.12(c) shows the voltage follower; it is just a buffer with amplification equal to -1 (inverting circuit). It is also the principle of a constant amplitude voltage supply. The purpose is to read a voltage without loading (drawing current) from the measured point. Often the opamp may be brought as near to the recording electrode as possible. Then the

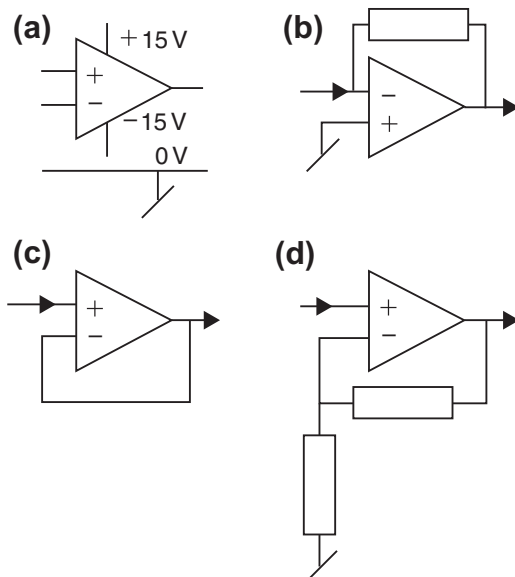


Figure 8.12: Operational amplifier circuits. The details shown in (a) are always present but usually omitted.

output wire is not critical and need not necessarily be shielded. A shield for the input wire may preferably be connected to the output instead of ground, because the capacitance between inner wire and shield is then eliminated (bootstrapping). By adding two resistors (d), it is possible to obtain amplification.

The current measuring circuit is very attractive instead of introducing a current reading shunt resistor with the necessary (even if small) voltage drop. The voltage drop in this circuit is virtually zero.

The circuit of (b) can be used also as a constant current circuit. A constant amplitude voltage and a resistor are used to supply the input current. The load is the feedback resistor; the constant input current will pass the feedback resistor for any resistance value up to the voltage limit of the operational amplifier. In this way, we can measure the current without any shunt.

8.3.2 Instrumentation Differential Amplifiers

The signal input of electronic amplifiers may be designed single-ended (two input wires) or differential (three input wires). Single-ended input (Figure 8.13(b)) is an asymmetrical two-wire input circuit; one wire for the signal and one wire for the indifferent electrode. The reference wire, grounded or not, is common for the input, output, and power supply. The circuit is a two-port, three-terminal input device. Figure 8.13(a) shows the three-terminal input system. More details are given in Figure 8.14.

Figure 8.14 shows an instrumentation biopotential preamplifier. The input signal comes from an electrode pair PU1 and PU2. A third electrode is an indifferent electrode (Ind)

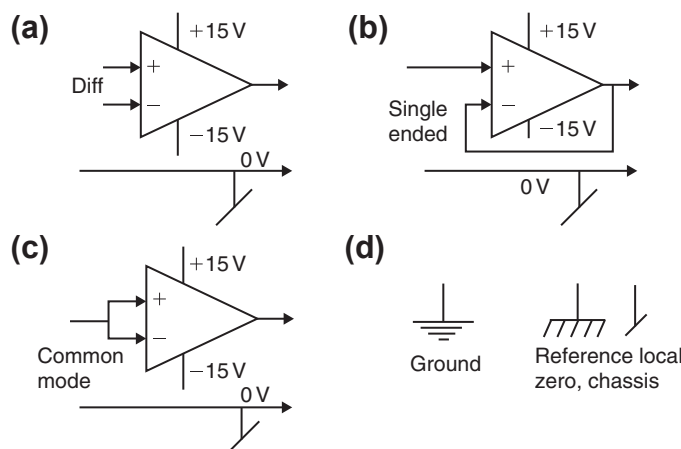


Figure 8.13: (a) Differential (instrumentation amplifier) input. (b) Single-ended input. (c) Common mode coupled input. (d) Symbols for ground and local reference.

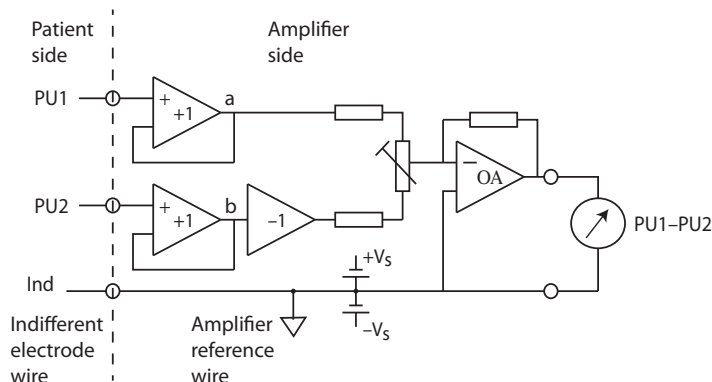


Figure 8.14: Differential preamplifier well adapted for serving as biopotential preamplifier. Input equipped with three-wire connections for two PU electrodes and one Ind electrode. The indifferent electrode is coupled to the amplifier reference wire. The purpose is to equipotentialize patient and preamplifier.

that is coupled to the reference wire of the electronic amplifier, so that the human body is equipotential with the amplifier. The power supply is from batteries ($+V_s$ and $-V_s$) so the patient is not grounded by the amplifier reference wire.

In Figure 8.14, the input amplifiers are so-called *buffer amplifiers*, with extremely high input resistance, low input capacitance, extremely low input current, and amplification exactly equal to 1.00000. At points a and b, the input voltages are found again but now transformed to robust extremely low impedance and accordingly with little need for screening. The signal can then be used for checking whether the electrode is on an active or passive skin site. OA is an ordinary operational amplifier equipped with a feedback resistor determining the gain.

As shown in Figure 8.14, differential input amplifiers are symmetrical three-wire input circuits, two wires for the input differential signal, (PU1 is the +wire in phase with the amplifier output, PU2 is the -wire 180° out of phase with the output). The signal between the differential wires PU1 and PU2 is the differential, desired signal. If these two wires are shorted together, the differential input voltage is zero. The voltage between the shorted input wires and the indifferent wire is the *common mode voltage* (CMV, Figure 8.13(c)). The amplifier should be as insensitive to CMV as possible, and this is expressed by the amplifier's *common mode rejection ratio* (CMRR), usually given in decibel (dB). A CMRR of 100 dB ($=10^5$) means that, for example, a CMV input signal of 1 V (between the two input wires connected together and the indifferent wire) is equivalent to a differential input signal of $10 \mu\text{V}$. The circuits are equipped with a trim potentiometer to make the amplification in the plus and minus channels exactly equal and thereby maximize the CMRR.

The CMV must usually be within limits set by the power supply of the amplifier. If the supply is ± 12 V, the CMV input range is perhaps ± 9 V. For this reason, the patient/test person usually must have a third electrode connected to the reference wire of the input amplifier. Without this third wire, the input amplifier's CMV range may easily be exceeded. Both DC and AC must be considered in this respect. In BF and CF equipment (c.f. Section 10.16.6), the third electrode is a floating reference electrode, in B equipment the amplifier common reference wire is grounded and therefore grounds the patient.

An operational or instrumentation amplifier of the applied part is usually galvanically coupled to the patient. If it has infinitely high CMRR, then with respect to CMV noise cancellation, it would be the same as if input and output were galvanically separated. But with respect to safety, it is not ideal because the CMV input range is restricted to less than the power supply voltage to the amplifier. Outside that linear range, the junctions of the input transistors may enter a nonlinear breakdown region. To keep it inside the CMV range, a third electrode is usually necessary. An input circuit is therefore only galvanically separated if its energy supply is from batteries or transformers, and if the signal output is by optical, transformer or radio signal (telemetry) coupling. Then the allowed CMV may be in the kilovolt range. A transformer winding input is the nearly perfect input both for safety and DC CMV cancellation, but unfortunately not for broadband amplification and high input impedance.

The patient has been considered equipotential in this analysis. From the human body segmental resistances described in Section 4.2.7, the chest has a segmental resistance of the order of 10Ω . With $1 \mu\text{A}$ flowing, the voltage difference is of the order of $10 \mu\text{V}$. In the limbs, the segmental resistances are much higher. If this is critical, care must be taken as to where to locate the reference and CC electrodes of the clamping circuit, and where to locate measuring electrodes with respect to noise current flow paths (see [Figure 8.18](#)).

[Figure 8.16](#) shows a combined stimulus neurogenerator and two-channel electromyographic amplifier with display. This is for helping the surgeon to navigate and cut the correct nerves in the *facialis*. The stimulator is coupled with two wires. One is a deeply inserted needle serving as indifferent electrode. The other is the active handheld surface probe. Each electromyelogram channel has bipolar coupling and a common indifferent electrode.

8.3.3 Interface Patient and Amplifier, Risk Considerations

In [Figures 8.14 and 8.15](#), one could be led astray if believing that the electrodes on a patient are to be coupled directly to the amplifier. Some risk situations must be considered, as shown in [Figure 8.17](#).

1. Amplifier failure so that the amplifier sends uncontrolled error currents into the patient.
It may for instance be that the input transistor has broken down so that the power

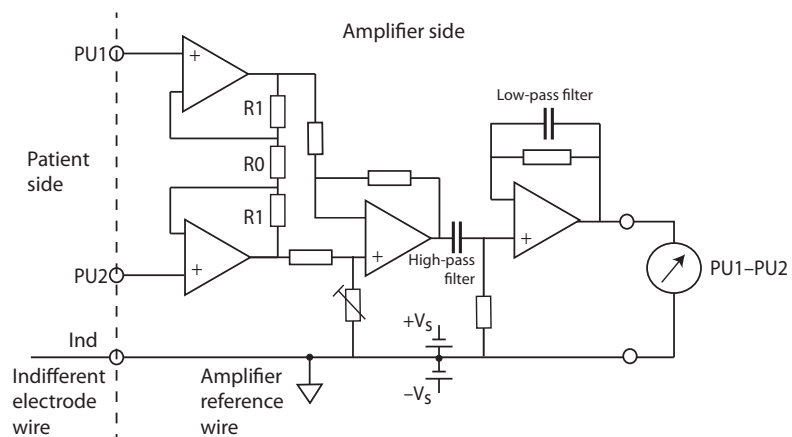


Figure 8.15: Differential preamplifier, another version of Figure 8.14, with band-pass filters included. The individual PU_1 and PU_2 potentials are not directly accessible because they are at points a and b in Figure 8.14.

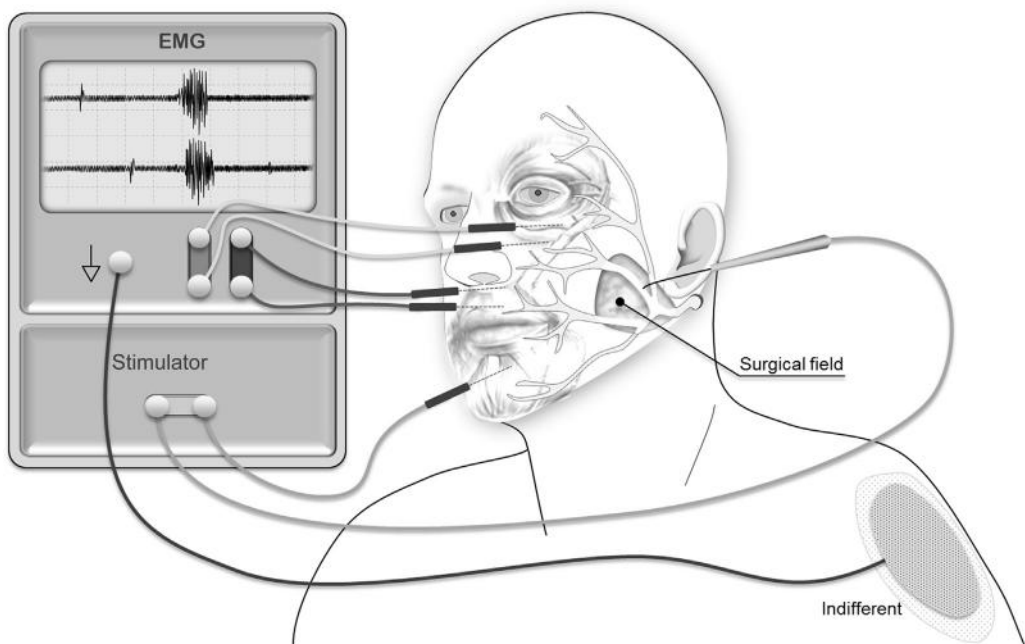


Figure 8.16: Mapping of *facialis* nerve before surgery. Courtesy: Tormod Martinsen.

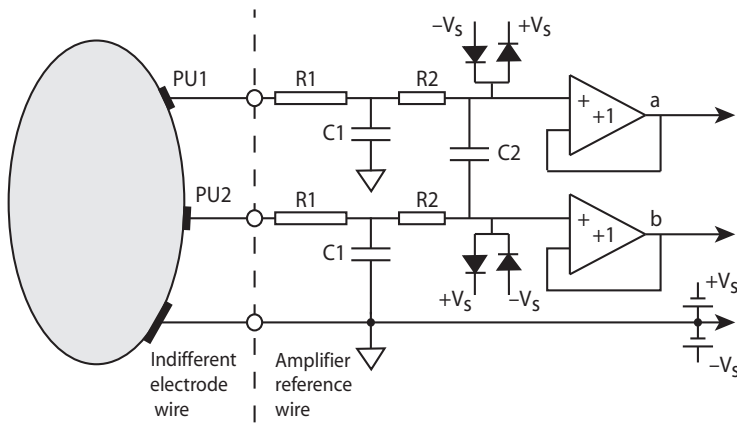


Figure 8.17: Safety components between patient and preamplifier (see Figure 8.14).

supply voltage is sent directly to one of the PU electrodes. The two resistors in series R1 and R2 shown on Figure 8.17 limit this to a maximum current of $V_s/(R_1 + R_2)$.

2. Static electricity generated, for example, when the patient's bed is made, and it is during wintertime with low air humidity. Static discharges can have destroyed the input transistor. The risk is reduced by the two resistors R1 + R2 and the two capacitors C1 + C2 forming two LPFs. A static discharge is usually very rapid (e.g., 5 μ s, c.f. Figure 10.33) so the damping can be substantial. In Figure 8.17, the four protective diodes shown hinder voltages much higher than Vs reaching the input of the input buffer amplifier.
3. The patient is defibrillated while coupled to the amplifier. A defibrillator shock can be up to 5 kV and is applied via two large electrodes to the thorax. A substantial part of this voltage can appear between PU1 and PU2. The frequency is much lower and the LPFs will damp the signal much less than the static discharge case. But the protection diodes will play an important role.
4. The patient coupled to the amplifier may be in the operating room and electrosurgery is going to be used. The frequency band will stretch from about 100 kHz to 10 MHz during fulguration, maximum voltage radiofrequency (RF) peak 5 kV. The LPFs will again be important (Figure 8.17).

Usually the value of R1 is chosen larger than R2. The R1 resistors must therefore be dimensioned to endure both the current duration, and the voltage rating is important (e.g., >1 kV). Therefore, the R1 resistors are drawn longer than the R2 resistors in Figure 8.17.

8.3.4 Power Line Noise Cancellation

Figure 8.18 shows a commonly used circuit for power line noise cancellation. Figure 8.19 shows three situations of power line capacitively coupled noise voltage. Suppose first (left)

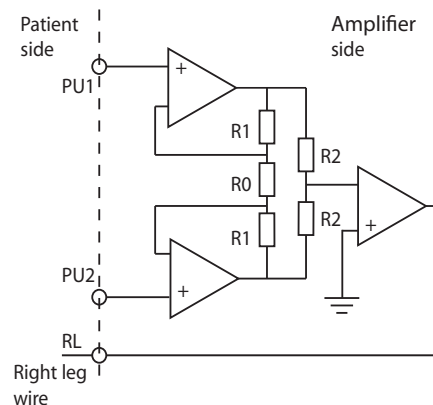


Figure 8.18: Driven right leg (RL) circuit for reduced common mode voltage. Differential preamplifier. Input equipped with three-wire connections for two PU electrodes and one RL drive wire.

The purpose is to equipotentialize human body and instrument and to reduce the common voltage between electrodes. Note power line ground symbol. See text.

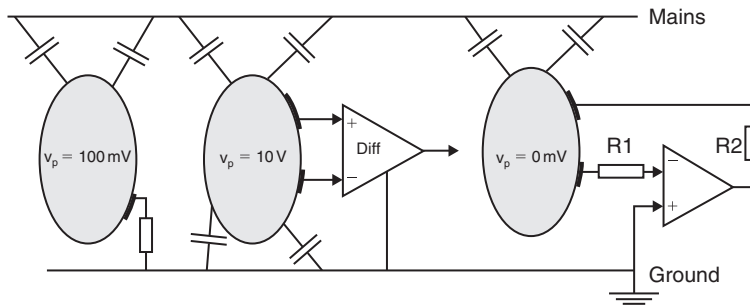


Figure 8.19: Three noise reduction approaches. Left: grounded patient. Middle: floating patient with instrumental amplifier. Right: ground-clamping circuit. v_p is typical patient AC voltage with respect to ground. v_p is in practice nonsinusoidal. Because of the high-pass filtering effects, the harmonics of the mains supply are expanded.

that leakage current is passing through a grounded electrode on the patient. The skin impedance under such electrode may easily attain $100 \text{ k}\Omega$ at 50/60 Hz. With a leakage current of $1 \mu\text{A}$, the voltage on the patient with respect to ground is 100 mV. With a single-ended signal amplifier (two electrodes on patient: signal and ground), the 100 mV is superimposed on the signal of interest. To reduce the influence of the noise voltage, either the coupling to the mains must be reduced (increase distance to source, shield, Faraday cage), or the impedance of the ground electrode (dominated by skin impedance) must be reduced.

Another approach (middle) is to convert the noise voltage to a common voltage by applying an instrumental amplifier (two measuring electrodes on patient). With a

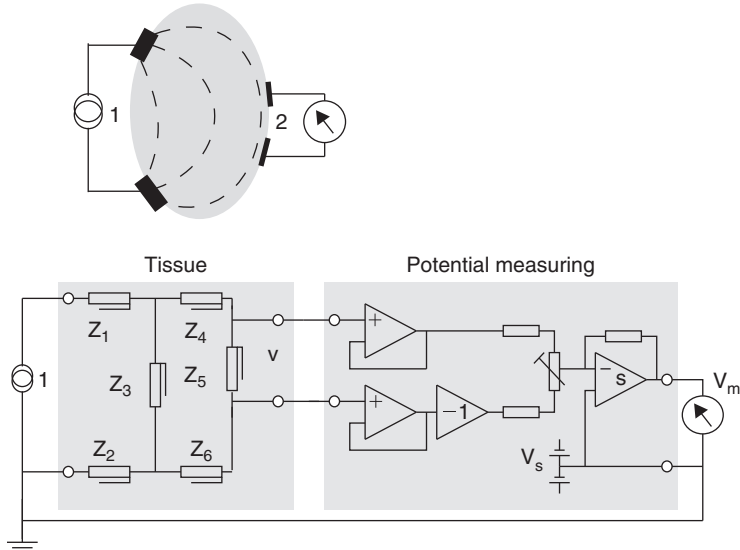


Figure 8.20: Equivalent circuits for tissue and potential amplifier. The bioimpedance symbols are for frequency dependent components. Note the grounded tissue (Z_2), amplifier, and output. Note also symbol for power line ground. Simplified circuit of the Solartron 1260 model.

floating patient the voltage may be about 10 V, so a common mode rejection ratio of 120 dB (10^6) would be needed to reduce the noise contribution to 10 μV . In addition the CMV must be within the linear range of the instrumentational amplifier. By also grounding the patient (three electrodes on patient), the CMV range is better controlled.

Figure 8.20 illustrates how the common-mode voltages are controlled in an often used configuration, by grounding one side of the signal source (Grimnes and Martinsen, 2007). In medical instrumentation terms, this means that the instrument is a class B device (Section 10.16.6). Even so, a differential amplifier is used.

A third approach (Figure 8.18 and Figure 8.19, right) is to clamp the patient to a ground potential by an active operational amplifier circuit (two electrodes on patient). The reference electrode picks up the voltage of the deeper skin layers (skin impedance independent: no current flow and no voltage drop in the stratum corneum). The operational amplifier sets up a current in the CC electrode to just counterbalance the capacitively coupled noise current; the reference electrode is virtually grounded. It is also possible to put in safety resistors (R_1 and R_2) without reducing the effect of the circuit. In that way the patient is not directly grounded even if the semiconductor circuits break down. Of course, this is also possible to do in the instrumentational amplifier input wires.

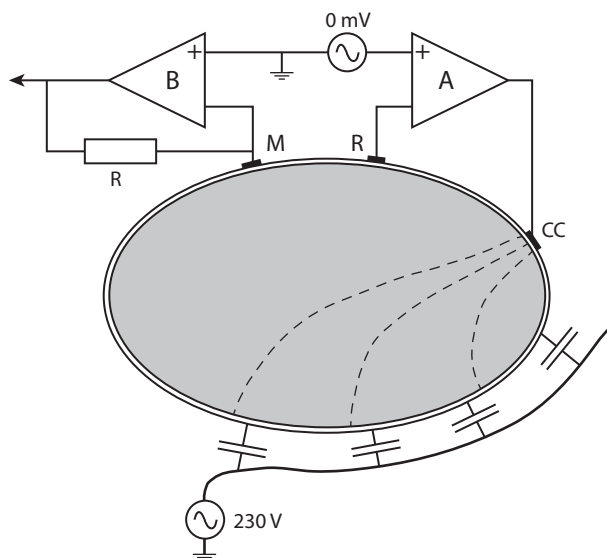


Figure 8.21: Capacitively coupled power line noise. Note the symbol for power line ground, not floating reference!

Figure 8.21 shows an admittance-measuring circuit. $Y = i/v$, v is constant AC generator output and i is measured AC current. M is the measured electrode, and monopolar function is obtained by opamp A in a circuit with three electrodes. The signal generator output is normally, for example, 30 mV so that A sets up a current from CC to M so that R has the same potential as the signal generator output. R is a reference PU electrode with no current flow. The resulting current i is measured by opamp B.

Figure 8.21 shows the capacitively coupled noise current path, for clarity, the signal generator output is regulated to zero so no measuring current flows. A sets up a current through CC so that R continuously is at signal generator output level, that is zero volts.

Now the point is that the noise current does not go to M, so it is not measured, it is canceled! A condition is that A is able to give the necessary current and the necessary output voltage to overcome the voltage drop in the skin impedance under the CC electrode.

8.3.5 Measuring DC Potential and AC Admittance Simultaneously at the Same Skin Site

A two-electrode monopolar electrode system is used as shown in Figure 8.22. DC voltage measurement is very simple. The potential of the monopolar electrode is coupled directly

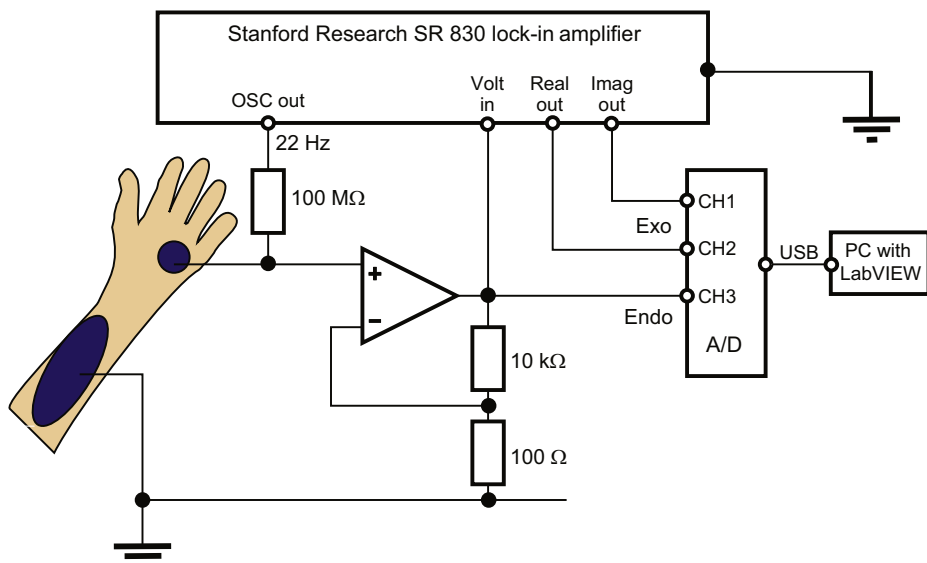


Figure 8.22: Circuit for measuring DC potential and AC admittance simultaneously at the same skin site. Note the symbol for power line ground.

to a noninverting opamp having a gain of 100. The amplified signal is connected to channel 3 on the analog/digital (A/D) converter. A very small constant AC current is supplied to the monopolar electrode and the resulting AC voltage is also amplified with $G = 100$. The combined amplified DC–AC signal is sent to the lock-in amplifier and the in-phase and quadrature outputs are sent to channels 1 and 2 on the A/D converter. The digital output is sent to a PC with Labview software. In the computer, the impedance signal is inverted so we also have an admittance output signal. In Section 10.3.4 we show some results with the circuit of Figure 8.22.

8.3.6 Bridges, Synchronous Rectifiers, Fast Amplifiers

Bridges

A variety of bridges have been used for immittance measurements. The general principle of an AC bridge is illustrated as an admittance bridge in Figure 8.23, where $\mathbf{Y}_1 = 1/\mathbf{Z}_1$ is a parallel circuit of a variable resistor and a variable capacitor, and $\mathbf{Y}_2 = 1/\mathbf{Z}_2$ is the measured sample.

By balancing the bridge so that the signal measured by the detector is equal to zero, the unknown admittance \mathbf{Y}_2 can be calculated using the relation $\mathbf{Y}_1\mathbf{Y}_4 = \mathbf{Y}_2\mathbf{Y}_3$.

The advantage of bridges is their high-resolution capabilities, a feature very important for extending dielectric measurements to low frequencies in tissue (see Section 3.8).

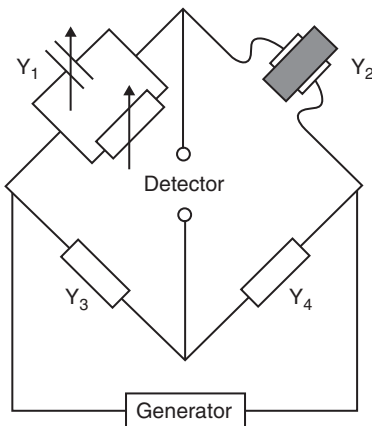


Figure 8.23: Admittance measurement with an AC bridge.

Blood, for instance, has a conductivity of about 1 S/m and ϵ_r' of 1500, frequency independent up to 100 kHz. A conduction resolution of about 10^5 is necessary for a precision of 10% at 1 kHz, (Schwan, 1963). Schwan (1963) discussed both low- and high-frequency bridges, and Schwan and Ferris (1968) discussed high-resolution tetrapolar bridges. Hayakawa et al. (1975) have further increased the precision of bridge instrumentation.

However, manual bridges are slow and not suited for measurements on dynamic systems. Although automated bridges are commercially available, they have given way to other methods for bioimpedance measurements, such as lock-in amplifiers.

The lower practical frequency limit for an AC bridge is about 10 Hz if it is transformer coupled, and down to DC if it is directly coupled. The upper frequency limit may be high in the MHz region with special constructions.

8.3.7 Lock-in Amplifiers

Lock-in amplifiers are commonly used to detect minute signals buried in noise. This can only be accomplished, however, if the signal of interest appears as an amplitude modulation on a reference frequency. The ideal lock-in amplifier will then detect only the part of the input signal having the same frequency and phase as of the reference signal.

Lock-in amplifiers are based on the multiplication of two sine waves (see [Eq. 8.22](#) and [Figure 8.4](#)), one being the signal carrying the amplitude modulated information of interest, and the other being a reference signal with the chosen frequency and phase.

If the reference signal is given (assuming amplitude of unity) by:

$$v_r = \sin(\omega_r t) \quad (8.41)$$

and the input signal is:

$$v_i = V_i \cdot \sin(\omega_i t + \varphi) \quad (8.42)$$

the output signal will be (see Section 8.2.2):

$$\begin{aligned} v_o &= V_i \cdot \sin(\omega_i t + \varphi) \cdot \sin(\omega_r t) \\ &= \frac{V_i}{2} \cdot [\cos((\omega_i - \omega_r)t - \varphi) - \cos((\omega_i + \omega_r)t + \varphi)] \end{aligned} \quad (8.43)$$

A LPF will follow this multiplier module, and the right hand higher frequency cosine expression may therefore be ignored. In fact the only DC signal that will appear at the LPF output, will be the one corresponding to $\omega_i = \omega_r$, which gives:

$$v_o = \frac{V_i}{2} \cdot \cos \varphi \quad (8.44)$$

A lock-in amplifier is perfect for immittance measurements. Two amplifiers could be used, one with a reference signal identical to or in phase with the excitation signal, and another with a reference signal 90° out of phase with the excitation signal (Figure 8.24). If the excitation signal is a voltage, the measured current should be converted to voltage using, for example, a transimpedance (or transresistance) amplifier (Figure 8.12(b)). In that case, the DC outputs from the lock-in amplifiers will be proportional to the parallel admittance values of the measured object, for example, conductance and susceptance, respectively. Using a current as excitation will correspondingly produce a measured voltage that can be separated into signals proportional to the series impedance values, which are resistance and reactance. Lock-in amplifiers can be basically digital or analog. Digital ones are more flexible and precise, but analog lock-in amplifiers consume much lower power and can operate at higher frequencies (Figure 8.24).

Digital Lock-in Amplifiers

Digital lock-in amplifiers perform digital multiplication of digitized input and reference signals. High precision multiplication is available, but also a high resolution (16–18 bit) and high speed (10 MHz sampling rate) analog-to-digital converter (ADC) is required to achieve the typically needed dynamic range of at least from 80 to 100 dB. Also, digital averaging (integration) is used for extracting the output signal from the multiplication product.

Total suppression of noise is possible only if the integration time is infinite (i.e., the multiplication is carried out over an infinite number of signal cycles). Gabrielli (1984)

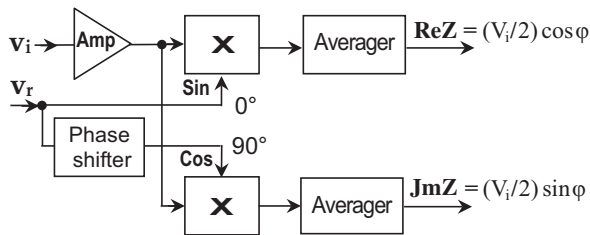


Figure 8.24: Two-phase (quadrature) lock-in amplifier.

showed that the suppression of random white noise is given by an equivalent filter function with a bandwidth Δf given by

$$\Delta f = \frac{f_r}{N} \quad (8.45)$$

where f_r is the analyzed frequency and N the number of cycles. Hence, in a 10-Hz measurement, the bandwidth is 0.1 Hz when integrating over 100 cycles, but only 2 Hz when integrating over only five cycles of the signal. The corresponding transfer function is given by

$$|H(\omega)| = \frac{2}{\pi N} \left[\frac{\sin\left(\frac{N\pi\omega}{\omega_0}\right)}{1 - \left(\frac{\omega}{\omega_0}\right)^2} \right] \quad (8.46)$$

where ω/ω_0 is the normalized angular frequency. The transfer function is also shown in **Figure 8.25** as a function of number of integration cycles.

Digital lock-in amplifiers have virtually no low-frequency limitations. Commercial amplifiers typically operate down to 1 mHz, but, for example, the Solartron 1260 is

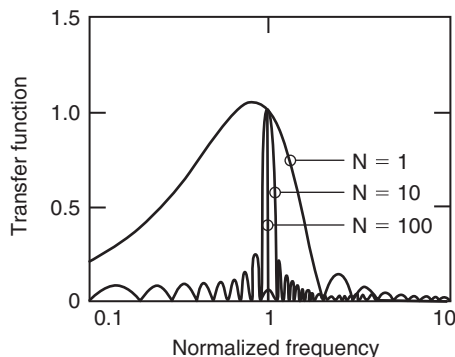


Figure 8.25: Absolute value of transfer function for digital lock-in amplifier as a function of normalized frequency and number of integration cycles.

constructed for measurements down to $10 \mu\text{Hz}$ (corresponding to a period of about 28 h). The upper frequency limit is about 100 kHz mainly limited by the conversion time in the ADCs. Above this frequency, heterodyne undersampling can be used as described in [Section 8.3.9](#), which extends the range of Solartron 1260 to 32 MHz . Another example of a radiofrequency down-converting digital lock-in amplifier is the SR844 from Stanford Research Systems. It has a frequency range from 25 kHz to 200 MHz with an *absolute* phase error better than 2.5° below 50 MHz , increasing to a maximum of 10.0° at 200 MHz . However, the *relative* phase error is less than 2.5° , which can be used in a practical experimental situation by measuring, for example, before and after biomaterial is added to an electrolyte solution.

Analog Lock-In Amplifiers and Synchronous Rectifiers

The heart of the analog lock-in amplifier is the synchronous rectifier that includes a phase-sensitive detector (PSD) and a LPF. Typically, a rectangular (square wave) reference signal controlling an analog switch is used. Hence, multiplication by a square wave reference signal is performed and a LPF is used for averaging ([Figure 8.26](#)). It is necessary to emphasize that the square wave signal contains odd higher harmonics (see [Eq. 8.31](#)).

The PSD in [Figure 8.26](#) comprises an inverter and the analog switch. The switch is connected to the in-signal in the positive half periods of the reference signal and to the inverted in-signal in the negative half periods. Hence, if the in-signal and reference signals are in phase, the detector will act as a full wave rectifier, providing a maximum DC signal out from the LPF. If the in-signal and reference signal are 90° out of phase, the resulting signal out from the PSD will be without any DC component as shown in [Figure 8.26](#), and

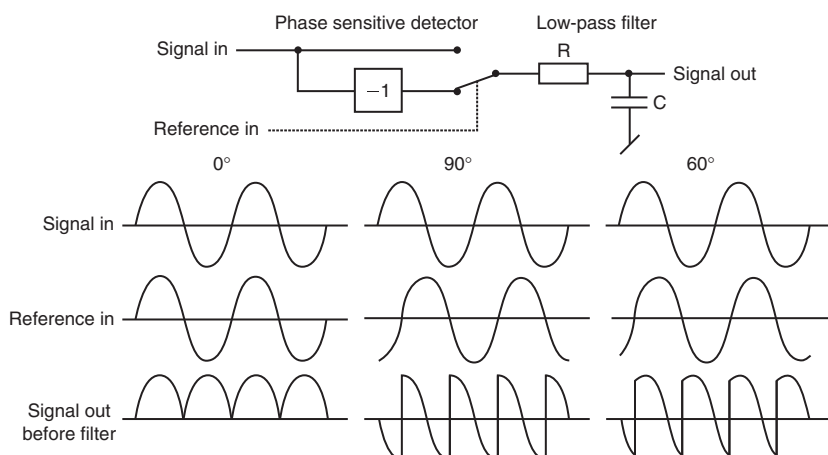


Figure 8.26: Synchronous rectifier with 0° , 90° , and 60° phase shift between signal and reference.

the LPF will produce no output signal. A phase shift between 0° and 90° will accordingly produce a DC signal lying between these two limits (see Eqs 8.22–8.24 and Figure 8.4). It can easily be shown that the output signal from the synchronous rectifier is given by the equation:

$$V_o = V_i(\text{avrect})\cos \varphi \quad (8.47)$$

where V_o is the DC voltage out from the LPF, $V_i(\text{avrect})$ is the average rectified value of the AC in-signal, and φ is the phase shift between the in-signal and the reference.

We should take into account that the Fourier components of the square wave signal include all the odd harmonic frequencies. The synchronous rectifier will hence be sensitive to both the main reference frequency and to all odd harmonic components, but with sensitivity proportional to $1/n$ where n is the odd harmonic number (see Eq. 8.31).

Analog lock-in amplifiers have a practical lower frequency limit of about 1 Hz, owing to the necessity of AC coupled inputs. Because any DC signal will influence the results, the method requires pure AC signals. The upper frequency limit of the analog lock-in technique is typically about 100 kHz to 1 MHz, and is mainly due to problems of stray capacitance. The dynamic range can reach over 100 dB.

8.3.8 Microelectronic Lock-in Amplifiers

Today microelectronic lock-in amplifiers are mostly based on mixed-signal integrated circuits combining both analog and digital processing in the best suitable way. Signal processing has traditionally been confined to manipulating electrical voltages, and current signals are typically transformed into voltages in electronic instruments. However, in semiconductor devices, it has proved to be advantageous to use current mode signal processing in modern applications (Min et al., 2006), especially in low-power implantable medical devices such as described by Silveira and Flandre (2004).

The basic idea for using current mode analog lock-in technique is that currents may be driven with relatively low voltages in discrete time-switching circuits. Thus, high-level signals are not expressed through higher voltages, but through the level of currents, which remains low in the pico- and microampere range. As a result, battery-supplied low-voltage (1.0–2.5 V) and low-power (microwatt range) microelectronic circuits can be designed and fabricated. Also the charging time of stray capacitance is reduced, which shortens signal propagation time and enables precise measurements at higher frequencies. A low-cost current mode lock-in amplifier has been presented by Min and Parve (1997).

As shown in Figure 8.27, it comprises a programmable oscillator that provides a symmetrical controlled current through the specimen of interest, Z_X . The voltage across the same specimen is again converted into a current by a differential input voltage-to-current

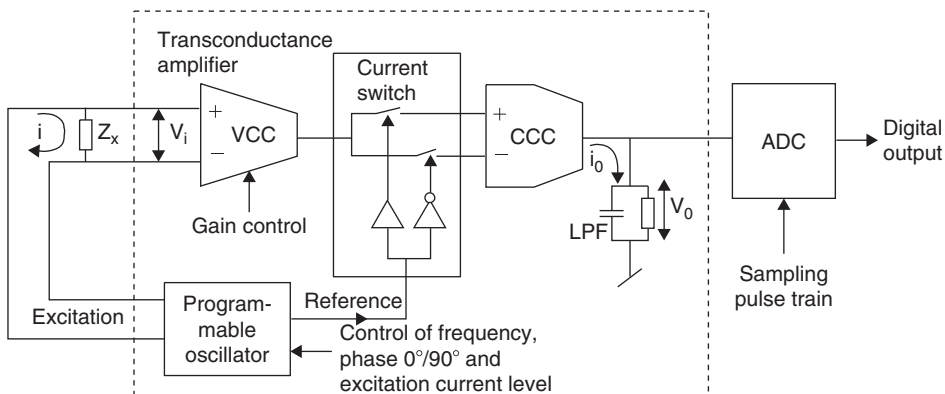


Figure 8.27: On-chip current mode lock-in amplifier. VCC = voltage to current converter, CCC = current to current converter, ADC = analog to digital converter

converter, which is also termed a transconductance amplifier or transor (see Min et al., 2006). The current from the transconductance amplifier is then decomposed into its in-phase and quadrature component by means of current mode switches that are driven by the reference signal from the programmable oscillator. Hence, to measure the quadrature component, the oscillator has also a second reference signal that is 90° out of phase. A differential current-to-current converter produces the output current i_o , which is filtered and converted into output voltage V_o by the LPF.

To avoid aliasing, the measured signal is filtered out by the LPF before reaching the ADC. The final averaging of the result is performed using digital averaging (Figure 8.27). The application specific integrated circuits (ASIC)-based measurement systems are able to operate at 10–50 MHz frequencies. Commercially available microelectronic lock-in amplifiers for impedance measurement systems are produced by several companies as Analog Devices (AD630, AD5933/34, ADUCM350) and National Instruments (AFE4300, ADS1298).

Significant efforts have been devoted to suppressing the sensitivity of synchronous rectifiers to higher odd harmonics, proportional to $1/n$, where n is the order number of the odd harmonics (see Section 8.3.7). Min et al. (2002) described a solution in which a very rough approximation of sine waves with only some single discrete levels is used in both the excitation and reference signals. It is important that the excitation and reference signals should be approximated differently. The idea is based on the fact that the synchronous rectifier is sensitive only to these higher harmonics, which are present simultaneously in both the excitation and reference signals. In Figure 8.28 is shown the case where two-level ($p = 2$, levels $g_{2,1}$ and $g_{2,2}$) and three-level ($q = 3$, levels $g_{3,1}$, $g_{3,2}$, and $g_{3,3}$) approximations are used by switching on and off the parallel connected current limiting resistors.

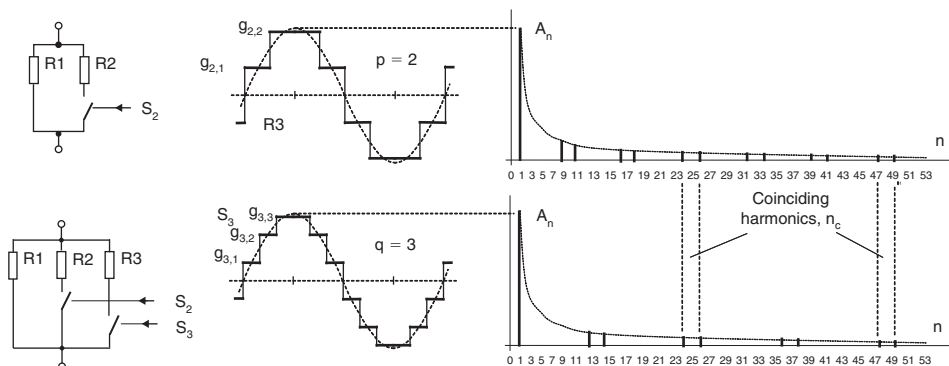


Figure 8.28: Two-level ($p = 2$) and three-level ($q = 3$) approximations of sine waves and their spectra.

The spectra in Figure 8.28 show that the harmonic contents of differently approximated waveforms ($p = 2$ and $q = 3$) are also different, although the most significant odd harmonics (the third and fifth) are absent in both. The orders of higher harmonics (n_c) that coincide in the excitation ($p = 2$) and reference ($q = 3$) signals, and to which the instrument is sensitive, can be found from the general equation

$$n_c = (4p \cdot q)i \pm 1, \quad \text{where } i = 1, 2, 3, 4, \text{ etc.} \quad (8.48)$$

In our case, where $p = 2$ and $q = 3$, the orders of common harmonics $n_c = 23; 25$ ($i = 1$), $47; 48$ ($i = 2$), $71; 73$ ($i = 3$), etc. The residual sensitivity to these harmonics is very low, proportional to $1/(n_c)^2$.

An even simpler solution is described in Min and Parve (2007), where only $+1, -1$, and 0 levels are used for approximations of the sine waves. Figure 8.29 shows a practical case where the two 0-level sections, lasting $1/6$ of each half-period $T/2$ ($\beta_1 = \pi/6 = 30^\circ$) remove the third harmonic, and lasting $1/10$ of the half-periods $T/2$ ($\beta_2 = \pi/10 = 18^\circ$) remove the fifth harmonic. As the result, the rectifying synchronous detector will not be sensitive to the third and fifth harmonics anymore, only the degraded sensitivity remains to the seventh, 11th, 13th, 19th, and so on odd harmonics. Publication by Min et al. (2007a) describes the digital version of a similar device, which uses synchronous sampling of the response voltage.

A fast impedance spectrometer may generate simultaneously several sine wave-based (multisine, chirp) (see Min et al., 2008; Sanchez et al., 2011, 2013; Trebbels et al., 2012) or discrete level excitations (binary pseudorandom or chirping sequences, multifrequency binary sequences) and process the response signals also simultaneously during a short observation time (Sun et al., 2007; Annus et al., 2012; Min et al., 2014). One effective solution is given by Min et al. (2007b), where the synchronous sampling performs the spectral analysis without any multiplication operations. Overview about contemporary

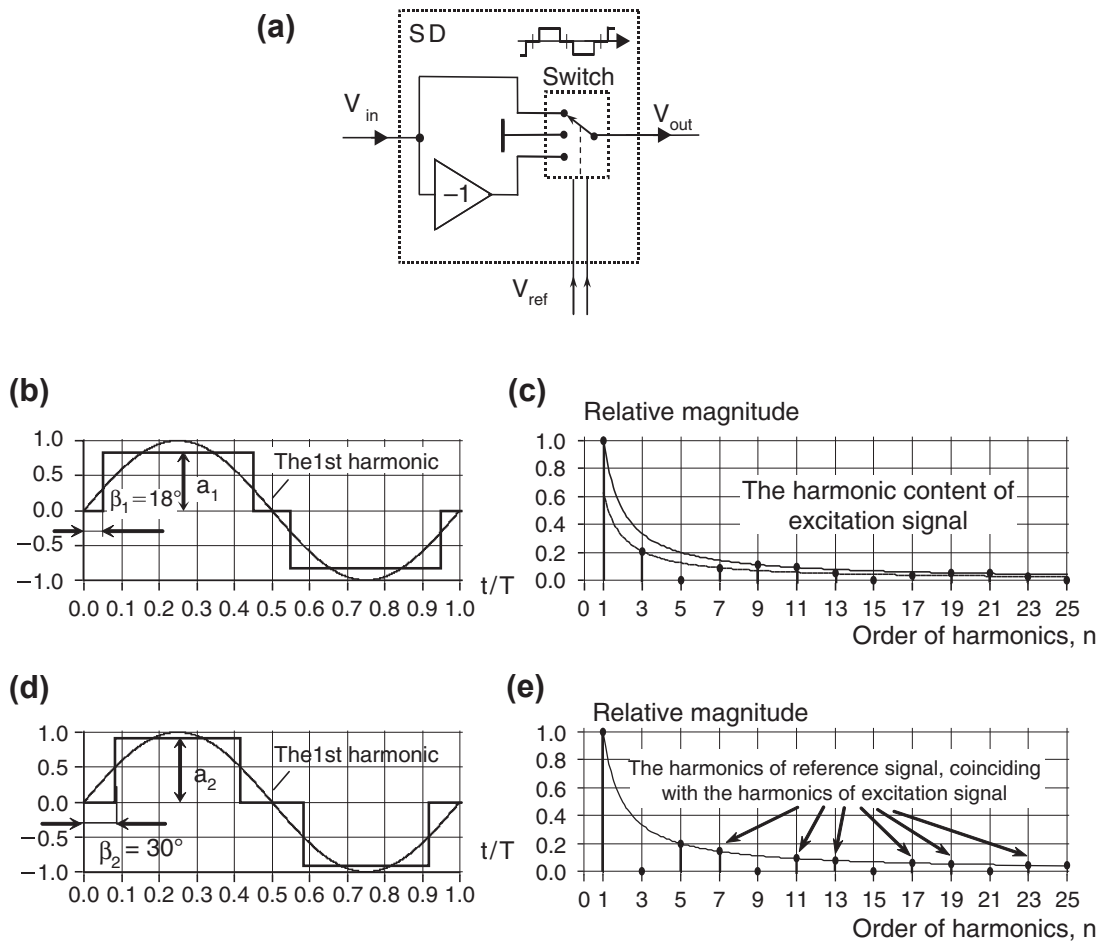


Figure 8.29: Circuit diagram of the modified synchronous detector (a), and the approximated sine waves with suppressed fifth harmonic (b) and its spectrum (c), and with suppressed third harmonic (d) and its spectrum (e).

ASIC solutions for medical devices is given in Yan et al. (2013), including an excellent design of the 13 μ A consuming intracardiac impedance measurement device for using in implantable pacemakers.

8.3.9 Impedance Analyzers and LCR Meters

When measuring electrical impedance, the main specifications are frequency and impedance measurement ranges, precision, speed, and points per sweep. Just as important are requirements of the test setup like two-, three-, or four-electrode configuration, bias control and scalability—when it comes to multichannel or high

throughput problems. Because most applications of bioimpedance require special care contacting a “device under test” (e.g., biochips, skin electrodes, special preamplifiers), the interface and extension possibilities of the instruments are also to be considered. When looking at instruments for impedance spectroscopy it is essential to look deeper than just the plain key specification from a product summary. Both precision and speed are at least dependent on frequency and absolute value of the measured impedance. Thus it is important to look at the range-precision plots showing which precision can be obtained at what absolute value and frequency. Some manufacturers also have tuneable precision settings to optimize the tradeoff between speed and accuracy. Determining the actual precision and speed at a certain target impedance requires a closer look at instrument datasheets and manuals. In general, it will be a good idea to contact the instrument manufacturer for support—either way, one has to beware of simplification to data sheet facts.

Impedance Analyzer

The best solution for broad measurement range, large-frequency spans, and high-resolution impedance spectroscopy without a doubt are dedicated precision impedance analyzers. Manufacturers of precision impedance analyzers are for example Agilent, Inphaze, Novocontrol, Solartron Analytical, Sciospec, or Zurich Instruments. Three very prominent examples are Agilent 4294A, Solartron 1260A, and Sciospec ISX-3.

The versatile precision impedance analyzer Agilent 4294A has been around for many years and has become a standard instrument in research. It uses an advanced type of the autobalancing bridge method allowing for measurements from $m\Omega$ to $30 M\Omega$ (range with 10% precision) in a frequency range from 40 Hz to 110 MHz. The maximum precision of 0.08% is available between 100Ω and $20 k\Omega$ up to 1 MHz. A maximum of 801 points per sweep allows for high-resolution spectroscopy and with minimum bandwidth setting the instruments performs relatively fast measurements (e.g., 3 ms/point at $f \geq 500$ kHz). The 4294A also covers a large DC bias range of ± 40 V/100 mA. Interface options are GPIB and Ethernet; for synchronization, one external TTL logic trigger is available and—showing just how long the instrument has been around—there is a 3.5" floppy drive. The 4294A has a base price of 36 k€ and can be combined with a broad choice of measurement adapters for component, material, or fluidic tests. Although the standard configuration uses four measurement ports, for many applications the 4294A does not allow for proper four-electrode measurements because the voltage and current electrodes must be connected together at the device under test. However, Gersing (1991) designed a special preamplifier for these analyzers that gives separate connections for the voltage and current electrodes. Such front-end amplifiers for increased measurement accuracy have also later been designed by e.g., Yelamos et al. (1999).

Just as well-established in electrochemistry and material test is Solartron Analytical's 1260A impedance analyzer. This instrument ranges from 100 to 100 M Ω (10% precision range) at frequencies from 10 μ Hz to 32 MHz. The maximum precision of 0.1%, 0.1° is available between 10 Ω and 100 k Ω up to 100 kHz. The system includes two differential voltage ports and one current measurement port supporting true two, three, and four terminal configurations and polarization voltages of up to \pm 40.95 V. The 1260A comes at a base price of 30 k€. Internally the system uses a single-sine correlation technique similar to digital lock-in after sampling the signals with 16-bit ADCs. For the highest frequency range (65.5 kHz to 32 MHz), an analog phase-locked loop system is used generating both the high-frequency output waveform to the sample under test and an internal high-frequency reference signal, which is arranged to be at a slightly different frequency than the output waveform. The input waveform is mixed (heterodyned) by this reference waveform to produce a sum and difference frequency. The sum frequency is filtered leaving the low-frequency waveform, which can then be analyzed using the ADC. A digital heterodyning process is used for measurements in the mid-frequency band (300 Hz to 65.5 kHz) to mix the input signals down to low frequency. Low-frequency measurements up to approximately 300 Hz are measured directly by the ADC. Although this technique yields very good precision, it makes the measurements inherently slow (minimum measurement time 10 ms per point). To make up for this, Solartron also offers fast Fourier transform-based multisine measurements speeding up the measurements at the price of lower precision. To further improve the instrument's performance in four-electrode measurements, the 1294 dielectric interface has been developed by Solartron as a preamplifier for the 1260A impedance analyzer (or any other frequency response analyzer). The 1294 makes use of driven shields, balanced generator, and high-input impedance voltage sense inputs to minimize stray currents to ground and hence maximize accuracy when measuring in difficult four-terminal conditions. In addition, this interface has been developed to comply with the IEC-60601 standard for connection of electrical equipment to live subjects. The 1294 can also be used for two- or three-electrode measurements.

Entirely dedicated to impedance measurement, Sciospec Scientific Instruments offers a range of standard laboratory products and original equipment manufacturer solutions. The basic Sciospec ISX-3 is a small form factor laboratory bench single-channel impedance analyzer supporting two-, three, and four-electrode configurations. The default front end option in I–V measurement topology offers a measurement range from DC to 10 MHz (optional extension up to 100 MHz) and m Ω to G Ω (10%). Maximum precision of 0.05% is available between 10 Ω and 1 M Ω over the entire frequency range. Measurement rates in sweep mode can be tuned, for example, down to 400 μ s at 500 kHz and in burst mode using internal data storage even further down to 10/f. The kinetic mode enables high time resolution measurements with single frequency points. For very high-resolution spectra,

the instrument supports up to 2048 points per sweep. Because of the lower hardware complexity required, using proprietary SineFit technology the ISX-3 starts at 6500 €. The default measurements work with single sine voltage excitation, but the generator also allows for complex excitation, multisine, and DC bias options. In combination with optional electrochemical modules, potentiо- or galvanostatic control is available.

Measurements are performed with high input impedance instrumentation amplifier circuits (voltage) and virtual ground biased transimpedance amplifier topology (current). Next to default coaxial measurement ports, the instrument also includes a general purpose extension port for application specific front ends and modules like Sciospec's multiplexers or the MEArack biochip/sensor adapter. Besides the ports for four electrode measurements, the extension port also carries supply rails and configurable digital IOs that can also be used as UART, SPI, or I2C interfaces. The port's specifications and interface are open access enabling users to build their own application specific modules such as adapters, multiplexers, fluidic chambers, and amplifiers. High-speed USB, Ethernet, or optional wireless interface are used for control from a PC and the system can be optionally extended with integrated graphical user interfaces, data analysis, and storage for stand-alone instrument use. The Com-Interface allows for full instrument control from Java, C, LabView, Matlab, and so on. Additional fast hardware synchronization is possible through several sync in/out ports.

Electrochemistry Instruments

For applications with primary focus on electrochemistry potentiostats/galvanostats with impedance measurement option are also to be considered. Although some have integrated modes for impedance spectroscopy, others require a so-called frequency response analyzer (FRA) module—a separate instrument that uses the potentiostat/galvanostat as front end for the impedance measurements. Solartron dielectric front ends such as the 1287A can be combined with an FRA like the 1255B to enable impedance spectroscopy. The well-known Metrohm Autolab product range also has impedance measurement capabilities with the additional FRA32M module. Electrochemical systems with integrated impedance functionality can be found in potentiostats/galvanostats from several manufacturers such as Ivium, Gamry, Sciospec, or PalmSens. Although most are rather slow and have limited specifications compared with actual impedance analyzers, the advantages of these configurations lie within the very good electrochemical control options and high current/voltage range options.

LCR Meter

Another option to measure electrical impedance are inductance (L), capacitance (C), and resistance (R) (LCR) meters, typically using various bridge circuits, adjusting variable reference elements until a detector signal becomes null. Newer generations also make use of the more general I–V-measurement approach. These are very common

instruments for electronics engineers, which results in a great variety of instruments and manufacturers to choose from, most of which at a rather small price tag—especially the very basic handheld LCR meters. Common manufacturers include IET Labs, Hameg, Sourcetronic, Agilent, GW Instek, Wayne Kerr, and many more. Most of these devices are rather simple instruments intended not for impedance spectroscopy, but for testing electrical components for their specifications (e.g., ESR, ESL measurements on capacitors). For this purpose, no spectral resolution is required because component specification is given only at singular frequency points. Thus LCR meters usually only have a few selectable test frequencies. More advanced instruments also offer sweep functions but typically only with 5–20 points per sweep. A quite typical example for a precision LCR meter would be the Hameg HM8118, which comes at a typical price of 1600 €. It offers precisions better than 0.5% between 10 and 10 MΩ for frequencies from 20 Hz to 200 kHz at up to 80 ms measurement rate, but will only measure at one frequency point per setup. Maximum precision of 0.05% is achieved from 100 Ω to 1 MΩ up to 1 kHz. The Sourcetronic ST2827A (1800 €) offers similar specifications and also includes a 10-point list sweep option with up to 13 ms measurement rate. The precision of an LCR meter measurement greatly degrades with speed and specifications for the base precision are always given for the “slow” modes. In case of the ST2827A, a measurement with 0.1% precision for a 1 pF capacitance will take 187 ms. In terms of range, speed, and sweep functionality, there are also exceptions in the high-end system range. Those already come close to actual impedance analyzer functionality, but of course also have significantly higher price tags. For example, the Agilent E4980A (13.5 k€) will measure mΩ to 100 MΩ (10% precision range) in the range between 20 Hz and 2 MHz. The downside is the speed: full range can only be met in slow configuration with 180 ms per point at $f > 1$ kHz. Nonetheless, the performance and the list sweep function with up to 201 points enable the device to acquire impedance spectra. For high-frequency demands, there are also RF LCR meters such as the Agilent E4982A (25 k€), which will measure mΩ to kΩ in the range from 1 MHz to 3 GHz. Bottom line—LCR meters are in general relatively affordable but rather slow instruments with limited frequency and impedance range, suited for only single frequency or small sweep measurements. LCR meters in general are perfect for electrical component test, but not well suited for precision high-resolution impedance spectroscopy.

Network Analyzer

For RF measurements, another class of instruments is available. Modern high-end network analyzers range up to 110 GHz. These instruments use reflexion measurements to determine ratios of inserted to reflected power. Because of the use of directional couplers, the lower frequency limit will typically not go below a few kHz. To obtain complex impedance values, a vector network analyzer (VNA) is needed, because scalar network analyzers give absolute values only. Measurements can be conducted very fast

with up to 10 μs per point and sweeps with high frequency point counts are available. Though the frequency range is enormous, even high-end VNAs with a large dynamic range only support relatively small impedance ranges. Because VNAs are designed for characterization of electrical networks, antennas, RF-circuit board traces, or RF-interconnect assemblies, the systems are optimized for impedances around 50 Ω for general purpose or 75 Ω for video applications. Accordingly, the optimum precision will be achieved in this range and resolution degrades rapidly for larger impedances. Typical maximums are around a couple of kilo-Ohms. Also care must be taken for measurement evaluation, because most VNAs display results as S-parameters and only few have integrated calculation of impedance, capacitance, or other typical electrical parameters. Typical network analyzers are built by Rohde & Schwarz, Agilent, or Anritsu and range from around 25 k€ up to well over 100 k€ for high-end devices. Over the past few years, some other instruments with less range, less precision but also significantly lower price tag have emerged, such a Omicrons Bode 100 (4200 €). Another noteworthy instrument is the Agilent E5061B (starting at around 26 k€) that comes with an LF option for combination of LF impedance measurement and RF network analysis. The instrument operates in referenced gain-phase mode (true impedance) for 5 Hz to 30 MHz and has a 10% precision range from 3 Ω to 40 k Ω . There are at least three other modes, for example, single port reflection (up to 3 GHz between 1 Ω and 2 k Ω), but the use of full ranges will require switching modes and ports resulting in nonuniform spectra and piecewise measurements that require additional user calibration. Although the overall frequency coverage is impressive, the downside is a rather low precision of only 3% and a small impedance range that is typical for network analyzers. In summary, network analyzers are almost unavoidable for frequencies higher than 100 MHz, but are limited in low-frequency ranges and even high-priced devices offer limited precision and relatively small impedance ranges usually not extending above a couple of kilo-ohms.

Spectrum Analyzers

Frequency domain dedicated instrumentation such as, for example, spectrum analyzers and Fourier analyzers, can also be used for impedance measurements. In combination with a suitable signal generator, a variety of excitation functions may be chosen and the transfer function of the measured object can hence be found by analyzing the response spectrum. Spectrum analyzers are typically swept-tuned, superheterodyne receivers that display amplitude versus frequency. However, unlike the Fourier analyzers, spectrum analyzers do not provide phase information. Fourier analyzers use digital sampling and mathematical algorithms to form a Fourier spectrum of a signal, and they can be used for both periodic and transient signals. In comparison to bridge circuits and single sine correlation or lock-in techniques, the precision of these frequency domain techniques is usually limited to a

few percent and care must be taken to eliminate artifacts, distortion, and other complex phenomena to achieve high precision results.

Scalability, Multichannel and Portable Devices

Typical issues beyond the measurement parameters themselves arise with the need for multichannel measurements, portability, or other requirements deviating from standard single-channel laboratory bench solutions or requiring atypical measurement modes. For multichannel needs without true parallel requirements, multiplexers are offered by some of the manufacturers already mentioned (e.g., PalmSens, Sciospec), but true multichannel is rare. Solutions with parallel impedance measurements within one instrument are available with Uniscan, Solartron ModuLab, Solartron 1470E, Multi-Autolab Series, and Sciospec ISX-5. In theory, most of the multichannel devices have the capability to perform nonstandard measurement modes, but only few incorporate more than an additional bias sweep or the choice between synchronous and asynchronous measurements. The ISX-5 system also allows for multiple analysis ports with single excitation source (including focused impedance method) and nonlinear impedance spectroscopy. Portable devices are uncommon as well. Except for simple and not very precise portable LCR meters, commercially available portable solutions are just now emerging: for example, Sciospec IsX3 mini has just been released and the newest PalmSens portable potentiostats also include small range EIS capability. A couple of publications have been reported that present self-made solutions for compact portable systems, most of which are based upon the AD5933 integrated impedance front end chip by AnalogDevices. Another way to cover special application needs is highly specialized systems, such as for typical cell tests. In recent years, a number of such devices have been commercialized. Good examples are the ACEA Xcelligence, NanoAnalytics CellZscope, or the more recent Nanson cardioExcite systems, all of which make use of impedance measurements but are not capable of performing general impedance spectroscopy experiments. The Xcelligence for example does not give complex impedance values but rather calculates an abstract cell index parameter that represents certain physiological changes in cell cultures. In impedance-based biomass monitoring, there are also specialized solutions from companies like Aber Instruments or Hamilton (former Fogale). A more general approach is provided by Sciospec with a modular instrumentation platform specifically targeting affordable application specific solutions. The system concept allows for simple scalability and migration between laboratory setups and original equipment manufacturer developments. The modular structure also extends beyond plain impedance spectroscopy. Impedance measurement modules can be used in combination with electrochemical control units, high-speed massive multichannel data acquisition cards for electrophysiological field potential measurements, temperature control, laser control, or optical measurement modules all in the same modular concept for complex measurement tasks.

8.3.10 Time Domain Spectroscopy

The time domain approach is advantageous for fast measurement requirements. Given the hardware available today, the accuracy can compete with that of measurements in the frequency domain (Feldman et al., 2003). The most important excitation signal in the early days was either a pulse (square or Dirac function) or a rectangular wave. Today new concepts such as multisinus excitation, ultra-wide band pseudo-noise sequences (Sachs, 2007), or wavelets have emerged. The purpose of the new concepts is to emphasize important regions of the spectrum while maintaining a low crest factor.

An advantage of time domain-based measurements is the option to compensate for parasitic reflections and transmission losses at specific parts of the measurement arrangement, such as connectors or cables. In the frequency domain, the excitation frequency is swept over a range that can be longer than eight decades for some commercial devices. The sweep time depends on the range and numbers of frequencies. This can be easily tens of seconds up to several minutes.

The basic feature of time domain spectroscopy (TDS) is the application of a broad bandwidth signal containing all the frequencies together. A typical signal with broad bandwidth is the square wave (Teorell, 1946). Other popular signals are the Dirac pulse, the multisinusoidal excitation, and the Gauss burst or wavelets.

Using Fourier transformation, the signal can be transformed into the frequency range, yielding the phase-sensitive amplitude for discrete frequencies ([Figure 8.30](#)).

Thus, a broad frequency range (several decades) can be obtained at once. Because the amplifiers need to have an adequately high bandwidth, different from the selective

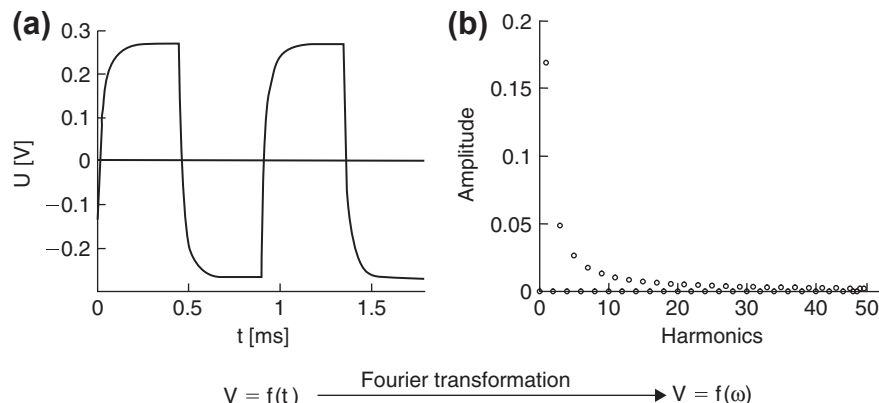


Figure 8.30: Basics of transformation from time to frequency domains.

amplifiers used in the frequency domain, the measurement chain is sensitive to noise. The highest measurement speed in TDS can be achieved when only one period is acquired. However, the noise will limit the useful bandwidth. When the speed of measurement is not so strict, averaging of several periods is possible, thereby enhancing the SNR greatly.

As an example, Sanches et al. (2013a,b,c) developed methods and instrumentation that created an optimal broadband multisine signal in a given frequency range, by using other a priori information like the expected shape of the impedance spectrum. They were able to acquire an impedance spectrum about every 5 ms (1 kHz–1 MHz) and applied mathematical methods to identify nonlinearities and other limitations of the measurement system and also identify the object under test in the case of time-varying impedances.

Fast measurements also require fast and robust parameter extraction. Büschel et al. (2011) compared the usability of stochastic algorithms, evolution, simulated annealing, and particle filter for robust parameter extraction from impedance spectra and concluded that particle filter delivered the most reliable results.

8.3.11 Time Domain Transmissometry

For low-frequency application (mHz to MHz), the classical approach using two or four electrodes interfaces are commonly used. The three electrodes interface is usually employed in conjunction with active electrical properties at surfaces, such as sensor surfaces. Because the behavior within the immediate vicinity of the working electrode overwhelms the measurement, the results are basically monopolar measurements.

The front ends used in time domain transmissometry are similar to those employed in frequency domain measurements. However, extra care should be taken to ensure high linearity and stability against transient voltage or current changes.

A very simple approach is shown in [Figure 8.31](#). The material under test (MUT), which may be, for instance, a cell suspension or tissue, is connected in series with a resistor R_m . It should be noted that the electrodes for such a simple arrangement should be large to ensure a low current density. Otherwise, the electrode polarization will dominate in the result of the measurement.

The broad bandwidth signal, which may be simply a rectangular wave, is applied to the MUT and the deformation of the voltage response is then measured ([Figure 8.31](#), right panel).

The voltage across the MUT (V_{MUT}) is deformed with respect to the stimulus V_{applied} , as a consequence of capacitance charging (e.g., cell membranes). In the simple case of a

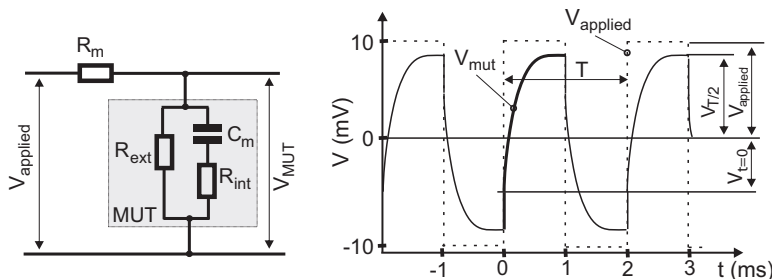


Figure 8.31: Simple arrangement for time domain measurements and the corresponding waveforms when using a square wave excitation. V_{applied} is the stimulus and voltage across the MUT (V_{MUT}) the voltage response. R_m is a measuring resistor. T is the duration of one period. $V_{t=0}$ is the voltage immediately after a positive step and $V_{T/2}$ the voltage immediately before a negative step.

typical three-element circuit, the deformed signal is an exponential function. Provided that the applied and the response signal are monitored, acquired, and transmitted to a computer, then these time domain signals can be converted to the frequency domain using standard engineering calculations (e.g., Fourier transformation).

Besides this, using relaxation theory, the resistance and capacitance values of the elements of the equivalent circuit can be directly calculated from the V_{MUT} . One half period of the deformed signal (Figure 8.31, right panel, thick line) yields an exponential function for V_{MUT} . If the time constant of the MUT is short compared with the period T (i.e., V_{MUT} becomes almost steady at $T/2$), then V_{MUT} is related to the elements of the equivalent circuit as follows:

$$V_{\text{MUT}} = \frac{V_{\text{applied}}}{R_{\text{ext}} + R_{\text{int}}} \left(R_{\text{ext}} - \frac{2 R_{\text{ext}} R_{\text{int}} R_m}{R_{\text{ext}} R_{\text{int}} + R_{\text{ext}} R_m + R_{\text{int}} R_m} e^{-t/\tau} \right) \quad (8.49)$$

$$\tau = \frac{(R_{\text{ext}} R_{\text{int}} + R_{\text{ext}} R_m + R_{\text{int}} R_m) C_m}{R_{\text{ext}} + R_{\text{int}}} \quad (8.50)$$

which can be fitted (e.g., Levenberg–Marquardt algorithm) to a simple model

$$V_{\text{MUT}}(t) = A_0 - A_1 e^{-t/\tau} \quad (8.51)$$

This is the typical result in TDS yielding the time constant τ , and the relaxation strength A . In contrast to a three element circuit, more complicated objects yield several time constants over a wide frequency range. More sophisticated is the calculation of distributed time constant as it would be required for the Cole model.

The direct result of the measurement and calculations are the time constants and the relaxation strength. Furthermore, if one seeks the impedance of the elements of the equivalent circuit, it can be calculated for the condition shown in Figure 8.31 using:

$$\begin{aligned} R_{\text{ext}} &= \frac{A_0 R_m}{V_{\text{applied}} - A_0} & R_{\text{int}} &= \frac{2 V_{\text{applied}} R_{\text{ext}}^2 R_m - A_1 R_{\text{ext}} R_m (R_{\text{ext}} + R_m)}{A_1 (R_{\text{ext}} + R_m)^2} \\ C_m &= \frac{\tau (R_{\text{ext}} + R_{\text{int}})}{R_{\text{ext}} R_{\text{int}} + R_{\text{ext}} R_m + R_{\text{int}} R_m} \end{aligned} \quad (8.52)$$

The presented equations are the solutions only for the example shown in Figure 8.31. The solution to any other system can be found using linear system theory. It should be noted that this simple arrangement works in practice, if the rectangular wave is nearly ideal with fast rising and falling edge. Moreover, electrodes should be large enough to keep electrode polarization at a minimum.

Additionally, another often used approach is the application of a voltage clamped stimulus and converting the current through the MUT into a voltage by means of a transimpedance circuit as shown in Figure 8.32.

The current I_{MUT} is related to the elements of the equivalent circuit as follows:

$$I_{\text{MUT}} = V_{\text{applied}} \left(\frac{1}{R_{\text{ext}}} + \frac{2}{R_{\text{int}}} e^{-t/\tau} \right) \quad (8.53)$$

Together with $V_{\text{out}} = -I_{\text{MUT}} R_m$, the calculation of the three elements is straightforward. Note that the doubling of the second term in the parenthesis is the result of the applied voltage step from $-V_{\text{applied}}$ to $+V_{\text{applied}}$.

The very simple approaches shown in Figures 8.31 and 8.32 rely on some assumptions. First, the rectangular wave is nearly ideal with instantaneous rise and quite stable during a half period. Second, the electrodes are big enough to keep electrode polarization at a minimum.

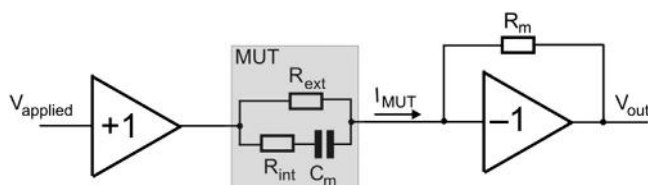


Figure 8.32: Arrangement for voltage clamped stimulus and monitoring of the current I_{MUT} as voltage output of a transimpedance.

A more sophisticated approach is the application of a current signal to the MUT and to monitor the voltage developed across it. Moreover, the use of a second pair of electrodes for voltage monitoring reduces greatly the electrode polarization (Figures 8.33 and 8.34).

To illustrate the method, the measurement on a potato is shown in Figure 8.35. The electrode system consists of four needles (20 mm long, inner electrodes 20 mm apart, diameter of one needle 3 mm).

The calculation of the equivalent circuit becomes very simple when the period is much larger than the time constant for charging the membranes, $T \gg \tau$, i.e., at $t = T/2$ the steady-state voltage is already reached.

$$R_{\text{ext}} = \frac{V_{T/2}}{I_{\text{applied}}} \quad R_{\text{int}} = \frac{R_{\text{ext}}(V_{T/2} + V_{t=0})}{V_{T/2} - V_{t=0}} \quad C_m = \frac{\tau}{R_{\text{ext}} + R_{\text{int}}} \quad (8.54)$$

This very simplified approach yields a rough approximation of the impedance but works for a variety of applications. It is more accurate to use both current and voltage for the calculation

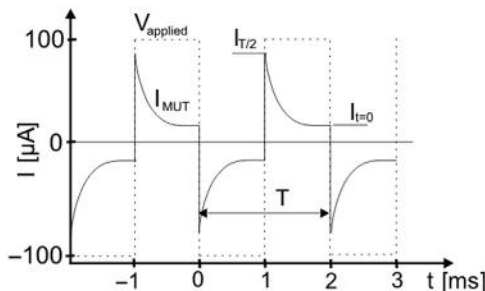


Figure 8.33: Current I_{MUT} as response to a voltage clamped square wave (dashed line).

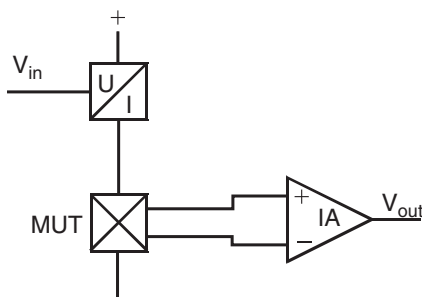


Figure 8.34: Impedance measurement using current excitation and a tetrapolar interface. The V/I-converter supplies the current, whereas the high impedance instrumentation amplifier yields the voltage difference across the inner electrodes.

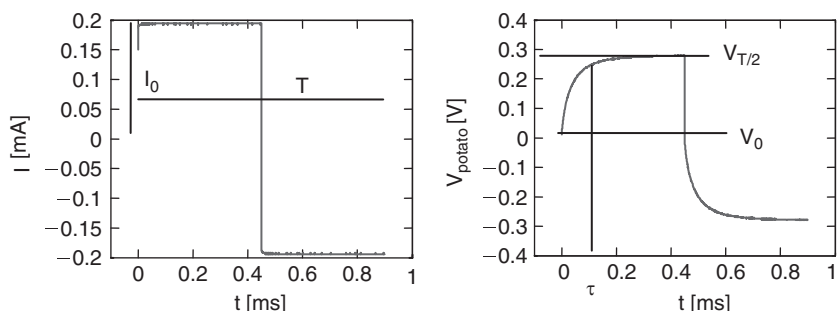


Figure 8.35: Typical signal captured with an oscilloscope. The applied current I_{applied} is $\pm 190 \mu\text{A}$ and the period is 0.9 ms.

and not only some indicative points but the entire trace. The common approach is to calculate the impedance as the ratio between the Fourier-transformed voltage and current.

$$Z(j\omega) = \frac{F(V(t))}{F(I(t))} \quad (8.55)$$

In the special case with no DC offset, we find the zeroth coefficient (DC component) zero as well. Because of the symmetry, each even coefficient will also be zero. Note that several programs, such as Matlab (The Mathworks Inc.), start with the first coefficient which is then the DC part ([Figure 8.36](#)).

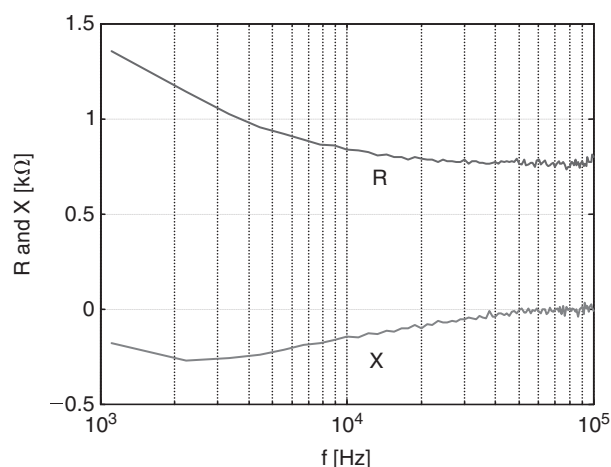


Figure 8.36: Impedance spectrum of a potato measured in time domain.

8.3.12 Time Domain Reflectometry

The MUT is placed at the end of a transmission line (i.e., coaxial cable). The cable has a characteristic impedance (Z_0), whereas the MUT in the case of biological matter shows a capacitive behavior (Figure 8.37).

An incident wave (E_{INC}) propagates through the transmission line up to a point where the dielectric behavior is changing (end of the line). This yields reflection and the reflected wave (E_{REF}) travels back.

The reflection coefficient is

$$r = \frac{E_{REF}}{E_{INC}} \quad (8.56)$$

which in terms of voltage monitored at one point of the line is

$$r = \frac{V_{REF}}{V_{INC}}. \quad (8.57)$$

The voltage at any point of the line is the sum of both, the voltage of reflected (V_{REF}) and the incident (V_{INC}) wave (Figure 8.38).

$$V = V_{INC} + V_{REF} \quad (8.58)$$

But, because the direction of both waves is opposite, the currents also (I_{INC} , I_{REF}) have opposite direction. Therefore, the current is

$$I = I_{INC} - I_{REF} \quad (8.59)$$

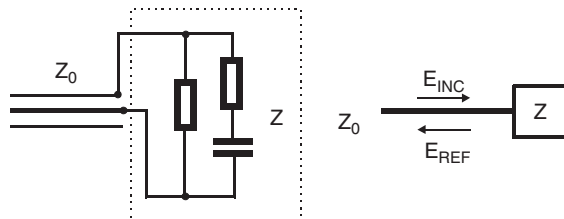


Figure 8.37: Coaxial transmission line connected to a complex impedance. The incident wave E_{INC} is applied, whereas the reflected wave E_{REF} is reflected at the MUT.

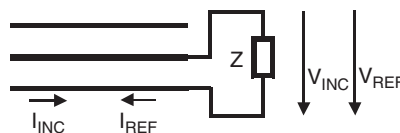


Figure 8.38: Voltage and current at the object and inside the transmission line.

According to Ohm's law, the impedance of the MUT is

$$Z = \frac{V}{I} = \frac{V_{INC} + V_{REF}}{I_{INC} - I_{REF}}. \quad (8.60)$$

Because the current at the transmission line is

$$I = \frac{V}{Z_0} = \frac{V_{INC} - V_{REF}}{Z_0} \quad (8.61)$$

we find

$$Z = \frac{V_{INC} + V_{REF}}{V_{INC} - V_{REF}} Z_0 \quad \text{or in terms of } r \quad Z = Z_0 \frac{1+r}{1-r} \quad (8.62)$$

It should be noted at this point that this simple approach is only valid for MUT with no spatial distribution. If the chamber does not have negligible geometrical length or the measurement aims in the assessment of higher frequencies, one has to account for the field distribution within the chamber. For more information, refer to Cole et al. (1989).

There are three special cases—the open line, the short circuit, and the termination with a matching resistor.

1. Open line $\lim Z \rightarrow \infty$

In case of an open line, no energy can be dissipated at the end of the line, thus all energy is reflected and the reflected voltage equals the voltage of the incident wave: $V_{REF} = V_{INC}$. The reflection factor is $r(Z \rightarrow \infty) = \frac{V_{REF}}{V_{INC}} = 1$.

2. Matched line $Z = Z_0$

If the impedance of the MUT equals the characteristic impedance of the cable, all the energy is dissipated by the MUT. Because nothing is reflected, r becomes zero.

3. Short circuit $Z = 0$

Because no voltage drops across an open circuit, no energy is dissipated by the MUT. Therefore, all energy is reflected but with the opposite polarity: $V_{REF} = -V_{INC}$. The superposition of the incident and the reflected voltage is zero. In case of sinusoidal voltage, the reflected wave shows a phase jump of 180° at the MUT.

$$\text{The reflection factor is } r(Z = 0) = \frac{V_{REF}}{-V_{INC}} = -1$$

Measurement Using Time Domain Reflectometry

We consider a transmission line consisting of a 50Ω coaxial cable (RG58, RG174), which is terminated by different loads. A square pulse (50 mV, 200 ns) travels along the cable

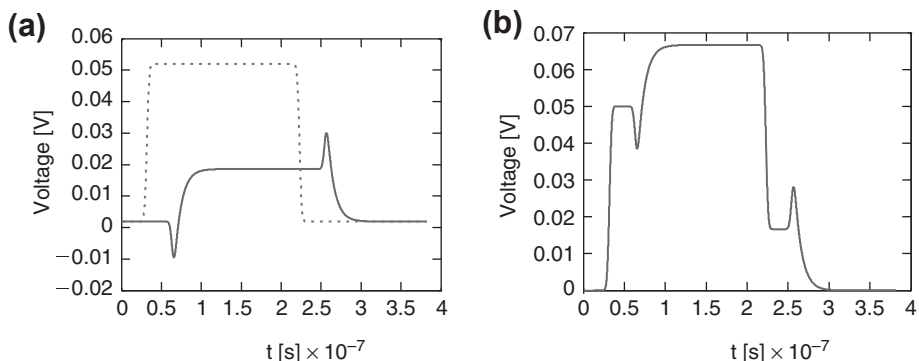


Figure 8.39: (a) Incident (dotted) and reflected (solid) waveform for the three element impedance and the corresponding voltage at the monitor (b).

(Figure 8.39). To make things simple, we are not going to consider any distortion caused by the cable itself.

The reflected voltage at a certain distance is shifted along the time axis since the speed is limited to $v = \frac{c_0}{\sqrt{\epsilon}}$ where c_0 is the speed of light in vacuum and ϵ is the permittivity of the material between the inner and the outer conductor of the cable.

The simulation shows the voltage at the entry of a 3-m-long cable terminated with a three-element impedance consisting of a 100Ω resistor in parallel with a serial combination of a 20Ω resistor and a 1 nF capacitor (Figure 8.39). The excitation pulse (dotted) has an amplitude of 50 mV and a rise time of 4 ns. The delay between the signals is caused by the delay time along the cable. First the reflected voltage becomes negative because of the impedance at high frequency (100Ω parallel to 20Ω) is less than the characteristic impedance of the cable resulting in a negative reflection factor. With consecutive pulses, the capacitive elements become increasingly charged. This decreases the current through the MUT and thus the impedance becomes bigger than that of the cable and the reflected wave becomes positive. The voltage monitored for instance by an oscilloscope at the entry of the cable is the sum of the incident and the reflected voltage as seen in the right panel of Figure 8.39.

Electrode Polarization

A conductive sample yields electrode polarization that is evident even at frequencies above 10 kHz. A simple correction is the modeling of electrode behavior using a capacitor for the double layer. Because the current will be known, one can calculate the voltage across the capacitor and correct the voltage across the MUT. For more sophisticated procedures, consult the literature (Schwan, 1992a). More on electrode polarization can be found in Section 7.9.

Besides of partly mathematical correction of the electrode polarization, it is a challenge to find the right electrode configuration and the right electrode material. A widely used electrode is the open-ended coaxial probe. Besides this, coaxial chambers (see example) are often used, especially for cell suspensions. This works well up to the frequency where the center electrode acts as antenna and disturbs the impedance because of its resonance behavior. The correction of this can be found in Cole et al. (1989). Another approach is the use of antennas, which needs some more attention because of multiple reflection and the relatively weak reflected signal.

8.4 Nonlinear Phenomena

In Section 8.1, the conditions for black box theory are found. To be valid the network must be *linear*, passive, and causal. A nonlinear system is a system that does not obey the superposition theorem, the output of a nonlinear system is not proportional to the input.

If linear, a sine excitation input results in a sine response. However, the admittance concept can be extended to nonlinear networks, where a sine wave excitation leads to a nonsinusoidal response. Including a separate admittance value for each harmonic component of the response performs the necessary extension. In the linear region, the principle of superposition is valid. This means, for example, that the presence of strong harmonics in the applied current or voltage would not affect admittance determination at the fundamental frequency or a harmonic (Schwan, 1963). Some lock-in amplifiers can measure harmonic components, making it possible to analyze nonlinear phenomena and extend measurement to nonsinusoidal responses.

In the nonlinear region, the principle of superposition is not valid. When measuring in the nonlinear region, it is necessary to state whether the system uses constant amplitude current (current clamp) or constant amplitude voltage (voltage clamp). With, for example, constant amplitude voltage, the voltage per definition is sinusoidal, but the current is not. If the measuring system is able to measure selectively sufficiently many current harmonic components (and a possible DC component, rectification), the actual current waveform in the time domain is defined. Such a steady-state nonlinear analysis is well suited in the low excitation energy end of the nonlinear region. At higher current densities used for instance in defibrillator shocks, steady state cannot be obtained (temperature rise and destruction), and all measurements must be performed during one single pulse of energy.

8.4.1 Electrolyte Nonlinearity

The bulk electrolyte solution obeys Ohm's law (Eq. 2.2), which is linear. If the E-field changes the viscosity η in Eq. 2.6 or the number of ions per volume n in Eq. 2.1, then the system is nonlinear and does not obey Ohm's law (Wien, 1928; Onsager, 1934). This will

be the case at very high electric field strengths. According to the Debye–Hückel theory, the ionic atmosphere is symmetrical around the ion in the absence of an external electric field. In an electric field the ion migrates, but its atmosphere (ionic and hydrational) is retarded by friction and is no longer symmetrical around the ion (asymmetry effect). Accordingly, at high electric fields the conductivity increases because the ions move so fast that the retarding ionic atmosphere does not have time to form, it is stripped off (Wien⁵ effect; Wien, 1931).

8.4.2 Electrode Nonlinearity

From Figure 7.20 and the Butler–Volmer Eq. 7.15, it is clear that the DC resistance is strongly dependent on the DC current through the electrode. With an AC superimposed on a DC, the resultant AC is dependent on the incremental resistance/conductance of the DC curve. If excitation is sinusoidal, and the measured AC voltage or current also is sinusoidal, then the system is linear with the amplitudes used. By increasing the amplitude, there will always be a level when nonlinearity is reached.

A DC or pulse current polarizes the electrode, and from the electrolytic basic experiment described in Section 2.2 it is also clear that faradaic current flow changes the chemical environment at the electrode surface. Current carrying electrodes are used in such different applications as nerve stimulation, pacemaker catheter stimulation; and defibrillation with 50 A passing for some milliseconds. Often a square wave pulse is used as stimulation waveform (e.g., pacemaker), and the necessary overvoltage is of great interest (see Section 9.1). In such applications a clear distinction must be made between tissue nonlinearity (Section 8.4.3) and electrode nonlinearity (this section). Nonlinearity network theory is treated in Section 7.9.3.

For the electrode polarization impedance, it has been shown that it was possible to state a frequency independent *voltage* amplitude limit for linear behavior (Onaral et al., 1982). This limit is about 100 mV (average, corresponding to about 30 mV_{pp}) AC. The corresponding *current* limit will of course be frequency dependent, and be as low as 5 μA/cm² in the lower millihertz range and as high as 100 mA/cm² in the higher kilohertz range. A typical current limit for a platinum black electrode in saline is 1 mA/cm² at 1 kHz (Schwan, 1963). There is reason to believe that as the frequency approaches zero, the current limit of linearity flattens out around 5 μA/cm² where the electrode impedance becomes resistive (Onaral and Schwan, 1982).

With composite waveforms, the electrode may therefore operate in the nonlinear region for the low-frequency components, and in the linear region for the high-frequency components.

⁵ Max Karl Werner Wien (1866–1938), German physicist. Cousin of Wilhelm Wien (1864–1928), famous for the Wien displacement law, 1911 Nobel Prize laureate in physics.

The current density under a surface plate electrode is not uniform, with larger densities at the edge (Figure 6.6). The fractal properties of the electrode surface also create local areas of high current densities. The onset of nonlinearity may therefore be gradual, and start very early at very limited areas on the electrode surface. By harmonic analysis (see the following section), it has accordingly been found that very weak nonlinearity is measurable at much lower voltages than 100 mV.

In a practical case when current carrying electrodes are used with tissue, it may also be difficult to differentiate between the nonlinearity of the electrode processes and the tissue processes.

Electrode behavior in the nonlinear region may be studied by electrode polarization impedance $Z = R + jX$ measured as a function of sinusoidal amplitude. The limit current of linearity i_L may, for instance, be defined as the amplitude when the values of R or X deviate more than 10% from low current density values. Often i_L is increasing with frequency proportional to f^m (Schwan's law of nonlinearity) (Onaral and Schwan, 1982; McAdams and Jossinet, 1991a, 1994). m is the constant phase factor (as defined in this book) under the assumption that it is obeying Fricke's law and is frequency independent (Section 9.2.5). When the measuring current is kept $< i_L$ they showed that Fricke's law is valid down to 10 mHz. The limit current of linearity will usually be lower for X than for R.

Nonlinearity

Pulse polarization nonlinearity may occur during a single pulse if it lasts long enough to cause irreversible electrolysis. Pulses < 1 ms are mostly transferred to the tissue by capacitive current paths not implying electrolysis (non-faradaic current). The same rules are valid for *large AC current polarization*: the higher the frequency, the better the linearity.

A fractal model was used by Ruiz et al. (2005) to explain the nonlinear behavior of an electrode–electrolyte interface.

Metal–Liquid Overvoltage

During exogenic current flow, an overvoltage is created as well in the double layer, the diffusion layer, and the resistance in the bulk electrolyte. Many applications are in the nonlinear region of current–voltage ratios. With DC currents, the overvoltage may increase gradually and attain many volts with polarizable electrodes, accompanied by several possible effects of electrolysis at the electrode surface.

Neurostimulation is usually performed with needles, and square wave pulses of amplitude < 5 mA and duration < 1 ms are common. Nerve stimulators may be with or without a net DC component. With skin surface electrodes, the current used may be larger.

Pacemaker pulses are usually short AC pulses with a zero DC component, and the overvoltage is mainly determined by the double layer capacitance (Jaron et al., 1969).

In *iontophoresis or antihyperhidrosis* treatment (Section 10.4.3), electrodes are used with continuous DC current. During such conditions, the volume of the electrolyte compartment is of interest with respect to the buffering capacity for the products of electrolysis.

Geddes et al. (1975a) measured the current/voltage characteristics with a 5 ms duration heavily damped sinusoidal *defibrillator* pulse. Standard defibrillator electrodes 3.5" in diameter (60 cm^2) were used with current pulses up to 80 A. The electrodes were face-to-face at 1 cm distance with the space filled with a $8.4 \Omega\text{-cm}$ electrode paste. It was found that the impedance of both electrodes (defined as the ratio of *peak* voltage to *peak* current) at such current levels was only a fraction of 1Ω . With the usual thorax tissue impedance of about 50Ω , little energy therefore is lost in electrode polarization processes. The 0.01 Hz impedance of the same electrode pair with small linear AC current levels was found to be about $2 \text{ k}\Omega$. This shows the extreme degree of nonlinearity.

8.4.3 Tissue and Cell Nonlinearity

Nonlinear behavior in suspensions has been studied, for example, Block and Hayes (1970) and Jones (1979); for electroporation, see Section 10.11.1; for defibrillation, see Section 10.9.1. Memristive elements are described in Section 9.2.11.

At a sufficiently low volume power density, every biomaterial is linear. At a sufficiently high volume power density, every biomaterial is nonlinear. Many applications make use of the nonlinear region, where the principle of superposition no longer is valid. The nonlinearity may be a property of the biomaterial, or of the electrode/electrolytic systems used.

At the *atomic and molecular* levels, some of the charge displacements will reach saturation at high E-field strength levels (Section 8.4.1). The alignment of dipoles in a polar dielectric will reach a maximum when the field energy is of the same order of magnitude as the Boltzmann factor kT .

At the *cellular* level, the cell membranes of polarized cells are of the order of 10 kV/mm , and additional field strengths may easily bring the membrane into a nonlinear region even without cell excitation. Cell excitation, the opening of membrane channels, and the creation of an action potential are the result of nonlinear processes. Electroporation and electrofusion of cells *in vitro* (Section 10.11) are also processes in the nonlinear region.

In human *skin*, Yamamoto et al. (1981) found the upper limit of linearity to be about $10 \mu\text{A/cm}^2$ at 10 Hz and $100 \mu\text{A/cm}^2$ at 100 Hz. Ionic flow through human skin *in vivo* is

probably constrictional through special zones of high conductance (Grimnes, 1984). Thus nonlinear phenomena may occur at such low average current densities.

They ascribe this phenomenon to the ionic conduction in the keratins of the stratum corneum. Electro-osmosis in the sweat ducts causes strong nonlinear effects with only a few volts DC (Grimnes, 1983b; Figure 8.40). A dielectric breakdown will occur at very high electrical fields in the stratum corneum. Grimnes (1983c) found that dry skin on the dorsal side of the hand did withstand 580 V DC for more than 3 s, but that breakdown was immediate at 935 V (Figure 8.41). These are astonishing high values remembering that the stratum corneum often is of the order of 15 μm thickness. With negative polarity, the breakdown is much more pronounced caused by electro-osmotic transport of electrolyte solution from deeper living parts of the skin.

There are some important *clinical* applications involving nonlinearity:

Defibrillator current of >50 amps over a 60 cm^2 electrode area implies a current density around 1 A/cm^2 (Section 9.10). This is clearly in the nonlinear region both for skin and living tissue, and actually the skin is reddened particularly under the electrode edge after a shock has been given. Geddes et al. (1976) reported that the resistance found from measured peak voltage with a 20 A peak current pulse with two 60 cm^2 electrodes corresponded with the small signal impedance measured at 30 kHz. During successive defibrillator shocks, a decrease in transthoracic impedance has been reported (Geddes et al., 1975b). After ten 400 J shocks, the impedance fell to 80% of the initial value. These effects must probably be contributed to cell membrane and myocardium

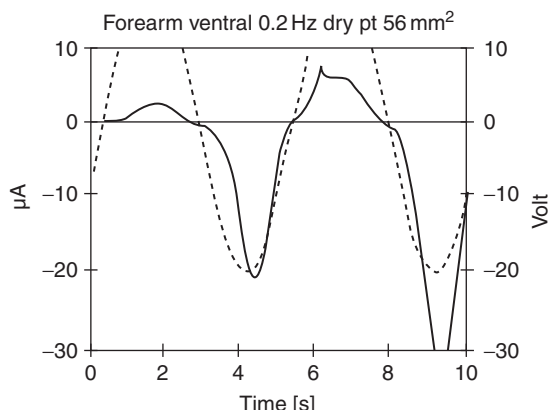


Figure 8.40: Voltage—current curves showing electro-osmosis and strong nonlinearity in human skin *in vivo*. From Grimnes (1983b) by permission.

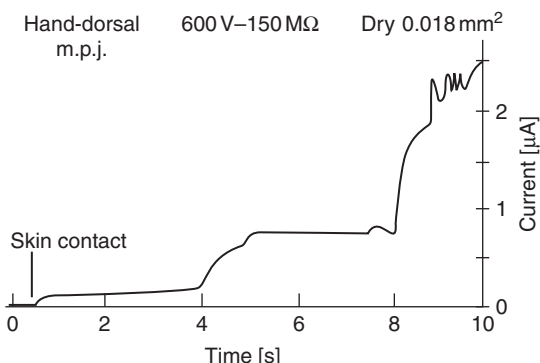


Figure 8.41: Thin stratum corneum dielectric strength, human skin *in vivo*. *From Grimnes (1983c), by permission.*

damage. Because of the current constriction near the electrodes, the highest current densities and largest effects are presumably there.

In *electrosurgery* (Section 10.10), the current density near the electrode is much higher than during defibrillation, and current duration is much longer. In cutting mode, the cell interior is brought up to 100 °C in just a few milliseconds, and the cells explode. Tissue destruction is the goal.

Iontophoresis (Section 10.4.3) for sweat sampling using DC current through the skin is presumably carried out in the nonlinear region.

An *electrostatic discharge* (Section 10.16.1) with an electric arc as contact medium may imply very high current densities on the affected area.

Incremental Impedance for Nonlinear, Time-Variant Objects

The impedance is usually measured by means of small voltage and current to ensure a linear behavior of the material under test. Many of the biological objects show active electrical behavior interfering with impedance measurements. The simple ratio between voltage and current becomes meaningless. This, for instance, happens when the impedance of single membranes is assessed. Especially, if these membranes are excitable or contain any voltage controlled ionic channels, they show nonlinear and time variant passive electrical properties. The adequate parameter describing this is the small signal response or the incremental impedance. Because it adds a degree of freedom (voltage at operating point or offset), its result is a field of spectra ([Figure 8.42](#)). For instance, at cell membranes, the most important spectrum is at the resting voltage.

For resistance or impedance measurements at materials driven into a nonlinear voltage region, it is often more informative to calculate the dynamic impedance dU/dI (also

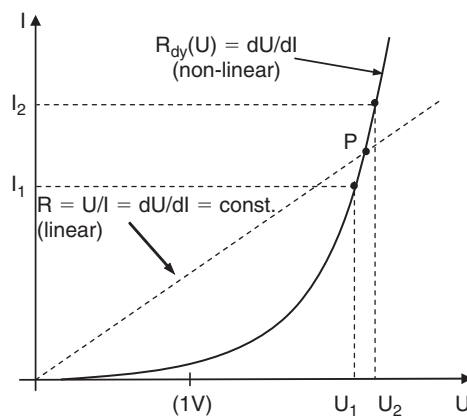


Figure 8.42: Linear and nonlinear behaviors of a material under test.

differential impedance or small signal behavior). Because the voltage is a parameter, it should be known for any dynamic impedance measured.

Nonlinearity of Membranes at Low Electric Field

Lipid Membrane

The biological membrane bases on a lipid bilayer. The polar head groups of the lipids are hydrophilic, thus they are arranged to contact the water. Because the aliphatic tails are hydrophobic, they face each other in the inner of the membrane, thereby minimizing the energy of the entire system (Alberts et al., 2007). Because of the hydrophobic interior of the membrane, hydrated charged ions cannot cross this structure, which yields insulating behavior. However, because the membranes are a two-dimensional liquid, meaning that a lipid molecule is highly mobile within the xy -layer but almost fixed along the z -axis, there is still a probability to find defects which can permit the passage of ions. Because this probability is very small, lipid membranes show a resistivity up to $\text{G}\Omega\text{cm}^2$.

An additional driving force such as an electric field can enhance the probability for the ion passage. This results in progressive increasing of the current with increased transmembrane voltage even for a pure lipid membrane.

Most of the biological membranes carry charges at the head groups, responsible for the appearance of an electric double layer in contact with electrolytes. This incorporates two parts, the directly adsorbed layer (Helmholtz layer) and a more diffuse layer (Guy-Chapman layer). The entire arrangement is called the Stern layer ([Figure 8.43](#)).

The outer electric field can modulate the behavior of the Stern layer, which has implications for impedance measurements with respect to the voltage applied but also to

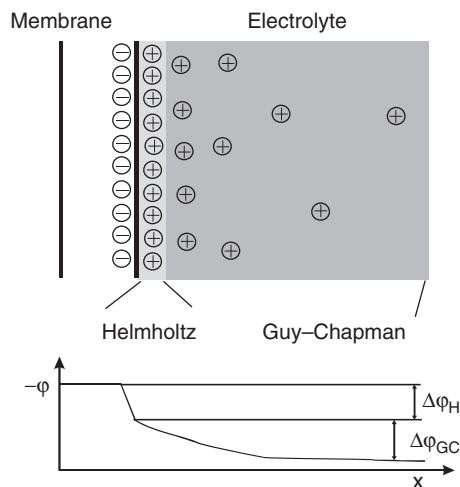


Figure 8.43: Electric double layer at a cell membrane. The potential across the Helmholtz layer drops linearly while the further drop in the Guy–Chapman layer is exponential.

the frequency. The ions within the double layer are less mobile, therefore increasing the resistance of the entire system. The mobility increases with higher field strength, thereby increasing the probability of ions reaching the cell membrane and in rare cases crossing it. This effect is more pronounced at a higher frequency where a net transport across the membrane is not necessary. The increased mobility of ions within the double layer will considerably decrease its resistance.

The capacity of the membrane is governed by the high electric resistance of the aliphatic tails within the membrane. The electric thickness of the membrane depends on the region without mobile charges as well. If this thickness decreases because of the outer electric field or even more pronounced, if ions are driven into the region of the head groups, this thickness decreases, resulting in increased capacitance of the membrane. Although this effect is not important for DC measurements, it will influence the AC measurements.

Cell Membrane

The membranes surrounding each cell (plasma membrane) and the intracellular structures (endoplasmatic reticulum, Golgi apparatus, nuclear membrane, mitochondria membranes, other organelle membrane) are not only composed of lipids but incorporate proteins and steroids as well. Besides this, adsorbed proteins will greatly influence the functionality of the membrane. Integral proteins can span the entire membrane. A considerable fraction of these proteins facilitates transmembrane transport of species usually not permeating the membrane. The transport mechanism may be very different. One group involves carriers

which need several steps of structural changes for the transport. Some carriers are powered externally (i.e., by dephosphorylation of ATP) and can facilitate transport against the electrochemical gradient (i.e., NA/K ATPase, sodium–potassium pump).

Other proteins build up channel structures providing access to a number of ions. Most of these channels are ion-selective (Na^+ , K^+ , Cl^- , Ca^{2+}) and can be controlled by external forces such as ligand binding (acetylcholine receptor), mechanical (sensing cell in the ear), or electrically (Na channels in excitable cell membranes).

Because of a great number of voltage-sensitive channels, they are mostly responsible for nonlinear properties of cell membranes at low voltage (<100 mV).

Since many cells are arranged in series and parallel by measurements in a tissue it is vague to get information about single cell membranes in an electrode arrangement cm-dimension.

A suitable method to study nonlinear behavior of cell membranes is the Whole Cell Path technique (Figure 8.44): (a) the cell in suspension is clamped by a micropipette (opening $\approx 1 \mu\text{m}$). To avoid electrode polarization both electrodes are AgAgCl electrodes consisting of a chloridized Ag wire. The counter electrode is immersed in 3 M KCl, which is arranged as gel in another pipette with bigger opening. Because the electrolyte of the suspension medium has a constant Cl^- concentration, the potential drop at the electrode is constant as well and can be compensated, either by adjusting the equipment or mathematically. (b) CHO cell (Chinese hamster ovary cell) attached to the micropipette. The cell diameter is about 16 μm .

To test the electrical behavior of the cell, one can apply a voltage stimulus (i.e., voltage ramp or step) and monitor the current (voltage clamp). Other than in technical systems, the application of a current ramp (or step) and monitoring the voltage

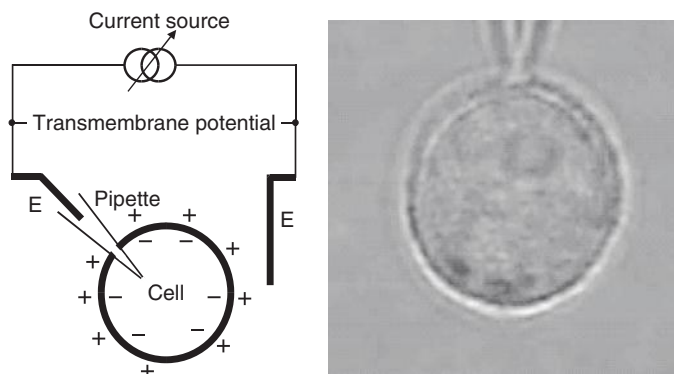


Figure 8.44: Arrangement for whole cell clamp (Frantescu et al., 2004).

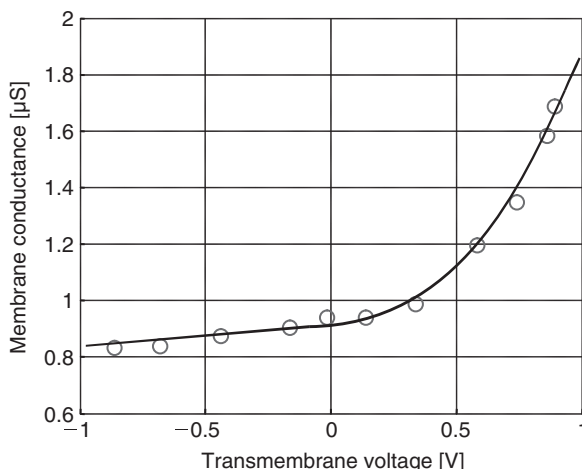


Figure 8.45: Membrane conductance depending on the voltage applied to a CHO cell membrane. The stimulus was a 1 ms long rectangular current pulse. The figure shows an average (current and voltage) over a greater number of experiments with always new cells. Error bars would be on the order of $0.4 \mu\text{S}$ and are omitted for showing a nicer picture. It should be noted that CHO cells do not have an excitable membrane.

(current clamp) yields different results and therefore additional information (Pliquett et al., 2005).

The slope of the ramp applied is critical because biological membranes show PI behavior. This means that the response to a stimulus is only partly proportional to the stimulus. Another, often greater part, is an integrating response (dose effect) (Figure 8.45).

The result shown in Figure 8.45 is within the limits where all changes are fully reversible and are only interpreted as happen without structural changes of the membrane itself (i.e., it is most likely but not only) a result of manipulating the open/closed state of channels.

8.4.4 Instrumentation Nonlinearity

The biopotential preamplifiers shown in Figures 8.14 and 8.15 are often DC coupled, a high-pass filter dropping DC values comes later in the chain, it is not a part of the front end. This means that the DC coupled preamplifier easily approaches saturation level. As described in Chapter 7, electrodes with different metals can easily generate hundreds of millivolt DC. The signal to be picked up may be in the microvolt range and with a large DC volt superimposed the system can be in the nonlinear range. The signal of interest can be distorted, or even become blind if the preamplifier has become saturated.

8.5 Problems

1. In tissue, sinusoidal current waveform generates potential differences that are also sinusoidal if the system is linear. Is the current amplitude for onset of nonlinearity dependent on the sine frequency?
2. Suppose we have a system where reciprocity is valid for a four-electrode setup. Will it then also be valid for a three-electrode system and a two-electrode system?
3. How is AC defined?
4. Are there lock-in amplifier models that can measure nonlinearity on a continuous basis?
5. What is an Amplifier Reference Wire?
6. What is the difference between the frequency spectra of a periodic and not-periodic signal?
7. In human skin, what is the upper current density limit of linearity [$\mu\text{A}/\text{cm}^2$] at 10 and 100 Hz?
8. Is the unit of transfer impedance ohm?

Data and Models

9.1 Models, Descriptive and Explanatory

We will see in [Section 9.2.3](#) that, when measuring on a parallel circuit with controlled voltage, the real part of the resulting current will be proportional to the conductance and the imaginary part will be proportional to the susceptance. And furthermore, that if the physical reality is a series circuit, this simple proportionality will be absent, and the values must be mathematically calculated in each case. The same proportionality is also present for controlled current measurements on a series circuit. Values for conductance and susceptance of the skin are thus always related to an opinion on whether these phenomena electrically exist in series or parallel.

The problem when trying to make an electrical model of the physical or chemical processes in tissue is often that it is not possible to mimic the electrical behavior with ordinary lumped, physically realisable components such as resistors (R), capacitors (C), inductors, semiconductor components, and batteries. Let us mention three examples: 1) The constant phase element (CPE), not realizable with a finite number of ideal resistors and capacitors. 2) The double layer in the electrolyte in contact with a metal surface. Such a layer has capacitive properties, but perhaps with a capacitance that is voltage or frequency dependent. 3) Diffusion-controlled processes (see [Section 2.4](#)). Distributed components such as a CPE can be considered composed of an infinite number of lumped components, even if the mathematical expression for a CPE is simple.

In this section, we will use electrical models for human skin as examples in a general discussion on the use of electrical models. An electrical model of the skin with only two components will obviously not be able to simulate the frequency response measured on skin—it is certainly too simple compared with the complex anatomy of human skin. We suggest three solutions to this problem, which would result in the following archetypes:

Model 1 (explanatory): One solution is to make a complete distinction between the different structures of the skin and hence make an electrical model as complex as the skin itself. Lipid membranes would then typically be replaced by capacitors, electrolytes by resistors, and semipermeable membranes by voltage sources. The model will, without compromise on the cellular level, aim to reflect the electrical properties of the various *microanatomical* structures.

Model 2: A different solution would be to focus on those structures of the skin that make the largest contributions to the electrical properties, decide whether each of these structures should be represented by a resistor or a capacitor, and finally find the simplest electrical equivalent that comprises all these structures. This *organ-oriented* model is thus a simplified version of model 1.

Model 3 (descriptive): A third solution would be to consider the skin as a *black box*, make extensive measurements on it, and find the electric circuit that matches the admittance levels and frequency response measured. The anatomy of the skin is not considered in this model.

These three models appear very different, but they are all electrical models of the skin. Is one of them more “correct” or “better than” the other models—and if so, why?

9.1.1 The Model Concept

The word *model* is ambiguous. A model can be a three-dimensional representation of an object, but it can also be a person presenting fashion clothing, an object used to produce casting molds, a person who is portrayed, an instrument for physical model experiments, a substitute for something, an illustration of a mathematical expression, and so on. The word *model* has essentially two different interpretations: *prototype/picture* and *equivalent/substitute*. Mathematical models should also be mentioned, which are a sort of predictive substitute for reality. A characteristic of models is that they represent selected properties of the reality they reflect.

Models that serve as visual pictures of reality have a geometric resemblance to the original, but can be scaled compared with it. The substitute models depict other properties than the visual. They can, with regard to these properties, act as substitutes for the original. (As an alternative, one could claim that pictorial models serve as substitutes with regard to visual properties, and include them also in this group.) Their predictive function is of great interest, because they are often used to investigate a specific side of the functionality or structure of the original, or its response to given stimuli. Such models might be flight simulators, models of the hull of a ship, miniature railroads, mathematical models, or electrical models or maps. Hence, for each of these models, one has chosen to emphasize one or more attributes from the original, and has thus made them selective acting substitutes. The models to be discussed here are substitute models, in which the electrical properties are important.

9.1.2 Description or Explanation?

Let us return to the question of which model is the best or most correct. The question as posed is obviously not precise enough to be given an exact answer. What is required from a good or correct model?

The term “electrical equivalent” is as frequently used as “electrical model” in the literature. The more rigorous word “equivalent” has a more precise meaning than “model.” An electrical equivalent is a circuit that electrically behaves exactly like the original when studied from predefined terminals. Model 3 is in this respect the best electrical equivalent and consequently also the best model, if the overall object is to describe the electrical properties of the skin. The descriptive models should therefore in this context be separated from the explanatory.

The descriptive models characterize the skin electrically by means of both known electric components and algorithms. The models reflect primarily the phenomena (i.e., the measured values and time courses) and the theories are not to any great extent connected to the microanatomy of the skin. The entities of the model do not necessarily exist as isolated biological structures, and even though the model includes known electric components, they do not necessarily resemble corresponding electrophysiological processes in the skin.

The explanatory models are based on the basic concepts of electrical theory—potential, conductance, polarization, induction, etc. Knowledge about the physical mechanisms behind these phenomena is used to provide understanding of similar phenomena in biological materials, and the models are largely influenced by theories concerning the relationship between microanatomy and fundamental electrical properties. It is vital that these models only include discrete electric components for which the essential mode of operation is known. The models are explanatory because one believes that the components of the model represent isolated anatomical structures or physical processes, such that the dominating electrical property can be explained by means of the properties of the component.

9.1.3 The Best Model

The best model takes all recent knowledge about relaxation processes, frequency dispersion, diffusion, fractals, and so on into account. It is an electrical equivalent to the skin (i.e., it has the same frequency response). Furthermore it is simple and uses symbols in a way that makes it easy to understand the outlines of the electrical properties of the different substructures of the skin. The model takes care of all requirements of an electrical model of the skin—but unfortunately it does not exist! The most correct of the existing models is therefore the one best adapted for the target group.

The realism of the lumped element models is not easy to assert in view of modern theories and measurement techniques, and these models can be regarded as pragmatic explanatory models. They are, however, the only models that differentiate between substructures of the skin and have clinical value in that they aid in choosing measuring technique.

The pure instrumentalism of the descriptive models is also questionable. There is an obvious need to correlate the parameters τ and α with well-defined mechanisms in the

skin, particularly regarding the use of skin admittance measurements as a diagnostic tool. The descriptive models can therefore be considered as essential intermediate stages in the development of better explanatory models. The new explanatory models will comprise discrete, passive components, but there will be a change in the use of symbols compared with the descriptive models as the relationship between anatomical structure and electrophysiological mechanisms are revealed. These new models should be able to explain the so-far empirically disclosed connections between skin diseases and the frequency response of the skin by showing how changes within a substructure in the skin influence one or more of the components of the model, and hence how this can be detected by choosing the appropriate measuring technique.

9.2 Equations, Laws, and Equivalent Circuits

A mathematical equation is also a model, and a very ideal one. There is an important interaction between these two model forms: the mathematical equation and the equivalent circuit diagram, with respect to the phenomena to be described.

9.2.1 Coulombs Law

See Section 3.1.1.

9.2.2 Maxwell–Heaviside Equations

Maxwell's famous four equations are found in many versions, for example, in differential or integral form and with different parameters involved. Equations 9.1–9.4 show one example set (the Minkowski formulation). The differential form relates the time and space derivatives at a point (in an infinitesimal small *volume*) to the current density at that point. The integral form relates to a defined finite *volume*. Ideal charge distributions are often discontinuous, and so not differentiable; *therefore, the integral form is a more generally applicable form*.

	Differential Form	Explanation by Integral
Eq. 9.1 Gauss law	$\nabla \cdot \mathbf{E} = q_v/\epsilon_0$	Flux of \mathbf{E} through a closed surface = net enclosed charge/ ϵ_0
Eq. 9.2 Faraday's law of induction	$\nabla \times \mathbf{E} = -\partial \mathbf{B}/\partial t$	Line integral of \mathbf{E} around a loop = –rate of change of flux of \mathbf{B} through the loop
Eq. 9.3	$\nabla \cdot \mathbf{B} = 0$	Flux of \mathbf{B} through a closed surface = 0
Eq. 9.4 Ampere's law	$\nabla \times \mathbf{H} = \mathbf{J}_f + \partial \mathbf{D}/\partial t$	Line integral of \mathbf{H} around a loop = current density of free charges through the loop + rate of change of flux of \mathbf{D} through the loop

Local symbols in this chapter are: c = velocity of light [m/s], \mathbf{B} = magnetic flux density [Vs/m²], \mathbf{H} = magnetic field strength [A/m], q is charge [C], q_v is charge density [C/m³], and q_{vf} is density of free charges not including dipole charges bound (q_{vb}) in the material, $q_v = q_{vf} + q_{vb}$.

∇ is the differential *vector operator* called *nabla* or *del*: $\nabla = \mathbf{i}\partial/\partial x + \mathbf{j}\partial/\partial y + \mathbf{k}\partial/\partial z$, where \mathbf{i} , \mathbf{j} and \mathbf{k} are unity vectors in a Cartesian coordinate system.

$\nabla\Phi$ is the *gradient* of Φ (the gradient of a scalar is a vector), $\nabla \cdot \mathbf{B}$ is the *divergence* of \mathbf{B} (the divergence of a vector is a scalar), and $\nabla \times \mathbf{B}$ is the *curl* of \mathbf{B} (the curl of a vector is a vector).

They describe almost all known electrical effects in one complete, concentrated, powerful set. They were very much based on Faraday's discoveries, for example, Eq. 9.2 is a more general formulation of Faraday's law of induction. The equations state that a *variable* electrical field can only exist together with a magnetic field and vice versa. They are based upon the presupposition that a charge cannot be created anywhere; it can just be moved. They apply to any inertial reference frame: the *charge* of a particle moving at an increasing velocity is constant, whereas the *mass* increases. The Maxwell equations themselves are linear: they do not contain products of two or more variables. They are extremely robust valid also for nonlinear, nonhomogenous, and anisotropic systems.

Most other equations describing electrical effects are derivable from the Maxwell's equations. In bioimpedance, Gauss law is important, describing how the E-field is changed by the existence of net space charges. It is equally valid for net free or bound charges. However, $\nabla \cdot \mathbf{D} = q_{vf}$ is related to free charges, meaning that the flux of \mathbf{D} through a closed surface = net enclosed free charges inside. If we replace E by $-\nabla\Phi$, we obtain the *Poisson equation*:

$$\nabla^2\Phi = \frac{-q_v}{\epsilon_0} \quad \text{or} \quad \frac{\partial^2\Phi}{\partial x^2} + \frac{\partial^2\Phi}{\partial y^2} + \frac{\partial^2\Phi}{\partial z^2} = \frac{-q_v}{\epsilon_0} \quad (9.5)$$

∇^2 is called the *Laplacian*. The special case of the volume charge density q_v being zero is called the Laplace equation:

$$\nabla^2\Phi = 0 \quad (\text{Laplace equation}) \quad (9.6)$$

From Eq. 9.2, the following relationship can be deduced: $\mathbf{D} = \epsilon_0\mathbf{E} + \mathbf{P}$ (Eq. 3.5), it is valid also for nonisotropic, nonlinear materials. Other equations derivable from the Maxwell's equations for linear and isotropic materials are, for example, Ohm's law $\mathbf{J} = \sigma\mathbf{E}$, the power density law (Joule heat) $W_v = \sigma'E^2$ [watt/m³], and the stored energy density law $\hat{E}_v = 1/2 \mathbf{E} \cdot \mathbf{D}$ [joule/m³]. Maxwell's equations are valid for all kinds of electromagnetic radiation and contain the speed of light in the fourth equation (Eq. 9.4) (in another version than Minkowski's). Heaviside played a special role in the development of the Maxwell equations (see Chapter 11).

Maxwell introduced the term *displacement current* for the current through free space and the local displacement of the *bound* charges (dipoles) in the dielectric, as opposed the movement of *free* charges.

From Maxwell's equations, the fundamental difference between static near fields (electromagnetic *fields*) and radiation (electromagnetic *waves*) is demonstrated. In Section 6.2, we treated the dipole. Consider that the dipole moment varies as a sine function with time. Now if the frequency is very high, the time delay will be noticeable if we are at a distance much longer than the wavelength $\lambda = c/f$ from the dipole.

In the *near-field* (distance to the source $\ll \lambda$), electric and magnetic fields are independent of each other and it is possible to have, for example, a pure 50 Hz electric field with a negligible magnetic field.

Bioimpedance and the Maxwell Equations

The Maxwell equations most relevant to bioimpedance are Eq. 9.4 and Eq. 3.5: $\mathbf{D} = \epsilon_0 \mathbf{E} + \mathbf{P}$. If the magnetic component is ignored, Eq. 9.4 is reduced to:

$$\frac{\partial \mathbf{D}}{\partial t} = -\mathbf{J}. \quad (1)$$

[Equations 1](#) and 3.5 are extremely robust and also valid both under *nonhomogeneous, nonlinear, and anisotropic* conditions. To be more useful for bioimpedance, four restrictions are introduced:

1. Use of sufficiently small voltage amplitude across the material so the system is *linear*.
2. Use of *sinusoidal* functions so that in complex notation, a derivative (e.g., $\partial E/\partial t$) is simply the product $j\omega E$ (j is the imaginary unit and ω the angular frequency; see Section 12.1).
3. Use of $\mathbf{D} = \epsilon \mathbf{E}$ (space vectors), where the permittivity $\epsilon = \epsilon_r \epsilon_0$. This implies that D , P , and E all have the same direction and therefore that the dielectric is considered isotropic.
4. No fringe effects in the capacitor model of Figure 3.1.

Let us now apply [Eq. 1](#) on the capacitor model of Figure 3.1 with the metal area equal to A and the dielectric thickness equal to L . However, [Eq. 1](#) is in differential form, and the interface between the metal and the dielectric represents a discontinuity. Gauss law as an integral form is therefore used, and we imagine a thin volume straddling an area of the metal/dielectric interface. According to Gauss law, the outward flux of D from this volume is equal to the enclosed free charge density on the surface of the metal. With an applied voltage v , it can be shown that $D = v \epsilon / L$. By using [Eq. 1](#), we then have $\partial D / \partial t = j\omega v \epsilon / L = J$ and $i = j\omega v \epsilon A / L = v j \omega C$.

We now leave the dielectric and take a look at the external circuit where the current \mathbf{i} and the voltage \mathbf{v} (time vectors) are measured and the immittance determined. The admittance is $\mathbf{Y} = \mathbf{i} / \mathbf{v}$. With no losses in the capacitor, \mathbf{i} and \mathbf{v} will be phase shifted by 90° (the quadrature part). The conductance is $G = \sigma' A / L$ and the basic equation of bioimpedance is then (time vectors):

$$\mathbf{Y} = G + j\omega C. \quad (2)$$

Three important points must be made here:

First, Eq. 2 shows that the basic impedance model actually is an *admittance* model. The conductive and capacitive (quadrature) parts are physically in parallel in the model of Figure 3.1.

Second, the model of Figure 3.1 is predominantly a dielectric model with *dry* samples. In bioimpedance theory, the materials are considered to be *wet*, with double layer and polarization effects at the metal surfaces. Errors are introduced, however, that can be reduced by introducing three- or four-electrode systems (Section 7.10). Accordingly, in dielectric theory, the dielectric is considered as an *insulator* with dielectric losses; in bioimpedance theory, the material is considered as a *conductor* with capacitive properties. Dry samples can easily be measured with a two-electrode system. Wet, ionic samples are prone to errors and special precautions must be taken.

Third, the Maxwell equations used are valid at a point. With a homogeneous and isotropic dielectric material in Figure 3.1, the variables have the same values all over the sample. With inhomogeneous and anisotropic materials, the capacitor model implies values averaged over the volume. Then under *linear* (small signal) conditions the equations are still correct, but the measured values are difficult to interpret. The capacitor is basically an *in vitro* model with a biomaterial placed in a measuring chamber. The average anisotropy can be measured by repositioning the sample in the capacitor. *In vivo* measurements must be analyzed with sensitivity fields as shown in Section 6.4.

9.2.3 Two Ideal Components Equivalent Circuits

We will now discuss the simplest equivalent circuits mimicking the immittance found in tissue measurements. In this section, the R-C components are considered *ideal*; that is, frequency independent and linear. Immittance values are examined with sine waves, relaxation times with step functions. A sine wave excitation results in a sine wave response. A square wave excitation results in a single exponential response with a simple R-C combination.

The two-component model with one resistor and one capacitor is a one-port network and is the simplest and most important model because every measurement on a specific frequency is reduced to such a circuit. The results are given as complex immittance values with two figures corresponding to the two components: one resistor and one capacitor. Inductive properties and corresponding resonance phenomena are possibilities that are found, for example, in membranes, but here we limit the treatment to capacitive systems.

Admittance and the Parallel Model

In the parallel two-component model circuit, there is direct access to both components from the external terminals (Figure 9.1). Therefore the voltage can be externally controlled, but not the current division. Accordingly a *constant amplitude voltage v* is

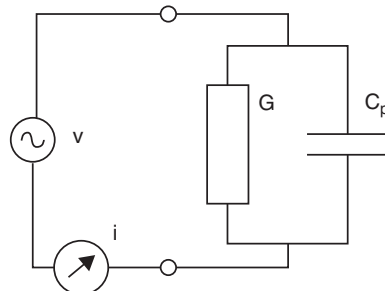


Figure 9.1: Parallel circuit driven from an ideal voltage source ($R_i = 0$), the response recorded by an ideal current reading device ($R_i = 0$).

applied across the model parallel circuit and the current \mathbf{i} is measured. The admittance \mathbf{Y} has a direct relationship with a parallel G-C circuit, the real part \mathbf{Y}' is G , and the imaginary part \mathbf{Y}'' is $B = \omega C$.

The parallel values are measured directly because it is proportionality between admittance \mathbf{Y} and measured \mathbf{i} . v is the independent reference sine wave, with zero phase shift per definition, and therefore here designated as a scalar:

$$\mathbf{Y} = \frac{\mathbf{i}}{v} \quad (9.7)$$

$$\mathbf{Y} = G + j\omega C_p \quad (9.8)$$

$$\varphi = \frac{\arctan \omega C_p}{G} \quad (9.9)$$

$$\epsilon' = C_p \quad (\text{unity cell})$$

$$\epsilon'' = \frac{G}{\omega} \quad (\text{unity cell}) \quad (9.10)$$

$$\tau = \frac{C_p}{G}$$

The circuit has some very characteristic properties:

- The admittance diverges at higher frequencies (Eq. 9.8); here, the model is not in agreement with biomaterial properties.
- It does let DC pass.
- The phase angle is positive, meaning the current (dependent variable) is leading the voltage. Because \mathbf{i} is the dependent variable, for causality it cannot lead the start of the sine wave, only after steady-state conditions have been obtained.
- The time constant τ of Eq. 9.10 is not found with a controlled step voltage excitation as shown in Figure 9.1; the capacitor will be charged in zero time during the voltage step.

The characteristic time constant of the parallel circuit alone *can only be found* with a *constant amplitude current* ($R_i = \infty$) excitation.

Time Constant of the Parallel G-C Circuit

The time constant τ of the parallel circuit depends on how it is driven. With a controlled step *current* across the circuit (not constant amplitude voltage as shown in [Figure 9.1](#)), the voltage across the G-C combination increases exponentially from zero to $V = I/G$. The time constant is $\tau = C_p/G$. Driven by a controlled *voltage* step V , the starting current is infinitely high, and the time constant is zero.

If the Parallel Model is to be Characterized with Impedance

We may express the impedance Z of the parallel circuit using the parallel values G and C_p , $Y^2 = G^2 + B^2$ and $\tau_Y = C_p/G$ (Y^2 means $|Y|^2$):

$$R = \frac{G}{Y^2}$$

$$X = \frac{-B}{Y^2}$$

$$Z = \frac{1}{Y} = \frac{1 - j\omega\tau_Y}{G(1 + \omega^2\tau_Y^2)}$$

$$Z' = \frac{1}{G(1 + \omega^2\tau_Y^2)} \quad (9.11)$$

$$Z'' = \frac{-j\omega\tau_Y}{G(1 + \omega^2\tau_Y^2)}$$

$$C_s = C_p \left(1 + \frac{1}{\omega^2\tau_Y^2} \right)$$

[Equation 9.11](#) illustrates the extreme importance of choosing the best model circuit:

- Z' will be frequency dependent, even if G is not.
- The series capacitance C_s *diverges toward infinite capacitance values at low frequencies*. This will, for instance, be experienced with a measuring bridge if an unknown parallel combination is to be zeroed by a series combination in the balancing arm (Section 8.3.6).

Impedance and the Series Model

In the series two-component model circuit, there is no direct access to both components from the external terminals, Figure 9.2. Because the two components are in series, the current can be externally controlled, but not the voltage division. Accordingly, a *constant amplitude current* i is applied across the model series circuit, and the voltage v is measured. The impedance Z has a direct relationship with a series R-C circuit, because the real part Z' is R , and the imaginary part Z'' is $X = -1/\omega C$. The series values are measured because it is proportionality between impedance Z and measured v . i is the independent reference sine wave, with zero phase shift per definition, and therefore here is designated as a scalar:

$$Z = \frac{v}{i} \quad (9.12)$$

$$Z = R - \frac{j}{\omega C_s} \quad (9.13)$$

$$\varphi = \arctan\left(\frac{-1}{\omega\tau}\right) \quad (9.14)$$

$$\tau = RC_s \quad (9.15)$$

Important properties of the series circuit are:

- The impedance converges at higher frequencies (Eq. 9.14).
- It does not allow the passage of DC.
- The phase angle is negative. This means that the voltage as dependent variable is lagging the current (see current leading in the parallel circuit).
- The time constant τ of Eq. 9.15 is not found with constant amplitude current excitation as shown in Figure 9.2; the capacitor will be charged ad infinitum during the current step. The characteristic time constant of the parallel circuit alone *can only be found with a constant amplitude voltage* ($R_i = 0$) excitation.

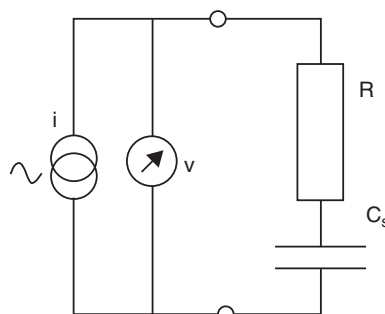


Figure 9.2: Series circuit driven from an ideal current source ($R_i = \infty$), the response recorded by an ideal voltage reading device ($R_i = \infty$).

Time Constant of the Series R-C Circuit

The time constant τ of the series circuit depends on how it is driven. With a controlled step *voltage* V across the circuit (not controlled current as shown in Figure 9.2), R is effectively in parallel with C_s , and the current decays exponentially from an initial value of $i = V/R$ to $i = 0$ with a time constant $\tau = RC_s$. The voltage across the capacitor increases exponentially with time from $v = 0$ to $v = V$ with the same time constant. Driven by a controlled *current* step I , the total series resistance is effectively infinite, and the voltage across the circuit (after a transient period) increases linearly with time with a velocity $\Delta v/\Delta t = I/C_s$. The time constant is therefore infinitely large.

If the Series Model is to be Characterized with Admittance

We may express the admittance \mathbf{Y} of the series circuit with the series values R and C_s , $Z^2 = R^2 + X^2$ and $\tau_Z = RC_s$ (Z^2 means $|\mathbf{Z}|^2$)

$$\begin{aligned}
 G &= \frac{R}{Z^2} \\
 B &= \frac{-X}{Z^2} \\
 \mathbf{Y} &= \frac{1}{Z} = \frac{\omega^2 C_s \tau_Z + j\omega C_s}{1 + \omega^2 \tau_Z^2} \\
 \mathbf{Y}' &= \frac{\omega^2 \tau_Z^2}{R(1 + \omega^2 \tau_Z^2)} \\
 \mathbf{Y}'' &= \frac{C_s \omega}{1 + \omega^2 \tau_Z^2} \\
 C_p &= \frac{C_s}{1 + \omega^2 \tau_Z^2} \\
 \epsilon' &= \frac{C_s}{1 + \omega^2 \tau_Z^2} \quad (\text{unity cell}) \\
 \epsilon'' &= \frac{\omega C_s \tau_Z}{1 + \omega^2 \tau_Z^2} \quad (\text{unity cell})
 \end{aligned} \tag{9.16}$$

Equation 9.16 illustrates the extreme importance of choosing the best model circuit:

- Y' will be frequency dependent, even if R is not.
- The parallel capacitance C_p will be frequency dependent, even if C_s is not. C_p converges to zero at high frequencies. C_p is now the capacitance as seen from the outside (C_{ext}), different from C_s because we do not have direct access to C_s from the model terminals.

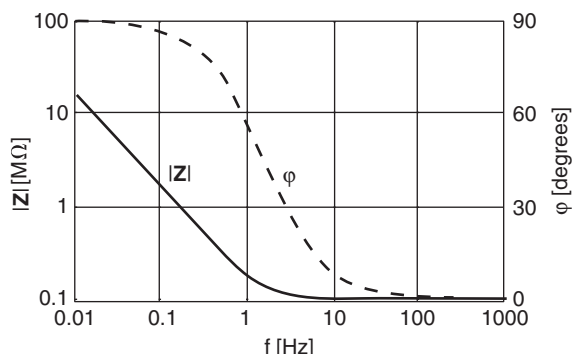


Figure 9.3: Impedance of the series model of Figure 9.2 presented in a Bode diagram: frequency and impedance scales logarithmic, phase scale linear. $R = 0.1 M\Omega$, $C_s = 10^{-6} F$, ($\tau = 0.1 s$, $f_c = 1.6 \text{ Hz}$).

Bode and Wessel Diagram Presentations

Figure 9.3 shows an example of how a model series circuit will look like in a Bode diagram. Most of the phase shift is within a frequency range of two decades, centered on the characteristic frequency 1.592 Hz where $\varphi = 45^\circ$. $|Z|$, however, has hardly started to increase at the characteristic frequency when passing toward lower frequencies.

Figure 9.4 illustrates the *parallel* circuit in the Wessel diagram. In a Y-plot representation, the locus is a straight line. Because of the frequency scale direction, it is reasonable to interpret this as an infinitely high characteristic frequency or an infinitely small time constant, as if the circuit was voltage driven. However, *in the impedance plane (Z-plot), the parallel circuit has a half-circle locus*. Then the characteristic frequency of the apex is $f_c = G/2\pi C_p$, as if the circuit were current driven. Notice how the Z-plot enlarges the low-frequency part and the Y-plot the high-frequency part.

Figure 9.5 illustrates the *series* circuit in the Wessel diagram. In a Z-plot representation, the locus is a straight line. Because of the frequency scale direction, it is reasonable to interpret this as zero characteristic frequency or an infinitely high time constant, as if the circuit were current driven. However, *in the admittance plane (Y-plot), the series circuit has a half-circle locus*. Then the characteristic frequency of the apex is $f_c = 1/2\pi R C_s$, as if the circuit were voltage driven. Notice how here also the Z-plot enlarges the low-frequency part and the Y-plot the high-frequency part.

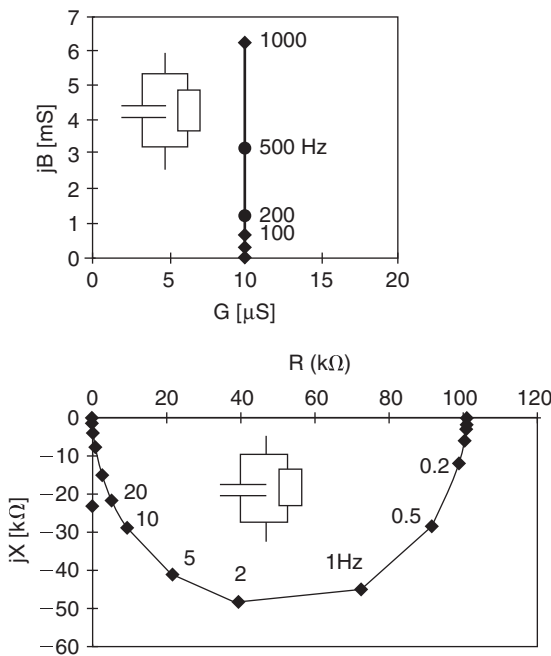


Figure 9.4: Wessel diagrams for the parallel model circuit. $G = 10 \mu\text{S}$, $C_s = 10^{-6} \text{ F}$ ($\tau = 0.1 \text{ s}$, $f_c = 1.6 \text{ Hz}$).

In conclusion, the parallel and series two-component circuits are *complementary models* and very different from each other. A choice of model is unavoidable when electrical data are to be analyzed and presented. The choice must be based upon a presumption on the actual physical arrangement in the biomaterial/electrode system to be modeled.

Parallel- and series-equivalent circuits contain the same information in ideal systems. *The choice is often actually done in the measurement setup* by choosing constant amplitude voltage or current modus from the signal generator or by choosing parallel or series coupling in the bridge arm.

Of course it is also possible to use nonideal sources and measure both voltage and current at the terminals of the system under examination. By special feedback circuits, it is also possible to control, for example, the power dissipation in the unknown (e.g., isowatt modus). It must still be decided whether admittance or impedance values are to be calculated and presented.

If the system under examination is nonlinear, the information in the parallel and series models is not equal. Series values cannot be calculated from parallel values and vice versa, and the actual measuring circuit determines the variables and the model chosen.

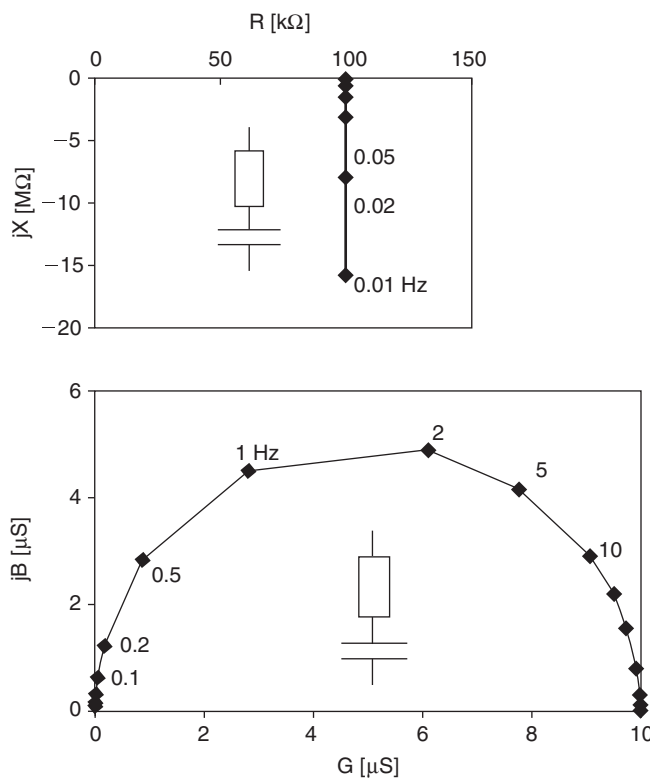


Figure 9.5: Wessel diagrams for the series model circuit. $R = 100\text{ k}\Omega$, $C_s = 10^{-6}\text{ F}$ ($\tau = 0.1\text{ s}$, $f_c = 1.6\text{ Hz}$).

9.2.4 Debye Models, Three Ideal Components

Usually the two-component circuit is too simple to mimic with sufficient precision the frequency dependence of the variables measured. The three-component model combines features of both the series and parallel models. It may consist of two capacitors and one resistor (dielectrics with bound electric charges) or two resistors and one capacitor (conductors with free charge carriers). Detailed equations can be found in Section 12.2.

Two Resistor and One Capacitor Circuits (2R-1C, Conductors)

The only two basically different versions are illustrated in Figure 9.6. Both allow DC, and both guarantee current limitation at high frequencies. The detailed equations are found in the appendix (Section 12.2). The two circuits are very similar because *it is possible to obtain the same immittance values for all frequencies with only two sets of component values*. As we have seen, this was not possible with the two-component series and parallel circuits. Their descriptive powers are therefore identical, and a choice must be

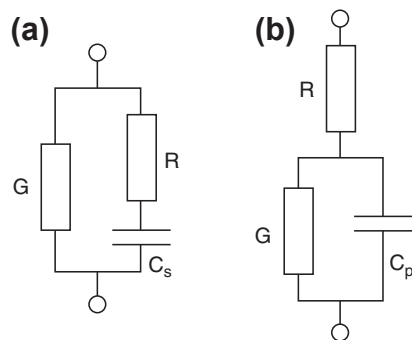


Figure 9.6: Conductor 2R-1C models. (a) Parallel version and (b) series version.

made on the basis of their explanatory possibilities. However, the choice is important because the component values for the same frequency dependence are not identical. It is easy to see that the limiting cases at very low and very high frequencies determine the resistor values.

The *parallel* version is best characterized by admittance because the *time constant then is uniquely defined* (Section 12.2). It has been used for cells and living tissue, with C for cell membranes, R for intracellular, and G for extracellular liquids.

The *series* version is best characterized by impedance because the *time constant then is uniquely defined* (Section 12.2). It has often been used as a skin electrical equivalent, with R for deeper tissue in series and the skin composed of G and C in parallel.

One Resistor and Two Capacitors Circuit (1R-2C, Dielectrics)

Detailed equations for such circuits with ideal components are found in Section 12.2. The only two basically different versions are illustrated in Figure 9.7. Neither allows DC, and neither guarantees current limitation at high frequencies. The two circuits are similar because it is possible to obtain the same immittance values for all frequencies with only

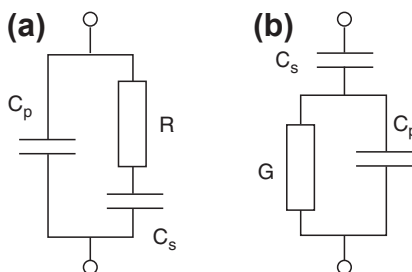


Figure 9.7: Dielectric 1R-2C models. (a) Parallel version and (b) series version.

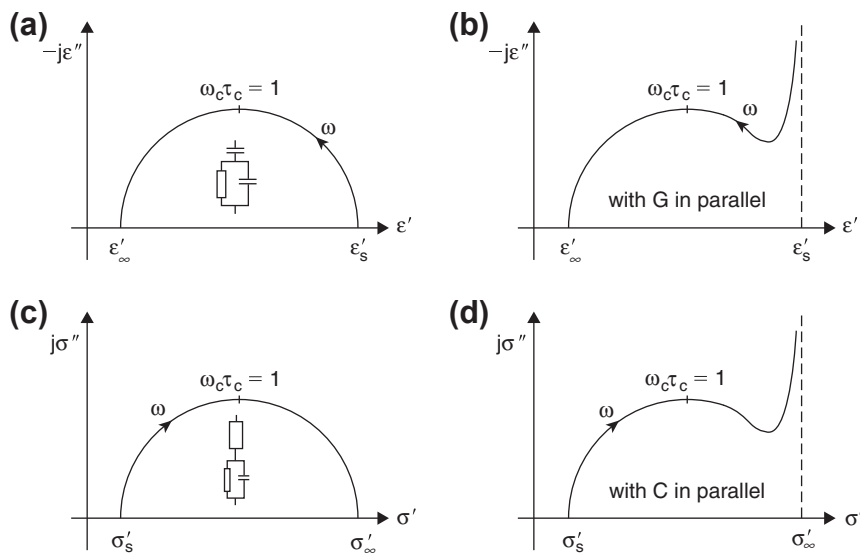


Figure 9.8: (a),(b) The effect of a parallel conductor added to the 1R-2C dielectric circuit of Figure 9.7. (c),(d) The effect of a parallel capacitor added to the 2R-1C conductor circuit of Figure 9.6.

two sets of component values. With one set of component values, they cannot be made equal to the (1C-2R) models at more than one frequency. Their descriptive powers are identical, and a choice must be made on the basis of their explanatory possibilities. However, the choice is important because the component values for the same frequency dependence are not identical. It is easy to see that the limiting cases at very low and high frequencies determine the capacitor values. The parallel version is an important model for a simple relaxation process. It is the preferred version because it can be defined *with one unique time constant* (Section 12.2), and is according to the Debye equation Eq. 3.15 treated in Section 3.4 on relaxation.

The Effect of Additional Parallel Conductors and Capacitors

The permittivity locus of a Debye dispersion in the Wessel diagram is a complete half circle with the center on the real axis, Figure 9.8(a). An ideal resistor in parallel destroys the circle at low frequencies, upper right (see Figure 9.8(b)). The conductivity locus is equally sensible for an ideal capacitor in parallel at high frequencies, Figure 9.8(d) lower right.

9.2.5 Constant Phase Element

The two-component equivalent circuit models presented in the last section are of course too simple to mimic the admittance found with real biomaterials at all

frequencies. A much better agreement can often be obtained by allowing the components to be nonideal; that is, frequency dependent. In particular, the frequency dependence can be modeled so that the *phase* of the immittance is *independent* of frequency.

Let us calculate the characteristic properties of a general CPE as a conductor and a susceptor in parallel, both frequency dependent. The frequency dependence of the admittance $Y = G + jB$ is sought so that the phase angle ($\varphi_{cpe} = \arctan B/G$) becomes frequency *independent*:

$$\frac{B_{cpe}}{G_{cpe}} = k \quad (9.17)$$

From Eq. 9.17, it is clear that to keep the phase angle constant, both G and B must be dependent on the frequency in the same way:

$$G_{cpe} = G_{\omega=1} \omega^m \quad B_{cpe} = B_{\omega=1} \omega^m \quad (9.18)$$

The dimension of G_{cpe} and B_{cpe} is siemens [S], so the dimension of $G_{\omega=1}$ and $B_{\omega=1}$ is not so simple: $[S/\omega^m]$ or $[S s^m]$.

Here the introduction of a parameter τ with the dimension of time and forming the product $\omega\tau$ is of interest for two reasons:

- τ represents a useful frequency scale factor
- the product $\omega\tau$ is dimensionless (an angle)

Equation 9.18 is then changed to (G_1 and B_1 are values at $\omega\tau = 1$):

$$G_{cpe} = G_1 (\omega\tau)^m \quad B_{cpe} = B_1 (\omega\tau)^m \quad (9.19)$$

The introduction of τ has the interesting consequence that it changes the dimension of G_1 and B_1 to also be that of an ideal conductance: siemens.

$$Y_{cpe} = (\omega\tau)^m (G_1 + jB_1) \quad (9.20)$$

$$\varphi_{cpe} = \arctan \left(\frac{B_1}{G_1} \right) \quad (9.21)$$

Equations 9.20 and 9.21 define a general CPE, determined by $\omega\tau$, m , G_1 , and B_1 . There is no correlation between m and φ_{cpe} , and there are no restrictions to the value of m . m does not determine the constant phase value, but it defines the frequency dependence of the Y_{cpe} and the frequency scale together with τ .

If the m values are restricted to positive values in the range $0 \leq m \leq 1$, then the admittance Y_{cpe} is increasing with frequency, in accordance with what is found for tissue. As can be seen from Eq. 9.21, this also implies the intrinsic property of zero DC conductance and

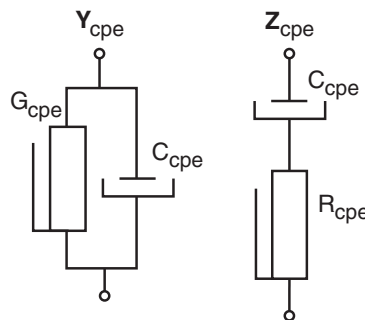


Figure 9.9: Equivalent circuits of parallel and series CPEs. The symbols are for nonideal, frequency-dependent components.

susceptance. By also specifying the susceptance to be capacitive, obeying the equation $B = \omega C$ and therefore $B_1 = (1/\tau)C_1$ ($C_1 = C_{\omega\tau=1}$), we get for the *admittance parallel* version:

$$Y_{cpe} = (\omega\tau)^m G_1 + j\omega^m \tau^{m-1} C_1 \quad 0 \leq m \leq 1 \quad (9.22)$$

$$\varphi_{cpe} = \arctan\left(\frac{C_1}{\tau G_1}\right) \quad (9.23)$$

$$C_{cpe} = C_1(\omega\tau)^{m-1} \quad (\text{falling with increasing frequency when } 0 \leq m \leq 1) \quad (9.24)$$

Let us examine the extreme values of frequency:

When $f \rightarrow \infty$, $Y_{cpe} \rightarrow \infty$ (Eq. 9.22), even when $C_{cpe} \rightarrow 0$! (Eq. 9.24).

When $f \rightarrow 0$, $Y_{cpe} \rightarrow 0$, even when $C_{cpe} \rightarrow \infty$!

Let us examine the extreme values of $m = 0$ and $m = 1$:

$m = 0$: $G_{cpe} = G_1$, an ideal (frequency independent) resistor. $C_{cpe} = C_1/\omega\tau$, a very special capacitor.

$m = 1$: $G_{cpe} = G_1 \omega\tau$, a very special resistor. $C_{cpe} = C_1$, an ideal (frequency independent) capacitor.

In both cases, the constant phase character is valid with $\varphi_{cpe} = \arctan C_1/\tau G_1$, not necessarily 0° or 90° . But with $G_1 = 0$: $\varphi_{cpe} = 90^\circ$; and with $C_1 = 0$: $\varphi_{cpe} = 0^\circ$.

The *impedance series* version show similar properties. The equivalent circuits are shown in Figure 9.9.

In the Wessel diagram of Figure 9.10 the loci of the Y_{cpe} and Z_{cpe} , both the parallel and series circuits are straight lines, with no circular arcs as seen in Figures 9.4 and 9.5. The choice between parallel or series representation is not important for a CPE, and using a series or parallel circuit as shown in Figure 9.10 is arbitrary. In particular, by inverting,

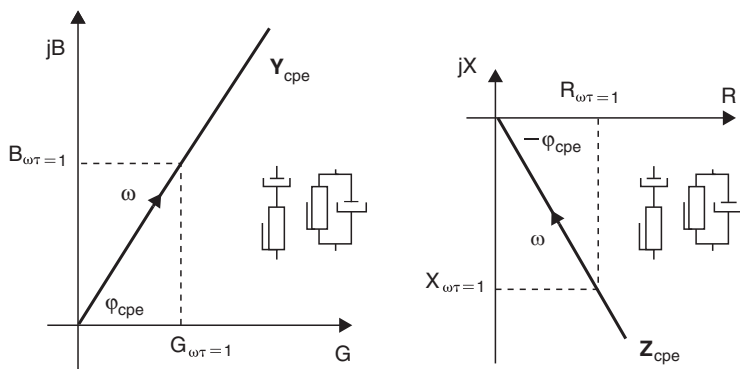


Figure 9.10: Immittance of an isolated CPE. There is no difference between series and parallel representation, in contrast to Figures 9.4 and 9.5.

for example, the admittance of a parallel CPE into an impedance Wessel diagram, the locus will still be a line (Figure 9.10), not a circular arc.

A CPE comprises a frequency-dependent capacitor and resistor. From an electronic point of view a CPE is a two-component descriptive model. If the mechanism behind is seen as one process, it is a one-component explanatory model.

CPE in Accordance with Fricke's Law (CPE_F)

According to Fricke's law, *there is* a correlation between the frequency exponent m and the phase angle φ in many electrolytic systems: when experiments show that $C = C_1 f^{m-1}$, then $\varphi = m\pi/2$. As pointed out by Fricke, m is often also found to be frequency dependent. However, it can be shown that Fricke's law is not in agreement with the Kramers-Kronig transforms *if m is frequency dependent* (Daniel, 1967). If we therefore also presuppose m and φ to be frequency independent, we have a CPE. For such a Fricke CPE_F, it is usual practice to use the exponent symbol α ($m = \alpha$). The immittance of a Fricke CPE_F can then be written in a very simple way in complex notation (remembering that $j^\alpha = \cos \alpha\pi/2 + j\sin \alpha\pi/2$, cf. Eq. 12.6):

$$\begin{aligned} \mathbf{Y}_{\text{cpeF}} &= G_1(j\omega\tau)^\alpha = \omega^\alpha \tau^\alpha G_1 \left(\cos \frac{\alpha\pi}{2} + j \sin \frac{\alpha\pi}{2} \right) \\ \mathbf{Z}_{\text{cpeF}} &= R_1(j\omega\tau)^{-\alpha} = \omega^{-\alpha} \tau^{-\alpha} R_1 \left(\cos \frac{\alpha\pi}{2} - j \sin \frac{\alpha\pi}{2} \right) \end{aligned} \quad (9.25)$$

The factor α intervenes *both* in the constant phase expression ($\cos \alpha\pi/2 + j\sin \alpha\pi/2$) and the frequency exponent, in accordance with Fricke's law. The dimension of \mathbf{Y}_{cpeF} and G_1 is siemens [S] and R_1 ohm [Ω]. The values of \mathbf{Y}_{cpeF} at extreme frequencies are like the general CPE: zero DC conductance and no admittance limit at very high frequencies.

The admittance at the extreme values of $\alpha = 0$ and $\alpha = 1$ must not be confused with the extreme values of m given in the general discussion of [Eq. 9.22 to Eq. 9.24](#) above:

$\alpha = 0$: $\varphi_{\text{CPEF}} = 0^\circ$. $\mathbf{Y}_{\text{CPEF}} = \mathbf{G}_1$: the Fricke CPE_F is an ideal conductance.

$\alpha = 1$: $\varphi_{\text{CPEF}} = 90^\circ$. $\mathbf{Y}_{\text{CPEF}} = j\omega\tau\mathbf{G}_1$. The Fricke CPE_F is an ideal capacitor, with $C = \tau G_1$.

A CPE_F has the locus of a straight line through the origin in the Wessel diagram, just as the general CPE, [Figure 9.10](#). Notice that the factor $(j\omega)^\alpha$ implies a Fricke-compatible CPE_F, but the factor $j^\alpha\omega^m$ ($m \neq \alpha$) implies a Fricke (and Cole) noncompatible CPE.

In conclusion: For a general CPE, there is no correlation between the frequency exponent m and the constant phase angle φ_{CPE} . However, for a Fricke CPE_F, $\varphi_{\text{CPEF}} = m\pi/2 = \alpha\pi/2$.

Control of Fricke Compatibility

For a data set, one procedure is to plot the data in a Wessel diagram, and then do a best fit to adapt a circular arc to the data. The extension of this arc gives, for example, G_o , G_∞ , and α . τ_c is found from the characteristic frequency f_c corresponding to the apex of the arc, from the equation $\omega_c\tau_c = 1$. *However, this is under the assumption that the data set is in accordance with Fricke's law and a CPE.* As shown in [Section 9.2.5](#), there are CPEs that do not have the link between the frequency exponent m and the constant phase angle φ . If the data are in disagreement with Fricke's law, the parameters found from the arc in the Wessel diagram do not correspond to the parameters G_o , G_∞ , α , and τ of the Cole equation. A perfect circular arc locus is not a proof of accordance with the rule of Fricke or the equations of Cole, as shown, for example, by [Eq. 9.27](#) and [Figure 9.12](#). A data check for Fricke compatibility can be done by plotting, for example, R or X or C_s or G or B or C_p as a function of log-frequency and determine the frequency exponent m , and then check whether m corresponds to the α found in the Wessel diagram. With reference to [Figure 9.15](#) and the ratio u/v , it can be shown that $u/v = (\omega\tau)^\alpha$ for admittance and $(\omega\tau)^{1-\alpha}$ for permittivity. $\log(u/v)$ plotted as a function of $\log(f)$ is therefore a straight line for a circular arc. α can be found from the slope being equal to $\alpha\pi/2$. The characteristic time constant τ_c can be found from the intercept of the straight line and the vertical axes at $\log(f) = 0$, this $\log(u/v)$ -value is equal to $\alpha \log(\tau_c)$.

9.2.6 Cole Equations (1940)

Immittance is the dependent variable in the Cole equations. For most biological systems, it is observed that the center of the impedance circular arc locus is situated below the real axis in the Wessel diagram. This was clear from the late 1920s, and Cole and Fricke published diagrams and equations based upon a frequency-independent phase angle. But in 1940, Kenneth S. Cole proposed the following empirical equation: $z = z_\infty + (r_o - r_\infty)/(1 + (j\omega\tau)^\alpha)$ to describe tissue impedance. The basis was findings

he presented in 1928 and onwards. In 1940, he explained the frequency dependence as membrane capacitive effects, and not relaxation as he did one year later together with his brother. Actually the term z_∞ is misleading and is replaced by an ideal resistor R_∞ in the usually quoted version of the *Cole_z equation*:

$$Z = R_\infty + \frac{\Delta R}{1 + (j\omega\tau_z)^\alpha} \quad [\Omega] \quad \Delta R = R_o - R_\infty \quad (9.26)$$

The subscripts for the resistances relate to frequency. The simplest equivalent circuit for this equation is with two ideal resistors and one CPE immittance. Examining the equations in Section 12.2, we see that the *series* version has the advantage that $R = R_\infty$ and $\Delta R = \Delta R$ directly and that the circuit is characterized with only one time constant. The simplest equivalent circuit for the Cole_z Eq. 9.26 is therefore the one shown in Figure 9.11. Here $\Delta G = 1/\Delta R$, the symbol ΔG is preferred to G_o because it is not the DC value of the system.

If we omit the series resistance R_∞ in Eq. 9.26, we find the admittance of the remaining parallel part of the circuit to be: $Y_{Cole} = \Delta G + \Delta G(j\omega\tau_z)^\alpha$. This admittance is difficult to handle because it has no characteristic time constant of finite value; the admittance locus of Y_{Cole} is a line. τ is merely a frequency scaling factor (see Section 9.2.5). By using the impedance form, the locus becomes a circular arc with a characteristic time constant τ_Z :

$$Z_{Cole} = \frac{1}{\Delta G + \Delta G(j\omega\tau_z)^\alpha} \quad [\Omega] \quad (9.27)$$

Equation 9.27 describes an ideal conductance in parallel with a Fricke CPE_F; we may call it the *parallel Cole element*. Together with the series resistor R_∞ , they form a

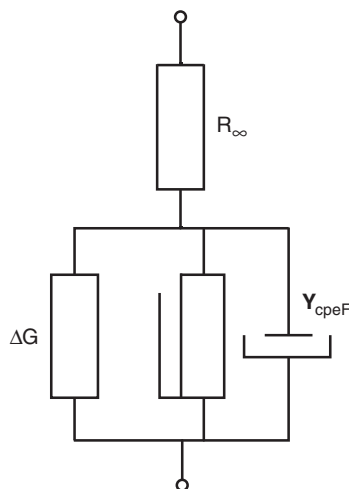


Figure 9.11: The complete Cole_z-system.

complete Cole series system. The impedance and capacitance of the Fricke CPE_F alone is:

$$\begin{aligned} Z_{\text{cpeF}} &= \frac{1}{\Delta G(j\omega\tau_Z)^\alpha} \quad [\Omega] \\ C_{\text{cpeF}} &= \omega^{\alpha-1} \tau_Z^\alpha \Delta G \sin \frac{\alpha\pi}{2} = \frac{\Delta G}{\omega} (\omega\tau_Z)^\alpha \sin \frac{\alpha\pi}{2} \quad [\text{farad}] \end{aligned} \quad (9.28)$$

The Cole element is a very special combination of a Fricke CPE_F and a parallel ideal (DC) conductance ΔG , so that ΔG also controls the magnitude of the CPE_F admittance. A change in a parallel conductance influences the magnitude (not the α) of the Z_{cpeF} so the parallel conductance is not a separate mechanism, but a part of the Cole dispersion mechanism. The Cole_Z equation does not allow an independent variable DC conductance in parallel with the CPE_F without disturbing the components of the CPE. This may limit the applicability of the Cole_Z equation in many real systems, because parallel processes are often independent of the CPE_F. For example, in the skin, with sweat duct conductance in parallel with the capacitive properties of the stratum corneum, the series model has serious limitations. However, the series resistance R_∞ of the Cole_Z equation is not correlated with the parameters of the Z_{elem} : ΔG , τ , or α . R_∞ may therefore freely be regarded as an independent access resistance to the parallel Cole element.

In the *impedance* (Z-plot) Wessel diagram, the series resistance R_∞ of the Cole system moves the arc of the Cole element to the right along the real axis a distance equal to the value of R_∞ , and with no influence on the characteristic frequency (Figure 9.12).

Cole Equation in Admittance Form

By examining the equations for the equivalent circuits in Section 12.2, we find that it is the *parallel* 2R-1C circuit that is best suited. Then the components in the equivalent circuit are directly equal to the parameters in the equation (G_0 and ΔG). Accordingly, the Cole_Y equation in admittance form is:

Cole equation :

$$Y = G_0 + \frac{\Delta G}{1 + (j\omega\tau_Y)^{-\alpha}} \quad [S] \quad \Delta G = G_\infty - G_0 \quad (9.29)$$

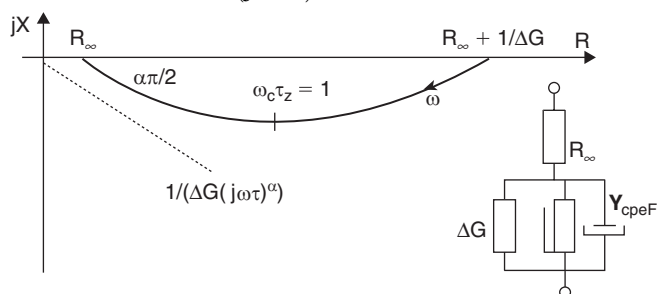


Figure 9.12: The impedance locus (ZARC) of the Cole_Z system.

Equation 9.29 may be decomposed in its real and imaginary parts:

$$Y' = G_0 + \Delta G \frac{1 + (\omega\tau)^{-\alpha} \cos\left(\frac{\alpha\pi}{2}\right)}{1 + 2(\omega\tau)^{-\alpha} \cos\left(\frac{\alpha\pi}{2}\right) + (\omega\tau)^{-2\alpha}} \quad [S] \quad (9.30)$$

$$Y'' = \Delta G \frac{(\omega\tau)^{-\alpha} \sin\left(\frac{\alpha\pi}{2}\right)}{1 + 2(\omega\tau)^{-\alpha} \cos\left(\frac{\alpha\pi}{2}\right) + (\omega\tau)^{-2\alpha}} \quad [S] \quad (9.31)$$

Such decompositions can of course also be made of the Cole impedance equation as well as the conductivity and permittivity equations. Equations 9.30 and 9.31 illustrate how extremely compact the Cole and Cole–Cole equations are.

The subscripts for the conductors relate to frequency. The best equivalent circuit is shown in Figure 9.13. The resistor $\Delta R (=1/\Delta G)$ and the CPE_F are now in series, and it is better to operate with the impedance of the CPE_F :

$$\begin{aligned} Z_{cpeF} &= \Delta R(j\omega\tau_Y)^{-\alpha} = \Delta R(\omega\tau_Y)^{-\alpha} \left(\cos\left(\frac{\alpha\pi}{2}\right) - j \sin\left(\frac{\alpha\pi}{2}\right) \right) \quad [\Omega] \\ C_{cpeF} &= \frac{\omega^{\alpha-1} \tau_Y^\alpha}{\Delta R \sin\left(\frac{\alpha\pi}{2}\right)} = \frac{(\omega\tau_Y)^\alpha}{\omega \Delta R \sin\left(\frac{\alpha\pi}{2}\right)} \quad [\text{farad}] \end{aligned} \quad (9.32)$$

In the Cole parallel model, the capacitance of the Fricke element C_{cpeF} is dependent on ΔR , α , ω , and τ_Y . A variable G_0 will not disturb the locus curve form in the admittance

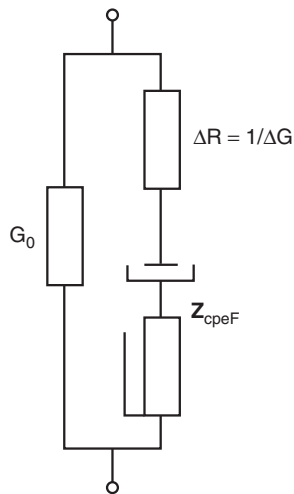


Figure 9.13: The complete Cole_Y system.

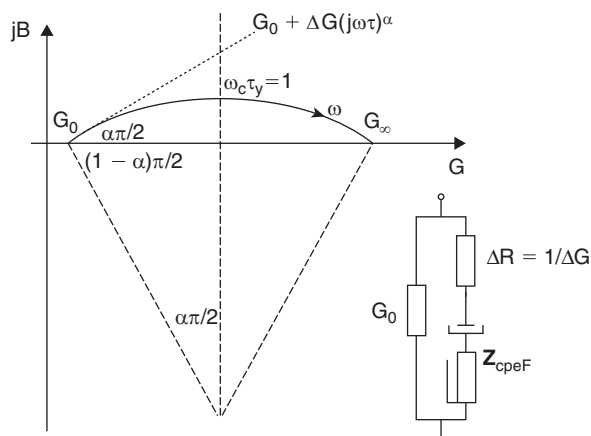


Figure 9.14: The admittance locus (YARC) of the Cole_Y system.

Wessel diagram, but move the arc along the real axis, Figure 9.14. C_{cpeF} , α , ΔR , the characteristic frequency, and the frequency scale on the arc will not change, but G_∞ will change.

Because $\mathbf{Y} = \sigma A/d$, and A/d is equal for all the components, Eq. 9.29 may be written:

$$\sigma = \sigma_0 + \frac{\Delta\sigma}{1 + (j\omega\tau_Y)^{-\alpha}} \quad [\text{S/m}] \quad (9.33)$$

If we omit the parallel conductance G_0 in Eq. 9.29, we find the impedance of the remaining part of the circuit to be $Z_{Cole} = \Delta R + \Delta R(j\omega\tau)^{-\alpha}$, or

$$\mathbf{Y}_{Cole} = \frac{1}{\Delta R + \Delta R(j\omega\tau_Y)^{-\alpha}} \quad [\text{S}] \quad (9.34)$$

This is a Fricke CPE_F in series with an ideal resistor; we may call it the *series Cole element*. Together with the parallel conductance G_0 , they form the *complete Cole parallel system*.

The term ΔR is found *both* in the Cole CPE_F and the series resistance of Eq. 9.34. A change in a series resistance influences the value of the CPE_F, so the series resistance is *not a separate mechanism*, but a part of the Cole polarisation mechanism. The Cole_Y equation does not allow an *independent* variable DC resistor in series with the CPE_F. This limits the applicability of the Coley equation in many real systems, because often series processes are processes independent of the CPE_F. However, the parallel conductance G_0 of the Cole_Y equation is not correlated to ΔR , nor to τ or the α of the Z_{Cole} . G_0 may therefore freely be regarded as an *independent* parallel conductance to the series Cole element. For example, in the skin, with sweat duct conductance in parallel with the

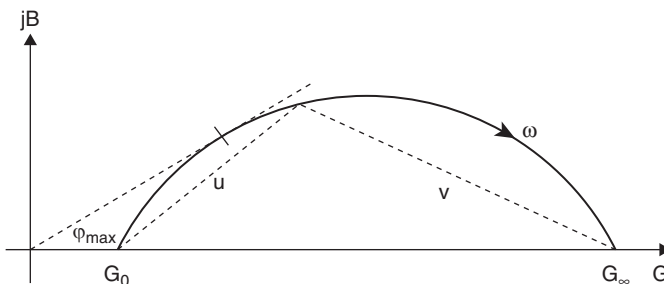


Figure 9.15: YARC plot showing the u - v variables and the maximum possible measured phase angle φ_{\max} .

capacitive properties of the stratum corneum, the parallel Cole model may therefore be a better choice than the series model.

Figure 9.15 shows the admittance locus of a Coley system with the u and v lengths defined (to be used for control of Fricke compatibility). Measured phase angle φ is smaller than $\alpha\pi/2$, φ_{\max} , and the corresponding angular frequency are shown on the figure.

In Conclusion

For Cole-compatible systems, the immittance arc locus is completely defined by three parameters, for example, G_0 , ΔG , and α . Vice versa: A given arc completely defines three parameters: G_0 , ΔG , and α .

The fourth parameter is the characteristic time constant τ_c , which defines the frequency scale. Vice versa: a given frequency scale defines the characteristic time constant.

These four parameters are independent as variables. τ is so only because one of the two ideal resistors of a Cole system is correlated with the CPE.

The Cole equations are descriptive in their nature. Even so, many have tried to use them for explanatory purposes but usually in vain. If a Cole model all the same is to be used not only for descriptive, but also for explanatory purposes, it is necessary to discuss the relevance of the equivalent circuit components with respect the physical reality that is to be modeled. Because the Cole models are in disagreement with relaxation theory, this is not easy. A more general dispersion model, Eq. 9.43, may help circumvent problems occurring when the characteristic frequency is found to vary and DC paths with independent conductance variables cannot be excluded.

The Alpha (α) Parameter

Characterizing tissue with the α parameter has the advantage that the parameter is not dependent on the geometry of the tissue sample as long as the measured tissue volume is constant and not a function of frequency. α is then a material constant like ϵ .

Table 9.1: The Exponent α in Cole Equations

Equation	Exponent	Equivalent Circuit Components	
		$\alpha = 0$	$\alpha = 1$
Z	α	Ideal resistors	Ideal resistors and capacitor
Y	$-\alpha$	Ideal resistors	Ideal resistors and capacitor
ϵ	$1 - \alpha$	Ideal resistor and capacitors (Debye)	Ideal capacitors

It is a common observation that the value of Z for tissue decreases with frequency, Y increases with frequency, and ϵ decreases with frequency. By choosing α as an exponent in the Z equation (Cole 1940), $-\alpha$ in the Y equation, and $1 - \alpha$ (equivalent to the loss factor of a capacitor: the phase angle of an ideal capacitor is 90° , but the loss angle is 0°) in the ϵ equation (Cole, 1940; Cole–Cole, 1941), the correct frequency dependence is taken care of *with the same α value independently of model, α being always positive: $1 \geq \alpha \geq 0$.* It is possible to regard the parameter α in several ways:

- As a measure of a distribution of relaxation times (DRT).
- As not due to a DRT, but based upon the theory of many body interactions between clusters in the material. Such a nonempirical model has been developed by Dissado-Hill (1979).
- As a measure of the deviation from an ideal resistor and capacitor ($\alpha = 0$) in the equivalent circuit.
- According to energy models (e.g., charge carriers trapped in energy wells).
- According to physical processes such as Warburg diffusion.

According to the first interpretation, the spread of relaxation times may be due to:

- (1) different degrees of molecular interaction (no interaction $\alpha = 1$, ideal capacitor),
- (2) cellular interactions and properties of gap junctions,
- (3) anisotropy,
- (4) cell size,
- (5) fractal dimensions.

Table 9.1 shows a summary according to Interpretations 1 and 3. $\alpha = 0$ corresponds to the lossy case, $\alpha = 1$ for the permittivity corresponds to the no loss case. α is therefore analogue to the phase angle, $1 - \alpha$ to the loss angle (see Section 3.3).

Augmented Fricke CPE_F

Freely Chosen Augmenting Ideal Resistor

We may *augment* the Fricke CPE_F by adding a resistor G_{var} (an ideal, frequency independent DC conductance) to a CPE_F. Let us consider the case with G_{var} in *parallel* with the CPE_F (Eq. 9.35). With an ideal resistor augmenting a CPE in *series*, the case will be similar.

The *admittance* locus will still be a line, but not through the origin, Figure 9.16.

$$Y_{\text{cpeFA}} = G_{\text{var}} + G_1(j\omega\tau)^\alpha \quad (9.35)$$

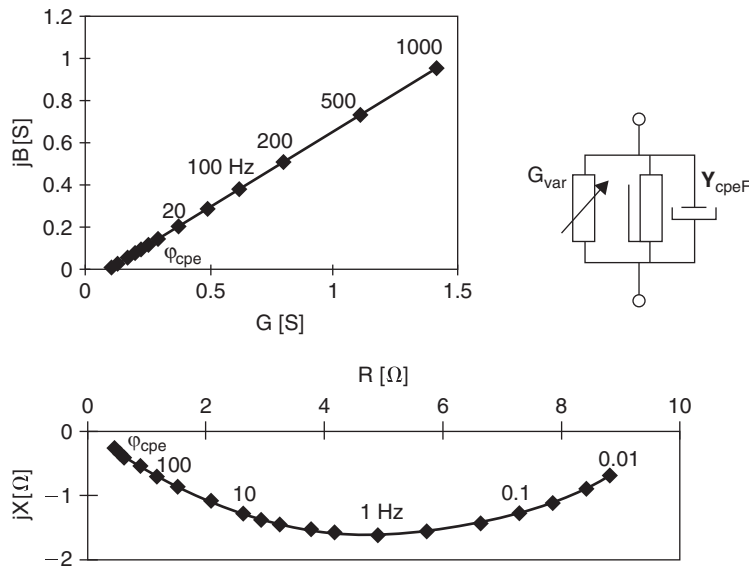


Figure 9.16: Y-Plot and Z-Plot for a CPE_F with a freely chosen $G_{var} = 0.1$ [S]. $\alpha = 0.4$ ($\varphi = 36^\circ$), $G_1 = 0.1$ [S], $\tau = 0.1$ [s].

In the admittance plane, the parallel combination will not have a finite characteristic time constant, and τ has the character of being just a frequency scale factor. Inverted to the impedance plane, *the added conductor G_{var} causes the locus to be a circular arc with a characteristic time constant $\tau_c = \tau_Z$ and frequency ω_c corresponding of the apex (the point of maximum magnitude of reactance) of the arc.*

In general, τ_Z will be dependent on G_{var} , this easily shown by programming these equations in a spreadsheet, an example is illustrated in [Figure 9.17](#).

This model with a free variable conductance in parallel with a CPE or CPE_F is often found in the literature and analyzed as if being in agreement with the Cole model which it is not. [Equation 9.35](#) is a non–Cole-compatible model that can be used if both conductance and characteristic frequency or time constant are found *to vary during an experiment*.

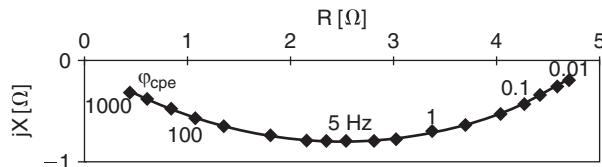


Figure 9.17: Demonstration of τ_Z being dependent on the augmenting conductor G_{var} . Higher conductance leads to higher characteristic frequency. Parameters as for [Figure 9.16](#) except that $G_{var} = 0.2$ [S].

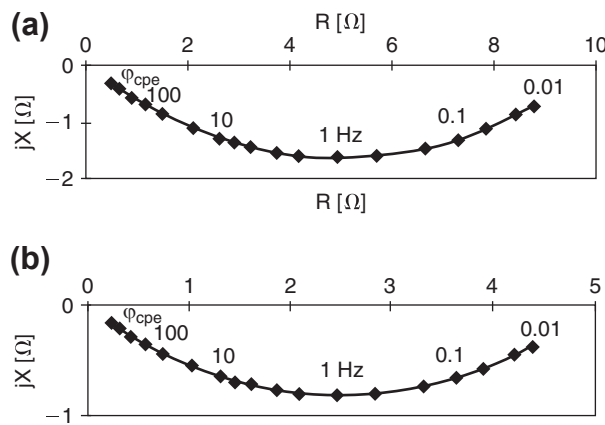


Figure 9.18: Demonstration of τ_Z being *independent* of the augmenting conductor (Cole case). Z-plot for a CPE_F with a Cole-compatible parallel conductor. No change of characteristic frequency; the only changes are the scales on the axes. (a) $G_{\text{var}} = G_1 = 0.1 \text{ [S]}$; (b) 0.2 [S] ; other parameters as for Figure 9.16.

Cole Compatible Augmented CPE_F

Restricting the value of G_{var} ($=1/R$) so that it is equal to the G_1 of the CPE_F element, gives a special case with different properties. The impedance of such a Cole element is:

$$Z_{\text{Cole}} = \frac{R}{1 + (j\omega\tau_Z)^{-\alpha}} \quad (9.36)$$

Equation 9.36 describes a parallel Cole element (see Eq. 9.32), G_{var} is now a dependent variable. With ideal components, the time constant of a parallel circuit is $\tau = C/G$, and thus dependent on the parallel conductance. In Eq. 9.27, the characteristic time constant is dependent on the parallel conductance G_{var} . However, in the special case of Eq. 9.28, the parallel conductance *does not* influence the characteristic time constant. τ_Z and the characteristic frequency ω_c corresponding to the apex of the ZARC is determined by the equation $\omega_c\tau_Z = 1$ and is independent of $G_{\text{var}} = G_1$ and α . This is the Cole case and has been obtained by linking the DC conductance value G_{var} to the magnitude of the immittance value of the CPE. The case is illustrated in Figure 9.18.

Equation 9.28 is a part of the Cole equation (see Section 9.2.6). If the characteristic frequency ω_c is found to vary during an experiment, it is a reason to believe that this is due to an independent parallel conductance, the process cannot be modeled with Eq. 9.28, and the process is Cole incompatible.

In conclusion, a circular arc locus in the immittance Wessel diagram can:

- not be due to a CPE alone
- be due to a general CPE augmented by an ideal resistor in parallel or series (not Fricke, not Cole compatible)
- be due to a Fricke CPE_F augmented by an ideal resistor of freely chosen value in parallel or series (not Cole compatible)
- be due to a Fricke CPE_F augmented by an ideal resistor of a particular value in parallel or series (Cole compatible)

9.2.7 Cole–Cole Equations (1941)

Permittivity is the dependent variable in the Cole–Cole equations. In 1941, Cole and Cole proposed the following version:

Cole–Cole equation

$$\epsilon = \epsilon_\infty + \frac{\Delta\epsilon}{1 + (j\omega\tau_0)^{1-\alpha}} \quad \epsilon_s - \epsilon_\infty = \Delta\epsilon \quad [\text{F/m}] \quad (9.37)$$

Here ϵ_s is used for static values (and not ϵ_0 which is reserved for vacuum permittivity). This is in agreement with the complex permittivity as $f \rightarrow 0$: in this model ([Figure 9.19](#)) there is no DC conduction and accordingly electrostatic conditions.

As $C = \epsilon A/d$, the Cole–Cole equation [Eq. 9.37](#) may equally well be written as a capacitance equation:

$$C = C_\infty + \frac{\Delta C}{1 + (j\omega\tau_0)^{1-\alpha}} \quad [\text{F}] \quad (9.38)$$

By inspection of the equations for the two-capacitor models found in [Section 12.2](#), we find the parallel version best adapted. According to [Eq. 12.24](#), it can be characterized by one single time constant. The equivalent circuit is shown on [Figure 9.19](#).

Notice that when $\omega \rightarrow \infty$, $C_{\text{cpeF}} \rightarrow 0$ ([Eq. 9.32](#)), thus decoupling ΔC (even if the fact that $Z_{\text{cpeF}} \rightarrow 0$ ([Eq. 9.32](#)) could lead to the false conclusion that ΔC actually is in the circuit).

A *Cole–Cole plot* is permittivity plotted in a Wessel diagram. If the permittivity is according to the Cole–Cole equation, the locus will be a circular arc. The permittivity used in the Cole–Cole equations implies that the model is changed from regarding tissue as a conductor (2R-1C model) to regarding tissue as a dielectric (1R-2C model) with only bound charges and dielectric losses. A 2R-1C model cannot have the same spectrum as a 1R-2C model with a fixed set of component values, so an arc locus in one model will not result in an arc locus in the other model. In living tissue, there is a substantial DC conductance. Such

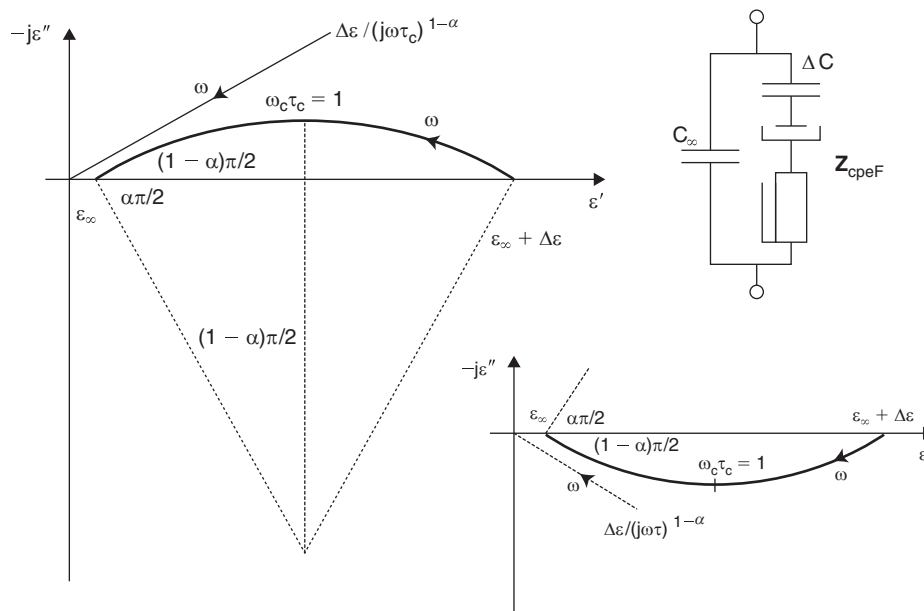


Figure 9.19: Equivalent circuit for the Cole–Cole permittivity equation.

conductance in parallel disturbs the circular arc locus (see Figure 9.19, upper part) and *must be subtracted for permittivity circular arc analysis*. Vice versa: if the admittance values are represented by a circular arc locus, the permittivity derived from it *will not* be a circular arc. In conclusion, admittance is linked with a 2R-1C equivalent circuit, and permittivity is linked with a 1R-2C circuit. With fixed component values, these equivalent circuits cannot be made to have the same frequency dependence.

9.2.8 Symmetrical Distribution of Relaxation Times

Perfect Circular Arcs, Cole-Compatible Distribution of Relaxation Times

The characteristic time constant τ_c in the form of τ_Z and τ_Y of Eqs (9.26) and (9.29) deserves some explanation. A two-component RC circuit with ideal components has a time constant $\tau = RC$. A step excitation results in an exponential response. With a CPE, the response will not be exponential. In Section 9.2.5, the time constant was introduced simply as a frequency scale factor. However, the *characteristic* time constant τ_c may be regarded as a mean time constant because of a DRT. When transforming the Cole_Z impedance \mathbf{Z} to the Cole_Y admittance \mathbf{Y} or vice versa, it can be shown that the α s of the two Cole Eqs 9.26 and 9.29 are invariant, but the characteristic time constants τ_c are not. In fact:

$$\tau_Y = \tau_Z (\Delta G R_\infty)^{1/\alpha} = \tau_Z \left(\frac{R_\infty}{R_0} \right)^{1/\alpha} \quad (9.39)$$

$\tau_Y < \tau_Z$ because R_∞ is always less than R_0 .

It is possible to determine the relationship between the DRT and the two parameters α and τ in the Cole–Cole equation (Cole and Cole, 1941):

$$p(\ln \tau) = \frac{1}{2\pi} \frac{\sin \alpha \pi}{\cosh \left[(1 - \alpha) \ln \frac{\tau}{\tau_0} \right] - \cos \alpha \pi} \quad (9.40)$$

Where $p(\ln \tau)$ is the spectral density of time constants and τ_0 is the mean relaxation time. This Cole–Cole distribution is the only distribution corresponding to a Fricke CPE_F. The distribution is broad, allowing for a considerable density two decades away from the mean (characteristic) time constant (Figure 9.20).

Quasi-Circular Arcs

Other distributions than the Cole–Cole of Eq. 9.40 are possible; for instance, a constant function extending over a limited range of time constants. Such different distributions result in Wessel diagram loci surprisingly similar to circular arcs, Schwan (1957). High-precision measurements, calculations, and plotting is necessary to determine the type of DRT. Actually a plot in the complex plane is much more sensitive to whether the distribution is logarithmically symmetrical. *An estimation in the Wessel diagram is therefore more about whether the time constants are logarithmically symmetrical distributed than whether the data actually are in agreement with a Cole–Cole model.* The popularity of the Cole–Cole model is due to the fact that by choosing the arc as the best regression curve to the data points found, the mathematical

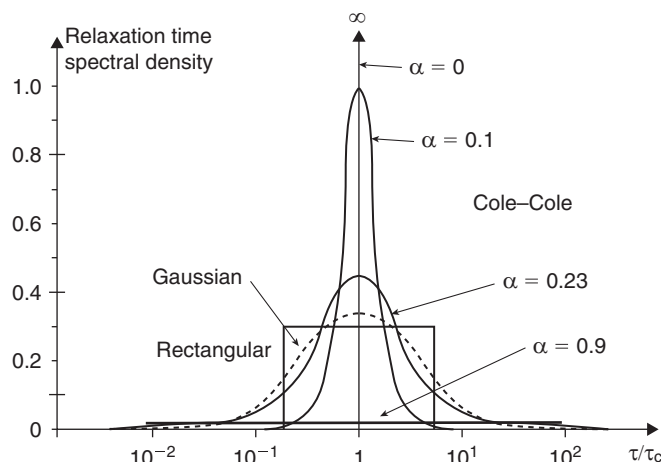


Figure 9.20: Time constant distribution for four different Cole (immittance) cases, and in addition the log-normal (*Gaussian*) and rectangular distributions. They are all symmetrical around the characteristic time constant τ_c , and correspond to circular arcs (Cole) or near-circular arcs. $\alpha = 0$ is a single time constant (Debye) case.

equations become apparently simple (the Cole equations), and the corresponding equivalent circuits also become simple.

9.2.9 Nonsymmetrical DRT and Multiple Cole Systems

Davidson and Cole (1951) proposed another version of the Cole–Cole equation:

$$\epsilon = \epsilon_\infty + \frac{\Delta\epsilon}{(1 + j\omega\tau)^\beta} \quad (9.41)$$

Havriliak and Negami (1966) and Williams and Watts (1970) proposed even more general versions of the form:

$$\epsilon = \epsilon_\infty + \frac{\Delta\epsilon}{[1 + (j\omega\tau)^\alpha]^\beta} \quad (9.42)$$

These equations do not correspond to circular arcs in the complex plane, but to a nonsymmetrical DRT with a larger density of relaxation times on the low-frequency side.

With measured data showing a nonsymmetrical DRT, the choice of model is important; for example, a model according to this section or a model with multiple Cole systems (see the next section).

Parameters similar to those, for example, of the Cole equation, can also be computed without choosing a model. Jossinet and Schmitt (1998) suggested two new parameters that were used to characterize breast tissues. The first parameter was the distance of the 1 MHz impedance point to the low-frequency intercept in the complex impedance plane and the second parameter was the slope of the measured phase angle against frequency at the upper end of the spectrum (200 kHz–1 MHz). Significant differences between carcinoma and other breast tissues were found using these parameters.

Dispersion Model in Accordance with Relaxation Theory

The Cole single-dispersion impedance model (Eq. 9.26) is based upon an ideal conductance as a dependent variable and a characteristic time constant as an independent variable. Usually, however, the characteristic time constant of tissue or cell suspensions is a function of conductance according to relaxation theory (see Section 3.4). The Cole model is therefore not in accordance with relaxation theory (Figures 9.21 and 9.22).

A more general dispersion model can be deduced from the already presented Eq. 9.35 and is found to be (Grimnes and Martinsen, 2005):

$$Z = R_\infty + \frac{1}{G_{\text{var}} + G_1(j\omega\tau_Z)^\alpha} \quad (9.43)$$

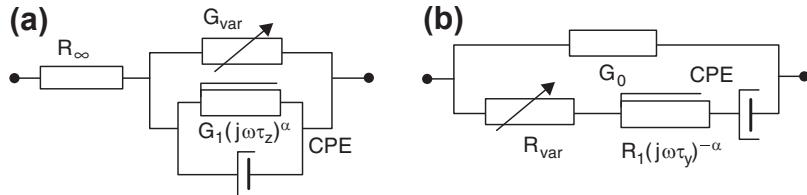


Figure 9.21: Dispersion model in accordance with relaxation theory (Eq. 9.43).
 (a) Impedance model and (b) admittance model.

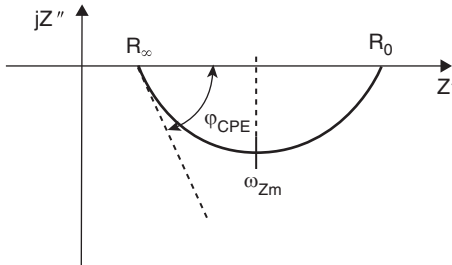


Figure 9.22: A circular arc locus in a Z-plot example is determined from measured spectrum data. The arc defines three parameters: R_0 , R_∞ , and φ_{CPE} . ω_{Zm} is taken from the apex of the arc. These values are put into Eq. 9.44, and variations in, for example, α and G_1 can be followed separately.

Here τ_Z is a nominal time constant according to the Cole model when τ_Z is a free variable but G_1 and G_{var} are not, $G_1 = G_{var}$. The time constant as a dependent variable is expressed by Eq. 9.39. τ_{Zm} is the time constant changing with changing conductance. If G_{var} increases, the time constant τ_{Zm} decreases, and this is in accordance with relaxation theory.

$$\tau_{Zm} = \frac{1}{\omega_{Zm}} = \tau_Z \left(\frac{G_1}{G_{var}} \right)^{1/\alpha} \quad \text{or} \quad G_1 = \frac{G_{var}}{(\tau_Z \omega_{Zm})^\alpha} \quad (9.44)$$

The equivalent circuit is shown on Figure 9.21 for the impedance and admittance cases.

A consequence of the model is that the apex of an immittance locus no longer necessarily corresponds to the Cole characteristic time constant, it corresponds to τ_{Zm} and Eq. 9.44.

Let us see how we proceed from measurement results to model variables. We start by making, for example, a Z-plot in the Wessel plane with measured values; let us assume that we are dealing with a single dispersion. The three variables R_0 , R_∞ , and φ_{CPE} are determined from the arc position and geometry, and from them $G_{var} = (R_0 - R_\infty)^{-1}$ and $\alpha = \varphi_{CPE}/90^\circ$ are calculated. The characteristic frequency ω_{Zm} is taken from the apex of the arc, and the time constant $\tau_{Zm} = 1/\omega_{Zm}$ calculated. From Eq. 9.39 we can then follow

variations in G_1 by choosing an arbitrary nominal time constant τ_Z , for example, equal to 1 s. With the Cole model, four parameters are determined from a measured data set; in the new model, five parameters are determined. With the new model, it is possible to test such hypotheses as whether the CPE has remained constant during an experiment or whether the free conductance G_1 value alone has changed. Such tests are impossible with the Cole model.

Multiple Cole Systems

With a given data set obtained from measurements, it must be decided how the data are to be interpreted and presented (see [Section 9.1](#)). This immediately leads to the question of which model should be chosen. The same data can be interpreted using Cole variables such as α and τ , but also with many non-Cole models as explained in earlier chapters. As we shall see, many datasets can be explained with multiple dispersions, for example, multiple Cole systems. As we now present multiple Cole systems, it must always be kept in mind that the tissue dataset certainly could have been made to fit other models. The ability to fit the multiple Cole model to the data set *is not a proof* that this model is the best one for describing, or explaining, the data found. Skin is, for instance, used as an example in this chapter, and we know that skin data are not necessarily in agreement with the Cole–Cole model.

As stated in [Section 9.2.6](#), the four-component equivalent circuit may be used as a model for the Cole equation. The Cole equation represents a single electrical dispersion with a given distribution of relaxation times and can hence be an interesting model for a macroscopically homogenous tissue within a limited range of frequencies. A practical experimental setup will, however, in most cases involve a measured object that can be divided in two or more separate parts, where each of these parts can be modeled by an individual Cole equation. Furthermore, when measuring over a broader frequency range, different dispersion mechanisms will dominate in different parts of the frequency range, and each of these mechanisms should also be ascribed to an individual Cole equation. We will suggest using the phrase *Cole system* for any system comprising one predominating dispersion mechanism that is decided to be adequately represented by one single Cole equation. This section deals with the necessity and problems of identifying more than one Cole system in a measured object.

Consider an assembly of Cole systems like the one shown in [Figure 9.23](#). This electrical equivalent corresponds with the object under investigation when doing impedance measurements on human skin. Measured data may represent contributions from electrode polarization, stratum corneum, sweat ducts, and deeper tissue, and furthermore several dispersions of some of these components. Only one Cole system is shown for the electrode polarization, although two dispersions have been found in some studies (Onaral and Schwan, 1982). The stratum corneum is dominated by one broad dispersion

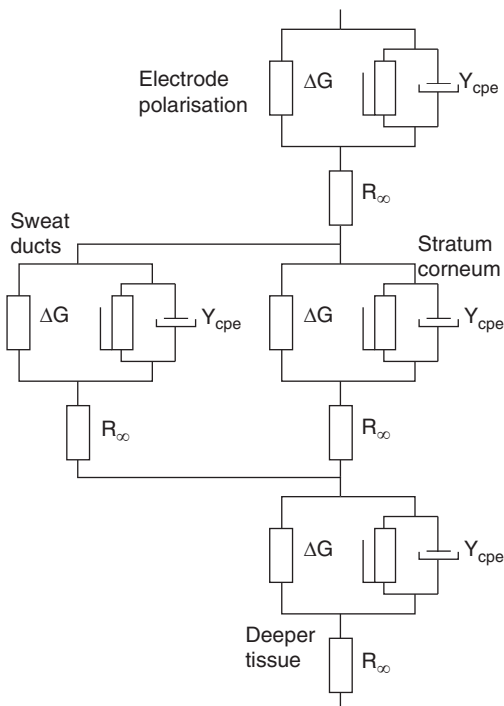


Figure 9.23: Assembly of Cole systems for measurements on skin.

(Yamamoto and Yamamoto, 1976) and the sweat ducts may exhibit dispersion because of counter-ion relaxation (Martinsen et al., 1998a). The viable skin will probably have several dispersions as explained in Section 4.2.6.

This rather incomprehensible equivalent circuit may of course be simplified on the basis of existing knowledge about the different parts of the circuit. The Cole system representing the sweat ducts will, for example, be reduced to a simple resistor because the polarization admittance most probably is negligible (Martinsen et al., 1998a). This corresponds to α being close to zero in the Cole equation. The beta and gamma dispersions of deeper tissue may be dropped if the measurements are made at sufficiently low frequencies, and there may likewise be rationales for neglecting the electrode polarization in a given set of data. It is nevertheless of great importance to recognize all relevant Cole systems that may influence the interpretation of measured data, and then carefully make the necessary simplifications. (We choose to use the Cole system as the basic model for any separate part of the measured object because, for example, a pure resistor can readily be achieved by choosing $\alpha = 0$ in the Cole equation.)

The subsequent discussion will be restricted to the case of two Cole systems in series or parallel, and how the measured data in those two cases will appear in the complex admittance (Y-plot) or impedance (Z-plot) plane.

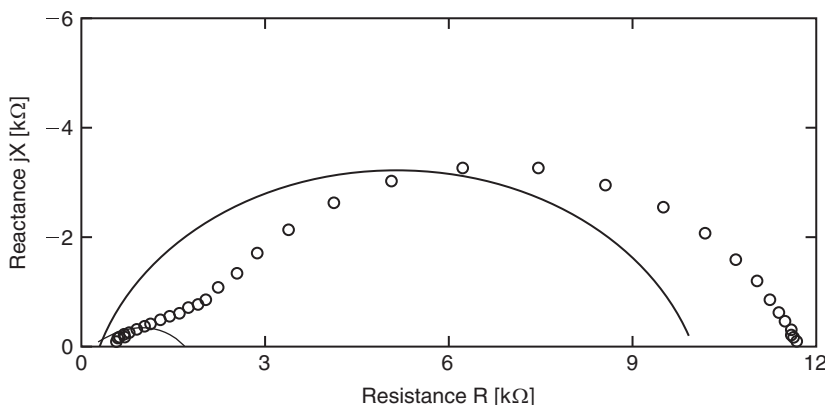


Figure 9.24: Cole plot in the impedance plane (Z-plot) for values given in [Table 9.2](#) showing system 1 (small solid arc), system 2 (large solid arc), and measured values (circles).

Consider two Cole systems in series having the following arbitrarily chosen parameters (τ is given for the impedance plane):

Each of these two Cole systems will produce a circular arc in the complex impedance plane as shown in [Figure 9.24](#), and when impedance measurements are done on the total system, complex values such as the ones indicated by circles in the diagram will be obtained.

Measurements will hence in this case reveal the presence of two Cole systems if the measured frequency range is broad enough. Measurements up to about 1 kHz will, however, only disclose one circular arc, corresponding to system 2 shifted to the right approximately by the value of R_0 in system 1.

The same data are plotted in the complex admittance plane in [Figure 9.25](#). The small arc representing system 1 in [Figure 9.24](#) has now become a large arc because of the low value of R_∞ . This illustrates the importance of using descriptions such as “small” or “large” dispersions in connection with Cole plots with considerable care. The existence of two dispersions will be revealed in this plot also, provided the frequency range exceeds 1 kHz.

The analysis will become more troublesome if the relaxation times of the two Cole systems are closer. Consider now two new Cole systems, system 3 and system 4, having almost identical parameters to the systems in [Table 9.2](#), but with the relaxation time of system 1 increased from 20 μ s to 2 ms as shown in [Table 9.3](#).

A dotted arc in [Figure 9.26](#) represents each of the two systems. The corresponding measured values show that *the existence of two Cole systems cannot be discovered in the*

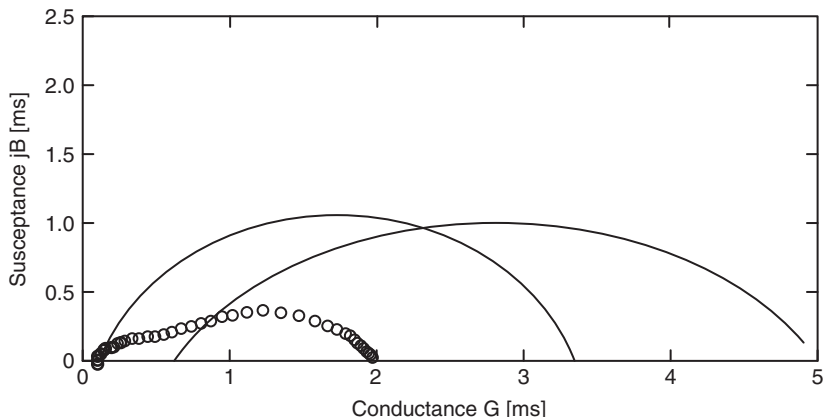


Figure 9.25: Cole plot in the admittance plane (Y-plot) for values given in [Table 9.2](#) showing system 1 (right solid arc), system 2 (left solid arc), and measured values (circles).

Table 9.2: Parameters for the Two Cole Systems in Series

	R_0	R_∞	τ_Z	α
System 1	1.7 k Ω	200 Ω	20 μ s	0.55
System 2	10 k Ω	300 Ω	5 ms	0.75

Table 9.3: New Parameters for the Two Cole Systems in Series

	R_0	R_∞	τ_Z	α
System 3	1.7 k Ω	200 Ω	2 ms	0.55
System 4	10 k Ω	300 Ω	5 ms	0.75

diagram. The natural thing will thus be to attempt to fit one circular arc to the measured values, as indicated by the solid line in [Figure 9.26](#). The parameters of this fitted arc are given in [Table 9.4](#). The values of R_0 and R_∞ are of course the sum of the corresponding values for the two isolated systems, but the most interesting features are the values of τ_Z and α . The value of τ_Z will be close to the value of the dominating system (i.e., the largest arc in the impedance plane). (For two Cole systems in parallel, this will be the largest arc in the admittance plane.) The value of α will be closer to the value of the dominating system, but may still be significantly different from either of the systems.

The same data are presented in the complex admittance plane in [Figure 9.27](#). In this plot, the arcs are about equal in size, but they produce total values that coincide well with a single circular arc. The parameters of this arc are given in [Table 9.4](#), and the most interesting thing is the value of α , which is roughly the mean of the two original values.

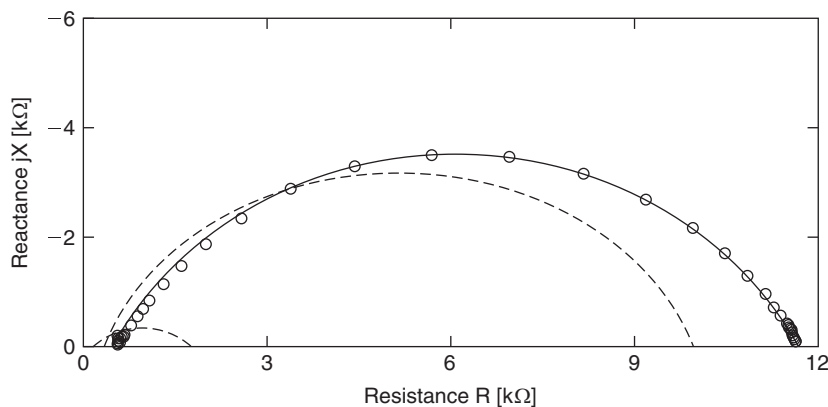


Figure 9.26: Cole plot in the impedance plane (Z-plot) for values given in [Table 9.3](#) showing system 3 (small dotted arc), system 4 (large dotted arc), measured values (circles), and fitted circular arc (solid line).

Table 9.4: Parameters for Arcs Fitted to Measured Values for the Two Cole Systems in Series

	R_0	R_∞	τ	α
Fitted impedance arc	11.7 kΩ	500 Ω	~5 ms	0.72
Fitted admittance arc	11.7 kΩ	500 Ω	~5 ms	0.67
Fitted admittance arc (low-frequency only)	11.7 kΩ	500 Ω	~5 ms	0.72

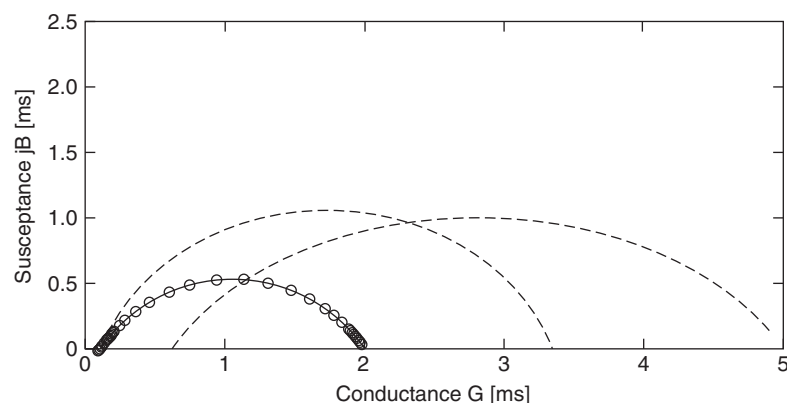


Figure 9.27: Cole plot in the admittance plane (Y-plot) for values given in [Table 9.3](#) showing system 3 (right dotted arc), system 4 (left dotted arc), measured values (circles), and fitted circular arc (solid line).

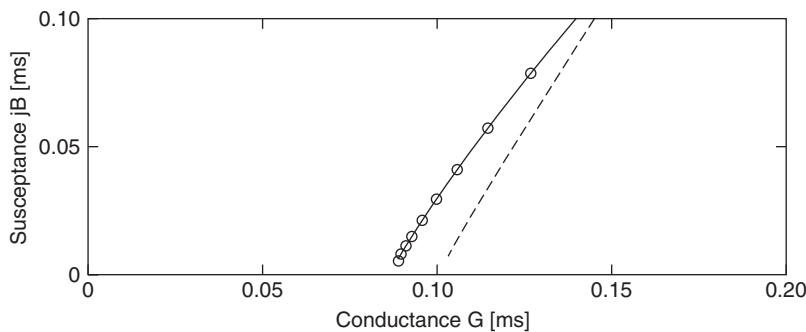


Figure 9.28: Low-frequency part of Figure 9.27, showing system 4 (dotted arc), measured values (circles), and fitted circular arc (solid line).

However, when plotting only the low-frequency part (Figure 9.28), the calculated value of α will be closer to that of system 4 as shown in Table 9.4, and, in this case, equal to the value found in the impedance plane.

The preceding examples demonstrate how two Cole systems in series influence on the measured electrical data. Two parallel Cole systems will behave in a similar manner, and we leave to the reader to investigate how systems with two parallel dispersions behave. We encourage the use of simulations such as this in order to acquire a general sense of how changing one parameter or part of a system comes out in different plots.

9.2.10 Bidomain Model

Equation 2.2: $\mathbf{J} = \sigma\mathbf{E}$ is not valid in anisotropic materials if σ is a scalar. Tissue as a rule is anisotropic. Plonsey and Barr (2000) discussed some important complications posed by tissue anisotropy and also emphasized the necessity of introducing the concept of the *bidomain* for cardiac tissue. A bidomain model is useful when the cells are connected by two different types of junctions: tight junctions and gap junctions with the cell interiors directly connected. The intracellular space is one domain and the interstitial space the other domain. Bidomain models have also been used for neural tissue (Sadleir, 2010).

9.2.11 Memristor Nonlinear Model

We are all familiar with the classic, passive circuit components; resistor, capacitor, and inductor. In a 1971 paper, however, Leon Chua argued that there was room for a fourth basic component, which he called *memristor*, short for memory resistor (Chua, 1971). The memristor is a special kind of resistor in which the resistance is dependent on the net amount of charge having passed through it. Hence, sending a current in one direction



Figure 9.29: Circuit symbol for the memristor.

through the memristor may make the resistance increase. Then stopping the current makes the resistance stay at its last value and finally sending a current in the opposite direction will make the resistance go down again. This ability to “remember” the amount of electric charge having passed it is the reason for calling it a memory resistor.

If you consider the four basic circuit variables from electromagnetism; current I , voltage V , charge Q , and magnetic flux F , then these can be combined two and two in six different combinations. Five of them are already well-known: Resistance $R = dV/dI$, capacitance $C = dQ/dV$, inductance $L = dF/dI$, Faraday’s law of induction $V = -dF/dt$, and the definition of electric current $I = dQ/dt$. The combination of magnetic flux F and charge Q is missing and from this Chua defined the memristor (or actually its property *memristance*) in the following way:

$$\text{Memristance } M = \frac{dF}{dQ} \quad (9.45)$$

He also proposed the circuit symbol shown in [Figure 9.29](#) for the memristor. Looking back, it seems the discovery by Leon Chua did not get as much attention as we today realize it deserved. One reason may be that combining magnetic flux and charge, one could not readily see how this new component could be used in practice. However, using Faraday’s law of induction and the definition of electric current in [Eq.9.45](#), it simplifies to:

$$M = \frac{dF}{dQ} = \frac{vdt}{idt} = \frac{v(t)}{i(t)} \quad [\Omega] \quad (9.46)$$

Thus, the memristor can be treated as a nonlinear resistor. The nonlinearity lies in the fact that the memristance is a function both of time and an internal state variable x , that is $M(x,t)$. This state variable is often (but not always) proportional to the electric charge Q .

Johnsen et al. (2011) showed that the measurements of electro-osmosis in human skin, shown in [Figure 8.40](#), can be closely mimicked by using memristor theory. They also explain the memristive mechanisms involved in electro-osmosis. An introduction to using memristor theory in bioimpedance and bioelectricity is given in Johnsen (2012). The whole concept has also been expanded to include memcapacitors and meminductors (Di Ventra et al., 2009).

9.2.12 Universality

There are numerous examples from the literature that disordered solids show remarkably similar frequency dependence of AC conductivity, both for electronic and ionic materials (Dyre and Scrøder, 2000). This is seen if one considers the conductivity $\sigma(\omega)$ as function of frequency ω at different temperatures. It is found that the curves for different temperatures collapse on a single universal curve if scaled according to the equation

$$\frac{\sigma(\omega)}{\sigma_{DC}} = F\left(\frac{\omega}{T\sigma_{DC}}\right) \quad (9.47)$$

where $\sigma_{DC} = \sigma(0)$ is the DC conductivity. That is, when the conductivity is normalized (each measured value divided by the DC conductivity) and the frequency is normalized with regard to both DC conductivity and temperature, the curves showing the conductivity as a function of frequency for different temperatures overlap. This phenomenon is commonly called *universality*. Such a scaling implies that the only relevant scaling parameter in the system is $1/T\sigma_{DC}$. It is well known that the DC conductivity of many disordered systems is determined by the percolating cluster (Dyre and Scrøder, 2000), and the previously mentioned scaling law implies that the DC percolation cluster determines also the AC properties of the sample, at least up to a certain frequency at which the frequency dependence saturates and the universal scaling law is no longer valid. A full understanding of the underlying reasons for universality and the conditions under which it will appear seems not to exist at present. These particular *scaling properties* have been shown both for electronic and ionic conductors (Jonscher, 1996), but to the knowledge of the authors, little has been done on biological materials. The same universal behavior will probably also be found when for example, the moisture content of the material is altered instead of the temperature (Martinsen et al., 2013).

Jonscher (1983, 1996) was very well aware of the discrepancy of dielectric discharge curves in the time domain. The Debye model was based upon supposed exponential discharge curves, but most dielectrics actually show fractional power law discharge curves. Because “most” dielectrics follow fractional power law behavior, such behavior was called the “universal” behavior.

But Jonscher was apparently not aware that Cole already in 1928 used the circle segment analysis in the Wessel plane and found many circular arcs with suppressed circle centers. The concept of CPE was introduced, and in Cole and Cole (1941), the idea was introduced that a dielectric could have a distribution of many relaxation time constants. The Debye model with ideal components presupposed one single relaxation time constant and therefore a complete semicircle. However, the Cole–Cole model implied that the distributed time constants do not correspond to one exponential, but a fractional power law. It seems that Jonscher (1996) did not accept the theory of distributed

time constants and therefore pursued the idea that the findings were due to other “universality” laws.

9.3 Data Calculation and Presentation

9.3.1 Measured Data, Model Data

Measured data and model data: the one cannot live without the other. A clear distinction is necessary between measured “raw” data, *calculated measured* data, and *derived* data. All these data are both obtained and analyzed according to models, equations included, as described in Sections 8.1, 9.1, and 9.2.

The measuring setup determines which data are *raw* data. If a constant amplitude current is applied to a set of electrodes and the corresponding voltage is measured, this voltage is directly proportional to the impedance of the unknown. Then raw data and the measured variable are impedance.

Raw data have to be presented in some chosen form. Some of the data is collected as a function of time, some as a function of frequency. If data are collected as a function of both frequency and time, the need for a three-dimensional presentation is present.

By a simple mathematical operation, the inverse values of impedance may be *calculated*, the admittance values found contain no additional information, and the calculations do not contain any apparent conditions with respect to any disturbing influence such as temperature, atmospheric pressure etc.: it is a purely mathematical operation. Therefore the admittance data are correct to the extent that the impedance data are correct; it is just two different ways presenting the measured data.

The problem of *derived* data is much larger, the variable of interest may be nonelectrical (e.g., tissue water content), derived from electrical variables. Then a new question arises: what *other* variables influence the correlation between the water content and the measured electrical variable? This is a *selectivity* problem and a *calibration* problem.

If the measured volume can be defined (not always possible in measurements *in vivo*), admittivity may be calculated, and also permittivity. Permittivity cannot be measured, only be calculated; capacitance can be measured. If instead an index is calculated (see the next section), knowledge of dimensions is not needed, but it must be ascertained that measured data are from the same tissue volume.

The interpretation of the measured data is always linked to some sort of model: an equation or a black box concept. Choosing a model is a major decision, and so is whether it is to be a descriptive or explanatory (see Section 9.1). The task is to choose a productive model, for example, as simple as possible but not too simple, allowing conclusions and predictions.

9.3.2 Indexes

An index is the ratio between two measurements made under different conditions but *on the same sample volume*. The index can be calculated from measurement results with respect to the results from a “gold” standard or be based, for instance, upon the same parameter measured at different energies or frequencies. Indexes can also be made by a mathematical operation on the combination of measurement results and other parameters such as, for example, height or weight of the measured person. Actually the phase angle $\varphi = \arctan(B/G)$ is an index.

An index is often useful because it is a relative parameter that becomes independent on, for example, sample dimensions (as long as it is invariable) or some invariable material property. By calculating several indexes, one may be able to choose one that is particularly well correlated with clinical judgments. An index may be based on a clear understanding of the underlying physical process, for instance, the admittance ratio of high- and low-frequency values referring to the total and the extracellular liquid volumes. But indexes may also be a “blind” route when they are used without really knowing why the correlation with clinical judgments is high. It has, however, long and very positive traditions in medicine, as for instance in the interpretation of electroencephalograph waveforms.

9.4 Statistical Methods for Bioimpedance Analysis¹

This chapter gives an overview of relevant statistical methods for the analysis of bioimpedance measurements, with an aim to answer questions such as: How do I begin with planning an experiment? How many measurements do I need to take? How do I deal with large amounts of frequency sweep data? Which statistical test should I use? How do I validate my results?

The topic of time-series is relevant for bioimpedance and especially bioelectricity analysis, but is not covered in this chapter on statistical methods. The methods covered are applicable for time-series after a suitable approach is employed for parameterization. All the examples in the text are given for bioimpedance measurements.

When doing measurements, statistics are needed if we want to describe the data (descriptive statistics) or if we want to draw conclusions based on the data (inferential statistics). There is a vast amount of statistical methods in the literature, and the choice of method depends on what we want to know and what type of data we have. In this chapter, we will give an overview of the most basic and the most relevant methods for

¹ This section is based on Tronstad and Pripp (2014), with permission.

bioimpedance analysis along with examples within the bioimpedance field. Because bioimpedance measurements often are done as frequency sweeps, producing large amounts of correlated and possibly redundant data, the implications for inferential statistics are discussed together with data reduction solutions. A goal of bioimpedance research is often to develop methods for prediction of a biological variable or state, and an overview is given for the most relevant methods for development and testing of a prediction model. At last, the validation of a new measurement technology employs distinct statistical methods, and an overview is given on the concepts, terms, and methods for evaluating performance.

9.4.1 Hypothesis and Research Design

Instead of beginning with the type of measurement as a basis for selecting the statistical method, we expand the perspective by beginning with the hypothesis and research design that should come before the measurements are acquired. The reason is that we generally have an idea about what we want to investigate with our bioimpedance measurement, and we do not perform measurements completely randomly. To do our investigation properly, we begin with a research hypothesis in which we formulate what we want to investigate in a testable way. For instance, if we want to find out whether gel electrodes provide lower bioimpedance measurement than textile electrodes, our hypothesis can be formulated as: “Bioimpedance is lower when using gel electrodes compared with using textile electrodes.” We now have a testable hypothesis, and our hypothesis can either be accepted or rejected by experiments. It is much easier to dismiss a hypothesis than to prove a hypothesis, because it takes only one piece of solid evidence to reject it, but an endless amount to prove it correct. That is why the statistical methods are based on rejecting an opposite hypothesis, called a *null hypothesis*, instead of attempting to prove the hypothesis. In our example, we test whether “Bioimpedance is *not* lower when using gel electrodes compared with using textile electrodes,” which is our null hypothesis. We reject the null hypothesis and thereby accept our original hypothesis if the statistical analysis of our measurements find that the null hypothesis is improbable. The statistical analysis provides a *p value*, which is the probability of our measurement result or larger deviations from the null hypothesis, assuming that the null hypothesis is actually true. Whether or not to reject the null hypothesis is based on whether the *p* value is lower than a predetermined threshold, the *alpha* (α) (i.e., *the significance level*). α is conventionally set to 0.05 in medicine and biology, implying that we reject the null hypothesis if our measurement result is less than 5% probable with the assumption that the null hypothesis is true.

The hypothesis example above is very general and the testability could be improved by making it more specific, such as “Transthoracic bioimpedance is lower when measured by gel electrodes than measured by textile electrodes using a two-electrode setup” if this is the relevant setup we want to test. It is easier to test this hypothesis because it implies only one certain type of measurement, and reduces the chance of an inconclusive result. A

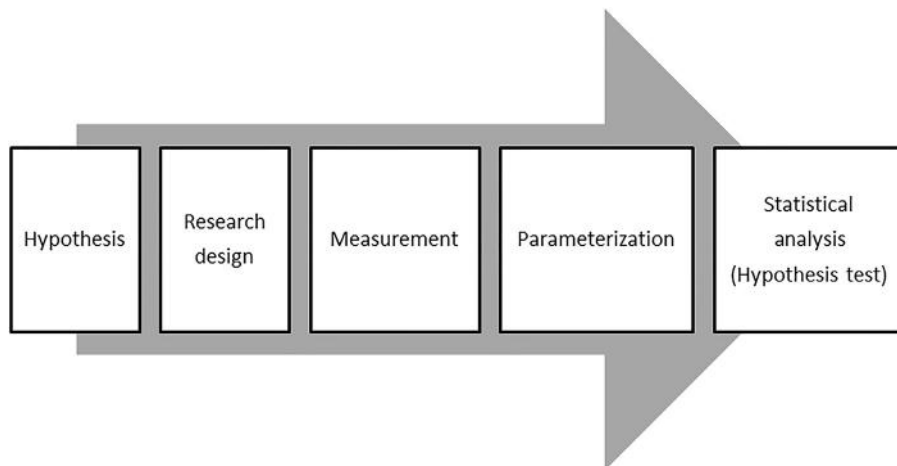


Figure 9.30: The steps from the formulation of a hypothesis to the testing of the hypothesis by statistical methods.

hypothesis should be *simple, specific, and stated in advance* (Hulley et al., 2001). It is the hypothesis that determines the research design, the type of experiments we need to conduct and the type of measurements we need to take. It is also the hypothesis that mainly determines what type of statistical test is appropriate. As an example, if we want to investigate whether the bioimpedance of two types of tissue samples are significantly different, this means that we have to assess the difference between two groups of bioimpedance measurements from a number of tissue samples of each type, and that the appropriate statistical test will be a test for comparison of two means in the groups such as the Student's t-test. We can also do a power analysis to estimate how many tissue samples we need in order to have a good chance of finding a difference if there actually is one. Hence, the planning of a study should begin with a clear hypothesis. The whole process from the planning of the study to the statistical analysis of the measurements is illustrated in Figure 9.30.

How Many Subjects Are Needed?

It is a good idea to know how many units (i.e., items or subjects) are needed to test our hypothesis. Unless we test all the units in a population, we are only testing a sample of the whole population. To make a general conclusion about the population, we need to show that the effect that we observed was not likely the result of chance from random variation in our sample. If we choose too few units, we may end up with an inconclusive result and a worthless study, and if we choose too many, we are wasting resources (e.g., sacrificing more animals than needed). Hence, sample size consideration is of ethical relevance (Baccetti et al., 2005).

In hypothesis testing, we want to reduce the chances of two types of errors: incorrectly rejecting a true null hypothesis (type I error), and the failure to reject a false null hypothesis (type II error). The type I error probability is determined by the α (i.e., 5% usually). With a given α , we can also calculate the *beta* (β), which is the probability of a type II error. As an example, let us say you want to replicate a pilot study you did on the bioimpedance of two materials, materials A and B. You want to test whether they are different based on a t-test, but you are not sure what sample size (N) you need in order to test the hypothesis. Based on the pilot data, you can estimate how large a difference between the materials you expect, and also how much variation there is within each material. With an expected difference in means of $10\ \Omega$ and a standard deviation also of $10\ \Omega$ as an example, $N = 5$ (for each material) gives a beta of 71%, which is too large a chance of a type II error. Increasing N to 10, we obtain a beta of 44%, and with $N = 20$, the β is down to 13%. The statistical *power* of the test is $1 - \beta$, and can be viewed as the ability to correctly reject the null hypothesis when it is false. The power requirement in a study depends on the type of investigation, but a power >0.8 is often considered acceptable.

The *effect size* is the relative magnitude of the effect we are investigating. When comparing groups, the effect size could for example be the difference in $|Z|$ between the groups divided by the pooled standard deviation or for testing associations the effect size could for instance be the coefficient of determination R^2 . It follows that smaller effect sizes require larger samples in order to be detectable and avoid a type II error. In the example here, the effect size was 1 ($10\ \Omega/10\ \Omega$). If the effect size was 2, only $N = 6$ would be required to obtain the same power as with $N = 20$ for an effect size of 1. The minimum amount of information needed to do a sample size estimation for a given statistical test is:

- Desired α (probability of incorrectly rejecting a true null hypothesis)
- Desired β (probability of failing to reject a false null hypothesis)
- Expected sample distribution (type of distribution and variance)
- Expected magnitude of difference or association

Estimation of sample sizes is not an exact science, and often these inputs will be “a qualified guess,” even so it is still important to assess whether we need something like 10 or 100 subjects/items. We already have decided our type of test based on the hypothesis, and our α will conventionally be set to 0.05 with a beta somewhere above 0.8. What is left for us to provide is the effect size. If this is not known, the first place to look is in similar studies. Perhaps other investigators have published data with similar measurements on a similar sample. If no previous data are available, conducting a pilot study can give a good indication of these values. Perhaps we gather information that suggests that the sample variance may be somewhere between 100 and 500 Ω , and that the

difference between means is between 1 k to 2 k Ω . In such cases it is best to account for the worst case (variance = 500 Ω and difference between means = 1 k Ω) in the sample size determination.

In practice, the sample size calculation is not done by hand, but by computer programs (such as the free G*Power \odot), which lets you choose a statistical test, asks for the necessary inputs (i.e., α , β , variance, and effect size), and gives you the minimum required sample size. They can also be used to determine the power of your test given the sample size, α , β , and effect size. Because of all these unknowns, it is a good idea to consult a biostatistician on these matters if possible.

9.4.2 Multiple Variables and Data Reduction (Parameterization)

Often in bioimpedance measurements, we want to examine more than one bioimpedance variable per sample or measurement. Sometimes, we have limited knowledge beforehand on effects in bioimpedance in our study. To maximize the changes of a finding, we may acquire several bioimpedance parameters (i.e., $|Z|$, G , theta) at multiple frequencies from one measurement. Say this gives us a set of 100 variables for comparing two different tissue types, it is very probable that we will find a significant difference in at least one of the variables purely by chance. It is possible to do adjustments for such multiple comparison tests by, for example, the Bonferroni correction method (Bonferroni, 1936; Miller, 1981), which adjusts the significance level threshold by dividing the single-comparison level by the number of multiple comparisons included in the analysis. For bioimpedance analysis, this approach is often insufficient because of the large number of comparisons. Unless the numbers of comparisons are few, a better approach is to reduce the number of variables by data reduction— or model-based approaches. Quite often, and especially for bioimpedance frequency sweeps, the data will be highly correlated and can be reduced into a small set of variables that account for most of the information in the measurements. A common method in the bioimpedance field is to assume that the electrical properties of the sample can be described by an electrical equivalent model (Section 9.2) such as the Cole model, and to estimate the component values by fitting the measurement to the mathematical expression of the model. With a good agreement between the model and the measurement, this approach reduces the measurement into a few uncorrelated parameters that are easier to handle statistically. Data reduction can also be done without equivalent model assumptions. One such way to reduce the data is to computationally transform the data into a set of uncorrelated components using principal component analysis (PCA). The transformation works in the way that linear combinations of the data are used to construct components, which explain as much as possible of the variance in the data, with the constraint that all components must be

uncorrelated. The PCA may provide a data subset by which almost all the information (i.e., 99%) is accounted for by just a few components. The disadvantage of PCA compared with the model-based approach is that the transformation is a “black-box” and the principal components are meaningless with respect to what we are measuring.

9.4.3 Choice of Statistical Method

After the data have been reduced to a practical set of parameters (if necessary), the next step is to perform a statistical analysis to test whether our null hypothesis can be rejected or not. The choice of statistical method is mainly determined by the hypothesis, but the measurements may also influence the selection of the most appropriate method.

Figure 9.31 provides a flowchart for selection of statistical method based on the type of study.

Comparing Two Groups

Let us go back to the example of the alpha parameter of two tissue types, with the hypothesis that the alpha is different between the two tissue types. Our natural choice of test is a two-sample Student’s t-test, which is designed to test whether the means of two sets of data are different. If however, our hypothesis is also on the *direction* of the difference between the tissue types, such as “the alpha parameter of tissue A is *larger* than for tissue B,” the statistical testing must also include this direction. Imagine if we throw five coins, the probability of getting all heads or all tails is 0.03 (0.5^5), but twice (0.06) for getting either all heads or all tails. In the first hypothesis (one-sided), getting all heads would be statistically significant by $p < 0.05$, but not for the second hypothesis (two-sided). When comparing two groups for one direction of the difference, the one-sided (also called one-tailed) t-test takes this into account. In medicine, the two-sided hypothesis and tests should be used unless there is a very good reason for doing otherwise, and if one-sided tests are used, the direction of the test must be specified in advance (Bland and Bland, 1994).

The t-test belongs to the family of *parametric* tests, which assume that our data follows a mathematical probability distribution, in this case the normal distribution, which is something we usually do not know before all the measurements are done. Our distribution of alpha values may be asymmetrical with an overweight of alphas close to one and fewer and fewer alphas toward zero. We then have two options, either to mathematically transform our data into a normal distribution or use a type of statistical test which does not require such a distribution. The alternative type of test for unpaired data that does not satisfy an assumption about normal distribution is the Wilcoxon rank-sum test (also called the Mann–Whitney U test), which is based on comparing the ranks of the values within the groups. This type of test does not rely on any parameter for describing the distribution of data (such as the standard deviation), and belongs to the nonparametric family of

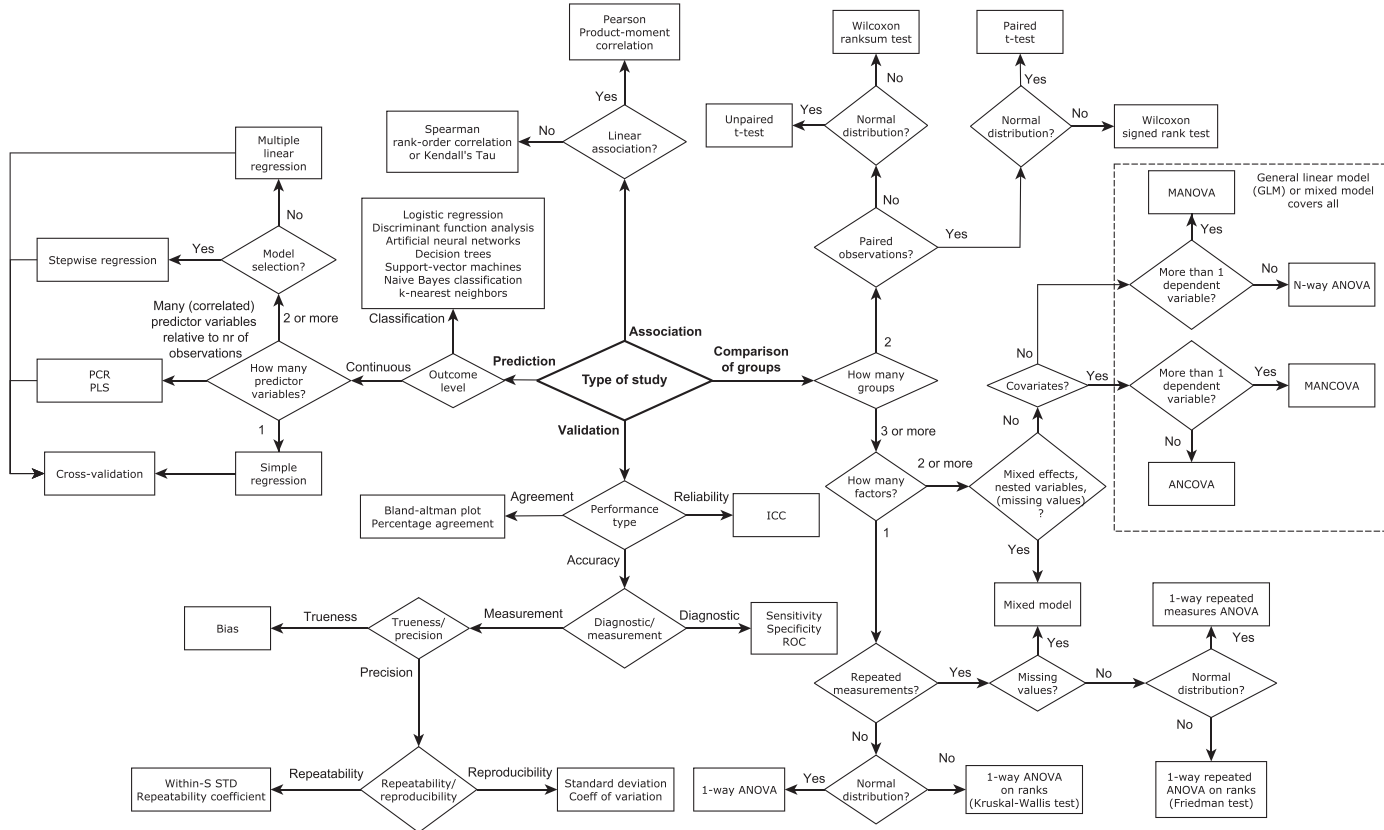


Figure 9.31: Flowchart for selection of statistical method based on the type of study.

statistical tests, which handles different types of hypothesis testing, typically based on data ranking. In general, the parametric tests are a better choice if possible because of a higher statistical power. In bioimpedance analysis, we often do mathematical transformations of our measurements to interpret or graph them differently. When doing statistical analysis, we need to keep in mind that the transformations may also change the distribution of the data. For instance, when transforming a normally distributed set of $|Z|$ measurements to $|Y|$, the distribution is likely to change into a non-normal one.

In the previous example, the measurements came from independent samples. If we have pairs of tissue types with each pair coming from the same animal, we cannot consider the samples from the two tissue types independent and we have to use statistical tests that account for the correlations within each pair, such as the paired t-test or the nonparametric Wilcoxon signed-rank test. A typical situation in which these tests are recommended is for testing the change in bioimpedance before versus after a treatment.

Comparing More Than Two Groups

If we want to statistically compare more than two groups of measurements, another type of test is better suited—the analysis of variance (ANOVA). This test compares the variance within each group to the variance between the groups, and also overcomes the problem of multiple pairwise comparisons (as described in [Section 9.4.2](#)). The ANOVA has the following assumptions: independence between groups, normal distribution, and equal variances within the groups. For more detail on theory, testing, and violations of these assumptions, see, for example, (Dowdy et al., 2004). For nonnormal data, most statistical packages offer rank-based ANOVAs, and the ordinary ANOVA is also regarded as robust against violations of the normality assumption (Schmider et al., 2010). The one-way ANOVA, which is used for comparing more than two independent groups, first calculates an F-statistic (based on the ratio between between-group variability and within-group variability) that, together with the degrees of freedom, determines a p value for the null hypothesis that the data from all groups are drawn from populations with the same mean. Further on, the difference between each pairwise combination of the groups can be tested similar to the t-test but with correction for the multiple testing.

Factor Analysis

The one-way ANOVA is useful when we study only one factor that groups the measurements (e.g., tissue type). If we, for example, want to study how electrode configuration in addition to tissue type affects the bioimpedance, we have a *factorial design* with two factors and may use the two-way ANOVA. The output of this test gives us the statistics (F-statistic, p value) that tell us whether each of the two factors have a significant effect on the bioimpedance. In addition, the two-way ANOVA can test whether there is a significant interaction between the two factors; the difference in bioimpedance

among tissue types may depend on the electrode system. As a procedure for two or more factors, it is advised to first test for all possible interaction terms and to continue with an ANOVA without these terms if none are found significant. If there are significant interaction terms, the main effects (e.g., the influence of tissue type and electrode system on bioimpedance) may essentially be rendered meaningless, because both effects will have to be qualified in reference to another factor. The most logical approach in this case is to do one-way ANOVAs for evaluating all levels of one factor across only one level of the other factor (also called *simple effects*). If one or more simple effects are significant, additional comparisons between specific groups within given factor levels can be conducted (for instance, tissue type A vs. tissue type B when using the four-electrode system). The advantages of the factorial design and the factorial ANOVA are that it allows the same set of hypotheses to be evaluated (at a comparable level of power) by using only a fraction of the subjects that would be required if separate experiments were conducted, and also the possibility to evaluate the interaction between the experimental conditions (Sheskin, 2011).

In the same way as the unpaired or paired t-tests are suited for comparing independent and dependent groups respectively, there are also ANOVA methods that are suitable for dependent groups, the *repeated measures ANOVAs*. Consider the example of comparing the bioimpedance measurement from three different electrode positions. If all measurements are on different subjects, the one-way ANOVA is the appropriate test, but if you measure several times on each subject (with the different electrode positions), the one-way *repeated measures ANOVA* is the appropriate test. The repeated measures tests have a higher statistical power, and fewer subjects are needed with the repeated experimental design. Repeated measures ANOVA can also be done for factorial designs (e.g., two-way repeated measures ANOVA), and for nonparametric data (e.g., repeated measures ANOVA on ranks, Kruskal–Wallis test). However, some care should be taken when performing factorial ANOVA on ranks as the rank transform procedure may be erratic for certain designs (Sawilowsky et al., 1989).

In factorial repeated measures design, the effect of time (or the repeated experimental condition) can be investigated by including it as a factor in the two-way repeated measures ANOVA. It is important to know that the ANOVA does not consider the order of the time points, only the difference between them, and if we want to evaluate a trend or relationship, it is better to use a regression approach.

In experiments, there may be other observable variables than the experimental factors, which have an influence on the dependent variable. This variable may be continuous, and therefore problematic to add as a factor in the design. In this case, the variable can be added as a *covariate* in the design. Let us use the example of measuring impedance in solutions during different chemical reactions. The temperature changes may be unknown

and uncontrollable, but possibly influence the impedance. The temperature can then not be added as a factor in the analysis, but as a covariate. The appropriate statistical method is the ANCOVA (analysis of covariance), which is a combination of ANOVA and regression. With this method, we will find out whether there is a significant difference between the impedance of the different chemical reactions when also controlling for the temperature effect. In some cases, we want to examine more than one dependent variable. If they are related, such as the $|Z|$ and phase of the same measurement, both the dependent variables can be studied in the same test while controlling for the correlation between them by the MANOVA (multivariate analysis of variance). If the dependent variables are not correlated, separate ANOVAs are appropriate. The MANOVA assesses the effect of each factor on each of the dependent variables (with p values for each case), and also the interactions both among the independent variables and among the dependent variables. The advantages of this method is that several dependent variables can be studied in one test, which avoids the increased type I error rate from multiple comparisons, the correlations between the dependent variables will be incorporated in the analysis, and the test may even find a significant result for the combined effect of all dependent variables when the effect on each of them are not strong enough. For adding covariates to the MANOVA, the appropriate test is the MANCOVA (multivariate analysis of covariance), which is the same analysis as the MANOVA, but adds control of one or more covariates that may influence the dependent variables.

One type of test that incorporates all of these (t-test, ANOVA, ANCOVA, MANOVA, and MANCOVA and also ordinary linear regression) is the *general linear model*. This method is included in several statistical software packages and is a convenient tool for analyzing many different types of data.

Mixed Models

Until now, we have discussed group comparison or factor analysis with *fixed effects*. Fixed effects means that the levels of our independent variables will be the same (fixed) in any attempted replication of our experiment. We have chosen a certain selection of levels that are of interest and do not attempt to generalize beyond these levels. As an example, let us consider a comparison of the impedance of electrode types. We could do a study in which the aim is to compare a certain selection of electrode types with different characteristics, and electrode type would then be a fixed factor. We could also do a study in which the aim is to assess whether the electrode type has an effect on the measured impedance *in general*. The electrode type would then be a random factor, and our sample of electrode types (levels) would be treated as a random selection of the overall population of possible electrode types/manufacturers. In the first case, our test result will be the explicit differences between the impedance of the selected electrode types, but for the second case the test result will be the general effect of electrode type on the impedance. In some cases,

our experiment may include both fixed and random factors, and the analysis model is then called a mixed-effects model. Tremendous advances have been made over the past several years in the methods for mixed model analysis, and the current tools available offer a lot of different features and advantages over other “traditional” methods. For instance, a mixed model analysis is not weakened by missing values in the same way as repeated ANOVA. The mixed model can also deal with hierarchies in our data. For instance, we may study samples of different electrode types from different producers and have different types of electrodes from each of the different producers. In the statistical terms, we have two factors (electrode type and producer) in which different levels of one factor do not occur at all levels of the other factor, which is called a *nested (or hierarchical) design*. A third advantage of the mixed model method is that our measurements do not need to be taken at the same time points. For instance, if we are following the impedance of different materials during a time-dependent process, but are unable to measure at all materials simultaneously, we can add all measurements with their individual timestamp to the mixed model and examine the effects of both material type and time even though we only have one measurement per time point. To sum it up, mixed model analysis is recommended for repeated (with missing values) and/or nested data. The analysis can be performed in statistical packages such as R, SPSS, STATA, and SAS. The procedure is more advanced compared with methods such as the ANOVA because of the number of choices and settings. Before embarking on the mixed model, it is advised to read up on the subject (e.g., Demidenko, 2013) or consult a biostatistician.

Association Analysis

Until now, we have been dealing with methods for investigating differences between groups and the effect that different factors have on these differences. Now we move over to the methods that assess associations between variables. The most basic case is testing for a *linear* relationship between two variables (also called bivariate association) by the Pearson Product–Moment correlation coefficient. The output of this test is the r statistic, which indicates the strength (0–1 in absolute value) and direction (positive or negative depending on the sign of r) of the relationship between the two variables. The r does not say anything about the causality or dependency of the relationship; r will be the same whether X was dependent on Y or Y was dependent on X or if they were independent of each other but dependent on another factor. The r also does not say anything about the agreement between X and Y . You can get an $r = 1$ (perfect correlation) with paired observations on completely different scales. This makes the r insufficient for testing agreement between two methods, but is useful for exploring associations between two variables under a linear assumption. Statistical inference (p value and hypothesis test) on the correlation can be conducted (see e.g., Eq. 28.3 in Sheskin (2011)). The squared r is also frequently used and is called the *coefficient of determination*. R^2 is more convenient to interpret, especially for larger r , because it expresses the proportion of variance of one

variable which can be accounted for by the variance of the other variable. For instance if we measure body mass index (BMI) and total body $|Z|$ and get an $r = 0.5$, then we can say that 25% of the variance in $|Z|$ could be explained by the BMI.

The Pearson Product–Moment correlation coefficient (and also the coefficient of determination) is based on an assumption of equal variance (in statistical terms called *homoscedasticity*). If we graph two variables against each other, and the scatter is roughly of the same size across the whole range, then the data are homoscedastic. In violation of this (called *heteroscedasticity*), the correlation will not be consistent across the full range of both variables. Different tests for homoscedasticity are available in most statistical software. Another pitfall of this method is that it is sensitive to outliers or extreme values in a way that they lead to overestimation of the correlation. Another matter is that a restriction of the range in either of the variables directly reduces the value of r . In general, it is recommended to begin with plotting the variables against each other to investigate the relationship and these assumptions, and also provide these graphs together with the statistics in publication of the results (completely different graphs can correspond to the same r !). Graphing the variables also lets us know whether a linear relationship should be assumed. Perhaps we see a quadratic or exponential relationship, and in this case we may simply transform one variable and use the linear methods for simplicity. If we do not want to consider the function of the relationship, but simply test whether there is a monotonic relationship (both variables increasing in the same or the opposite direction), we can apply the Spearman's rank-order correlation.

Regression Methods

The relationship between two variables can also be described mathematically by *regression* methods. Perhaps we have found a significant association between bioimpedance and total body water (TBW), and we want to find the function that expresses their relationship. The basic method is simple linear regression. It estimates the straight line that best fits with the variables plotted against each other and provides the intercept and slope of this line. Using the intercept and slope values together with the bioimpedance measurements, we can make *predictions* about the TBW. The difference between the measured TBW and the predicted TBW is called the *residuals*. The residuals can be used for inspecting whether the selected model (in this case linear) is valid. A scatterplot of the residuals (in this case, bioimpedance vs. residuals) provides information on linearity, homoscedasticity, normality, and independence of the error terms, which are all assumptions for doing regression analysis. If, for instance, we see that the distribution of points is asymmetrical around the x -axis (also called skewed), the normality assumption might be violated (the *robust regression* method is an alternative to the ordinary method using least squares, which can be appropriately used for nonnormal distributions or outliers). From the residuals we also obtain a value for the error of the

prediction, such as the root-mean-square error (RMSE), which is the average of how close the regression line is to all of the points. The r , R^2 , and RMSE are measures for goodness of fit, but the RMSE is better at telling us how large an error is in terms of the quantity we are trying to predict. It is important to note that the RMSE or similar error values represent the error in the sample of measurements we have analyzed, and not the whole population.

Perhaps we have found that the RMSE of our TBW prediction based on bioimpedance was rather large, and that we need to reduce this error if we want to develop a TBW device. We might know of other factors that are also related to TBW, or factors that give changes in bioimpedance but are not related to TBW (confounding variables). If these variables are independent, we may be able to reduce the prediction error by including them as predictor variables in a *multiple linear regression*. For instance, we may add BMI and age together with the assumption that they will correct for the discrepancies in the estimation of TBW from bioimpedance. The multiple regression gives us an R^2 , and the same error quantities such as the RMSE. Again, these statistics represent the sample and not the population, and the results from a multiple regression are optimized for the sample it is based on. The chance of spurious inflation of the statistics and a type I error increases as more predictor variables are added, and it has been recommended that the number of data points should be at least 10 times the number of predictor variables (Mariscuilo and Levin, 1983, p. 1456). It is advised to keep the number of predictor variables low (five or less), and that these variables are close to uncorrelated to find the simplest possible predictive model. Including all points of a bioimpedance frequency sweep is an example of a bad prediction set for multiple regression. Selection of the prediction variables may be done based on preexisting empirical data or theory, but there are also semiautomatic methods that can assist in sifting out redundant predictors. One of these methods is called *stepwise regression*, which suggests a model based on successively adding or removing variables based on the t-statistics of their estimated coefficients. This procedure can either be *forward* or *backward*. In the forward procedure, variables are added one by one based on the degree to which they produce a significant increase in prediction until the addition of more variables no longer make significant contributions. A similar procedure is employed for backward selection, but beginning with a model including all predictor variables. In general, the forward procedure is best suited for finding few significant predictors among many candidates, whereas the backward procedure is best suited for elimination of few variables for fine-tuning of a preselected model. Still, there is always a chance of overfitting (obtaining a poor model with spuriously inflated statistics), and it is always recommended that the resulting regression model is validated (more on this in [Section 9.4.4](#)).

For data as, for example, bioimpedance frequency sweeps, when we may have many predictor variables compared with the number of observations and/or highly correlated

predictor variables, there are other type of regression methods that could be more suitable such as *principal components regression (PCR)* and *partial least squares regression (PLS)*. Both methods employ transformations of the initial set of predictor variables by constructing linear combinations of these into a new set of orthogonal (independent) components. In PCR, these components, which may explain most of the variance of the predictor variables, are regressed against the dependent variable. Often the first few principal components explain most (typically more than 90%) of the variance, and these components are used in the PCR model. However, this selection of regression set is based on including the largest variance of the predictor variables, not the independent variable. The PLS deals with this problem by finding the components of the predictor variable set that are most relevant to the dependent variable (by a simultaneous decomposition of both the predictor variables and the dependent variable with the constraint of explaining as much as possible of the covariance between them). Selecting how many components to include is a matter for both PCR and PLS and has for a long time been subject for discussion in the statistical field (see e.g., Peres-Neto (2005)). In general, some kind of cross-validation (see [Section 9.4.4](#)) should be used to compare the predictive ability as a function of the number of components included.

Classification Methods

Until now, we have been dealing with predictions of a continuous outcome as the dependent variable. Suppose we have investigated bioimpedance with respect to tissue type and found a significant difference between two types of tissue, and now we want to test how well bioimpedance could be used to discriminate between these tissue types.

Logistic regression is such a method, which finds an optimal model based on the predictors and calculates the percentage of correct classification for each of the categories and for the overall classification. For more than two outcomes, the method is referred to as *multinomial logistic regression*. The independent variables can be continuous and real-valued, binary, categorical, or a combination of these types. The R^2 statistic (calculated as in linear regression) gives a misleading indication of the goodness of fit for logistic regression, and several alternative analogues have been suggested (see e.g., Chapter 9.5.1. in Ryan (2008)). In the case that the outcome is ordinal (i.e., good, better, best), another variant called *ordered logistic regression* is suitable. The logistic regression methods do not require normal distribution of the predictor variables (Tabacknick and Fidell, 1996, p. 575).

Another classification method is the *discriminant function analysis*, which instead of regression as the mathematical framework is based on the same principle as the MANOVA. Whereas the MANOVA deals with whether a number of groups differ significantly with respect to differences on a number of dependent variables, the discriminant function analysis deals with whether a linear combination of predictor

variables can differentiate between the groups. The assumptions are normality of the predictor variables, homoscedasticity, linear relationships between all predictor variables within each group, and absence of multicollinearity and outliers in the predictor variables (same as for MANOVA) (Sheskin, 2011). The discriminant function analysis is in general reasonably robust against violations of these assumptions, especially for large samples and equal number of observations per group (Sheskin, 2011).

Other classification methods used in biomedical research include *artificial neural networks (ANN)*, *decision trees*, *support-vector machines (SVM)*, *naïve Bayes classifier*, and *k-nearest neighbors*. These methods are important approaches in the field of *machine learning*, where algorithms are being developed by learning from sample data in order to classify unseen data. These methods are increasingly being adopted in the biomedical engineering fields, including bioimpedance.

ANN is a classification method inspired by the workings of the central nervous system. By constructing a network of interconnected nodes (“neurons”) organized in layers, a classification algorithm is developed (also called *trained*) by optimizing the weights of each node-to-node connection, representing the connection strength between them. As new inputs of selected features are fed through the network, the output layer at the end of the network will provide the suggested classification.

Decision trees are based on an algorithm for splitting the input data in a way that maximizes the separation of the data, resulting in a tree-like structure (Breiman et al., 1984). There are algorithms that can suggest the structure of the tree such as the Hunt’s algorithm, but these algorithms usually employ a greedy strategy that grows a tree by making a series of locally optimum decisions. Another drawback with the method is that continuous variables are implicitly discretized by the splitting process, losing information along the way (Dreiseitl et al., 2003).

SVM has become popular because of the performance the method has demonstrated in problems such as handwriting recognition. The principle is based on representing the data as points in space, and then finding an optimal surface called a hyperplane, which maximizes the margin between the classes. If the classes are not linearly separable in the original data space, the data are mapped into a much higher dimensional space (called *feature space*) by employing a mathematical projection called the *kernel trick*, where a new hyperplane is found. This makes the SVM also efficient for nonlinear classification.

Naïve Bayes classification uses the Bayes’ theorem together with a “naïve” independence assumption to calculate probabilities of class membership. Predicting class membership can be done directly using Bayes’ theorem with only one feature and the prior probability. As an example, consider that we are investigating bioimpedance as a marker

for wound healing. Suppose we gathered 100 measurements after wounding in an experiment where 50 of the wounds healed by themselves. Among the wounds that healed, the impedance increased during the healing process in 35 of the 50 wounds, and in five of the 50 wounds that did not heal. We can now calculate the conditional probability of a wound belonging to the “healing” class based on whether or not the impedance increases using the Bayes’ Theorem, giving us 88% if impedance increases and 25% if the impedance does not increase. When including several conditional features, the mathematics would normally become problematic because of the relations between the features, but the naive Bayes classifier assumes that all the features are independent, which allows for easy computation.

The k-Nearest Neighbors (kNN) algorithm predicts the class of a point in a feature space based on the known attributes of the neighboring k number of points in this space. For instance, say we want to predict tissue status based on a set of independent bioimpedance features, such as the Cole parameters. Using a dataset of measurements with known tissue states, the kNN algorithm will first construct class-labeled vectors in a multidimensional space with one dimension for each feature. Class prediction of a new measurement will then be done based on the majority of class-memberships of the k number of nearest neighbors based on the distance (usually Euclidian) to the new point.

These classification methods use different principles and rules for learning and prediction of class membership, but will usually produce a comparable result. Some comparisons of the methods have been given (i.e., Kotsiantis, 2007; Rani et al., 2006). Although the modern methods such as SVM have demonstrated very good performance, the drawback is that the model becomes an incomprehensible “black-box” that removes the explanatory information provided by, for example, a logistic regression model. However, classification performance usually outweighs the need for a comprehensible model. PCA has been used for classification based on bioimpedance measurements. Technically, PCA is not a method for classification but rather a method of data reduction, more suitable as a parameterization step before the classification analysis.

9.4.4 Validation Methods

Until now, we have been dealing with exploratory methods, in which the bioimpedance measurements have been used to explore differences between groups of measurement, effects of different factors, or associations between bioimpedance and other parameters. We have also been dealing with predictions of either continuous or discrete outcomes, but not the validation² of these. If we have come one step further and developed a potentially

² Provision of objective evidence that a given item fulfills specified requirements, where the specified requirements are adequate for an intended use (JCGM 200:2012).

useful method based on our research, we need other types of testing and statistical methods to validate its performance. These statistics are very important because they will mainly determine how good the developed method is, together with for instance availability, usability, price, and so on.

Evaluating Performance

For bioimpedance measurements, the performance is in most cases determined by the agreement between a developed bioimpedance parameter and a reference (“gold standard”). For example, if we develop a probe to detect breast cancer, we need to find out how often it correctly detects cancerous tissue (the sensitivity) and how often it correctly detects healthy tissue (the specificity). These two statistics are what the potential users will mainly look for when considering the method. Our approach will then be as follows. We have already explored the difference in bioimpedance between healthy and cancerous tissue by the procedure shown in [Figure 9.30](#), and based on our previous results we have also selected which bioimpedance parameters and algorithm we will use for discriminating between the two tissue types. We now do a new study using the selected method on a new sample of subjects. The sample size should be adequate to obtain an estimate with acceptable precision, and can be estimated based on the prevalence and the anticipated sensitivity and specificity (Buderer, 1996; Malhotra and Indrayan, 2010). Say we did 500 measurements, among which 100 were confirmed positive by a reference measurement. Among these 100, our method detected 85 as positive, and among the 400 negative, our method detected 350 as negative. We can now calculate the sensitivity and specificity by (see also [Section 9.5.2](#)):

$$\text{Sensitivity} = \frac{TP}{TP + FN}$$

$$\text{Specificity} = \frac{TN}{TN + FP}$$

Where TP is the number of true positives (85), FN is the number of false negatives ($100 - 85 = 15$), TN is the number of true negatives (350) and FP is the number of false positives ($400 - 350 = 50$). Our sensitivity and specificity then becomes 85% and 87.5%, respectively. It is also often of interest to see how the sensitivity and specificity depends on the decision threshold (i.e., the level of our bioimpedance parameter which separates healthy and cancerous tissue). The ROC (receiver operating characteristic) curve is constructed by plotting the sensitivity (the TP rate) against 1-specificity (the FP rate) for the whole range of decision thresholds. This plot allows us to see what kind of sensitivity and specificity we may obtain according to what we consider important with respect to the application. The area under the curve (AOC) is usually reported together with the ROC curve as a measure of total classification performance.

A very relevant case in the field of bioimpedance is the validation of an estimate of a continuous physiological parameter, where we want to find out how well our estimate agrees with a reference measurement of this parameter. Among the methods used for evaluating agreement in medical instruments measuring continuous variables, the Bland–Altman method (Bland and Altman, 1986) is the most popular (Zaki et al., 2012). By this method, a plot is constructed with the means of all measurement pairs (estimate and reference pairs) on the x -axis and the difference between them on the y -axis. In addition to this, the mean difference line is plotted along with two lines representing the 95% limits of agreement (LOA), given by the mean difference ± 1.96 standard deviation of the difference. By this simple method, the reader can easily see how much the two measuring methods differ according to the magnitude of the measurement, and also inspect for systematic differences such as bias or trends. The LOA tell us that most (95%) of the measurements had a difference within the upper and lower LOA. It is not possible to give any general criterion for an acceptable LOA because it depends on the intended use of the proposed method. As an example, limits of agreement of up to $\pm 30\%$ have been recommended as acceptable for introducing new techniques within cardiac output measurements (Critchley and Critchley, 1999). It is important to note that the correlation coefficients or the coefficient of determination is not sufficient for reporting agreement, because two variables may have a perfect linear relationship but at the same time be very different in magnitude. Another type of correlation which avoids this problem is the *intraclass correlation coefficient* (ICC). Although it was originally devised to assess reliability (see later in this section), it has also been used to assess agreement (Zaki et al., 2012). The appropriateness for this use of the ICC has been criticized (Bland and Altman, 1990) and considered doubtful (Zaki et al., 2012), but also regarded as the best traditional approach for assessing agreement (Lin, 2007).

Cross-validation

Models should always be validated to avoid overfitting and inflated performance results. When a predictive model, such as a regression model, is developed and tested based on the same sample of measurements, there is a chance that the model parameters are optimized in a way that fits better with the sample than the population it comes from and produces an overoptimistic result. This is more relevant the more complex (i.e., number of independent variables) the model is. Therefore, the model should always be tested against an independent sample to see how well the model will generalize and perform in practice. The model can be validated by replicating the results on one or more independent samples from the same population, but in most cases it is more practical to split the data in one part that is used to develop the model parameters (the training sample) and use the remaining data (the validation sample) to test the performance of the model. The validation data can then play the role of “new data” as long as the data are independent and identically distributed (Arlot and Celisse, 2010). This is called the *hold-out method*.

(Devroye and Wagner, 1979) and is performed by splitting the data in a training sample and a validation sample with, for example, 2/3 for training and 1/3 for validation. The training sample is used to fit the model parameters against the independent variable, and the model along with its fitted parameters is then used to predict the independent variable in the validation sample based on the predictor variables in the validation sample. A large difference between the results of training and validation is an indication that the model is wrong. Whereas one such split yields a validation estimate, averaging over several splits is called *cross-validation* (Geisser, 1975). Cross-validation overcomes the risk of a misleading performance (i.e., accuracy, sensitivity, specificity) estimate from an “unfortunate” split in the hold-out method. There are several procedures that can be employed for cross-validation: see Arlot and Celisse, 2010, for a comprehensive list of cross-validation procedures):

- *Random subsampling.* The data are split by random selection of data points without replacement into training and validation samples. The model is then fitted to the training sample and the performance of the model is evaluated on the validation sample. This is repeated a number of times, and the total performance is found by averaging the performance of all iterations. This process is similar to the hold-out method and is also referred to as *repeated hold-out*. A drawback of this method is that different validation sets may overlap.
- *k-Fold Cross-Validation.* The data are first divided into k (e.g., 10) parts as evenly as possible. Each part is used in turn as a validation sample and the remaining for training. The performance results are then averaged from the k runs to provide an overall estimate.
- *The leave-one-out method.* Each data point is successively “left out” from the sample and used for validation. The performance is calculated for the left-out data point based on the fitted model obtained from the remaining data. The average of all iterations gives an estimate of the overall performance. This method makes maximum use of the data, but is also computationally expensive because the number of iterations is the same as the number of data points.

Concepts of Performance

There are several terms that are important in validating a new measurement method. A list of the most relevant aspects of validation is given in Table 9.5, along with a definition of each term and how it is usually reported. The definitions of the terms vary among different fields and standards, sometimes giving an inconsistent meaning. The table is an attempt at giving an unambiguous overview of the terms based on the most common uses.

The concept of *error* in a measurement is quite straightforward and is the difference between the measured value and a reference value. If the error in replicate measurements remains constant or varies in a predictable manner, the error is referred to as a *systematic*

Table 9.5: List of Important Terms in the Validation of New Measurement Technology and the Most Usual and Recommended Ways of Reporting

Term	Definition ^a	Reported as
Measurement error	<p>Measured quantity value minus a reference quantity value (JCGM 200:2012)</p> <p>Systematic measurement error: component of measurement error that in replicate measurements remains constant or varies in a predictable manner (JCGM 200:2012)</p> <p>Random measurement error: component of measurement error that in replicate measurements varies in an unpredictable manner (BIPM, 2012)</p>	<p>Quantity on the same scale as the measurement scale, relative error, percentwise error, mean square error, root-mean square error.</p> <p>Systematic measurement error: bias</p> <p>Random measurement error: standard deviation, variance, coefficient of variation</p>
Sensitivity	The sensitivity of a clinical test refers to the ability of the test to correctly identify those patients with the disease (Lalkhen and McCluskey, 2008)	<p>Equation 1 A part of the ROC curve which shows the relation between sensitivity, specificity and the detection threshold</p>
Specificity	The specificity of a clinical test refers to the ability of the test to correctly identify those patients without the disease (Lalkhen and McCluskey, 2008)	<p>Equation 2 A part of the ROC curve, which shows the relation between sensitivity, specificity, and the detection threshold</p>
Agreement	The degree to which scores or ratings are identical (Kottner et al., 2011)	<p>Continuous: Bland-Altman plot Discrete: percentage agreement</p>

Trueness	Closeness of agreement between the average value obtained from a large series of results of measurement and a true value (ISO 5725-1)	Bias (i.e., the difference between the mean of the measurements and the true value)
Precision	Closeness of agreement between independent results of measurements obtained under stipulated conditions (ISO 5725-1)	Standard deviation, coefficient of variation
Repeatability	Precision determined under conditions in which independent test results are obtained with the same method on identical test items in the same laboratory by the same operator using the same equipment within short intervals of time (ISO 5725-1)	Within-subject standard deviation (Bland and Altman, 1999) Repeatability coefficient (Bland and Altman, 1999)
Reproducibility	Precision determined under conditions where test results are obtained with the same method on identical test items in different laboratories with different operators using different equipment (ISO 5725-1)	Standard deviation, coefficient of variation
Accuracy ^b	Closeness of agreement between the result of a measurement and a true value (both trueness and precision) (ISO 5725-1) Measurement accuracy: closeness of agreement between a measured quantity and a true quantity value of a measurand (JCGM 200:2012)	Bias (trueness) and standard deviation/coefficient of variation (precision) Diagnostic accuracy: sensitivity and specificity Sensitivity and specificity corrected for prevalence as: (sensitivity) (prevalence) + (specificity) (1 – prevalence) (Metz, 1978)
Reliability	Ratio of variability between subjects or objects to the total variability of all measurements in the sample (Kottner et al., 2011)	Intraclass correlation coefficient Kappa statistics (categorical data)

^aThere are numerous different definitions in the literature, which can be inconsistent and confusing. These definitions provide one version with the aim of reducing ambiguity.

^bAccuracy has previously been defined as the same as trueness only, but with ISO 5725-1 (1994), and reflected in the JCGM 200:2012, the definition of accuracy has for the most changed to include both trueness and precision as given here. The old definition is still in use in some areas.

measurement error. If the error varies in an unpredictable manner, it is referred to as *random measurement error*. The measurement error can be a combination of the two.

The term *agreement* can be regarded as a general term for the degree to which the measurements are identical (either in nominal, ordinal, or continuous variables) and it is of main interest in method comparison studies. *Accuracy* is the closeness of agreement between the result of a measurement and a true value, and depends on both *trueness* and *precision*. The difference between trueness and precision is easiest explained through the example of throwing darts. Trueness is high if the darts are centered around the middle, but low if they are all on one side of the board (bias), regardless of how much they are spread. Precision is high if they are close and low if they are spread far apart, regardless of the center they are spread around. Precision is further divided into *repeatability* and *reproducibility* according to the measurement condition. When new measurements are taken with the same setup by the same operator on the same items/subjects (i.e., replicated), the repeatability of the method is tested. When new measurements are taken with the same method on the same items/subjects but with different devices and operators, the reproducibility is tested. Repeatability can be thought of as the minimum variability between results, and reproducibility the maximum variability between the results. With measurement of thoracic bioimpedance as an example, the repeatability of the method can be assessed by replicating the measurement by the same operator using the same equipment (i.e., device and electrodes) on the same subjects, with measurements taken in quick succession such as on the same day. When clinical implementation is considered, it is also important to know how large this variation becomes under realistic conditions. Factors such as electrode positioning (operator-related), calibration (device-related), and ambient humidity (laboratory-related) may cause variations in the measurement. The reproducibility of the method can then be assessed by performing measurements on the same subjects at two or more different laboratories having different operators and equipment (but of the same type), providing a realistic estimate of the precision. Specific reproducibility, such as interelectrode reproducibility, can be assessed for the factors which influence the measurement, telling us how these factors influence the measurement precision.

Agreement and reliability are two distinct concepts in the medical literature (De vet et al., 2006; Kottner et al., 2011, Barlett and Frost, 2008). Although agreement is the degree to which scores or ratings are identical, reliability is the ability of a measuring device to differentiate among subjects, or objects (Kottner et al., 2011). Agreement concerns the measurement error whereas reliability relates the measurement error to the variability between the subjects or items that are tested (De Vet et al., 2006). Reliability is assessed during certain conditions such as different equipment or users (interrater reliability) or with the same equipment and users (intrarater or test-retest reliability). As an example, if we test our impedance measurement system against a set of calibration resistors once each month and each time measure a 10% positive offset, the system has a low agreement

(and accuracy), but a high test-retest reliability. Given these definitions, the test-retest reliability may seem to be the same as the repeatability of a measurement, but we make a distinction here. Repeatability is assessed through repeated measurements on identical subjects/items within a short time relative to any changes in the property being measured, whereas test-retest reliability is assessed from measurements taken at different occasions with the same conditions and allowing changes in the property being measured. The same goes for reproducibility versus interrater reliability in that reproducibility is assessed using identical test items under different conditions (which is the source of variation) while interrater reliability also involves testing under different conditions, but in addition allows changes in the property being measured. This also implies that precision and reliability are two different concepts.

An advantage of using reliability to compare measurement methods is that it can be used to compare methods when their measurements are given on different scales or metrics (Barlett and Frost, 2008). For continuous variables, reliability is usually determined by the ICC. The ICC is a ratio of variances derived from ANOVA, with a maximum value of 1.0, indicating perfect reliability. There are different types of the ICC, including one- or two-way model, fixed- or random-effect model, and single or average measures (see Weir, 2005, for more on selection), and the type should be reported in a reliability study (Zaki et al., 2013). For assessing reliability in categorical data, *kappa* statistics such as Cohen's kappa provide useful information (Kottner, 2011). Instead of simply taking the percentage of equal decisions relative to the total number of cases, Cohen's kappa provides a measure of association that is corrected for equal decisions due to chance.

Which of these measures to report should be chosen based on the how the measurements are to be used in the future? The same goes for the importance of the measurement performance. A certain degree of measurement error may be acceptable if measurements are to be used as an outcome in a comparative study such as a clinical trial, but the same errors may be unacceptably large in individual patient management such as screening or risk prediction (Barlett and Frost, 2008). For some applications, there are specific ways of reporting performance which have become standard, such as the Clarke-Error Grid together with mean absolute relative deviation for blood glucose measurement. At last, it is important to also mention the concept of *validity*, originating from psychometrics and addresses the inference of truth of a set of statements (Nunnally and Bernstein, 1994). A study may provide perfect test results on accuracy, but if the experiments are not testing what they are supposed to, the results are not valid. For instance, testing the agreement between a new method and an existing method with barely acceptable clinical accuracy may provide a good agreement between the two, but the results are not valid with respect to the accuracy of the new method. Validity is also used to describe the same concept as trueness within psychometrics.

9.5 More Data Analysis Methods

9.5.1 Multivariate Analysis

Multivariate analysis is a set of techniques used for analysis of data sets that contain more than one variable, and the techniques are especially valuable when working with correlated variables. The techniques provide an empirical method for information extraction, regression, or classification; some of these techniques have been developed quite recently because they require the computational capacity of modern computers.

As a trivial example, say that you wanted to use impedance measurements to assess the quality or texture of the inside matter of an apple. One approach would be to develop an electrical model for the apple and figure out how texture differences depend on things such as cell structure and water content. Based on these assumptions, you could try to postulate how differences in texture will influence the impedance spectrum and then seek to have this confirmed by experiments. Referring to [Section 9.1.2](#) this would be the explanatory approach, whereas a more descriptive approach could be the use of multivariate analysis.

To use a multivariate regression technique, you would need another way of measuring or assessing the apple's texture as a golden standard to calibrate your model against. The measured impedance values will in this case often be called X-variables and the measurements from the calibration instrument is called Y-variables.

There may exist a mechanical instrument for measuring the softness of the apple material or you may simply use a taste panel to score each apple on a scale from 1 to 10. What the multivariate regression software program then will do for you is basically to produce a model that you can use to calculate the softness of each apple (Y-variable) from the measured impedance data (X-variables) or from any data derived from the measured data, such as Cole parameters.

The main purpose of multivariate methods would be information extraction. The simplest form of information extraction and data reduction is the PCA technique. The history of PCA can be traced to an article by Pearson (1901). It is a statistical method that can be performed in a wide variety of mathematical, statistical, or dedicated computer software such as Matlab (The MathWorks, Inc.), SPSS (SPSS, Inc.), or The Unscrambler (Camo, Inc.). We will here give a short nonmathematical introduction to this method, and we refer the reader to one of the many available text books on this topic for a more in-depth, formal presentation.

PCA is mathematically defined as an orthogonal linear transformation that transforms the data to a new coordinate system such that the greatest variance by any projection of the data come to lie on the first coordinate (called the first principal component), the second greatest variance on the second coordinate, and so on.

In Figure 9.32 the samples are plotted as circles according to their measured impedance values in the n -dimensional space, where n is the number of measured values in each impedance spectrum. For obvious reasons, only three orthogonal directions are shown in the figure. Hence, a frequency scan using 19 discrete frequencies (three frequencies per decade from 1 Hz to 1 MHz) measuring resistance and reactance, would give data points plotted in the 38-dimensional space. The longest axis inside the “volume” occupied by the data points in this space will be the first principle component (PC1). The second longest axis orthogonal to PC1 will be PC2, and so on. In this way, a new coordinate system that emphasizes the greatest variances in the data set, is constructed.

Certain plots and graphical presentations are frequently used in multivariate analysis and the most frequently used is perhaps the *score plot*. This is a two-dimensional scatter plot (or map) of scores for two specified components (PCs), in other words a two-dimensional version of Figure 9.32. The plot gives information about patterns in the samples. The score plot for PC1 and PC2 may be especially useful because these two components summarize more variation in the data than any other pair of components. One may look for groups of samples in the score plot and also detect outliers, which may be due to measurement error. In classification analysis the score plot will also show how well the model is able to separate between groups. An example is given in Section 10.4.3.

The *loading plot* is the corresponding map of the variables for two specified PCs. Looking at both the score plot and the loading plot for the same two components can help you determine which variables are responsible for differences between samples. For example, samples to the right of the score plot will usually have a large value for variables to the right of the loading plot, and a small value for variables to the left of the loading plot.

The score s_i for sample i for one PC is given by

$$s_i = \sum_{j=1}^n p_j x_{ij} \quad (9.48)$$

where p_j is the loading associated with variable x_j for the given component.

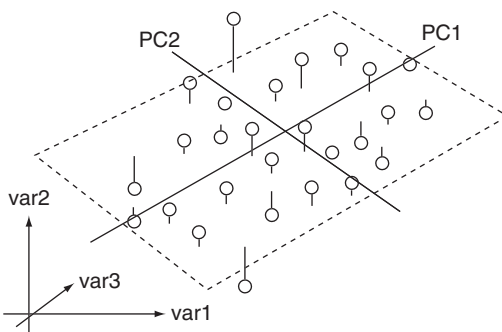


Figure 9.32: Samples plotted with each individual measured variable on orthogonal axes. The samples are projected down on the plane given by principal components PC1 and PC2.

Another popular method is called PLS regression. This method also creates a new coordinate system based on orthogonal linear transformations, but the optimization criterion is different. Whereas PCA maximizes the variance in X, PLS will maximize covariance between X and Y.

For classification, one may use a method called Soft Independent Modeling of Class Analogies in which one PCA model is constructed for each group of samples, but a range of other methods are also available.

9.5.2 Clinical Performance

ROC graphs are useful for visualizing the performance of binary (having two possible outcomes) classifiers. It is a well-known means for evaluating diagnostic tools in medicine, but in general it can be used for evaluation of all kinds of classification algorithms (Fawcett, 2005).

The obvious example from bioimpedance applications in medicine would be the possible diagnosing or classification of human tissue as normal or cancerous from a measured impedance spectrum. After measurements and the pertinent treatment of the data, the possible outcomes from the classifier are denoted positive (p') or negative (n') with regard to cancer or not, in [Figure 9.33](#). The true classes are correspondingly denoted p or n.

ROC graphs are commonly used to assess the performance of a classifier. Sensitivity is plotted on the y-axis and 1-specificity on the x-axis.

Classifiers producing results on the diagonal, dashed line in [Figure 9.34](#) have the same performance as random guessing or coin flipping. Results toward the upper left corner of the graph are better and a result in the point (0, 1) represents a perfect classifier.

		Actual value		
		p	n	
Classification outcome		TP True positives	FP False positives	Accuracy = $\frac{TP + TN}{P + N}$
		FN False negatives	TN True negatives	Sensitivity = $\frac{TP}{TP + FN}$
Total:	P		N	Specificity = $\frac{TN}{FP + TN}$

Figure 9.33: Confusion matrix showing the four outcomes of a binary classification process.

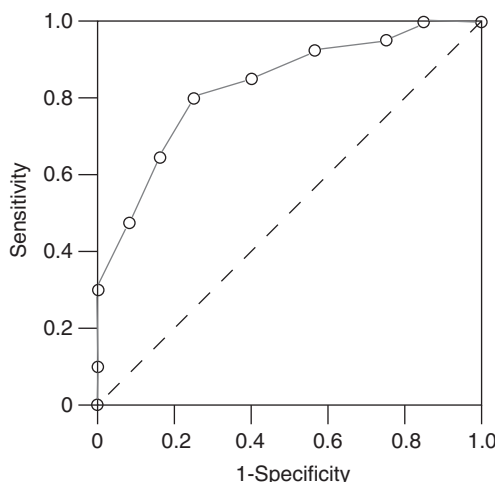


Figure 9.34: A basic ROC graph.

As an example, say that the classifier calculates a number from 1 to 10 from the measured impedance data, where low numbers represent normal tissue and high numbers cancerous tissue. In most real cases, the distributions of normal and cancerous tissues will overlap on this scale. Setting the cutoff value to 6 may for instance classify 80% of the cancerous tissues correctly, but at the same time erroneously classify 20% of the normal tissue as cancerous. This corresponds to $TP = 0.8$ and $FP = 0.2$ and a point at $(0.2, 0.8)$ in the ROC graph. Changing the cutoff value from the lowest to the highest value in steps, and calculating the corresponding TP and FP for each value will produce a curve in the ROC graph, similar to the one shown in Figure 9.34. The area under the curve is commonly used as a measure of classifier performance. An area of 1.0 indicates a perfect classifier, whereas 0.5 is equal to random guessing. Values below 0.5 can be made equally larger than 0.5, just by negating the prediction.

9.5.3 Neural Networks

A neural network is a system of interconnected processing elements called neurones or nodes. Each node has a number of inputs and one output, which is a function of the inputs. There are three types of neurone layers: input, hidden, and output layers. Two layers communicate via a weight connection network. The nodes are connected together in complex systems, enabling comprehensive processing capabilities. The archetype neural network is of course the human brain, but there is no further resemblance between the brain and the mathematical algorithms of neural networks used today.

A neural network performs parallel and distributed information processing that is learned from examples, and can hence be used for complex bioimpedance signal processing.

The “learning” capabilities of neural networks are by far their most fascinating property. The processing may be simulated in a computer program, but because of the sequential nature of conventional computer software, the parallel feature of the neural network will be lost and computation time will increase. However, simulation on a computer gives the great advantage of full control over the network algorithm at any time. Physical neural networks are most often implemented as very large-scale integrated electronic circuits, and sometimes a hybrid solution is chosen.

Neural networks may be constructed in many ways, and those presented so far in the literature can be classified as follows:

Feedforward networks: These networks are usually used to model static systems. Data from neurones of a lower layer are propagated forward to neurones of an upper layer, and no feedback is used.

Recurrent networks: These networks include feedback, and are usually used to model dynamic systems.

Associative memory networks: A type of recurrent network whose equilibrium state is used to memorize information.

Self-organizing networks: The neurones are organized on a sort of dynamic map that evolves during the learning process, in a way that is sensitive to the history and neighboring neurones. Clustering of input data is used to extract extra information from the data.

The most commonly chosen approach is the feedforward network using a so-called back-propagation algorithm. The back-propagation algorithm can be thought of as a way of performing a supervised learning process by means of examples, using the following general approach: A problem, for example, a set of inputs, is presented to the network, and the response from the network is recorded. This response is then compared to the known “correct answer.” The result from this comparison is then fed back into the system to make the network adapt according to the information inherent in the examples. This adaptation is accomplished by means of adjustable parameters that control the behavior of the network. The act of repeatedly presenting inputs to the network, and providing it with feedback regarding its performance, is called *training*, and the network can be said to be *learning*.

9.5.4 Chaos Theory and Fractals

An exciting development has for some years been seen in the use of chaos theory in signal processing. A chaotic signal is not periodic; it has random time evolution and a broadband spectrum and is produced by a deterministic nonlinear dynamical system with an irregular

behavior. The evolution in state space (also called phase space) of a chaotic signal must take place on a *strange attractor* of volume zero, which requires sensitive dependence to initial conditions. An attractor is a set of values to which all nearby values converge in an iterative process. To classify the attractor as strange, this set of values must be a fractal. Consider for example the sequence produced by the iterative process:

$$S_n = (\cos x)^n \quad (9.49)$$

This sequence appears when you, for example, repeatedly press the cosine button on a pocket calculator and it converges to 0.739 if x is an arbitrary number in radians. Other iterative processes do not converge to a specific number, but produce what seems like a random set of numbers. These numbers may be such that they always are close to a certain set, which may be a *fractal*. This set is called a fractal attractor or strange attractor.

Fractal patterns have no characteristic scale, a property that is formalized by the concept of *self-similarity*. The complexity of a self-similar curve will be the same regardless of the scale to which the curve is magnified. A so-called fractal dimension D may quantify this complexity, which is a noninteger number between 1 and 2. The more complex the curve, the closer D will be to 2. Other ways of defining the fractal dimension exist, such as the Haussdorff-Besicovitch dimension.

Self-affine curves resemble self-similar curves, but have weaker scale-invariant properties. Whereas self-similarity expresses the fact that the shapes would be identical under magnification, self-affinity expresses that the two dimensions of the curve may have to be scaled by different amounts for the two views to become identical (Bassingthwaighe et al., 1994). A self-affine curve may hence also be self-similar; if it is not, the curve will have a local fractal dimension D when magnified a certain amount, but this fractal dimension will approach 1 as an increasing part of the curve is included. Brownian motion plotted as particle position as a function of time gives a typical example of a self-affine curve.

The theory of fractal dimension may be used in bioimpedance signal analysis, for example, for studying time series. Such analysis is often done by means of *Hurst's rescaled range analysis* (R/S analysis), which characterizes the time series by the so-called *Hurst exponent* $H = 2 - D$. Hurst found that the rescaled range often can be described by the empirical relation

$$\frac{R}{S} = \frac{N^H}{2} \quad (9.50)$$

where R is the peak-to-peak value of the cumulative deviation from the average value of the signal, and S is the corresponding standard deviation over a time period of N sampling intervals. Natural phenomena such as temperature and rainfall figures are

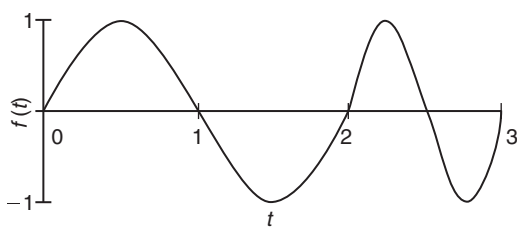


Figure 9.35: Sequence of two single-period sine wave signals.

found to have Hurst exponents more or less symmetrically distributed around 0.73 (SD = 0.09) (Feder, 1988).

9.5.5 Wavelet Analysis

It is difficult to give an introduction to wavelet analysis without reference to Fourier analysis, which is discussed in Section 8.2.

Consider the following signal:

$$f(t) = \sin(\omega_0 t) = \sin\left(\frac{2\pi}{T}t\right) = \begin{cases} \sin(\pi t), & 0 \leq t \leq 2 \\ \sin(2\pi t), & 2 < t \leq 3 \end{cases} \quad (9.51)$$

which is the sum of two single-period sine signals, as shown in [Figure 9.35](#).

The Fourier transform for this signal will be

$$\mathbf{F}(\omega) = \int_0^2 \sin(\pi t) e^{-j\omega t} dt + \int_2^3 \sin(2\pi t) e^{-j\omega t} dt \quad (9.52)$$

which solves to

$$\mathbf{F}(\omega) = \frac{\pi}{\omega^2 - \pi^2} (e^{-j2\omega} - 1) + \frac{2\pi}{\omega^2 - 4\pi^2} (e^{-j3\omega} - e^{-j2\omega})$$

The modulus response of $F(\omega)$ is shown in [Figure 9.36](#).

[Figure 9.36](#) shows that you need an infinite number of sine waves to reconstruct the original signal perfectly, or at least a large number of sine waves to get close to the original.

Looking at [Figure 9.36](#), it is obvious that the signal could be represented by only one or two frequency components if the transformation was performed within a moving time window. This kind of time-frequency analysis is available in the so-called short-time Fourier transform (STFT). The problem with STFT is that the resolution in time and

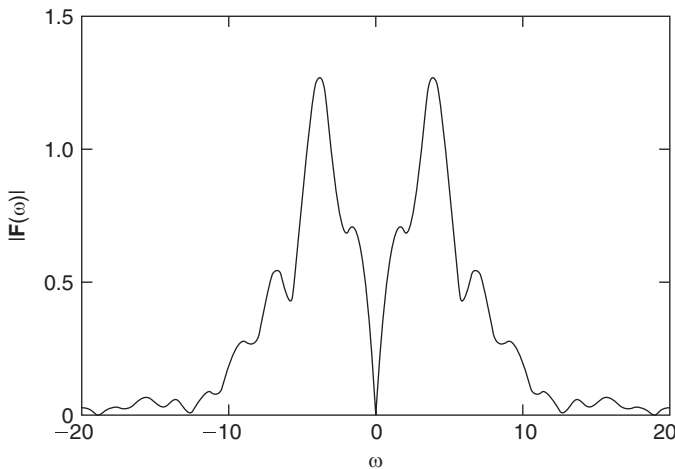


Figure 9.36: Modulus response of the signal in Figure 9.36.

frequency is restricted once you have selected the kind of window you want to use for your analysis.

An intuitive solution to this problem would be to allow for sine waves with finite duration to appear as building blocks in the transformed data. This is the basis of wavelet analysis. The wavelet transform is based on such building blocks or elementary functions, which are obtained by dilatations, contractions, and shifts of a unique function called the wavelet prototype (or mother wavelet) $\psi(t)$.

There are four different types of wavelet transforms:

1. *The continuous wavelet transform.* This transform is given as

$$CWT(a, \tau) = \frac{1}{\sqrt{a}} \int_{-\infty}^{\infty} f(t)\psi\left(\frac{t-\tau}{a}\right)dt \quad (9.53)$$

It has a parallel in the Fourier transform, and the variable t , scale a , and shift τ are all continuous.

2. *The discrete parameter wavelet transform (DPWT, or wavelet series).* Here the parameters a and τ are discretized to $a = a_0^m$ and $\tau = n\tau_0 a_0^m$. The parameters m and n are integers and the function $f(t)$ is still continuous. The transform is then given as

$$DPWT(m, n) = a_0^{-\frac{m}{2}} \int_T f(t)\psi(a_0^{-m}t - n\tau_0)dt \quad (9.54)$$

The wavelet prototype $\psi(t)$ is hence shifted in time by increasing n or in frequency by increasing m . An increased m will reduce the time duration and thereby increase the center frequency and frequency bandwidth of $\psi(t)$.

3. *The discrete time wavelet transform.* This is a version of the DPWT with discrete time where $t = kT$ and the sampling interval $T = 1$, given as

$$DTWT(m, n) = a_0^{-\frac{m}{2}} \sum_k f(k) \psi(a_0^{-m}k - n\tau_0) \quad (9.55)$$

4. *The discrete wavelet transform.* This is defined as

$$DWT(m, n) = 2^{-\frac{m}{2}} \sum_k f(k) \psi(2^{-m}k - n) \quad (9.56)$$

The discrete wavelet $\psi(k)$ can be, but not necessarily is, a sampled version of a continuous counterpart.

Let us now see how discrete parameter wavelet transform can be applied to the simple example given above. The transform coefficients were given as:

$$DPWT(m, n) = a_0^{-\frac{m}{2}} \int_T f(t) \psi(a_0^{-m}t - n\tau_0) dt \quad (9.57)$$

Considering the signal in Figure 9.35, one could choose the mother wavelet to be a single period of a sine wave, for example,

$$\psi(t) = \sin\left(\frac{2\pi}{T}t\right) = \sin(\pi t) \quad (9.58)$$

and furthermore choose $a_0 = \frac{1}{2}$ and $\tau_0 = 2$, giving transform coefficients on the form:

$$DPWT(m, n) = 2^{\frac{m}{2}} \int_T f(t) \psi(2^m t - 2n) dt \quad (9.59)$$

where the baby wavelets are

$$\psi_{m,n}(t) = 2^{\frac{m}{2}} \psi(2^m t - 2n) \quad (9.60)$$

The procedure is then to compare the value of this wavelet with $f(t)$ for one period of the wavelet, i.e., $0 \leq t < 2$, which gives you $DPWT(0,0) = 0$. Then increase m and n individually in positive unit steps, to get $DPWT(0,0)$ equal to:

	$n = 0$	$n = 1$	$n = 2$
$m = 0$	1	0	0
$m = 1$	0	0.707	0
$m = 2$	0	0	0

Hence, $f(t)$ can be represented by two terms only:

$$f(t) = \psi_{0,0}(t) + \frac{1}{\sqrt{2}} \psi_{1,1}(t) \quad (9.61)$$

An in-depth description of wavelets and their use in biomedical signal processing is given by Akay (1998).

9.6 Problems

1. An ideal resistor of $1 \text{ k}\Omega$ is coupled in parallel with an ideal capacitor with capacitance $2.2 \mu\text{F}$. Calculate the complex impedance and the complex admittance at 314 Hz.
2. Suppose that we have obtained the measurement results shown in [Table 9.6](#). The table contains raw data, as for instance obtained directly from a lock-in amplifier. It is admittance data according to $Y = G + jB$, and the results are given in microsiemens.
 - a. Calculate the corresponding impedance values at each frequency.
 - b. Plot complex admittance as a function of logarithmic frequency, with linear and logarithmic conductance/susceptance scales. Is there a second dispersion below 0.1 Hz?
 - c. Plot the admittance and impedance data in a Wessel diagram and compare. From this presentation, is there a second dispersion below 0.1 Hz?
 - d. Plot of the admittance magnitude and phase (called a *Bode*³ plot if it is presented with logarithmic amplitude scales, linear phase scale, and logarithmic frequency

Table 9.6: Measured Data

F [Hz]	G [μS]	B [μS]
0.01	23.0	0.5
0.03	23.1	0.7
0.1	23.2	0.7
0.3	23.4	1.6
1	23.8	3.7
3	25.1	7.7
10	29.8	16.4
20	36.3	23.6
50	52.5	31.8
100	68.3	32.2
200	82.0	27.0

Continued

³ Hendrik W. Bode, research mathematician at Bell Telephone laboratories, author of the book *Network Analysis and Feedback Amplifier Design* (1945).

Table 9.6: Measured Data—cont'd

F [Hz]	G [μ S]	B [μ S]
500	92.6	17.4
1000	96.3	11.4
3000	98.7	5.6
10,000	99.5	2.4
30,000	99.8	1.1
100,000	99.9	0.5

scale on the x -axis). With linear scales, the characteristic frequency coincides with the geometrical mean of the dispersion; is this changed with the logarithmic scales used in Bode plots?

- e. Let us assume that we know the dimensions of the sample in problem 2 to be $d = 1 \text{ mm}$ and $A = 1 \text{ cm}^2$. We can then calculate the relative permittivity according to the equations in Section 3.3. Calculate the complex capacitance and permittivity and plot the results in Bode and Wessel diagrams. Compare the spectra with the admittance plots.

Selected Applications

Bioelectric sources are endogenous sources found in the body. At a short distance the signals may be dominated by the nervous parts of the organ, at larger distance by the muscle mass under nervous control. The signals are generated by the electrical activity of the cell membranes.

Bioimpedance sources are often exogenous signals derived from mechanical activities in the source (e.g., plethysmographic signals from respiration (air) and pumping action (heart)). Electrocardiography (ECG) measures the *electrical* activity of the heart; impedance cardiography (ICG) measures the *mechanical* pumping activity of the heart. A heart may exhibit electrical activity without mechanical blood pumping action.

When we present some selected applications, we have therefore often made two different groups of sources: bioelectric and bioimpedance types.

10.1 Heart as a Bioelectric Source (ECG)

ECG is an important clinical examination routinely performed with 12 leads and 10 electrodes (nine skin surface electrodes plus an indifferent electrode). ECG is also important for long-term monitoring in intensive care units and is extremely important during resuscitation and defibrillation.

During a routine ECG examination, four electrodes are connected to the limbs. Three of these are for ECG signal pick-up and one is a reference electrode (right leg) for noise reduction. In addition, six electrodes are connected in the thorax region at well-defined positions near the heart.

10.1.1 Three Limb Electrodes (Six Limb Leads)

The most basic ECG examination is with three skin surface electrodes on the limbs: one at the left arm (LA), one at the right arm (RA), and one at the left leg (LL). [Figure 10.1](#) illustrates how six limb leads are derived from these three electrodes.

It is unusual that pick-up electrodes are placed so far away from the source organ; the main reasons in ECG are standardization and reproducibility. In our language, the limbs are salt bridges to the thorax. By this, the coupling to the thorax is well-defined and ECGs can be compared even when recorded in different hospitals and at long intervals.

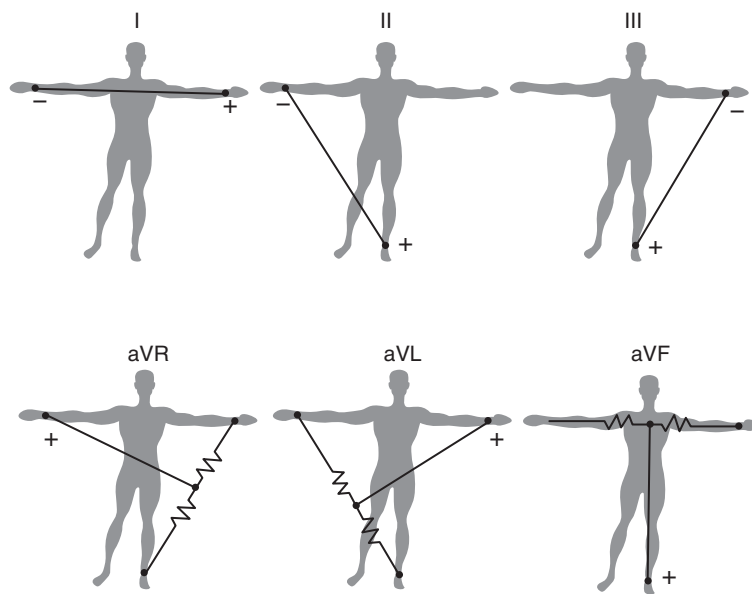


Figure 10.1: The six limb leads derived from three limb electrodes (both arms and left leg). Here, a indicates augmented.

The position of the electrodes on each limb is uncritical because the distal part of each limb is isoelectric (with respect to ECG, not with respect to, for example, electromyography (EMG) sources of the arm muscles). Such is the reproducibility that the bipolar leads form the basis for determining the axis of the electric heart vector.

Three Bipolar Leads: I, II, III

Channel I is the voltage difference RA–LA; channel II: RA–LL; channel III: LA–LL. Einthoven found the following relationship between the scalar lead voltages: $u_{II} = u_I + u_{III}$. [Figure 10.2](#) shows an example of a typical ECG waveform.

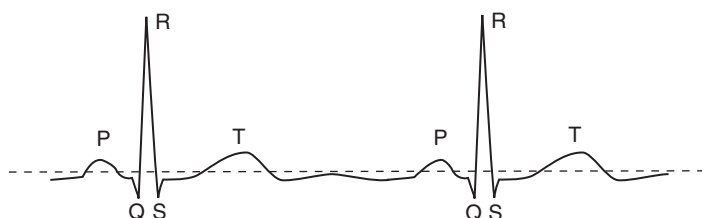


Figure 10.2: ECG waveform lead II. The dashed line indicates zero voltage and is determined by the electronic circuit high-pass filter functioning so that the negative and positive areas become equal.

The Three Unipolar Limb Leads: aVR, aVL, aVF

In the days of the first publications of Einthoven,¹ no amplification tube had yet been invented, and the signal from the electrodes had to drive a galvanometer directly. Later the *unipolar augmented* leads were invented; they were called augmented because the signal amplitudes were higher. A “reference” voltage was obtained by summing the voltage from two of the limb electrodes (Figure 10.1). More important, these vector leads have the interesting property of interlacing the vector lead angles of I, II, and III (0° , 60° , and 120°) so that each 30° is covered. This is shown in Figure 10.3, in which both an example of the heart vector \mathbf{m} and the six lead directions are shown.

Figure 10.4 shows the six limb leads arranged in a so called Cabrera sequence. The text box on Figure 10.4 contains a set of data extracted from the six ECG lead waveforms.

Einthoven Triangle and the Lead Vector

Einthoven (1913) proposed an equilateral triangle model with the center in the heart center, Figure 10.5. Each side of the triangle corresponded to each of the three bipolar leads I, II, and III. He proposed the heart modeled as a bound dipole vector (he did not use that expression), and that a lead voltage was the projection of the heart vector on a corresponding triangle side (actually a dot product). He proposed that his model could

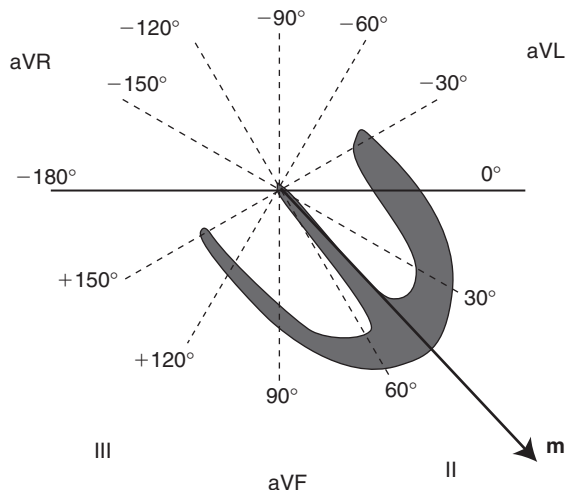


Figure 10.3: Myocard of left (thick) and right (thin) ventricles, the Einthoven triangle in the frontal plane. QRS heart vector \mathbf{m} , normal angle values are between -30° and $+90^\circ$.

¹ Willem Einthoven (1860–1927), Dutch physician. Nobel prize laureate in medicine 1924 (on ECG).

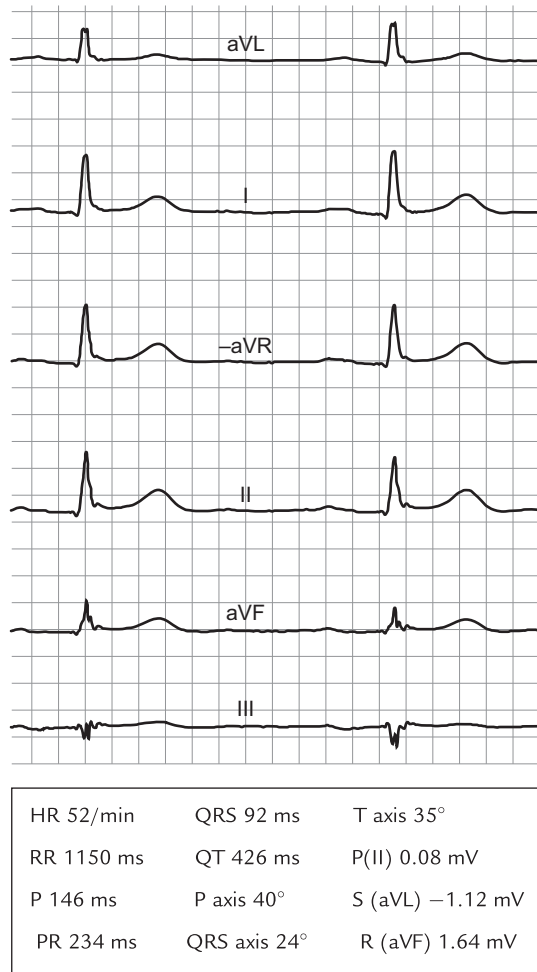


Figure 10.4: ECG waveforms of the six standard extremity leads shown with the augmented leads interlaced between the bipolar limb leads (Cabrera sequence).

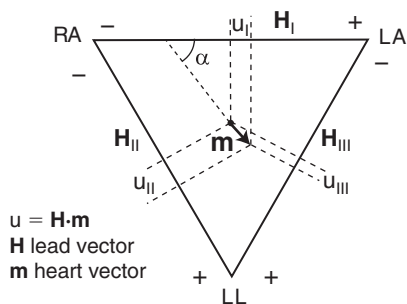


Figure 10.5: Einthoven's triangle. The triangle is in the frontal plane of the patient. \mathbf{m} is the heart vector bound to the “center” of the heart; u is the instantaneous scalar voltage measured in a respective lead; α is the instantaneous angle of the electric axis of the heart.

be used for determining the heart vector axis. This means that he saw a solution to the inverse problem: from measured lead voltages to the heart vector, from measured surface potentials to source characterization. He regarded the triangle apexes as corresponding to right and left shoulder and the symphysis. The triangle is in the frontal plane of the patient, and the heart vector has no component perpendicular to the frontal plane. He considered the heart vector to be very short.

Burger and Milan (1946) formalized Einthoven's idea and introduced the concept of the *lead vector*, Eq. 6.30. The lead vectors \mathbf{H} of the I, II, and III leads correspond to the sides of the Einthoven triangle with corners corresponding to the anatomy: the shoulders and the symphysis. The measured lead voltage u [V] is a scalar and according to Eq. 6.31 $u = \mathbf{H} \cdot \mathbf{m}$ so that u is the projection of \mathbf{m} in the direction of a lead vector \mathbf{H} , Figure 10.5. \mathbf{H} [Ω/m] for each lead is obtained from the Einthoven triangle, and the heart vector \mathbf{m} [Am] is the unknown. The magnitude and direction of \mathbf{m} can be determined from measured potentials of at least two leads, Figure 10.5.

\mathbf{m} represents a bound vector with the fixed origin in the “center” of the heart, the lead vectors \mathbf{H} are free vectors. Sampling the u values of leads I, II, and III at a given moment in Figure 10.5 defines the *instantaneous* value and direction (angle α in Figure 10.5) of the heart vector \mathbf{m} . The mean direction during the QRS complex defines the *electrical axis* of the heart. Mean direction is used because the R tags are not completely concurrent for the I, II, and III leads. The electrical axes for the P, QRS, and T complexes have different directions (see the text box in Figure 10.4). During a QRS complex, the locus of the vector arrow describes a closed loop in the frontal plane, Figure 10.6.

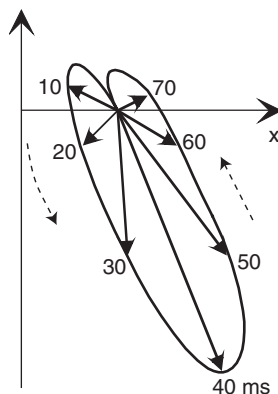


Figure 10.6: Locus of the heart vector \mathbf{m} given each 10 ms in the QRS diastole. Derived from the Einthoven triangle (Figure 10.5). The graph is in the frontal plane and the x -axis has the direction of the lead vector \mathbf{H}_I ($\alpha = 0$).

The electrical axis of the heart can roughly be determined by looking at the net area of a QRS complex. A net positive area means that the heart vector has the same direction as the lead vector. A small net area means that the heart vector is perpendicular to the lead vector. A negative net area means that the heart vector has the opposite direction of the lead vector. It is interesting to compare this interpretation, which is based upon a bound heart vector with changing length and direction, with the model used for Figure 6.11. The model for Figure 6.11 is a current dipole moving but having constant length and direction. With \mathbf{m} and \mathbf{H}_{II} parallel, the waveform will be monophasic; with \mathbf{m} and \mathbf{H}_{III} perpendicular, the waveform will be biphasic.

The *dipole* model in electrocardiography has been a hot topic.² Einthoven (1913) did not use the dipole concept, but referred to the potential difference [V] between two close points in the center of the heart. He thus defined a current vector with the voltage difference between its poles. There is an ambiguity here: A potential difference may be regarded as a scalar [V], but may also be regarded as an electric field [V/m] vector. A bipolar lead may be regarded as an electric field transducer with scalar voltage [V] output. Einthoven used the concept of electromotive force (emf) that may be considered to have direction when related to the transducing mechanism of the force exercised on a charge in an electric field, but may also be regarded as a scalar potential [V]. So the heart dipole has a vector moment [Am], the heart dipole moment has a direction from plus pole to minus pole, the resulting current density in the thorax is a vector field [A/m^2], the current density \mathbf{J} , and the electric field strength \mathbf{E} are in isotropic media proportional and simply related by Eq. 2.2: $\mathbf{J} = \sigma\mathbf{E}$. Einthoven did not use the vector concept neither the dipole concept. He referred to the direction of maximum potential difference, and this is in accordance with the Maxwell equation $\mathbf{E} = -\nabla\Phi$.

The Einthoven triangle gained more and more acceptance, but was also heavily criticized. In particular, four aspects have been attacked:

1. *Redundancy*: Of course, $u_I + u_{II} + u_{III} = 0$ (Kirchhoff's law) in a linear system. Because the two input wires of the amplifier of lead II are swapped, lead II has changed sign so that: $u_{III} = u_{II} - u_I$. Theoretically, a third lead contains no new information; in practice, however, it represents a quality control and eases rapid waveform interpretations.

² “Unfortunately, the application of the long known and well understood principles of potential theory to electrocardiography was not in general well received. Many of the more or less theoretic and mathematical papers along these lines aroused a storm of opposition. Some of the criticism came from physicians who felt that electrocardiography was a purely empiric science and that progress in the field could come only from comparison of the electrographic findings with clinical and post mortem data. Much opposition came from physiologists, many eminent in their field, who not only discounted any article of theoretical nature but also regarded the dipole hypothesis as rank heresy.” Wilson (1953).

2. *One bound dipole vector alone:* It is not a great surprise that an equivalent to the electrical activity of the whole myocard, the transmission from the sources to the different lead electrodes included, cannot be modeled as one bound dipole vector alone. The surprise is that the accordance is so good. As shown by Plonsey (1966), refinements can only include expansion with spherical harmonic multipoles such as a quadrupole, not with moving dipoles, electromotive surfaces, or multiple dipoles.
3. *Lack of three-dimensional (3D) data:* The Einthoven triangle is flat as if all electrical activities in the heart occur in a thin vertical sheet. An additional back electrode would, for instance, represent a first primitive approach to a lead perpendicular to the classical Einthoven triangle.
4. *Model with two ideal dipoles:* The triangle is actually based upon a model with two ideal dipoles (see Section 6.4.3). This presumption is broken because the distance between the dipoles is not very much longer than the dipole lengths and the medium is not infinite and homogeneous.

Torso models were built filled with electrolytes and with an artificial heart in the natural heart position. Burger and Milan (1946) used two copper plates 2 cm in diameter and 2 cm apart with two wires supplying a current as an artificial heart. The dipole concept was not used, but the lead vector and an oblique triangle instead of the equilateral Einthoven triangle. The heart vector was defined as the direction a heart propagates current flow; the dimension was given as [V cm²]. It is still easy to mix the dimensions; in [Figures 10.2 and 10.4](#), it is easy to believe that the heart vector is some strange voltage vector created by projections of the lead voltages. But the heart vector is a dipole vector according to $\mathbf{m} = i\mathbf{L}_{cc}$ [Am]. The direction of the vector is the electrical axis of the heart, and this is clinically used. The split components of \mathbf{m} : the dipole current i and the distance vector \mathbf{L}_{cc} are not used clinically.

[Table 10.1](#) shows time intervals and heart vector axis as shown in [Figure 10.3](#).

10.1.2 Six Chest Electrodes (Six Unipolar Precordial Leads)

A larger signal with higher information content is obtained by placing surface electrodes as near to the heart as possible. The drawback is that the exact electrode positions become critical, and it is difficult to obtain the same positions next time by another person or clinic. Six unipolar pick-up electrodes are positioned on the skin around the heart in a

Table 10.1: Normal Values of Time Intervals and Direction of the Heart Vector

Normal Values		
0.12 s < PQ < 0.25 s	QRS < 0.12 s	-30° < QRS axis < +90°

transverse plane. The lead vector of each of the six electrodes has the direction of the line from the heart center to the unipolar electrode in the transversal plane. The “reference” electrode system may be simply the RA electrode alone (CR lead). A more common “reference” is obtained (V lead) by summing the voltage from all three extremities; this is the Wilson reference used as an indifferent site for obtaining the six monopolar leads.

The 12-lead ECG clinical diagnostic test is composed of the six limb leads and the six unipolar precordial leads; an example is shown in [Figure 10.4](#).

Other Unipolar Leads

During open heart surgery, a net of 11 sterile electrodes are used for epicardial mapping. They have direct contact with the surface of the heart, and the spread of signal on the heart surface is examined by sampling at millisecond intervals in the systole. The signal amplitude is large, and the discriminative power also. The position of infarcted regions is revealed by abnormal epicardial potential spread.

Another invasive ECG recording is with intracardial catheter electrodes, e.g., for *His*³ bundle transmission. Both unipolar and bipolar leads are used, and the catheter is always advanced into the right atrium via the venous vessels. From there, it is further advanced through the tricuspidal valve into the ventricle. Being so near to the source, only small position changes have a large influence on the recorded waveform. This is acceptable because usually the time intervals are of greatest interest. Because the electrodes are very near or on the myocard, the recorded signals have several millivolts of amplitude and with a frequency content up to more than 500 Hz.

10.1.3 Cardiac Electrophysiology

The heart is a large muscle group (myocard) driven by a single firing unit followed by a special network for obtaining the optimal muscle squeeze for ventricle filling and blood acceleration. It is a very important organ and a very well-defined signal source; therefore, all sorts of recording electrodes have been taken into use: from invasive intracardiac catheter electrodes for local His-bundle recording to multiple sterile electrodes placed directly on the heart surface during open heart surgery (epicardial mapping).

The cardiac cycle in the normal human heart is initiated by the sinoatrial (SA) node. The excitation wave spreads through the atria at a velocity of about 1 m/s. The electroanatomy of the heart separates the atria and ventricles (two-chamber heart) so that the excitatory wave can be delayed before it reaches the ventricles. This delay of about 0.15 s is performed in the zone of the atrioventricular (AV) node, and permits a filling of the

³ Wilhelm His Jr. (1863–1934), Swiss physician.

ventricles before their contraction. Beyond the AV node, the excitation spreads rapidly (2–4 m/s) in the networks of His and Purkinje. These networks consist of specialized muscular (not nerve) tissue. From these networks, the excitation wave spreads in the myocard at a much lower speed (0.3 m/s). The myocard cells communicate by channels that connect the intracellular electrolytes directly. Each muscle cell is therefore triggered by its neighbor myocard cell but guided by the Purkinje network. Myocard lacks direct nerve control, although the SA node is under nerve control. The intracellular volume is like one volume of cytoplasm with many nuclei (*syncytium*), and electrical models are based upon the concept of the *bidomain*, the extracellular and intracellular domains. The tissue mass of the network is much smaller than the mass of the myocard and the electrical signal from myocard dominates the surface ECG.

Important clinical use of ECG data is to look for beat-to-beat differences, both waveform and repetition rate (variation in the beat-to-beat Q-T interval is called *dispersion*), arrhythmias, blocks, detection of ischemia, and infarcted muscle volumes and their positions.

10.1.4 Vector Cardiography

Figure 10.6 actually shows a two-dimensional vector cardiogram in the *frontal* plane. 3D vector-cardiography according to Frank is based upon the heart vector in a 3D Cartesian diagram. Five strategically positioned skin surface electrodes define the heart vector in the *transversal* plan, and two additional electrodes on the head and left leg take care of the vertical vector component. The heart vector is calculated from the recorded lead voltages and projected into the three body planes. Three loci curves of the vector tip in the three planes are the basis for the doctor's description. In principle, the 12-channel registration is reduced to three; even so, this 3D data set contains more information than the two-dimensional data set from leads I, II, and III. However, the problem for vector cardiography is that it is very difficult to throw overboard the long tradition of interpreting curves obtained with the old standardized electrode positions. From long experience, a clinical information bank has been assembled giving the relation between waveform and diagnosis. The reason for these relationships may be unknown, and is not of great concern as long as the empirical procedure furnishes precise diagnostic results. All doctors the world over are trained according to this tradition (the interpretation of EEG waveforms is another striking example of such a practice). For special diagnostic problems the vector cardiograph has some distinct advantages (e.g., the vector display of the QRS complex has a much better resolution than the narrow QRS waveform obtained with a standard 12-lead ECG). Also the vector cardiograph is valuable for training purposes to obtain a better understanding of the spatial distribution of the electrical activity of the heart.

10.1.5 Forward and Inverse Problems

The purpose of the ECG examination is to find electrical properties of the heart by measuring potential differences on the skin surface. The emfs in the heart produce currents in the surrounding tissue. The anatomy of the thorax and the conductivity distribution determine how the current flow spreads and which potential differences are to be found at the skin surface. It is generally accepted that the thorax tissue is linear with the usual endogenous current density/electrical field amplitudes generated by the heart itself. The different contributions of different myocard volumes can therefore simply be added. On the other hand, the tissue may be anisotropic and the transfer impedance is frequency-dependent. A rough demonstration of that can be obtained by measuring the transfer impedance between the arms and a bipolar skin surface pick-up electrode pair positioned over the apex and the sternum, [Figure 10.7](#). Because of reciprocity, the transfer impedance is the same if the current is applied to the electrodes on the thorax and the potential difference between the hands is measured. From [Figure 10.7](#), the frequency components of the P and T waves are not much attenuated, but the frequency components of the QRS above 50 Hz are attenuated by a factor of about 10 or more.

To find the electrical properties of the heart is an *inverse* problem, and in principle it is unsolvable, it is infinitely many source configurations that may result in the measured skin potentials.

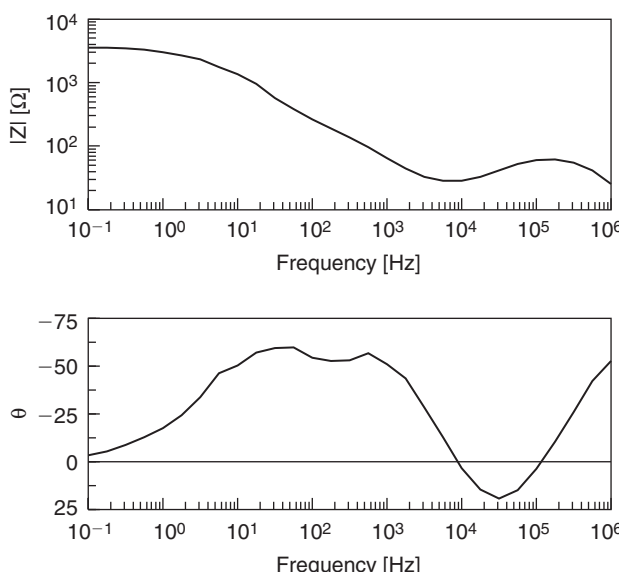


Figure 10.7: Transfer impedance between two chest surface electrodes (apex-sternum) and two electrodes in each of the hands.

We therefore start with the forward problem: from heart models in a conductive medium to surface potentials. Those problems are solvable, but it is difficult to model the heart and it is difficult to model the signal transmission from the heart up to the surface. The model may be an infinite homogeneous volume or a torso filled with saline or with a heterogeneous conductor mimicking the conductivity distribution of a thorax.

The most basic electrical model of the heart is a bound vector with the variable vector moment $m = iL_{cc}$; see Eq. 6.10. Plonsey (1966) showed that a model with more than one dipole is of no use because it will not be possible from surface measurements to determine the contribution from each source. The only refinement is to let the single bound dipole be extended to a multipole of higher terms (e.g., with a quadrupole).

The Einthoven triangle was an early solution to the inverse problem: how to characterize the source from surface electrode-derived data. It is astonishing how the original Einthoven triangle still is the basis for standard clinical ECG interpretations all over the world, even if many improvements have been proposed. Actually the tradition of using a simple theoretical model with an ideal dipole in an infinite, homogeneous volume conductor is uninterrupted. The six limb leads have been heavily attacked for their redundancy. There must be some reason why they have endured all these attacks and reached the overwhelming global spread and acceptance they have today. The large amount of clinical data is one reason; perhaps the value of these data is based upon the exceptional reproducibility of their lead vectors. The salt bridge principle assures a well-defined coupling to the shoulders and symphysis, and the position of the electrodes on the limbs is totally uncritical. The chest electrode positions are critical both for the precordial leads and the vector cardiographic leads.

10.1.6 ECG Technology

Signal Amplitude, Limb Lead II

The R voltage amplitude is usually around 1 mV. Amplitudes <0.5 mV are characterized as “low-voltage” cases, and are pathological. Obesity does not change the ECG waveforms; the R amplitude may be somewhat reduced but not into the “low-voltage” region.

Frequency Spectrum

Routine bipolar diagnostic ECG is performed with a pass band of, for example, 0.05–60 Hz. The American Heart Association recommends 150 Hz as minimum bandwidth and 500 Hz as minimum sampling rate for recording pediatric ECG. DC voltage is thus filtered out because it is related to the electrodes and not to tissue electrophysiology. In monitoring situations, the low-frequency cut-off frequency may be

increased to 0.5 Hz or more because the patient-induced motion artifacts are reduced. With skin surface electrodes, only the QRS complex has frequency components above 60 Hz; however, in the QRS there are components up to and above 1000 Hz (Franke et al., 1962) that are not used clinically. With electrodes in direct connection with the heart, the useful frequency spectrum extends to 500 Hz and more. With a pacemaker-assisted heart, the pacemaker pulses may have a width of <1 ms, and the frequency spectrum extends far above 1 kHz.

Zero Line and Isoelectric Level

Because the ECG amplifier is AC coupled, no true zero voltage is recorded. Instead the zero is a line defined by the low pass filter of the ECG amplifier so that the positive and negative areas of the total ECG waveform are equal. The zero line can be determined by simply shorting the two input wires of a lead (no signal).

10.1.7 Noise

True Physiological Signals

The limb leads presuppose that the patient is lying down so that EMG signals from the limb and body muscles do not intervene. Slow baseline respiration waves are seen if the characteristic frequency of the low-pass filter is 0.05 Hz or lower.

Exogenous Noise

- 50/60 Hz mains noise is electric or magnetic field coupled from power line wires to patient wires or patient body.
- Patient movement generates triboelectricity which may severely disturb the ECG waveform (electrostatic noise).

Solutions are shielding, active opamp circuit clamping the body to ground (Chapter 8), increased distance to the noise source, increased common mode rejection circuitry (Chapter 8), averaging over several heart beats, and wireless telemetry of electrode pick-up signals.

See Section 7.11 on indifferent electrodes and ground electrodes.

10.2 Other Organs as Bioelectric Sources

10.2.1 Brain (EEG, Electroencephalography)

EEG is recorded with three types of electrodes: scalp, cortical, and depth. The electrical activity of 10^{11} brain cells can be recorded on the skin of the scalp with a standardized electrode network of 21 electrodes. The leads may be bipolar or unipolar. The signal amplitude is only of the order of 50 μ V, and the frequency content 1–50 Hz, so DC

voltages are filtered out. The low-frequency content and the low amplitudes are a clear sign that the scalp has a detrimental effect on the signal transmission. Even so, the number of electrodes indicates that the information content is sufficient to roughly localize a source. It is believed that the brain centers are less synchronized, the higher their activity, resulting in smaller amplitude and more high frequency content of the EEG. At sleep, the waves have the largest amplitudes and lowest frequency content. The electrodes used are rather small (e.g., made of tin/lead with collodion as contact/fixation medium). Collodion is a syrupy compound of pyroxylin (nitrocellulose), ether, and alcohol that dries into a transparent, tenacious film used as a typical protectant. The brain can be stimulated, for example, by a sound or by looking at changing visual patterns. The EEG signal can be time averaged based upon synchronization pulses from the stimulator. Electrical activity and the brain's electric response can by this method be extracted from noise. In this way, hearing sense of small children and babies can be examined.

10.2.2 Brain (ECoG, Electrocorticography)

Brain (ECoG, electrocorticography) monitoring is with electrodes placed directly on the cortex when the brain cortex has been exposed by removal of a scull flap. This permits direct recording of high-amplitude, high-frequency EEG. Cortex is pulsating with the heart beats and this may cause pulse artifacts in the ECoG. The artifacts can be removed by using cotton wicks soaked with saline between the cortex surface and an electrode fixed to the scull.

10.2.3 Eye (EOG, Electrooculography)

Eye (EOG, electrooculography) is an electrophysiological method in which DC potentials are registered, and therefore AgCl electrodes are used. The DC potential is dependent on the position of the eye, and is of particular interest, for instance, when the eyelids are closed (REM sleep). As a DC recording method, EOG tends to be prone to drift that makes the spatial localization of the point of gaze problematic. It is also sensitive to facial muscle activity and electrical interference. The signals are due to a potential between the cornea and the fundus of an eye with a functioning retina, and are not from the ocular muscles (Geddes and Baker, 1989).

10.2.4 Eye (Electronystagmography)

Eye (electronystagmography) is also the recording of corneo-retinal potentials, usually used to confirm the presence of nystagmus (special eye movements). The electrodes are placed to the side (lateral), above, and below each eye. A reference electrode is attached to the forehead. A special caloric stimulation test is performed, with cold and/or hot water

brought into the canal of one ear. The electrodes record the duration and velocity of eye movements that occur when the ear is temperature stimulated.

10.2.5 Eye (ERG, Electroretinography)

Eye (ERG, electroretinography) records the AC potentials from the retina. The electrode system is unipolar, with a gold foil or AgCl recording electrode embedded in a special saline-filled contact lens in contact with the cornea. The eye may be considered as a fluid-filled sphere in contact with the retina as a thin, sheet-like bioelectric source. The ERG signal caused by a light flash is a very rapid wave with an initial rise time less than 0.1 ms (early receptor potential) and an amplitude around 1 mV, followed by a late receptor potential lasting many milliseconds.

10.2.6 Stomach (EGG, Electrogastrography)

The typical EGG signal from stomach activity is recorded with a bipolar lead using a pair of standard ECG electrodes on the skin (e.g., 4 cm apart). The signal is typically of about 100 μ V amplitude, and periodic with a period of about 20 s (0.05 Hz fundamental). Best position for the EGG electrodes is along the projection of the stomach axis on the abdomen.

Internal electrodes are also used, but are in general not considered to provide more information than external EGG recording. Of course, the internal electrodes are nearer to the source, implying higher amplitude signals with more high-frequency content. Because of the very low-frequency spectrum, external noise from, for example, slowly varying skin potentials, tends to be a greater problem than with internal recordings.

10.2.7 Muscles (EMG, Electromyography)

To record signals from active muscles, both skin surface electrodes and invasive needles are used. The distance to the muscle is often short, and the muscle group large, so signals have high-amplitude and high-frequency content. But the signal is usually composed of many muscle groups, and the signal looks rather chaotic. The muscle activity is related to the root-mean-square (rms) value of the signal. If the muscle activity is low and controlled, single motor units become discernible with needle electrodes. EMG is often recorded in connection with active neurostimulation involving both the muscle and the nervous system.

The frequency EMG spectrum covers 50–5000 Hz, and the amplitude may be several millivolts with skin surface electrodes.

10.2.8 Nerves (Electroneurography)

The sum of activities from a nerve bundle may be picked up by skin surface electrodes (e.g., on the arm where the distance from the electrodes are not too many millimeters). Action potentials from single nerve fibers must be measured with invasive needle electrodes. They may be bipolar or unipolar, Section 7.12.3. To find the right position, the signal is monitored during insertion, often guided by sounds in a loudspeaker.

Stimulation may be done with the same electrode designs: either transcutaneous right above the bundle of interest, or by needles. Muscles, for example, in the hand are stimulated by stimulating efferent nerves in the arm. EMG electrodes can pick up the result of this stimulation, for instance for nerve velocity determination. It can also be picked up by neurographic electrodes, but the signal is much smaller and must therefore be averaged with multiple stimuli. However, the method is more interesting because there is more information in the response waveforms.

Afferent and efferent nerves are often in the same nerve bundle. A stimulation signal can therefore go both ways, and from the central nervous system (CNS) side signals can be delayed and returned back to the signal origin.

10.2.9 Urology

Bioimpedance techniques are interesting candidates for diagnosing disorders in the urinary system. There are many possible applications, ranging from measurements of uterine tone and contractility to assessment of prelabor ripening and detection of cervical cancer. Some examples are as follows.

Mudraya et al. (2007) used different instruments such as a multichannel impedance spectrometer for tetrapolar measurements on an array of nine electrodes, enabling simultaneous recording of six locations along the urinary tract. They found such measurements to be valuable for quantitative assessment of ureteric peristalsis, and they could also locate stricture regions by monitoring the ratio between low and high frequency impedance, $Z_{\text{low}}/Z_{\text{high}}$.

Abdul et al. (2005) developed a tetrapolar probe for impedance measurements in the frequency range 2–1200 kHz. They found their system to give similar sensitivity and specificity to currently used screening tests for cervical intraepithelial neoplasia, but with the evident advantage of providing instant results.

Gandhi et al. (2006) measured cervical stromal impedance in nonpregnant women and women in different stages of pregnancy. They found the impedance to increase during

pregnancy, and their results suggest potential utility of cervical stromal impedance measurement for quantifying gestation-dependent changes in cervical stromal tissue.

10.3 Electrodermal Activity, Psychophysiology

Electrodermal activity (EDA)⁴ signals can be compared with ECG signals. Both are due to autonomous neurogenic control of their source activity. The heart muscle generates for each heart beat currents from myocardium circulating in the thorax. These currents generate potential differences that are picked up at the skin surface by ECG electrodes. In the same way, the sweat glands are under autonomous nerve control from the hypothalamus in the brain. For each EDA response, sweat glands produce a quantity of sweat that is propelled up the sweat ducts. This has two important effects: (1) High conductivity sweat brings the negative potential of the duct content in better contact with the potential reading electrode resulting in an increased negative electrode voltage. (2) The filling of the sweat ducts increases the conductance recorded by an exogenous current carrying electrode. The EDA signal source can therefore be considered either as endogenous [V], or exogenous [conductance, Siemens]. The skin conductance response (SCR) is due to the filling of the ducts with sweat having a much higher conductivity than the stratum corneum.

10.3.1 Physiology, Psychophysiology, Stimuli

Some skin properties are well-adapted to be controlled by autonomous sweat gland activity:

1. *Skin friction*
2. *Body temperature*
3. *Water loss prevention*
4. *Prevention of microorganisms entering the body*

In acute situations, *skin friction* is important, in particular on palmar and plantar skin sites. Examples are: best foothold for escape or attack based on very fast fight-flight decision, best finger hold, baby's best finger grasp to mother. On palmar and plantar sites, the skin must be thick and strong. Very dry stratum corneum, and thick as it is on palmar and plantar sites, is brittle and with low friction. Too wet skin gets slippery. It is therefore no surprise that the autonomous nerve system regulates the sweat activity very precisely at such sites, from low activity during sleep to a quick increase during wakening or unexpected surprises. This is what the psychologists call "arousal." It has a

⁴ EDA includes, among others, EDR (electrodermal response), GSR (galvanic skin response), and PGR (psychogalvanic reflex).

wide meaning and is therefore often called “emotional sweating.” Stimuli includes a touch, expectations, anticipations, speaking to many people, telling lies, feeling anger, stress, fear or pain, feeling incompetent, and elicit fight reflexes. Sometimes a response comes without any known external stimulus. Some of these situations may be static, you can be afraid for hours. To study the sensitivity for eliciting different types of EDA responses, the best thing is to start with the person as relaxed as possible. A stimulus may then be presented short and unexpected, or started and stopped—e.g., performing a given mathematical task.

Emotional sweating is in contrast to the sweat activity for thermoregulation of the body. This regulation is a slower system and may cover the skin of the whole body.

10.3.2 DC and AC Exogenous Measurements

Skin Conductance DC Method

For a long time, today included, DC conductance has been the most important parameter in electrodermal routine measurements. The method is exogenous, an externally applied voltage (or current) is applied to two electrodes, the resulting current (voltage) is measured and the conductance (resistance) is calculated. The SCR waveform is very simple: always a conductance increase reaching a maximum after a second or so, and then the curve relaxing back toward the starting level. Usually the constant applied voltage is 0.6 V DC, and the measurement implies that up to 50 μ A DC current can flow through the electrodes and the skin. Even if this is acceptable in routine electrodermal work, it represents a problem in research because DC current flow polarizes the electrodes, electrolyzes the skin, disturbs the measurement of conductance by varying counter-emf in the circuit, and impedes the registration of the skin endosomatic DC potential. DC conductance data may contain both conductance and potential contributions. In the public recommendations on electrodermal measurements, Fowles et al. (1981), resistance is not a recommended parameter but conductance is.

In both cases, this implies an exogenous, continuous DC current flow through the electrodes and the skin. Even if such a system is simple and practical, it is not particularly suitable for many purposes: (1) DC current flow polarizes the electrodes and electrolyzes the skin, (2) the measurement of conductance is disturbed by possible varying emfs in the circuit, and (3) skin endosomatic DC potential cannot be registered simultaneously with DC conductance because of the DC current used.

EDA is divided into *tonic* (level) and *phasic* (response) phenomena. Both tonic levels (skin conductance level, skin potential level) and responses (SCR, skin potential response) are of interest working with EDA. They are generated under autonomous nerve control of the active organs of the skin, in particular the sweat glands.

AC Method: Conductance and Capacitance (Susceptance)

As we have seen in the previous section, the DC method has been used for more than 100 years, in spite of the problems listed. The reason for this is (1) the simpler and more standardized curve forms obtained with DC and (2) the early start in the 1890s long before technology advances had made the AC method feasible. The simplest method of them all was of course the endogenous potential measurement, but the disadvantage of that method was a more difficult interpretation of the many waveforms that could come up.

The AC method also has problems of its own. We have a new parameter, the measuring frequency, which must be chosen. But perhaps the largest problem is that impedance is a complex quantity related to a capacitor and a resistor coupled in series, and the inverse quantity admittance is related to a capacitor and resistor coupled in parallel. Resistance and conductance are inverse when using DC excitation, but with AC the resistance will not be the inverse of the conductance. In this case, it is obvious that resistance and conductance are no longer inverse, as discussed in Section 3.3, and conductance should be preferred to resistance since ionic conduction and polarization basically appear in parallel in biological tissue.

10.3.3 Skin as an Endogenous Bioelectric Source, Skin Potential

The skin potential (SP) method measures potential *difference* between two skin electrodes without current flow. It is the endogenous potential level and response generated by the body itself. Usually the palmar and plantar skin sites are active during a response; other sites are passive if the person is relaxed. Both SP electrodes must not be placed on active sites, because if they are equally active no change in potential difference will occur. If both sites are more or less active, the measured potential difference may be small or even with reversed polarity. One electrode is placed at an active site (e.g., the hypothenar), and the other must be at a passive skin site (e.g., the forearm). See more about passive skin sites in Chapter 7.11, Electrode Terminology.

10.3.4 Potential and Impedance from Same Skin Site

Earlier Measurement of Both Skin Potential and Skin Conductance

Skin conductance (SC) has a simple curve form always with an initial rapid increase and a slower recovery. SP curves are more complicated. Many papers, such as Edelberg et al. (1962), Gaviria et al. (1969), Lykken et al. (1968), Venables et al. (1967), Venables et al. (1963), Yokota et al. (1959), have presented results with both conductance and potential parameters and found this an interesting research area even without having the chance of measuring both parameters simultaneously at the same skin site. They pointed out different correlations between potential and conductance both with respect to responses

and levels. It is clear that the variables may contain different information from sweat glands, sweat ducts, membranes and epidermal responses.

Wilcot (1958) defended the opinion that it is not possible to record potential and resistance from the same skin area simultaneously. Measuring with the same electrode is important because of the often large skin site—dependence of levels and response waveforms. However, a measuring system in which DC current is *replaced* by a small AC current in a monopolar system enables DC potential and AC conductance to be measured simultaneously at the same skin site (Grimnes et al., 2011). They found examples of skin potential response waveforms also with diphasic sharp edges not appearing in the conductance waveforms. The mechanism of conductance and potential signal generation may therefore be different. The potential responses were found to be more robust with respect to movement artifacts, and the instrumentation could discern whether the indifferent electrode really was on an inactive skin site.

The shapes of potential EDA and AC conductance are often similar, but can also be very different because of an unexplained cause, Tronstad et al. (2013). Using the new method of measuring SP and SC independently they examined the waveforms of both signals (Section 8.3.5 and [Figure 10.8](#)).

Skin sites are preferably palmar or plantar, using bipolar or monopolar leads. SCR is largely determined by the low conductivity stratum corneum shunted by the high but very variable conductance contribution of the sweat content in the ducts in parallel (Boucsein, 1992: p. 59; Edelberg, 1968; Venables et al., 1980). Although SC mainly is a sweat duct—filling variable, the SP is a skin membrane parameter (Venables et al., 1967).

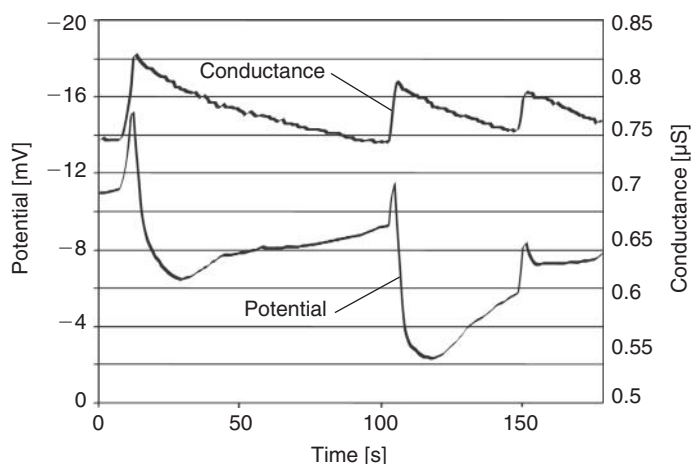


Figure 10.8: Simultaneous registration of exogenic AC conductance and endogenic DC voltage. (Courtesy of Azar Jabbari).

Applications

Basically EDA has been measured using three different parameters: skin potential, skin DC conductance, and skin AC admittance. In humans, the skin is the largest body organ, with very important tasks with respect to protection against microorganisms, wound healing, temperature control, and water loss. With very easy sensor access, it is easy to measure dielectric and electrical properties of the skin. Pharmaceutical drug delivery can be monitored.

In Figure 10.9 both hands show clear conductance waves, but no substantial susceptance waves. No time delay can be seen between the onset of the conductance waves in the two hands, but the almost undetectable susceptance waves appear a few seconds after the changes in conductance. This indicates that these changes have different causes. The rapid conductance change is presumably a sweat duct effect and the slower change in susceptance is most probably from a resultant increased hydration of the stratum corneum itself. There are no susceptance waves that could indicate any significant capacitance in the sweat ducts.

Venables and Christie (1980) give a detailed suggestion on the analysis of EDR conductance waves based on the calculation of amplitude, latency, rise time, and recovery time. They also give extensive statistical data for these parameters in different age groups. As already mentioned several times in this book, the use of absolute values for the electrical properties of tissue is hazardous because of their liability to measurement error

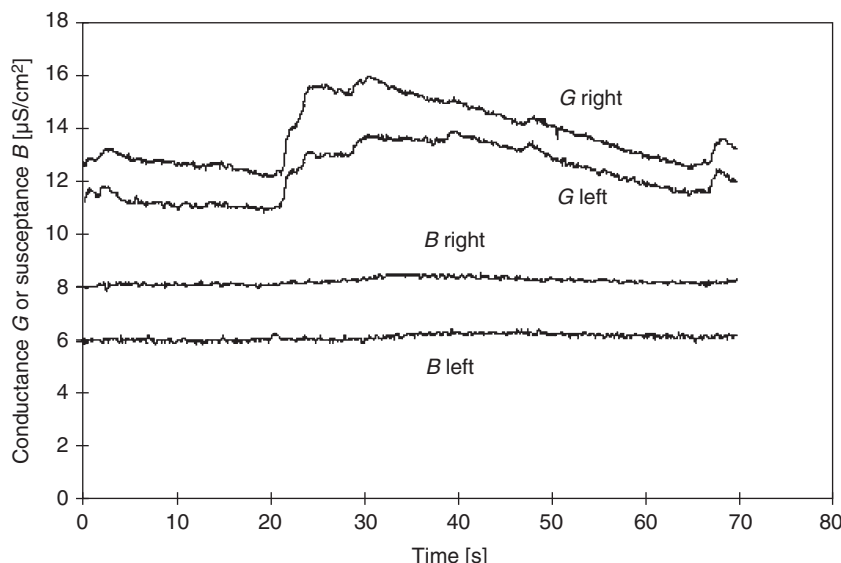


Figure 10.9: Measured 88 Hz admittance galvanic skin response activity on palmar skin sites. A deep breath at approximately 20 s on the time scale triggered the response.

and their dependence on, for example, electrode size, gel composition and ambient environment. The use of indexes or other relative parameters would presumably prove beneficial also in EDR measurements. Mørkrid and Qiao (1988) analyzed the use of different parameters from the Cole admittance equation in EDR measurements and proposed a method for calculating these parameters from measurements at only two frequencies.

10.4 Other Skin Applications

10.4.1 Sweat Activity Measurement (*Sudologger*)

Quantitative assessment of sweat activity is of great importance also for other purposes than the measurement of EDA. Tronstad et al. (2008) have reported on the development of a portable multichannel instrument for long-term logging of sweat activity (*Sudologger*). The instrument is based on conductance measurements and has been developed primarily for the assessment before and after treatment of patients with *hyperhidrosis*. Because the instrument is portable, it can also be used in sports and during other kinds of physical activities, and with four independent channels it can monitor different body parts simultaneously. Their measurements indicate that the sweat activity of different skin sites behaves differently under physical stress. Hence, such measurements will be valuable for obtaining a better understanding of the physiology controlling thermal sweating.

We have found that the AC SCR amplitude for instance may be doubled at the hypothenar with respect to the thenar site and be fourfold as high on the long finger. This is in agreement with earlier findings, Fowles et al. (1981).

10.4.2 Skin Hydration Measurement

Stratum corneum hydration is essential for proper function and appearance of the skin. The moisture content can be measured in vitro by means of gravimetry or electron microscopy, or by magnetic resonance techniques in vivo. The resolution of the latter technique is, however, currently not sufficiently high to enable isolated measurements on the stratum corneum. Compared with these techniques, assessment of stratum corneum hydration by means of electrical measurements (susceptance) represents an important reduction in instrumental cost and complexity.

A prerequisite for using electrical measurements in this way is a detailed knowledge of how the different parts of the skin influence electrical impedance. Furthermore, the current and potential distribution in the skin will also be determined by the electrode geometry, which must be taken into account. As explained in Section 4.2.6, the complex conductance of the stratum corneum and the viable skin converge as the measuring frequency is increased. Measurements at high frequencies will hence normally be largely influenced by

the deeper layers of the skin. The frequency must therefore be kept low in order to achieve isolated measurements of the stratum corneum. A frequency scan (i.e., impedance spectroscopy) cannot be used in stratum corneum hydration measurements, owing to the problems of interacting dispersion mechanisms explained in Section 9.2.9. Contrary to certain opinions (Salter, 1998), the mere fact that the current distribution in the different skin layers will differ between different measuring frequencies is enough to discard the multiple frequency approach on stratum corneum *in vivo* (Martinsen et al., 1999). Further complications are introduced by the dispersions of the electrode polarization impedance and deeper skin layers, and also by the Maxwell–Wagner type of dispersion that is due to the interface between the dry stratum corneum and the viable epidermis.

Because the sweat ducts largely contribute to the DC conductance of the skin, the proper choice of electrical parameter for stratum corneum hydration assessment is consequently low-frequency AC conductance (where DC conductance has been removed), or susceptance.

There are a number of instruments for skin hydration assessment on the market. Most of them measure at rather high frequencies, which means that they measure deep into the viable skin. Some instruments use closely spaced interdigitated microelectrodes. This somewhat reduces the contribution from viable skin layers, but the chance of only measuring in redundant moisture on the skin surface is obvious for such systems.

Rationales for using a low-frequency electrical susceptance method for skin hydration assessment and description of a method for absolute calibration of the measurements can be found elsewhere (Martinsen et al., 1998b, 2008; Martinsen and Grimnes, 2001).

10.4.3 Skin Diseases

Hyperhidrosis

Hyperhidrosis is a state of extreme sweat secretion in palmar, plantar, or axillary skin sites. The disorder can be treated with drugs (e.g., anticholinergics), tap water iontophoresis, or surgical sympathectomy. Tap water iontophoresis has been in use for more than 100 years and represents a simple, effective, but somewhat painful cure. In its simplest form, the set-up comprises two water-filled metal tubs and a DC supply. In case of palmar hyperhidrosis, the hands are placed in the two tubs and a DC current is driven from one hand to the other through the upper body. This treatment has now been stopped in Norway because the current is driven through the heart region. The Drionic is an example of an alternative device for the treatment of palmar hyperhidrosis where this problem is solved. When one hand is placed on the Drionic, half the hand is connected to one electrode through a wet sponge, and the other half to the other electrode through another wet sponge. The current is hence driven locally in the hand, and only one hand is treated at a time.

How tap water iontophoresis can impede excess sweating is still not fully understood. One theory suggests abnormal keratinization in the epidermis as a result of the current being shunted through the sweat ducts, leading to a plugging of the sweat orifices. This plugging can not be found on microographies of the skin, however, and a more plausible theory is presumably that the current leads to a reversible destruction of the sweat glands.

Skin Irritation

Irritant contact dermatitis is a localized, superficial, nonimmunological inflammation of the skin resulting from the contact with an external factor. The dermatitis may be acute, for example, if the influence from the external source was strong and of short duration, or of a more chronic kind if the influence is weaker but prolonged. The difference between irritant and allergic contact dermatitis is subtle, and depends mainly on whether the immune system is activated or not. Established signs of irritation are edema, erythema, and heat, and any electrical parameter sensitive to these physiological changes could serve as a possible parameter for the assessment of skin irritation. As for other diagnostic bioimpedance measurements, the parameter should be immune to other, irrelevant changes in the skin. To eliminate the large variations in interpersonal electrical impedance baseline, normalization by means of indexes are often used rather than absolute impedance values (see Section 9.3.).

A depth-selective skin electrical impedance spectrometer (formerly called SCIM) developed by S. Ollmar at the Karolinska Institute is an example of a commercial instrument intended for quantification and classification of *skin irritation*. It measures impedance at 31 logarithmically distributed frequencies from 1 kHz to 1 MHz, and the measurement depth can to some extent be controlled by electronically changing the virtual separation between two concentric surface electrodes (Ollmar, 1998).

Ollmar and Nicander (1995), Nicander et al. (1996), and Nicander (1998) used the following indices:

$$\text{Magnitude index (MIX)} = \frac{|Z|20 \text{ kHz}}{|Z|500 \text{ kHz}}$$

$$\text{Phase index (PIX)} = \phi |Z|20 \text{ kHz} - \phi |Z|500 \text{ kHz}$$

$$\text{Real part index (RIX)} = \frac{R20 \text{ kHz}}{|Z|500 \text{ kHz}}$$

$$\text{Imaginary part index (IMIX)} = \frac{X20 \text{ kHz}}{|Z|500 \text{ kHz}}$$

where Z, R, X, and ϕ have their usual meaning. The authors found significant changes in these indexes after treatment with sodium lauryl sulfate, nonanoic acid, and benzalkonium chloride, and the measured changes correlated well with the results from subsequent

histological examinations. The stratum corneum is soaked with saline before the measurements to provide good contact between the electrode system and the skin surface and to focus the measurements on the viable skin, although the barrier function of intact stratum corneum will still give a considerable contribution. The choice of frequencies for the indices hence seems reasonable. The group has also extended its impedance spectroscopy technology to further applications. Examples are the detection of other conditions and diseases in the skin or oral mucosa (Emtestam and Nyrén, 1997; Lindholm-Sethson et al., 1998; Norlén et al., 1999), the early detection of transplanted organ complications (Ollmar, 1997; Halldorsson and Ollmar, 1998), and assessment of skin cancer (Emtestam et al., 1998).

After publication of a paper by Nicander et al. (1996) in which it was demonstrated that skin reactions elicited by three irritants of different polarity created three different histologic patterns and that each pattern could be correlated to corresponding patterns in the impedance indices, the Ollmar group has taken steps away from the data reduction technique based on the four indices to extract more information from the original impedance spectra. However, the indices are still useful for quantification of various aspects of responses to treatment or test substances, an example of which is given by Emtestam et al. (2007).

The finding of correlation between tissue structures (as seen in the microscope) with impedance properties (Nicander et al., 1996) triggered the idea of a potential diagnostic decision support tool intended to assist the doctor in a clinical environment. This idea is not new (e.g., Fricke and Morse found a difference in capacity of tumors of the breast compared with normal breast tissue in 1926). However, this finding is completely unspecific. Almost any tissue alteration can be detected by electrical impedance, but to be clinically useful, the method has to be able to differentiate benign alterations from malignant alterations, or be able to distinguish one disease from another to select a specific and adequate therapy. In other words: There is a difference between statistical significance and clinical significance. A p -value <0.001 may sound convincing in a statistical comparison, but may mean nothing in the clinic unless both sensitivity and specificity are good enough in the intended application (see Section 9.4.1). Thus, more information had to be extracted from the impedance spectra, and both the electrical impedance indices, which were sufficient for characterizing elicited skin reactions, and classical Cole-style models, were found inadequate to distinguish various disorders, according to the Ollmar group.

In skin testing, the central area of the volar forearm is very popular, mainly because of ease of access. It is also considered very homogeneous and stable, compared with other areas of the human body, and in extrapolation of this belief there have been studies without randomization of test sites within the volar forearm region. In search of suitable

statistical tools to enhance discrimination power, this belief was challenged by Åberg et al. (2002), who used linear projection methods (in this case PARAFAC) to extract clinical information from the impedance spectra. The results showed systematic differences within the test area, which may not be important in comparison of strong reactions to, for example, detergents, but would have devastating impact on the outcome of a comparison of cosmetic preparations, where only small differences would be expected on normal skin, unless randomization of test sites is built into the study protocol.

Diabetics

It is known that diabetics are prone to develop ulcers difficult or impossible to heal, and therefore some difference in the skin properties might be present even when no clinical signs of ulceration, not even slight erythema, are present. Lindholm-Sethson et al. (1998) found such a difference in the skin between diagnosed diabetics without clinical signs in comparison with a healthy control group, but the difference was hidden behind more pronounced factors, such as age and sex, which were identified using PCA (principal component analysis). It seems that multivariate methods, such as PCA, make better use of the information inherent in electrical impedance spectra than simple indices or lumped parameter models, and that the extracted information sometimes reflects clinically interesting physiological or pathological conditions. In certain cases, it might be possible to establish a strong correlation between specific principal components and well-defined physiological or pathological conditions.

To date, most skin studies involving electrical impedance are based on pure surface electrodes. Because of the extreme heterogeneity of the skin, such measurements (at least at low frequencies, as demonstrated in a simulation study by Martinsen et al., 1999), reflect mainly the conditions in the stratum corneum and the integrity of its inherent skin barrier. However, only living cells get irritated or sick, and if important information about an alteration in the living strata of skin resides in a relatively low-frequency range, such information will be overshadowed or diluted by the intact stratum corneum. The dilution factor might be 1:100 or even 1:1000, and strongly frequency dependent! In several skin reactions or diseases, the skin barrier will be more or less destroyed by the chemical assault from the outside (fast event), or by sloppy maintenance of the stratum corneum provided by the damaged or sick living epidermis from the inside (slow event), and then surface electrodes would be sufficient. If not, something has to be done about the stratum corneum, and a number of methods have been tried, such as aggressive electrode gels (which will add to tissue damage), peeling creams, or simply grinding or stripping off the outermost layer. The effect of tape stripping to various degrees of damage on skin impedance is illustrated in a book chapter by Ollmar and Nicander (2005) and shows the dramatic overshadowing power of the intact stratum corneum on properties residing in the living strata of skin.

Metal Electrode Part with Small Spikes

A new approach toward solving the stratum corneum dilemma has been presented by Griss et al. (2001), using electrodes furnished with micromachined conductive spikes, thin enough not to leave any damage after removal and short enough to only short-circuit the stratum corneum without reaching blood vessels and nerve endings in deeper strata. This concept, originally developed as an improvement of ECG and EEG electrodes, has been further developed by the Ollmar group (Åberg et al., 2003a) to an electrode system intended to facilitate skin cancer detection even when the stratum corneum happens to be intact on top of any skin tumor.

Skin Cancers

For a clinical diagnostic decision support tool, it is not enough to detect an alteration; it must also reliably distinguish disease from other alterations. Key concepts in this context are sensitivity and specificity, as well as receiver operating characteristic (ROC) curves (see Section 9.5.2). In the skin context, reasonable clinical requirements on area under ROC curve have been published by Lee and Claridge (2005). Several classifiers have been tried on data sets prepared by data decomposition techniques using indices as well as PCA, and using impedance data from both surface electrodes and spiked electrodes, by Åberg et al. (2003b, 2004, 2005). It seems that non-melanoma skin cancers, which are slow-growing, degrade the skin barrier enough to make it more conductive and in this case there would be no need for demolition or short-circuiting of the stratum corneum, whereas for example, malignant melanoma at an early stage the stratum corneum can be quite normal (electrically insulating) and in this case the spiked electrodes increase diagnostic power.

Figure 10.10 illustrates a PCA plot of non-melanoma skin cancer and other lesions (neither normal skin nor malignant melanoma) using two principal components that in this case describe 84% of the variation in the data set that was obtained with noninvasive probes (without spikes). It is obvious that different ways to cut out the data volume including the cancer lesions would include different amounts of noncancer data points, and that it is generally impossible to avoid classification of at least some harmless lesions as harmful. The choice of classifier and cut-off levels is a matter of risk assessment, common sense, and data characteristics. In the case of malignant melanoma, missing a tumor might be assigned an unacceptable risk (life at stake), and therefore an almost 100% sensitivity required, which would entail a reduced specificity at a given area under ROC curve. In other cases, it might be more important with high specificity to avoid painful and costly interventions, because a wrong diagnosis is not dangerous and the patient simply could come back if the complaint remains.

Åberg et al. (2013) and Mohr et al. (2013) are based on large patient cohorts, and show step-by-step development and validation of a clinical device. The device, now named Nevisense®, www.scibase.se, was released autumn 2013.

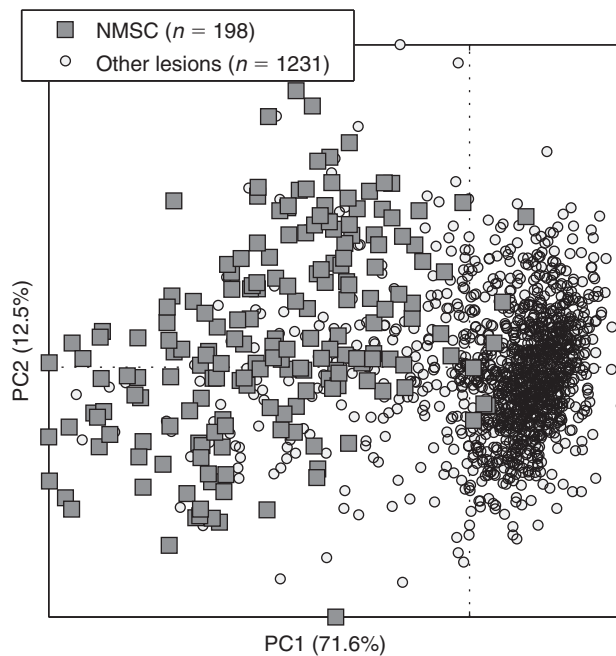


Figure 10.10: PCA plot of non-melanoma skin cancer.

An update on this group's latest work on validation of their skin cancer detector in multicenter clinical studies can be found in Malvehy et al. (2014).

Skin Fibrosis

Subcutaneous fibrosis is a common side effect of radiotherapy given, for example, to women with breast cancer. Nuutinen et al. (1998) measured the relative permittivity of the skin at 300 MHz with an open-ended coaxial probe and found that the permittivity values were higher in fibrotic skin sites than in normal skin. Based on in vitro experiments with protein-water solutions indicating that the slope of the dielectric constant vs. the electromagnetic frequency is a measure of the protein concentration, Lahtinen et al. (1999) demonstrated that skin fibrosis can also be measured with the slope technique. Both Nuutinen et al. (1998) and Lahtinen et al. (1999) found a significant correlation between the permittivity parameters and clinical score of subcutaneous fibrosis obtained by palpation. Finally, radiation-induced changes in the dielectric properties were also found in subcutaneous fat by modeling the skin as a three-layer dielectric structure (Alanen et al., 1998).

Other Diseases

The transport of charged substances through the skin (*iontophoresis and transdermal drug delivery*) was shown early by the famous experiment by Munk (1873). He applied an

aqueous solution of strychnine in HCl under two electrodes attached to the skin of a rabbit. Without current flow nothing happened to the rabbit; with application of a DC current for 45 min, the rabbit died.

Abramson and Gorin (1939, 1940) found that timothy pollen could be transported into the skin by electrophoresis. They studied the transport of dyes into human skin by electrophoresis. Without the application of electricity, no particular skin marks were seen after the dye had been in contact with the skin for some minutes. With an applied DC current, and after the superfluous dye had been wiped off, small dots were seen corresponding to the pores of the skin. Positively charged methylene blue was transported into the skin under an anode and negatively charged eosin under a cathode. Some pores were colored with only one of the types.

Iontophoresis of pilocarpine is the classical method for obtaining sweat for the cystic fibrosis test (Gibson and Cooke, 1959). The penetration of pilocarpine in the skin enhances sweat production. The test is usually performed on children with both electrodes placed on the underarm (for safety reasons, the current should not pass the thorax). A 0.5% solution of pilocarpine is placed under the positive electrode, and the DC current is slowly increased to a maximum of about 1.5 mA. The iontophoresis time is about 5 min.

A skin surface negative electrode attracts water from deeper layers, a positive electrode repels water. This is an electro-osmotic effect and not iontophoresis (Abramson and Gorin, 1939; Grimnes, 1983b).

The conductivity of human skin is very unevenly distributed. The current pathways have been found to be the pores of the skin, particularly the sweat ducts, only to a small extent through the hair follicles (Abramson and Gorin, 1940; Grimnes, 1984).

Transdermal drug delivery through iontophoresis has received widespread attention. A long-term delivery with transdermal DC voltage of <5 V was used (Pliquett and Weaver, 1996). High-voltage pulses up to 200 V decaying in about 1 ms have also been used on human skin for enhancement of transport by electroporation (Pliquett and Weaver, 1996). The effect was found to be due to the creation of aqueous pathways in the stratum corneum.

10.4.4 Fingerprint Detection

Electronic fingerprint systems will in the near future eliminate the need for keys, pin-codes and access cards in a number of everyday products. While fingerprint recognition traditionally has been used only in high security applications, it is now gaining acceptance in mainstream consumer applications worldwide. One such large-scale application will be the need for secure mobile transactions when paying for the groceries with your mobile

phone at the local supermarket. Several bioimpedance-based fingerprint sensors have been developed, such as the electrode array–based sensor from the company Idex ASA (www.idex.no). An array of electrodes is scanned as the fingertip is swept over the sensor stripe, giving a 500 dpi resolution impedance image of the fingerprint.

The fingerprint sensor market also demands systems for detecting fake fingers on the sensor, and a bioimpedance-based solution for spoof detection was described by Martinsen et al. (2007). Their system is based on the simultaneous measurement of skin impedance at different depths, and the use of multivariate models to classify the fingers as living or fake.

10.5 Impedance Plethysmography

Plethysmography is the measurement of volume. Dynamic plethysmography is usually associated with volume changes caused by the heartbeats, but may also be related to, for example, respiration or peristaltic movements of the alimentary canal. During heart systole with increased blood flow, the volume, for example, of a limb increases due to the inflow of blood (*swelling*). Impedance may in many cases be regarded as measuring both volume and flow, a volume change must be due to a flow. Measurements may be based upon, for example, mechanical dimensional change (strain-gauge plethysmography, light absorption (photo-plethysmography), X-ray absorption or impedance change). Application areas are rather diversified, for example, heart stroke volume (SV), cardiac output (CO), respiration volume, fluid volume in pleural cavities, edema, urine bladder volume, uterine contractions, and detection of vein thrombosis.

10.5.1 Ideal Cylinder Models

By ideal we mean that the biomaterial is considered incompressible and homogeneous. The right section of the cylinder may be cylindrical, elliptical, or have any plane form. Estimation of volume from immittance measurement is based upon two effects:

1. A geometry-dependent effect illustrated by the cylinder model and the ratio A/L in the equation $G = \sigma A/L$. The resulting effect will be dependent on the constraints on the measured tissue volume: If the volume increase results in a swelling of length L, conductance will fall. If the volume increase results in a swelling of cross-sectional area A, the conductance will increase. If the volume increase occurs outside the measured tissue volume, the measured conductance will not change with the geometrical volume increase.
2. A conductivity-dependent component. Of special interest is the flow dependence of the conductivity of blood.

For the further analysis of these effects it is useful to set up some simple cylinder models.

The geometry is shown in [Figure 10.11](#). For the single cylinder shown at the top of [Figure 10.11](#), the volume v is easily found from $G = \sigma A/L$ or $R = \rho L/A$:

$$v = G\rho L^2 = R\sigma A^2 = \frac{1}{R} \frac{L^2}{\sigma} \quad (\text{exact}) \quad (10.1)$$

Notice that with the presumption $L = \text{const}$, the volume v is proportional to G . If the presumption is that $A = \text{const}$ the volume v is proportional to R . *If swelling is longitudinal*, the volume increase Δv is best modeled as a resistance increase in a series model. *If swelling is transverse (as supposed in many cases)*, the volume increase Δv is best modeled as a conductance increase in a parallel model. If it is not known whether the tissue swells in longitudinal or transverse direction, the conductance versions may be preferred because they lead to simpler and more exact expressions.

1. One-compartment model. Cylinder surrounded by air. See the top of [Figure 10.11](#).

In many applications, the absolute volume may remain unknown; the emphasis is instead on the *relative* volume change $\Delta v/v$. Also the relative conductance change $\Delta G/G$ is of special interest, because the ratio is related to the signal-to-noise ratio, which should be as high as possible. From [Eq. 10.1](#):

$$\frac{\Delta G}{G} = \frac{\Delta v}{v} \quad \text{or} \quad \frac{\Delta G}{\Delta v} = \frac{\sigma}{L^2} \quad \text{or} \quad \Delta v = \Delta G \rho L^2 \quad (\text{exact}) \quad (10.2)$$

From the equation, it is clear that relative volume changes can be found without knowing the dimensions of the cylinder. To have a high sensitivity (large ΔG) for a given volume change Δv , the length L should be as short as possible.

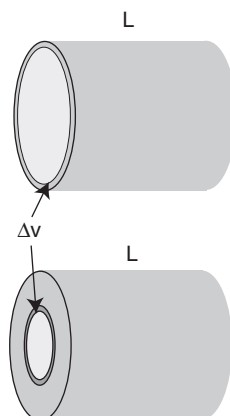


Figure 10.11: Cylinder models of length L and a small parallel volume increment Δv . Upper: one-compartment, lower: two-compartment model.

Under the presumption that $L = \text{const}$, the conductance model is preferred. If we still use a resistance model, we have from [Eq. 10.1](#):

$$\Delta v = \left(\frac{1}{R + \Delta R} - \frac{1}{R} \right) \rho L^2 = -\frac{\Delta R}{R} \frac{1}{R + \Delta R} \rho L^2 \quad (\text{exact}) \quad (10.3)$$

[Equation 10.3](#) becomes linear only if $\Delta R \ll R$:

$$\Delta v \approx -\Delta R \rho \left(\frac{L}{R} \right)^2 \quad (\Delta R \ll R) \quad (10.4)$$

The minus sign in [Eqs 10.3 and 10.4](#) is because a resistance *increase* corresponds to a volume *decrease*.

2. Two-compartment model: an inner cylinder surrounded by an outer cylinder of same resistivity. [Figure 10.11](#) bottom.

$$\frac{\Delta G}{G} = \frac{\Delta v}{\Delta v + v_A + v_t} \quad (\text{exact}) \quad (10.5)$$

In the two-compartment model, the two cylinders are physically in parallel, and the conductance model is preferred with $L = \text{const}$. $\Delta v + v_A$ is the volume of the inner cylinder, v_t is the volume of the outer cylinder and considered constant (implying that both the inner tube and outer tube swell when $\Delta v > 0$). [Equation 10.5](#) shows that the sensitivity falls with a larger surrounding volume v_t . In plethysmography, the measurement should be confined as much as possible to the volume where the volume change occurs. Thus the problem of high-sensitivity plethysmography poses the same problem as in electrical impedance tomography (EIT): to selectively measure immittance in a selected volume.

10.5.2 The Effect of Different Conductivities

In the two-compartment, constant length, parallel cylinder model analyzed previously, the conductivities in the inner and outer cylinders were considered equal. Different conductivities will of course also change G . With a conductivity σ_t of tissue outer cylinder and σ_b of blood in inner cylinder, and with constant geometry, the conductance is found from $G = \sigma A/L$:

$$G = (\sigma_A A_A + \sigma_t A_t) \frac{1}{L} \quad (\text{constant volume}) \quad (10.6)$$

[Equation 10.6](#) is not really a plethysmographic equation when the assumption is that no geometrical change shall occur. However, it relates to flow systems with a varying conductivity of the passing liquid, and flow with time is volume.

10.5.3 Models with Any Geometry and Conductivity Distribution

Figure 10.12 shows a dynamic system in a vessel where, for example, a blood bolus volume on its passage leads to a temporal local volume increase during heart systole. The measured zone in the inner cylinder is filled with blood (inflow phase). Later, during the diastole, the blood is transported further (outflow phase), but also returned via the venous system. Figure 10.12 shows a tetrapolar electrode system for the measurement of G.

In general a *tetrapolar* system is preferable; it may then be somewhat easier to confine the measured tissue volume to the zone of volume increase. The sensitivity for bolus detection with a tetrapolar electrode system will be dependent on the bolus length with respect to the measured length.

To analyze the situation with a tetrapolar electrode system in contact with, for example, a human body, we must leave our simplified models and turn to lead field theory (see Section 6.4). The total measured transfer impedance measured is the ratio of recorded voltage to injected current according to Eq. 6.39. The impedance is the sum of the impedance contributions from each small volume dv in the measured volume. In each small volume, the resistance contribution is the resistivity multiplied by the vector dot product of the space vectors $\mathbf{J}'_{\text{reci}}$ (the local current density from a unit reciprocal current applied to the recording electrodes) and \mathbf{J}'_{cc} (the local current density from a unit current applied to the true current carrying electrodes). With disk-formed surface electrodes, the constrictional resistance increase from the proximal zone of the electrodes may reduce sensitivity considerably. A prerequisite for two-electrode methods is therefore large band electrodes with minimal current constriction.

If the system is reciprocal, the swapping of the recording and current carrying electrode pairs shall give the same transfer impedance. It is also possible to have the electrode system situated *into the volume* of interest, for example, as needles or catheters. Such volume calculation, for example, of cardiac output, is used in some implantable heart pacemaker designs (see Section 10.12.3).

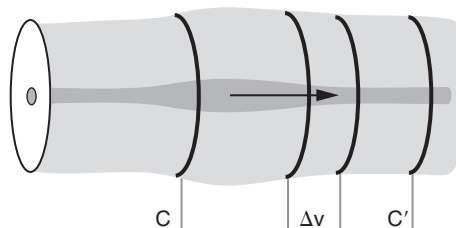


Figure 10.12: Tetrapolar electrode system and the effect of a bolus of blood passing the measured volume.

Changes in Conductivity

Conductivity may change as a function of time, for example, caused by flow. The special case of a changing conductivity with a general but constant geometry was analyzed by Geselowitz (1971) who developed an expression for ΔZ based upon the potential field. Lehr (1972) proposed to use current density instead of potential in the development. Using the nomenclature of our book and putting $\mathbf{E} = -\nabla\Phi$ and as $\mathbf{J} = \sigma\mathbf{E}$ in isotropic media, we have:

$$\Delta Z = \frac{-\Delta\sigma}{\sigma_0^2} \iiint \mathbf{J}'_0 \cdot \mathbf{J}'_{\Delta\sigma} dv \quad [Ω] \quad (10.7)$$

Here the integration is in the volume of conductivity change. The volume is homogeneous but with changing conductance, at a given moment of integration σ , is therefore constant and is put outside the integral. \mathbf{J}'_0 is the lead field at $t = 0$ and conductivity σ_0 , $\mathbf{J}'_{\Delta\sigma}$ is the reciprocal lead field dependent on $\Delta\sigma$. The choice of which port is to be current carrying and which is to be potential reading is arbitrary. \mathbf{J}' is current density with unit current excitation [$1/m^2$]. If $\Delta\sigma$ is positive, ΔZ is negative because of the minus sign in Eq. 10.7. If $\Delta\sigma$ is zero, ΔZ is zero, this is not the case for Eq. 25.1 in Malmivuo and Plonsey (1995).

Sigman Effect

Sigman et al. (1937) were the first to report that the resistivity of blood is flow-dependent. They found that the resistivity fell about 7% when the blood velocity was increased from 10 to 40 cm/s. This is an application area for the Geselowitz (1971) equation, a change in measured conductance not related to volume and therefore not plethysmographic. It is a source of error in volume estimations, but not necessarily in flow estimations.

No Sigman effect is found in plasma or electrolytes, Geddes and Baker (1989). The Sigman effect is due to the nonspherical bodies in the blood, in particular the erythrocytes. At higher velocities but still linear flow the erythrocytes reorient into the flow direction, and in a tube they also clump together around the central axis. The erythrocyte orientation means less hindrance to electric current flow and lower resistivity if resistance is measured in the axial direction. Kanai et al. (1976) reported that resistivity changes occurred at double the flow pulsation frequency, and that the magnitude became very small (>3 Hz). This means that the orientation and clumping effects are rather slow.

10.5.4 Electrical Impedance Myography

Electrical impedance myography (EIM) refers to a group of impedance-based methods for the clinical assessment of muscles. This includes primary disorders of muscle such as myopathic conditions (Rutkove et al., 2002; Tarulli et al., 2005) and the sarcopenia of aging (Aaron et al., 2006) as well as diseases that affect the nerve, such as localized

neuropathies or nerve root injuries (Rutkove et al., 2005) and generalized problems, such as amyotrophic lateral sclerosis (Esper et al., 2005). This neuromuscular disease-focused application of bioimpedance is built upon the earlier experimental and theoretical work of Shiffman and Aaron (see Aaron et al., 1997; Shiffman et al., 1999; Aaron and Shiffman, 2000). Importantly, the goal of EIM is not to image the muscle, but rather to assess quantitatively changes in its microscopic structure induced by neuromuscular disease states.

All methods use a tetrapolar technique and rely upon the placement of voltage-sensing electrodes along a muscle or muscle group of interest. Depending upon the application, current-injecting electrodes can be placed in close proximity to or at a distance from the voltage electrode array. Both single-frequency (50 kHz) and multifrequency (up to 2 MHz) methods have been studied, with the former showing very high reproducibility of the major outcome variable, the spatially averaged phase θ_{avg} (Rutkove et al., 2006). The application of EIM in the setting of voluntary or stimulated muscle contraction represents another provocative and potentially important area of investigation that may allow assessment of the contractile apparatus (Shiffman et al., 2003).

Some limited animal work has also been performed. Nie et al. (2006) showed that consistent measurements could be obtained on the hamstring muscles of the rat and that substantial changes occur after experimental sciatic crush, including reductions in the measured phase and loss of the normal frequency dependence. Future animal work will be geared at disease differentiation and determining the relationship between muscle states and their impedance patterns.

The most straightforward application of the technique of EIM for clinical care is for its use as a quantifiable measure of muscle health, such that treatment or rehabilitation programs can be effectively monitored. Indeed, EIM has the potential to serve as a useful new outcome measure in clinical trials work (Tarulli et al., 2005) and studies are ongoing to verify the role of EIM as an outcome measure in amyotrophic lateral sclerosis, spinal muscular atrophy, and exercise interventions in aging. It is uncertain whether the technique has the potential of supplanting standard neuromuscular diagnostic methods, most notably needle electromyography, and this remains a subject of ongoing research.

10.5.5 Rheoencephalography

Rheoencephalography (REG) is a plethysmographic bioimpedance method widely used in countries such as Russia and China, but not very well known in the United States and Europe. The ambition is to assess cerebral blood flow (Geddes and Baker, 1989); however, only a little part of the REG signal is caused by changes in brain conductivity, the rest relates to the pulsating blood flow of the scalp. REGs use has been limited because the reading is so highly contaminated by this scalp component. The anatomical background of

REG is not clearly understood, and a multilayer spherical model of the head has been used so that the REG information is split into the extracranial and intracerebral flow signals.

The US Food and Drug Administration (FDA) definition states (1997): “(a) Identification. A rheoencephalograph is a device used to estimate a patient’s cerebral circulation (blood flow in the brain) by electrical impedance methods with direct electrical connections to the scalp or neck area.” In other words, the FDA definition includes the word “flow.” On the basis of previous data, REG is actually a reflection of volume rather than flow (Nyboer, 1960). REG and cerebral blood flow (CBF) correlation have been described earlier (Hadjiiev, 1968; Jacquy et al., 1974; Moskalenko, 1980; Jenkner, 1986). However, the correlation of global, local CBF, and carotid flow was not investigated.

REG pulse amplitude change reflects arteriolar, capillary, and venular volume changes together rather than absolute brain blood flow. Early CBF-REG studies did not focus on this topic. It was previously described that the involvement of a vessel in CBF autoregulation is size-dependent: larger arteries are less involved than arteriola (Kontos et al., 1978). Consequently, the arteriolar change observed in brain by REG reflects arteriolar function more than it reflects functions in larger arteries (e.g., carotid). The clinical importance of these findings is that REG can be measured more conveniently and continuously in humans than Doppler ultrasound. Therefore, measurement of CBF autoregulation by REG has potential for use as a life sign monitoring modality.

REG is a potential method for cerebrovascular diagnostics as well. To reach the potential of widespread application of REG, there is a need for research to clarify the physiological and pathophysiological correlations and adequate data processing (partially mentioned by Bodo et al., 2007). Additionally, as Jenkner proposed in 1983 International Conference on Electrical Bio-Impedance, there is a need to create REG standards.

The physical basis of the REG measurement is based on the fact that blood and cerebrospinal fluid are better conductors than the brain or other “dry” tissue. The REG signal reflects the impedance change: during blood inflow into the cranial cavity, electrical conductivity is increased (resistance decreased) represented by increasing REG pulse amplitude. The same electrical impedance change occurs generating a pulse wave on peripheral site, as it was first described by Nyboer (1970) in the parallel-column model. In the skull, the input is the volume of the arterial pulse, and the output is the venous outflow and the cerebrospinal fluid together. The resulting impedance change—REG curve—is the result of the equation—involving all mentioned factors but not detailed individually. The measured electrical impedance value offers the basis of several volume calculations, detailed by Jenker (1986).

A typical REG change is known to occur as a consequence of arteriosclerosis, expressed as elongation of REG pulse amplitude peak time or decreased slope of anacrotic part

(Jenckner, 1986). The possible cause of this alteration is the decreased elasticity of arteriolar wall, which is the most sensitive indicator of disease progression.

Animal studies (Bodo et al., 2004, 2005a,b, 2007) show that REG can be measured more conveniently and continuously in humans than Doppler ultrasound. Therefore, measurement of CBF autoregulation by REG has potential for use as a life sign monitoring modality.

Studies on humans have shown that reproducibility and sensitivity of the bioimpedance measurement—including REG—were comparable to the sensitivities of the pulse oximeter, laser Doppler, and Doppler ultrasound. Results demonstrated that bio-impedance offers potential for use as a multifunctional, continuous, noninvasive life sign monitor for both military and civilian purposes (Bodo et al., 2006).

In a comparative population screening study (546 volunteers), REG measurements revealed symptoms of arteriosclerosis in 54% of the subjects; within the identical population the Doppler ultrasound measurements showed 30% with arteriosclerosis (Sipos et al., 1994; Bodo et al., 1995a).

REG may have potential for noninvasive continuous life sign monitoring and detection of early cerebrovascular changes. Since the early days of REG research, advances in the development of electronics, computation, and signal processing techniques offer the possibility to reconsider the feasibility of implementing a portable or even wearable version of the REG monitoring technique to evaluate the adequacy of CBF reactivity. REG is also used in cardiac applications and evaluation of edema in the legs.

To fulfill some of the expectations, REG must reach a much higher level of standardization of both instrumentation and electrode geometry. The lack of electrode sensitivity analysis of the REG techniques has severely reduced the scientific soundness of the method.

10.6 Impedance Cardiography

10.6.1 Stroke Volume Measurements

ICG is impedance plethysmography based upon the measurement of thoracic electrical bioimpedance. It may also include a component from the resistivity dependence on blood flow (Sigman effect). If so this is not a plethysmographic but a blood velocity component. Usually a measuring frequency of 50–100 kHz has been used. A thoracic electrical bioimpedance measurement picks up both cardiac and respiration signals. The ambition is that the SV [L] and therefore CO [L/min] can be calculated with ICG, as well as the total thoracic fluid volume, for example, according to Eq. 10.1: $v = GpL^2$.

Nyboer (1950) used two band electrodes around the neck, one band electrode corresponding to the apex of the heart, and a fourth band further in caudal direction. Nyboer regarded the thorax as a cylinder volume of length L and used the expression:

$$\Delta v = \Delta Z \rho \left(\frac{L}{Z_0} \right)^2 [m^3] \quad (\text{Nyboer}) \quad (10.8)$$

which is in accordance with Eq. 10.4. The ICG tradition has since then been to use impedance Z instead of resistance R, and to use the series model. Equation 10.8 is surely valid as the condition $\Delta Z \ll Z_0$ is fulfilled in ICG, but the $\Delta Z/Z_0^2$ term is not so directly evident as the simple ΔG term in Eq. 10.2. Also, an increased volume corresponds to a conductance increase, but to an impedance decrease. Therefore a minus sign is often introduced as in Eq. 10.4, Geddes and Baker (1989). Typically, values for Z_0 are 25Ω and $\Delta Z 0.2 \Omega$. The Z waveform is similar to the aorta blood pressure curve.

SV as developed by Kubicek et al. (1966) is still compatible with a basic physical model:

$$SV = \left(\frac{dZ}{dt} \right)_{\max} T \rho \left(\frac{L}{Z_0} \right)^2 [m^3] \quad (\text{Kubicek}) \quad (10.9)$$

The *first time derivative* dZ/dt is called the ICG. T is the ventricular ejection time. Because the pick-up electrodes are positioned near the heart, they also pick up the ECG signal; this is used for the time estimation.

In the original Nyboer model, the changes in conductance were associated with cylinders of different and changing cross-sectional areas. The blood distribution process is of course much more complicated. With chest electrodes, we have plethysmographic signals from the filling and emptying of the heart, the filling and emptying of the aorta, the filling and emptying of the lungs, the filling and emptying of the muscles of the chest, as well as the Sigman effect.

Many electrode geometries have been used, in particular the old four-band technique and newer spot electrodes with four, eight, or more electrodes. Some systems use two current-carrying systems with four excitation and four recording electrodes, for eight electrodes in total. Four electrodes are connected around the neck, the others on the lower thorax. With two current sources, the sensitivity field is complicated, and many algorithms are possible when weighing the results obtained in the two channels. Kauppinen et al. (1998) compared four different electrode systems using either band or spot electrodes. They used a 3D computer model with data from the US Library of Medicine's Visible Human Project. They found that more than 55% of the measured transfer impedance was due to the skeletal muscle mass in the thorax and only about 15% originated from blood, heart, and lungs. The sensitivity field for the four tested systems showed only small differences in total sensitivity, but all the same each was a complicated mixture of many factors.

Sramek (1981) and Bernstein (1986) further developed empirical equations also with biometrical data such as patient height, actual weight, ideal weight, body surface area, age, and gender. Other transthoracic equations have also appeared (reviewed by Moshkovitz et al., 2004), partly with proprietary modifications, making methods more accurate but perhaps less robust in the case of, for instance, critically ill patients or validity before and after surgery. Bernstein and Osypka (2003) and Bernstein and Lemmens (2005) introduced an index of transthoracic aberrant conduction (e.g., by excess extravascular lung water) in their equations. Suttner et al. (2006) tried it on critically ill patients with acceptable results.

Because ICG is a very simple and low-cost technique, very valuable applications may appear. It must be remembered that a gold standard method for SV and CO does not exist; the intramethod variability may be larger than the intermethod variability. Reference methods have been thermodilution, dye dilution, oxygen Fick technique, radionuclear radiography, and transesophageal Doppler echocardiography.

Almost all of these estimates are essentially based on the assumption that the major fluctuations in the ICG signal originate from small fluctuations in a simply distributed electrical field caused by blood volume changes, mainly in the aorta. Meanwhile, several studies have shown that these assumptions may be too simplistic (e.g., Visser et al., 1976; Sakamoto et al., 1979; Meijer et al., 1982; Patterson et al., 1990, 2010; Gaw et al., 2009) because the distribution of the electrical field in the thorax is inhomogeneous, the locations of the probably multiple origins of the signal are uncertain, and the fluctuating orientation of erythrocytes in pulsating blood flow may contribute substantially to the amplitude of the signal. This orientation of the erythrocytes has been put forward as the basis of the signal and to be used for SV assessment (Bernstein, 2010). However, it is evident that the thorax holds multiple, strongly different organs and is very inhomogeneous in composition. The heart itself consists of four compartments, rhythmically containing and pumping blood, most of it forward but also some backward, while both halves of the heart pump the same volume of blood more or less simultaneously around. This means that it may be futile to make a clinically or physiologically useful interpretation of the amplitude of the ICG signal based on simplistic physiological models and simplistic field distribution models.

10.6.2 Time Relationships in the Cardiac Cycle

Although the interpretation of the amplitude of the ICG is obscured by many complicating factors, a more relevant aspect of the ICG signal may be found in the time relationships, especially when the timing of specific marker points in the ICG signal is compared with that of marker points in the ECG. Regardless of the multiple sources of the signal, the ICG reflects the mechanical/hydrodynamical aspects of the cardiac cycle, as described by

Lababidi et al. (1970), whereas the ECG reflects the electrical aspects. Therefore, time differences between the two signals can be interpreted as the time difference between electrical and mechanical aspects of the cardiac activity (Meijer et al., 2007, 2008). By recording both signals simultaneously, the time difference between specific events in the cardiac cycle can be studied under various circumstances and in various diseases or physiological conditions. In the past, several studies have related a specific time difference in the cardiac cycle, the preejection period (PEP), to autonomous nervous activation (Schweiger et al., 1998; Schächinger et al., 2001; Burgess et al., 2004). These studies showed that PEP shortened as sympathetic activity increased; for example, when a beta-adrenergic agonist such as norepinephrine was administered. In contrast, PEP increased when a sympathetic antagonist (e.g., metoprolol) was used. PEP is obtained from the time difference between the Q-point (onset of the Q-wave) in the ECG and the B-point in the ICG signal. These marker points, however, are not always present and are difficult to trace automatically (van Lien et al., 2013)—especially the existence of the so called B-point. The end marker of the PEP is uncertain, because this B-point may well originate from two, more or less coinciding, waves in the ICG (Ershishkin et al., 2012, 2013), of which the second wave (called the ejection wave) is assumed to coincide with the left ventricular ejection phase.

To skirt around these problems, Meijer et al. (2007) advocated the use of the initial systolic time interval (ISTI), which is defined as the time difference between the R-peak in the ECG and the minimum (C-point) of the ejection wave (C-wave) in the ICG. Because the R-peak in the ECG represents the maximal electric activity of the ventricles and because it was established that the C-point in the ICG coincides with the maximum of the diameter of the aortic arch during the cardiac cycle (van Eijnatten et al., 2014), it is realistic to interpret ISTI as a noninvasive parameter indicating the velocity of the left ventricular contraction. It has been observed that ISTI depends on the level of physical training (Hoekstra et al., 2010). Disturbances of the velocity of contraction, reflected in ISTI, were observed in patients with diseases or lesions of the autonomic nervous system, suffering from Parkinson's disease or spinal cord injuries (Meijer et al., 2011; Hoekstra et al., 2012). ISTI is also influenced by the amount of circulating blood volume after cardiac surgery and during hemodialysis (Smorenberg et al., 2013; Biesheuvel et al., 2013), as can be expected because this strongly influences the preload of the heart (Meijer et al., 2010).

Most of the problems encountered in ICG, such as uncertainty about the distribution of the electrical field and dependence on electrode position, concern an influencing of the impedance signal by amplitude modulation. The timing, however, of the points and waves in the ICG signal is mostly independent of these problems. Therefore, the use of the time relationships instead of the amplitude of the ICG offers more fruitful perspectives for clinical and physiological applications. The method is noninvasive, without adverse

effects, and can be used for continuous monitoring. The technical equipment is inexpensive and easy to operate. The measurements can be performed both inside and outside the hospital, both in clinical and physiological situations.

10.7 Imaging of Lungs

In Section 6.6 a general description of EIT was given. In this section, we will give an example of an innovation that ended up with a bioimpedance imaging solution that filled a vacuum that neither magnetic resonance imaging nor computed tomography imaging could meet. It illustrates many of the characteristic properties of an innovation process: it must be based upon a new idea for solving a problem in medical imaging. The problem and the solution must be of a quality that can compete with already known methods. The new tomographic instrumentation is with an imaging resolution that is much worse than that of a microscope, X-ray generator, computed tomography, magnetic resonance imaging, or ultrasound image. Even so it can compete because of a few, but unique features: (1) imaging done bedside and (2) it can monitor a patient continuously for many hours.

The idea is based upon a relatively small device, being able to take up to 50 frames per second, connected with noninvasive sensors fixed to the skin and without being held by an operator but being able to monitor 24 h without intervention.

The description is partly based on a booklet that appeared in 2011: Electrical impedance tomography: The realization of regional ventilation monitoring (Teschner and Imhoff, 2011). The product is PulmoVista 500, fabricated and marketed by Dräger, Germany.

A more detailed history of EIT is found in Chapter 6.6. The first research models appeared in the 1980s (Sheffield group with Barber and Brown), and a European concerted action project backed by European Union financing resulted in a bioimpedance research take off, and the first algorithms for the construction of images appeared. Around 1995, more than 30 research groups worked with EIT, mostly in Europe. Little by little, it became clear that imaging lungs gave promising results. It also became clear that image resolution did not increase very much by increasing the number of electrodes beyond 16. A research group in Göttingen developed an EIT prototype suited for not only laboratory research, but also clinical research. In 2001, the Göttingen group and Dräger started a joint effort to develop a commercial instrument. They started by pursuing a fundamental question: why had the large effort during the past 20 years not resulted in clinical practice when laboratory results had pointed out the interesting field of regional lung monitoring? One important reason was that prototypes had been based upon careful fixation of individual electrodes as shown in [Figure 10.13](#) left, a procedure taking more than 20 min. By putting all the electrodes into a belt, [Figure 10.13](#) right, a much quicker electrode fixation to the

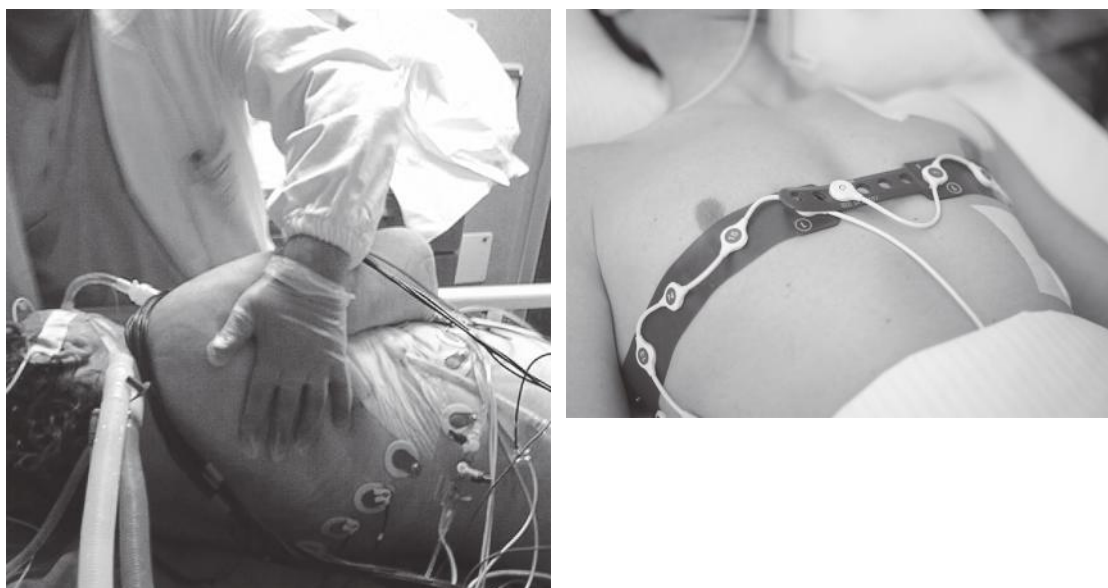


Figure 10.13: Left: Early solution with separate electrodes fixed to the patient. Right: Individual electrodes have been replaced by the electrode belt.

patient became possible. In addition it facilitated more accurate electrode positioning. After 5 years of research, a small prototype series was built and spread out to selected clinics.

At last, around 2011, the PulmoVista 500 appeared on the market. The instrument was particularly well-adapted to be used at the bedside, and with a screen where the lung regional activity could be followed, [Figure 10.14](#). The computer solution allowed follow-up and trend analysis in a simple way. Take notice that in spite of the poor image resolution, it is sufficient for answering very important clinical therapeutic questions.

10.8 Body Composition

The parameters of interest in body composition analysis (bioelectric impedance analysis, BIA) are total body water (TBW), extracellular/intracellular fluid balance, fat-free mass (lean body mass or muscle mass), and fat mass. Application areas are as diversified as sports medicine, nutritional assessment, and fluid balance in renal dialysis and transplantation.

One of the first to introduce the method was Thomasset (1965), using a two-electrode method and 1 kHz signal frequency. With just two electrodes, it is important to use large-area band electrodes to reduce the contribution from the current constrictional zones near the electrodes. With a tetrapolar electrode system, it is easier to select the preferred

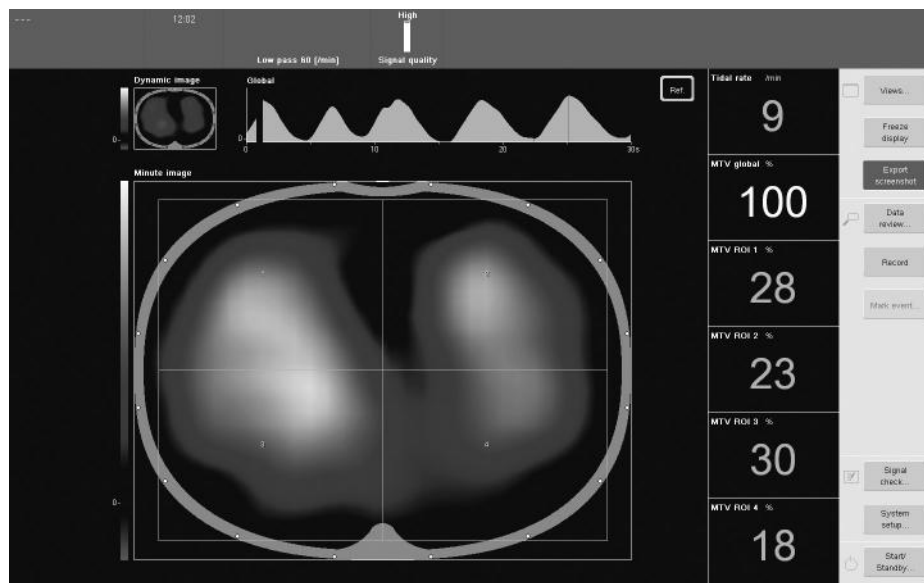


Figure 10.14: Bedside screen where the patient's lung images can be continually followed.

volume to be measured and this is now the method exclusively used. The small circumference of the lower arm, wrist, and fingers causes those body segments to dominate measured impedance in a so-called whole body measurement (see Figure 4.26). With measuring electrodes, for example, on one hand and one foot, the chest contribution is very small. The impedance of the chest segment is the most difficult one to determine directly and accurately, both because it is much lower than the impedance of the limbs and because it varies with respiration and heartbeats, as exploited in ICG (Section 10.6). It may, however, be determined by invoking the principle of equipotentials (Cornish et al., 1999). Thoracic measurements were compared with whole body measurements by Nescolarde et al. (2006).

By using more than four electrodes, it is possible to measure more than one body segment. One method uses eight electrodes, two electrodes at each hand and foot. The body impedance is then modeled in five segments: arms, legs, and chest (Figure 10.15). One segment impedance is determined by letting two limbs be current-carrying and use a third limb for zero current potential reading (five-electrode lead, pentapolar). The leads are then varied in succession. The system will be highly sensitive for the detection of asymmetrical limb bioimpedance. Standardization of the type of electrodes used and their placement is a major concern (Kyle et al., 2004). Bogonez-Franco et al. (2009) studied the effect of electrode impedance mismatch in segmental bioimpedance measurements. They found that measurement errors for commercial instruments are bigger than expected when measuring segments with low impedance. Cornish et al.

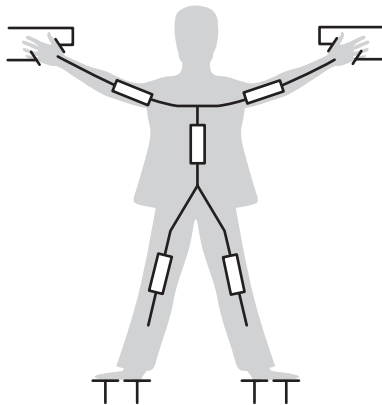


Figure 10.15: Human body divided in five impedance segments, octopolar electrodes.

(1999) provided a set of standard electrode sites for bioimpedance measurements. Standardization has been achieved by the introduction of commercial impedance devices with stand-on and handgrip contact electrodes (Bosy-Westphal et al., 2013). Marques et al. (2013) studied different types of textile electrodes (textrodes) for body composition measurements and found that a larger sensor area, a high conductive material, and an appropriate design can compensate, to some degree, for the charge transfer deficiency of the skin electrode interface.

Calibration is also a major concern in BIA. Calibration can be done with more accurate but cumbersome methods such as using deuterium, underwater weighing or dual energy X-ray absorption. However, dilution methods have their own errors (>2 L for TBW) and yield different results (e.g., 4% difference between the deuterium-TBW method and the ^{18}O -TBW method). Although body impedance reflects tissue hydration, soft-tissue mass (lean and fat) can also be empirically derived by correlation in healthy subjects because the compartments of soft tissue are correlated with each other through physiological constants. However, physiological constants become flawed in patients with fluid disorders, which accounts for some of the conflicting results in the literature (Kyle et al., 2004).

Body *position* is important because of gravitational influences on the distribution both of blood and the fluids in the stomach/intestine tissue. Direct body segment to body-segment skin contact must be avoided to have stable readings. The feet should therefore be kept at a distance from each other, and the arms should be held out from the chest. Scharfetter et al. (1998) also analyzed the artifacts produced by stray capacitance during whole body or segmental bioimpedance spectroscopy, and proposed a model for simulating the influence of stray capacitance on the measured data.

BIA as a tool for assessment of the hydration of soft tissue may be divided into *four methods of body fluid volume assessment*.

The first and the most validated method is prediction of TBW from whole body impedance measurements, often 50 kHz. Either the series impedance electrical model (often with the reactance component X neglected), or the parallel equivalent has been used. Several dependent variables may be introduced to increase the accuracy, for example, gender, age and anthropometric data such as total body weight and height. An often used index is H^2/R_{segm} , where H is the body height and R_{segm} the resistance of a given segment. Because of the $1/R_{\text{segm}}$ term, this is therefore actually a *conductance* index. Calibration can then be done by determining the k-constants in the following equations:

$$\text{TBW} = k_1 \frac{H^2}{R_{\text{segm}}} + k_2 \quad (10.10)$$

$$\text{TBW} = k_1 \frac{H^2}{R_{\text{segm}}} + k_2 W + k_3 \quad (10.11)$$

Such equations are not directly derived from biophysical laws, but have been empirically selected because they give the best correlation. The correlation according to Eq. 10.10 can be better than 0.95, and it can be slightly improved by also including other predictive variables such as body weight W, Eq. 10.11. Hundreds of validation studies with isotope dilution as the reference method have established a solid relation between whole-body impedance at 50 kHz and body fluid volume (Kyle et al., 2004). Complex impedance data can be given also as modulus and phase. Phase has been used as an index of *nutrition*. This is true only in comparison between vectors with the same modulus. For instance, short vectors with a small phase angle are associated with edema, whereas long vectors with an increased phase angle indicate dehydration. *Fat free mass* (FFM) is then predicted either from TBW ($\text{TBW}/0.73$) or through specific regression equations calibrated against direct measurement of FFM such as by dual-energy X-ray absorptiometry, with different partial regression coefficients than for TBW (Sun et al., 2003; Kyle et al., 2004) (the factor 0.73 is the hydration fraction of FFM). *Fat mass* is calculated by difference. The prediction error of best equations, although suitable for epidemiological studies, is generally considered too high for the clinical use (standard error of the estimate in the order of 2–3 L for TBW and 2–3 kg for the FFM) (Sun et al., 2003).

The second method is use of bioimpedance spectroscopy (BIS) following the Cole model approach (many groups call it a Cole–Cole model, but that is a permittivity model), earlier used by Cornish et al. (1993). R values are extrapolated at extreme limit frequencies (infinity and zero) for prediction of TBW and extracellular water, respectively, and by difference intracellular water (ICW), most commonly by a method known as mixture theory that uses assumed values for tissue fluid resistivities instead of empirical regression approaches. *Body cell mass* is then predicted as a function of the ICW (De Lorenzo et al., 1997). The results of Lozano et al. (1995) showed that there is a sharp

disequilibrium between the intracellular and extracellular compartments in the very first dialysis period and they stressed the importance of continuously monitoring segmental impedance during dialysis. BIS may be accurate with cell suspensions (the basis of mixture theory), but unfortunately it is impossible to estimate the extracellular electric volume of tissues because of anisotropy and limited low-frequency data. It is common practice not to measure below 1 kHz, and low-frequency dispersions are therefore neglected. The measuring current is usually around 0.20–0.35 mA, higher current levels are difficult to use because the threshold of perception is reached at the lowest frequencies (see Section 10.17).

The third method is prediction of *extracellular water* and TBW with low- (1–5 kHz) and high- (100–500 kHz) frequency impedance data (dual- or multifrequency BIA), with the ICW calculated by difference. Volume calibration is obtained with regression equations as in single-frequency BIA. Like BIS, multifrequency BIA relies on the wrong assumption of tissue isotropy with low-frequency current only flowing around cells. If the hydration of the FFM is not fixed at 73%, (e.g., in hemodialysis, in patients with edema or heart failure) or when body weight is meaningless for body compartments (e.g., in ascites, pregnancy, severe obesity), then BIA, multifrequency BIA, and BIS prediction equations should not be used.

The fourth and more recent method is use of the direct impedance vector measurement (Z vector, with R and Xc components) at 50 kHz in a probabilistic Wessel diagram. Such vector BIA (or BIVA) is based on patterns of the impedance vector relating body impedance to body *hydration* (Piccoli et al., 1994). BIVA is a single-frequency BIA that follows a black-box approach considering Z as a random output of a stochastic system (current flow through anisotropic tissues). The method consistently applies to whole body or segmental measurements normalized by the conductor length (height [H] for whole body, body segment length for segmental). BIVA only needs to take care of the measurement error (in the order of 3% at 50 kHz) and of the biological variability of subjects in any clinical condition. The intersubject variability of Z is represented with the bivariate normal distribution (i.e., with elliptical sex-specific probability regions [50%, 75%, and 95% tolerance ellipses] in the Wessel plane). Vector components are normalized by the subject's height (R/H , and X/H , in Ω/m , where R is the vector components' resistance, X is reactance, and H is the subject's height). Upper and lower poles of the 75% tolerance ellipses represent bioelectrical thresholds for dehydration and the fluid overload, respectively. Vector components can also be transformed into dimensionless z-scores that allow comparisons of vector position between different analyzers (Piccoli et al., 2002). Clinical information on hydration is obtained through patterns of vector distribution with respect to the healthy population of a same race, sex, and class of body mass index and age (Figure 10.16). From clinical validation studies in adults, vectors falling out of the 75% tolerance ellipse indicate abnormal tissue impedance. Vector

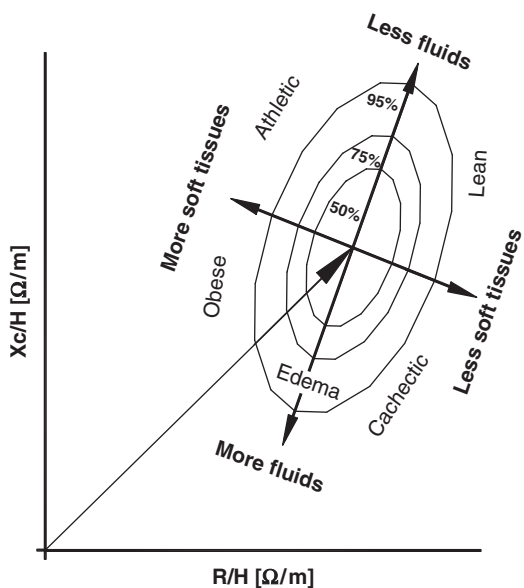


Figure 10.16: Z probability graph. Vector position and migration in the Wessel plane are interpreted and ranked according to directions: (a) Vector displacement parallel to the major axis of an ellipse is associated with a progressive change in soft tissue hydration (short-term changes: hours, days). (b) A vector lying on the left or right side of the major axis of an ellipse is associated with more or less cell mass respectively (long-term changes: weeks, months).

position is interpreted and ranked following two directions in the Wessel plane, as depicted in Figure 10.16. The basic pattern has been validated with deuterium dilution (Lukaski et al., 2007).

Body composition instruments that use complex impedance values (e.g., resistance and reactance) must either be able to measure both parameters, or to calculate one from the other. Nordbotten et al. (2011) compared the Kramers-Kronig method to regression using the Cole equation for calculating phase angle from impedance modulus in whole body measurements. They concluded that both methods were suitable, but that using the Cole model in some cases gave better accuracy. A different solution was presented by Paterno et al. (2009). Maundy et al. (2012) developed an integrator-based setup to extract the four Cole parameters without actually measuring the complex impedance.

10.9 Defibrillation and Electroshock

10.9.1 Defibrillator

Defibrillator shocks are the largest electric shocks used in clinical medicine, up to 50 A is applied for some milliseconds through the thorax, driven by approximately 5 kV. The

electrode system is usually bipolar with two equal electrodes of surface about 50 cm^2 (adult; defibrillation of children is rare). They are positioned so that as much as possible of the current is passing the heart region. With a more unipolar system with one electrode under the shoulder, the current path is more optimal, and this is used if the defibrillation is planned (electroconversion).

Previously, conductive paste was used on the skin, today contact pads are used because they are quick to apply. They also make it possible to avoid usual contact paste that is easily smeared out on the skin surface and causes stray currents (either short-circuiting the shock energy, or representing a hazard for the personnel involved). The current density is so high that reddening of the skin often occurs, especially at the electrode edge (see Section 6.2.4). The large electrode and the large current cause an extremely low-ohmic system. A total of 50Ω is the standardized resistance of the complete system with two electrodes and the tissue in between. The resistance is falling for each shock given, and this is attributed to tissue damage.

We must assume that it is the local current density in the heart that is the determining parameter for a successful conversion. Because this is unknown, it is usual practice to characterize the shock in energy (watt seconds = joules). This refers to the capacitor used to store the energy, Figure 10.17. Stored energy is $\text{CV}^2/2$, so a shock dose is simply chosen by choosing charging voltage. Maximum stored energy is usually 400 Ws. Not all the energy will be dissipated in the patient system, a part will be dissipated in the internal resistance R_i of the coil used to shape the waveform of the discharge current pulse.

External shock is given transcutaneously, so the voltage must be high enough to break down the skin even at the lowest dose. For internal, direct epicardial application (internal shock), sterile electrode cups are used directly on the heart without any paste or pad. The necessary dose is usually less than 50 Ws.

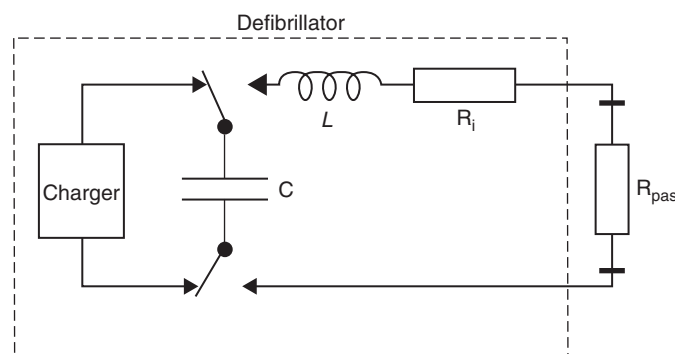


Figure 10.17: Classical defibrillator circuit. Typical values are $C = 20\mu\text{F}$, $L = 100\text{ mH}$, $R_i = 15\Omega$, $R_{pas} = 50\Omega$.

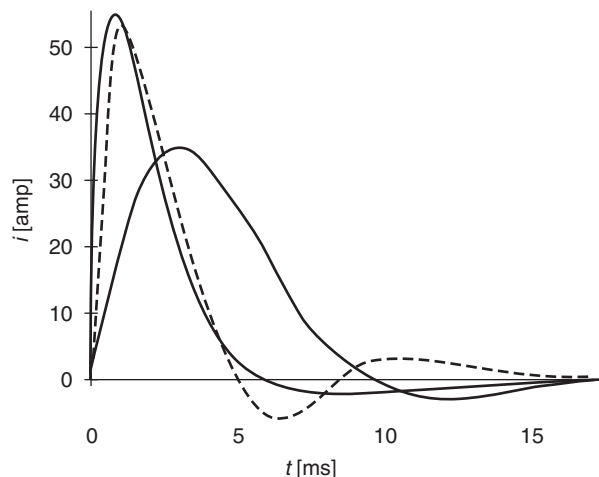


Figure 10.18: Some classical current discharge waveforms.

There is a certain range of accepted current duration. Figure 10.18 shows some current discharge current waveforms. Note that some models use biphasic waveforms, some use truly monophasic.

Defibrillators are also made as implanted types, using intracardial catheter electrodes. To reduce energy consumption, new waveforms have been taken into use: the exponential truncated waveform. It may be monophasic or biphasic. The idea of the biphasic waveform is that the second pulse shall cancel the net charge caused by the first pulse and thereby reduce the chance of fibrillation.

Tissue impedance measurements with the defibrillator electrodes are used both in some external and internal defibrillator models. Measuring current and voltage during a shock gives a high current level, minimum value, nonlinear region, peak voltage to peak current ratio. Between shocks, the small signal, linear impedance is also monitored. The measured impedance value is used to customize both waveform and energy level for each shock given.

10.9.2 Electroshock (Brain Electroconvulsion)

Electroshock therapy is a somatic method in psychiatry for the treatment of depression. The traditional current waveform is a quarter-period power line 50 Hz sine wave, starting at the waveform maximum. Pulse duration is therefore 5 ms, followed by a pause of 15 ms. Automatic amplitude increase, or pulse grouping, is used. It is now often replaced by another waveform, a train of pulses of 1 ms duration with a total energy around 20 J. It is believed that with this waveform, the memory problems are less. The corresponding voltage and current are several hundred volts and millamps. Large bipolar electrodes are used on the temples. The positioning is usually bilateral, but ipsilateral positioning is also used.

ECT is a much discussed procedure, partly because it has been perceived as a brutal medical treatment. It is performed under anesthesia, and because of the heavy muscle contractions, muscle relaxants are given. The shock elicits a seizure not very different from a grand mal epileptic attack; the seizure is to last longer than 25 s. The effect is presumably from the enormous synchronized activity of the whole central nervous system. The treatment is usually repeated several times within a few weeks' span. The treatment is often followed by a loss of memory for recent events, and the therapeutic effect is not permanent.

10.10 Electrosurgery

In electrosurgery, high-frequency (also called radio frequency, RF) current is used to cut or coagulate living tissue. The method should not be confused with *electrocautery*, where the current is passed through a wire and not through tissue, and the wire is accordingly heated. In electrosurgery heat is developed in the tissue where current flows, but the electrodes are cold. Bioimpedance is involved in different ways:

- Determining the RF current path and the influence from metal implants if such are present.
- Controlling the RF output characteristic.
- Controlling special coagulation processes.
- Safety monitoring the important neutral return plate functions.

Thus the bioimpedance participation concerns both functions and safety. It illustrates a typical feature often found with bioimpedance: bioimpedance devices are embedded in larger instrumentation as rather anonymous parts. This is especially true because use of RF high power directly to patient tissue implies high risk factors imposing strict safety requirements.

A unipolar (in the field of surgery called monopolar) circuit is used in general surgery, [Figure 10.19](#). The active electrode has a very high local current density in the tissue near the electrode, and the return current is taken care of by a large area neutral electrode. The neutral electrode is often covered with sticky hydrogel for direct fixation to the skin. The active electrode may be handheld and free, or may be endoscopic: long and thin insulated types either flexible or rigid and with an open metal sphere at the end (see Section 6.2.1).

Bipolar forceps are used for microsurgery, they represent a dipole current source in the tissue and no neutral return electrode is used (see Section 6.2.3).

The waveform used is more or less pure sinusoidal in *cut mode*, but highly pulsed with a crest factor of 10 or more for the *spread coagulation mode*. In spread coagulation, tissue contact is not critical; the current is passed to the tissue mostly by *fulguration*

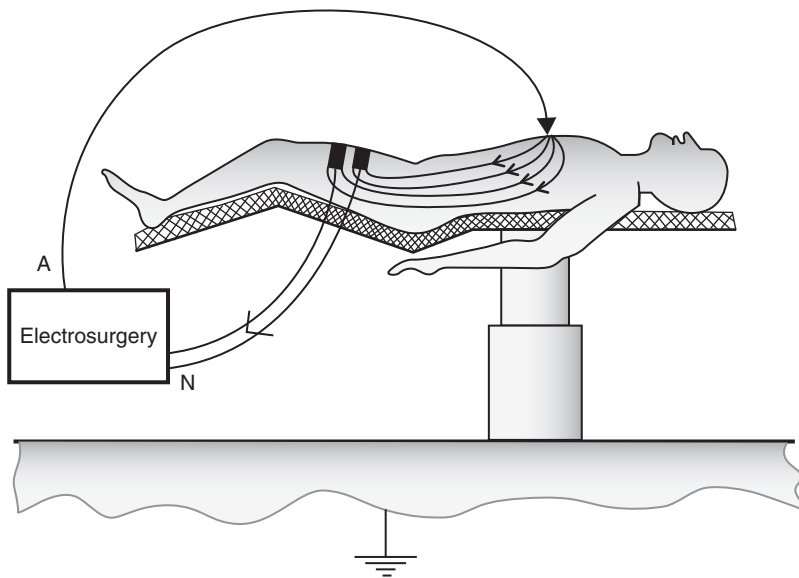


Figure 10.19: Monopolar electrosurgery.

(electric arcs). The electromagnetic noise generated may be severe over a broad frequency spectrum, causing trouble for other medical instrumentation connected to the same patient.

Electrosurgery is based upon the *heat effect* of the current, and this is proportional to tissue *conductivity* σ and the square of the *current density* (and the electric field). The power volume density W_v is falling extremely rapidly with distance from the electrode, as shown by the equation for a voltage driven half sphere electrode at the surface of a half infinite homogeneous medium: [Eq. 10.12](#). With constant amplitude current i the power volume density W_v is:

$$W_v = \frac{i^2}{4\pi^2\sigma r^4} \quad (\text{half sphere}) \quad (10.12)$$

Tissue destruction therefore occurs only in the very vicinity of the electrode. Power dissipation is linked with conductance, not admittance, because the reactive part just stores the energy and sends it back later in the AC cycle. Heat is also linked with the rms values of voltage and current, ordinary instruments reading average values cannot always be used. The temperature rise ΔT is given by Eq. 6.8. Because heat is so current *density*-dependent, the heat effect is larger the smaller the cross-sectional area of the electrode, or in a tissue zone constriction. This is an important reason for the many hazard reports with the use of electrosurgery in hospitals.

High frequencies have been chosen to avoid nerve and muscle stimulation; see the sensitivity curve of [Figure 10.20](#).

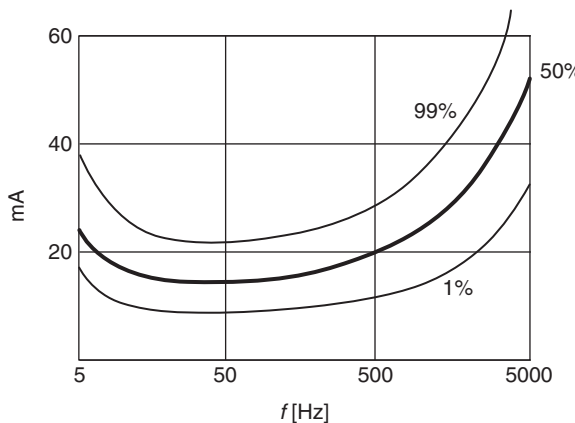


Figure 10.20: Frequency dependence of let-go currents. Statistic for 134 men and 28 women.
According to Dalziel (1954, 1972).

Typical power levels in unipolar electrosurgery is about 80 W (500Ω , 200 V, 400 mA rms), in bipolar work 15 W (100Ω , 40 V, 400 mA rms). The frequency content of the sine wave is of course just the repetition frequency, usually around 500 kHz. In pulsed mode, the frequency content is very broad, but most of the energy will be in the frequency band 0.5–5 MHz. In pulsed mode, the peak voltage can reach 5000 V, so insulation in very humid surroundings is a problem.

Argon gas is sometimes used as an arc guiding medium. The argon gas flows out of the electrode mainly for two purposes: to facilitate and lead the formation of an arc between the electrode and tissue surface, and to impede oxygen in reaching the coagulation zone. In this mode of operation, no physical contact is made between the metal electrode and the tissue, the surgeon points the pen toward the tissue and coagulation is started just as if it was a laser beam (which it is often mixed up with). The gas jet also blows away liquids on the tissue surface, thus facilitating easy surface coagulation.

Ablation

Through catheters it is possible to destroy tissue with RF currents in a minimally invasive procedure. In cardiology, this is called *ablation*. Both DC and RF current have been tried for this purpose. Choice of bipolar or monopolar technique is important, Anfinsen et al. (1998).

10.10.1 Risk Analysis

The number of reported incidents and accidents has been higher for electrosurgery apparatus than other electromedical instrumentations. One reason for this is that it is made for therapeutic interventions with use of high RF power, implying that wire lengths of 2–3 m do exhibit strong antenna effect.

Burns

The whole patient is electroactive in monopolar mode. The RF potentials of many body segments may easily attain some tenths of volt rms, and insulation of these body segments is critical. The current path in the body is much shorter in bipolar modus, this is therefore a preferred lower risk modus.

Unintended tissue destruction occurs at tissue constriction sites where the current density is high. Burns can occur at current densities above about 100 mA/cm^2 in 10 s. Peak voltage above 3 kV due to high crest factors in coagulation makes the insulation critical and high voltage insulation breakdowns may result in tissue burns.

Noise Source

An electrosurgery unit is a 2–300 W radio transmitter in the medium wave band around 1 MHz and connected to antenna wires of about 3 m lengths. In coagulation mode the power is strongly pulsed with peak powers of 1 kW or more. In fulguration modus, the contact between active electrode and tissue is to a large extent by electric arcs, which in themselves are powerful noise transmitters.

Nerve Excitation

High-frequency current used in electrosurgery does not result in living tissue excitation. However, electric arcs imply a local rectifying effect generating nerve and muscle excitation in the very vicinity of an arc. In the active electrode wire, a blocking safety capacitor is inserted so the rectified voltage shall result in only small AC low-frequency currents; see [Figure 10.21](#).

Even so, there may be local low-frequency current loops in multiple arc situations, Slager et al. (1993). Rectification is strongly unwanted, and the resulting nerve stimulation still is a problem in certain surgical procedures.

10.10.2 Embedded Bioimpedance Devices

Controlling the RF Output Power Characteristic

The optimal output characteristic is linked with the very variable load resistance. Tissue resistivity increases when coagulated. Fat has higher resistivity than muscles and blood, and the contact geometry is very dependent on the electrode chosen and the way it is held by the operator. If constant amplitude current is chosen, power would be proportional to load resistance, and tissue would quickly be carbonized in high resistance situations. If constant amplitude voltage were chosen, power would be inversely proportional to load resistance, and when tissue layers around the electrode coagulate, current stops flowing. Modern instrumentation therefore measures both

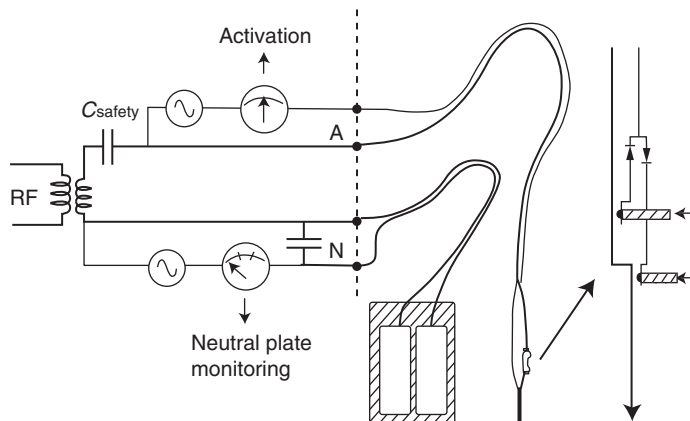


Figure 10.21: Typical electrosurgery output circuit. Notice double plate neutral electrodes for monitoring of skin contact. Safety blocking capacitor shall prevent rectified low-frequency currents in tissue.

output voltage and current, and the output impedance regulates for an isowatt characteristic delivery.

Determining the RF Current Path in Monopolar Modus

The current path between the active electrode and the neutral plate will depend on the tissue conductivity volume distribution. The site of the surgical intervention is given, but the site of the neutral electrode can be more freely chosen for optimum safe delivery.

Patients with Metallic Implants

The use of electrosurgery on patients with metallic implants or cardiac pacemakers may pose problems. Metallic implants are usually considered not to be a problem if the form is round and not pointed, Etter et al. (1947). The pacemaker electrode tip is a small area electrode, where relative small currents may coagulate endocardial tissue. The pacemaker catheter positioning should therefore not be parallel with the electrosurgery current density lines. This is illustrated in [Figure 10.22](#) for a heart pacemaker implant.

Controlling Critical Coagulation Processes in Vessel Sealing (LigaSure)

Vessel sealing for stopping bleeding is a critical process; if it fails, it may result in reopening the patient. Using the special bipolar electrode shown in [Figure 10.23](#) it is possible both to seal and to cut the vessel. When the vessel is positioned in the jaw, the tissue is pressed together by the grip. The impedance is increasing during the denaturation and impedance is monitored with the two electrodes shown. When the tissue impedance has reached a correct level, the power is switched off automatically (and not by the surgeon). When the pressure, the high frequency current level and the time is correct the

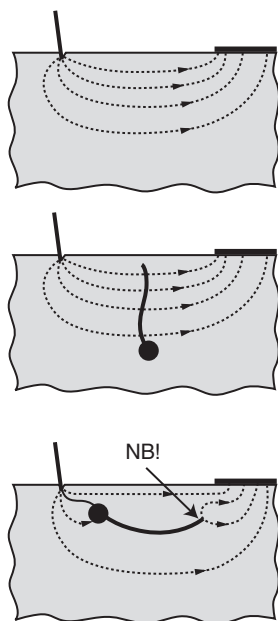


Figure 10.22: Monopolar electrosurgery and an implant; for example, a pacemaker with intracardial catheter electrode. Importance of catheter direction with respect to current density direction.

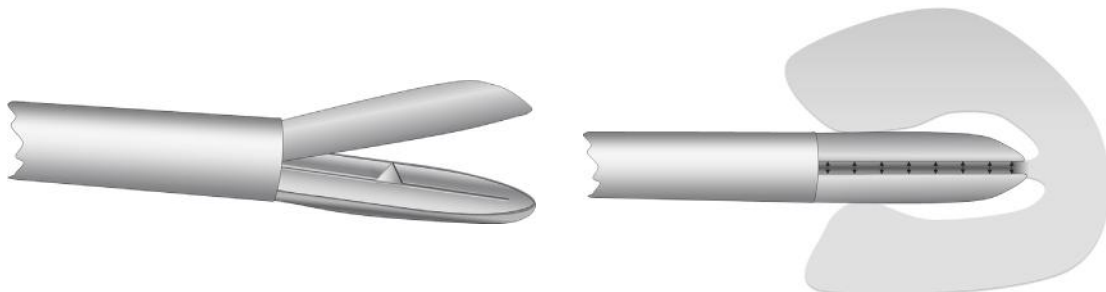


Figure 10.23: Control of critical coagulation (Ligasure). Left: Open gap with cutting device. Right: Closed gap and coagulation under controlled pressure. Courtesy: Tormod Martinsen.

inner walls of the vessel has melted together with little tissue damage and the knife can be used to cut the vessel so that both ends are sealed. [Figure 10.23](#) left shows the cutting blade that is used after the coagulation is completed and the ends of the vessels have been sealed off. The outer surface of the jaw is made of electrically insulated material so that other tissues in unintended contact will not be injured, [Figure 10.23](#) right.

Safety Monitoring of the Neutral Return Plate Function

The neutral plate is often split in two, and a small current is passed between the two plates via the skin and tissue. Impedance is measured, and if this impedance is outside preset or memory set limits, the unit will warn to inform about poor and dangerous plate contact (cf. Figure 10.21).

10.11 Cell Suspensions

10.11.1 Electroporation and Electrofusion

Electroporation is the phenomenon in which cell membrane permeability to ions and macromolecules is increased by exposing the cell to short (microsecond to millisecond) high-voltage electric pulses (Weaver, 2003). Although the mechanism for electroporation is not yet completely understood, experiments show that the application of electrical pulses can have different effects on the cell membrane as a function of various pulse parameters—such as amplitude, duration, pulse shape, and repetition rate (Mir, 2001). As a function of these parameters, the application of the electrical pulse can have no effect, can have a transient effect known as reversible electroporation, or can cause permanent permeation known as irreversible electroporation (IRE) which leads to nonthermal cell death by necrosis (Weaver, 2003; Davalos et al., 2005). It is thought that the induced potential across the cell membrane causes instabilities in the polarized lipid bilayer (Weaver and Chizmadzhev, 1996; Weaver and Barnett, 1992; Edd et al., 2006). The unstable membrane then alters its shape-forming aqueous pathways that possibly are nano-scale pores through the cell's plasma membrane (Weaver, 1995; Neumann et al., 1989; Neumann and Rosenheck, 1972). Irreversible behavior is attributed to bilayer rupture by uncontrolled pore growth and the outcome is governed by the local plasma membrane potential, $\Delta\psi_{PM}$, behavior, and the relative large membrane tension (Esser et al., 2007).

Irreversible Electroporation for Tissue Ablation

IRE has been studied extensively with in vitro cellular systems. IRE has also been studied as method to destroy prokaryotic (Sale and Hamilton, 1967) and eukaryotic cells in vitro and has gained momentum recently as a method to kill microorganisms (Vernhes et al., 1999), mammalian normal cells (Vernhes et al., 1999), and mammalian cancer cells (Miller et al., 2005) in vitro and tumors (Nuccitelli et al., 2006). These studies have demonstrated the ability of IRE to completely eradicate an entire population of cells in vitro without inducing any thermal damage.

Lee et al. hypothesized that electrical injury is often characterized by the preferential death of large mammalian cells (skeletal muscle, nerves) in tissue regions where insignificant temperature rise occurs (Esser et al., 2007; Bhatt et al., 1990; Lee et al., 2000). With the key distinction between shock trauma and temperature change, this

research group opened the door to the application of IRE as an alternate tissue ablation technique (Lee and Despa, 2005).

Davalos, Mir, and Rubinsky recently postulated that irreversible electroporation can be used as an independent drug-free tissue ablation modality for particular use in cancer therapy (Davalos et al., 2005). This minimally invasive procedure involves placing electrodes into or around the targeted area to deliver a series of short and intense electric pulses that induce irreversible structural changes in the cell membrane (Edd and Davalos, 2007). This induced potential is dependent on a variety of conditions such as tissue type and cell size (Edd and Davalos, 2007). Because of the changes in the cell membrane resistance during electroporation, the technique can be controlled and monitored with electrical impedance tomography, a real-time imaging method that maps the electrical impedance distribution inside the tissue (Davalos et al., 2004). Ivorra et al. concluded in Ivorra and Rubinsky (2007) that impedance measurements can be employed to detect and distinguish reversible and irreversible electroporation in *in vivo* and *in situ* liver tissue. IRE produces a well-defined region of tissue ablation, without areas in which the extent of damage changes gradually as during thermal ablation (Rubinsky, 2007). A single cell is either destroyed by irreversible electroporation or not (Rubinsky, 2007). The IRE pulses do not compromise the blood vessel matrix and appears to be safe and cause no complications as suggested in Maor et al. (2007). In addition, it has been shown through mathematical modeling that the area ablated by irreversible tissue electroporation before the onset of thermal effects is substantial and comparable to that of other tissue ablation techniques, such as cryosurgery (Davalos et al., 2005). Thus, for certain medical applications, IRE alone could be used as an effective technique for tissue ablation without the use of cytotoxic drugs as in chemotherapy (Davalos et al., 2005).

Electrical Properties of Tissue during Electroporation

The electrical properties of any material, including biological tissue, can be broadly separated into two categories: conducting and insulating. In a conductor, the electric charges move freely in response to the application of an electric field, whereas in an insulator (dielectric), the charges are fixed and not free to move.

If a conductor is placed in an electric field, charges will move within the conductor until the interior field is zero. In the case of an insulator, no free charges exist, so net migration of charge does not occur. In polar materials, however, the positive and negative charge centers in the molecules do not coincide. An electric dipole moment, p , is said to exist. An applied field, E_o , tends to orient the dipoles and produces a field inside the dielectric, E_p , which opposes the applied field. This process is called polarization. Most materials contain a combination of orientable dipoles and relatively free charges so that

the electric field is reduced in any material relative to its free-space value. The net field inside the material, E , is then

$$E = E_o - E_p \quad (10.13)$$

The net field is lowered by a significant amount relative to the applied field if the material is an insulator and is essentially zero for a good conductor. This reduction is characterized by a factor ϵ_r , which is called the relative permittivity or dielectric constant, according to

$$E = \frac{E_o}{\epsilon_r} \quad (10.14)$$

Biological systems are electrically heterogeneous (Gift and Weaver, 1995). Application of an electric field pulse results in rapid polarization changes that can deform mechanically unconstrained cell membranes (e.g., suspended vesicles and cells) followed by ionic charge redistribution governed by electrolyte conductivities and distributed capacitance (Ivorra and Rubinsky, 2007; Weaver, 2000). For most cells and tissues, the latter charging times are of order $\tau_{\text{CHG}} \approx 10^{-6}$ s. Thus, if U_m is to exceed 0.5–1 V, much larger pulses must be used if the pulse is significantly shorter than τ_{CHG} (Weaver, 2000).

Electroporation is hypothesized to involve inhomogeneous nucleation of primary hydrophilic pores based on transitions from much more numerous hydrophobic pores (Weaver, 2000). The basic idea is that a circular region of membrane is replaced with a pore. As primary pores appear in the membrane, its resistance drops, and the voltages within the system redistribute on a time scale governed by the instantaneous values of the various conductivities and capacitance (Weaver, 2000). Both experiment and theory show that the membrane capacitance change is small (Chernomordik et al., 1982; Freeman et al., 1994), so that the main electrical result is drastically decreased barrier resistance. Overall, bilayer membrane electroporation results in dynamic, nonlinear changes as a heterogeneous pore population evolves rapidly in response to the local value of the transmembrane voltage U_m, local along the surface of a cell membrane (Weaver, 2000). At the time of maximum membrane conductance, pores are nevertheless widely separated, occupying only about 0.1% of the electroporated membrane area (Hibino et al., 1991; Freeman et al., 1994). In this sense, electroporation is catalytic (Weaver, 1994). Not only is there the possibility of binding and lateral diffusion to the other side of the membrane as pores form and then vanish, the tremendous increases in rate (of transport) is due to small entities (pores) that occupy a small fraction of the membrane (Weaver, 2000).

Because of the changes in the cell membrane resistance during electroporation, the technique can be controlled and monitored with electrical impedance tomography, a real-time imaging method that maps the electrical impedance distribution inside the tissue (Davalos et al., 2004). Ivorra et al. concluded in (Ivorra and Rubinsky, 2007) that

impedance measurements can be employed to detect and distinguish reversible and irreversible electroporation in *in vivo* and *in situ* liver tissue.

Single-Cell Microelectroporation Technology

There are different techniques to overcome the cell membrane barrier and introduce exogenous impermeable compounds, such as dyes, DNA, proteins, and amino acids into the cell. Some of the methods include lipofection, fusion of cationic liposome, electroporation, microinjection, optoporation, electroinjection, and biolistics. Electroporation has the advantage of being a noncontact method for transient permeabilization of cells (Olofsson et al., 2003). In contrast to microinjection techniques for single cells and single nuclei (Capecci, 1980), the electroporation technique can be applied to biological containers of sub-femtoliter volumes, that are less than a few micrometers in diameter. Also, it can be extremely fast and well-timed (Kinoshita et al., 1988; Hibino et al., 1991), which is of importance in studying fast-reaction phenomena (Ryttse et al., 2000).

In addition to bulk electroporation methods, instrumentation has been developed that can be used for electroporation of a small number of cells in suspension (Chang, 1989; Kinoshita and Tsong, 1979; Marszalek et al., 1997) and for a small number of adherent cells grown on a substratum (Teruel and Meyer, 1997; Zheng and Chang, 1991). These electroporation devices create homogeneous electric fields across fixed distances of 0.1–5 mm, several times larger than the size of a single mammalian cell (Ryttse et al., 2000). Also, there are numerous experimental methods for the biochemical and biophysical investigations of single cells. Such methods include (1) patch-clamp techniques for measuring transmembrane currents through a single ion channel (Hamill et al., 1981), (2) scanning confocal and multiphoton microscopy for imaging and localizing bioactive components in single cells and single organelles (Maiti et al., 1997), (3) near-field optical probes for measuring pH in the cell interior (Song et al., 1997), (4) ultramicroelectrodes for monitoring the release of single catechol- and indol-amine-containing vesicles (Chow et al., 1992; Wightman et al., 1991), (5) optical trapping and capillary electrophoresis separations for analyzing the chemical composition of individual secretory vesicles (Chiu et al., 1998), (6) electroporation with solid microelectrodes (Lundqvist et al., 1998), (7) electroporation with capillaries and micropipettes (Nolkrantz et al., 2001; Haas et al., 2001; Rae and Levis, 2002), and (8) microfabricated chips and multiplexed electroporation system (Huang and Rubinsky, 1999; Lin, 2001).

Rubinsky's group presented the first microfluidic device to electroporate a cell (Davalos et al., 2000; Huang and Rubinsky, 1999). Their devices consisted of three silicon chips bonded together to form two chambers, separated by a 1 μm thick silicon nitride membrane with a 2–10 μm diameter hole. Because silicon nitride is nonconductive, any electrical current flowing from the top chamber to the bottom chamber must pass through this microhole. A cell suspension was introduced into the top chamber, followed by the immobilization of one cell in the hole by lowering the pressure in the bottom chamber.

Because the trapped cell impedes the system's electrical path, only low voltage pulses are needed to induce large fields near the trapped cell and only the trapped cell is electroporated. With this chip, they were able to show the natural difference in electroporation behavior between human prostate adenocarcinoma and rat hepatocyte cells by studying the process using current–voltage measurements (Huang and Rubinsky, 1999). Davalos and colleagues advanced this technology by making the chambers and electrodes off-chip, simplifying it to one silicon chip. Such changes enabled ease of use, accessibility of the device, and reusability (Lee et al., 2006; Robinson et al., 2007).

In recent years, several microfluidic electroporation designs for the analysis, transfection, or pasteurization of biological cells have been reported (Fox et al., 2006). The range of applications for microfluidic electroporation coupled with advances in microfabrication techniques, specifically the use of structural photoresist for soft lithography, has resulted in a variety of designs: microchips in which cells move through a treatment zone (Gao et al., 2004), microchips in which cells are trapped at a specific location (Huang and Rubinsky, 1999), and devices in which the cells are surface-bound (Lin and Huang, 2001; Fox et al., 2006). Of all the types of designs created, only the few designs in which a cell is trapped at a specific location enables us to study the biophysics of electroporation at the single cell level. In addition to the original devices described in the previous paragraph, other designs have been developed in which a cell is trapped at a specific location and electroporated. For example, Huang and Rubinsky advanced their technology using structural photoresist to create microfluidic channels on top of their silicon wafer (Huang and Rubinsky, 2003). Khine et al. fabricated a device using soft lithography that was originally developed as a multiple patch clamp array. Their device contains a main channel with multiple perpendicular small side channels. The individual cells in the main channel are brought into contact with the opening of a side channel using pressure. The cell does pass the constriction because its diameter (12–17 μm) is approximately four times larger than the constriction (3.1 μm). The constriction enables potentials of less than 1 V to deliver the high fields needed to induce electroporation, which is applied using an Ag/AgCl electrode (Khine et al., 2005a,b). Such devices are useful to study the biophysical process of electroporation because the changes in electrical properties of an individual cell as well as the molecular transport into the cell can be tracked (Davalos et al., 2000).

Supraelectroporation

If the applied electric field is very high ($>10 \text{ kV/cm}$) and the pulses are very short (ns-range), not only the plasma membrane of a cell is rendered permeable but so are intracellular structures (Schoenbach et al., 2004; Vasilkoski et al., 2006). This opens new perspectives for treatment of cells, especially involving intracellular structures.

Electroporation theory works well up to about 2 kV/cm applied electric field. At higher field strength, some effects appear that are hardly explainable just by pore formation.

The cell membrane has a capacity of the order of $1 \mu\text{F}/\text{cm}^2$. At 30 MHz, its capacitive resistance is small compared with the resistance of the electrolytes (i.e., the membranes are de facto shortened). The conductivity at this frequency is therefore a good guide for the maximum extent of electroporation, which would be when all membranes contain 100% pores. Even if it is practically irrelevant, it gives an idea about the absolute maximum of conductance.

As shown in [Figure 10.24](#), the conductance exceeds this maximum value considerably when the field exceeds about 5 kV/cm. An early explanation involved some kind of Wien effect. The first Wien effect is due to the liberation of ions from the counterion cloud around charged particles such as proteins, whereas the second one describes the creation of new charge carriers by field dissociation of weak electrolytes. Both of these effects together can explain a conductivity increase by several percent but not by 40% as seen in [Figure 9.24](#). Moreover, this dramatic conductivity increase is only found in solution containing aggregated amphiphiles like lipids.

The creation of very dense electropores (supra electroporation) is probably the initial step to a complete disintegration of the membrane. If the electric field is sufficiently high, micelles instead of membrane structures become stable. Because of the higher mobility of ions in the vicinity of the membrane, a significant increase in conductivity happens.

Electrofusion is the connection of two separate cell membranes into one by a similar pulse. It is believed that the process is based on the same field-induced restructuring of the bilayer lipid membranes, a process that may be reversible or irreversible.

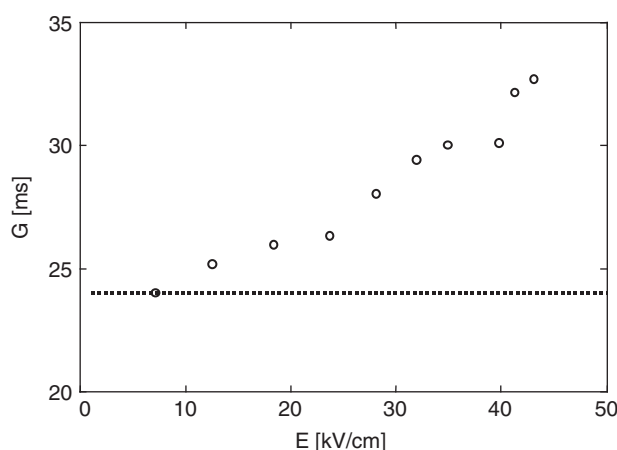


Figure 10.24: Measured conductance versus the field strength for a suspension of Jurkat-cells. The dashed line indicates the conductance at 30 MHz. *From Pliquet et al. (2007).*

It is known that an ordinary cell membrane cannot withstand a prolonged DC potential difference ΔV_m more than about 150–300 mV without irreversible damage. For short pulses in the μs range, it has been found that at a threshold voltage Δv_m of about 1 V, the cell membrane becomes leaky and rather large macromolecules pass in and out of the cell (lysis). The following expression for the electric field in the membrane E_m is valid if the membrane thickness d is much less than cell radius r , and that the conductivity of the membrane material is much less than both the internal and external (σ_o) electrolyte conductivity:

$$E_m = 1.5 \left(\frac{r}{d} \right) E (1 - e^{-Kt}) \cos \theta \quad (10.15)$$

E is the electric field in the external homogenous medium, $K = \sigma_o / 3rC_m$, and θ the angle between the E -field and the cell radius r (cell center is origin).

For electroporation, a threshold voltage of about 1 V across the cell membrane has been found. The relationship between the cell membrane potential difference (corresponding to the order of 2–20 kV/cm in the suspension according to cell size, type etc.), it may still be a reversible electroporation as long as it is caused by a single pulse of a short time duration (e.g., of the order of 20 μs). If a train of such pulses is applied, the cell is killed because of the excessive material exchange. It is believed that a large part of the material exchange (lysis) is an *after-field* effect lasting up to 0.1 s or more. If the electroporation is reversible, the pores or cracks then reseal. Electrofusion is certainly an irreversible after-field effect.

The primary field effect shows threshold behavior, about the same value for poration and fusion. The electric field effect in the cell membrane lipid bilayer is a molecular rearrangement with both hydrophobic and hydrophilic pore formation. Hydrophilic pores are considered to be water filled, with pore walls that may comprise embedded lipids. The threshold field strength has been found to be inversely proportional to the cell diameter. At the time of pulse application, cell fusion may occur if two cells are in contact with each other; DNA uptake may occur if DNA is adsorbed to the cell surface. Cells may be brought in contact with each other by means of the pearl chain effect (see the following section). The electroporative cell transformation probability from DNA entrance is low, typically 10^{-5} . Field values above threshold are believed to increase the pores in number and size, until a critical value is reached where complete membrane rupture occurs (irreversible nonthermal breakdown). The difference between the threshold level and the critical level is not large, so overdoses easily kill the cells. It is interesting to speculate whether electroporation is a mechanism in defibrillator shock treatment. The field strength used is lower (on the order of 500 V/cm); however, the pulse duration is longer, on the order of some milliseconds.

The usual source for the electric field pulse is to discharge a charged capacitor (e.g., a 25 μF capacitor charged to 1500 V). The charge voltage and the distance between the

capacitor plates determine the E-field strength, and the capacitance together with the system resistance determines the time constant of the discharge current waveform. The circuitry is very similar to the defibrillator circuit shown in Figure 10.17, except that the inductor extending the time constant into the millisecond range, is not necessarily used. The pulse is accordingly a single exponentially decaying DC pulse, and the time constant is dependent on the liquid conductivity. With more complicated circuitry, it is possible to make a square-wave high-voltage pulse generator. Because it is DC, it may be an appreciable electrolysis and change in pH near the electrodes. To keep the necessary voltage low, the distance between the electrode plates is small.

It is possible to use an RF pulse instead of DC. The RF causes mechanical vibrations in addition to the electrical effects, and this may increase the poration or fusion yield. Because the effect is so dependent on the cell diameter, it may be difficult to fuse or porate cells of different sizes with DC pulses. The threshold level for the smallest cell will kill the largest.

10.11.2 Cell Sorting and Characterization by Electrorotation and Dielectrophoresis

The principles behind electrorotation, dielectrophoresis, and other electrokinetic effects are described in Section 2.5. A good basic understanding of the various AC-electrokinetic effects is also provided by Gimsa (2012). The direction and rate of movement of bioparticles and cells due to these mechanisms depend on the dielectric properties of, for example, the cell. These dielectric properties may to some extent reflect the type of cell or the condition of the cell and there is consequently a significant potential in the use of these techniques for cell sorting or characterization.

Electrorotation was used, for example, to differentiate between viable and nonviable biofilms of bacteria. Because of their small size, determination of the dielectric properties of bacteria by means of electrorotation is impractical. By forming bacterial biofilms on polystyrene beads; however, Zhou et al. (1995) were able to investigate the effect of biocides on the biofilms.

Masuda et al. (1987) introduced the use of a traveling wave configuration for the manipulation of particles. The frequency used was originally relatively low, so that electrophoresis rather than dielectrophoresis was predominant. The technique was later improved by, among others, by Fuhr et al. (1991) and Talary et al. (1996), who used higher frequencies where dielectrophoresis dominates. Talary et al. (1996) used traveling wave dielectrophoresis to separate viable from nonviable yeast cells and the same group have used the technique to separate erythrocytes from white blood cells (Burt et al., 1998).

Hydrodynamic forces in combination with stationary electric fields have also been used for the separation of particles. Particles in a fluid flowing over the electrodes will to a

different extent be trapped to the electrodes by gravitational or dielectrophoretic forces. Separation is achieved by calibration of, for example, the conductivity of the suspending medium or the frequency of the applied field. This approach has been used for separation between viable and nonviable yeast cells (Markx et al., 1994), different types of bacteria (Markx et al., 1996), and leukemia and breast cancer cells from blood (Becker et al., 1994, 1995). Dielectrophoresis has also been successfully used for other types of bioparticles like DNA (Washizu and Kurosawa, 1990), proteins (Washizu et al., 1994), and viruses (Schnelle et al., 1996).

More recently, dielectrophoretic studies have for instance been reported on T-lymphocytes (Pethig and Talary, 2007) and on how cell destruction during dielectrophoresis can be minimized (or used) by appropriate choice of AC frequency and amplitude (Menachery and Pethig, 2005). Dielectrophoresis has also been used for measurement of membrane electrical properties such as capacitance and conductance for insulin-secreting pancreatic cells (Pethig et al., 2005).

Another interesting approach to particle separation is called field-flow fractionation, and this technique can be used in combination with dielectrophoresis (Davis and Giddings, 1986). Particles are injected into a carrier flow and another force, for example, by means of dielectrophoresis, is applied perpendicular to the flow. Dielectric and other properties of the particle will then influence the particles distance from the chamber wall and hence its position in the parabolic velocity profile of the flow. Particles with different properties will consequently be released from the chamber at different rates and separation hence achieved. Washizu et al. (1994) used this technique for separating different sizes of plasmid DNA.

Some commercial applications of DEP are now also on the market. Examples are the Bacterial Counter® from Panasonic for measurement of oral bacteria (Hamada et al., 2013), the ApoStream® from ApoCell Inc. for isolation and recovery of cancer cells from blood (Gupta et al., 2012), and the DEPArray® from Silicon Biosystems for identification, quantification and recovery of individual rare cells.

10.11.3 Cell-Surface Attachment and Micromotion Detection

Many types of mammalian cells are dependent on attachment to a surface in order to grow and multiply. Exceptions are the different cells of the blood and cancer cells which may spread aggressively (metastases). To study cell attachment, a microelectrode is convenient: as shown in Chapter 5.2, the half-cell impedance is more dominated by electrode polarization impedance the smaller the electrode surface is. [Figure 10.25](#) shows the setup used by Giaever's group (Giaever and Keesee, 1993):

A monopolar electrode system with two gold electrodes is used. A controlled current of 1 µA, 4 kHz is applied to a microelectrode <0.1 mm², and the corresponding voltage is

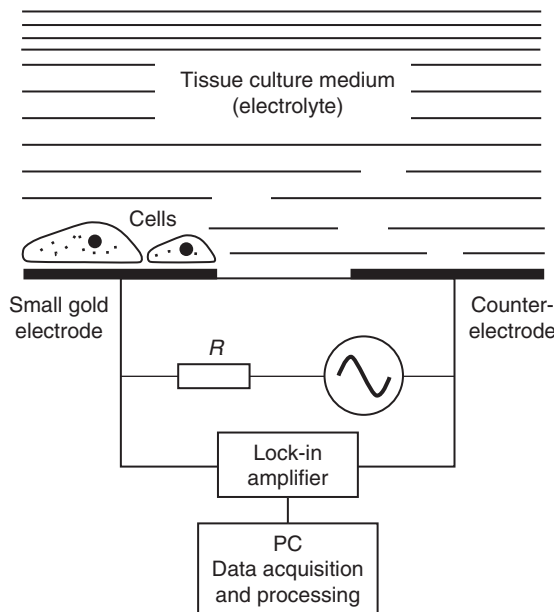


Figure 10.25: Impedance motion sensing with cells on a small gold electrode.

measured by a lock-in amplifier. With cell attachment and spreading, both the in-phase and quadrature voltage increase as the result of cell surface coverage. It is possible to follow cell motion on the surface, and the motion sensitivity is in the nm range. The method is very sensitive to subtle changes in the cells (e.g., by the addition of toxins, drugs, and other chemical compounds). It is also possible to study the effect of high-voltage shocks and electroporation.

[Figure 10.26](#) shows an example of cell attachment and motion as measured with the Electric Cell-substrate Impedance Sensing instrument, which is a commercially available version of this system (Applied BioPhysics Inc., Troy, New York, USA).

10.11.4 Coulter Counter

The principle of the Coulter counter is based on letting cells in suspension pass a narrow orifice. If a cell has different electrical properties than the liquid, the impedance of the pore will change at each cell passage. Cell counting is possible, and it is also possible to have information about each cell's size, form, or electrical properties. [Figure 10.27](#) shows the basic setup of the two-electrode conductance measuring cell. Typical dimensions (diameter, length) for a capillary is 50 and 60 µm (erythrocytes); 100 and 75 µm (leukocytes).

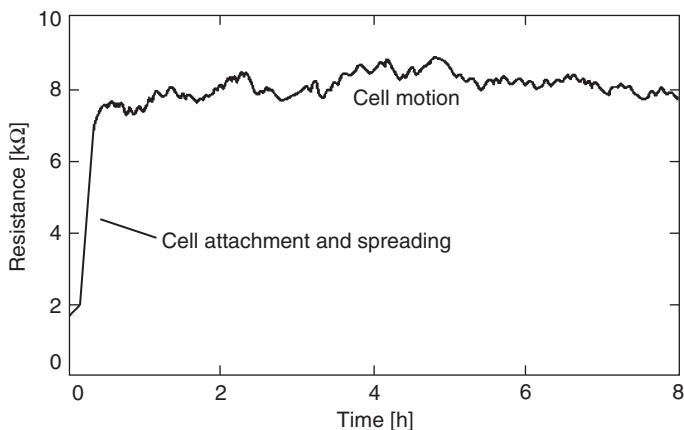


Figure 10.26: Changes in electrical resistance reflecting attachment and motion of cells on a small gold electrode.

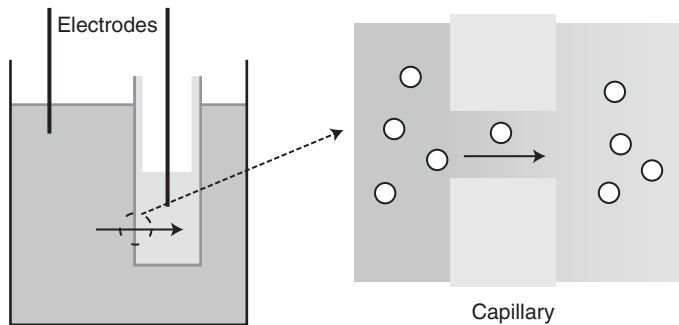


Figure 10.27: The measuring capillary cell of a coulter counter.

10.12 Implanted Active Thoracic Devices

Bioimpedance is especially attractive as a potentially useful transducing mechanism in implantable devices such as pacemakers (including pacemakers with cardiac resynchronization therapy and internal cardioverter defibrillators) for several reasons. First, the device circuitry and electrode vector configurations to perform such measurements is relatively simple and already exists in many of the current implantable devices and lead configurations. However, sampling resolution is limited in many of these circuits, preventing sufficient data for detecting changes in cardiac impedance waveforms. Therefore, low-resolution impedance measurements that provide information on fluid status or respiratory impedance trends as a function of time (day(s)/month(s)) are currently used. Improved circuit designs planned for future generation devices will be ideally suited for implantable impedance applications where high-resolution, real-time complex impedance waveform data are required. Second, impedance may be able to provide useful

diagnostic information about multiple physiologic parameters including heart rate, cardiac output, respiratory rate, minute ventilation, thoracic fluid accumulation, myocardial contractility, and ischemia detection. Third, impedance is a well-established sensing means that may provide relevant clinical diagnostic information used independently or in conjunction with other sensors such as pressure transducers or accelerometers.

10.12.1 Physiologic Impedance Components

Impedance signals are acquired from selected implantable electrode vector configurations, defined in this context as the electric field generated by the injection current field electrodes and the voltage measured by the sense field electrodes. Signals acquired from each electrode vector configuration can be either bipolar where the injection current electrodes and sense field electrodes are the same, or tetrapolar, where the injection current electrodes and sense field electrodes are isolated from each other. Electrodes in implantable pacing devices consist of unipolar or bipolar electrodes positioned on the distal end of conventional pacing leads. Pacing and internal cardioverter defibrillator leads can be implanted in the right atrium, right ventricle, superior vena cava, and left ventricular cardiac vein.

Data acquired from the various possible electrode vectors typically contain three major physiologic components that may provide useful information for diagnostics or implantable device control:

- A low-frequency respiratory component (fundamental <1 Hz);
- A higher frequency cardiac component (fundamental = 1–3 Hz);
- A calculated mean impedance (0 Hz).

As shown in [Figure 10.28](#), the higher frequency cardiac component is superimposed on the low-frequency respiratory component. The higher frequency cardiac component represents the impedance change during each cardiac cycle that occurs immediately after the QRS deflection on the electrocardiogram. The low-frequency respiratory component represents the impedance change during respiration because of the expansion of the lungs and thorax. Moreover, each component has a different fundamental frequency, typically 1.0–3.0 Hz for cardiac activity and 0.1–1.0 Hz for respiratory activity (Hettick and Zielinski, 2006). This frequency differentiation allows extraction of each signal by specific filtering techniques. Mean impedance, as represented by a “DC shift” in impedance, changes according to the amount of static conductive fluid in the electrode vector lead field configuration as a function of time (hours/days).

More specifically, change in impedance waveform morphologies may be an indicator of change in blood volume, interstitial volume, or tissue integrity. Deviations in the impedance waveform morphologies such as in the positive or negative slope, time duration

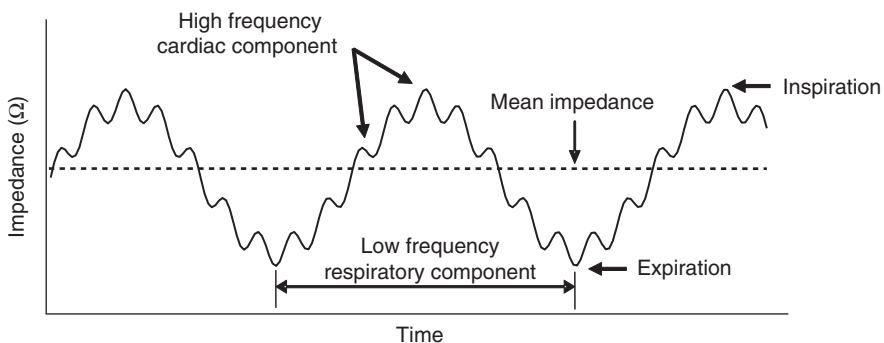


Figure 10.28: Simulated impedance waveform consisting of a higher frequency cardiac component superimposed on a low-frequency respiratory component: The dotted line is the calculated mean impedance (measured during two respiratory cycles). An implantable impedance sensor may be able to leverage all three signal components in order to provide useful diagnostic or device control information.

between minimum and maximum magnitudes, delta between the minimum and maximum magnitudes, changes in the minimum and maximum first derivative, changes in the area under a specific waveform, or other deviations in the waveform morphology of complex impedance may be indicative of a vector specific change in chamber or vessel blood volume, such as in heart disease, tissue degradation, such as in myocardial ischemia, or interstitial fluid accumulation, such as in peripheral or pulmonary edema, all secondary to cardiac, vascular, or renal disease.

10.12.2 Fluid Status Monitoring

Externally measured transthoracic impedance techniques have been shown to reflect alterations in intrathoracic fluid and pulmonary edema in both acute animal and human studies (Fein et al., 1979). The electrical conductivity and the value for transthoracic impedance are determined at any point in time by relative amounts of air and fluid within the thoracic cavity (Gotshall and Davrath, 1999). Additional studies have suggested that transthoracic impedance techniques provide an index of fluid volume in the thorax (Ebert et al., 1986; Pomerantz et al., 1969). Wang et al. (2005) employed a pacing-induced heart failure model to demonstrate that measurement of chronic impedance using an implantable device effectively revealed changes in left ventricular end-diastolic pressure in dogs with pacing-induced cardiomyopathy. Several factors were identified that may influence intrathoracic impedance with an implantable system. These include: (1) fluid accumulation in the lungs from pulmonary vascular congestion, pulmonary interstitial congestion, and pulmonary edema; (2) as heart failure worsens, heart chamber dilation and venous congestion occur and pleural effusion may develop; and (3) after implant, the tissues near the pacemaker pocket swell and surgical trauma can cause fluid build-up (Wang et al., 2005).

Yu et al. (2005) also showed that sudden changes in thoracic impedance predicted eminent hospitalization in 33 patients with severe congestive heart failure (New York Heart Association Class III–IV). During a mean follow-up of 20.7 ± 8.4 months, 10 patients had a total of 25 hospitalizations for worsening heart failure. Measured impedance gradually decreased before admission by an average of $12.3 \pm 5.3\%$ ($p < 0.001$) over a mean duration of 18.3 ± 10.1 days. The decline in impedance also preceded the symptom onset by a mean lead-time of 15.3 ± 10.6 days ($p < 0.001$). During hospitalization, impedance was inversely correlated with pulmonary wedge pressure and volume status with $r = -0.61$ ($p < 0.001$) and $r = -0.70$ ($p < 0.001$), respectively. Automated detection of impedance decreases was 76.9% sensitive in detecting hospitalization for fluid overload with 1.5 false-positive (threshold crossing without hospitalization) detections per patient-year of follow-up. Thus, intrathoracic impedance from the implanted device correlated well with pulmonary wedge pressure and fluid status, and may predict imminent hospitalization with good sensitivity and low false alarm rate in patients with severe heart failure. Figure 10.29(a) shows operation of an algorithm for detecting decreases in impedance over time. Differences between measured impedance (bottom; circles) and reference impedance (solid line) are accumulated over time to produce fluid index (top). Threshold values are applied to fluid index to detect sustained decreases in impedance which may be indicative of acutely worsening thoracic congestion. Figure 10.29(b) shows an example of impedance reduction before heart failure hospitalization (arrow) for fluid overload and impedance increase during intensive diuresis during hospitalization. The label indicates reference baseline (initial reference impedance value when daily impedance value consistently falls below reference impedance line before hospital admission). Magnitude and duration of impedance reduction are also shown. Days in hospital are shaded.

Some commercially available implantable devices for the treatment of congestive heart failure and/or ventricular tachyarrhythmias now continually monitor intrathoracic impedance and display fluid status trends. This information is then provided to the clinician via direct device interrogation or by remote telemetry. Recent reports based on actual clinical experience with this feature have attested to critical reliability and utility (Vollmann et al., 2007) and good correlation with other traditional tools such as brain natriuretic peptide (Luthje et al., 2007).

However, besides lung fluid, other physiologic parameters might explain device-measured changes in intrathoracic impedance. Some of these factors include ventricular dilation, atrial, or pulmonary vascular dilation, anemia, hyper or hypovolemia, right and left ventricular preload, hematocrit, electrolyte balance, pocket infection, kidney dialysis, pneumonia, bronchitis; weight change (not related to fluid accumulation), lymphatic fluid changes, and so on.

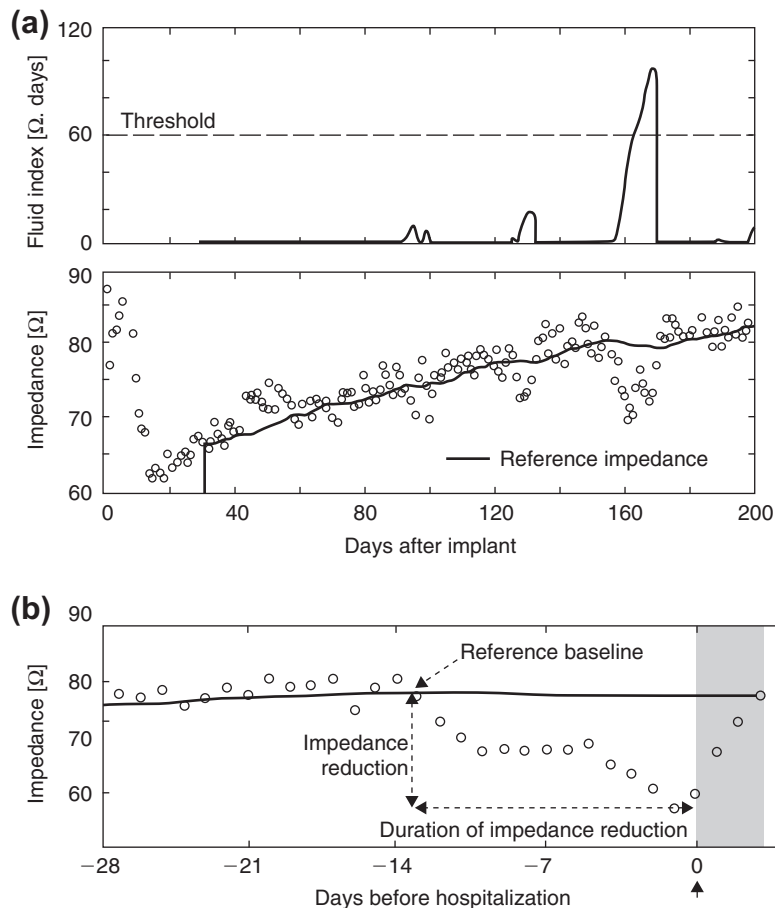


Figure 10.29: (a) Fluid index and impedance over 6 months; (b) example of impedance reduction before heart failure hospitalization (arrow) for fluid overload and impedance increase during intensive diuresis during hospitalization. *Reproduced with permission: Yu et al. (2005).*

10.12.3 Cardiac Pacemakers

Pacing of the heart may be done transcutaneously, but this is accompanied by pain. The usual method is with two epicardial electrodes and leads out through the chest to an external pacemaker, or with an implanted pacemaker.

The implanted pacemakers are of many models. Let us consider a demand pacemaker, with special recording ring electrodes on the catheter for the demand function. If QRS activity is registered, pacing is inhibited. The pacemaker housing may be of metal (titan) and function as a large neutral electrode. Pacing is done with a small catheter tip electrode, either unipolar with the neutral electrode or bipolar with a catheter ring proximal to the tip electrode.

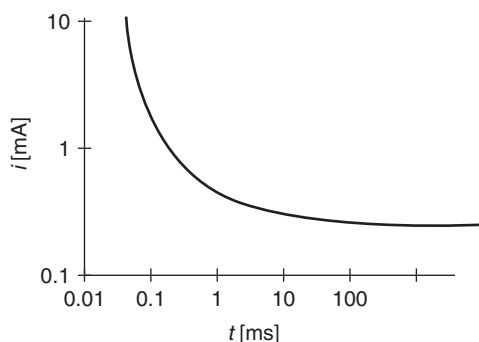


Figure 10.30: Current-time curves for heart pacing with a square wave pulse delivered during diastole with intracardial catheter electrode.

As can be seen from Figure 10.30, the chronaxie is less than about 500 μ s, so there is an energy waste choosing the pulse duration much larger than 100 μ s.

A pacemaker may be externally programmed by magnetic pulses. Also because of this, a pacemaker is to a certain degree vulnerable to external interference. Typical limits are: static magnetic field <1 G, 40 kV arcing >30 cm distance (car ignition system), and radar 9 GHz E-field <1.2 kV/m. Typical pacemaker data are: pulse amplitude 5 mA, impedance monopolar electrode system 1 k Ω , load voltage 5 V, and a lithium battery 6.4 V with capacity of 1800 mAh. The stimulus electrodes are ac coupled in the pacemaker's output stage, so that no DC can pass and unduly polarize the electrodes. The electrodes are made of noble metals to be biocompatible, and consequently they are highly polarizable (Section 7.3.1). The monopolar electrode system impedance is not very dependent on faradaic impedance because the admittance of the double layer capacitance is large at the frequencies used.

Pacemaker implant and the use of electrosurgery are treated in Section 10.10.

10.13 Electrotherapy

Transcutaneous stimulation

Transcutaneous electrical nerve stimulation (TENS) is electrical stimulation through surface electrodes. The advantage of not using syringe injections is obvious; the electrical pulses stimulate the body's own mechanisms for obtaining pain relief. There are three theories as to how the pain relief is achieved:

1. Gating theory

Pain perception is controlled by a gate mechanism in the synapses, particularly in CNS of the spine. This gate is controlled by separate nerve fibers, and by stimulating with

pulses of high frequency (50–200 Hz), these fibers are stimulated and pain relief is obtained.

2. Endorphins

The body uses natural forms of morphine called endorphins for pain relief. The secretion of endorphins is obtained with low frequency (2–4 Hz) stimulation. These low frequencies correspond to the rhythmic movement of an *acupuncture* needle (in classical acupuncture it is necessary also to stimulate motor nerve fibers). The effect of endorphins is probably in the higher centers of the CNS.

3. Vasodilatation

This effect is usually linked to pain in cold extremities. Increased blood flow may increase the temperature from the range 22–24 °C to 31–34 °C, also in extremities not stimulated. The effect must therefore be elicited in higher centers of the CNS.

The afferent pain nerves have a higher threshold and rheobase than sensory and motor nerves. Thus it is possible to stimulate sensory and motor nerves without eliciting pain. Very short pulses of 10–400 µs duration are used, with constant amplitude current up to about 50 mA and treatment duration of 15 min or more. The skin electrodes may be bipolar or monopolar. The position is in the pain region; an electrode pair may, for example, be positioned on the skin on the back of the patient, or implanted with thin leads out through the skin. The electrode pair may also be positioned outside the pain area (e.g., at regions of high afferent nerve fiber densities in the hand).

Electroacupuncture

The secretion of endorphins is obtained with low frequency (2–4 Hz) stimulation, corresponding to the rhythmic movement of an *acupuncture* needle. Instead of, or in addition to the mechanical movement, the needle is used as monopolar electrode, pulsed by a low frequency in the same frequency range (1–4 Hz). This is not a TENS method strictly speaking, because the electrode is invasive and the current not transcutaneous.

10.13.1 Electrotherapy with DC

Applied DC through tissue for *long* duration (e.g., >10 s), is a method almost 200 years old, and is traditionally called *galvanization*. Today the DC effect is often ignored, even if it is quite clear that DC through tissue has some very special effects. Generally the physical/chemical effect of a DC through tissue is:

- electrolysis (local depletion or accumulation of ions)
- electrophoresis (e.g., protein and cell migration)
- iontophoresis (ion migration)

- electro-osmosis (volume transport)
- temperature rise.

Some of these effects are special for long duration (>10 s) DC or very low-frequency AC; in particular, electrolysis. Other effects are in common with AC.

Short-term effects of DC through the skin is limited to the sweat ducts. The current density is much smaller in the stratum corneum, but long-term currents may have an effect. Proximal to the electrode electrolytic effects influences the skin. Possible effects in deeper layers are erythema (skin reddening) and hyperemia (increased blood perfusion) from the stimulation of vasomotor nerves. If DC is applied transcutaneously, there is always a chance of unpleasant pricking, reddening, and wound formation in the skin under the electrode.

Iontophoresis

See also [Section 10.4.3](#) for iontophoresis in the skin. If a drug is in ionic form, the migration velocity and direction are determined by the polarity of the DC. It was a very famous experiment whereby strychnine was applied to one of the electrodes attached to a rabbit (Munk, 1873). With one polarity the rabbit died, with the reverse polarity nothing happened. The ions may be transported from the electrode, and thus have an effect both in the tissue during passage, and when assembled under the other electrode. Anesthetic agents may be introduced in the skin by iontophoresis for minor surgery or the treatment of chronic pain. Also antibiotics and metallic silver has been introduced iontoporetically, as has zinc for ischemic ulcers. The mechanism of iontophoresis is of course accompanied by a possible electrophoretic action (see the following section), but is not necessarily so pH-dependent as the latter. The advantage of iontoporetic instead of local syringe injection is not always obvious.

Electrotonus

Tonus is the natural and continuous slight contraction of a muscle. Electrotonus is the altered electrical state of nerve or muscle cells from the passage of a DC. Subthreshold DC currents through nerves and muscles may do the tissue more (excitatory effect) or less (inhibitory effect) excitable. Making the outer nerve cell membrane less positive lowers the threshold and has an excitatory effect (at the cathode, *catelectrotonus*), the anode will have a certain inhibitory effect (*anelectrotonus*). This is used in muscle therapy with diodynamic currents (see the following section).

Wound Healing

Many controlled studies have shown that a small microampere current as a long-term treatment leads to accelerated healing. There are two classes of cases: accelerated

healing of bone fractures and of skin surface wounds. Ischemic dermal ulcers are treated with DC, and the healing rate is approximately doubled. It has been found that a monopolar cathodic application the first days followed by an anodic application gives the best results. In a skin wound, it is believed that positive charge carriers (ions and proteins) are transported to the liquid wound zone by endogenic migration.

An increased rate of bone formation has also been found when small currents are applied to each side of a bone fracture (bipolar electrode system). This is of particular interest in cases of bone fractures that will not grow the natural way: so called *nonunion*.

Nordenström (1983) described the use of DC treatment by applied needles into tumors for the treatment of cancer.

DC Ablation

At higher current densities, the acid under the anode leads to coagulation, and the alkali under the cathode to liquidification of the tissue. Warts can thus be treated, and with a needle cathode in the hair follicle, the local epidermis is destroyed and the hair removed.

DC Shock Pulses

DC shock pulses have also been used for destroying calculi in the urinary tract, *electrolithotripsy*.

Hydrogen Production

The application of a DC current to the inside of the eyeball by a needle electrode is used to produce bubbles of hydrogen in the aqueous humor, *electroparacentesis*.

10.13.2 Electrotherapy of Muscles

Electrotherapy is a broad term, and should for instance include pacing, defibrillation, and electroconvulsion. Here we will keep to the traditional meaning, however, which is more limited to methods stimulating *muscles*, either directly or via the nerves. Usually such stimulation also brings data of diagnostic value.

Figure 10.31 shows the minimum stimulus current to an efferent nerve fiber as a function of pulse duration for obtaining a certain muscle response. The coupling (synapses) between the nerve axon end plates and the muscle cells is an important part of this signal transmission line. It is not possible to lower the current under a certain minimum level, the *rheobase* value. The pulse length with current amplitude two x rheobase value is called the *chronaxie*.

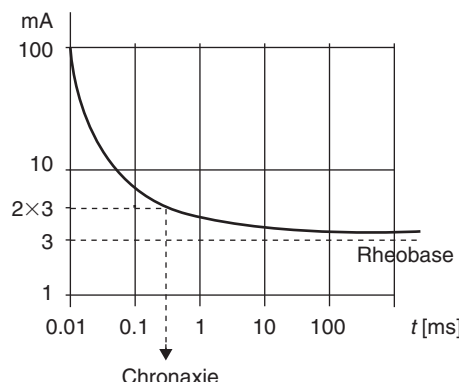


Figure 10.31: Minimum stimulus current to an efferent nerve fiber bundle for obtaining a certain muscle response, as a function of pulse duration.

Pflüger's law relates the muscle effect to the leading or trailing edge of the pulse, and to anodal or cathodal polarity:

leading edge cathodal	strongest effect
leading edge anodal	
trailing edge anodal	
trailing edge cathodal	weakest effect

If a linear triangular current pulse is used instead of a square wave pulse, an *accommodation* effect will appear, particularly at pulse duration >1 ms. A slowly increasing DC does not excite a nerve to the same extent as a DC step change, and the accommodation implies that the threshold current amplitude will be larger with triangular than with squared waveform. The current–time curves can be recorded for diagnostic purposes; the curves are quite different for degenerated muscles.

The pulses may be of unidirectional current (interrupted DC, *monophasic*), which implies that the current has a DC component. High-voltage pulsed galvanic stimulation is also used, with pulse currents up to some amperes, but pulse duration only a few microseconds. If DC effects are to be avoided (e.g., to reduce electrolytic effects or electrode metal corrosion), the current is *biphasic*. *Faradic* currents are biphasic currents of the type generated by an induction coil. If the pulses are slowly increased in amplitude, then reduced, and after a pause again increased, we have a *ramp* or *surged* current. Because many effects are current controlled, it is often better to use a constant amplitude current mode than a constant amplitude voltage mode of the stimulator output.

Pulse Waveform Treatment of Innervated Muscles (Faradization)

Short (0.5–5 ms) triangular pulses for tetanic muscular contractions, interrupted or with varying amplitude. Interval between pulses 10–25 ms. For muscle pain relief, rectangular pulses of length 2 ms and interval 7 ms are used. TENS for pain relief is different. It is based on stimulating afferent nerve fibers with much shorter pulses (e.g., 0.2 ms).

Pulse Waveform Treatment of Denervated Muscles

Because there are no innervations, the stimulation is directly to the muscle. The paralyzed part of the muscle mass can be stimulated selectively because such muscles have a smaller accommodation at long pulse duration. Very long (1 s) triangular waveforms are used, with even longer intervals between the pulses.

Diodynamic Currents for the Treatment of Pain and Increase of Blood Perfusion

This is the summation of two currents: a pulse current superimposed on a DC. Each current is separately adjusted. Often the DC level is first increased slowly so that no perception occurs (*electrotonus*), and then with a constant DC flowing the pulse amplitude is increased until a weak vibration is felt. The pulse waveform may be a power line 50 Hz half-rectified (50 Hz) or fully rectified (100 Hz) current.

Interferential Currents

Two electrode pairs are used to set up two different current paths crossing each other in the target tissue volume. Each pair is supplied by a separate oscillator, adjusted to, for example, 5000 and 5100 Hz. The idea is that the target volume is treated with the frequency difference, 100 Hz. The advantage is the possible selective choice of a limited treated volume deep in the tissue, together with lower electrode polarization and skin impedance, plus less sensation in the skin and the tissue outside the treated volume.

If the current level is low enough for linear conditions, the resultant current density in the tissue is the linear summation of the two current densities (see Chapter 8.2.2). According to the superposition theorem in network theory and Fourier analysis, the new waveform $f(t)$ does not contain any new frequencies. The linear summation of two currents at two different frequencies remains a current with a frequency spectrum with just the two frequencies; no current at any new frequency is created.

The current density in the treated volume must be high enough to create nonlinear effects. The process can then be described mathematically by a multiplication (see Chapter 8.2.2). If $\omega_1 \approx \omega_2 \approx \omega$, $f(t)$ is a signal of double frequency and half the amplitude, together with a signal of the low beat frequency $\omega_1 - \omega_2$, also of half the amplitude. The double frequency signal is not of interest, but the low beat frequency $\omega_1 - \omega_2$ is now present in the tissue.

A third electrode pair can be added, with additional flexibility of frequency and amplitude selection. In any case, it must be taken into account that muscle impedance may be strongly anisotropic, with a possible 1:10 ratio between two directions.

10.14 Nonmedical Applications

- Fingerprint detection as described in [Section 10.4.4](#) is a measurement on humans, but not for a medical purpose.
- The monitoring of fermentation processes in beer brewing or pharmaceutical industry is measuring on different sort of cell suspensions.
- Plant tissue is both strongly similar and very different from animal tissue; the cell membranes for instance are quite different.
- Meat quality can be estimated from bioimpedance measurements; see e.g., Oliver et al. (2001) and Guerro et al. (2004).
- In geophysics, impedance measurements were used as early as in the 1920s for oil exploration (Schlumberger, 1920). Impedance measurements are also used for monitoring volcanic activity, for example, on Iceland.

10.15 Discoveries, Innovations

A discovery leading to a new electrical method for medical use is one thing, the start-up of industrial production and marketing of suitable equipment is another. As we already have seen in this chapter, discoveries have often appeared without being followed by any industrial production. Scientific experimentation with electricity applied to animals and humans was going on since the first practical sources of electricity were invented. By 1740, the electrostatic machine was in widespread use all over Europe, partly from influence of the French court. The lightning in nature was explained as dangerous large electric discharges, and the invention of lightning rods reduced risk for animals, people, and buildings. Other sources of electricity became available, and electricity started to be used in treatment of patients. Medical doctors were appointed at University clinics (e.g., at Rikshospitalet in Oslo the first medical *electriseur* appeared in 1863). The electrical treatments were not very efficient and not very successful. The first use of electricity for medical use that spread all over the world in just a few years after the discovery (1895) was made of the mystical X-rays. X-ray tubes and high-voltage, high-power generators were needed. That led to expensive instrumentation, and industrialization.

Innovation (from Latin *innovare* and *novus*, new) means “bringing something new, making something new.” In contrast to research, which in short can be described as a systematic and open development of new knowledge. Innovation is more about development of new

products and services that someone is willing to pay for. The concept of innovation is therefore something more commercial, even if innovation also can appear in connections that we do not consider commercial. Patenting may be an important requirement for innovation.

Innovation is the process of bringing an idea all the way from sketches and simple prototypes to a marketed product. It may comprise:

- Discovery of a new way of doing a medical procedure by means of a new device, for example, EIT.
- Building of research prototypes by different university centers. Perhaps supported by European Union—concerted actions.
- Testing research prototypes technically and in clinics; make improvements.
- Specialize and find the most promising medical application (e.g., lung imaging at bedside).
- Analyze the market; what is the need? Analyze competition and patenting.
- Set up a small-scale industrial prototype production line.
- Set up clinical trials to obtain public approvals by national bodies.
- Optimize efficiency; determine prices.
- Market the product.

The time from discovery to industrial production may be long, very long, and difficult. The list does not represent a strict time series; many of the activities are run in parallel. The process would often take between five and 10 years.

Bioimpedance represents a general transducing mechanism for many physiological events, and the instrumentation is low cost. Sometimes the situation may have the aspect of a technology seeking a problem, but this must be reverted by taking the other approach: go to the clinics and start with their problems and needs and see whether bioimpedance technology has any solution. Many of the transducing mechanisms can indeed offer solutions, but they must compete with the other solutions already in clinical use.

Ultrasound imaging instrumentation for example can measure many of the parameters that bioimpedance also can measure. When a medical doctor already has the ultrasound probe in his or her hand as a multiparameter measuring device, the bioimpedance technology must offer some definite advantages. The task is to select the application which is sufficiently adequate for the purpose.

Another job is to standardize methods used by different models and companies. A problem related to standardization arises when different models use nonscientific methods being based upon nonpublished algorithms. Another problem is that it is difficult to describe the clinical applications in detail because the more important they are the more patent rights and commercial interests complicate the picture.

10.16 Electrical Safety

10.16.1 Threshold of Perception

The perception of a current through human skin is dependent on frequency, current density, effective electrode area, and skin site/condition. Current duration also is a factor, in the case of DC determining the quantity of electricity and thereby the electrolytic effects according to Faraday's law (see Section 7.8).

DC

If a DC source coupled to two skin surface electrodes is suddenly switched on, a transient sensation may be felt in the skin. The same thing happens when the DC current is switched off. This proves that many nerve endings are only sensitive to *changes* in a stimulus and not to a *static* stimulus. At the moment a DC is switched on, it is not only a DC, it also contains an AC component. DC must therefore be applied with a slow increase from zero up to the desired level, if the threshold of DC perception is to be examined.

DC causes ion migration (iontophoresis) and cell/charged particle migration (electrophoresis). These charge carriers are depleted or accumulated at the electrodes, or when passing ion-selective membranes in the tissue. In particular, almost every organ in the body is encapsulated in a *macro-membrane* of epithelia tissue. There are, for example, three membranes (meninges) around the brain and central nervous system (pia mater, arachnoidea, dura mater). There are membranes around the abdomen (peritoneum), fetus, heart (pericardium), lungs (pleura), inside the blood vessel (endothelium), and around the nerves (myelin, neurolemma in the hand). At some tissue interfaces and at the electrodes, the chemical composition will gradually change.

A sensation will start either under one of the electrodes (anode or cathode), or in the tissue between. The chemical reaction at an electrode is dependent on the electrode material and electrolyte, but also on the current level (see Section 7.7). A sensation around threshold current level is slowly developing and may be difficult to discern from other sensations (e.g., the mechanical pressure or the cooling effect of the electrode). After the sensation is clear and the current is slowly reduced to avoid ac excitation, the sensation remains for some time. That proves that the current does not trigger nerve ends directly, but that the sensation is of a chemical, electrolytic nature as described by the law of Faraday. The after-current sensation period is dependent on the perfusion of the organ eliciting the sensation.

On palmar skin, with a surface electrode of varying area A, the current I_{th} or current density J_{th} at the threshold of perception follows the following equation for a sensation within 3 min after current onset (Martinsen et al., 2004)

$$J_{th} = J_0 A^{-0.83} \quad \text{or} \quad I_{th} = I_0 A^{0.17} \quad (10.16)$$

The perception was only localized under the monopolar electrode, never in the tissue distal to the electrode. Surprisingly, according to Eq. 10.16, the threshold as a function of electrode area A is more dependent on *current* than current density. There may be more than one reason for this:

1. A spatial summation effect in the nervous system. The current *density* is reduced when the same current is spread by a larger electrode, but at the same time a larger number of nerve endings are excited. Consequently, the current threshold is not so much altered when electrode area is changed
2. The DC current is not evenly distributed under a plate electrode (Section 6.2.4), the current density is higher at the edge. The conductance of a surface sphere or plate electrode is proportional to radius or circumference, not to area (Eqns 6.1 and 6.9).
3. The DC current is probably concentrated to the sweat ducts and the nerve endings there (Grimnes, 1984).

A practical use of DC perception is the old test of the condition of a battery by placing the poles at the tongue. This test is actually also done clinically: *electrogustometry* is the testing of the sense of taste by applying a DC to the tongue.

Sine Waves

The lowest level ($<1 \mu\text{A}$) of 50/60 Hz perception is caused by *electrovibration*, Grimnes (1983d), Figure 10.32. It is perceived when the current carrying conductor slides on dry skin. Dry skin is a poor conductor, so that potential differences of several tenths of volts may exist across the dielectric which is the stratum corneum of the epidermis. With dry skin, only a small microampere current flows. The electric field sets up an electrostatic compression force in the dielectric, pressing the stratum corneum to the metal plate. In the stratum corneum, there are no nerve endings and consequently no perception. However, if the skin is made to slide along the metal, the frictional force will be modulated by the electrostatic force and be felt as a lateral mechanical vibration synchronous with the double frequency of the AC voltage. Even if the voltage across the dielectric is $>20 \text{ V}$ at

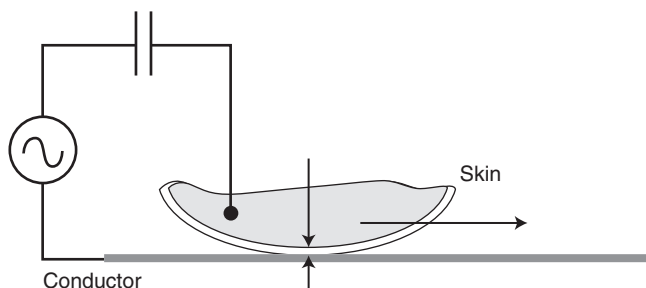


Figure 10.32: Electrovibration perception mechanism.

threshold, the corresponding (mainly capacitive) current may be $<1\text{ }\mu\text{A}$. If the skin is at rest, or if the skin is wet, no sensation is felt.

The second level (1 mA) is due to the *direct electric excitation* of nerve endings, which must be a function of the local current (density). The electric current threshold of perception with firm hand grip contact and contact area several square centimeters, is around 1 mA. Threshold current has a surprisingly small dependence on contact area. The reason for this is mentioned previously in the chapter on DC perception. With a small area contact around 1 mm^2 , the threshold of perception is around 0.1 mA, corresponding to 100 A/m^2 .

Interpersonal variations and the dependence on age and sex are small. Skin condition is not important as long as there are no wounds. Skin site may be important. On the fingertips the density of nerve ending is large, but the stratum corneum is thick and the current will be rather uniformly distributed. Other skin sites may have much thinner skin and lower density of nerve endings, but conductive sweat ducts that canalize the current.

Frequency Dependence

For sine waves, the maximum sensitivity of our nervous system is roughly in the range 10–1000 Hz, (see also Figure 10.20). At lower frequencies, each cycle begin to be discernible, and during each cycle it may be charge enough to give electrolytic effects. At frequencies $>1000\text{ Hz}$, the sensitivity is strongly reduced, and at $>100\text{ kHz}$ no perception remains, because the levels are so high that electric stimulation are shadowed by the heat effect of the current. That is the frequency range for electrosurgery.

A single pulse or a repetitive square wave may give both DC and AC effects. In both cases, the duration of the pulse or square wave is an important variable (see rheobase and chronaxie).

The exponential decaying discharge waveform is the case of electrostatic discharges; see the following section.

Electrostatic Discharge Pulse

The perception of an electrostatic discharge is an annoyance, and in some situations a hazard. It is particularly troublesome in-door during the winter with low relative humidity. Low relative humidity reduces the conductivity of most dielectrics (e.g., the stratum corneum; see Section 4.2.6), and also the conductivity of clothing, construction materials, tree, or concrete. A person may be charged up to more than 30 kV under such circumstances, and with a body capacitance to the room (ground) of about 300 pF, the electrical energy of the person is of the order of 0.1 J. A smaller discharge, near the threshold of perception, is typically within a time constant of a few μs , and the peak current around 100 mA, Figure 10.33. It is obtained by discharging a capacitor of 100 pF

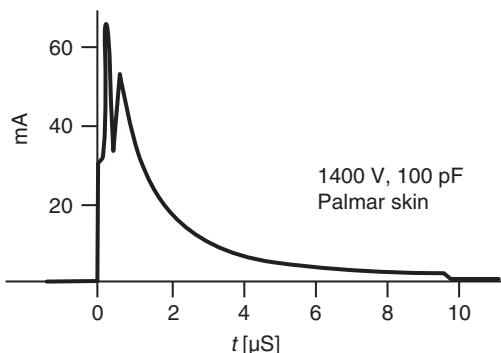


Figure 10.33: Capacitor discharge current flow through palmar skin. Monopolar electrode: 1.3 mm diameter pin of steel, sharpened at the tip. Indifferent electrode on the underarm.

charged to 1.4 kV. The point electrode is approached to the skin until an arc is formed, heard, and perceived in the skin.

The maximum current is determined by the voltage drop in the arc (probable less than 100 V) and the resistance in the skin. The arc probably has a very small cross-sectional area, so most of the resistance is in the proximal zone in the stratum corneum. The current density is probably far out in the nonlinear breakdown region of the skin, but because of the short pulse duration the impedance is presumably also determined by the capacitive properties of stratum corneum. A rough calculation based on Eq. 6.1 with $\sigma = 0.1 \text{ S/m}$ and calculated resistance from measured current maximum: $20 \text{ k}\Omega$, gives the arc contact diameter with the skin: $2a = 200 \mu\text{m}$.

The charge transferred around threshold level is of the order of 0.2 C. The threshold of perception as a function of stored energy is about $10 \mu\text{J}$. The formation of an arc in the air between the conductor and the skin is possible when the voltage difference is larger than about 400 V. The arc discharge can be heard as a click and felt as a prick in the skin.

10.16.2 Electrophysiological Hazards

Electromagnetic Field Effects

Coupling without galvanic tissue contact is covered in Section 7.4.2. However, electromagnetic hazards are outside the scope of this book. There is a vast amount of experimental data on this subject, and the interested reader is recommended the CRC *Handbook of Biological Effects of Electromagnetic Fields* (Barnes and Greenbaum, 2006).

Continuous Current

The risk of sudden death is related to stimulating the cells of three vital organs of the body: the heart, the lungs, and the brain stem. Involuntary movements may indirectly lead

to sudden deaths (loss of balance, falling). Heat and electrochemical effects may also be fatal by inducing injuries that develop during hours and days after the injury. In electrical injuries, the question often arises as to whether the current is evenly distributed in the tissue or follows certain high-conductance paths. Current marks and tissue destruction often reveal an uneven current distribution; see Ugland (1967).

The current path is important, and organs without current flow are only indirectly affected: to be directly dangerous for the healthy heart, the current must pass the heart region.

Cell, nerve, and muscle excitation

Heat effects are certainly related to current density in volume conductors, but this is not necessarily so for nerve and muscle excitation. Excitation under a plate electrode on the skin is more highly correlated to current than current density (see [Section 10.16.1](#)). The stimulus summation in the nerve system may reduce the current density dependence if the same current is spread out over a larger volume of the same organ. Therefore, and for practical reasons, safe and hazard levels are more often quoted as current, energy or quantity of current in the external circuit, and not current density in the tissue concerned.

Macroshock/Microshock

A *macroshock* situation is when current is applied to tissue far from the organ of interest, usually the heart. The current is then spread out more or less uniformly, and rather large currents are needed in the external circuit (usually quoted $>50\text{ mA}$ at $50/60\text{ Hz}$) to attain dangerous levels, [Figure 10.34](#).

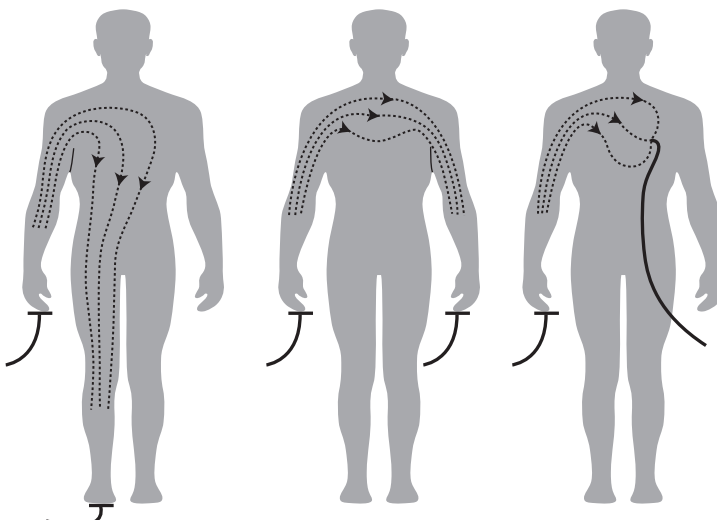


Figure 10.34: Macroshock (left) and microshock (right) situations.

The heart and the brain stem are particularly sensitive for small areas of high current density. Small area contacts occur, for example, with pacemaker electrodes, catheter electrodes, and current-carrying fluid-filled cardiac catheters. Small area contact implies a monopolar system with possible high local current densities at *low current levels* in the external circuit. This is called a *microshock* situation. The internationally accepted 50/60 Hz safety current limit for an applied part to the heart is therefore 10 µA in normal mode, and 50 µA under single fault condition (e.g., if the patient by insulation defects is in contact with mains voltage). The difference between macro- and microshock safety current levels is therefore more than three decades.

The heart is most vulnerable for an electric shock in the repolarization interval; that is, in the T-wave of the ECG waveform. Therefore the probability of current passage during the approximately 100 ms duration of the T-wave is important. If the current lasts more than one heart cycle, the T-wave is certainly touched. For short current durations <1 s, the risk of heart stop is determined by the chance of coincidence with the T-wave.

Let-go Current

Let-go current threshold (15 mA at 50/60 Hz) is the current level when the current density in muscles and nerves is so large that the external current controls the muscles. Just as the grip muscles are stronger than the opening muscles of the hand, a grip around the current carrying conductor cannot be loosened by the person himself. Let-go current levels are therefore the most important data for safety analysis. The result on [Figure 10.20](#) shows that 1% of the population has a let-go threshold as low as 9 mA at power line frequencies.

Fatal levels are reached at current levels >50 mA at 50/60 Hz if the current path is through vital organs: heart, lung, or brain stem (see the electric chair, [Section 10.16.3](#)).

Heat Effects

Jouleian heat is dependent on the in-phase components of potential difference and current density. The resulting temperature rise is dependent on the power density, the specific heat of the tissue, and the cooling effect of the blood perfusion (see Eq. 6.8).

The tissue damage is very dependent on exposure time; cells can tolerate long time exposure of 43 °C. Above about 45 °C, the time duration becomes more and more critical. In high-voltage accidents, the heat effect may be very important, and patients are treated as thermal burn patients. In particular, special attention is paid to the fluid balance, because electrical burn patients tend to go into renal failure more readily than thermal burns of equal severity. As electric current disposes thermal energy directly into the tissue, the electric burn is often deeper than a thermal burn caused by thermal energy penetrating

from the surface. The general experience is therefore that an electrical burn is more severe than it may look like the first hours after the injury.

Electrolytic Effects

Electrolytic effects are related to DC, applied or rectified by nonlinear effects at the electrodes or in the tissue. Also with very low-frequency AC (e.g., <10 Hz), each half period may last so long as to cause considerable nonreversible electrolytic effects. With large quantities of electricity ($Q = It$) passed, the *electrolytic* effects may be systemic and dangerous (lightning and high-voltage accidents). The risk of skin chemical burns is greater under the cathode (alkali formation) than the anode (acid formation), the natural skin pH is on the acidic side ($pH < 5.5$).

Nerve damage is often reported in high-voltage accidents.

Current Limiting Body Resistance

The most important current limiting resistance of the human body is the dry skin. This may be impaired by high-field electrical breakdown, skin moisturizing, or a skin wound. Skin breakdown may occur at less than 10 V AC 50/60 Hz from electro-osmotic breakdown (Grimnes, 1983b).

Without the protective action of the skin, the *internal body resistance* may be divided into a *constrictional zone resistance* with increased current density near an electrode, and *segmental resistances* of each body segment with rather uniform current density. With small area electrode contact, the constrictional zone resistance will dominate (see Section 6.2.2). The segmental resistance may be estimated from the equation $R_{sr} = L/\sigma A$. With constant σ , the segmental resistance depends on the ratio L/A , and accordingly varies according to body or limb size.

Table of Threshold Values

From the threshold current levels, the corresponding voltages are found by estimating the minimum current limiting resistance. These worst case minima are found by assuming no protective action from the skin at all, only from the volume resistance of the living parts of the body. The levels are summarized in [Table 10.2](#).

The question of current canalizing effects in tissue is one of the issues of our field. It is well known that the myelin sheet around the nerves serves electrical insulation and current canalization to the Ranvier nodes. But the extent of current canalization in many parts of the body is largely unknown. The blood has a high conductivity, but what are the electrical properties of the endothelium? Does electrosurgery current follow the bile duct? The current through skin is canalized through the sweat ducts. The high acid concentration in the stomach must have high electrical conductivity.

Table 10.2: 50/60 Hz Threshold Levels of Perception and Hazard

Current Threshold	Voltage Threshold Very Approximate	Organs Affected	Type	Comments
0.3 µA	20 V	Skin	Perception threshold	Electrovibration, mechanical
10 µA	20 mV	Heart	Microshock hazard	Myocard excitation
1 mA	10 V	Skin	Perception threshold	Nerve excitation
15 mA	50 V	Muscles	Let-go	Loss of muscle control
50 mA	250 V	Heart, lung, brain stem	Macroshock hazard	Nerve excitation

Single Pulses

Trigger and safety levels have been examined by Zoll et al. (1964) for external pacing of the heart. For TENS, single monophasic pulses of duration <1 ms FDA have set up the following values for the electric charge through the thorax (Table 10.3).

10.16.3 Lightning and Electrocution

Lightning

An average lightning stroke may have a rise time of 3 µs and duration of 30 µs, energy dissipated 10^5 J per meter, length 3 km, peak current 50,000 A, power 10^{13} W. After the main stroke there are continuing currents of typically 100 A and 200 ms duration.

The mechanical hazards are due to the pressure rise in the lightning channel. The energy per meter is equivalent to about 22 g of TNT per meter. A direct hit from the main stroke

Table 10.3: Electric Charge Values
(microcoulomb) for Single Monophasic Pulses
through the Chest

	µC
TENS threshold	3
TENS, max	7
Safe level	20
Hazard threshold	75
Heart pacing	100

is usually lethal, but often the current path is via a tree, the ground (current path from foot to foot, current through tissue determined by the *step voltage*), or from a part of the house or building. The current path is of vital importance; for humans, a current from foot to foot does not pass vital organs, for a cow it may.

It is believed that there are around 500 deaths caused by lightning per year in the United States.

Electrocution

The current path in an electric chair is from a scalp electrode to a calf electrode. The current is therefore passing the brain and the brain stem, the lung, and the heart. It is believed that the person gets unconscious immediately after current onset, but it is well known that death is not immediate. The electric chair was used for the first time in 1890, and the first jolt was with 1400 V 60 Hz applied for 17 s, which proved insufficient. At present a voltage of about 2000 V applied for 30 s is common, followed by a lower voltage for about a minute. The initial 60 Hz AC current is about 5 A, and the total circuit resistance is therefore around $400\ \Omega$. The power is around 10 kW and the temperature rise in the body, particularly in the regions of highest current densities in the head, neck, and leg region, must be substantial. Because of the cranium, the current distribution in the head may be very nonuniform. Temperature rise is proportional to time and the *square* of current density according to Eq 6.8, so there are probably local high temperature zones in the head.

The scalp electrode is a concave metal device with a diameter about 7 cm and an area of about 30 cm^2 . A sponge soaked with saline is used as contact medium.

10.16.4 Electric Fence

The electric fence is used to control animals and livestock. There are two types of controllers: One type delivers a continuous controlled AC current of about 5 mA. The other delivers a capacitive discharge, like the working principle of a defibrillator. The repetitive frequency is around 1 Hz, and the capacitor is charged to a DC voltage up to 10 kV. The large voltage secures that the shock will pass the animal's hair-covered skin. The shock is similar to an electrostatic discharge, even if the electric fence shock energy is higher and the duration longer. The capacitor is charged to energy typically in the range 0.25–10 J.

10.16.5 Electroschok Weapon (Taser)

The Taser X26 is the handgun-shaped electroschok weapon most widely sold in the United States. Two dart electrodes are driven by compressed nitrogen and connected to the gun by wires. One of the electrodes is coupled to a laser aiming device. The other electrode is

sent out at an angle of 8° , so that the distance between the electrodes increases with the distance to the victim. The electroshock is meant to elicit neuromuscular inhibition so that the person falls paralyzed to the ground in pain, harmless for the police long enough to gain control.

The dart electrodes have a length of 9–14 mm. The shock is given by a constant current generator with a voltage limitation of 50 kV. This is sufficient to form an arc if the dart tip does not reach the skin. The output is pulsed with pulse duration about 0.1 ms, delivered pulse charge 0.1 mC, current 1 A, and repetition frequency 19 Hz for duration 5 s.

The Taser X26 is sold as a nonlethal weapon. The shock should therefore be delivered to electrode sites so that the heart is not directly included in the current path but perhaps so that maximum muscle mass or motor nerve tissue is included. On the other hand, the two electrodes can both hit near the heart so that heart pumping action is impaired and blood pressure falls so that the person loses consciousness and may go into ventricular fibrillation and die. Zipes (2014) claims that the Taser X26 can cause cardiac arrest in humans.

10.16.6 Electrical Safety of Electromedical Equipment

Special safety precautions are taken for electromedical equipment. Both patient and operator safety is considered (as well as damage of property). *Electromedical equipment* is equipment situated in the patient environment and is in physical contact with the patient, or which can deliver energy (electrical, mechanical, or radiation) to the patient from a distance. Equipment for in vitro diagnosis is also important for patient safety with respect to correct diagnostic answers, but as long as it is not in the patient environment, the safety aspects are different.

The basis for the national or international standards (IEC, UL, VDE, MDD [the European Medical Device Directive]) is to reduce the risk of hazardous currents reaching the patient under normal conditions. Even under a *single fault condition*, patient safety shall be secured.

The part of the equipment in physical contact with the patient is called the *applied part*. It may ground the patient (type B applied part) or keep the patient floating with respect to ground (BF—body floating, or CF—cardiac floating) by *galvanic separation* circuitry (magnetic or optical coupling, battery-operated equipment). In most situations, higher safety is obtained by keeping the patient floating. If the patient by accident comes in contact with a live conductor the whole patient will be live, but *little current* will flow.

Figure 10.35 shows the most important parts of an electromedical device. The power line and earth connection are shown to the right. The signal connections to the outside world

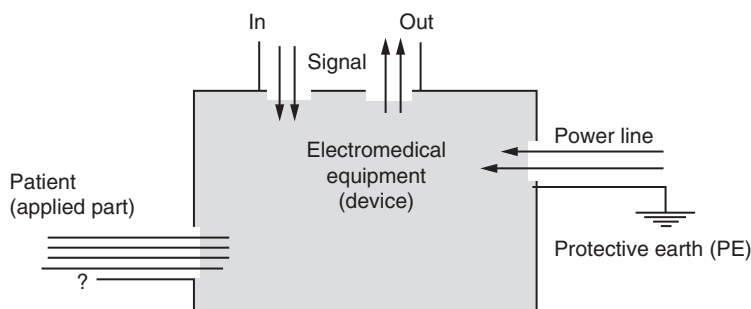


Figure 10.35: Basic parts of a grounded (class I) electromedical device.

are shown at the upper part. Important safety aspects are linked with these signal input and output parts: they may be connected to recorders, printers, data loggers, data networks, coaxial video cables, synchronization devices, and so on. These devices may be remotely situated and outside the electrical control of the patient room. With a floating applied part, hazardous currents from the outside do not reach the patient, the galvanic separation protects both ways.

The device may be grounded for safety reasons (safety class I, as shown in [Figure 10.35](#), maximum resistance in the *protective earth* conductor between power plug and chassis $0.2\ \Omega$), or double insulated (safety class II).

Leakage currents are currents at power line frequency (50 or 60 Hz), they may be due to capacitive currents even with perfect insulation, and are thus difficult to avoid completely.

Patient leakage currents are the leakage currents flowing to the patient via the applied part. *Patient auxiliary currents* are the functional currents flowing *between* leads of the applied part (e.g., for bioimpedance measurement). They are not leakage currents and therefore usually not at power line frequency. *Earth leakage current* is the current through the ground wire in the power line cord (not applicable for double insulated devices).

According to IEC, it shall be $<500\ \mu\text{A}$ during normal conditions for all types B, BF, or CF, [Table 10.4](#). *Enclosure leakage current* is a possible current from a conductive accessible part of the device to earth. Grounded small devices have zero enclosure current during normal conditions, but if the ground wire is broken the enclosure leakage current is equal to the earth leakage current found under normal conditions.

The current limits according to IEC-60601-1 (2005) are shown in [Table 10.4](#).

The insulation level is also specified. It is defined in kV, creepage distances, and air clearances in millimeters. Important additional specifications are related to maximum exposed surface temperature, protection against water penetration (drop/splash proof), cleaning-disinfection-sterilization procedures, technical and user documentation ([Figure 10.35](#)).

Table 10.4: Allowable Values of Continuous Leakage and Patient Auxiliary Currents (μA) According to IEC-60601

	Type B		Type BF		Type CF		
Currents	N.C.	Single Fault	N.C.	Single Fault	N.C.	Single Fault	
Earth leakage	500	1000	500	1000	500	1000	Higher values (e.g., for stationary equipment)
Patient leakage	100	500	100	500	10	50	
Patient leakage				5000		50	Mains on applied part
Patient leakage		5000					Mains on signal part
Patient auxiliary	100	500	100	500	10	50	AC
Patient auxiliary	10	50	10	50	10	50	DC

N.C. = normal conditions.

A nonmedical device such as a PC may be situated within a patient environment (instrument B in [Figure 10.36](#)), but in itself it must not have an applied part. An electromedical device (instrument A) must be inserted between the B and the patient. The connection between A and B is via the signal input/output of device A. If the instrument B has higher earth leakage current than 500 μA , an insulation power line transformer or extra ground must be provided. The reason for this is that a person can transfer the enclosure leakage current by touching the enclosure of B and the patient simultaneously. During the single-fault condition of a broken ground wire to B, the earth leakage current of B may then be transferred to the patient. This would not happen with the interconnected signal ground wires as shown in [Figure 10.36](#), but could happen if A and B were in the same rack with one common power cord.

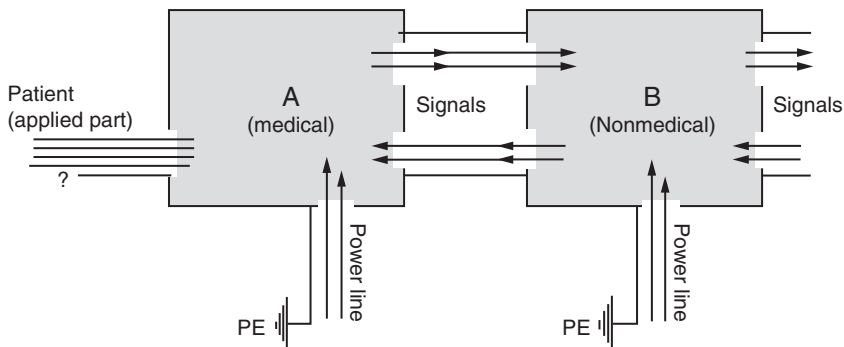


Figure 10.36: A nonelectromedical device (B) within the patient environment. According to IEC-60601-1 (2005).

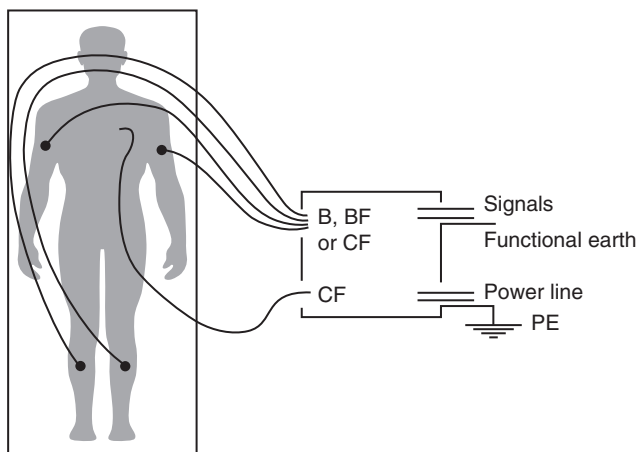


Figure 10.37: Electomedical equipment with two applied parts.

An electomedical device may have more than one applied part, [Figure 10.37](#). The producer must basically declare the intended use of his or her equipment. If an applied part is intended to be used in direct connection with the heart, it must be of type CF. The same instrument may have another applied part intended to be used with skin surface electrodes or sensors. That applied part may be of type B, BF, or CF. A plug in the instrument may be marked with type B, but a box with a galvanic separation may be inserted in the cable so that the applied part is converted from type B to BF or CF.

History of Bioimpedance and Bioelectricity

We may imagine that the first sensory experience with electricity was electrostatic discharges by rubbing. Magnetic stones have also been known very early, and the Arabs are believed to have used such a stone floating as a compass around 700.

Leonardo da Vinci experimented with lodestone and iron, and knew that the forces penetrated a wood wall. *William Gilbert*¹ is the first scientist who devoted a whole book exclusively to electromagnetism: “*De Magnete*” from the year 1600, written in Latin. The book is actually considered to be the first real scientific work published in England. Gilbert was the first to use the word “electricity”; to distinguish between static electricity and magnetism; and to consider the earth as a giant magnet.

Bioelectricity was not mentioned.

A device generating static electricity was first made by *Otto von Guericke* in 1663. He used a rotating sphere of sulfur. A more efficient machine with a rotating glass sphere was invented by *Francis Hauksbee* in 1704. He also experimented with evacuated glass bottles and observed the light generated in high electric fields. By 1740, electrostatic machines with a rotating glass disc had become popular and were in widespread use in Europe. In 1745, a new cheap and convenient source of static electricity was invented: the low-loss, high-voltage capacitor in the form of the Leyden jar. It was a glass bottle with a metal foil on the outside and a conductor at the inside. Not surprisingly, the ability of storing electricity in a jar that can be “filled” and “emptied” made people think of electricity as a fluid. The Leyden jar spread very rapidly in Europe and America.

*Benjamin Franklin*² had an electrostatic machine in Philadelphia, and in the winter of 1746–1747 he began to investigate electrical phenomena. He suggested an experiment to prove the identity of lightning, but this was first carried out in France. He is believed to have tried the dangerous experiment of flying a kite in a thunderstorm. In 1763, professor Richman in St. Petersburg was killed by such an experiment. He is believed to be the first victim of experimenting with electricity. Franklin and his associates concluded early that the corona discharge “electrical fire” or “St. Elmo’s fire” was a discharge that equalized

¹ William Gilbert (1544–1603), British physician/physicist/natural philosopher at the court of Queen Elizabeth I.

² Benjamin Franklin (1706–1790), an American printer and publisher, author, inventor and scientist, diplomat, and a religious protestant. Stayed several times in London and Paris.

bodies with an excess and deficiency of “electrical fire.” Franklin introduced the concept of positive and negative electricity. He suggested that buildings could be protected from lightning by erecting pointed iron rods. The term *Franklin currents* means currents of electrostatic origin and is named after him. His papers were collected in 1751 in the book *Experiments and Observations on Electricity*, soon translated into French (1752), German (1758), and Italian (1774).

The French abbot *Jean-Antoine Nollet*³ was interested in bioelectric phenomena and made use of electrostatic machines and Leyden jars for electrotherapy. His book *Lettre sur l'electricite* was published in Paris in 1753, and in it he referred to Franklins's work. It is said that under the French king Louis XV (reigned 1715–1774), the whole court “se fait électriser.”

All these experiments where carried out with static electricity. The history of continuously flowing electricity *started* with *bioelectricity*, and in particular with *Luigi Galvani* (1737–1798) at the University of Bologna. On November 6, 1780, he discovered that while an assistant was touching the sciatic nerve of a frog with a metal scalpel, the frog's muscle moved when he drew electric arcs on a nearby electrostatic machine (Galvani's first experiment, performed in his home). Galvani's frogs were placed on iron gratings, and he used bronze hooks to move them. He then discovered that the muscle twisted at the mere touch of the hook to the spinal cord. This is known as Galvani's second experiment. His explanation based on “animal electricity” was challenged by Volta, leading to the famous Galvani–Volta controversy. Galvani was a physician (obstetrician) and a natural philosopher, and he also examined the organs of electric fishes. Many expressions reveal this historical origin, we speak of *galvanism*, *galvanic current* (= DC), and galvanic separation; in modern terms, galvanic means related to DC current. A *galvanostat* is a DC constant current source, and a *galvanometer* a DC current meter.

It was *Alessandro Volta* (1745–1825), professor in physics at Como (later in Pavia and then Padua), who found the correct explanation of Galvani's second experiment: Galvani actually experimented with DC created by different metals in contact with the same electrolyte: the animal's own body fluids. He used the frog muscle both as a part of a battery and as the first ammeter! The concept of animal electricity was

³ L'Abbé Nollet was a member of the l'Académie Royale des Sciences in Paris, the Royal Society in London, and the Institute of Bologna, professor at the College of Navarra, and “Maitre de Physique” for the Dauphin. His favorite public experiment was to discharge a Leyden jar through many series-coupled persons. On one occasion he did it in front of King Louis XV with a chain of 180 Royal Guards, on another through a row of Carthusian monks *more than a kilometer long*. At the discharge, the white-robed monks reportedly leapt simultaneously into the air. He also discovered the osmotic pressure across semipermeable membranes.

abandoned, but reappeared later under the term animal magnetism, meaning hypnosis (mesmerism). He invented the new source of continuous electricity, the Volta battery.⁴

The work of *Michael Faraday* was important both in electrochemistry and for the discovery of magnetic induction. He was also interested in bioelectricity. On his European tour, he passed Genoa in 1813, where he studied electrical discharge from the torpedo fish. In 1820, *Hans Christian Ørsted* in Copenhagen published his discovery of the relationship between flowing electricity and magnetism. It was presented in Latin, but within the same year it was translated into French, Italian, German, English, and Danish. In 1831, Faraday invented the induction coil, which became very important for bioelectric research and practical use. *Faraday stimulation* means stimulation with high-voltage/current pulses, faradaic current. The induction coil was further developed by *Nikola Tesla*, who discharged a capacitor through a coil with just a few windings, air coupled to a secondary coil of several 100 windings. Tesla currents were therefore high voltage damped oscillating pulses in the lower MHz range.

Parallel with the discovery of new sources of electricity, the *detection* of small bioelectric currents became possible. Soon after Ørsted's discovery in 1820, the first *galvanometers* appeared. The problem was twofold: to increase sensitivity and to make the new sources follow the rapid changes of muscle and nerve currents.

Johannes Peter Müller published his *Elements of Physiology* in 1840. Müller had a keen interest in to what extent life processes can be explained from the “dead” laws of mechanics, physics and chemistry. He thought it useful as long as we keep to the solid ground of observation and experiment. Müller clearly represented a mind fitted to carry on physical researches into the phenomena of living things in a legitimate way. In 1840, Müller made *Du Bois-Reymond* his assistant in physiology; as a starting point for an inquiry, he did put into Du Bois-Reymond's hands the essay that the Italian *Carlo Matteucci* had just published on the electric phenomena of animals. Matteucci measured muscle current impulses as early as in 1838.

From 1850 to 1900, we had a parallel development of important medical use of endogenic bioelectric sources in the body.

11.1 Electrocardiogram—Heart Muscle Activity

August Waller recorded human electrocardiogram (ECG) in 1887 with the capillary electrometer (a voltage-reading device), but the QRS complex was highly distorted

⁴ In 1801, Volta demonstrated his battery in Paris before Napoleon, who made Volta a count and senator of the Kingdom of Lombardy.

because of too slow a response. Willem Einthoven presented a new sensitive and quick quartz *string* galvanometer in 1903, and with this device he registered correct ECG curves.

11.2 *Electroencephalogram—Brain, Nervous Tissue*

Richard Caton registered currents from the brain (early form of electroencephalogram [EEG]) in 1875. The problem of registering the activity of the heart was more difficult because the galvanometers of the time were not sufficiently quick.

11.3 *Electrodermal Activity—Skin, Sweat Activity*

Du Bois-Raymond started a long series of investigations on *bioelectricity* by studying fishes that are capable of generating electrical currents; he registered electrodermal responses with his hands or feet submerged in an electrolyte of zinc sulfate. His book *Untersuchungen über die Tierische Elektrizität* in 1848 was a very early work. In 1888, Féré discovered electrodermal activity by measuring the drop in DC skin resistance elicited by an emotional stimulus.

An important reason for the parallel development of these three methods was their equal dependence on technology. In the beginning, it was a common lack of sensitivity and speed. The amplifying vacuum tube had not yet been invented, and the most used sensor device also that allowed time registrations on photo paper was a galvanometer with a coil suspended in a magnetic field. The sensitivity was dependent on the magnetic field strength and the number of coil windings. The speed was dependent on the moving mass of the coil. By fixing a very small mirror to the coil thus omitting the large mass of an arrow, using a narrow light beam and long distance from the coil mirror to the scale, it little by little ended up with the galvanometer Einthoven presented in 1903.

EEG needed the highest sensitivity, speed was less demanding. ECG needed quick response times. Electrodermal activity galvanometers were not so critical of either speed or sensitivity ([Figure 11.1](#)).

The ECG method spread worldwide much more quickly than the other two. But the world record had the spread of X-ray imaging technology. Within months, the first images were taken all over United States and Europe. Medical technology spread much faster than today.

Hermann von Helmholtz was a student of Du Bois-Reymond. He measured the conduction velocity of a nerve cell axon around 1850. He formulated the very basic theorems of superposition and reciprocity, and also some very important laws of



Figure 11.1: Electrotherapy around 1890? The first electrotherapeutic congress was held in Frankfurt am Main in 1891.

acoustics. *Hermann Müller* in Königsberg/Zürich during the 1870s found the capacitive properties of tissue and the anisotropy of muscle conductance, based also on AC measurements.

Based upon Faraday's work, *James Clerk Maxwell*⁵ published his famous equations in 1873. He more specifically calculated the resistance of a homogeneous suspension of uniform spheres (also coated, two-phase spheres) as a function of the volume concentration of the spheres. This is the basic mathematical model for cell suspensions and tissues still used today. However, it was not Maxwell himself who in 1873 formulated the four equations we know today as Maxwell's equations. Maxwell used the concept of quaternions, and the equations did not have the modern form of compactness; he used 20 equations and 20 variables. It was *Oliver Heaviside* (1850–1925) who first expressed them in the form we know today. It was also Heaviside who coined the terms *impedance* (1886), *conductance* (1885), *permeability* (1885), *admittance* (1887), and “permittance,” which later became *susceptance*.

Around 1900, it was well-known that large high-frequency currents of more than 1 A could pass through the human body with only heat sensation (*Arsène d'Arsonval*, 1893), but that small low-frequency currents excited the nerves without heat effects.

⁵ James Clark Maxwell 1831–1879, British mathematician and physicist, founder of the electromagnetic field theory and the kinetic theory of gases.

The study of bioelectricity before 1900 can be divided in five periods according to the sources of electricity available:

- Continuous static electricity from 1663—*von Guericke*'s electrostatic device (high voltage);
- Static electricity discharge pulses from 1745—the *Leyden* jar (high-voltage discharge);
- Continuous DC current from 1800—*Volta* electrochemical battery (low voltage, high current);
- High-voltage/current pulses from 1831—*Faraday*'s induction coil;
- Continuous AC current from 1867—*Werner von Siemens*' rotating dynamo (high power).

These were the giants of the past centuries. We call them giants also because their influence was of a very general and deep nature, and all of whole society was somewhat aware of their achievements. The nineteenth century was important for a broad understanding of some of the chemical and physical processes behind bioelectricity. In the twentieth century, specialization has gradually increased. The achievements are more specialized with a more narrow impact and not so well-known to the “public at large.”

On the other hand, the *technology*, in the basic sense of the word: the know-how about how to construct devices and have them produced and marketed, all belong to the twentieth century. These products and their importance for new medical procedures can be seen by everyone. Bringing medical instrumentation to the marketplace started with the X-ray machine and ECG at the beginning of the twentieth century, electrosurgery and diathermy equipment appeared in the 1930s, the EEG in the 1940s, and the pacemaker and the defibrillator in the 1960s.

Rudolf Hoeber discovered the frequency dependence of conductivity of blood and postulated the existence of cell membranes (1911). *Philippson* in 1921 measured tissue impedance as a function of frequency and found that the capacitance varied approximately as the inverse square root of the frequency. He called this a polarization capacitance similar to that found for the metal/electrolyte interphase. In the late 1920s, *Gildemeister* found the constant phase character of tissue, and *Herman Rein* found electro-osmotic effects.

11.4 Kenneth S. Cole (1928a,b Papers)

It was the Cole brothers who paved the way for an analytical, mathematical treatment of tissue immittivity and permittivity. K.S. Cole worked for a period in Debye's laboratory. In the theoretical part (1928a), he *calculated* the impedance of a suspension of spheres in which each sphere was coated with a layer having capacitive properties. He found expressions for the impedance at DC and infinite frequency (r_0 and r_∞ , both purely resistive).

He introduced a constant phase element (CPE), defined in the paper by the phase angle $\phi_3 = \arccotan(m)$, and $m = r_3/x_3$, accordingly using m completely differently from Fricke: ideal resistor has $m = \infty$ and $\phi_3 = 0^\circ$, and found the impedance locus for such a system was a circular arc with the center below the real axis in the Wessel diagram. *A plot of complex immittance or immittivity in the Wessel diagram with the purpose of searching for circular arcs, may according to this book, be called a Cole-plot.*

He discussed the three-component electric equivalent circuit with two resistors (one ideal, lumped, physically realizable electronic component; one frequency-dependent not realizable) and a capacitor (frequency-dependent) in two different configurations. He discussed his model first as a descriptive model, but later discussed Philippson's explanatory interpretation (extra-/intracellular liquids and cell membranes).

In the experimental paper (1928b), he presented the measuring cell and tube oscillator used and the results obtained with a suspension of small eggs. The results were in accordance with the theory outlined in the previous paper (1928a).

11.5 Peter Debye (1929 Book)

In Debye's classical book *Polar Molecules*, he regarded molecules as spheres in a continuous medium having a macroscopic viscosity. The model was particularly based upon gases and dilute solutions of polar liquids. From the model, he deduced the equation:

The Debye equation

$$\epsilon^* - \epsilon_\infty = \frac{\epsilon_0 - \epsilon_\infty}{1 + j\omega\tau_0} \quad (11.1)$$

where ϵ^* is the complex permittivity

Debye's work was not centered on biological materials; it was hardly known at the time that many large organic molecules are strongly polar.

11.6 Hugo Fricke (1932 Paper)

Hugo Fricke showed that, for example, the electrode polarization capacitance often varies as f^{-m} (in this book written⁶ as f^{m-1}), and that there is a basic empirical relationship between the exponent m and the phase angle of the electrode polarization impedance (*Fricke's law*): $\varphi = (1 - m)90^\circ$ (in our book, $\varphi = m 90^\circ$). He found that the frequency

⁶ The use of phase angles, loss angles, and the parameters m and α has been very confusing since the days of Cole and Fricke. This book is based on the following philosophy: The use of the phase angle coefficient α follows the Cole equations, and the frequency exponent m must then be defined according to $\varphi = m\pi/2$. The frequency dependence of a capacitance is then $C = C_1 f^{m-1}$, $0 \leq m \leq 1$, according to Eq. 8.25.

exponent m usually is frequency-dependent; accordingly, Fricke's law does not necessarily imply a CPE. However, for certain electrodes, m is frequency-independent over an extended frequency range. Such a CPE, we may call a Fricke CPE. Fricke did not use circular analysis in the Wessel plane. He laid the basis for the Maxwell-Wagner dispersion model.

The ideal capacitor has (Fricke's symbols) $m = 0$ and $\phi = 90^\circ$, ideal resistor $m = 1$, and $\phi = 0^\circ$. His model was a purely descriptive one.

11.7 Kenneth S. Cole (1932 Paper)

Kenneth S. Cole repeated the presentation from 1928, but now with a quasi-four-element equivalent circuit with two static resistors, his z_3 is a CPE. *His model implies that the two resistors are not a part of the polarization process.* This is explicitly stated in Cole (1934). He did not discuss a microanatomical or relaxation-theory explanatory model. He pointed out that different equivalent circuits may equally well mimic measured data: all are possible descriptive models. He did point out the similarity between data from tissue/cell suspensions and polarization on metal-electrolyte interphases.

11.8 Kenneth S. Cole (1940 Paper)

This is an important and original paper. Here the famous Cole equation was presented in this way:

$$z = z_\infty + \frac{r_0 - r_\infty}{1 + (j\omega\tau)^\alpha} \quad (11.2)$$

For the first time, there was a mathematical expression for the *impedance* dispersion corresponding to the circular arc found experimentally. The equation introduced a new parameter: the somewhat enigmatic constant α . He interpreted α as a measure of *molecular interactions*, with no interactions $\alpha = 1$ (ideal capacitor). Comparison was made with the impedance of a semiconductor diode junction (selenium barrier layer photocell). It is logical and has become common practice to replace z_∞ with r_∞ .

In fact, the Cole-Cole (1941) permittivity equation (see Eq. 11.3) was briefly introduced in this paper ("in manuscript").

11.9 Kenneth S. Cole and Robert H. Cole (1941 Paper)

Here the famous Cole-Cole equation was presented. The emphasis was turned from impedance to permittivity. The two brothers did not link the paper to biological data (with the exception of two references); it is a general paper about dielectrics. It is the first

paper by Kenneth S. Cole in which the concepts of dielectrics, Debye- and relaxation-theory and dispersion are used. The Cole–Cole *equation* was presented:

$$\varepsilon^* - \varepsilon_\infty = \frac{\varepsilon_0 - \varepsilon_\infty}{1 + (j\omega\tau_0)^{1-\alpha}} \quad (11.3)$$

As a permittivity equation, they used $1 - \alpha$, not α , as the exponent. The equation was derived from the Debye equation simply by analogy, based upon the overwhelming amount of experimental data for all sorts of dielectrics giving impedance loci of *arcs* of depressed circles (and not complete Debye half circles) in the Wessel diagram.

It is an empirical, purely descriptive equation, with no direct explanatory power. The problem with the Cole–Cole equation has always been its small explanatory power, and it has led to endless debates about its interpretation. However, the original paper had already introduced the concept of a distribution of relaxation times and linked this with α . This is then the beginning of an explanatory model.

The paper also presented an equivalent electric circuit for the Cole–Cole equation. The permittivity was modeled as two ideal, lumped capacitors and one frequency-dependent impedance (not physically realizable) modeled as a CPE. They stressed that this impedance was *merely one way of expressing the experimental facts, and that it and its real and imaginary parts have no conventional meaning*. The constant phase impedance was purely a descriptive model.

From this paper, a Cole–Cole plot should be defined as a plot of the complex *permittivity* in the Wessel diagram to search for one or more circular arcs.

In the late 1930s, *Cole and Curtis* extended their investigations to the nonlinear effects of excitable membranes. After World War II, *Hodgkin and Huxley* revealed some of the main mechanisms of nerve transmission, for which they won the Nobel Prize in 1963.

11.10 Herman Paul Schwan (1915–2005)

Schwan was one of the founders of biomedical engineering as a new discipline.⁷ Before World War II, in the laboratory of Rajewski at the Frankfurter Institut für Biophysik, he had started with some of the most important topics of the field: on low-frequency blood and blood serum conductivity, counting of blood cells, selective heating and body tissue properties in the ultra-high-frequency range, electromagnetic hazards and safety standards for microwaves, tissue relaxation, and electrode polarization. He also worked with the acoustic and ultrasonic properties of tissue. In 1950, he revealed for the first time the frequency dependence of muscle

⁷ Working to establish a new discipline. Herman P. Schwan and the roots of biomedical engineering. In: Nebecker F. (1993), Sparks of genius, IEEE Press.

tissue capacitance and interpreted it as a relaxation phenomenon. He introduced the concept of dispersion and was first to describe the α dispersion in muscle tissue (Schwan, 1954). Two of the most cited articles in the field of biomedical engineering appeared in 1957 and 1963: “Electrical properties of tissue and cell suspensions” and the more methodology focused article “Determination of biological impedances.” In the 1957 article, he introduced the α , β , and γ classifications (see Chapter 3.8). He pioneered low-frequency precision measurements (Schwan et al., 1962), four-electrode techniques, and gigahertz measurements. Later he turned also to dielectrophoresis, electro-rotation, and nonlinear phenomena of interfacial polarization (Schwan’s law of linearity, McAdams et al., 1994). He is very appreciated for a number of much-cited review articles, lately also about the history of our field (Schwan, 1992b, 1993). Some of his students and close collaborators at the University of Pennsylvania were: Edwin Carstensen, Kenneth Foster, David Geselowitz, Dov Jaron, Mariam Moussavi, Banu Onaral, and Shiro Takashima.

The most important papers by Herman Schwan were selected in close cooperation with him and were published in 2001: *Selected Papers by Herman P. Schwan*, editors Sverre Grimnes and Ørjan G. Martinsen.

11.11 Surface Potentials Generated by a Bioelectric Source in a Volume Conductor

The historic development in this area includes Helmholtz (1853), Einthoven et al. (1913), Burger et al. (1946), McFee and Johnston (1953), Schmitt (1957), and Geselowitz (1971).

It was a long way to go before the genesis of the surface potential differences caused by action potentials deep in the thorax was understood. It was the work of Einthoven and the lead concept that paved the way. It was Burger and van Milaan who introduced the *lead vector*, making it possible to find the direction to go. Richard McFee replaced the lead vector by the *lead field*, defined as the electric field set up in the body by a unit current applied to the pick up electrode pair. Otto Schmitt reintroduced the old Helmholtz concept about reciprocity and introduced the concept of *transfer impedance* already known from the use of four-electrode technique. And it was David Geselowitz who finally put it in the elegant mathematical form. A certain similarity with the Faraday–Maxwell intellectual process runs in our minds.

Appendix

12.1 Vectors and Scalars, Complex Numbers

Suppose we have a black box with one port = two terminals. Suppose that with sinusoidal excitation, all voltage differences and all currents inside are also sinusoidal. Suppose that inside there are only resistors. Then all current maxima and voltage maxima occur simultaneously, there are no delays, no phase shifts.

Suppose that inside the box there is a circuit with resistors and capacitors. Then the voltage across a capacitor is also sinusoidal, but the voltage maximum occurs *after* the current maximum. There is a time lag, a phase shift. The phase shift is measured in degrees, and one complete period is 360° . In such circuits, we must keep track not only of the magnitude, but also on the phase. Two voltages cannot just be added, they must be added as *vectors*. Two voltages *added* are actually *subtracted* if they are 180° out of phase, and equal magnitudes then cancel. Each vector quantity must therefore be given with *two* numbers. We must introduce mathematical tools to deal with such double-numbered quantities.

A *vector* or a *complex number* is the answer, both are characterized by two numbers (e.g., by magnitude and direction). A vector or complex number symbol is written with **bold** characters in our book, so if a symbol is written in bold it may either be a vector in space or a complex number referring to a plane, the Wessel plane.

12.1.1 Vectors and Scalars

Mathematically, a vector in space is defined as a directed line segment (an arrow), with its initial point undefined. As long as it has the same length and is not rotated, the vector may be translated anywhere in space, it is the same vector. However, in physics, we may impose restrictions on the initial point of the vector. A force may for instance be applied anywhere along its line of action to a rigid body, this is a *sliding* vector. The same force applied to an elastic body must be defined at a single initial point, it is a *fixed* or *bound* vector.

A vector is not necessarily referred to a Cartesian coordinate system, but, for example, to a neighbor vector with respect to magnitude and direction. Rules about the addition, subtraction, and multiplication (dot and cross products) of two vectors are a part of vector algebra.

Temperature, for instance, has no direction in space, so it is a *scalar*. However, a temperature *gradient* has a direction, so it is a vector.

In addition to vectors in the *space* domain, vectors may also be defined in the *time* domain, in particular rotating vectors with a fixed initial point at the origin of a Cartesian coordinate system. A variable such as the electric field strength may be a vector *both* in time and space. Every space vector may also be a time vector, and often it is not clear what sort of vector an author actually is dealing with. Vectors in the time domain are used for sine waves when the maxima do not occur simultaneously. These two-dimensional (planar) time vectors are more conveniently represented by complex numbers.

12.1.2 Complex Numbers

A complex number is an ordered pair of real numbers, for instance G and B . Introducing the *imaginary unit* $j = \sqrt{-1}$, the complex number $\mathbf{Y} = G + jB$. G is the *real* part and can be written Y' , and B the *imaginary* part written Y'' . Y or $|\mathbf{Y}|$ is called the *absolute value*, *magnitude*, or *modulus*, and the phase angle is $\phi = \arctan B/G$.

A real number G can be regarded as a position on a number *line*. A complex number \mathbf{Y} can be regarded as a point in the *plane* of a special Cartesian coordinate system: the complex plane, also called the Argand¹ or Wessel² diagram. G is an ordinary real number situated on the real x -axis. j (actually \mathbf{j}) indicates that B is to be situated on the imaginary y -axis. B is a *real* number, jB is an *imaginary* number, \mathbf{Y} is a *complex* number.

Complex numbers such as \mathbf{Y} are written in **bold** in this book. \mathbf{Y} is represented by a point in the Wessel diagram determined by G and B , the *locus* of \mathbf{Y} (see Figure 12.1).

$\mathbf{Y}^* = G - jB$ is called the complex *conjugate* to \mathbf{Y} . Often the complex conjugate is used to obtain positive values for the imaginary component in the Wessel diagram. Impedance loci for instance are usually plotted with the circular arcs up, so instead of $\mathbf{Z} = R + jX$, $\mathbf{Z}^* = R - jX$ is plotted.

Summing up: What is the difference between a space vector and a complex number in our context?

A space vector represents a quantity having a magnitude and direction in 3-D space; reference to a co-ordinate system is not necessary. A complex number is a time vector in a 2-D plane and always referred to a Cartesian co-ordinate system.

¹ Jean Robert Argand (1768–1822), French/Swiss mathematician. Proposed the complex plane presentation in 1806.

² Caspar Wessel (1745–1818), Norwegian surveyor. Proposed the complex plane presentation in 1797, 9 years before Argand. Presentation in the imaginary plane is accordingly called a Wessel diagram in this book.

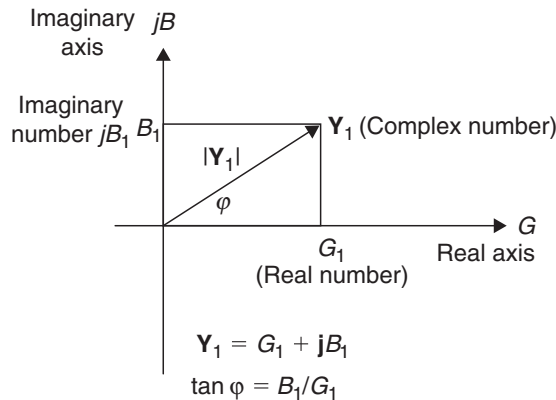


Figure 12.1: The complex plane (Wessel diagram).

Ohm's law in scalar form is written for AC (small i and u indicate sinusoidal varying quantities): $i = uG$. There is no time lag in the circuit (e.g., just resistors). i , u , and G are scalars, all maxima occur simultaneously. Under the condition that *all waveforms are sinusoidal*, Ohm's law is written:

$$i = uY = uG + u j\omega C \quad (12.1)$$

u is still a scalar, because it is chosen as the reference, the *independent* variable (e.g., coming from the signal generator). Phase shift is measured with reference to this sinusoidal voltage. i and Y are printed with bold characters, indicating that they are complex quantities. They are given by:

$$\mathbf{i} = i_i + j i_q \quad (12.2)$$

i_i is the real part, the *in-phase* current component, meaning that this current is in phase with the imposed sine wave voltage. i_q is the imaginary part, the *quadrature* current component. The phase shift φ (relative to the voltage u and the in-phase current i_i) is given by

$$\varphi = \arctan \frac{i_q}{i_i} \quad (12.3)$$

Y is the complex *admittance*, composed of *conductance* G (in-phase with the voltage) unit: [siemens], and *susceptance* B (quadrature component) unit: siemens; in parallel:

$$Y = G + jB = G + j\omega C \quad (12.4)$$

For a capacitor $B = \omega C$, that is proportional to frequency. $f = 0$ gives $B = 0$, this is the direct current (DC) case, with no influence on admittance from the capacitance. If $C = 0$, we have no capacitor, then $i_q = 0$, and $\varphi = 0^\circ$, there is no phase shift, and the expressions reduce to contain only real quantities.

A complex number may also be given in *polar form* based upon *Euler's formula*:

$$e^{j\varphi} = \cos\varphi + j \sin\varphi \quad (12.5)$$

Then $\mathbf{Y} = Ye^{j\varphi} = Y\cos\varphi + jY\sin\varphi$. Because φ is the argument of sine and cosine functions, it is to be an angle; that is, dimensionless.

Another important formula in polar form is that of *De Moivre*:

$(\cos\varphi + j \sin\varphi)^\alpha = \cos\alpha\varphi + j \sin\alpha\varphi$. With $\varphi = \pi/2$, we have the more specialized version used in the Cole equations:

$$j^\alpha = \cos\left(\frac{\alpha\pi}{2}\right) + j \sin\left(\frac{\alpha\pi}{2}\right) \quad (12.6)$$

12.1.3 Sign Conventions

The convention in the electrical sciences is that in the complex plane (Wessel diagram) the counterclockwise direction corresponds to a positive phase shift between two vectors. From this, some sign rules can be deducted:

Admittance

The capacitor model of Figure 3.1 and the Wessel diagram of Figure 12.1 is defined with admittance $\mathbf{Y} = G + jB$. This corresponds to a *parallel* GC circuit where both components have the same voltage. The current is the dependent parameter and the current through G is in phase with the voltage. The current through the capacitor leads the voltage, that by convention is defined as a positive phase shift and the current and admittance vector is counterclockwise to the real axis, $B = +\omega C$. With a GL parallel inductive circuit, $B = -1/\omega L$.

Impedance

Impedance is the inverse of admittance: $\mathbf{Z} = 1/\mathbf{Y} = 1/(G + j\omega C) = (G - j\omega C)/|Z|^2 = R + jX$. This corresponds to a *series* RC circuit where both components pass the same current. The voltage is the dependent parameter and divided between the R and C components. The voltage in the capacitor lags the current and the voltage across the resistor. By the same convention, this is defined as a negative phase shift and the voltage and impedance vector is clockwise to the real axis, $X = -1/\omega C$ and for inductance $X = +\omega L$.

Material Constant Signs in Capacitive Materials

Complex conductivity $\sigma = \sigma' + j\sigma''$

Complex resistivity: $\rho = \rho' - j\rho''$

Complex permittivity: $\epsilon = \epsilon' - j\epsilon''$. In the parallel GC circuit, the current through C corresponds to ϵ' and through G to ϵ'' . The current through G lags the current through C, this corresponds to a negative sign for the current through G and for ϵ'' .

12.1.4 Phasor, Sine Wave, and Operator $j\omega t$

A complex number in the time domain is introduced under the assumption that the independent variable is a sinusoidal function of time.

What is so fundamental about the sine wave? It is the only signal containing only one frequency; it is the perfect and simplest form of *periodicity*. The sine wave is closely linked with the *circle*. A point on a circle rotating with constant frequency draws a sine wave if projected on a paper moving with uniform speed. A complex number vector of unity magnitude rotating as a function of time around the origin is called a *phasor*. A phasor is best represented with polar coordinates: $\mathbf{Y} = G + jB = Y(\cos\varphi + j \sin\varphi) = Ye^{j\varphi}$. If the angle φ is increasing uniformly with time, $\varphi = \omega t$ (radians), then the phasor is: $e^{j\omega t} = \cos\omega t + j \sin\omega t$. A clear distinction is made between *frequency* and *angular frequency*. Both terms imply dimension [1/second], but ωt is an angle. In the expression $\cos(\omega t)$, the product ωt is not an angle and the expression is meaningless: in complex signal analysis the operator is $j\omega t$, not $j\omega$.

A more general mathematical treatment is possible by introducing the complex frequency $s = \sigma + j\omega$, allowing sine waves of variable amplitude, pulse waveforms etc. Such Laplace analysis is outside the scope of this book, however.

Implicit in the complex notation is an important mathematical simplification. Because $\partial(e^{j\omega t})/\partial t = j\omega e^{j\omega t}$, the necessary differential equations are transformed to algebraic equation: the operator $\partial/\partial t$ becomes the factor $j\omega$.

12.1.5 Some Algebraic Rules for Sine Wave Complex Numbers

1. When a complex number is multiplied by j , the phase angle is increased by 90° ($\pi/2$).
2. When a complex number is divided by j , the phase angle is decreased by 90° ($\pi/2$).
3. $di/dt = i j \omega$ (i is complex sine wave).
4. $\int idt = i/j\omega$ (i is complex sine wave).
5. $e^{j\varphi} = \cos\varphi + j \sin\varphi$ (Euler's formula).
6. $\mathbf{YY^*} = \mathbf{Y}^2 = |\mathbf{Y}|^2 = G^2 + B^2$.
7. $j^\alpha = \cos(\alpha\pi/2) + j \sin(\alpha\pi/2) = e^{j\alpha\pi/2} |j^\alpha| = 1$.

12.2 Equivalent Circuit Equations

All the circuits in this chapter are with ideal components, that is, frequency independent resistance, conductance, and capacitance. Derived parameters, however, are often

frequency dependent (see, C_{ext} in Eq. (12.14)). C_{ext} is the capacitance as seen from the outside at the terminals. Two-component circuits are treated in Chapter 9.2.3.

12.2.1 Equations for Two Resistor + One Capacitor Circuits

2R–1C series circuit (Figure 12.2)

$$\begin{aligned} Z &= R + \frac{G - j\omega C}{G^2 + \omega^2 C^2} \\ Z &= R + \frac{1 - j\omega\tau_Z}{G(1 + (\omega\tau_Z)^2)} \\ Z &= R + \frac{1}{G(1 + j\omega\tau_Z)} \end{aligned} \quad (12.7)$$

$$\tau_Z = \frac{C}{G} \quad (12.8)$$

$$\begin{aligned} \varphi &= \arctan \frac{\omega C}{G(1 + RG) + \omega^2 C^2 R} \\ \varphi &= \arctan \frac{\omega C}{G(1 + RG + \omega^2 \tau_Z \tau_2)} \end{aligned} \quad (12.9)$$

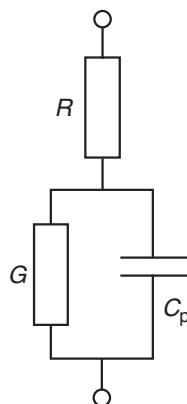


Figure 12.2: 2R–1C series model, ideal components.

$$\mathbf{Y} = \frac{G(1 + RG) + \omega^2 C^2 R + j\omega C}{(1 + RG)^2 + \omega^2 C^2 R^2} \quad (12.10)$$

$$\mathbf{Y} = \frac{G(1 + RG + \omega^2 \tau_Z \tau_2 + j\omega \tau_Z)}{(1 + RG)^2 + (\omega \tau_2)^2}$$

$$\tau_2 = CR \quad (12.11)$$

$$C_{ext} = \epsilon' = \frac{C}{(1 + RG)^2 + (\omega \tau_2)^2} \quad (\text{unity cell}) \quad (12.12)$$

$$\epsilon'' = \frac{G(1 + RG + \omega^2 \tau_Z \tau_2)}{\omega [(1 + RG)^2 + (\omega \tau_2)^2]} \quad (\text{unity cell}) \quad (12.13)$$

Impedance is the preferred parameter characterizing the two resistors, one capacitor series circuit, because it is defined by one unique time constant τ_Z (Eq. (12.8)). This time constant is independent of R , as if the circuit was current driven. The impedance parameter therefore has the advantage that measured characteristic frequency determining τ_Z is directly related to the capacitance and parallel conductance (e.g., membrane effects in tissue), undisturbed by an access resistance. The same is not true for the admittance: the admittance is dependent both on τ_Z and τ_2 , and therefore on both R and G .

$$\begin{aligned} \text{When } \omega \rightarrow 0: \quad \mathbf{Y} &\rightarrow \frac{G}{1 + RG} \\ \mathbf{B} &\rightarrow \frac{\omega C}{(1 + RG)^2} \\ C_{ext} &\rightarrow \frac{C}{(1 + RG)^2} \\ \varphi &\rightarrow 0^\circ \end{aligned}$$

$$\begin{aligned} \text{When } \omega \rightarrow \infty: \quad \mathbf{Y} &\rightarrow \frac{1}{R} \\ \mathbf{B} &\rightarrow \frac{\omega C}{\omega^2 C^2 R^2} \rightarrow 0 \\ C_{ext} &\rightarrow \frac{C}{\omega^2 C^2 R^2} \rightarrow 0 \\ \varphi &\rightarrow 0^\circ \end{aligned} \quad (12.14)$$

Equation (12.14) is of particular interest. C_{ext} is the capacitance measured on the terminals (e.g., with a bridge or a lock-in amplifier). At high frequencies, the susceptance part $B = Y''$ is small, and C_{ext} is strongly frequency dependent ($1/\omega^2$). In this frequency range, the strong capacitance increase with decreasing frequency is externally true as measured at the network port, but it does not reflect any frequency dependence of the internal capacitor component. It only reflects the simple fact that we do not have direct access to the capacitor, only through the—at high frequencies—dominating series resistance R .

Selectivity

It is important to analyze this circuit with respect to selectivity: let us assume that our black box contains the two resistors—one capacitor series circuit. Under what conditions will measured Y' be proportional to the unknown G and not be disturbed by variations in R and C ? And correspondingly: under what conditions will measured Y'' be proportional to unknown C and not be disturbed by variations in R and G ?

From Eq. (12.10) we see that Y' is proportional to G only if the following three conditions are met:

1. $RG \ll 1$
2. $\omega^2 C^2 R^2 \ll 1$
3. $\omega^2 C^2 G \ll 1$

Y'' will be proportional to C only if the following two conditions are met:

1. $RG \ll 1$
2. $\omega^2 C^2 R^2 \ll 1$

If the conditions for Y'' are satisfied, it will be possible to follow, for example, the unknown C directly by single frequency measurement of Y , without calculations based on results from measurements on several frequencies.

2R–1C parallel circuit (Figure 12.3)

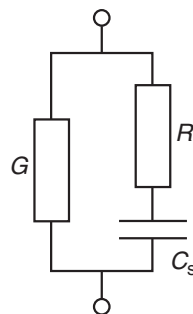


Figure 12.3: 2R–1C parallel model, ideal components.

$$Y = \frac{G + (\omega^2 C^2 R + j\omega C)}{(1 + \omega^2 C^2 R^2)} \quad (12.15)$$

$$Y = \frac{G + (\omega^2 C \tau_Y + j\omega C)}{1 + (\omega \tau_Y)^2}$$

$$\tau_Y = CR \quad (12.16)$$

$$\phi = \arctan \frac{\omega C}{G + \omega^2 C^2 R (1 + RG)} \quad (12.17)$$

$$\phi = \arctan \frac{\omega C}{G [1 + \omega^2 \tau_Y \tau_2 (1 + RG)]}$$

$$Z = \frac{G + \omega^2 C^2 R (1 + RG) - j\omega C}{G^2 + \omega^2 C^2 (1 + RG)^2} \quad (12.18)$$

$$Z = \frac{1 + \omega^2 \tau_Y \tau_2 (1 + RG) - j\omega \tau_2}{G [1 + (\omega \tau_2)^2 (1 + RG)^2]}$$

$$\tau_2 = \frac{C}{G}$$

$$\epsilon' = C_{ext} = \frac{C}{1 + \omega^2 C^2 R^2} \quad (\text{unity cell}) \quad (12.19)$$

$$\epsilon'' = \frac{G}{1 + \omega^2 C^2 R^2} \quad (\text{unity cell})$$

The admittance time constant is uniquely defined by τ_Y , independent of G , as if the circuit were voltage driven. The admittance parameter therefore has the advantage that the measured characteristic frequency determining τ_Y is directly related to the capacitance (membrane effects) and series resistance in tissue. The same is not true for impedance: the impedance is defined by both τ_Y and τ_2 .

When $\omega \rightarrow 0$:

$$Y \rightarrow G$$

$$B \rightarrow \omega C$$

$$\phi \rightarrow 0^\circ$$

$$\epsilon' = C_{ext} = C \quad (\text{unity cell})$$

$$\epsilon'' \rightarrow \infty \quad (\text{unity cell}) \quad \text{NB! Loss per cycle diverges!}$$

$$\begin{aligned}
 \text{When } \omega \rightarrow \infty : & \quad \mathbf{Y} \rightarrow G + \frac{1}{R} \\
 & \quad B \rightarrow \frac{\omega C}{\omega^2 C^2 R^2} \\
 & \quad \varphi \rightarrow 0^\circ \\
 \varepsilon' = C_{\text{ext}} &= \frac{C}{\omega^2 C^2 R^2} \rightarrow 0 \quad (\text{unity cell}) \\
 \varepsilon'' &\rightarrow 0 \quad (\text{unity cell})
 \end{aligned}$$

12.2.2 Equations for One Resistor + Two Capacitor Circuits

1R–2C series circuit (Figure 12.4)

$$\begin{aligned}
 \varepsilon' = C_{\text{ext}} &= \frac{C_s [G^2 + \omega^2 C_p (C_p + C_s)]}{G^2 + \omega^2 (C_p + C_s)^2} \quad (\text{unity cell}) \\
 \varepsilon' = C_{\text{ext}} &= \frac{C_s (1 + \omega^2 \tau_2 (\tau_1 + \tau_2))}{(1 + \omega^2 (\tau_1 + \tau_2)^2)} \quad (\text{unity cell}) \\
 \varepsilon'' &= \frac{\omega C_s^2 G}{G^2 + \omega^2 (C_p + C_s)^2} \quad (\text{unity cell}) \tag{12.20} \\
 \varepsilon'' &= \frac{C_s \omega \tau_1}{1 + \omega^2 (\tau_1 + \tau_2)^2} \quad (\text{unity cell}) \\
 \varepsilon &= \frac{C_s (1 + \omega^2 \tau_2 (\tau_1 + \tau_2)) - j \omega \tau_1 C_s}{1 + \omega^2 (\tau_1 + \tau_2)^2} \quad (\text{unity cell})
 \end{aligned}$$

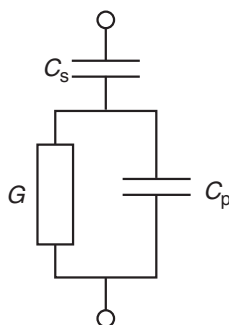


Figure 12.4: 1R–2C series model, ideal components.

$$\tau_1 = \frac{C_s}{G} \quad (12.21)$$

$$\tau_2 = \frac{C_p}{G} \quad (12.22)$$

$$Z = \frac{\omega C_s G - j(\omega^2 C_s C_p + \omega^2 C_p^2 + G^2)}{\omega C_s (\omega^2 C_p^2 + G^2)} \quad (12.23)$$

$$Z = \frac{\omega \tau_1 - j(\omega^2 \tau_1 \tau_2 + (\omega \tau_2)^2 + 1)}{\omega C_s [(\omega \tau_2)^2 + 1]}$$

$$\phi = \arctan \frac{\omega^2 C_p (C_p + C_s) + G^2}{\omega C_s G} \quad (12.24)$$

$$\phi = \arctan \frac{\omega^2 \tau_2 (\tau_1 + \tau_2) + 1}{\omega \tau_1}$$

$$Y = \frac{\omega^2 C_s^2 G + j\omega C_s (G^2 + \omega^2 C_p (C_p + C_s))}{G^2 + \omega^2 (C_p + C_s)^2} \quad (12.25)$$

$$Y = \frac{\omega^2 C_s \tau_1 + j\omega C_s (1 + \omega^2 \tau_2 (\tau_1 + \tau_2))}{1 + (\omega (\tau_1 + \tau_2))^2}$$

This is not a preferred one resistor, two capacitors circuit, because no parameters are uniquely defined with one unique time constant.

When $\omega \rightarrow 0$: $\epsilon' = C_s$ (unity cell)

$$\epsilon'' \rightarrow 0$$

$$Y \rightarrow 0$$

$$B \rightarrow \omega C_s$$

$$C_{ext} \rightarrow C_s$$

$$\phi \rightarrow 90^\circ$$

$$\text{When } \omega \rightarrow \infty : \quad \epsilon' = \frac{C_s \tau_2}{\tau_1 + \tau_2} \quad (\text{unity cell})$$

$$\epsilon'' \rightarrow 0$$

$$Y \rightarrow \infty$$

$$B \rightarrow \frac{\omega C_p C_s}{C_p + C_s}$$

$$C_{\text{ext}} \rightarrow \frac{C_p C_s}{C_p + C_s}$$

$$\phi \rightarrow 90^\circ$$

1R–2C parallel circuit (Figure 12.5)

$$\epsilon' = C_{\text{ext}} = \frac{C_p + C_s}{1 + (\omega \tau_Y)^2} \quad (\text{unity cell})$$

$$\epsilon'' = \frac{C_s \omega \tau_Y}{1 + (\omega \tau_Y)^2} \quad (\text{unity cell}) \quad (12.26)$$

$$\epsilon = \frac{C_p + C_s}{1 + j\omega \tau_Y} \quad (\text{unity cell})$$

$$Y = \frac{j\omega C_p + (\omega^2 C_s^2 R + j\omega C_s)}{1 + \omega^2 C_s^2 R}$$

$$Y = \frac{j\omega C_p + j\omega C_s}{1 + j\omega C_s R} \quad (12.27)$$

$$Y = \frac{j\omega C_p + j\omega C_s}{1 + j\omega \tau_Y}$$

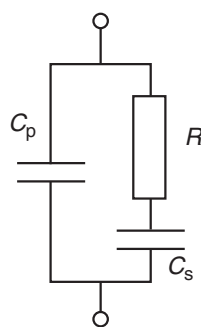


Figure 12.5: 1R–2C parallel model, ideal components.

$$\tau_Y = C_s R \quad (12.28)$$

$$\phi = \arctan \frac{-(C_p + C_s + \omega^2 C_s^2 R^2 C_p)}{\omega C_s^2 R} \quad (12.29)$$

$$\phi = \arctan \frac{[C_p + C_s + (\omega \tau_Y)^2 C_p]}{\omega \tau_Y C_s}$$

$$Z = \frac{\omega C_s^2 R - j(C_p + C_s + \omega^2 C_s^2 R^2 C_p)}{\omega [(\omega C_s C_p R)^2 + (C_p + C_s)^2]} \quad (12.30)$$

$$Z = \frac{\omega \tau_Y C_s - j(C_p + C_s + (\omega \tau_Y)^2 C_p)}{\omega [(\omega \tau_Y C_p)^2 + (C_p + C_s)^2]}$$

This is a preferred one resistor, two capacitors circuit, because all parameters are uniquely defined with one unique time constant.

$$\text{When } \omega \rightarrow 0: \quad \epsilon' = C_{\text{ext}} \rightarrow C_p + C_s \quad (\text{unity cell})$$

$$\epsilon'' \rightarrow 0 \quad (\text{unity cell})$$

$$Y \rightarrow 0.$$

$$B \rightarrow \omega(C_p + C_s)$$

$$C_{\text{ext}} \rightarrow (C_p + C_s)$$

$$G \rightarrow \omega^2 C_s^2 R \rightarrow 0$$

$$\phi \rightarrow 90^\circ$$

$$\text{When } \omega \rightarrow \infty: \quad \epsilon' = C_{\text{ext}} \rightarrow C_p \quad (\text{unity cell})$$

$$\epsilon'' \rightarrow 0 \quad (\text{unity cell})$$

$$Y \rightarrow \infty$$

$$B \rightarrow \omega C_p$$

$$G \rightarrow \frac{1}{R}$$

$$\phi \rightarrow 90^\circ$$

12.2.3 Equations for Four-Component Series Circuit (Simple Maxwell–Wagner Model) (Figure 12.6)

This is the Maxwell–Wagner model of a capacitor with two dielectric layers. Even with only two layers, the equations are complicated; with three layers, they become much

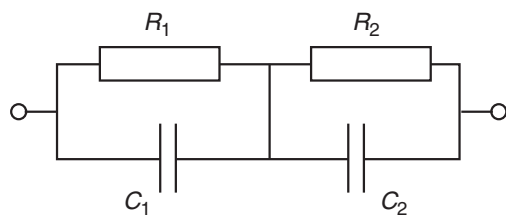


Figure 12.6: 2R-2C series circuit, ideal components.

worse. The equations become somewhat simpler by bringing them to the Debye equation form: $Y = Y_0 + \Delta Y/[1 + (\omega\tau_Y)^2]$.

$$Y' = \frac{(G_1 + G_2)(G_1 G_2 - \omega^2 C_1 C_2) - \omega^2 (C_1 + C_2)(C_1 G_2 + C_2 G_1)}{(G_1 + G_2)^2 + \omega^2 (C_1 + C_2)^2} \quad (12.31)$$

$$Y'' = \frac{\omega [(G_1 + G_2)(C_1 G_2 + C_2 G_1) - (C_1 + C_2)(G_1 G_2 - \omega^2 C_1 C_2)]}{(G_1 + G_2)^2 + \omega^2 (C_1 + C_2)^2}$$

When $\omega \rightarrow 0$: $Y' \rightarrow \frac{G_1 G_2}{G_1 + G_2}$

$$Y'' \rightarrow 0$$

$$C_{\text{ext}} \rightarrow \frac{C_1 G_2^2 + C_2 G_1^2}{(G_1 + G_2)^2}$$

$$\varphi \rightarrow 0^\circ$$

When $\omega \rightarrow \infty$: $Y' \rightarrow \frac{C_1 C_2 (G_1 + G_2) - (C_1 + C_2)(C_1 G_2 + C_2 G_1)}{(C_1 + C_2)^2}$

$$Y'' \rightarrow \frac{\omega C_1 C_2}{C_1 + C_2}$$

$$C_{\text{ext}} \rightarrow \frac{C_1 C_2}{C_1 + C_2}$$

$$\varphi \rightarrow 90^\circ$$

12.3 Global Symbols ([Table 12.1](#))

A *quantity* is usually defined as the product of a *numerical value* and a *unit*. A current is 4 A: current is the quantity, 4 is the numerical value and [ampere] is the unit. In equations,

Table 12.1: Global Symbols

Symbol (in Equations)		Quantity	[Unit] or [Dimension] Dimensionless = [1]
Scalar	Vector in space		
r	\mathbf{r}	Radius (variable)	[Meter], [m], SI system base unit.
	$\hat{\mathbf{r}}$	Unity radius vector	[1]
a	\mathbf{a}	Radius (constant)	[m]
L	\mathbf{L}	Length	[m]
v		Volume	[Liter], [L], [m^3]
v	\mathbf{v}	Velocity	[m/s]
v		ac voltage	[Volt]
d	\mathbf{d}	Diameter, thickness,	[m]
A	\mathbf{A}	(Cross sectional) area	[m^2]
f	\mathbf{f}	Force	[Newton], [N]
mol		Number of particles, relative mass	[1]. Amount of substance of 6×10^{23} particles. SI system base unit.
c		Concentration	[Mol/l], %weight or %volume of total [1].
η		Viscosity	[Pa s]
q,		Charge, quantity of electricity	[Coulomb], [C], [As]
F		Faradays constant	$1 F = 96,472$ [C/mol]
q_v		Volume charge density	[C/ m^3]
q_s		Surface charge density	[C/ m^2]
e		Elementary charge (one proton or electron)	$1.6 \cdot 10^{-19}$ C, + or -
z		Number of electrons for transfer (electrovalency)	[1], + or -
n		Number of ions pr volume	[1/L], + or -
N		Number of molecules pr volume	[1/L]
μ		Ionic mobility	[m^2/Vs] ($\mu = v/E$)
I (dc)		Current	[Ampere], [A], SI system base unit
i (ac)		Current	[Ampere], [A]
J	\mathbf{J}	Current density	[A/ m^2]
J'	\mathbf{J}'	Unit current density	[1/ m^2]
emv*		Electromotive voltage	[Volt]

Continued

Table 12.1: Global Symbols—cont'd

Symbol (in Equations)		Quantity	[Unit] or [Dimension]
Scalar	Vector in space		Dimensionless = [1]
Φ		Potential (in space)	[Volt]
U, V (dc)		Voltage (in circuit)	[Volt]
u, v (ac)		Voltage (in circuit)	[Volt]
ϵ		Permittivity = $\epsilon_r \epsilon_0$	[F/m]
ϵ_0		Permittivity of vacuum	8.8×10^{-12} [F/m]
ϵ_s		Static permittivity, bound charges	[F/m]
ϵ_r		Relative permittivity (dielectric constant)	[1]
ϵ_∞		Permittivity, infinite high frequency	[F/m]
M		Modulus function = $1/\epsilon$	[m/F]
E	E	Electric field	[Volt/m]
D	D	Electric flux density (displacement)	[C/m ²]
P	P	Polarization	[Cm/m ³] or [C/m ²]
P	P	Electric dipole moment	[Cm], debye (D) = 3.3 10^{-30} [qm]
m	m	Current dipole moment = iL	[Am]
C		Capacitance	farad [F]
C_p		Parallel capacitance	[F]
C_s		Series capacitance	[F]
t		Time	[second], [s]. SI system base unit
τ		Time constant	[s]
f, v		Frequency	hertz (Hz), periods/s, [1/s]
ω		Angular frequency, $2\pi f$	Angle/s, [1/s]
σ		Conductivity	[S/m]
ρ		Resistivity	[Ω m]
G		Conductance	[Siemens], [S], [1/ Ω], [mhos], [\mathcal{G}]
B		Susceptance	[S]
Y		Admittance	[S]
R		Resistance (in series)	[Ohm], [Ω]
X		Reactance	[Ω]
Z		Impedance	[Ω]

Table 12.1: Global Symbols—cont'd

Symbol (in Equations)			[Unit] or [Dimension] Dimensionless = [1]
Scalar	Vector in space	Quantity	
Z_c		Transfer impedance	[Ω]
m		Frequency exponent, f^m	[1], $0 \leq m \leq 1$
φ		Phase angle	[1], degrees (°)
α		Phase angle coefficient and frequency exponent combined	[1], $\alpha = \varphi/90^\circ$, $0 \leq \alpha \leq 1$ for CPE: $\alpha = m$
δ		Loss angle	[1], $\delta = 90^\circ - \varphi$
\hat{E}		Energy, work	$1 \text{ J} = 1 \text{ wattsecond}$ [Ws], $eV = 1.6 \cdot 10^{-19} \text{ J}$
\hat{E}_v		Energy density	[J/m ³]
W		Power = energy per second	watt = [J/s]
W_v		Power density	[W/m ³]
T		Temperature	[°C], [K]. °K = −273,16 °C. SI system base unit
j		Imaginary unit	$\sqrt{-1}$
h		Planck's constant	$6.6 \cdot 10^{-34} \text{ Js}$
k		Boltzmann's constant	$1.38 \cdot 10^{-23} \text{ J/}^\circ\text{K}$
\approx		Approximately equal to	
\sim		Proportional to	
z		Volume impedance density	[Ω/m ³]
g		Volume conductance density	[S/m ³]
r		Volume resistance density	[Ω/m ³]

*Also called electromotance or electromotive force (emf). The term *force* was used by Maxwell because a potential difference exerts a force on a charge. The use of emf in this book is limited to potential differences caused by chemical or thermal energy, or induced in a circuit by a changing magnetic flux. Thus a potential difference across a resistor or a charged capacitor as ideal components is not termed emf. In the literature before 1940, emf was often used more generally about the voltage difference across any component.

we use *symbols* for the quantities (e.g., the symbol for current is I). For the units, we also use symbols or abbreviations. The symbol for current is I, the abbreviation for the unit [ampere] is [A]. The SI system defines seven base units: meter, kilogram, second, ampere, kelvin, mol, and candela. The *dimension* of a derived unit is the product of the powers of the base units. A quantity with dimension [1] is called *dimensionless*. A number of electrons, for example, is dimensionless. A symbol within square brackets is a unit or a dimension.

Global symbols are symbols used in all the chapters of our book, if not otherwise stated. In equations, large letters are often used for DC quantities, small letters for alternating currency (AC) quantities (DC voltage V , AC voltage v). The quantity called *voltage* is used in electric circuits, and *potential* in space. Vectors and complex quantities are printed in **bold**. All space vectors may also be time vectors, and all scalar variables may be time vectors. The subscripts 0 and ∞ are used for frequency extremes, except for ϵ_0 , in which the subscript is for vacuum. The subscript s sometimes means static in the electrostatic meaning, which is without current flow and must therefore not be confused with DC conditions when current *is* flowing.

The printing fonts for the Greek letters are not quite standardized: Φ is the large but both ϕ and φ are the small “phi,” θ and ϑ are the small “theta,” v and υ are the small “ny” and “upsilon,” respectively.

12.3.1 Physical Dimensions ([Table 12.2](#))

The physical dimension of a particle is an important parameter: e.g., the smaller a sphere, the larger the surface to volume ratio ($= 3/r$). The smaller a sphere, the more surface properties dominate. [Table 12.2](#) shows some important dimensions of the components we are dealing with. The dimensions of most single atoms are of the same order of 0.1 nm ($\text{nm} = \text{nanometer} = 10^{-9}\text{ m}$), but dependent on measuring conditions and bonds (free, covalent, ionic). Because this is such an important dimension, it was given a special unit, the ångstrom (\AA). However, in the internationally accepted SI system, the ångstrom unit is not used and it is not recommended. Even so, it is used in some disciplines.

$$1\text{\AA} = 10^{-10}\text{ m} = 0.1\text{ nm}.$$

When the dimension is smaller than the order of 1 nm , the rules of quantum mechanics prevail. The concept of a single, well-defined particle must be abandoned; we know neither the exact dimension nor position nor velocity of each particle. Our picture of a single electron is more like an electron gas or cloud, with a certain probability of finding it at a certain position. So it is also for the atoms of a gas. However, atoms in a solid evidently have more well-defined positions (e.g., in a crystal). But because of thermal vibrations, it is even here a question of a most probable position. Thermal (Brownian) movements are proportional to thermal energy and the Boltzmann factor kT , indicating an increasing uncertainty with temperature.

Our experienced macro-world where the laws of Newtonian physics are valid is based upon so many particles that the law of large numbers dominate. There is a gradual transition from single or a few particles quantum mechanical laws, to the classical laws governed by many particles in sum. *Tunnelling* is an example of a quantum mechanical effect violating macro-laws, where single electrons may cross an energy barrier over small distances of some 100 pm (e.g., from a metal electrode to an ion in the solution).

Table 12.2: Dimension of Particles

Particle	Dimensions	Remarks
Electron	10^{-15} (=1 fm)	Gas-like probability
Nuclei, most atoms	10^{-14}	Gas-like probability
Proton	10^{-14} (?)	Nucleus without electrons
Hydrogen	0.037 nm	Radius
Oxygen	0.066 nm	Radius
Nitrogen	0.07 nm	Radius
ions: Na^+ , O^- , Cl^-	0.10; 0.13; 0.18 nm	Solid state
Water molecule, approx.	0.1 nm	
Electric double layer	0.1–10 nm	Strong/diluted solution
Amino acid	0.5 nm	alanine
Small protein	3.6 nm	Myoglobin
Bilayer membrane, liposome	5 nm	
Membrane, human cell	7 nm	
Molecule, m.weight 14,000	1.5 nm	Myoglobin
Molecule, m.weight 500,000	50 nm	Myosin, length
Molecule, m.weight 4,000,000	120 nm	DNA, double helix length
Debye length	10 nm	Space charge region around an ion
Ribosome	15 nm	
Liposome sphere	25 nm	
Virus	20–200 nm	
Synaptic cleft	20 nm	
Mitocondries	0.1–5 μm	
Cell	2 μm	<i>Escherichia coli</i>
Cell	20 μm	Liver
Cell	5 μm ; 1 m	Nerve, diameter, length
Colloidal particles	1 nm–1 μm	Three-dimensional unlimited
Erythrocyte (red blood cell)	2; 8 μm	Thickness; diameter
Bacteria	0.2–2; 1–400 μm	Diameter; length
Electrode diffusion zone	0.01–0.5 mm	Stirred/unstirred

f(femto) = 10^{-15} , p(pico) = 10^{-12} , n(nano) = 10^{-9} , μ (micro) = 10^{-6} , m(milli) = 10^{-3} .

Defining the dimensions for a molecule may be difficult. Is a whole crystal to be regarded as a macromolecule? The large organic molecules may form a helix or a double helix, with a total string length many times the external helix length. The dimensions may change as a function of, for example, water content, and the whole molecule may be more or less rigid under stretch and torsion. The shape may vary from one moment to the next. Because molecules are continually rotating, their effective (apparent) volume is greater than their real volume. Two parameters are often used to specify dimensions: end-to-end distance and radius of gyration.

Of course, *volume* is sometimes a more relevant quantity than a linear dimension. Also weight and therefore density may be of interest. In molecular biology the *dalton* (Da) unit is sometimes used; it is the same as the relative atomic weight (without unit), with carbon-12 defined as 12 dalton.

References

Recommended Books and Review Articles

General Topics

- Attwood, S.S., 1956. Electric and Magnetic Fields, third ed. Dover Publications.
Castellan, G.W., 1971. Physical Chemistry. Addison-Wesley.
CRC, 1998. Handbook of Chemistry and Physics, 79th ed. CRC Press.
Gilbert, W., 1600. De Magnete. Dover.
Kreyszig, E., 1988. Advanced Engineering Mathematics. John Wiley.
Kuo, F.F., 1962. Network Analysis and Synthesis. Wiley International Edition.
Lorrain, P., Corson, D.P., Lorrain, F., 1988. Electromagnetic Fields and Waves. W H Freeman & Comp.
Maxwell, J.C., 1873. Treatise on Electricity and Magnetism. Oxford University Press.

Specialized Topics, in Chronological Order

- Akay, M., 1998. Time Frequency and Wavelets in Biomedical Signal Processing. IEEE Press.
Alberts, B., Bray, D., Lewis, J., 2007. Molecular Biology of the Cell. Taylor & Francis, London, England.
Bassingthwaite, J.B., Liebovitch, L.S., West, B.J., 1994. Fractal Physiology. Oxford University Press.
Berardesca, E., Elsner, P., Maibach, H.I., 1995. Bioengineering of the Skin. Cutaneous Blood Flow and Erythema. CRC Press.
Blaustein, M.P., 1984. Electrogenic Transport: Fundamental Principles and Physiological Implications. Raven Print.
Böttcher, C.J.F., 1973. Theory of Electric Polarisation. In: Dielectrics in Static Fields, second ed., vol. I. Elsevier.
Böttcher, C.J.F., Bordewijk, P., 1978. Theory of Electric Polarisation. In: Dielectrics in Time Dependent Fields, second ed., vol. III. Elsevier.
Cole, K.S., 1972. Membranes, Ions and Impulses. Univ. of California Press.
Cooper, R., Osselton, J.W., Shaw, J.C., 1980. EEG Technology. Butterworth.
Craig, D.Q.M., 1995. Dielectric Analysis of Pharmaceutical Systems. Taylor&Francis.
Daniel, V.V., 1967. Dielectric Relaxation. Academic Press.
Davis, M., 1965. Some Electrical and Optical Aspects of Molecular Behaviour. Pergamon.
Debye, P., 1929/45. Polar Molecules. Dover Publications.
Duck, F.A., 1990. Physical Properties of Tissue. A Comprehensive Reference Book. Academic Press.
Durney, C.H., Christensen, D.A., 1999. Basic Introduction to Bioelectromagnetics. CRC Press.
Elsner, P., Baradesca, E., Maibach, H., 1994. Bioengineering of the Skin: Water and the Stratum Corneum. CRC Press.
Feder, J., 1988. Fractals. Plenum Press.
Fluhr, J., Elsner, P., Berardesca, E., Maibach, H.I., 2005. Bioengineering of the Skin. Water and the Stratum Corneum. CRC Press.
Frölich, H., 1958. Theory of Dielectrics, second ed. Oxford Univ Press.
Gabler, R., 1978. Electrical Interactions in Molecular Biophysics: An Introduction. Acad. Press.
Geddes, L.A., Baker, L.E., 1989. Applied Biomedical Instrumentation. Wiley-Interscience.

- Geddes, L.A., 1972. *Electrodes and the Measurement of Bioelectric Events*. Wiley-Interscience.
- Grant, E.H., Sheppard, R.J., South, G.P., 1978. *Dielectric Behaviour of Biological Molecules in Solution*. Oxford Univ Press.
- Hasted, J.B., 1973. *Aqueous Dielectrics*. Chapman and Hall.
- Hill, N., Vaughan, W.E., Price, A.H., Davies, M., 1969. *Dielectric Properties and Molecular Behaviour*. Van Norstrand.
- Holder, D.S. (Ed.), 2005. *Electrical Impedance Tomography. Method, History and Applications*. Institute of Physics Publishing (IOP).
- Jonscher, A.K., 1983. *Dielectric Relaxation in Solids*. Chelsea Dielectrics Press.
- Koryta, J., 1991. *Ions, Electrodes and Membranes*. John Wiley.
- Low, J., Reed, A., 1994. *Electrotherapy Explained. Principles and Practice*. Butterworth-Heinemann.
- Macdonald, J.R., 1987. *Impedance Spectroscopy, Emphasizing Solid Materials and Systems*. John Wiley.
- Malmivuo, J., Plonsey, R., 1995. *Bioelectromagnetism*. Oxford Univ. Press.
- Miller, H.A., Harrison, D.C., 1974. *Biomedical Electrode Technology. Theory and Practice*. Acad. Press.
- Morucci, J.-P., Valentiniuzzi, M.E., Rigaud, B., Felice, C.J., Chauveau, N., Marsili, P.-M., 1996. Bioelectrical impedance techniques in medicine. *Crit. Rev. Biomed. Eng.* 24, 223–681.
- Neumann, E., Sowers, A.E., Jordan, C.A., 1989. *Electroporation and Electrofusion in Cell Biology*. Plenum Press.
- Nordenstrøm, B., 1983. *Biologically Closed Electric Circuits*. Nordic Medical Publications.
- Nunnally, J.C., Bernstein, I.H., 1994. *Psychometric Theory*. McGraw-Hill, New York.
- Nyboer, J., 1970a. *Electrical Impedance Plethysmography*. Charles Thomas.
- Nyboer, J., 1970b. Electrorheometric properties of tissues and fluids. *Ann. N.Y. Acad. Sci.* 170, 410–420.
- Pethig, R., 1979. *Dielectric and Electronic Properties of Biological Materials*. John Wiley.
- Plonsey, R., Barr, R.C., 1988. *Bioelectricity. A Quantitative Approach*. Plenum Press.
- Plonsey, R., Collin, R.E., 1961. *Principles and Applications of Electromagnetic Fields*. McGraw-Hill.
- Plonsey, R., Barr, C., 2000. *Bioelectricity, a Quantitative Approach*, second ed. Kluwer Academic/Plenum Publishers.
- Polk, C., Postow, E., 1996. *CRC Handbook of Biological Effects of Electromagnetic Fields*.
- Rajewsky, B., 1938. *Ergebnisse der Biophysikalischen Forschung*. Georg Thieme, Leipzig.
- Reilly, J.P., 1998. *Applied Bioelectricity. From Electrical Stimulation to Electropathology*. Springer.
- Riu, P.J., Rosell, J., Bragos, R., Casas, O., 1999. Electrical bioimpedance methods: applications to medicine and biotechnology. *Ann. N.Y. Acad. Sci.* 873.
- Schanne, O.F., Ruiz, P., Ceretti, E., 1978. *Impedance Measurements in Biological Cells*. John Wiley.
- Schwan, H.P., 2001. Selected Papers by Herman P Schwan. In: Grimnes, S., Martinsen, Ø.G. (Eds.). *Medisinskt teknisk avdelings forlag*, Norway.
- Silveira, F., Flandre, D., 2004. *Low Power Analog CMOS for Cardiac Pacemakers: Design and Optimization in Bulk and SOI Technologies*. Kluwer Academic Publishers, Boston, MA (USA).
- Smyth, C.P., 1955. *Dielectric Behaviour and Structure*. McGraw-Hill.
- Takashima, S., 1989. *Electrical Properties of Biopolymers and Membranes*. Adam Hilger.
- Tregear, R.T., 1966. *Physical Functions of Skin*. Academic Press, New York.
- Webster, J.G., 1990. *Electrical Impedance Tomography*. Adam Hilger.
- Webster, J., 1992. *Medical Instrumentation*. Houghton Mifflin.
- Zimmermann, U., Neil, G.A., 1996. *Electromanipulation of Cells*. CRC Press.

References

- Aaron, R., Esper, G.J., Shiffman, C.A., Bradonjic, K., Lee, K.S., Rutkove, S.B., 2006. Effects of age on muscle as measured by electrical impedance myography. *Physiol. Meas.* 27, 953–959.
- Aaron, R., Huang, M., Shiffman, C.A., 1997. Anisotropy of human muscle via non-invasive impedance measurements. *Phys. Med. Biol.* 42, 1245–1262.

- Aaron, R., Shiffman, C.A., 2000. Using localized impedance measurements to study muscle changes in injury and disease. *Ann. N.Y. Acad. Sci.* 904, 171–180.
- Abdul, S., Brown, B.H., Milnes, P., Tidy, J.A., 2005. A clinical study of the use of impedance spectroscopy in the detection cervical intraepithelial neoplasia (CIN). *Gynecol. Oncol.* 99, S64–S66.
- Åberg, P., Geladi, P., Nicander, I., Ollmar, S., 2002. Variation of skin properties within human forearms demonstrated by non-invasive detection and multi-way analysis. *Skin Res. Technol.* 8, 194–201.
- Åberg, P., Nicander, I., Ollmar, S., 2003a. Minimally invasive electrical impedance spectroscopy of skin exemplified by skin cancer assessment. In: Proceedings of the Annual International Conference of the IEEE Engineering in Medicine and Biology, pp. 3211–3214.
- Åberg, P., Nicander, I., Holmgren, U., Geladi, P., Ollmar, S., 2003b. Assessment of skin lesions and skin cancer using simple electrical impedance indices. *Skin Res. Technol.* 9, 257–261.
- Åberg, P., Nicander, I., Hansson, J., Geladi, P., Holmgren, U., Ollmar, S., 2004. Skin cancer identification using multi-frequency electrical impedance – a potential screening tool. *IEEE Trans. Biomed. Eng.* 51, 2097–2102.
- Åberg, P., Geladi, P., Nicander, I., Hansson, J., Holmgren, U., Ollmar, S., 2005. Non-invasive and microinvasive electrical impedance spectra of skin cancer – a comparison between two techniques. *Skin Res. Technol.* 11, 281–286.
- Åberg, P., Birgersson, U., Elsner, P., Mohr, P., Ollmar, S., 2013. Electrical impedance spectroscopy and the diagnostic accuracy for malignant melanoma. *Exp. Dermatol.* 20, 648–652.
- Abramson, H.A., Gorin, M.H., 1939. Skin reactions VII. Relationship of skin permeability to electrophoresis of biologically active materials into the living human skin. *J. Phys. Chem.* 43, 335–346.
- Abramson, H.A., Gorin, M.H., 1940. Skin reactions IX. The electrophoretic demonstration of the patent pores of the living human skin; its relation to the charge of the skin. *J. Phys. Chem.* 44, 1094–1102.
- Ackmann, J.J., Seitz, M.A., 1984. Methods of complex impedance measurements in biological tissue. CRC Crit. Rev. Biomed. Eng. 11 (4), 281–311.
- Ahn, A.C., Gow, B.J., Martinsen, O.G., Zhao, M., Grodzinsky, A.J., Baikie, I.D., June 2012. Applying the Kelvin probe to biological tissues: theoretical and computational analyses. *Phys. Rev. E Stat. Nonlin. Soft Matter Phys.* 85 (6 Pt 1), 061901.
- Akay, M., 1998. Time Frequency and Wavelets in Biomedical Signal Processing. IEEE Press.
- Alanen, E., Lahtinen, T., Nuutinen, J., 1998. Measurement of dielectric properties of subcutaneous fat with open-ended coaxial sensors. *Phys. Med. Biol.* 43, 475–485.
- Aliau-Bonet, C., Pallas-Areny, R., 2012. On the effect of body capacitance to ground in tetrapolar bioimpedance measurements. *IEEE Trans. Biomed. Eng.* 59, 3405–3411.
- Aliau-Bonet, C., Pallas-Areny, R., 2013. A novel method to estimate body capacitances to ground at mid frequencies. *IEEE Trans. Instrum. Meas.* 62, 2519–2525.
- Almasi, J.J., Schmitt, O.H., 1970. Systemic and random variations of ECG electrode system impedance. *Ann. N.Y. Acad. Sci.* 170, 509–519.
- Amoussou-Guenou, K.M., Teyssier, F., Squitiero, B., Voutay, M., Rusch, Ph., Healy, J.C., 1995. Second generation of cell transit analyzer. *Innov. Technol. Biol. Med.* 16 (5), 609–622.
- Anfinsen, O.-G., Kongsgaard, E., Foerster, A., Aass, H., Amlie, J.P., 1998. Radio frequency current ablation of porcine right atrium: Increased lesion of bipolar two catheter technique compared to unipolar application in vitro and in vivo. *Pacing Clin. Electrophysiol.* 21, 69–78.
- Annus, P., Min, M., Ojarand, J., Paavle, T., Land, R., Ellerjee, P., Parve, T., 2012. Multisine and Binary Multifrequency Waveforms in Impedance Spectrum Measurement - A Comparative Study. In: IFMBE Proceedings, 37. Springer-Verlag, Berlin Heidelberg, pp. 265–268.
- Anonymous 1, 1997. Rheoencephalograph. (a) Identification. Code of Federal Regulations. Sec. 882.1825, vol. 8. U.S. Government Printing Office, Washington, DC. Title 21, Parts 800 to 1299; revised April 1. [CITE: 21CFR882.1825].
- Arlot, S., Celisse, A., 2010. A survey of cross-validation procedures for model selection. *Stat. Surv.* 4, 40–79.
- Arnold, W.M., Zimmerman, U., 1982. Rotating-field-induced rotation and measurement of the membrane capacitance of single mesophyll cells of *Avena sativa*. *Z. Naturforsch.* C37, 908–915.

- Asami, K., Gheorghiu, E., Yonezawa, T., 1999. Real-time monitoring of yeast cell division by dielectric spectroscopy. *Biophys. J.* 76, 3345–3348.
- Bacchetti, P., Wolf, L.E., Segal, M.R., McCulloch, C.E., 2005. Ethics and sample size. *Am. J. Epidemiol.* 161 (2), 105–110.
- Baden, H.P., 1970. The physical properties of nail. *J. Invest. Dermatol.* 55, 115–122.
- Baikie, I.D., Estrup, P.J., 1998. Low cost PC based scanning Kelvin probe. *Rev. Sci. Instrum.* 69 (11), 3902–3907.
- Baikie, I.D., Venderbosch, E., Meyer, J.A., Estrup, P.J.Z., 1991a. Analysis of stray capacitance in the Kelvin method. *Rev. Sci. Instrum.* 62 (3), 725–735.
- Baikie, I.D., Mackenzie, S., Estrup, P.J.Z., Meyer, J.A., 1991b. Noise and the Kelvin method. *Rev. Sci. Instrum.* 62 (5), 1326–1332.
- Baikie, I.D., Smith, P.J.S., Porterfield, D.M., Estrup, P.J., 1999. *Rev. Sci. Instrum.* 70, 1842.
- Balleza, M., Fornos, J., Calaf, N., Feixas, T., Gonzalez, M., Anton, D., Riu, P., Casan, P., 2007. Monitoring of breathing pattern at rest by electrical impedance tomography. *Arch. Bronconeumol.* 43 (6), 300–303.
- Barker, A.T., Jalinous, R., Freeston, I.L., 1985. Non invasive magnetic stimulation of the human motor cortex. *Lancet* 1, 1106–1107.
- Barlett, J.W., Frost, C., 2008. Reliability, repeatability and reproducibility: analysis of measurement errors in continuous variables. *Ultrasound Obstet. Gynecol.* 31, 466–475.
- Barnes, F.S., Greenbaum, B., 2006. *Handbook of Biological Effects of Electromagnetic Fields*, third ed. CRC Press.
- Barnett, A., 1937. The basic factors involved in proposed electrical methods for measuring thyroid function. III The phase angle and the impedance of the skin. *West. J. Surg. Obstet. Gynecol.* 45, 540–554.
- Bayford, R., Tizzard, A., 2012. Bioimpedance imaging: an overview of potential clinical applications. *Analyst* 137, 4635–4643.
- Becker, F.F., Wang, X.-B., Huang, Y., Pethig, R., Vykoukal, J., Gascoyne, P.R.C., 1994. The removal of human leukaemia cells from blood using interdigitated microelectrodes. *J. Phys. D: Appl. Phys.* 27, 2659–2662.
- Becker, F.F., Wang, X.-B., Huang, Y., Pethig, R., Vykoukal, J., Gascoyne, P.R.C., 1995. Separation of human breast cancer cells from blood by differential dielectric affinity. *Proc. Natl. Acad. Sci. U.S.A.* 92, 860–864.
- Bedard, C., Destexhe, A., 2009. Macroscopic models of local field potentials and the apparent 1/f noise in brain activity. *Biophys. J.* 96, 2589–2603.
- Belmont, B., Dodde, R.E., Shih, A.J., 2013. Impedance of tissue-mimicking phantom material under compression. *J. Electr. Bioimp.* 4, 2–12.
- Bernstein, D.P., 1986. A new stroke volume equation for thoracic electrical bioimpedance: theory and rationale. *Crit. Care Med.* 14 (10), 904–909.
- Bernstein, D.P., 2010. Impedance cardiography: pulsatile blood flow and the biophysical and electrodynamic basis for the stroke volume equations. *J. Electr. Bioimp.* 1, 2–17.
- Bernstein, D.P., Lemmens, H.J.M., 2005. Stroke volume equation for impedance cardiology. *Med. Biol. Eng. Comput.* 43, 443–450.
- Bernstein, D.P., Osypka, M.J. Apparatus and Method for Determining an Approximation of the Stroke Volume and the Cardiac Output of the Heart. US Patent 6,511,438 B2, 2003.
- Bhatt, D.L., Gaylor, D.C., Lee, R.C., 1990. Rhabdomyolysis due to pulses electric fields. *Plast. Reconstr. Surg.* 86, 1–11.
- Bickford, R.G., Fremming, B.D., 1965. Neural stimulation by pulsed magnetic fields in animals and man. In: Digest of the 6th International Conference on Medical Electronics and Biological Engineering (Tokyo), Paper 7–6.
- Birgersson, U., Birgersson, E., Åberg, P., Nicander, I., Ollmar, S., 2011. Non-invasive bioimpedance of intact skin: mathematical modeling and experiments. *Physiol. Meas.* 32, 1–18.
- Birgersson, U., Birgersson, E., Nicander, I., Ollmar, S., 2013. A methodology for extracting the electrical properties of human skin. *Physiol. Meas.* 34, 723–736.
- Blad, B., 1996. Clinical applications of characteristic frequency measurements: preliminary in vivo study. *Med. Biol. Eng. Comput.* 34 (5), 362–365.

- Bland, J.M., Altman, D.G., 1986. Statistical methods for assessing agreement between two methods of clinical measurement. *Lancet* 8, 307–310.
- Bland, J.M., Altman, D.G., 1990. A note on the use of the intraclass correlation coefficient in the evaluation of agreement between two methods of measurement. *Comput. Biol. Med.* 20, 337–340.
- Bland, J.M., Altman, D.G., 1999. Measuring agreement in method comparison studies. *Stat. Methods Med. Res.* 8, 135–160.
- Bland, J.M., Bland, D.G., 1994. Statistics notes: one and two sided tests of significance. *BMJ* 309, 248. <http://dx.doi.org/10.1136/bmj.309.6949.248> (Published July 23, 1994) Cite this as: *BMJ* 1994;309:248.
- Block, H., Hayes, E.F., 1970. Dielectric behavior of stiff polymers in solution when subjected to high voltage gradients. *Trans. Faraday Soc.* 66, 2512–2525.
- Bodo, M., et al., 2004. Cerebral blood flow changes: rat studies in rheoencephalography. *Physiol. Meas.* 25, 1371–1384.
- Bodo, M., Pearce, F.J., Baranyi, L., Armonda, R.A., 2005a. Changes in the intracranial rheoencephalogram at lower limit of cerebral blood flow autoregulation. *Physiol. Meas.* 26, S1–S17.
- Bodo, M., et al., 2005b. Cerebrovascular involvement in liposome – induced cardiopulmonary distress in pigs. *J. Liposome Res.* 15, 3–14.
- Bodo, M., Pearce, F.J., Sowd, M., 2006. In vitro and In vivo Studies for a Bio-Impedance Vital-Sign Monitor. Technical report; Defense Technical Information Center; DTIC# ADA460555 Fort Belvoir, VA, USA. <http://www.dtic.mil/>.
- Bodo, M., Pearce, F., Van Albert, S., Armonda, R., 2007. Rheoencephalogram reflects cerebral blood flow autoregulation in pigs. In: Scharfetter, H., Merva, R. (Eds.), ICEBI 2007, IFMBE Proceedings, 17, pp. 695–698.
- Bogonez-Franco, P., Nescolarde, L., Bragos, R., Rosell-Ferrer, J., Yandiola, I., 2009. Measurement errors in multifrequency bioelectrical impedance analyzers with and without impedance electrode mismatch. *Physiol. Meas.* 30, 573–587.
- Bogonez-Franco, P., Nescolarde, L., Galvez-Monton, C., Bragos, R., Rosell-Ferrer, J., 2013. An implantable bioimpedance monitor using 2.45 GHz band for telemetry. *Physiol. Meas.* 34, 1–16.
- Bonferroni, C.E., 1936. Teoria statistica delle classi e calcolo delle probabilità. In: Pubblicazioni del R Istituto Superiore di Scienze Economiche e Commerciali di Firenze, vol. 8, 3–62.
- Bosy-Westphal, A., Schautz, B., Later, W., Kehayias, J.J., Gallagher, D., Müller, M.J., January 2013. What makes a BIA equation unique? Validity of eight-electrode multifrequency BIA to estimate body composition in a healthy adult population. *Eur. J. Clin. Nutr.* 67 (Suppl. 1), S14–S21.
- Bozler, E., Cole, K.S., 1935. Electric impedance and phase angle of muscle in rigor. *J. Cell. Comp. Physiol.* 6, 229–241.
- Bragos, R., Rosell, J., Riu, P., 1994. A wide-band AC-coupled current source for electrical impedance tomography. *Physiol. Meas.* 15 (Suppl. A), 91–99.
- Breiman, L., Friedman, J., Olshen, R., Stone, C., 1984. Classification and Regression Trees. Wadsworth, Belmont, California. Dowdy, Wearden, Chilko. Statistics for Research. (Wiley Series in Probability and Statistics).
- Brown, B.H., Barber, D.C., Wang, W., Lu, L., Leathard, A.D., Smallwood, R.H., Hampshire, A.R., Mackay, R., Hatzigalanis, K., 1994a. Multi-frequency imaging and modelling of respiratory related electrical impedance changes. *Physiol. Meas.* 15 (Suppl.), 1–12.
- Brown, B.H., Barber, D.C., Leathard, A.D., Lu, L., Wang, W., Smallwood, R.H., Wilson, A.J., 1994b. High frequency EIT data collection and parametric imaging. *Innov. Technol. Biol. Med.* 15 (1), 1–8.
- Bruggeman, D.A.G., 1935. Berechnung verschiedener physikalischer Konstanten von heterogenen Substanzen. *Ann. Phys. (Leipzig)* 24, 636–679.
- Brunner, P., Merwa, R., Missner, A., Rosell, J., Hollaus, K., Scharfetter, H., 2006. Reconstruction of the shape of conductivity spectra using differential multi-frequency magnetic induction tomography. *Physiol. Meas.* 27, S237–S248.

- Buderer, N.M., 1996. Statistical Methodology: I. Incorporating the Prevalence of Disease into the Sample Size Calculation for Sensitivity and Specificity.
- Burger, H.C., van Milaan, J.B., 1946. Heart vector and leads. *Br. Heart J. Part I*: 8, 157; *Part II* (1947): 9, 154; *Part III* (1948): 229.
- Burgess, H.J., Penev, P.D., Schneider, R., Van Cauter, E., 2004. Estimating cardiac autonomic activity during sleep: impedance cardiography, spectral analysis, and Poincaré plots. *Clin. Neurophysiol.* 115, 19–28.
- Burt, J.P.H., Pethig, R., Talary, M.S., 1998. Microelectrode devices for manipulating and analysing bioparticles. *Trans. Inst. Meas. Control* 20, 82–90.
- Büscher, P., Tröltzsch, U., Kanoun, O., 2011. Use of stochastic methods for robust parameter extraction from impedance spectra. *Electrochim. Acta* 56, 8069–8077.
- Capecci, M.R., 1980. High efficiency transformation by direct microinjection of DNA into cultured mammalian cells. *Cell* 22, 479–488.
- Casañas, R., Scharfetter, H., Altes, A., Remacha, A., Sarda, P., Sierra, J., Merwa, R., Hollaus, K., Rosell, J., 2004. Measurement of liver iron overload by magnetic induction using a planar gradiometer: preliminary human results. *Physiol. Meas.* 25 (1), 1095–1103.
- Casas, O., Bragos, R., Riu, P., Rosell, J., Tresanchez, M., Warren, M., Rodriguez-Sinovas, A., Carreño, A., Cinca, J., 1999. In-vivo and in-situ ischemic tissue characterisation using electrical impedance spectroscopy. *Ann. N.Y. Acad. Sci.* 873, 51–59.
- Chang, D.C., 1989. Cell poration and cell fusion using an oscillating electric field. *Biophys. J.* 56, 641–652.
- Chernomordik, L.V., Sukharev, S.I., Abidor, I.G., Chizmadzhev, Yu.A., 1982. The study of the BLM reversible electrical breakdown mechanism in the presence of UO_2^{2+} . *Bioelectrochem. Bioenerg.* 9, 149–155.
- Chilcott, T.C., Coster, H.G.L., 1991. AC impedance measurements on Chara Corallina. I: Characterization of the static cytoplasm. *Aust. J. Plant Physiol.* 18 (2), 191–199.
- Chiu, D.T., Lillard, S.J., Scheller, R.H., Zare, R.N., Rodriguez-Cruz, S.E., Williams, E.R., Orwar, O., Sandberg, M., Lundqvist, J.A., 1998. Probing single secretory vesicles with capillary electrophoresis. *Science* 279, 1190–1193.
- Chow, R.H., Von Ruden, L., Neher, E., 1992. Delay in vesicle fusion revealed by electrochemical monitoring of single secretory events in adrenal chromaffin cells. *Nature* 356, 60–63.
- Chua, L.O., 1971. Memristor – the missing circuit element. *IEEE Trans. Circuit Theory* 18, 507–519.
- Cole, K.S., 1928a. Electrical impedance of suspension of spheres. *J. Gen. Physiol.* 12, 29–36.
- Cole, K.S., 1928b. Electrical impedance of suspension of arbacia cells. *J. Gen. Physiol.* 12, 37–54.
- Cole, K.S., 1932. Electrical phase angle of cell membranes. *J. Gen. Physiol.* 15, 641–649.
- Cole, K.S., 1934. Alternating current conductance and direct current excitation of nerve. *Science* 79, 164–165.
- Cole, K.S., 1940. Permeability and impermeability of cell membranes for ions. *Cold Spring Harb. Symp. Quant. Biol.* 8, 110–122.
- Cole, K.S., Cole, R.H., 1941. Dispersion and absorption in dielectrics. I. Alternating current characteristics. *J. Chem. Phys.* 9, 341–351.
- Cole, R.H., Berberian, J.G., Mashimo, S., Chryssikos, G., Burns, A., Tombari, E., 1989. Time domain reflection methods for dielectric measurements to 10 GHz. *J. Appl. Phys.* 66, 793–802.
- Cooper, R., 1946. The electrical properties of salt-water solutions over the frequency range 1–4000 Mc/s. *J. Inst. Electr. Eng.* 93, 69–75.
- Cornish, B.H., Thomas, B.J., Ward, L.C., 1993. Improved prediction of extracellular and total body water using impedance loci generated by multiple frequency bioelectrical impedance analysis. *Phys. Med. Biol.* 38, 337.
- Cornish, B.H., Jacobs, A., Thomas, B.J., Ward, L.C., 1999. Optimising electrode sites for segmental bioimpedance measurements. *Physiol. Meas.* 20, 241–250.
- Critchley, L.A.H., Critchley, J.A.J.H., 1999. A meta-analysis of studies using bias and precision statistics to compare cardiac output measurement techniques. *J. Clin. Monit. Comput.* 15, 85–91.
- Dalziel, C.F., 1954. The threshold of perception currents. *AIEE Trans. Power App. Syst.* 73, 990–996.
- Dalziel, C.F., 1972. Electric shock hazard. *IEEE Spectr.* 9, 41.

- Danilov, A.A., Nikolaev, D.V., Rudnev, S.G., Salamatova, V.Y., Vassilevski, Y.V., 2013. Modelling of bioimpedance measurements: unstructured mesh application to real human anatomy. *Russ. J. Num. Anal. Mathem. Model.* 27, 431–440.
- Davalos, R., Rubinsky, B., Huang, Y., 2000. Electroporation: bio-electrochemical mass transfer at the nano scale. *Microscale Thermophys. Eng.* 4, 147–159.
- Davalos, R.V., Otten, D.M., Mir, L.M., Rubinsky, B., 2004. Electrical impedance tomography for imaging tissue electroporation. *IEEE Trans. Biomed. Eng.* 51, 761–767.
- Davalos, R.V., Mir, L.M., Rubinsky, B., 2005. Tissue ablation with irreversible electroporation. *Ann. Biomed. Eng.* 33, 223–231.
- Davidson, D.W., Cole, R.H., 1951. Dispersion and absorption in dielectrics. *J. Chem. Phys.* 9, 341–351.
- Davis, J.M., Giddings, J.C., 1986. Feasibility study of dielectric field-flow fractionation. *Sep. Sci. Technol.* 21, 969–989.
- De Lorenzo, A., Andreoli, A., Matthie, J., Withers, P., 1997. Predicting body cell mass with bioimpedance by using theoretical methods: a technology review. *J. Appl. Physiol.* 82, 1542–1558.
- De Vet, H.C.W., Terwee, C.B., Knol, D.L., Bouter, L.M., 2006. When to use agreement versus reliability measures. *J. Clin. Epidemiol.* 59, 1033–1039.
- Demidenko, E., 2013. Mixed Models: Theory and Applications with R, second ed. Wiley.
- Devroye, L., Wagner, T., 1979. Distribution-free performance bounds for potential function rules. *IEEE Trans. Inf. Theory* 25, 601–604.
- Di Ventra, M., Pershin, Y.V., Chua, L.O., 2009. Circuit elements with memory: memristors, memcapacitors and meminductors. *Proc. IEEE* 97, 1717–1724.
- Dissado, L.A., Hill, R.M., 1979. Non-exponential decay in dielectrics and dynamics in correlated systems. *Nature* 279, 685–689.
- Dreiseitl, S., Ohno-Machado, L., 2003. Logistic regression and artificial neural network classification models: a methodology review. *J. Biomed. Inform.* 35, 352–359.
- Dyre, J.C., Schröder, T.B., 2000. RMP Colloquia: universality of AC conduction in disordered solids. *Rev. Mod. Phys.* 72 (3), 873–892.
- d'Arsonval, M.A., 1893. Production des courants de haute fréquence et de grand intensité; leurs effets physiologiques. *Comptes Rendus Soc de Biol* 45, 122–124.
- Ebert, T., Smith, J., Barney, J., et al., 1986. The use of thoracic impedance for determining thoracic blood volume changes in man. *Aviat. Space Environ. Med.* 57, 49–53.
- Edd, J.F., Davalos, R.V., 2007. Mathematical modeling of irreversible electroporation for treatment planning. *Technol. Cancer Res. Treat.* 6, 275–286.
- Edd, J., Horowitz, L., Davalos, R., Mir, L., Rubinsky, B., 2006. In vivo results of a new focal tissue ablation technique: irreversible electroporation. *IEEE Trans. Biomed. Eng.* 53, 1409–1415.
- Einthoven, W., Fahr, G., de Waart, A., 1913. Über die Richtung und die manifeste Grösse der Potentialschwankungen in menschlichen Hertzen und über den Einfluss der Herzlage auf die Form des Elektrokardiogramms. *Pfluger Arch. ges. Physiol.* 150, 275–315.
- Emtestam, L., Nyrén, M., 1997. Electrical impedance for quantification and classification of experimental skin reactions. *Am. J. Contact Dermat.* 8 (4), 202–206.
- Emtestam, L., Nicander, I., Stenström, M., Ollmar, S., 1998. Electrical impedance of nodular basal cell carcinoma: a pilot study. *Dermatology* 197, 313–316.
- Emtestam, L., Kuzmina, N., Talme, T., 2007. Evaluation of the effects of topical clobetasol propionate by visual score, electrical impedance and laser Doppler flowmetry. *Skin Res. Technol.* 13, 73–78.
- Epstein, B.R., Foster, K.R., 1983. Anisotropy in the dielectric properties of skeletal muscles. *Med. Biol. Eng. Comput.* 21, 51.
- Ermishkin, V.V., Kolesnikov, V.A., Lukoshkova, E.V., Mokh, V.P., Sonina, R.S., Dupik, N.V., Boitsov, S.A., 2012. Variable impedance cardiography waveforms: how to evaluate the preejection period more accurately. *J. Phys. Conf. Ser.* 407, 012016.

- Ermishkin, V.V., Kolesnikov, V.A., Lukoshkova, E.V., Sonina, R.S., 2013. Simulation of ‘pathologic’ changes in ICG waveforms resulting from superposition of the ‘preejection’ and ejection waves induced by left ventricular contraction. *J. Phys. Conf. Ser.* 434, 0120007.
- Esper, G.J., Lee, K.S., Shiffman, C.A., Aaron, R., Bradonjic, K., Rutkove, S.B., 2005. Electrical impedance myography in the assessment of age-associated muscle change. In: 52nd Annual Scientific Meeting for the American Association for Neuromuscular and Electrodiagnostic Medicine. Monterey, CA, USA.
- Esser, A.T., Smith, K.C., Gowrishankar, T.R., Weaver, J.C., 2007. Towards solid tumor treatment by irreversible electroporation: intrinsic redistribution of fields and currents in tissue. *Technol. Cancer Res. Treat.* 6, 261–274.
- Etter, H.S., Pudenz, R.H., Gersh, I., 1947. The effects of diathermy on tissues contiguous to implanted surgical materials. *Arch. Phys. Med. Rehabil.* 28, 333–344.
- Fawcett, T., 2005. An introduction to ROC analysis. *Pattern Recognit. Lett.* 27, 861–874.
- Fein, A., Grossman, R.F., Jones, G., et al., 1979. Evaluation of transthoracic electrical impedance in the diagnosis of pulmonary edema. *Circulation* 60, 1156–1160.
- Feldman, Y., Ermolina, I., Hayashi, Y., 2003. Time domain dielectric spectroscopy study of biological systems. *IEEE Trans. Dielectr. Electr. Insul.* 10, 728–753.
- Fink, H.-W., Schönenberger, C., 1999. Electrical conduction through DNA molecules. *Nature* 398, 407–410.
- Forslind, B., 1970. Biophysical studies of the normal nail. *Acta Derm. Venereol. (Stockh)* 50, 161–168.
- Foster, K.R., Schwan, H.P., 1986. Dielectric properties of tissue. In: Polk, C., Postow, E. (Eds.), Part I: Dielectric Permittivity and Electrical Conductivity of Biological Materials. CRC Handbook of Biological Effects of Electromagnetic Fields. CRC Press.
- Foster, K.R., Schwan, H.P., 1989. Dielectric properties of tissue. *CRC Crit. Rev. Biomed. Eng.* 17, 25–104.
- Foster, K.R., Epstein, B.R., Gealt, M.A., 1987. “Resonances” in the dielectric absorption of DNA? *Biophys. J.* 52, 421–425.
- Fox, M.B., Esveld, D.C., Valero, A., Luttge, R., Mastwijk, H.C., Bartels, P.V., van den Berg, A., Boom, R.M., 2006. Electroporation of cells in microfluidic devices: a review. *Anal. Bioanal. Chem.* 385, 474–485.
- Franke, E.K., Braunstein, J.R., Zellner, D.C., 1962. Study of high-frequency components in electrocardiogram by power spectrum analysis. *Circ. Res.* 10, 870.
- Frantescu, C.G., Wesner, D., Pliquett, U., Neumann, E., 2004. Unsymmetrical non-linearity in cell membranes. In: Proceedings of the XII. International Conference on Electrical Bio-impedance, Gdansk, p. 41.
- Freeman, S.A., Wang, M.A., Weaver, J.C., 1994. Theory of electroporation of planar bilayer membranes: predictions of the aqueous area, change in capacitance, and pore-pore separation. *Biophys. J.* 67, 42–56.
- Freiburger, H., 1933. Der elektrische Widerstand des menschlichen Körpers gegen technischen Gleich – und Wechselstrom. *Elektrizitätswissenschaft* 32, 373–375, 442–446.
- Fricke, H., 1924. A mathematical treatment of the electrical conductivity and capacity of disperse systems. I. The electrical conductivity of a suspension of homogeneous spheroids. *Phys. Rev.* 24, 575–587.
- Fricke, H., 1925. A mathematical treatment of the electrical conductivity and capacity of disperse systems. II. The capacity of a suspension of conducting spheroids surrounded by a non-conducting membrane for a current of low frequency. *Phys. Rev.* 26, 678–681.
- Fricke, H., Morse, S., 1926. The electric capacity of tumors of the breast. *J. Cancer Res.* 10, 340–376.
- Fricke, H., 1932. Theory of electrolytic polarisation. *Philos. Mag.* 14, 310–318.
- Fuhr, G., Hagedorn, R., Müller, T., Benecke, W., Wagner, B., Gimsa, J., 1991. Asynchronous travelling-wave induced linear motion of living cells. *Stud. Biophys.* 140, 79–102.
- Fuhr, G., Zimmermann, U., Shirley, S.G., 1996. Cell motion in time-varying fields: principles and potential. In: Zimmermann, U., Neil, G.A. (Eds.), Electromanipulation of Cells. CRC Press, Boca Raton.
- Gabor, D., 1946. Theory of communication. *JIEE* 93, 429–457.
- Gabriel, C., Gabriel, S., Corthout, E., 1996a. The dielectric properties of biological tissue: I, literature survey. *Phys. Med. Biol.* 41, 2231–2249.
- Gabriel, S., Lau, R.W., Gabriel, C., 1996b. The dielectric properties of biological tissue: II. Measurements in the frequency range 10 Hz to 20 GHz. *Phys. Med. Biol.*, 2251–2269.

- Gabrielli, C., 1984. Identification of Electrochemical Processes by Frequency Response Analysis. Solartron Technical report number 004/83.
- Gandhi, S.V., Walker, D., Milnes, P., Mukherjee, S., Brown, B.H., Anumba, D.O.C., 2006. Electrical impedance spectroscopy of the cervix in non-pregnant and pregnant women. *Eur. J. Obstet. Gynecol. Reprod. Biol.* 129, 145–149.
- Gao, J., Yin, X.F., Fang, Z.L., 2004. Integration of single cell injection, cell lysis, separation and detection of intracellular constituents on a microfluidic chip. *Lab Chip* 4, 47–52.
- Gaw, R.L., Cornish, B.H., Thomas, B.J., 2009. Decay properties of the experimental electrical impedance of pulsatile blood flowing through rigid tubes. In: Dössel, O., Schlegel, W.C. (Eds.), WC2009, IFMBE Proceedings 25/XII, pp. 259–262.
- Geddes, L.A., Baker, L.E., 1966. The relationship between input impedance and electrode area in recording the ECG. *Med. Biol. Eng.* 4, 439–450.
- Geddes, L.A., Baker, L.E., 1967. The specific resistance of biological material – a compendium of data for the biomedical engineer and physiologist. *Med. Biol. Eng.* 5, 271–293.
- Geddes, L.A., Valentiniuzzi, M.E., 1973. Temporal changes in electrode impedance while recording the electrocardiogram with “dry” electrodes. *Ann. Biomed. Eng.* 1, 356–367.
- Geddes, L.A., Tacker, A., Cabler, B., Kidder, H., Gothard, R., 1975a. The impedance of electrodes used for ventricular defibrillation. *Med. Instrum.* 9, 177–178.
- Geddes, L.A., Tacker, A., Cabler, B., Chapman, R., Rivera, R., Kidder, H., 1975b. The decrease in transthoracic impedance during successive ventricular defibrillation trials. *Med. Instrum.* 9, 179–180.
- Geddes, L.A., Tacker, A., Schoenlein, W., Minton, M., Grubbs, S., Wilcox, P., 1976. The prediction of the impedance of the thorax to defibrillating current. *Med. Instrum.* 10, 159–162.
- Geisser, 1975. The predictive sample reuse method with applications. *J. Am. Stat. Assoc.* 60, 320–328.
- Gencer, N.G., Ider, Y.Z., 1994. A comparative study of several exciting magnetic fields for induced current EIT. *Physiol. Meas.* 15 (Suppl. 2A), 51–57.
- Gersing, E., 1991. Measurement of electrical impedance in organs – measuring equipment for research and clinical applications. *Biomed. Tech.* 36 (1–2), 6–11.
- Gersing, E., 1998. Impedance spectroscopy on living tissue for determination of the state of organs. *Bioelectrochem. Bioenerg.* 45 (2), 145–149.
- Gersing, E., Krüger, W., Osypka, M., Vanupel, P., 1995. Problems involved in temperature measurements using EIT. *Physiol. Meas.* 16 (Suppl. 3A), 153–160.
- Geselowitz, D.B., 1971. An application of electrocardiographic lead theory to impedance plethysmography. *IEEE Trans. Biomed. Eng.* 18, 38–41.
- Gheorghiu, E., 1993. The resting potential in relation with the equivalent complex permittivity of a spherical cell suspension. *Phys. Med. Biol.* 38, 979–989.
- Gheorghiu, E., 1994. The dielectric behaviour of suspensions of spherical cells: a unitary approach. *J. Phys. A: Math. Gen.* 27, 3883–3893.
- Gheorghiu, E., 1996. Measuring living cells using dielectric spectroscopy. *Bioelectrochem. Bioenerg.* 40 (2), 133–139.
- Gheorghiu, E., 1999. On the limits of ellipsoidal models when analyzing dielectric behavior of living cells: emphasis on red blood cells. *Ann. N.Y. Acad. Sci.* 873, 262–268.
- Gheorghiu, M., Gersing, E., Gheorghiu, E., 1999. Quantitative analysis of impedance spectra of organs during ischemia. *Ann. N.Y. Acad. Sci.* 873, 65–71.
- Gheorghiu, E., Balut, C., Gheorghiu, M., 2002. Dielectric behaviour of gap junction connected cells: a microscopic approach. *Phys. Med. Biol.* 47, 341–348.
- Giaever, I., Keesee, C.R., 1993. A morphological biosensor for mammalian cells. *Nature* 366. Product Review, 591–592.
- Gibson, L.E., Cooke, R.E., 1959. A test for concentration of electrolytes in sweat in cystic fibrosis of the pancreas utilising pilocarpine by iontophoresis. *Pediatrics* 23, 545–549.

- Gift, E.A., Weaver, J.C., 1995. Observation of extremely heterogeneous electroporative molecular uptake by *Saccharomyces cerevisiae* which changes with electric field pulse amplitude. *Biochim. Biophys. Acta* 1234, 52–62.
- Gimsa, J., 2012. AC-electrokinetic applications in cell chips: basic understanding and modeling of structural polarization effects. *IFMBE Proc.* 37, 1242–1245.
- Gisser, D.G., Isaacson, D., Newell, J.C., 1987. Current topics in impedance imaging. *Clin. Phys. Physiol. Meas.* 8 (Suppl. A), 39–46. PMID: 3568569.
- Goldman, D.E., 1943. Potential, impedance and rectification in membranes. *J. Gen. Physiol.* 27, 37–60.
- Gordon, D.H., 1975. Triboelectric interference in the ECG. *IEEE Trans. Biomed. Eng.*, 252–255.
- Gotshall, R., Davrath, L., 1999. Bioelectric impedance as an index of thoracic fluid. *Aviat. Space Environ. Med.* 70 (1), 58–61.
- Gougerot, L., Foucher, M., 1972. La membrane de l'hématie est-elle un dielectrique parfait? *Ann. Phys. Biol. Med.* 6, 17–42.
- Gow, B.J., Cheng, J.L., Baikie, I.D., Martinsen, O.G., Zhao, M., Smith, S., Ahn, A.C., 2012. Electrical potential of acupuncture points: use of a noncontact scanning Kelvin probe. *Evidence-Based Complementary Altern. Med.* 2012, 632838.
- Grahame, D.C., 1952. Mathematical theory of the faradaic admittance. *J. Electrochem. Soc.* 99, 370c–385c.
- Greatbatch, W., 1967. Electrochemical polarization of physiological electrodes. *Med. Res. Eng.* 6, 13–17.
- Griffiths, H., Ahmed, A., 1987. Applied potential tomography for non-invasive temperature mapping in hypertermia. *Clin. Phys. Physiol. Meas.* 8 (Suppl. A), 147–153.
- Grimnes, S., 1982. Psychogalvanic reflex and changes in electrical parameters of dry skin. *Med. Biol. Eng. Comput.* 20, 734–740.
- Grimnes, S., 1983a. Impedance measurement of individual skin surface electrodes. *Med. Biol. Eng. Comput.* 21, 750–755.
- Grimnes, S., 1983b. Skin impedance and electro-osmosis in the human epidermis. *Med. Biol. Eng. Comput.* 21, 739–749.
- Grimnes, S., 1983c. Dielectric breakdown of human skin in vivo. *Med. Biol. Eng. Comput.* 21, 379–381.
- Grimnes, S., 1983d. Electrovibration, cutaneous sensation of microampere current. *Acta Physiol. Scand.* 118, 19–25.
- Grimnes, S., 1984. Pathways of ionic flow through human skin in vivo. *Acta Derm. Venereol. (Stockh)* 64, 93–98.
- Grimnes, S., Martinsen, Ø.G., 2005. Cole electrical impedance model – a critique and an alternative. *IEEE Trans. Biomed. Eng.* 52 (1), 132–135.
- Grimnes, S., Martinsen, Ø.G., 2007. Sources of error in tetrapolar impedance measurements on biomaterials and other ionic conductors. *J. Phys. D: Appl. Phys.* 40, 9–14.
- Grimnes, S., Jabari, A., Martinsen, Ø.G., Tronstad, C., 2011. Electrodermal activity by DC potential and AC conductance measured simultaneously at the same skin site. *Skin Res. Technol.* 17, 26–34.
- Griss, P., Enoksson, P., Tolvanen-Laakso, H.K., Meriläinen, P., Ollmar, S., Stemme, G., 2001. Micromachined electrodes for biopotential measurements. *IEEE J. Microelectromech. Syst.* 10, 10–16.
- Grosse, C., Foster, K.R., 1987. Permittivity of a suspension of charged spherical particles in electrolyte solution. *J. Phys. Chem.* 91, 3073.
- Guerrero, L., Gobantes, I., Oliver, M.A., Arnau, J., Guardia, M.D., Elvira, J., Riu, P.J., Grebol, N., Monfort, J.M., 2004. Green hams electrical impedance spectroscopy (EIS) measures and pastiness prediction of dry cured hams. *Meat Sci.* 66, 289–294.
- Gupta, V., Jafferji, I., Garza, M., Melnikova, V., Hasegawa, D.K., Pethig, R., Davis, D.W., 2012. ApoStreamTM, a new dielectrophoretic device for antibody independent isolation and recovery of viable cancer cells from blood. *Biomicrofluidics* 6, 024133.
- Gursoy, D., Mamatjan, Y., Adler, A., Scharfetter, H., 2011. Enhancing impedance imaging through multimodal tomography. *IEEE Trans. Biomed. Eng.* 58, 3215–3224.

- Guy, A.W., Davidow, S., Yang, G.Y., Chou, C.K., 1982. Determination of electric current distribution in animals and humans exposed to a uniform 60Hz high intensity electric field. *Bioelectromagnetics* 3, 47.
- Haas, K., Sin, W.C., Javaherian, A., Li, Z., Cline, H.T., 2001. Single-cell electroporation for gene transfer in vivo. *Neuron* 29, 583–591.
- Hadjiev, D., April 1968. A new method for quantitative evaluation of cerebral blood flow by rheoencephalography. *Brain Res.* 8 (1), 213–215.
- Halldorsson, H., Ollmar, S., 1998. Signal analysis of non-invasive impedance spectra of transplanted kidneys in vivo. In: Proc. 10th Int. Conf. Electrical Bio-impedance, Barcelona, April 5–9, 1998, pp. 351–354.
- Hamada, R., Takayama, H., Shonishi, Y., Mao, L., Nakano, M., Suehiro, J., 2013. A rapid bacteria detection technique utilizing impedance measurement combined with positive and negative dielectrophoresis. *Sens. Actuators B Chem.* 181, 439–445.
- Hamill, O.P., Marty, A., Neher, E., Sakmann, B., Sigworth, F.J., 1981. Improved patch-clamp techniques for high-resolution current recording from cells and cell-free membrane patches. *Pflugers Arch.* 391, 85–100.
- Hanai, T., 1960. Theory of the dielectric dispersion due to the interfacial polarization and its application to emulsion. *Kolloid Z.* 171, 23–31.
- Harris, N.D., Suggett, A.J., Barber, D.C., Brown, B.H., 1987. Applications of applied potential tomography (APT) in respiratory medicine. *Clin. Phys. Physiol. Meas.* 8 (Suppl. A), 155–165.
- Havriliak, S., Negami, S., 1966. A complex plane analysis of α -dispersions in some polymer systems. *J. Polym. Sci. Part C* 14, 99–117.
- Hayakawa, R., Kanda, H., Sakamoto, M., Wada, Y., 1975. New apparatus for measuring the complex dielectric constant of a highly conductive material. *Jpn. J. Appl. Phys.* 14, 2039–2052.
- Helmholtz, H., 1853. Über einige Gesetze der Verteilung elektrischer Stroms in körperlichen Leitern, mit Anwendung auf die thierischelektrischen Versuche. *Ann. Physiol. Chem.* 29 (3), 222.
- Hetrick, D.A., Zielinski, T.M., 2006. Bioimpedance in Cardiovascular Medicine. *Encyclopedia of Medical Devices and Instrumentation*, second ed. John Wiley & Sons, Inc. pp. 197–216.
- Hibino, M., Shigemori, M., Itoh, H., Nagayama, K., Kinosita, K., 1991. Membrane conductance of an electroporated cell analyzed by submicrosecond imaging of transmembrane potential. *Biophys. J.* 59, 209–220.
- Hodgin, A.L., Huxley, A.F., 1952. A quantitative description of membrane current and its application to conductance and excitation in nerve. *J. Physiol.* 117, 500–544.
- Hoening, S.A., Gildenberg, P.L., Murthy, K., 1978. Generation of permanent, dry, electric contacts by tattooing carbon into skin tissue. *IEEE Trans. Biomed. Eng.* 25, 380–382.
- Holder, D.S., 1992. Detection of cortical spreading depression in anaesthetised rat by impedance measurement with scalp electrodes – implications for noninvasive imaging in the brain with electrical impedance tomography. *Clin. Phys. Physiol. Meas.* 13 (1), 77–86.
- Hollaas, K., Magele, C., Merwa, R., Scharfetter, H., 2004. Numerical simulation of the eddy current problem in magnetic induction tomography for biomedical applications by edge elements. *IEEE Trans. Magnetics* 40, 623–626.
- Huang, Y., Rubinsky, B., 1999. Micro-electroporation: improving the efficiency and understanding of electrical permeabilization of cells. *Biomed. Microdevices* 2, 145–150.
- Huang, Y., Rubinsky, B., 2003. Flow-through micro-electroporation chip for high efficiency single-cell genetic manipulation. *Sens. Actuators A Phys.* 104, 205–212.
- Hulley, S.B., Cummings, S.R., Browner, W.S., Grady, D., Hearst, N., Newman, T.B., 2001. Getting ready to estimate sample size: hypothesis and underlying principles. In: *Designing Clinical Research—an Epidemiologic Approach*, second ed. Lippincott Williams and Wilkins, Philadelphia, pp. 51–63.
- IEC 60601-1, 2005. Medical Electrical Equipment – Part 1: General Requirements for Basic Safety and Essential Performance. International Standard.
- ISO 5725-1, 1994. Accuracy (Trueness and Precision) of Measurement Methods and Results – Part 1: General Principles and Definitions.

- Ivorra, A., Rubinsky, B., 2007. In vivo electrical impedance measurements during and after electroporation of rat liver. *Bioelectrochemistry* 70, 287–295.
- Jacquy, J., et al., 1974. Cerebral blood flow and quantitative rheoencephalography. *Electroencephalogr. Clin. Neurophysiol.* 37, 501–511.
- Jahnke, H.G., Heimann, A., Azendorf, R., Mpoukouvalas, K., Kempski, O., Robitzki, A.A., Charalampaki, P., 2013. Impedance spectroscopy — an outstanding method for label-free and real-time discrimination between brain and tumor tissue *in vivo*. *Biosens. Bioelectron.* 46, 8–14.
- Jaron, D., Briller, A., Schwan, H.P., Geselowitz, D.B., 1969. Nonlinearity of cardiac pacemaker electrodes. *IEEE Trans. Biomed. Eng.* 16, 132–138.
- JCGM 200, 2012. International Vocabulary of Metrology — Basic and General Concepts and Associated Terms (VIM), third ed.
- Jenkner, F.L., 1986. Clinical Rheoencephalography. Vienna, Austria: Ertldruck.
- Jentsch, T.J., 2002. Chloride channels are different. *Nature* 415, 276–277.
- Johnsen, G.K., 2012. An introduction to the memristor — a valuable circuit element in bioelectricity and bioimpedance. *J. Electr. Bioimp.* 3, 20–28.
- Johnsen, G.K., Lütken, C.A., Martinsen, Ø.G., Grimnes, S., 2011. Memristive model of electro-osmosis in skin. *Phys. Rev. E* 83, 031916.
- Jones, P., 1979. High electric field dielectric studies of aqueous myoglobin solutions. *Biophys. Chem.* 9, 91–95.
- Jonscher, A.K., 1996. Universal Relaxation Law. Chelsea Dielectrics Press, London.
- Jossinet, J., 1996. Variability of impedivity in normal and pathological breast tissue. *Med. Biol. Eng. Comput.* 34 (5), 346–350.
- Jossinet, J., McAdams, E.T., 1991. The skin/electrode interphase impedance. *Innov. Technol. Biol. Med.* 12 (1), 22–31.
- Jossinet, J., Schmitt, M., 1998. Alternative parameters for the characterisation of breast tissue. In: Proc. X Int. Conf. Electr. Bioimpedance, pp. 45–48.
- Kao, T.-J., Boverman, G., Kim, B.S., Isaacson, D., Saulnier, G.J., Newell, J.C., Choi, M.H., Moore, R.H., Kopans, D.B., 2008. Regional Admittivity Spectra with Tomosynthesis Images for Breast Cancer Detection: Preliminary Patient Study. *IEEE Trans. Med. Imag.* 27, 1762–1768.
- Kauppinen, P.K., Hyttinen, J.A., Malmivuo, J.A., 1998. Sensitivity distributions of impedance cardiography using band and spot electrodes analyzed by a three-dimensional computer model. *Ann. Biomed. Eng.* 26 (4), 694–702.
- Khine, M., Lau, A., Ionescu-Zanetti, C., Seo, J., Lee, L.P., 2005a. A single cell electroporation chip. *Lab Chip* 5, 38–43.
- Khine, M., Lau, A., Zanetti, C.I., Seo, J., Lee, E., Davalos, R., Lee, L.P., 2005b. A low-voltage single cell electroporation array for intracellular compound delivery. In: 9th International Conference on Miniaturized Systems for Chemistry and Life Sciences. Royal Society of Chemical Special Publications, Boston, MA.
- Kinosita Jr., K., Tsong, T.Y., 1979. Voltage-induced conductance in human erythrocyte membranes. *Biochim. Biophys. Acta* 554, 479–497.
- Kinosita Jr., K., Ashikawa, I., Saita, N., Yoshimura, H., Itoh, H., Nagayama, K., Ikegami, A., 1988. Electroporation of cell membrane visualized under a pulsed-laser fluorescence microscope. *Biophys. J.* 53, 1015–1019.
- Kirkwood, J.G., 1939. The dielectric polarization of polar liquids. *J. Chem. Phys.* 7, 911.
- Kontos, H.A., et al., 1978. Responses of cerebral arteries and arterioles to acute hypotension and hypertension. *Am. J. Physiol.* 234, H371–H383.
- Korjenevsky, A.V., Cherepenin, V.A., 1998. Mesuring system for induction tomography. In: Proc X Int. Conf. Electr Bio-impedance, Barcelona, pp. 365–368.
- Kotsiantis, S.B., 2007. Supervised machine learning: a review of classification techniques. *Informatica* 31, 249–268.

- Kottner, J., Audige, L., Brorson, S., Donner, A., Gajewski, B.J., Hróbjartsson, A., Roberts, C., Shoukri, M., Streiner, D.L., 2011. Guidelines for reporting reliability and agreement studies (GRRAS) were proposed. *Int. J. Nurs. Stud.* 48, 661–671.
- Kramers, H.A., 1926. Theory of dispersion in the X-ray region. *Phys. Z.* 30, 52.
- Krizaj, D., Pecar, B., 2012. Analysis of impedance measurements of a suspension of microcapsules using a variable length impedance measurement cell. *J. Electr. Bioimp.* 3, 42–50.
- Kronig, R. de L., 1929. The theory of dispersion of X-rays. *J. Opt. Soc. Am.* 12, 547.
- Kubicek, W.G., Kamegis, J.N., Patterson, R.P., Witsoe, D.A., Mattson, R.H., 1966. Development and evaluation of an impedance cardiac output system. *Aerosp. Med.* 37, 1208–1212.
- Kwon, H., Lee, E.J., Seo, J.K., Wi, H., Karki, B., McEwan, A., Woo, E.J., Oh, T.I., Harrach, B., 2012. Bioimpedance spectroscopy tensor probe for anisotropic measurements. *Electron. Lett.* 48, 1252.
- Kyle, U.G., Bosaeus, I., De Lorenzo, A.D., Deurenberg, P., Elia, M., Gomez, J.M., Heitmann, B.L., Kent-Smith, L., Melchior, J.C., Pirlich, M., Scharfetter, H., Schols, A.M.W.J., Pichard, C., 2004. Bioelectrical impedance analysis – part I: review of principles and methods. *Clin. Nutr.* 23, 1226–1243.
- Lababidi, Z., Ehmke, D.A., Durnin, R.E., Leaverton, P.E., Lauer, R.M., 1970. The first derivative thoracic impedance cardiogram. *Circulation* 41, 651–658.
- Lademann, J., Jacobi, U., Surber, C., Weigmann, H.J., Fluhr, J.W., 2008. The tape stripping procedure—evaluation of some critical parameters. *Eur. J. Pharm. Biopharm.* 72, 317–323.
- Lahtinen, T., Nuutinen, J., Alanen, E., Turunen, M., Nuortio, L., Usenius, T., Hopewell, J.W., 1999. Quantitative assessment of protein content in irradiated human skin. *Int. J. Radiat. Oncol. Biol. Phys.* 43, 635–638.
- Lalkhen, A.G., McCluskey, A., 2008. Clinical tests: sensitivity and specificity. *Contin. Educ. Anaesth. Crit. Care Pain* 8, 221–223.
- Lapicque, L., 1907. Recherches quantitatives sur l'excitation électrique des nerfs traitée comme une polarization. *J. Physiol. Paris* 9, 620–635.
- Lee, T.K., Claridge, E., 2005. Predictive power of irregular border shapes for malignant melanomas. *Skin Res. Technol.* 11, 1–8.
- Lee, R.C., Despa, F., 2005. Distinguishing electroporation from thermal injuries in electrical shock by MR imaging. In: Engineering in Medicine and Biology 27th Annual Conference. IEEE, Shanghai, China.
- Lee, R.C., Zhang, D., Hannig, J., 2000. Biophysical injury mechanisms in electrical shock trauma. In: Yarmish, M.L., Diller, K.R., Toner, M. (Eds.), *Ann. Rev. Biomed. Eng.* Palo Alto. Annual Review Press.
- Lee, E.S., Robinson, D., Rognlien, J.L., Harnett, C.K., Simmons, B.A., Ellis, C.R.B., Davalos, R.V., 2006. Robust giant lipid vesicles and micro-electroporation technology for controllable manipulation of picoliter volumes on-chip. *Bioelectrochemistry* 69.
- Lehr, J., 1972. A vector derivation useful in impedance plethysmographic field calculations. *IEEE Trans. Biomed. Eng.* 19 (2), 156–157.
- de Lema, B., Casan, P., Riu, P.J., 2006. Electrical impedance tomography: standardizing the procedure in pneumology. *Arch. Bronconeumol.* 42 (6), 299–301.
- Lin, L., 2007. Overview of agreement statistics for medical devices. *J. Biopharm. Stat.* 18, 126–144.
- Lin, Y.-C., Huang, M.-Y., 2001. Electroporation microchips for in vitro gene transfection. *J. Micromech. Microeng.* 11, 542–547.
- Lindholm-Sethson, B., Han, S., Ollmar, S., Nicander, I., Jonsson, G., Lithner, F., Bertheim, U., Geladi, P., 1998. Multivariate analysis of skin impedance data in long term type 1 diabetic patients. *Chemometr. Intell. Lab. Syst.* 44, 381–394.
- Lionheart, W.R.B., 1997. Conformal uniqueness results in anisotropic electrical impedance imaging. *Inverse Probl.* 13 (1), 125–134.
- Liston, A., Bayford, R., Holder, D., 2012. A cable theory based biophysical model of resistance change in crab peripheral nerve and human cerebral cortex during neuronal depolarisation: implications for electrical impedance tomography of fast neural activity in the brain. *Med. Biol. Eng. Comput.* 50, 425–437.

- Logothetis, N.K., Kayser, C., Oeltermann, A., 2007. In vivo measurement of cortical impedance spectrum in Monkeys: Implications for signal propagation. *Neuron* 55, 809–823.
- Lozano, A., Rosell, J., Pallas-Areny, R., 1995. A multifrequency multichannel electrical impedance data aquisition system for body fluid monitoring. *Physiol. Meas.* 16, 227–237.
- Lu, Y.Y., Huang, J.J., Huang, Y.J., Cheng, K.S., 2013. Cell growth characterization using multi-electrode bioimpedance spectroscopy. *Meas. Sci. Technol.* 24, 035701.
- Lukaski, H.C., Hall, C.B., Siders, W.A., 2007. Assessment of change in hydration in women during pregnancy and postpartum with bioelectrical impedance vectors. *Nutrition* 8, 543–550.
- Lundqvist, J.A., Sahlin, F., Aberg, M.A., Stromberg, A., Eriksson, P.S., Orwar, O., 1998. Altering the biochemical state of individual cultured cells and organelles with ultramicroelectrodes. *Proc. Natl. Acad. Sci. U.S.A.* 95, 10356–10360.
- Luthje, L., Vollmann, D., Drescher, T., Schott, P., Zenker, D., Hasenfuss, G., Unterberg, C., 2007. Intrathoracic impedance monitoring to detect chronic heart failure deterioration: relationship to changes in NT-proBNP. *Eur. J. Heart Fail.* 9 (6–7), 716–722.
- Maiti, S., SHEAR, J.B., Williams, R.M., Zipfel, W.R., Webb, W.W., 1997. Measuring serotonin distribution in live cells with three-photon excitation. *Science* 275, 530–532.
- Maleev, V.T., Kashpur, V.A., Glibitski, G.M., Krasnitskaya, A.A., Veretelnik, Y.V., 1987. Does DNA absorb microwave energy? *Biopolymers* 26, 1965–1970.
- Malhotra, R.K., Indrayan, A., 2010. A simple nomogram for sample size for estimating sensitivity and specificity of medical tests. *Indian J. Ophthalmol.* 58, 519–522.
- Malvehy, J., Hauschild, A., Curiel-Lewandrowski, C., et al., 2014. Clinical performance of the Nevisense system in cutaneous melanoma detection: an international, multi-centre, prospective and blinded clinical trial on efficacy and safety. *Br. J. Dermatol.* <http://dx.doi.org/10.1111/bjd.13121>.
- Mandel, M., 1977. Dielectric properties of charged linear macromolecules with particular reference to DNA. *Ann. N.Y. Acad. Sci.* 303, 74–87.
- Mandel, M., Odijk, T., 1984. Dielectric properties of polyelectrolyte solutions. *Ann. Rev. Phys. Chem.* 35, 75–108.
- Mangnall, Y.F., Baxter, A.J., Avill, R., Bird, N.C., Brown, B.H., Barber, D.C., Seagar, A.D., Johnson, A.G., Read, N.W., 1987. Applied potential tomography: a new non-invasive technique for assessing gastric function. *Clin. Phys. Physiol. Meas.* 8 (Suppl. A), 119–130.
- Maor, E., Ivorra, A., Leor, J., Rubinsky, B., 2007. The effect of irreversible electroporation on blood vessels. *Technol. Cancer Res. Treat.* 6, 307–312.
- Marisculo, L.A., Levin, J.R., 1983. Multivariate statistics in the social sciences: a researcher's guide. Brooks/Cole Pub. Co., Monterey, Calif. ISBN: 0534011470.
- Markx, G.H., Talary, M., Pethig, R., 1994. Separation of viable and non-viable yeast using dielectrophoresis. *J. Biotechnol.* 32, 29–37.
- Markx, G.H., Dyda, P.A., Pethig, R., 1996. Dielectrophoretic separation of bacteria using a conductivity gradient. *J. Biotechnol.* 51, 175–180.
- Marquez, J.C., Seoane, F., Lindecrantz, K., 2013. Textrode functional straps for bioimpedance measurements—experimental results for body composition analysis. *Eur. J. Clin. Nutr.* 67, S22–S27.
- Marszalek, P.E., Farrell, B., Verdugo, P., Fernandez, J.M., 1997. Kinetics of release of serotonin from isolated secretory granules. II. Ion exchange determines the diffusivity of serotonin. *Biophys. J.* 73, 1169–1183.
- Martinsen, Ø.G., Grimnes, S., 2001. Facts and myths about electrical measurement of stratum corneum hydration state. *Dermatology* 202, 87–89.
- Martinsen, Ø.G., Grimnes, S., Henriksen, I., Karlsen, J., 1996. Measurement of the effect of topical liposome preparations by low frequency electrical susceptance. *Innov. Technol. Biol. Med.* 17 (3), 217–222.
- Martinsen, Ø.G., Grimnes, S., Sveen, O., 1997a. Dielectric properties of some keratinised tissues. Part 1: stratum corneum and nail in situ. *Med. Biol. Eng. Comput.* 35, 172–176.
- Martinsen, Ø.G., Grimnes, S., Kongshaug, E.S., 1997b. Dielectric properties of some keratinised tissues. Part 2: human hair. *Med. Biol. Eng. Comput.* 35, 177–180.

- Martinsen, Ø.G., Grimnes, S., Nilsen, S., 1997c. Absolute water content and electrical admittance of human nail. *Exp. Dermatol.* 6 (5), 264.
- Martinsen, Ø.G., Grimnes, S., Karlsen, J., 1998a. Low frequency dielectric dispersion of microporous membranes in electrolyte solution. *J. Colloid Interface Sci.* 199, 107–110.
- Martinsen, Ø.G., Grimnes, S., 1998b. On using single frequency electrical measurements for skin hydration assessment. *Innov. Technol. Biol. Med.* 19 (5), 395–399.
- Martinsen, Ø.G., Grimnes, S., Haug, E., 1999. Measuring depth depends on frequency in electrical skin impedance measurements. *Skin Res. Technol.* 5, 179–181.
- Martinsen, Ø.G., Grimnes, S., Mirtaheri, P., 2000. Non-invasive measurements of post mortem changes in dielectric properties of haddock muscle – a pilot study. *J. Food Eng.* 43, 189–192.
- Martinsen, Ø.G., Grimnes, S., Piltan, H., 2004. Cutaneous perception of electrical direct current. *Innov. Technol. Biol. Med.* 25 (4), 240–243.
- Martinsen, Ø.G., Clausen, S., Nysæther, J.B., Grimnes, S., 2007. Utilising characteristic electrical properties of the epidermal skin layers to detect fake fingers in biometric fingerprint systems – a pilot study. *IEEE Trans. Biomed. Eng.* 54 (5), 891–894.
- Martinsen, Ø.G., Grimnes, S., Nilsen, J.K., Tronstad, C., Jang, W., Kim, H., Shin, K., 2008. Gravimetric method for in vitro calibration of skin hydration measurements. *IEEE Trans. Biomed. Eng.* 55, 728–732.
- Martinsen, Ø.G., Grimnes, S., Bergli, J., Galperin, Y.M., 2013. Universality in the electrical conductance of human hair. *Proc. XV ICEBI*.
- Masuda, S., Washizu, M., Iwadare, M., 1987. Separation of small particles suspended in liquid by nonuniform travelling field. *IEEE Trans. Ind. Appl.* 23, 474–480.
- Maundy, B., Elwakil, A.S., 2012. Extracting single dispersion Cole-Cole impedance model parameters using an integrator setup. *Analog Integr. Circuits Signal Process.* 71, 107–110.
- McAdams, E.T., Jossinet, J., 1991a. DC nonlinearity of the solid electrode-electrolyte interface impedance. *Innov. Technol. Biol. Med.* 12, 330–343.
- McAdams, E.T., Jossinet, J., 1991b. The impedance of electrode-skin impedance in high resolution electrocardiography. *Automedica* 13, 187–208.
- McAdams, E.T., Jossinet, J., 1994. The detection of the onset of electrode-electrolyte interphase impedance nonlinearity: a theoretical study. *IEEE Trans. Biomed. Eng.* 41 (5), 498–500.
- McFee, R., Johnston, F.D., 1953. Electrocardiographic leads. *Circulation* 8, 554–568.
- Meijer, J.H., Reulen, J.P.H., Oe, P.L., Allon, W., Thijs, L.G., Schneider, H., 1982. Differential impedance plethysmography for measuring thoracic impedances. *Med. Biol. Eng. Comput.* 20, 187–194.
- Meijer, J.H., Boesveldt, S., Elbertse, E., Berendse, H.W., 2007. Using time interval parameters from impedance cardiography to evaluate autonomic nervous function in Parkinson's disease. In: Scharfetter, H., Merwa, R. (Eds.), *Proc. 13th Int. Conf. El. Bioimp. and 8th Conf. El. Imp. Tomography (Graz Austria 2007) (IFMB Proceedings)*, vol. 17. Springer, Berlin, Heidelberg, New York, pp. 596–599.
- Meijer, J.H., Boesveldt, S., Elbertse, E., Berendse, H.W., 2008. Method to measure autonomic control of cardiac function using time interval parameters from impedance cardiography. *Physiol. Meas.* 29, S383–S391.
- Menachery, A., Pethig, R., 2005. Controlling cell destruction using dielectrophoretic forces. *IEE Proc. Nanobiotechnol.* 152 (4), 145–149.
- Merwa, R., Hollaus, K., Brandstätter, B., Scharfetter, H., 2003. Numerical solution of the general 3D eddy current problem for magnetic induction tomography (spectroscopy). *Physiol. Meas.* 24, 545–554.
- Metherall, P., Barber, D.C., Smallwood, R.H., Brown, B.H., 1996. Three dimensional electrical impedance tomography. *Nature* 380 (6574), 509–512.
- Metz, C.E., 1978. Basic principles of ROC analysis. *Semin. Nucl. Med.* 8, 283–298.
- Miller, Rupert, G., 1981. *Simultaneous Statistical Inference*, second ed. Springer Verlag. pp. 6–8.
- Miller, L., Leor, J., Rubinsky, B., 2005. Cancer cells ablation with irreversible electroporation. *Technol. Cancer Res. Treat.* 4, 699–705.

- Min, M., Parve, T., Kukk, V., Kuhlberg, A., 2002. An Implantable Analyzer of Bio-Impedance Dynamics: Mixed Signal Approach. *IEEE Trans. Instrum. Meas.* 51 (4), 674–678.
- Min, M., Parve, T., Salo, R., 2006. Biomedical Electronics. In: Wiley Encyclopedia of Biomedical Engineering. Wiley-Interscience, Hoboken (NJ), USA, pp. 500–514.
- Min, M., Parve, T., 2007. Improvement of lock-in electrical bio-impedance analyzer for implantable medical devices. *IEEE Trans. Instrum. Meas.* 56, 968–974.
- Min, M., Annus, P., Land, R., Paavle, T., Haldre, E., Ruus, R., 2007a. Bioimpedance monitoring of tissue transplants. In: Proc. IEEE Instrumentation and Measurement Technology Conference – IMTC 2007, Warsaw, Poland, May 1–3, 2007, 4 pp.
- Min, M., Parve, T., Ronk, A., Annus, P., Paavle, T., 2007b. Synchronous sampling and demodulation in an instrument for multifrequency bioimpedance measurement. *IEEE Trans. Instrum. Meas.* vol. 56 (No. 4), 1365–1372.
- Min, M., Pliquett, U., Nacke, T., Barthel, A., Annus, P., Land, R., 2008. Broadband excitation for short-time impedance spectroscopy. *Phys. Meas.* 29, S185–S192.
- Min, M., Parve, T., Pliquett, U., 2014. Impedance detection. In: Springer Encyclopedia of Microfluidics and Nanofluidics, second ed. Springer-Verlag, Heidelberg.
- Mir, L.M., 2001. Therapeutic perspectives of in vivo cell electropermeabilization. *Bioelectrochemistry* 53, 1–10.
- Mirtaheri, P., Grimnes, S., Martinsen, Ø.G., 2005. Electrode polarization impedance in weak NaCl aqueous solutions. *IEEE Trans. Biomed. Eng.* 52 (12), 2093–2099.
- Mishra, V., Bouayad, H., Schned, A., Hartov, A., Heaney, J., Halter, R.J., 2012. A real-time electrical impedance sensing biopsy needle. *IEEE Trans. Biomed. Eng.* 59, 3327–3336.
- Mohr, P., Birgersson, U., Berking, C., et al., 2013. Electrical impedance spectroscopy as a potential adjunct diagnostic tool for cutaneous melanoma. *Skin Res. Technol.* 19, 75–83.
- Mørkrid, L., Qiao, Z.G., 1988. Continuous estimation of parameters in skin electrical admittance from simultaneous measurements at two different frequencies. *Med. Biol. Eng. Comput.* 26, 633–640.
- Mørkrid, L., Ohm, O.-J., Hammer, E., 1980. Signal source impedance of implanted pacemaker electrodes estimated from spectral ratio between loaded and unloaded electrograms in man. *Med. Biol. Eng. Comput.* 18, 223–232.
- Morucci, J.P., Marsili, P.M., Granie, M., Shi, Y., Lei, M., Dai, W.W., 1994. A direct sensitivity matrix approach for fast reconstruction in electrical impedance tomography. *Physiol. Meas.* 15 (Suppl. 2A), 107–114.
- Moskalenko, Y.E. (Ed.), 1980. Biophysical Aspects of Cerebral Circulation. Oxford, Pergamon.
- Moussavi, M., Schwan, H.P., Sun, H.H., 1994. Harmonic distortion caused by electrode polarisation. *Med. Biol. Eng. Comp.* 32, 121–125.
- Mudraya, I.S., Kirpatovsky, V.I., Martov, A.G., 2007. Bioimpedance methods in urology functional diagnostics. ICEBI 2007, Graz IFMBE Proc. 17, 707–710.
- Munk, H., 1873. Über die galvanische Einführung differenter Flüssigkeiten in der unversehrten lebenden Organismus. *Arch. Anat. Physiol. Wissen. Med.*, 505–516.
- Murphy, D., Burton, P., Coombs, R., Tarassenko, L., Rolfe, P., 1987. Impedance imaging in the newborn. *Clin. Phys. Physiol. Meas.* 8 (Suppl. A), 131–140.
- Nescolarde, L., García-González, M.A., Rosell-Ferrer, J., Doñate, T., Querfeld, U., 2006. Thoracic vs whole-body bioimpedance measurements: relation to hydration status and hypertension in peritoneal dialysis patients. *Physiol. Meas.* 27, 961–971.
- Neumann, E., Rosenheck, K., 1972. Permeability changes induced by electric pulses in vesicular membranes. *J. Membr. Biol.* 10, 279–290.
- Newell, J.C., Peng, Y., Edic, P.M., Blue, R.S., Jain, H., Newell, R.T., 1998. Effect of electrode size on impedance images of two- and three-dimensional objects. *IEEE Trans. Biomed. Eng.* 45 (4), 531–534.
- Nicander, I., 1998. Electrical Impedance Related to Experimentally Induced Changes of Human Skin and Oral Mucosa (Ph.D. thesis). Karolinska Institute, Stockholm.
- Nicander, I., Ollmar, S., Eek, A., Lundh Rozell, B., Emtestam, L., 1996. Correlation of impedance response patterns to histological findings in irritant skin reactions induced by various surfactants. *Br. J. Dermatol.* 134, 221–228.

- Nie, R., Chin, A.B., Lee, K.S., Sunmonu, N.A., Rutkove, S.B., 2006. Electrical impedance myography: transitioning from human to animal studies. *Clin. Neurophysiol.* 117, 1844–1849.
- Nolkrantz, K., Farre, C., Brederlau, A., Karlsson, R.I.D., Brennan, C., Eriksson, P.S., Weber, S.G., Sandberg, M., Orwar, O., 2001. Electroporation of single cells and tissues with an electrolyte-filled capillary. *Anal. Chem.* 73, 4469–4477.
- Nordbotten, B.J., Tronstad, C., Martinsen, Ø.G., Grimnes, S., 2011. Evaluation of algorithms for calculating bioimpedance phase angle values from measured whole-body impedance modulus. *Physiol. Meas.* 32, 755–765.
- Norlén, L., Nicander, I., Lundh Rozell, B., Ollmar, S., Forslind, B., 1999. Differences in human stratum corneum lipid content related to physical parameters of skin barrier function in vivo. *J. Invest. Dermatol.* 112, 72–77.
- Nuccitelli, R., Pliquett, U., Chen, X., Ford, W., Swanson, J.R., Beebe, S.J., Kolb, J.F., Schoenbach, K., 2006. Nanosecond pulsed electric fields cause melanomas to self-destruct. *Biochem. Biophys. Res. Commun.* 342, 351–360.
- Nuccitelli, R., Nuccitelli, P., Ramlatchan, S., Sanger, R., Smith, P.J., 2008. Wound Repair and Regen. 16, 432.
- Nuutinen, J., Lahtinen, T., Turunen, M., Alanen, E., Tenhunen, M., Usenius, T., Kolle, R., 1998. A dielectric method for measuring early and late reactions in irradiated human skin. *Radiother. Oncol.* 47, 249–254.
- Nyboer, J., 1950. Electrical impedance plethysmography. *Circulation* 2, 811–887.
- Nyboer, J., 1960. Regional pulse volume and perfusion flow measurement. *AMA Arch. Intern. Med.* 105, 264–276.
- Oh, S.H., Lee, B.I., Woo, E.J., Lee, S.Y., Kim, T.-S., Kwon, O., Seo, J.K., 2005. Electrical conductivity images of biological tissue phantoms in MREIT. *Physiol. Meas.* 26, S279–S288.
- Oh, T., Gilad, O., Ghosh, A., Schuetter, M., Holder, D.S., 2011. A novel method for recording neuronal depolarization with recording at 125–825 Hz: implications for imaging fast neural activity in the brain with electrical impedance tomography. *Med. Biol. Eng. Comput.* 49, 593–604.
- Oliver, M.A., Gobantes, I., Arnau, J., Elvira, J., Riu, P.J., Grebol, N., Monfort, J.M., 2001. Evaluation of the electrical impedance spectroscopy (EIS) equipment for ham meat quality selection. *Meat Sci.* 58, 305–312.
- Ollmar, S., 1997. Noninvasive monitoring of transplanted kidneys by impedance spectroscopy — a pilot study. *Med. Biol. Eng. Comput.* 35 (Suppl. Part 1), 336.
- Ollmar, S., 1998. Methods for information extraction from impedance spectra of biological tissue, in particular skin and oral mucosa — a critical review and suggestions for the future. *Bioelectrochem. Bioenerg.* 45, 157–160.
- Ollmar, S., Nicander, I., 1995. Information in multi frequency measurement of intact skin. *Innov. Technol. Biol. Med.* 16, 745–751.
- Ollmar, S., Nicander, I., 2005. Within and beyond the skin barrier as seen by electrical impedance. In: Fluhr, J., Maibach, H., Berardesca, E., Elsner, P. (Eds.), *Bioengineering of the Skin: Water and the Stratum Corneum*, second ed. CRC Press, Boca Raton, pp. 335–350.
- Olofsson, J., Nolkrantz, K., Ryttssén, F., Lambie, B.A., Weber, S.G., Orwar, O., 2003. Single-cell electroporation. *Curr. Opin. Biotechnol.* 14, 29–34.
- Onaral, B., Schwan, H.P., 1982. Linear and nonlinear properties of platinum electrode polarisation. Part I: frequency dependence at very low frequencies. *Med. Biol. Eng. Comp.* 20, 299–306.
- Onsager, L., 1934. Deviations from Ohm's law in weak electrolytes. *J. Chem. Phys.* 2, 599–615.
- Onsager, L., 1936. Electrical moments of molecules in liquids. *J. Am. Chem. Soc.* 58, 1486.
- Oostendorp, T.F., Delbeke, J., Stegeman, D.F., 2000. The conductivity of the human skull: results of in vivo and in vitro measurements. *IEEE Trans. Biomed. Eng.* 47, 1487–1492.
- Paterno, A.S., Stiz, R.A., Bertemes-Filho, P., 2009. Frequency-domain reconstruction of signals in electrical bioimpedance spectroscopy. *Med. Biol. Eng. Comput.* 47, 1093–1102.
- Patterson, R.P., 2010. Impedance cardiography: what is the source of the signal? *J. Phys. Conf. Ser.*, 224, 012118.

- Patterson, R.P., Wang, L., Raza, B., Wood, K., 1990. Mapping of the cardiogenic impedance signal on the thoracic surface. *Med. Biol. Eng. Comput.* 28, 212–216.
- Pauly, H., Schwan, H.P., 1959. Über die Impedanz einer Suspension von Kugelformigen Teilchen mit einer Schale. *Z. Naturforsch.* 14b, 125–131.
- Pauly, H., Schwan, H.P., 1966. Dielectric properties and ion mobility in erythrocytes. *Biophys. J.* 6, 621.
- Pearson, K., 1901. On lines and planes of closest fit to systems of points in space. *Philos. Mag.* 2, 559–572.
- Peres-Neto, P., Jackson, D.A., Somers, K.M., 2005. How many principal components? Stopping rules for determining the number of non-trivial axes revisited. *Comput. Stat. Data Anal.* 49, 974–997.
- Pethig, R., 2010. Review article—dielectrophoresis: status of the theory, technology, and applications. *Biomicrofluidics* 4, 022811.
- Pethig, R., 2013. Dielectrophoresis: an assessment of its potential to aid the research and practice of drug discovery and delivery. *Adv. Drug Del. Rev.* 65, 1589–1599.
- Pethig, R., Talary, M.S., 2007. Dielectrophoretic detection of membrane morphology changes in Jurkat T-cells undergoing etoposide-induced apoptosis. *IET Nanobiotechnol.* 1, 2–9.
- Pethig, R., Jakubek, L.M., Sanger, R.H., Heart, E., Corson, E.D., Smith, P.J.S., 2005. Electrokinetic measurements of membrane capacitance and conductance for pancreatic β-cells. *IEE Proc. Nanobiotechnol.* 152 (6), 189–193.
- Pettersen, F.J., Høgsetveit, J.O., 2011. From 3D tissue data to impedance using Simpleware ScanFE+IP and COMSOL Multiphysics – a tutorial. *J. Electr. Bioimp.* 2, 13–32.
- Piccoli, A., Rossi, B., Pillon, L., Buccianti, G., 1994. A new method for monitoring body fluid variation by bioimpedance analysis: the RXc graph. *Kidney Int.* 46, 534–539.
- Piccoli, A., Pillon, L., Dumler, F., 2002. Impedance vector distribution by sex, race, body mass index, and age in the United States: standard reference intervals as bivariate Z scores. *Nutrition* 18, 153–167.
- Pliquett, U., Weaver, J.C., 1996. Electroporation of human skin: simultaneous measurement of changes in the transport of two fluorescent molecules and in the passive electrical properties. *Bioelectrochem. Bioenerg.* 39, 1–12.
- Pliquett, U., Krassen, H., Frantescu, C.G., Wesner, D., Neumann, E., Schoenbach, K., 2005. Asymmetric changes in membrane conductance due to hyper- and depolarization: probing with current and voltage clamp. *IFMBE Proc.* 11, 1923.
- Pliquett, U., Joshi, R.P., Sridhara, V., Schoenbach, K., 2007. High electrical field effects on cell membranes. *Bioelectrochemistry* 70, 275–282.
- Pohl, H.A., 1958. Some effects of nonuniform fields on dielectrics. *J. Appl. Phys.* 29, 1182–1188.
- Pollack, G.H., 2001. Cells, gels and the engines of life. Ebner & Sons.
- Pomerantz, M., Baumgartner, R., Lauridson, J., Eiseman, B., 1969. Transthoracic electrical impedance for the early detection of pulmonary edema. *Surgery* 66, 260–268.
- Rabbani, K.S., Sarker, M., Akond, M.H.R., Akter, T., 1999. Focused impedance measurement (FIM): a new technique with improved zone localization. *Ann. N.Y. Acad. Sci.* 873, 408–420.
- Rae, J.L., Levis, R.A., 2002. Single-cell electroporation. *Pflugers Arch.* 443, 664–670.
- Ranck, J.B., 1963. Analysis of specific impedance of rabbit cerebral cortex. *Exp. Neurol.* 7, 153–174.
- Rani, P., Liu, C., Sarkar, N., Vanman, E., 2006. An empirical study of machine learning techniques for affect recognition in human-robot interaction. *Pattern Anal. Appl.* 9, 58–69.
- Riu, P.J., Lapaz, C., 1999. Practical limits of the Kramers-Kronig relationships applied to experimental bioimpedance data. *Ann. N.Y. Acad. Sci.* 873, 374–380.
- Riu, P., Rosell, J., Lozano, A., Pallas-Areny, R., 1992. A broadband system for static imaging in electrical impedance tomography. *Clin. Phys. Physiol. Meas.* 13 (Suppl. A), 61–66.
- Riu, P., Rosell, J., Lozano, A., Pallas-Areny, R., 1995. Multifrequency static imaging in electrical impedance tomography. Part 1: Instrumentation Requirements. *Med. Biol. Eng. Comput.* 33, 784–792.
- Robbins, C.R., 1979. Chemical and Physical Behaviour of Human Hair. Van Norstrand Reinhold, New York.
- Robinson, D., Lee, E.S., Iqbal, Z., Rognlien, J.L., Davalos, R.V., 2007. Reinforced vesicles withstand rigors of microfluidic electroporation. *Sens. Actuators B Chem.* 125, 337–342.

- Rosell, J., Riu, P., 1992. Common-mode feedback in electrical impedance tomography. *Clin. Phys. Physiol. Meas.* 13 (Suppl. A), 11–14.
- Rosell, J., Colominas, J., Riu, P., Pallas-Areny, R., Webster, J.G., 1988a. Skin impedance from 1 Hz to 1 MHz. *IEEE Trans. Biomed. Eng.* 35 (8), 649–651.
- Rosell, J., Murphy, D., Pallas-Areny, R., Rolfe, P., 1988b. Analysis and assessment of errors in a parallel data acquisition system for electrical impedance tomography. *Clin. Phys. Physiol. Meas.* 9 (Suppl. A), 93–100.
- Rosell, J., Casañas, R., Scharfetter, H., 2001. Sensitivity maps and system requirements for magnetic induction tomography using a planar gradiometer. *Physiol. Meas.* 22, 121–130.
- Rubinsky, B., 2007. Irreversible electroporation in medicine. *Technol. Cancer Res. Treat.* 6, 255–260.
- Ruiz, G.A., Felice, C.J., Valentinuzzi, M.E., 2005. Non-linear response of electrode–electrolyte interface at high current density. *Chaos, Solitons and Fractals* 25, 649–654.
- Rutkove, S.B., Aaron, R., Shiffman, C.A., 2002. Localized bioimpedance analysis in the evaluation of neuromuscular disease. *Muscle Nerve* 25, 390–397.
- Rutkove, S.B., Esper, G.J., Lee, K.S., Aaron, R., Shiffman, C.A., 2005. Electrical impedance myography in the detection of radiculopathy. *Muscle Nerve* 32, 335–341.
- Rutkove, S.B., Lee, K.S., Shiffman, C.A., Aaron, R., 2006. Test-Retest reproducibility of 50 kHz Linear-Electrical impedance myography. *Clin. Neurophysiol.* 117, 1244–1248.
- Ryan, T.P., 2008. Modern Regression Methods. Wiley Series in Probability and Statistics. Wiley. ISBN: 978-0-470-08186-0.
- Ryttsen, F., Farre, C., Brennan, C., Weber, S.G., Nolkrantz, K., Jardemark, K., Chiu, D.T., Orwar, O., 2000. Characterization of single-cell electroporation by using patch-clamp and fluorescence microscopy. *Biophys. J.* 79, 1993–2001.
- Sachs, J., Peyerl, P., Woeckel, S., Kmec, M., Herrmann, R., Zetik, R., 2007. Liquid and moisture sensing by ultra wideband pseudo noise sequence signals. *Meas. Sci. Technol.* 18, 1074–1087.
- Sadleir, R., 2010. A bidomain model for neural tissue. *Int. J. Bioelectromagn.* 12, 2–6.
- Sakamoto, K., Muto, K., Kanai, H., Lizuka, M., 1979. Problems of impedance cardiography. *Med. Biol. Eng. Comput.* 17, 697–709.
- Salazar, Y., Bragos, R., Casas, O., Cinca, J., Rosell, J., 2004. Transmural versus non-transmural in situ electrical impedance spectrum for healthy, ischemic, and healed myocardium. *IEEE Trans. Biomed. Eng.* 51 (8), 1421–1427.
- Sale, A.J., Hamilton, W.A., 1967. Effects of high electric fields on micro-organisms. 1. Killing of bacteria and yeasts. *Biochim. Biophys. Acta* 148, 781–788.
- Salter, D.C., 1981. Studies in Measurement, Form and Interpretation of Some Electrical Properties of Normal and Pathological Skin In vivo (Ph.D. thesis), Univ of Oxford.
- Salter, D.C., 1998. Examination of stratum corneum hydration state by electrical methods. In: Elsner, P., et al. (Eds.), *Skin Bioengineering. Techniques and Applications in Dermatology and Cosmetology*. Karger.
- Sanchez, B., Vandersteen, G., Bragos, R., Schoukens, J., 2011. Optimal multisine excitation design for broadband electrical impedance spectroscopy. *Meas. Sci. Technol.* 22, 115601 (11 pp).
- Sanchez, B., Louarroudi, E., Jorge, E., Cinca, J., Bragos, R., Pintelon, R., 2013a. A new measuring and identification approach for time-varying bioimpedance using multisine electrical impedance spectroscopy. *Physiol. Meas.* 34, 339–357.
- Sanchez, B., Louarroudi, E., Bragos, R., Pintelon, R., 2013b. Harmonic impedance spectra identification from time-varying bioimpedance: theory and validation. *Physiol. Meas.* 34, 1217–1238.
- Sanchez, B., Vandersteen, G., Martin, I., Torrego, A., Riu, P.J., Shoukens, J., Bragos, R., 2013c. In vivo electrical bioimpedance characterization of human lung tissue during the bronchoscopy procedure. A feasibility study. *Med. Eng. Phys.* 35, 949–957.
- Sarro, E., Lecina, M., Fontova, A., Sola, C., Godia, F., Cairo, J.J., Bragos, R., 2012. Electrical impedance spectroscopy measurements using a four-electrode configuration improve on-line monitoring of cell concentration in adherent animal cell cultures. *Biosens. Bioelectron.* 31, 257–263.

- Saulnier, G.J., Liu, N., Tamma, C., Xia, H., Kao, T.-J., Newell, J.C., Isaacson, D., 2007. An electrical impedance spectroscopy system for breast cancer detection. *Proc. IEEE-EMBS Conf.* 1, 4154–4157.
- Sawilowsky, S.S., Blair, R.C., Higgins, J.J., 1989. An investigation of the type I error and power properties of the rank transform procedure in factorial ANOVA. *J. Educ. Stat.* 14, 255–267.
- Scaife, J.M., Tozer, R.C., Freestone, I.L., 1994. Conductivity and permittivity images from an induced current electrical impedance tomography system. *IEE Proc. Sci. Meas. Technol.* 141 (5), 356–362.
- Schächinger, H., Weinbacher, M., Kiss, A., Ritz, R., Langewitz, W., 2001. Cardiovascular indices of peripheral and central sympathetic activation. *Psychosom. Med.* 63, 788–796.
- Schäfer, M., Schlegel, C., Kirlum, H.-J., Gersing, E., Gebhard, M.M., 1998. Monitoring of damage to skeletal muscle tissue caused by ischemia. *Bioelectrochem. Bioenerg.* 45, 151–155.
- Scharfetter, H., Hartinger, P., Hinghofer Szalkay, H., Hutten, H., 1998. A model of artefacts produced by stray capacitance during whole body or segmental bioimpedance spectroscopy. *Physiol. Meas.* 19 (2), 247–261.
- Scharfetter, H., Casañas, R., Rosell, J., 2003. Biological tissue characterization by magnetic induction spectroscopy (MIS): requirements and limitations. *IEEE Trans. Biomed. Eng.* 50, 870–880.
- Scharfetter, H., Brunner, P., Merwa, R., 2006a. Magnetic induction tomography: single-step solution of the 3-D inverse problem for differential image reconstruction. *Int. J. Inf. Syst. Sci.* 2 (4), 585–606.
- Scharfetter, H., Hollaus, K., Rosell-Ferrer, J., Merwa, R., 2006b. Single-step 3-D image reconstruction in magnetic induction tomography: theoretical limits of spatial resolution and contrast to noise ratio. *Ann. Biomed. Eng.* 34, 1786–1798.
- Schlumberger, C., 1920. Etude sur la Prospection Electrique du Sous-sol. Gauthier-Villars, Paris.
- Schmider, E., Ziegler, M., Danay, E., Beyer, L., Bühner, M., 2010. Is it Really Robust? Reinvestigating the Robustness of ANOVA against Violations of the Normal Distribution Assumption. *Schmider, Emanuel.*
- Schmitt, O.H., 1957. Lead vectors and transfer impedance. *Ann. N.Y. Acad. Sci.* 65, 1092–1109.
- Schnelle, T., Mueller, T., Fiedler, S., Shirley, S.G., Ludwig, K., Herrmann, A., Fuhr, G., Wagner, B., Zimmermann, U., 1996. Trapping of viruses in high-frequency electric field cages. *Naturwissenschaften* 83, 172–176.
- Schoenbach, K., Joshi, R.P., Kolb, J., Chen, N., Stacey, M., Blackmore, P.F., Buescher, E.S., Beebe, S.J., 2004. Ultrashort electrical pulses open a new gateway into biological cells. *Proc. IEEE* 92, 1122.
- Schwan, H.P., 1954. Die elektrischen Eigenschaften von Muskelgewebe bei Niederfrequenz. *Z. Naturforsch.* 9b, 245.
- Schwan, H.P., 1957. Electrical properties of tissue and cell suspensions. In: Lawrence, J.H., Tobias, C.A. (Eds.), *Advances in Biological and Medical physics*, vol. V. Acad. Press, pp. 147–209.
- Schwan, H.P., 1963. Determination of biological impedances. In: Nastuk, W.L. (Ed.), *Physical Techniques in Biological Research*, vol. 6. Acad. Press, pp. 323–406.
- Schwan, H.P., 1985. Dielectric properties of the cell surface and biological systems. *Stud. Biophys.* 110, 13–18.
- Schwan, H.P., 1988. Biological effects of non-ionizing radiations: cellular properties and interactions. *Ann. Biomed. Eng.* 16, 245–263.
- Schwan, H.P., 1992a. Linear and non-linear electrode polarisation and biological materials. *Ann. Biomed. Eng.* 20, 269–288.
- Schwan, H.P., 1992b. Early history of bioelectromagnetics. *Bioelectromagnetics J.* 13, 453–467.
- Schwan, H.P., September 1993. Early organizations of biomedical engineering in the US. *IEEE Eng. Med. Biol. Mag.*, 25–29.
- Schwan, H.P., Ferris, C.D., 1968. Four-electrode techniques for impedance measurement with high resolution. *Rev. Sci. Instrum.* 39 (4), 481–485.
- Schwan, H.P., Kay, C.F., 1957. The conductivity of living tissue. *Ann. N.Y. Acad. Sci.* 65, 1007.
- Schwan, H.P., Morowitz, H.J., 1962. Electrical properties of the membranes of the pleuro-pneumonia-like organism A5969. *Biophys. J.* 2, 295.
- Schwan, H.P., Sher, L.D., 1969. Electrostatic fields induced forces and their biological implications. In: Pohl, H.A., Pickard, W.F. (Eds.), *Dielectrophoretic and Electrophoretic Deposition. The Electrochemical Society, Inc.*, New York, pp. 107–126.

- Schwan, H.P., Schwartz, G., Maczuk, J., Pauly, H., 1962. On the low frequency dielectric dispersion of colloidal particles in electrolyte solution. *J. Phys. Chem.* 66, 2626–2636.
- Schwan, H.P., Takashima, S., Miyamoto, V.K., Stoeckenius, W., 1970. Electrical properties of phospholipid vesicles. *Biophys. J.* 10, 1102.
- Schwartz, G., 1962. A theory of the low frequency dispersion of colloidal particles in electrolyte solution. *J. Phys. Chem.* 66, 2636.
- Schweidler, E.R.V., 1907. Studien über die Anomalien im Verhalten der Dielektrika. *Ann. Phys.* 329, 711–770.
- Schweiger, E., Wittling, W., Genzel, S., Block, A., 1998. Relationship between sympathovagal tone and personality traits. *Pers. Indiv. Differ.* 25, 327–337.
- Serrano, R.E., de Lema, B., Casas, O., Feixas, T., Calaf, N., Casan, P., Sanchís, J., Riu, P.J., 2002. Use of electrical impedance tomography (EIT) for the assessment of unilateral pulmonary function. *Physiol. Meas.* 23 (1), 211–220.
- Serrano, R.E., Riu, P.J., de Lema, B., Casan, P., 2004. Assessment of the unilateral pulmonary function by means of electrical impedance tomography using a reduced electrode set. *Physiol. Meas.* 25 (4), 803–813.
- Sheskin, D.J., 2011. Handbook of Parametric and Nonparametric Statistical Procedures. CRC Press.
- Shiffman, C.A., Aaron, R., Amoss, V., Therrien, J., Coomler, K., 1999. Resistivity and phase in localized BIA. *Phys. Med. Biol.* 44, 2409–2429.
- Shiffman, C.A., Aaron, R., Rutkove, S.B., 2003. Electrical impedance of muscle during isometric contraction. *Physiol. Meas.* 24, 213–234.
- Sigman, E., Kolin, A., Katz, L.N., Jochim, K., 1937. Effect of motion on the electrical conductivity of the blood. *Am. J. Physiol.* 118, 708–719.
- Sipos, K., Bodo, M., Veer, A., Hagtvet, K.A., Banyasz, A., 1994. Neurosis, depression, anxiety and stroke risk factors in a Hungarian village. In: Kalokagathia (Review of the Hung. Univ. of Physical Education) vol. XXXII, pp. 94–114, Budapest.
- Slager, C.J., Schuurbiers, J.C.H., Oomen, J.A.F., Bom, N., 1993. Electrical nerve and muscle stimulation by radio frequency surgery: role of direct current loops around the active electrode. *IEEE Trans. Biomed. Eng.* 40, 182–187.
- Smallwood, R.H., Mangnall, Y.F., Leathard, A.D., 1994. Transport of gastric contents. *Physiol. Meas.* 15 (Suppl. 2A), 175–188.
- Song, A., Parus, S., Kopelman, R., 1997. High-performance fiber-optic pH microsensors for practical physiological measurements using a dual-emission sensitive dye. *Anal. Chem.* 69, 863–867.
- Song, C.G., Kim, S.C., Nam, K.C., Kim, D.W., 2005. Optimum electrode configuration for detection of leg movement using bio-impedance. *Physiol. Meas.* 26, S59–S68.
- South, G.P., Grant, E.H., 1973. The contribution of proton fluctuation to dielectric relaxation in protein solutions. *Biopolymers* 12, 1937–1944.
- Sramek, B.B., 1981. Noninvasive technique for measurement of cardiac output by means of electrical impedance. *Proc. Vth ICEBI Tokyo*, 39–42.
- Stuchly, M.A., Stuchly, S.S., 1990. Electrical properties of biological substances. In: Gandhi, O.P. (Ed.), Biological Effects and Medical Applications of Electromagnetic Energy. Prentice Hall.
- Sun, S.S., Chumlea, W.C., Heymsfield, S.B., et al., 2003. Development of bioelectrical impedance analysis prediction equations for body composition with the use of a multicomponent model for use in epidemiological surveys. *Am. J. Clin. Nutr.* 77, 331–340.
- Sun, T., Gawad, S., Bernabini, C., Green, N.G., Morgan, H., 2007. Broadband single cell impedance spectroscopy using maximum length sequences: theoretical analysis and practical considerations. *Meas. Sci. Technol.* 18, 2859–2868.
- Suttner, S., Schollhorn, T., Boldt, J., Mayer, J., Rohm, K.D., Lang, K., Piper, S.N., 2006. Noninvasive assessment of cardiac output using thoracic electrical bioimpedance in hemodynamically stable and unstable patients after cardiac surgery: a comparison with pulmonary artery thermodilution. *Intensive Care Med.* 32, 2053–2058.

- Takashima, S., Schwan, H.P., 1965. Dielectric dispersion of crystalline powders of amino acids, peptides and proteins. *J. Phys. Chem.* 69, 4176–4182.
- Talary, M.S., Burt, J.P.H., Tame, J.A., Pethig, R., 1996. Electromanipulation and separation of cells using travelling electric fields. *J. Phys. D: Appl. Phys.* 29, 2198–2203.
- Tarulli, A., Esper, G.J., Lee, K.S., Aaron, R., Schiffman, C.A., Rutkove, S.B., 2005. Electrical impedance myography in the bedside assessment of inflammatory myopathy. *Neurology* 65, 451–452.
- Teorell, T., 1946. Application of square wave analysis to bioelectric studies. *Acta Physiol. Scand.* 12, 235–254.
- Teruel, M.N., Meyer, T., 1997. Electroporation-induced formation of individual calcium entry sites in the cell body and processes of adherent cells. *Biophys. J.* 73, 1785–1796.
- Therkildsen, P., Hædersdal, M., Lock-Andersen, J., Olivarisu, F. dF., Poulsen, T., Wulf, H.C., 1998. Epidermal thickness measured by light microscopy: a methodological study. *Skin Res. Technol.* 4, 174–179.
- Thomasset, A.L., 1965. Mesure du volume des liquides extra-cellulaires par la methode electro-chimique signification biophysique de l'impedance a 1 kilocycle du corps humain. *Lyon Med.* 214, 131–143.
- Tozer, J.C., Ireland, E.H., Barber, Barker, 1998. Magnetic impedance tomography. In: Proc. X Int. Conf Elect. Bio-impedance, Barcelona, pp. 369–372.
- Trebbels, D., Fellhauer, F., Jugl, M., Haimerl, G., Min, M., Zengerle, R., 2012. Online Tissue Discrimination for Transcutaneous Needle Guidance Applications Using Broadband Impedance Spectroscopy. *IEEE Trans. Biomed. Eng.* 59 (2), 494–503.
- Tregear, R.T., 1965. Interpretation of skin impedance measurements. *Nature* 205, 600–601.
- Tronstad, C., Gjein, G.E., Grimnes, S., Martinsen, Ø.G., Krogstad, A.-L., Fosse, E., 2008. Electrical measurement of sweat activity. *Physiol. Meas.* 29, S407–S415.
- Tronstad, C., Johnsen, G.K., Grimnes, S., Martinsen, Ø.G., 2010. A study on electrode gels for skin conductance measurements. *Physiol. Meas.* 31, 1395–1410.
- Tronstad, C., Kalvøy, H., Grimnes, S., Martinsen, Ø.G., 2013. Waveform difference between skin conductance and skin potential responses in relation to electrical and evaporative properties of skin. *Psychophysiology* 50, 1070–1078.
- Tronstad, C., Pripp, A.H., 2014. Statistical methods for bioimpedance analysis. *J. Electr. Bioimp.* 5, 14–27.
- Ugland, O.M., 1967. Electrical burns. *Scand. J. Plast. Reconstr. Surg. (Suppl. 2)*, 1–74.
- Vasilkoski, Z., Esser, A.T., Gowrishankar, T.R., Weaver, J.C., 2006. Membrane electroporation: the absolute rate equation and nanosecond time scale pore creation. *Phys. Stat. Sol* 74, 021904.
- Venables, P.H., Christie, M.J., 1980. Electrodermal activity. In: Martin, I., Venables, P.H. (Eds.), *Techniques in Psychophysiology*. John Wiley & Sons.
- Vernhes, M.C., Cabanes, P.A., Teissie, J., 1999. Chinese hamster ovary cells sensitivity to localized electrical stresses. *Bioelectrochem. Bioenerg.* 48, 17–25.
- Visser, K.R., Lamberts, R., Korsten, H.H.M., Zijlstra, W.G., 1976. Observations on blood flow related electrical impedance changes in rigid tubes. *Pflügers Arch.* 366, 289–291.
- Vollmann, D., Nagele, H., Schauerte, P., et al., 2007. Clinical utility of intrathoracic impedance monitoring to alert patients with an implanted device of deteriorating chronic heart failure. *Eur. Heart J.* 28 (15), 1835–1840.
- Vrinceanu, D., Gheorghiu, E., 1996. Shape effects in the dielectric behaviour of arbitrarily shaped particles with particular reference to biological cells. *Bioelectrochem. Bioenerg.* 40, 167–170.
- Wagner, K.W., 1914. Explanation of the dielectric fatigue phenomena on the basis of Maxwell's concept. *Arch. Elektrotech (Berlin)* 2, 271.
- Wang, X.-B., Huang, Y., Hølzel, R., Burt, J.P.M., Pethig, R., 1993. Theoretical and experimental investigations of the interdependence of the dielectric dielectrophoretic and electrorotational behaviour of colloidal particles. *J. Phys. D: Appl. Phys.* 26, 312–322.
- Wang, L., Lahtinen, S., Lentz, L., et al., 2005. Feasibility of using and implantable system to measure thoracic congestion in an ambulatory chronic heart failure canine model. *PACE* 28, 404–411.
- Warburg, E., 1899. Über das Verhalten sogenannte unpolarisierbare Elektroden gegen Wechselstrom. *Ann. Phys. Chem.* 67, 493–499.

- Washizu, M., Kurosawa, O., 1990. Electrostatic manipulation of DNA in microfabricated structures. *IEEE Trans. Ind. Appl.* 26, 1165–1172.
- Washizu, M., Suzuki, S., Kurosawa, O., Nishizaka, T., Shinohara, T., 1994. Molecular dielectrophoresis of biopolymers. *IEEE Trans. Ind. Appl.* 30, 835–843.
- Weaver, J.C., Barnett, A., 1992. “Guide to Electroporation and Electrofusion” in *Progress toward a Theoretical Model of Electroporation Mechanism: Membrane Electrical Behavior and Molecular Transport*, 26.
- Weaver, J.C., 1994. Biomembrane electrochemistry. In: *Theory of Electroporation*, pp. 447–470.
- Weaver, J.C., 1995. *Electroporation Theory: Concepts and Mechanisms. Methods in Molecular Biology*. Humana Press, Inc., Totowa, NJ.
- Weaver, J.C., 2000. Electroporation of cells and tissues. *IEEE Trans. Plasma Sci.* 28, 24–33.
- Weaver, J.C., 2003. Electroporation of biological membranes from multicellular to nano scales. *IEEE Trans. Dielectr. Electr. Insul.* 10, 754–768.
- Weaver, J.C., Chizmadzhev, Y.A., 1996. Theory of electroporation: a review. *Bioelectrochem. Bioenerg.* 41, 135–160.
- Weir, J.P., 2005. Quantifying test-retest reliability using the intraclass correlation coefficient and the SEM. *J. Strength Cond. Res.* 19, 231–240.
- Weiss, G., 1901. Sur la possibilite de rendre comparables entre eux les appareils servant a l'excitation electrique. *Arch. Ital. Biol.* 35, 413–446.
- Wien, M., 1928. Über die Abweichungen der Elektrolyte vom Ohmischen Gesetz. *Phys. Z.* 29, 751–755.
- Wien, M., 1931. Über Leitfähigkeit und Dielektrizität Konstante von Elektrolyten bei Hochfrequenz. *Phys. Z.* 32, 545–547.
- Wightman, R.M., Jankowski, J.A., Kennedy, R.T., Kawagoe, K.T., Schroeder, T.J., Lesczyszyn, D.J., Near, J.A., Dilberto Jr., E.J., Viveros, O.H., 1991. Temporally resolved catecholamine spikes correspond to single vesicle release from individual chromaffin cells. *Proc. Natl. Acad. Sci. U.S.A.* 88, 10754–10758.
- Williams, G., Watts, D.C., 1970. Non-symmetrical dielectric relaxation behavior arising from a simple empirical decay function. *Trans. Faraday Soc.* 66, 80–85.
- Wilson, F.N., 1953. Foreword to “Electrocardiographic Leads” cf. McFee et al (1953).
- Wilson, M.T., Elbohouty, M., Voss, L.J., Steyn-Ross, D.A., 2014. Electrical impedance of mouse brain cortex in vitro from 4.7 kHz to 2.0 MHz. *Physiol. Meas.* 35, 267–281.
- Yamamoto, T., Yamamoto, Y., 1976. Electrical properties of the epidermal stratum corneum. *Med. Biol. Eng.* 14, 592–594.
- Yamamoto, T., Yamamoto, Y., 1981. Non-linear electrical properties of the skin in the low frequency range. *Med. Biol. Eng. Comput.* 19, 302–310.
- Yamamoto, Y., Yamamoto, T., Ozawa, T., 1986. Characteristics of skin admittance for dry electrodes and the measurement of skin moisturisation. *Med. Biol. Eng. Comput.* 24, 71–77.
- Yan, L., Pettine, J., Mitra, S., Kim, S., Jee, D.-W., Kim, H., Osawa, M., Harada, Y., Tamiya, K., Van Hoof, C., Yazicioglu, R.F., 2013. A 13 µA analog signal processing IC for accurate recognition of multiple intracardiac signals. *IEEE Trans. Biomed. Circuits Syst* 7 (6), 785–795.
- Yelamos, D., Casas, O., Bragos, R., Rosell, J., 1999. Improvement of a front end for bioimpedance spectroscopy. *Ann. N.Y. Acad. Sci.* 873, 306–312.
- Yu, T.H., Liu, J., Zhou, Y.X., 2004. Using electrical impedance detection to evaluate the viability of biomaterials subject to freezing or thermal injury. *Anal. Bioanal. Chem.* 378, 1793–1800.
- Yu, C., Wang, L., Chau, E., et al., 2005. Intrathoracic impedance monitoring in patients with heart failure. Correlation with fluid status and feasibility of early warning preceding hospitalization. *Circulation* 112, 841–848.
- Zaki, R., Bulgiba, A., Ismail, R., Ismail, N.A., 2012. Statistical methods used to test for agreement of medical instruments measuring continuous variables in method comparison studies: a systematic review. *PLoS One* 7, e37908.
- Zaki, R., Bulgiba, A., Nordin, N., Ismail, N.A., 2013. A systematic review of statistical methods used to test for reliability of medical instruments measuring continuous variables. *Iran. J. Basic Med. Sci.* 16, 803–807.

- Zhang, M.I.N., Repo, T., Willison, J.H.M., Sutinen, S., 1995. Electrical impedance analysis in plant tissues: on the biological meaning of Cole-Cole α in Scots pine needles. *Eur. Biophys. J.* 24, 99–106.
- Zheng, Q.A., Chang, D.C., 1991. High-efficiency gene transfection by *in situ* electroporation of cultured cells. *Biochim. Biophys. Acta* 1088, 104–110.
- Zhou, X.-F., Markx, G.H., Pethig, R., Eastwood, I.M., 1995. Differentiation of viable and non-viable bacterial biofilms using electrorotation. *Biochim. Biophys. Acta* 1245, 85–93.
- Zipes, D.P., 2014. Can TASER electronic control devices cause cardiac arrest? *Circulation* 129, 101–111.
- Zoll, P.M., Linenthal, A.J., 1964. External electrical stimulation of the heart. *Ann. N.Y. Acad. Sci.* III, 932–937.

Index

Note: Page numbers followed by f indicate figures; t, tables; b, boxes.

0–9

1R-2C model. *See* Debye relaxation model

A

Ablation, 455

Absolute value, 506

Accommodation effect, 478

Accuracy, 392

Action potential, 119, 122–127

Activation energy, 204–205

Acupuncture, 475

Adenosine triphosphate (ATP), 120

Adipose tissue, 92

Admittance, 2, 94f, 256–257, 335–337, 508
faradaic, 216–217

Adsorption, 104

specific, 194–195

After-field effect, 465

Aggregates, 70

Aliasing errors, 277

Alpha parameter (α parameter), 353–354

Alternating current (AC), 2, 263

Amino acids, 79–82

Ampereometry, 204

Amplifiers, 283–286, 285f

AC admittance, 293–294, 294f

black box analysis, 283–286

DC potential measurement, 293–294, 294f

filters, 283–286

instrumentation differential, 286–288

interface patient and, 288–290

lock-in, 295–299, 297f

microelectronic lock-in, 299–302

power line noise cancellation, 290–293, 291f

risk considerations, 288–290

reference wire, 283

Amplitude, 265

magnitude frequency spectrum, 270–271

Analog lock-in amplifiers, 298–299.

See also Digital lock-in amplifiers

Analog-to-digital converter (ADC), 296

Analysis of covariance (ANCOVA), 379–380

Analysis of variance (ANOVA), 378

Anelectrotonus, 476

Angular frequency, 264

Animal electricity, 496

Anisotropy, 110–117

Anode, 15–17

Antihyperhidrosis, 321

Aperiodic waveforms, 271–273

Application specific integrated circuits (ASIC),
300

Applied part, 282–283

Arachnoid, 129

Area under the curve (AOC), 387

Argand diagram, 506

Argand, Jean Robert, 506

Argon gas, 455

Arrhenius, Svante August, 17–18

Arsonval, Arsène d', 499

Artificial neural networks (ANN), 385

Association analysis, 381–382

Associative memory networks, 398

Atrioventricular node (AV node), 412–413

Autocorrelation, 277

Auxiliary currents, 492

Axon transmission, 131–138

B

Baby wavelet, 402

Back-propagation algorithm, 398

Band electrodes, 234

- Basic capacitor experiment, 42f, 45–47
 Basic electrolytic experiment, 13–17
 Basic measuring circuit, 286
 Basic membrane experiment, 67–70, 68f
 Basic suspension experiment, 70–71, 70f
 Bidomain model, 367
 Bilayer lipid membrane (BLM), 84, 84f, 119–120, 119f
 Bioelectric impedance analysis (BIA), 445
 Bioelectric signals, 119
 Bioelectric sources, 405
 brain, 416–417
 EDA, 420–425
 eye, 417–418
 heart as, 405–416
 muscles, 418
 nerves, 419
 skin applications, 425–433
 stomach, 418
 urology, 419
 Bioelectricity, 1, 3
 peoples working with, 7
 Bioimpedance spectroscopy (BIS), 448–449
 Bioimpedance, 1–3
 hypothesis and research design, 372–375
 peoples working with, 7
 quantities of, 4
 techniques, 419
 Biomaterial, 2, 77–85, 141
 Biometry, 442
 Biopermittivity, 2–3
 Biosensor, 233
 Bipolar leads, 406
 Bipolar measuring depth, 167–168
 Bispectral analysis, 278
 Bivariate association, 381–382
 Black box theory, 258–259
 Black-box, 255–262, 256f, 375–376
 Blood, 93–95
 coagulation, 25
 Bode diagram, 340–341
 Body Mass Index (BMI), 381–382
 Body segment resistance, 107f
 Body
 cell mass, 448–449
 composition, 445–450
 forces, 33
 liquids, 77–78
 position, 447
 Boltzmann equation, 193–194
 Bone tissue, 92
 Bootstrapping, 285–286
 Bound
 vector, 505
 water, 77–78
 Boundary value problem, 142
 B-point, 442–443
 Brain electroconvulsion. *See* Electroshock
 Brain, 416–417
 ECOG, 417
 EEG, 416–417
 and neurons, 129–130
 Brainstem, 129
 Breakdown, 84, 288, 322, 488
 Bridges, 294–295
 Buffer, 224, 287
 Bulk electrolytic DC conductance, 17–18
 conduction and semiconductor theory, 28–29
 conductivity
 of water itself, 22–23
 of weak acids, 24–25
 contributions to ionic conductivity, 19–22
 environment of ions, 18–22
 isoelectric point, 25–26
 materials, 29
 special electrolytes, 26–28
 Butler-Volmer equation, 217
- C**
- Cabrera sequence, 407
 Calibration, 447
 Capacitor experiment, basic, 45–47
 Carbohydrates, 83
 Carbon electrodes, 15
 Carbon tattoo, 191
 Cardiac electrophysiology, 412–413
 Cardiac output (CO), 433
 Cardiac pacemakers, 473–474
 Cardiac resynchronization therapy, 469–470
 Cartesian coordinate system, 505–506
 Cathode, 15–16, 198, 476, 482

- Cell membrane, 325–327. *See also* Lipid membrane
 cell clamp, 326f
 Cell oscillator, 127
 Cell polarization, 120–122
 Cell potential model, 125–126
 Cell sorting, 466–467
 Cell suspensions
 cell sorting and characterization, 466–467
 cell-surface attachment, 467–468
 coulter counter, 468
 electrofusion, 459–466
 electroporation, 459–466
 micromotion detection, 467–468
 Cell-attached patch clamp technique, 244
 Cell-surface attachment, 467–468
 Cellular spin resonance, 242–243
 Center of symmetry, 116
 Central nervous system (CNS), 127, 419
 Cerebellum, 129
 Cerebral blood flow (CBF), 439
 Cerebrospinal fluid (CSF), 88, 129
 Channel gating, 123–125
 Chaos theory, 398–400
 Characteristic relaxation frequency, 55
 Charge-dipole interactions, 44–45
 Chassis wire. *See* Amplifier reference wire
 Chemical bonds, 12
 Chest electrodes, 411–412
 Chirp-z-transformation, 280
 Chronaxie value, 477
 Classification methods, 384–386
 Clausius–Mosotti equations, 44
 Clinical applications, 5–6
 Clinical performance, 396–397
 Cole element, 350
 Cole equations, 348–357
 Coley system, 351f
 admittance locus, 352f
 Cole_z system, 349f
 impedance locus, 350f
 exponent α in, 354t
 Cole, Kenneth S., 500–503
 Cole, Robert, 502–503
 Cole–Cole equations, 357–358, 358f, 502–503
 Cole–Cole model, 72
 Cole plot, 500–501
 Cole–Cole plot, 357–358
 Collodion, 191, 416–417
 Colloid, 26
 Common mode feedback, 174–175
 Common mode rejection ratio (CMRR), 287
 Common mode voltage (CMV), 287
 Complex
 conductivity, 48
 permittivity, 47–48
 resistivity, 48
 variables, 47–51
 numbers, 505–508
 Concentration wave, 31
 Concentric ring electrodes, 235–236
 Conductance, 17–29, 59, 422
 Conduction
 band, 28
 theory, 28–29
 Conductivity
 complex, 48, 58f
 ionic, 12, 19–22, 63–64
 molar, 20, 22–23
 temperature dependence, 25
 tissue, 85, 88t, 454, 457
 Conductor, 1
 Conformal mapping, 41
 Constant amplitude
 current output, 281–282
 voltage output, 281
 Constant phase element (CPE), 38, 212, 329, 344–348, 346f–347f, 500–501
 Constricting zone, 146
 Contact electrolytes, 184, 213–214
 contact media descriptions, 185–188
 dry and dielectric contact, 188–191
 skin preparation, 191
 Continuous frequency spectrum, 272
 Continuous wavelet transform (CWT), 401
 Convolution, 277
 Correlation, 277
 Cortex, 129
 Coulomb's law, 39–41, 332

- Coulter counter, 468
 Counterions, 82
 adsorbed, 65–67
 Covalent bonds, 12–13, 13t. *See also* Ionic bonds
 Current clamp. *See* Constant amplitude—current output
 Current limiting body resistance, 488
 Current measuring circuit, 286
Current
 density field lines, 113, 114f
 density, 19
 step, 206, 260, 339
 dipole, 132–133, 147, 177
 auxiliary, 492
 electronic/ionic, 9
 Franklin, 495–496
 galvanic, 262, 496
 leakage, 127, 492
 diodynamic, 479
 interferential, 479–480
 Current-carrying electrodes (CC electrodes), 9, 141, 147–150, 179, 255
 Cyclic voltammetry, 206
 Cylinder monopolar sources, 155–157
- D**
 Da Vinci, Leonardo, 495
 Dalton unit (Da unit), 524
 Data
 analysis methods, 394–403
 calculation, 370–371
 presentation, 370–371
 reduction, 375–376
 DC potentials, 197–203
 Death process, 106–109
 Debye equations, 44
 Debye length, 19
 Debye models, 342
 2C-1R, 343–344, 343f–344f
 2R-1C, 342–343, 343f
 Debye relaxation model, 53–59
 Debye single dispersion, 53
 Debye unit, 42
 Debye, Peter, 501
 Debye-Falkenhagen effect, 25
 Debye-Hückel approximation, 194
 Defibrillation, 3
 Defibrillator shocks, 450–452, 451f
 Denaturation, 2, 81, 457–458
 Dendrite, 127–129
 Dental galvanism, 115
 Depolarization process, 3
 Descriptive models, 329–331
 Diabetics, 429
 Diodynamic currents, 479
 Dialysis, 25–26
Dielectric(s), 37
 AC polarization and relaxation, 51–61
 capacitor experiment, 45–47
 complex variables, 47–51
 constant, 39
 decrement, 40, 77
 dispersion and dielectric spectroscopy, 71–74
 increment, 66–67, 80
 interfacial polarization, 61–67
 material constants, 47–51
 membrane experiment, 67–70
 microscopic anisotropy, 110–111
 polarization in uniform, 38–45
 spectroscopy, 71–74
 suspension experiment, 70–71
 Dielectrophoresis (DEP), 33, 242
 traveling wave, 243–244
 Diffuse electric layer, 192–193
 Diffusion, 30–33
 Digital heterodyning process, 304
 Digital lock-in amplifiers, 296–298.
 See also Lock-in amplifiers
 Dimensionless, 518–521
 Dipolar ion, 79
Dipole
 electrostatic, 44–45, 147, 177
 current, 132–133, 147, 177
 Dipole–dipole interactions, 44–45
 Direct current (DC), 2, 262, 507
 ablation, 477
 conductance, 17–29
 conduction, 9–13
 conductivity, 24, 115–116
 potentials, 197–203
 shock pulses, 477

- Discharge, 446–447, 452f
 Discoveries, 480–481
 Discrete parameter wavelet transform (DPWT), 401
 Discriminant function analysis, 384–385
 Disk electrode, 151, 234
 Disk monopole source, 150–152
 Dispersing zone. *See* Constricting zone
 Dispersion, 51–52, 71–74, 360–362, 361f, 413
 Displacement current, 334
 Dissipation factor, 49
 Dissociation, 17–18, 24
 Distribution of relaxation times (DRT), 354, 358–367
 DNA molecule, 82–83
 Donnan effect, 122
 Donnan potentials. *See* Membrane equilibrium
 Double layer, electric, 85, 180, 192–197
 Drionic, 426
 Driving point immittance, 256
 Dry skin, 483–484
 Dura mater, 129
- E**
 Earth leakage current, 492
 Earth, 231
 Eddy currents, 245–246
 Effect size, 374
 Effective electrode area (EEA), 184
 Einthoven triangle, 407–411, 407f–408f
 Einthoven, Willem, 497–498
 Ejection wave, 442–443
 Electrets, 44
 Electric
 arc, 190–191
 dipole moment, 18
 electrical equivalent, 331
 fence, 490
 field sensor, 233
 fish, 496
 flux density, 43
 susceptibility, 43
 Electric, double layer, 85, 180, 192–197
 field coupling, 247–249
 axis of the heart, 409–410
 hazards, 485–489
 Electrical impedance myography (EIM), 437–438
 Electrical impedance tomography (EIT), 171–176, 435
 Electrical model, 130, 329, 415
 Electrical safety, 482–494
 Electricity, quantity of, 183, 208–209, 482
 Electroacupuncture, 475
 Electrocardiogram (ECG), 99, 185, 273–274, 497–498
 Electrocardiography (ECG), 405, 415–416
 standard extremity leads, 408f
 waveform lead II, 406f
 Electrocautery, 453
 Electrochemistry instruments, 305
 Electroconvulsion, 452–453, 477
 Electrocorticography (ECoG), 417
 Electrocution, 490
 Electrode area (EA), 184
 Electrode double layer, 191–192
 lateral fields, 196–197
 perpendicular fields, 192–195
 Electrode metals, 180
 metal and electronic conductor properties, 183–184
 test of polarizability, 180–182
 Electrode pair DC voltage, 200–201
 Electrode pairs, 179, 219–220
 Electrode polarization, 209, 317–318
 DC counter electromotive voltage, 209–210
 DC/AC circuit for electrode processes, 214–219
 immittance, 219
 impedance in saline, 210–214
 Electrode(s), 9
 contact electrolytes, 184–191
 current carrying (CC), 141, 179, 255
 DC current flow experiment, 203–208
 DC potentials, 197–203
 designs, 233–252
 double layer, 191–197
 equivalent circuit, 509–518
 Faraday’s law of electrolysis, 208–209
 indifferent, 227, 231
 invasive, 115, 152–153, 190
 metals, 180–184

- Electrode(s) (*Continued*)
multiple electrode systems, 219–226
needle, 89, 475, 477
neutral, 232
(non-) polarizable, 180
pair, 179
pick-up (PU), 147–148, 179
process, 214–219
proper, 1
reactions, 17
reference, 115, 202–203, 417–418
single electrode, 179–180
systems
 four-electrode, 223–226
 three-electrode, 220–223
 two-electrode, 166
terminology, 226–233
vulnerable electrode technology, 252–253
working, 204, 230
- Electrodermal activity (EDA),
 420, 498–500, 499f
AC method, 422, 423f
physiology, 420–421
psychophysiology, 420–421
skin conductance DC method, 421, 423f
SP, 422–423
stimuli, 420–421
- Electrodermal response (EDR), 278, 420–421
- Electrodialysis, 25–26
- Electrodiffusion, 31
- Electroencephalogram (EEG), 185–186,
 277, 498
- Electroencephalography (EEG), 191
- Electrofusion, 459–466
- Electrogastrography (EGG), 418
- Electrogenic transport, 31
- Electrogram
- Electrogustometry, 483
- Electrokinetics, 33
 exogen transport, 34
 flow-generated potentials, 35
- Electrolyte
 colloidal, 26–27
 contact, 184–191
 fused, 27
 solid gel (hydrogel), 188
- solid, 27
wet gel, 185–186
- Electrolyte, 9, 45
 concentrations, 21, 214
 effect, 488
- Electrolytic cell, 13–14
- Electrolytic experiment, basic, 14f
- Electrolytics
 electrolytic DC experiment, 13–17
 electron shell configuration, 10t
 ionic and electronic DC conduction, 9–13
 particle migration and diffusion, 30–33
- Electromagnetic field, 485
- Electromedical equipment, 491–494
- Electromotive voltage (EMV), 86
- Electromyography (EMG), 405–406, 418
- Electron
 affinity, 12
 transfer process, 214–215
 valence, 10–11
- Electronegativity, 11
 Pauling's scale of, 11t
- Electroneurography (ENeG), 419
- Electroneutrality, 20
- Electronic polarization, 41. *See also* Ionic polarization
- Electronystagmography, 41
- Electrooculography (EOG), 417
- Electro-osmosis, 34, 69
- Electrophoresis, 34
- Electrophysiological hazards, 485–489
- Electroporation, 459–466
- Electroretinography (ERG),
 418
- Electrorotation, 242–243, 466
- Electroshock, 452–453
 weapon, 490–491
- Electrostatic dipole, 44–45, 147, 177
- Electrostatic discharge pulse, 484–485
- Electrostriction, 116
- Electrosurgery, 453
 embedded bioimpedance devices, 456–459
 frequency dependence, 455f
 monopolar, 453, 454f, 458f
 output circuit, 457f
 risk analysis, 455–456

- Electrotherapy
 with DC, 475–477
 electroacupuncture, 475
 muscles, 477–480
 transcutaneous stimulation, 474–475
- Electrotonus, 476
- Electrovalency, 10–11
- Electrovibration perception, 483f
- Elementary charge, 208
- Ellipsoidal needle source, 152–154
- Embedded bioimpedance devices, 456–459
- Emotional sweating, 420–421
- Enclosure leakage current, 492
- Endogenic potentials. *See*
 Flow-generated potentials
- Endoneurium, 134
- Endorphins, 475
- Endosomatic measurements, 421
- Energy of waveform pulse, 275–276
- Equivalent circuit equations, 509–510
 four-component series circuit equations, 517–518
 resistor and capacitor circuits equations,
 510–517, 510f
- Equivalent conductance, 20
- Event-related signal, 278
- Evoked potentials, 278
- Evoked responses, 278
- Excitable tissue, 119
- Excitation, 135–136
- Exogen transport, 34
- Exogenous noise, 416
- Exosomatic measurements
- Explanatory models, 329–332
- Exponential discharge curve, 56, 260, 369
- External electric excitation, 136
 trigger parameters, 136–137
 waveforms, 137–138
- Eye**
 electronystagmography, 417–418
 EOG, 417
 ERG, 418
- F**
- Factor analysis, 378–380. *See also* Bioimpedance analysis
- False negatives (FN), 387
- Faradaic current, 208–209
- Faradaic impedance, 216–217
- Faraday constant, 199, 208
- Faraday stimulation, 497
- Faraday, Michael, 208–209
- Faraday’s law of electrolysis, 208–209
- Faraday’s law of induction, 245–246, 333, 368
- Fascicle, 134
- Fat free mass (FFM), 448
- Fatal levels, 487
- Feature space, 385
- Feedforward networks, 398
- Fick’s law, 31
- Field-flow fractionation, 467
- Fingerprint detection, 432–433
- Finite element method (FEM), 164, 169–171
- First principal component (PC1), 394–395
- Fixed recording lead, 158–160
- Fixed vector, 505
- Flow-generated potentials, 35. *See also* Streaming potential
- Fluid status monitoring, 471–472
- Flux density, 19, 208
- Flux, 208
- Focused impedance measurements (FIM), 226
- Forward problem, 142
- Four-component series circuit equations, 517–518
- Four-electrode systems, 223–226. *See also*
 Three-electrode systems monopolar recording
- Fourier
 analysis, 273–276
 series, 268–271
 transforms, 273–278
- Fractal
 attractor, 399
 patterns, 398–400
- Fractional power law discharge curve, 56, 260, 369
- Franklin currents, 495–496
- Franklin, Benjamin, 495–496
- Frequency response analyzer (FRA), 305
- Frequency
 dependence, 112, 484
 domain, 273–274, 278–279
 filtering
 high-pass filter, 280

- Frequency (*Continued*)
 low-pass filter, 280
 spectrum, 265, 273–276, 415–416
 vector, 279–280
- Fricke, Hugo, 501–502
- Fricke's law, 347–348
- Frictional charging. *See* Triboelectricity
- Fulguration, 453–454
- Functional grounding, 282–283
- G**
- Galvani, Luigi, 496
- Galvanic current, 262
- Galvanic electrode, 233
- Galvanic skin response (GSR), 115
- Galvanization, 475–476
- Galvanometer, 231, 496–498
- Galvanostat, 496
- Gap junctions, 135
- Gating theory, 474
- General network theory, 255–262
- Geometrical analysis, 141
 CC and pick-up dipoles, 147–150
 constricting zone, 146
 dielectric and conductor theory duality, 176–177
 disk monopole source, 150–152
 EIT, 171–176
 ellipsoidal needle source, 152–154
 FEM, 169–171
 ideal two-dimensional models, 155–158
 signal transfer, 158–169
 sphere monopole source, 143–146
 volume conductors, 141–142
- Global symbols, 518–521, 519t–521t
 physical dimensions, 522–524, 523t
- Glycocalyx, 85
- Gouy-Chapman theory, 193–194
- Gray matter, 129
- Grounded patient, 282–283
- Guericke, Otto von, 495
- Guldberg, Cato Maximilian, 24–25
- Guldberg-Waage law, 24
- H**
- Half cells, 219–220
- Hanai's equation, 64
- Heart dipole vector, 162
- Heat effects, 487–488
- Heaviside, Oliver, 499
- Helmholtz layer, 192–193, 324
- Helmholtz, Hermann von, 498–499
- Henderson equation, 201
- Heteroscedasticity, 382
- Hierarchical design. *See* Nested design
- High-frequency, 453
- High-pass filter, 280
- His Jr., Wilhelm, 412–413
- His-bundle, 412
- Hoeber, Rudolf, 500
- Hold-out method, 388–389
- Homoscedasticity, 382
- Human skin, 95–105
- Hurst exponent, 399–400
- Hydration, 18, 197
- Hydrogels, 188
 electrode, 212–213
- Hydrogen production, 477
- Hydronium. *See* Oxonium
- Hydroxonium. *See* Oxonium
- Hyperhidrosis, 426–427
- I**
- Ideal component equivalent circuits, 335–341
- Ideal cylinder models, 433–435, 434f
- Ideal two-dimensional models, 155–158
- Immittance, 2, 256, 348–349
 with endogenic signal source, 281
 theory, 260
- Impedance analyzer, 303–305
 electrochemistry instruments, 305
 LCR meters, 305–306
 multichannel and portable devices, 308
 network analyzer, 306–307
 scalability, 308
 spectrum analyzers, 307–308
- Impedance cardiography (ICG), 405
 stroke volume measurements, 440–442
 time relationships, 442–444
- Impedance, 2, 508, 511
 equation, 257
 spectrum, 314f

Implanted active thoracic devices, 469–470
 cardiac pacemakers, 473–474
 fluid status monitoring, 471–472
 physiologic impedance components, 470–471

In vitro measuring cells, 240–242

Incremental impedance, 323

Index, 371

Indifferent electrode, 227, 231

Induced dipole moments, 42–44

Inductance, capacitance, resistance meters (LCR meters), 305–306

Initial systolic time interval (ISTI), 443

Innovations, 480–481

Inside-out patch technique, 244–245

Instrumentation amplifier, 285, 286f

Instrumentation differential amplifiers, 286–288, 286f

Instrumentation nonlinearity, 327

Insulation, 133–134, 492

Insulator, 29, 47

Interface patient and amplifier, 288–290
 differential preamplifier, 289f–290f
 mapping of *facialis*, 289f

Interfacial polarization, 61–67

Interferential currents, 479–480

Internal Cardioverter Defibrillator (ICD), 469–470

Intracellular water (ICW), 448–449

Intraclass correlation coefficient (ICC), 388

Invasive needle electrodes, 236–238

Inverse Fourier transform, 274

Inverse problem, 142

Ion
 channel, 123
 exchanger, 26

Ionic
 atmosphere, 18–19
 bonds, 12
 polarization, 41

Ionization, 10–12

Iontophoresis, 321, 431–432, 476

Irreversible electroporation (IRE), 459
 electrical properties, 460–461
 for tissue ablation, 459–460

Isoelectric point, 25–26

J

Joule effect, 60–61

K

Kelvin probe, 251–252

Keratin, 27

Keratinized tissue, 95–105

Kernel trick, 385

k-fold cross-validation, 389

Kirchhoff's law, 410

k-Nearest Neighbors (kNN), 386

Kohlrausch, Friedrich Wilhelm Georg, 19

Kramers–Kronig transforms (KKTs), 260–262

L

Laboratory applications, 6

Laboratory on a chip, 6

Langmuir adsorption isotherm, 194–195

Laplace equation, 333

Laplace, Pierre Simon de, 259

Lead vector, 407–411

Leakage, 276
 currents, 492

Leave-one-out method, 389

Left arm (LA), 405

Left leg (LL), 405

Let-go current, 487

Levitation, 243

Ligands, 135

Lightning, 489–490

Limb electrodes, 405–411, 406f

Limb leads. *See* Limb electrodes

Limits of agreement (LOA), 388

Linear behavior, 319, 323

Lipids, 83–85
 membrane, 324–325

Liposome, 85

Liquid junction potential, 201–202

Loading plot, 395

Lock-in amplifiers, 295–299, 297f

Logarithmic potential, 156

Loss angle, 49

Loss factor, 48

Low-pass filter (LPF), 280

Lungs, imaging of, 444–445, 445f–446f

M

- Macroscopic anisotropy, 111–112
 Macroshock, 486–487, 486f
 Magnetic Induction Tomography (MIT), 174
 Magnetic Resonance Electrical Impedance
 Tomography (MREIT), 89
 Magnetic resonance imaging (MRI),
 245–246
 Mann-Whitney U test. *See* Wilcoxon
 rank-sum test
 Mass action law, 24
 Material constants, 47–51
 Material under test (MUT), 310, 313f
 Maxwell, James Clark, 499
 Maxwell's equations, 2, 38, 333, 410
 Maxwell-Fricke equation, 63–64
 Maxwell-Heaviside equations, 332–335
 Maxwell-Wagner effects, 61–63
 Medical
 applications, 6
 sensor, 233
 technology, 498
 Membrane
 equilibrium, 202
 experiment, basic, 67–70
 Memristor, 367–368, 368f
 nonlinear model, 367–368, 368f
 Mesh points, 169
 Metal/ion systems, 197
 Metal-liquid overvoltage, 320–321
 Microelectrodes, 239–240
 Microelectronic lock-in amplifiers, 299–302
 modified synchronous detector, 302f
 on-chip current mode, 300f
 sine waves spectra, 301f
 Microelectroporation, 462–463
 Micromotion detection, 467–468
 Microshock, 486–487, 486f
 Minimum phase shift network, 261
 Mixed models, 380–381
 Models, 4–5
 bidomain, 367
 two-component, 335–336, 338
 Modulus function, 49
 Molar conductivity, 20, 21t
 Molecular bonds, 12–13

Monopolar

- electrosurgery, 453, 454f, 458f
 sphere, 142
 system, 204
 Mother wavelet, 401–402
 Motor neuron, 128–129
 Multinomial logistic regression, 384
 Multiple Cole system, 362–367
 Cole plot, 364f–366f
 measurements on skin, 363f
 parameters, 365t–366t
 Multiple electrode systems
 electrode pairs, 219–220
 four-electrode systems, 223–226
 half cells, 219–220
 three-electrode systems monopolar recording,
 220–223
 Multiple linear regression, 383
 Multiple variables, 375–376
 Multiple-point electrodes, 235
 Multivariate analysis of variance (MANOVA),
 379–380
 Multivariate analysis, 394–396
 Muscle(s), 418
 group, 135
 tissue, 89–91
 Myelinated axons, 133–134, 134f

N

- Nafion, 27
 Nail, 2, 27, 89, 102–105
 Nanoelectrodes, 239–240
 Needle electrode, 89, 236–238, 237f, 477
 Neocortex, 129
 Nernst equation, 122, 199–200
 Nerve(s), 134, 419
 damage, 488
 excitation, 456
 tissue, 92
 Nested design, 380–381
 Network analyzer, 306–307
 Neural networks, 397–398
 Neuron, 127–130
 brain and, 129–130
 Neurostimulation, 320
 Neutral electrode, 144, 166–167, 232, 234, 453

-
- Node of Ranvier, 133–134
 Noise, 262–283, 416
 Nollet, Jean-Antoine, 496
 Nonbiological applications, 6
 Nongalvanic coupling to tissue
 capacitive coupling to tissue, 247
 endogenic current sources, 247
 far-field radiation, 249–251
 high-frequency electric field coupling to tissue, 248–249
 low-frequency electric field coupling to tissue, 247–248
 magnetic coupling to tissue, 245–246
 magnetic resonance imaging, 246–247
 static electric field coupling to tissue, 247
 Nonlinear system, 318
 cell membrane, 325–327
 cell clamp, 326f
 electrode nonlinearity, 319–321
 electrolyte nonlinearity, 318–319
 incremental impedance for nonlinear, 323
 instrumentation, 327
 lipid membrane, 324–325
 time-variant objects, 323
 voltage-current curves, 322f
 tissue, 321–327
 Nonmedical applications, 6, 480
 Nonpolarizable electrode, 207
 Not grounded patient, 282–283
 Null hypothesis, 372
 Nyquist criterion, 277
- O**
- Ohm's law, 316
 One-compartment model, 434–435. *See also* Two-compartment model
 One-sided t-test, 376
 One-tailed t-test. *See* One-sided t-test
 Onsager, Lars, 22
 Operational amplifiers, 285–286
 Ordered logistic regression, 384
 Orientational polarization, 41
 Ørsted, Hans Christian, 497
 Osmosis, 25–26
- Osmotic pressure, 101, 202
 Outside-out patch technique, 244–245
 Overvoltage, 179, 206
 Oxidizing agent, 198
 Oxonium, 23
- P**
- Pacemaker, 321, 473–474
 Pain, 5–6, 138, 474, 479
 Parallel cylinders, 157
 Parallel G-C circuit, 337
 Parallel model, 335–337, 336f
 Parallel version, 343
 Parameterization, 371, 375–376
 Partial least squares regression (PLS regression), 383–384
 Particle migration, 30–33
 Passive cell membrane, 83–85
 Passive tissue electrical properties
 biomaterials, 77–85
 special electrical properties, 110–117
 tissue and organs, 85–110
 Patch clamp electrode, 244–245
 Patient auxiliary currents, 492
 Pauling, Linus, 11
 Pauly-Schwan equation, 65
 Pearl chain formation, 244
 Peptides, 81
 Periodic waveforms, 263–271
 Peritoneum, 86
 Permanent dipole moments, 42–44
 Permittivity, 2, 39–41
 relative, 40t
 pH electrode, 27
 Phase
 angle, 49
 space, 398–399
 Phase-sensitive detector (PSD), 298, 298f
 Phasor, 264, 509
 Phospholipids, 84
 Pick-up electrodes (PU electrodes), 179, 255
 dipoles, 147–150
 Piezo electric effects, 116–117
 Plant tissue, 109–110
 Platinum
 black electrode, 210–211

- Platinum (*Continued*)
 electrodes, 15
- Plethysmography, 433
 conductivities effect, 435
- EIM, 437–438
- geometry and conductivity distribution, 436–437
- ideal cylinder models, 433–435, 434f
- REG, 438–440
- Poisson equation, 192–194, 333
- Polar substance, 26
- Polarizable electrode, 180, 200, 208, 228
- Polarization, 38
 process, 460–461
 types of, 41
- Polarography, 204
- Polyelectrolyte, 82
- Ponderomotive forces. *See* Body forces
- Ponderomotoric effects and electrodes, 242–244
- Postexcision changes, 106–109
- Potential
 action, 119, 122–127, 135, 147, 419
 cell, 125–126, 198–199
 Donnan, 202
 electrode, 14, 197, 203
 flow generated, 35
 injury, 116
 liquid junction, 115, 201–202
 redox equilibrium, 199–201
 sedimentation, 35
 streaming, 35, 115, 233–234
 zeta, 25, 34, 194–195
- Potentiometry, 197–198, 204
- Potentiostat, 305, 308
- Power density spectrum, 276
- Power spectrum, 276
- Power, 60, 145, 272, 290–293
- Preejection period (PEP), 442–443
- Primary hydration sphere, 197
- Principal component analysis (PCA), 375–376, 429
- Principal components regression (PCR), 383–384
- Probability density function, 278
- Protective earth, 492
- Proteins, 79–83
- Proton hopping mechanism, 23
- Q**
- Quadro-polar, 229t
- Quantity of electricity, 208
- Quasi-circular arcs, 359–360
- R**
- Radiofrequency (RF), 290
- Random measurement error, 389–392
- Random subsampling, 389
- Rayleigh scattering, 250
- Reactance, 69, 261
- Reactive power, 60
- Receiver operating characteristic (ROC), 387, 430
- Receptors, 138
- Reciprocal lead field, 163–164
- Reciprocity, 258–259
- Recurrent networks, 398
- Redox process, 17
- Redox systems, 197–199
- Reducing agent, 198
- Reference electrodes, 202–203
- Regression methods, 382–384
- Relative permittivity, 39, 40t, 57f, 461
- Relaxation, 51–52
 Debye model, 342–344, 369–370
 time, 19
- Repeated hold-out, 389
- Resistance, 105–106, 368, 422
- Resistivity, 2, 130, 437, 456–457
- Resonance, 52, 74, 318
- Reversible electroporation, 459
- Rheobase, 137f, 138, 477
- Rheoencephalography (REG), 438–440
- Right arm (RA), 405
- Ring monopolar source, 157–158
- Root-mean-square (rms), 61, 418
- Root-mean-square error (RMSE), 382–383
- S**
- Saccharides, 83
- Safety grounding, 282
- Salt bridges, 187–188, 201–202
 principle, 415
- Savart, Felix, 174–175
- Scalars, 505–506
- Schwan, Herman Paul, 503–504

- Schwarz theory
later improvements of, 196
for suspension of spheres, 196
- Score plot, 395
- Sedimentation potential, 35
- Self-organizing networks, 398
- Semiconductor theory, 28–29
- Sensitivity field, 166–167
- Sensor, 233, 433, 495, 498
- Series
model, 338
resistance, 215–216
version, 343
- Short-time Fourier transform (STFT), 400–401
- Siemens, Werner von, 500
- Sigman effect, 440
- Sign conventions, 508–509
- Signal transfer, 158, 257–258
bipolar measuring depth, 167–168
fixed recording lead, 158–160
reciprocal lead field, 163–166
sensitivity field, 166–167
spatial resolution and frequency content, 160–161
surface layer, 169
transfer lead vector, 161–163
- Signal
amplitude, 415
averaging, 278
generators, 281–282
processing forms, 278
- Silver chloride wet gel electrode, 211–212
- Silver/silver-chloride electrodes, 15
- Simple effects, 378–379
- Simple Helmholtz layer, 192–193
- Simple Maxwell-Wagner model. *See* Four-component series circuit equations
- Sine wave, 264, 483–484, 509
complex numbers, 509
sum and product, 265–268
- Single electrode, 179–180
- Single fault condition, 487, 491, 493
- Single-cell microelectroporation technology, 462–463
- Sinoatrial (SA), 412–413
- Skin conductance (SC), 422–423
- Skin conductance response (SCR), 420
- Skin potential (SP), 422
- Skin
cancer, 430–431, 431f
diseases, 426–432
electrodes, 233–236
wires, 236
fibrosis, 431
friction, 420–421
hydration measurement, 425–426
irritation, 427–429
- Skin, breakdown, 488
- Sliding vector, 505
- Sodium pump, 120
- Solid gel, 187–188, 253
- Solvation, 18
- Special electrolytes, 26–28
- Specific absorption rate (SAR), 250–251
- Specificity, 387, 419, 428
- Spectrum
analysis, 273–278
analyzers, 307–308
- Sphere monopole source, 143–146
- Spherical particles, suspension of, 63–65
- Spontaneous activity, 83–85
- St. Elmo's fire, 495–496
- Standardized conditions, 199
- Static electricity, 495
- Static values, 53, 263
- Statistical methods, 371–393
- Stepwise regression, 383
- Stern
layer, 324, 325f
theory, 194–195
- Stoke's law, 20, 59
- Stomach, 418
- Strange attractor, 399
- Stratum corneum (SC), 88
- Streaming potential, 35
- Stripe monopolar sources, 155–157
- Stroke volume (SV), 433
- Sudologger. *See* sweat activity measurement
- Support-vector machines (SVM), 385
- Supraelectroporation, 463–466

- Susceptance, 71, 89, 97–98, 102–104
 Susceptibility, 43–44
 Susceptivity, 51
 Suspension experiment, basic, 70–71
 Sweat activity measurement, 425
 Swelling, 433
 Symmetrical distribution of relaxation times
 Synapses, 135
 Synchronous rectifier, 294–295, 298–300
- T**
 Taser X26. *See* Electroshock—weapon
 Temperature coefficient, 25, 87
 TENS, 474–475, 479
 Tesla, Nikola, 497
 Tetrapolar electrode system, 436, 436f
 Tetrapolar systems. *See* Four-electrode systems
 Three-electrode systems monopolar recording, 220–223
 Threshold of perception, 482–485
 Time constant, 53, 59, 260, 339, 361
 Time domain reflectometry, 315–318
 coaxial transmission, 315f
 Time domain spectroscopy (TDS), 309–310, 309f
 Time domain, 273–274, 278–279
 transmissometry, 310–314
 arrangement for voltage, 311f–312f
 Time-variant objects, 323
 Tissue
 and organs, 85–110
 anisotropy, 110–113
 liquid electrolytes, 190
 Titanium alloys, 184
 Tomography, 171, 176
 Tonus, 476
 Total body water (TBW), 382–383, 445
 Transconductance, 257, 299–300
 Transcutaneous electrical nerve stimulation (TENS), 474–475
 Transdermal drug delivery, 431–432
 Transducer, 233
 Transfer
 admittance, 256–257
 coefficient, 217
 impedance, 256–257
 Transformation, remarks about, 279–280
 Transimpedance amplifiers, 285
 Transmembrane voltage, 324, 461
 Transmittance, 256
 Transresistance amplifiers, 285
 Traveling wave dielectrophoresis, 243–244
 Tribo electric effects, 116–117
 Triboelectricity, 116–117
 True negatives (TN), 387
 True physiological signals, 416
 Tunnelling, 522
 Two-compartment model, 435
 Two-port network, 257–258
 Two-sample Student's t-test, 376
- U**
 Unipolar precordial leads. *See* Chest electrodes
 Unipolar
 augmented leads, 407
 lead, 412
 limb leads, 407
 recording, 158–160
 Unit impulse waveform, 28
 Universal behavior, 369
 Universality, 369–370
 Unsolved basic problems, 6–7
 Urine, 22
 Urology, 419
 US Food and Drug Administration (FDA), 439
- V**
 Valence electrons, 10–11
 Validation methods, 386–393
 concepts of performance, 389–393
 cross-validation, 388–389
 evaluating performance, 387–388
 measurement technology, 390t–391t
 Van der Waals forces, 13
 Vasodilatation, 475
 Vector cardiography, 413
 Vector network analyzer (VNA), 306–307
 Vectors, 505–506
 Vessel sealing, 457–458
 critical coagulation control, 458f
 Volta, Alessandro, 496–497

-
- Voltage clamp. *See* Constant amplitude voltage output
Voltage, 522
Voltammetry, 204
Volume conductors, 141–142
Vulnerable electrode technology, 252–253
- W**
Waage, Peter, 24–25
Waller, August, 497–498
Warburg immittance, 217
Water liquids, 77–78
Wavelet analysis, 400–403
Wavelet prototype, 401
Wavelet series. *See* Discrete parameter wavelet transform (DPWT)
- Wessel diagram, 340–341, 506, 507f
for parallel model circuit, 341f
for series model circuit, 342f
Wessel, Caspar, 506
Wet gel electrolytes, 185–186
White noise waveform, 272–273
Whole-cell recording technique, 244
Wien effect, 318–319, 464
Wien, Max Karl Werner, 319
Wilcoxon rank-sum test, 376–378
Working electrode, 204
Wound healing, 476–477
- Z**
Zeta-potential, 194–195
Zwitterion, 79

This page intentionally left blank